Multiscale analysis of the landforms and sediments of palaeo-ice streams

Heather Channon

A thesis presented
for the degree of
Doctor of Philosophy in Geography

Queen Mary, University of London

For my parents, John and Barbara Channon.

Thank you for your endless support.

Acknowledgements

Firstly, I would like to thank my main supervisors Simon Carr and Chris Stokes for their extensive help, guidance and encouragement throughout my PhD. I am also grateful to Jaap van der Meer, who has given me valuable advice and help.

I am very thankful to my field assistants in Scotland and Canada: Dan Newby, William Channon and Danni Pearce, all of whom made fieldwork a great deal easier and more enjoyable. Regarding fieldwork, I would also like to acknowledge Dave Evans for valuable advice about my study site in Alberta; and to Dave Evans and Dave Roberts for advice in the Tweed Valley. I am also very thankful to Hester Jiscoot, for all her help and hospitality in Lethbridge, Alberta. I produced my thin sections at Royal Holloway, University of London, and I am very grateful for all the expert advice and help I received there from Adrian Palmer. I also would like to thank Emrys Phillips for his generous guidance and advice with the analysis of some of my thin sections. I also received valuable help from Eddie Channon with some of my statistical analyses, for which I am thankful.

The PhD has been much more enjoyable thanks to my fellow postgrads: Robert Grabowski, Lorna Linch, Danni Pearce and Helen Gibbs, and many others. I am grateful for all advice and support they have given over the years. Finally, I would like to thank my family and friends, including: John Channon, Barbara Channon, Mary Sell, Laura Channon, William Channon, Andrew Channon, Laura Findlay, and especially my fiancé David Mack. I couldn’t have done it without all of your fantastic support.

Abstract

Ice streams play a fundamental role in the stability and dynamics of ice sheets. They are defined by their rapid flow and this is enabled by conditions and processes at the ice-bed interface. A significant limitation to our understanding of this environment is that most studies, of both contemporary and palaeo-ice streams, have focussed on only one or two, discrete spatial scales of analysis and so integration between scales is restricted. This thesis investigates palaeo-ice streams at multiple scales in order to examine their subglacial processes and characteristics, and to assess the links between and the application of different spatial scales of analysis. Seven palaeo-ice streams from the British and Laurentide ice sheets were investigated at the macroscale, which involved geomorphological mapping, spatial analysis of subglacial lineations and examination of bed characteristics. Two ice streams were also investigated at smaller scales, which included sedimentological analysis (mesoscale) and micromorphological analysis (microscale).

Macroscale results showed that subglacial lineations display certain spatial characteristics, including: clustering according to elongation ratio; distribution of low elongation ratios throughout the ice streams; and a decrease in maximum elongation ratio towards the ice stream lateral margins. The latter of which is considered to reflect the transverse distribution of ice velocity. In some cases, a decline in subglacial lineation concentration and elongation ratio coincided with topographic obstacles at the ice stream bed. The most common bed characteristics identified were: widespread till, fine grained sedimentary bedrock with a moderate permeability, low relief and a flat topographic curvature.

Key subglacial processes identified included deformation, which was observed at all three scales, and high pore water pressures, for which multiple lines of evidence were found at the meso and micro scales. Spatial variability in both strain and pore water pressure was also common. The multiscale approach allowed robust interpretations of fast flow mechanisms, which furthers knowledge of the sediment and landform characteristics that may result from these flow mechanisms. A summary of the processes that can be identified at each of the spatial scales is given.

Contents

List of figures

List of tables

1. Introduction

1.1 Rationale

Present day ice sheets cover the Antarctic and Greenland land masses and lock up 80 % of global freshwater (Bamber *et al*., 2007). Ice sheets are primarily governed by climate, which controls key mass balance parameters, including input of snow and ice via precipitation, and the output of ice via melting and sublimation. Predicted and current climate warming will increase ice sheet melting, causing sea level rise, which potentially will have devastating impacts on low lying regions worldwide (Overpeck *et al*., 2006). Given these impacts, it is crucial that ice sheet responses to climatic changes are fully understood, to enable accurate prediction of their behaviour and contribution to sea level rise. Some studies have highlighted that ice sheets may exhibit discontinuous behaviour and may not respond to climate changes in a steady manner (e.g. Weertman, 1974; MacAyeal, 1992; Vaughan, 2008). This is a major limitation of the reliability of models that examine ice sheet response to climatic warming (Greve, 2000). To address this limitation, further understanding of ice sheet processes, characteristics and dynamics is required in order to constrain and test models.

Ice sheet flow primarily takes place within ice streams, which have a fundamental role in ice sheets. This is demonstrated by the fact that up to 90 % of discharge from the West Antarctic Ice Sheet takes place through ice streams (Bamber *et al*., 2000). Hence, ice stream behaviour and processes must be fully understood and characterised in order to accurately predict ice sheet behaviour. Ice streams may experience dynamic behaviour as a result of climatic or oceanic changes, or internal fluctuations in the ice or at the ice bed. Observations and evidence from contemporary and palaeo-ice streams demonstrate that ice streams can speed up, slow down, migrate, widen, narrow, shutdown and that a network of ice streams can even completely reorganise (e.g. Whillans *et al*., 1987; Retzlaff and Bentley, 1993; Echelmeyer and Harrison, 1999). Despite widespread dynamic behaviour, the underlying reasons for this are rarely clear, because the processes, behaviour and characteristics of ice streams are only partially understood (Alley *et al*., 2004).

Processes and conditions at the ice stream bed are crucial to the rapid flow of ice streams. In pure ice streams (i.e. not topographically controlled by a subglacial valley) subglacial water and/or subglacial sediments lubricate the bed, enabling rapid flow through subglacial sliding and subglacial sediment deformation (Alley *et al*., 2004). Despite the critical role of the subglacial environment to ice stream flow, our understanding of its controls on the ice stream processes and spatial variations, is incomplete. This is principally due to the inaccessibility of the ice stream bed. Studies of the beds of contemporary ice streams are limited to geophysical surveys, which cover large areas at relatively low resolutions (e.g. Blankenship *et al*., 1986; Gades *et al*., 2000); and to point samples or measurements, which are derived from boreholes (e.g. Engelhardt and Kamb, 1997; Tulaczyk *et al*., 1998; Kamb, 2001). These two approaches to the study of modern ice streams provide information at vastly different spatial scales, which can be difficult to reconcile, potentially leaving a considerable gap in our knowledge of the subglacial environment.

The exposed beds of palaeo-ice streams provide a way to access and study ice stream beds across a range of scales with relative ease. Palaeo-ice streams have provided considerable insight into ice stream basal processes and behaviour (e.g. Hicock and Dreimanis, 1992; Ó Cofaigh and Evans, 2001; Stokes and Clark, 2001; Ottesen *et al*., 2005) and the ability to reconstruct palaeo-ice streams has been enabled by the study of the processes and behaviour of both modern and past ice streams. The study of the macroscale geomorphology of palaeo-ice streams, in particular, has been considerable, owing to the availability of widespread remote sensing datasets (e.g. Stokes and Clark, 2001; Ottesen *et al*., 2002). In comparison, studies of palaeo-ice stream sedimentological analysis at a field scale and microscale analysis of sediments are few (e.g. Lian and Hicock, 2000; Ó Cofaigh *et al*., 2007). Most studies of palaeo-ice streams have focussed on one or two of these spatial scales, which relate to certain methodological techniques, and attempts to integrate between different scales is usually limited (e.g. Hicock and Fuller, 1995; Clark and Stokes, 2001; Sejrup *et al*., 2003; Graham *et al*., 2009; Reinardy *et al*., 2011). The use of these techniques and scales in isolation, may have allowed linkages and differences between these scales to be overlooked, and as such may be a limiting factor for our understanding of the ice stream subglacial environment.

Given the limitations of studying ice streams at a single scale, a more complete examination of an ice stream at multiple scales and where possible integrating between scales, should reveal a more comprehensive insight into subglacial processes. This study will take this approach, integrating geomorphology, sedimentology and micromorphology of palaeo-ice streams, in order to understand the full range of processes operating at the ice stream bed and the links between the different scales. Interrogation of specific scales will highlight any connections between them, which may indicate where key processes are manifest and if they migrate between spatial scales (for example from a micro scale to a macro scale). This may shed light on the knowledge gap that exists between point-scale processes and macro-scale products in the subglacial environment (Clarke, 2005). Furthermore, this would allow a more robust reconstruction of ice stream processes, as the employment of multiple methodologies may provide corroboration or disagreement between different results, thus increasing reliability. The overall aim of this thesis is as follows:

Aim

To investigate palaeo-ice stream beds at multiple spatial scales, in order to identify their subglacial characteristics and processes, and to assess the relevance of spatial scale.

1.2 Approach

This thesis will focus on three spatial scales of analysis. These are based on: geomorphology (referred to as macroscale, ranging from kilometres to metres); sediments (referred to as mesoscale, ranging from metres to centimetres); and micro sediments (referred to as microscale, ranging from centimetres to micrometres). The three spatial scales will be explored across selected palaeo-ice streams. This will allow the questions surrounding scale to be addressed, in addition to furthering understanding of the ice stream system and specific subglacial processes therein.

The core of this thesis comprises an examination of two palaeo-ice streams (the Tweed Ice Stream, UK and the Central Alberta Ice Stream, Canada) at all three of the aforementioned scales. Only two ice streams were studied to this degree because of the considerable time involved in the range of methods required to investigate each of the

scales. Further to this, a macroscale survey was conducted of the subglacial lineations of seven palaeo-ice streams (including the two aforementioned ice streams), allowing an investigation into macroscale spatial variability of the ice stream bed. These elements of the thesis are summarised in the following objectives:

Objectives

1. To conduct detailed mapping of the subglacial lineations and other glacial landforms of seven palaeo-ice streams, enabling characterisation of ice stream macroscale geomorphology and spatial heterogeneities (in both subglacial lineations and bed properties).

2. To conduct detailed studies of two palaeo-ice stream beds (the Tweed Ice Stream, UK and the Central Alberta Ice Stream, Canada) in order to examine their subglacial processes and characteristics at multiple scales (using geomorphology, sedimentology and micromorphology).

1.3 Thesis structure

The main body of this thesis is presented in three results chapters (chapters 4 to 6). Prior to this, Chapter 2 presents a review of the literature on ice streams and their subglacial processes and Chapter 3 presents the methods. The first results chapter, Chapter 4, presents glacial geomorphological mapping and associated spatial analysis of five palaeo-ice streams. Chapter 5 presents the results of the multiscale investigation of the Tweed Ice Stream and Chapter 6 presents the results of the multiscale investigation of the Central Alberta Ice Stream. Chapter 7 presents the discussion and Chapter 8 presents the conclusions of the thesis. Several electronic appendices are included, which correspond mainly to Chapters 5 and 6, and are referred to throughout the thesis.

2. Basal processes and characteristics of ice streams

Ice streams are defined as channels of ice that flow faster than surrounding ice within ice sheets (Swithinbank, 1954). They play a key role within ice sheets, exporting significant amounts of ice, which may be as much as 90 % of total ice sheet discharge (Bamber *et al*., 2007). Ice streams are dynamic entities and play a critical role in ice sheet response to changes in climate and sea level, and as such understanding them is critical for accurate forecasting of ice sheets. Understanding and prediction of ice stream dynamics and evolution remains a challenge, which is largely a result of their inaccessibility (Clarke, 2005; Smith *et al*., 2007). This problem is most pertinent for the understanding of the ice-bed interface. The ice-bed interface of an ice stream facilitates rapid ice flow, in other words, the functioning of the ice stream is dependent upon conditions and processes at the ice stream bed (Alley *et al*., 2004). The investigation of accessible palaeo-ice streams has improved understanding of the processes and characteristics of the ice stream subglacial environment (e.g. Clark and Stokes, 2001; Ó Cofaigh *et al*., 2005; Winsborrow *et al*., 2010) and may continue to do so. This chapter presents a review of the subglacial processes and characteristics of ice streams and outlines how this has been investigated at the macro, meso and micro scales, in contemporary and palaeo-ice streams.

2.1 Ice streams

Ice streams have certain distinctive characteristics. They can flow at speeds of up to 12 km per year (e.g. Jakobshavn Isbrae, West Greenland; Joughin, 2004a). Typically, they are tens of kilometres wide, hundreds of kilometres long and constitute a main trunk fed by several tributaries, as shown in Figure 2.1. Their lateral margins are characteristically abrupt and display a sharp lateral change from fast to slow moving ice, across a small proportion of their total width (Raymond *et al*., 2001). Whilst a slow moving ice dome typically characterises the centre of an ice sheet, ice streams often emerge at the peripheries of an ice sheet where they drain onto land, or into the sea at an ice shelf (as in Figure 2.1), or at a calving margin. The flow of ice within ice streams is controlled by its force balance, which refers to the balance between the gravitational driving forces and the opposing forces (van der Veen, 1999). The opposing forces include lateral shear

(which typically constitutes 50 % and in some cases near 100 % of the opposing forces; Raymond *et al*., 2001); basal shear (found to account for 29 % of opposing forces in MacAyeal Ice Stream; MacAyeal *et al*., 1995; and 40 – 50 % in Whillans Ice Stream; Beem *et al*., 2010); and longitudinal stresses (found to contribute 20 % of force balance of Bindschadler Ice Stream; Price *et al*., 2002). These opposing forces commonly vary between ice streams and along the length of an ice stream (Raymond *et al*., 2001; Price *et al*., 2002). A force balance is present in all glacier types and in a valley glacier the relative contributions of the resistive forces may vary dependent on various factors, including the geometry of the valley in which the glacier lies (Nye, 1957). In an ice stream, the specific conditions of high pore water pressures at an ice stream bed means that basal drag is likely to be relatively low compared to other glacier types, and lateral drag may have a greater significance (Raymond *et al*., 2001).

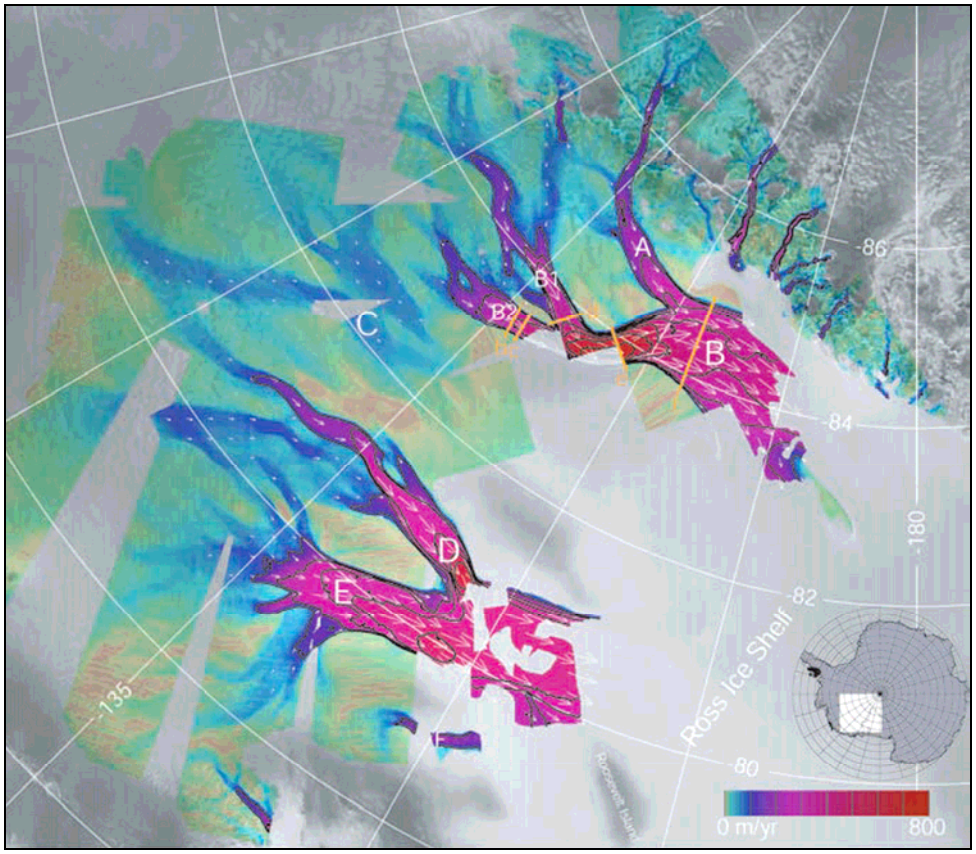

Figure 2.1 – Radar imagery of ice streams from the Siple Coast region of the West Antarctic Ice Sheet, displaying their velocities and characteristic form. The ice streams are labelled with their old names in the figure, and have since been renamed: Mercer Ice Stream (A); Whillans Ice Stream (B); Kamb Ice Stream (C); Bindschadler Ice Stream (D); and MacAyeal Ice Stream (E). Ice flow is towards the Ross Ice Shelf in the lower right of the image. From Joughin *et al*. (2004b).

2.1.1 Ice stream types

Ice streams can be classified into two types: ‘topographic’ ice streams and ‘pure’ ice streams (Truffer and Echelmeyer, 2003). Topographic ice streams, such as Jakobshavn Isbrae, are constrained within topographic lows, such as a bedrock trough, and their rapid flow results from high gravitational driving stresses, which is reinforced by high basal temperatures due to the insulation effects of the thick ice and dissipation of heat from fast flow (Payne, 1999). Conversely, pure ice streams are not controlled by topography and despite relatively low driving stresses, they flow rapidly over a well lubricated bed, resulting from pressurised water and in many cases also soft deformable sediments (Alley, 2004). However, in reality many ice streams fall into a broad spectrum of types, ranging from pure ice streams to topographic ice streams (Bentley, 1987; Truffer and Echelmeyer, 2003) and many ice streams are likely to contain characteristics of both types. Furthermore, outlet glaciers, which are fast flowing glaciers that are bounded by rock, may overlap with the classification of ice streams. Some outlet glaciers may be transitional with ice streams, such as Jakobshavn Isbrae, which is an ice stream at its upstream end and an outlet glacier at its terminal zone (Clarke, 1987) and as such is referred to as both an ice stream and an outlet glacier by different authors (e.g. Abdalati and Krabill, 1999; Alley *et al*., 2005; Holland *et al*., 2008).

2.1.2 Ice stream basal flow mechanisms

Mechanisms for ice flow within a glacier include: internal deformation, basal sliding, and subglacial deformation (Bennett and Glasser, 1996); as well as a fourth mechanism, comprising decoupling and sliding along a discrete layer within the substrate, as proposed by Kjær *et al*. (2006). These different mechanisms are illustrated in Figure 2.2. All of these may take place within ice streams, and which mechanism(s) operate depends on a range of factors such as: ice thickness and temperature; transport of water to the bed; permeability, thickness and deformability of the till/substrate; and permeability of the bedrock. Because ice deformation can only account for very low ice velocities (less than 10 m yr^{-1}; Alley and Whillans, 1991), one or more of the other flow mechanisms must operate for rapid ice stream flow. As mentioned, these take place at the ice-bed interface, which is why this environment is so critical to the functioning of an ice stream.

Rapid subglacial sliding results from highly pressurised water at the ice-bed interface (Kamb, 2001; Alley *et al*., 2004). Pressurised water decouples the ice from its bed, reducing friction and allowing the ice to slide over its bed. Sliding may take place over bedrock or over soft sediments. Subglacial deformation occurs where till is weaker than overlying ice, causing it to deform and, in turn, contribute to the forward motion of the overlying ice (Murray, 1997). It requires sediments to be saturated at sufficiently high pore water pressures. Subglacial deformation became widely recognised in the 1980s following several studies (e.g. Boulton, 1979; Boulton and Jones, 1979; Alley *et al*., 1986; Blankenship *et al*., 1986; 1987; Boulton and Hindmarsh, 1987). Of these the measurement and modelling of till below an Icelandic glacier provided key evidence for subglacial deformation (Boulton and Hindmarsh, 1987), whilst geophysical studies inferred the importance of this mechanism below the Whillans Ice Stream (Blankenship *et al*., 1986; 1987; Alley *et al*., 1986). The reliance of both subglacial sliding and subglacial deformation on high pore water pressures demonstrates that the subglacial drainage system is critical to ice stream flow.

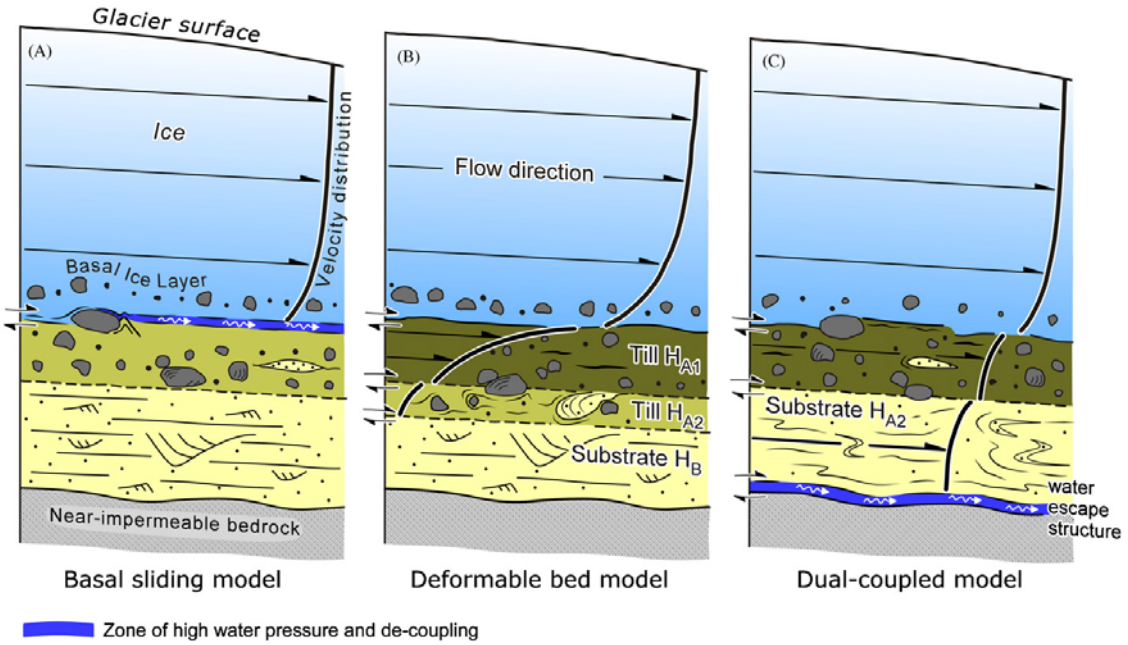

Figure 2.2 – Schematic model of different ice flow mechanisms that can operate and how they may be manifest through the ice and the substrate. Each diagram represents internal deformation (represented by the velocity distribution within the ice) and the following: (a) basal sliding; (b) subglacial deformation; (c) subglacial deformation in addition to sliding along a decoupled horizon between the till and underlying bedrock. From Kjær *et al*. (2006).

Several studies have demonstrated that both sliding and deformation may be spatially and temporally variable in the subglacial environment (e.g. Smith, 1997; Fischer and

Clarke, 2001; Smith *et al*., 2007; Murray *et al*., 2008). In ice streams they have been inferred to operate simultaneously but in different areas of an ice stream bed (e.g. Murray *et al*., 2008) and with alternation between the two mechanisms (e.g. Rattas and Piotrowski, 2003; Jørgensen and Piotrowski, 2003). Significantly, inferences of flow mechanism(s), their relative importance and their spatial distributions have only been made for a limited number of ice streams (e.g. Blankenship *et al*., 1986; Alley, 1989; Jørgensen and Piotrowski, 2003; Murray *et al*., 2008), and often for only a limited spatial area of the bed. As such, the relative distribution of these mechanisms, how they interact and change, and what ice stream or substrate characteristics determine these factors, is poorly known.

2.1.3 Ice stream dynamics

The significance of ice streams lies in their substantial contribution to ice sheet discharge and their potential for change, for example in their speed or force balance (Tulaczyk, 2006a; Stokes *et al*. 2007). Ice streams can experience a range of dynamic behaviour, which may have significant impacts on the ice sheet and on wider earth systems such as climate and oceans. Jakobshavn Isbrae, for example, has experienced an increase in velocity over the past decade, associated with thinning and loss of its buttressing ice tongue (Joughin *et al*., 2004a; Motyka *et al*., 2011). It is not clear what initiated these changes, but they may have a significant impact on ice sheet mass balance, which in turn affects sea level (Joughin *et al*., 2004a). In West Antarctica, the Kamb Ice Stream (Figure 2.1) shut down 130 years ago, in contrast to adjacent ice streams that continue to flow rapidly (Retzlaff and Bentley, 1993). Various theories have been proposed to explain its shutdown; including surging behaviour, freeze-on, loss of lubricating basal sediments and competition with the adjacent Whillans Ice Stream, and of these water piracy is the leading hypothesis (e.g. Thomas, 1988; Anandakrishnan and Alley, 1997; Bougamont *et al*., 2003).

Studies of palaeo-ice streams have found that ice streams may reorganise over time, as documented by overprinted ice stream signatures, which is particularly apparent at the macroscale in the landscape of North America (e.g. Hodgson, 1994; De Angelis and Kleman, 2007a; Ross *et al*., 2009). These large scale changes are inferred to result from various factors, including: changes in climate; changes at the ice stream bed; and inherent or cyclic instabilities within the ice sheet (e.g. MacAyeal, 1993; Clark *et al*.,

2000; Bennett, 2003; Stokes and Clark, 2006). Evidently, dynamic behaviour of ice streams is widespread and its forcing factors may be varied and ambiguous. This complexity is a result of the wide range of factors that influence ice stream behaviour, which commonly are difficult to observe due to the inaccessibility of ice streams, in particular the ice-bed interface.

2.2 Macroscale characteristics of ice stream beds

The macroscale characteristics of an ice stream bed can be considered as its geomorphology (e.g. bedforms) as well as any basal conditions and processes manifest across a large scale. For contemporary ice streams, geophysical methods have been employed to study the large scale characteristics of the bed, including seismic and radar surveys (e.g. Blankenship *et al*., 1987; Smith, 1997; Murray *et al*., 2008). For palaeo-ice streams, large scale geomorphology can be observed using satellite imagery, aerial photos, digital elevation models (DEMs) (e.g. Dyke and Morris, 1988; Stokes and Clark, 2003a), and in the case of offshore palaeo-ice streams; bathymetry, seismic and sonar data (e.g. Dowdeswell *et al*., 2004; Andreassen *et al*., 2008). Understanding of the macroscale characteristics and processes of ice streams may also be aided by modelling, whereby parameters (measured from any of the spatial scales) are inputted into ice stream or ice sheet models in order to reconstruct large scale observed trends or ice stream evolution (e.g. Alley *et al*., 1987; Tulaczyk *et al*., 2000a; Joughin *et al*., 2004b).

2.2.1 Subglacial bedforms

Subglacial bedforms have been identified in a handful of macroscale surveys of contemporary ice streams (e.g. Blankenship, 1986; Smith *et al*., 2007; King *et al*., 2007; King *et al*., 2009), but the vast majority of knowledge about subglacial bedforms stems from studies of palaeo-ice streams (e.g. Stokes and Clark, 2003a; De Angelis and Kleman, 2005; Ottesen *et al*., 2005a). Investigation of palaeo-ice stream beds has revealed a characteristic signature of ice stream bedforms and sediment features, including: characteristic shape and dimensions; convergent flow patterns; highly elongate bedforms; Boothia-type erratic trains; sharp lateral margins; lateral shear moraines; evidence of pervasively deformed till; and the existence of a submarine sediment fan or delta (Stokes and Clark, 1999). Some of these are apparent in Figure 2.3, which depicts a palaeo-ice stream signature from Norway. Potentially the most

significant ice stream characteristic is elongated subglacial lineations, which may be the most commonly invoked criterion for palaeo-ice stream identification (e.g. Stokes and Clark, 2003a; Everest *et al*., 2005; De Angelis and Kleman, 2005; Ottesen *et al*., 2005a). Albeit elongated subglacial lineations may form in other subglacial environments (e.g. surging glaciers), indicating that this characteristic alone is insufficient evidence to identify a palaeo-ice stream and several criteria are required for confident identification as such (Stokes and Clark, 1999).

a. Ice stream subglacial lineations

Ice stream subglacial lineations are streamlined bedforms aligned parallel to ice flow and may include drumlins, mega scale glacial lineations (MSGL), flutings, crag and tails, and streamlined bedrock (e.g. Clark, 1993; Jansson *et al*., 2003; Bradwell *et al*., 2007; Anderson and Fretwell, 2008). The most prolific of these is drumlins, which are found below both glaciers and ice streams, and for which there is a considerable body of research (e.g. Menzies, 1979; Hart, 1997; Rattas and Piotrowski, 2003; Clark *et al*., 2009). Subglacial lineations are usually located together in fields that may comprise thousands of individual features and they may also be found in close association with ribbed moraine (Benn and Evans, 2010). The various types of subglacial lineations, which are typically defined by their form, may represent a continuum of bedforms, in terms of characteristics including size and elongation ratio (Rose, 1987).

Drumlins are typically associated with soft sediments, but the internal composition of drumlins may vary considerably. Those reported include sorted sediments, till and bedrock, all of which may display varying degrees of deformation (see Stokes *et al*., 2011). This variation in properties has led to an array of hypotheses for drumlin formation. Menzies (1979) review of drumlins evaluates several different theories for their formation, which are: the accretion theory; the till squeeze theory; the dilatancy theory; the frost heave theory; and the glacial kinematic fluting theory. Additional theories have included: subglacial deformation; subglacial lodgement; melt out; and fluvial infills or remnants of subglacial floods (Bennett and Glasser, 1996). More recently two major theories have emerged as predominant, these are: (a) drumlin formation via subglacial sediment deformation (e.g. Boulton, 1987; Hindmarsh, 1998a; Fowler, 2000); and (b) drumlin formation via subglacial floods (e.g. Shaw *et al*., 1989; Shaw, 2002). The first of these theories, the deformation theory, put forward by Boulton

(1987) involves stronger parts of the bed remaining static, whilst weaker parts of the bed deform around them. The theory has several strengths including: its ability to explain many different types of subglacial landforms including megaflutes, drumlins and ribbed moraine; its ability to explain a range of different compositions found in subglacial lineations, such as till, bedrock and fluvial sediments; and it can also explain some of the rapid rates of drumlin formation that have been observed (Bennett and Glasser, 1996). However, critics of the theory argue that there is no direct evidence that deformation is widespread below ice sheets and that sedimentary evidence for tectonic structures is lacking (Bennett and Glasser, 1996). Albeit if deformation is pervasive it would be expected to remove traces of sedimentary features leaving a homogenised till. Modelling work has also lent support to components of the theory and has shown that an instability mechanism can allow the formation of two dimensional waves at glacier beds (Hindmarsh, 1998a, b; Fowler, 2000; Schoof, 2002). This theory is further strengthened by more recent studies from modern ice streams, in which geophysical imaging has revealed the mobilisation of sediment to form drumlins (King *et al*., 2007; Smith *et al*., 2007). Smith *et al*. (2007) found evidence for the development of a drumlin below the Rutford Ice Stream in West Antarctica, within a time span of seven years.

The subglacial megaflood theory, which evokes some controversy, states that drumlins form by catastrophic meltwater floods below ice sheets that are fed by large proglacial and subglacial lakes (Shaw, 1983; Shaw *et al*., 1989; Shaw, 1994). The theory advocates that a range of subglacial bedforms including drumlins are formed via the infilling of large scours cut into the base of the ice from turbulent subglacial floods. The premise is primarily based on the morphological similarity between drumlins and erosional scour structures that form at the base of turbulent underflows. The hypothesis has been subject to considerable criticism, such as a lack of rigorous hypothesis testing (Benn and Evans, 2006) and the infeasibility of the sudden release of water of sufficient volumes to create the bedforms (Clarke *et al*., 2005). Given the evidence against the megaflood theory its seems that the majority of researchers in the field do not favour the theory and the subglacial deformation theory provides the most satisfactory explanation (e.g. Bennett and Glasser, 1996; Clarke *et al*., 2005; Benn and Evans, 2006).

Another subglacial lineation type is MSGL, which are particularly large and elongate lineations or flutings and reportedly range in length from six to a hundred kilometres

(Clark, 1993). This particular bedform type has typically been identified in palaeo or contemporary ice streams (e.g. Ottesen *et al*., 2005a; Ó Cofaigh *et al*., 2005; Bradwell *et al*., 2007; King *et al*., 2009). A formation mechanism, which invokes ploughing of ice keels into underlying sediment, has been proposed for this bedform (Clark, *et al*., 2003).

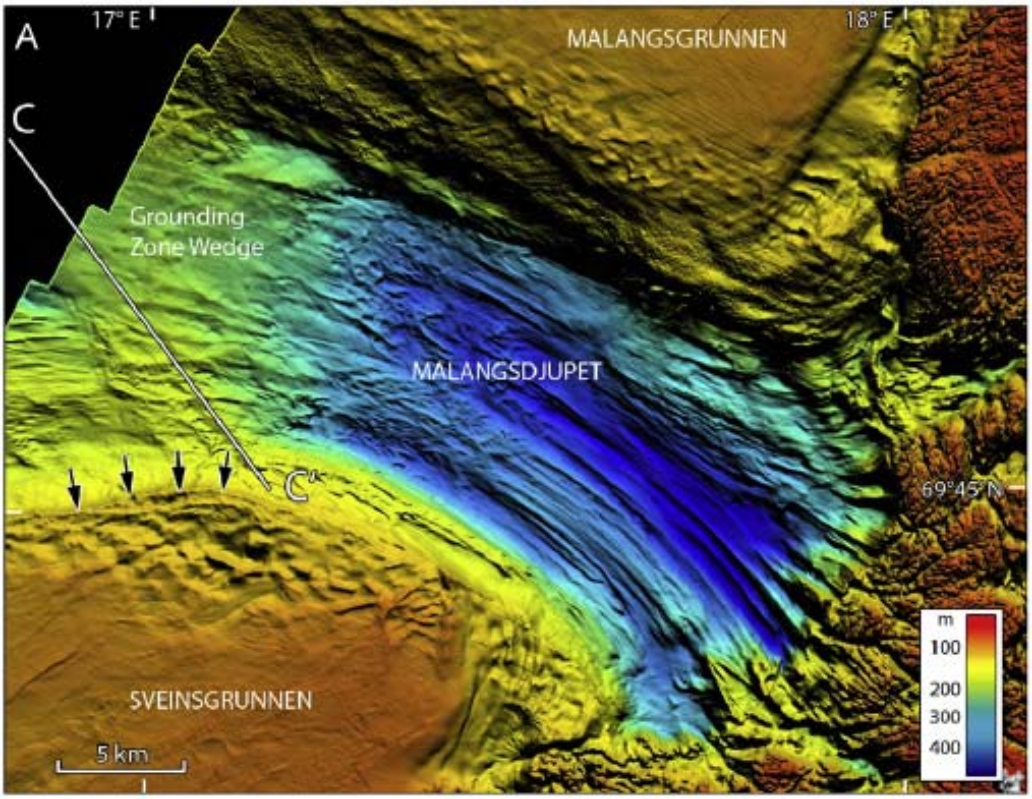

Figure 2.3 – Bathymetry of the palaeo-ice stream in Malangsdjupet Trough, off the West Coast of Norway. Ice flow direction is from the lower right to the upper left of the image. Note the upstream convergence zone, elongate MSGL and abrupt lateral margins. A lateral shear margin moraine is highlighted with black arrows. From Ottesen *et al*. (2008).

In palaeo-ice streams subglacial lineations are typically highly elongate, as illustrated in Figure 2.3. Stokes and Clark (1999) suggest an elongation ratio of 10:1 or higher as typical, and elongation ratios up to 70:1 have been reported (Bradwell *et al*., 2007). Several studies have argued that elongation ratio provides a proxy for ice velocity (Hart, 1999; Stokes and Clark, 2002a; Briner, 2007; King *et al*., 2009). These arguments are commonly based on comparisons between the spatial distribution of elongation ratio in a palaeo-ice stream to the spatial distribution of ice velocity within modern day ice streams, chiefly the decline in ice velocity from the centreline of an ice stream to its lateral margins (e.g. Hart, 1999; Briner, 2007; Stokes and Clark, 2003a). The relationship between ice flow and elongation of subglacial lineations may be envisaged whereby they initiate at a point and progressively elongate with time via substrate

deformation (Clark, 1993). This would mean that elongation ratio might provide a proxy for strain, as manifest via ice velocity and substrate characteristics. However, this would only be feasible in certain conditions, because if the ice was decoupled from its bed, substrate deformation would not control any elongation that was taking place (Stokes and Clark, 2002).

This proposed relationship between ice flow and elongation is complicated by other factors affecting bedform morphometry. Substrate properties in particular have been found to play a role in bedform morphometry. Piotrowski (1987) noted a correlation between till texture and drumlin morphometry, in that those composed of finer-grained sediment are smaller and more elongate than those composed of coarser sediment. This same relationship was also observed by Rattas and Piotrowski (2003) in an east Baltic palaeo-ice stream. They also noted that drumlins on more permeable bedrock were larger and those on less permeable bedrock were smaller and more elongate, within a drumlin field. If subglacial deformation is taken to be the formation mechanism for drumlins then evidently substrate properties will play a key role in forming the more resistant drumlin cores and facilitating the conditions for deformation.

Another factor that may contribute to elongation ratio is constancy of flow direction (Doornkamp & King 1971; Mills 1987). Mills (1987) found that more parallel drumlins, found in the central zone of a drumlin field had higher elongation ratios. Clark (1993) considered that MSGL may arise from high velocities over short timescales or slower velocities over shorter timescales, but Stokes and Clark (2002) argue that the increasing evidence for rapid changes to ice streams and ice sheets suggest that the former is more likely. Furthermore, in the context of an ice stream the constancy of flow direction or the time over which the subglacial lineations are elongated for will be the same in the centre of the ice stream as its lateral margins. Thereby the evidence from previous studies indicates that ice velocity has a fundamental control on elongation ratio (Hart, 1999; Stokes and Clark, 2002a; Briner, 2007; King *et al*., 2009). And with consideration for its limitations, elongation ratio could be used as a proxy to assess flow heterogeneities in a palaeo ice stream and specifically examine the link between flow speed and proposed ‘sticky spots’, such as till free areas (Stokes *et al*., 2007).

b. Other ice stream bedforms

Other bedforms observed on or around ice stream beds include eskers, ribbed moraine, lateral shear margin moraines, terminal moraines and hummocky moraine (e.g. Stokes, 2006; Stokes and Clark, 2002b; Ottesen *et al*., 2005b). Eskers are rarely reported from ice stream beds (e.g. Jørgensen and Piotrowski, 2003; Storrar and Stokes, 2007; Evans *et al*., 2008). This may be explained to a degree by the fact that many ice streams are located on sedimentary bedrock (Alley *et al*., 2004), which is less conducive to the formation of eskers than crystalline bedrock, because a canal system of subglacial meltwater drainage is considered to be more typical in these localities (Clark and Walder, 1994). Additionally, their lack of preservation and lack of identification in low resolution remotely sensed imagery may also be factors contributing to their limited sightings.

Ribbed moraine is a common subglacial landform and comprises irregular transverse ridges. They are frequently associated with ice divides although are not restricted to these areas (Dunlop and Clark, 2006). Several formation mechanisms have been proposed for these landforms, but as yet there is no consensus to this (e.g. Boulton, 1987; Fisher and Shaw, 1992; Hättestrand, 1997; Möller, 2006; Lindén *et al*., 2008). They are not typically associated with ice streaming but they have been found on some palaeo-ice stream beds, including an ice stream onset zone (Dyke *et al*., 1992), where they were interpreted as a reflection of the transition from cold to warm based ice (Hättestrand and Kleman, 1999); and they have also been found superimposed onto subglacial lineations (Stokes and Clark, 2003a; Dunlop and Clark, 2006). Superimposed ribbed moraine in the Dubawnt Lake Palaeo-Ice Stream (Nunavut, Canada) is interpreted as being representative of a change in basal conditions, specifically a manifestation of ice stream shutdown via basal freeze-on (Stokes and Clark, 2003a; Stokes, 2006; Stokes *et al*., 2008).

Several types of moraine may be associated with palaeo-ice streams. A handful of lateral shear margin moraines have been identified (e.g. Stokes and Clark, 2002b; Ottesen *et al*., 2005b; 2008; Figure 2.3) and this landform represents one of the diagnostic criteria for palaeo-ice stream identification (Stokes and Clark, 1999). Different formation mechanisms for this landform have been proposed including:

differential erosion rates relating to lateral variations in ice velocity; incursion from interstream ridges after ice stream retreat; deposition by meltwater; and melt-out of englacial debris (Stokes and Clark, 2002a; Hindmarsh and Stokes, 2008). Some of these may be considered more likely than others, but further investigation is required to ascertain the precise formation mechanism of this landform. Terminal moraines may be associated with terrestrial terminating ice streams and have been observed in a few palaeo settings (e.g. Patterson, 1998; Jennings, 2006). They commonly form a lobate shape, which reflects the terminal ice lobe that is characterised by a large surface area allowing high ablation, balancing the large flux of ice transported by the ice stream (Clark and Stokes, 2003). The terminus of a marine ice stream may be characterised by a trough mouth fan, grounding zone wedge or moraine(s) (e.g. Ó Cofaigh *et al*., 2003; Andreassen *et al*., 2008; Ottesen *et al*., 2008; Winsborrow *et al*., 2010). Hummocky moraine on or around ice streams has been reported from several locations in the Laurentide Ice Sheet (e.g. Shetsen, 1987; 1990; Eyles *et al*., 1999; Jennings, 2006; Ross *et al*., 2009). In these cases hummocky moraine is typically reported in inter-ice stream areas or moraines and is commonly thought to be associated with ice stagnation (Jennings, 2006; Eyles *et al*., 1999), although not exclusively so (e.g. Munro and Shaw, 1997). In summary, the range of bedforms found at the beds of palaeo-ice streams has brought significant insights to their interpretation (e.g. Stokes and Clark, 2003a; Ottesen *et al*., 2008). However, the incomplete understanding of many of these landforms limits analysis of palaeo-ice streams.

In the context of a palaeo-ice stream a distinction may be made between whether the bedforms were laid down time-trangressively (i.e. bedforms which reflect changing glacial conditions and geomorphic processes over time) or isochronously (i.e. bedforms which represent the glacial conditions in a single point in time) (Stokes and Clark, 2001). This consideration of temporal scale is important to allow reliable inferences to be made about former glacial conditions and subglacial processes. A time-transgressive ice stream signature may be expected to display characteristics such as overprinted bedforms, subglacial lineations with low parallel conformity and bedform morphometry that has abrupt spatial variations (Clark, 1999). In contrast, an isochronous ice stream signature is likely to have subglacial lineations with a high degree of parallel conformity and minimal association with end moraines or eskers (Clark, 1999). An isochronous ice stream signature may be considered to represent a snapshot in time (Clark, 1999) and as

such can provide a useful means to infer subglacial processes. However, this is an oversimplification because geomorphic processes do not happen instantaneously and different geomorphic processes may operate at different rates (Anderson and Anderson, 2010). Furthermore, bedforms may be subject to post depositional modification. Bedforms may be preserved subglacially where basal shear stress is lower than bed strength (Clark, 1999), such situations include cold based ice, slow moving ice, a shallowing deforming layer or basal decoupling. The last two of these may take place in an ice stream subglacial environment, thus providing potential for preservation of such bedforms. However, below a fast moving ice stream there is also potential for bedform modification (for example if ice is coupled to its bed, especially where pore water pressures are low; Clark, 1999) and this may vary spatially, which has significance if the spatial variations of bedforms is investigated.

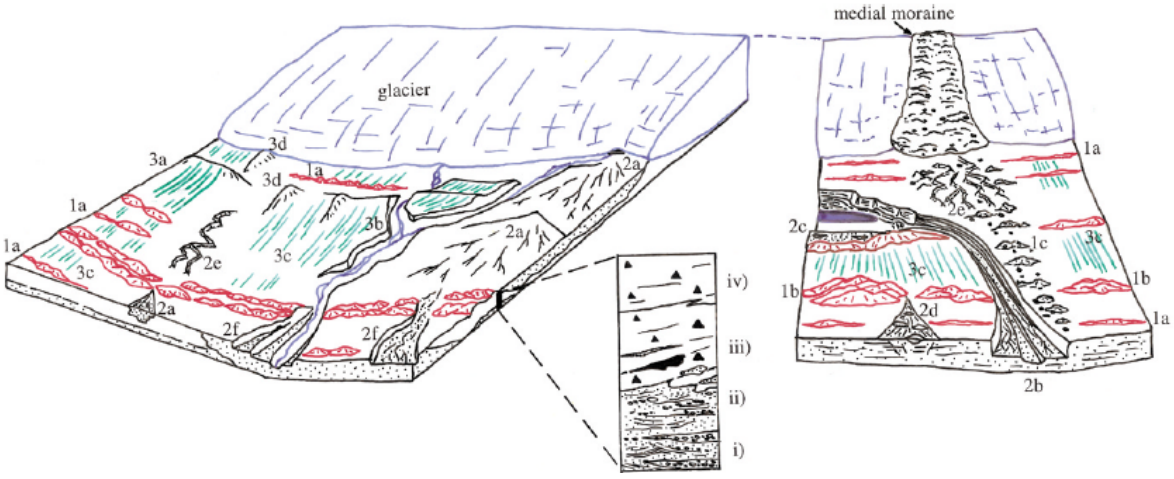

Figure 2.4 – Depiction of an active temperate glacial landsystem, from Evans and Twigg (2002). The numbers refers to a range of geomorphological and sedimentological features, including small push moraines (1a), ice contact sandur fans (2a), eskers (2e), flutes (3c) and drumlins (3d); see Evans and Twigg (2002) for further details. Comparison with Figure 2.3 enables identification of some of the key differences between ice streams and other glacial landsystems.

As the above paragraphs describe, certain landforms characterise the bed of an ice stream, most notably the elongated subglacial lineations as depicted in Figure 2.3 (Stokes and Clark, 1999). Whilst some of these landforms may be present in other subglacial environments, it is the combination of landforms that is most useful to characterise different glacial landsystems (see Evans, 2003). For example a temperate glacier landsystem is characterised by a range of landforms including push and squeeze moraines, glaciofluvial deposits, flutes and drumlins, as depicted in Figure 2.4 (Evans and Twigg, 2002). On a more theoretical level differences between an ice stream subglacial environment and a normal ice stream environment may display several key

differences at the macroscale. An ice stream bed has water at its bed, whereas glaciers in other environments may be frozen to their beds, such as small arctic glaciers (Benn and Evans, 2010). An subglacial ice stream environment is also likely be subject to high pore water pressures across much of its bed, which enables subglacial deformation and subglacial sliding, whereas this may not be the case for other subglacial environments and if they are frozen to their bed they will instead flow via internal deformation (Figure 2.2).

2.2.2 Macroscale evidence for subglacial deformation and basal sliding

Geophysical investigations beneath contemporary ice streams have revealed some of the characteristics of subglacial deformation and subglacial sliding, and have helped establish the importance of these processes to rapid ice flow. Blankenship *et al*. (1986) conducted a seismic survey across a 10 km^2 area of the Whillans Ice Stream (West Antarctica), which revealed a 5 to 6 m thick, porous, saturated till layer at a high pore water pressure. These characteristics indicated that the till was weak, leading them to infer that the till layer was deforming (Blankenship *et al*., 1986; Alley *et al*., 1986) and contributing to the idea that subglacial deformation is a key mechanism for ice stream flow.

Since then, further geophysical investigations of ice streams have found evidence for dilated subglacial till, leading to further inferences of subglacial deformation (e.g. Smith, 1997; Anandakrishnan, 2003; Vaughan *et al*., 2003), whilst some studies have found evidence for subglacial sliding (e.g. Smith 1997; Murray, 2008). The initial studies considered sediment deformation to be deep seated in the subglacial sediment layer (Alley *et al*., 1986; 1987; Blankenship *et al*., 1987), however, later studies found evidence that deformation was typically confined to the upper few centimetres of till (e.g. Engelhardt and Kamb, 1998; Kamb, 2001). The limited spatial extent of these investigations, in addition to the finding of spatial heterogeneities of bed properties and basal flow mechanisms (e.g. Atre and Bentley, 1993; Smith, 1997; Vaughan *et al*., 2003), suggests that further work is needed to characterise the spatial extent and distribution of ice stream basal flow mechanisms.

2.2.3 Subglacial water systems

Subglacial water pressure plays a critical role in the rapid flow of ice streams, as previously noted. It controls the degree of coupling between the ice and the bed, because the greater the water pressure the lower effective pressure will be, which results in a lesser transfer of stress from the ice to the bed, allowing it to slide more easily (Tulaczyk, 2003). Furthermore, water pressure affects sediment strength because it reduces internal friction and cohesion, and this mechanism is depicted in the Mohr-Coulomb equation:

$$\tau_y = c + p' \tan\phi$$

Where τ_y is yield strength,

c is cohesion,

ϕ is the angle of internal friction and

p' is the effective pressure, which is defined as:

$$p' = P - p_w$$

In which P is total stress and

p_w is the pore water pressure.

This crucial component of ice stream flow is closely linked with the ice stream subglacial water system. Ice stream subglacial water systems may include all of the types identified by Benn and Evans (1996), which are shown in Figure 2.5. A limited number of seismic and radar studies have identified subglacial water systems in contemporary ice streams. For example, King *et al*. (2007) and Murray *et al*. (2008) both found evidence for a subglacial canal system (e.g. Figure 2.5(6)) below areas of the Rutford Ice Stream. These observations support theoretical predictions that canals (subglacial channels cut into till) play a key role in subglacial drainage where ice flows over low gradient, soft sedimentary beds (Walder and Fowler, 1994; Ng, 2000). Another observation of Murray *et al*. (2008) is that small water bodies were characteristic in areas of subglacial sliding within their study area, which may represent a linked cavity system (e.g. Figure 2.5(5)). Tulaczyk *et al*. (2000b) also suggest that Whillans Ice Stream has no organised regional drainage, thus allowing the development of high pore water pressures.

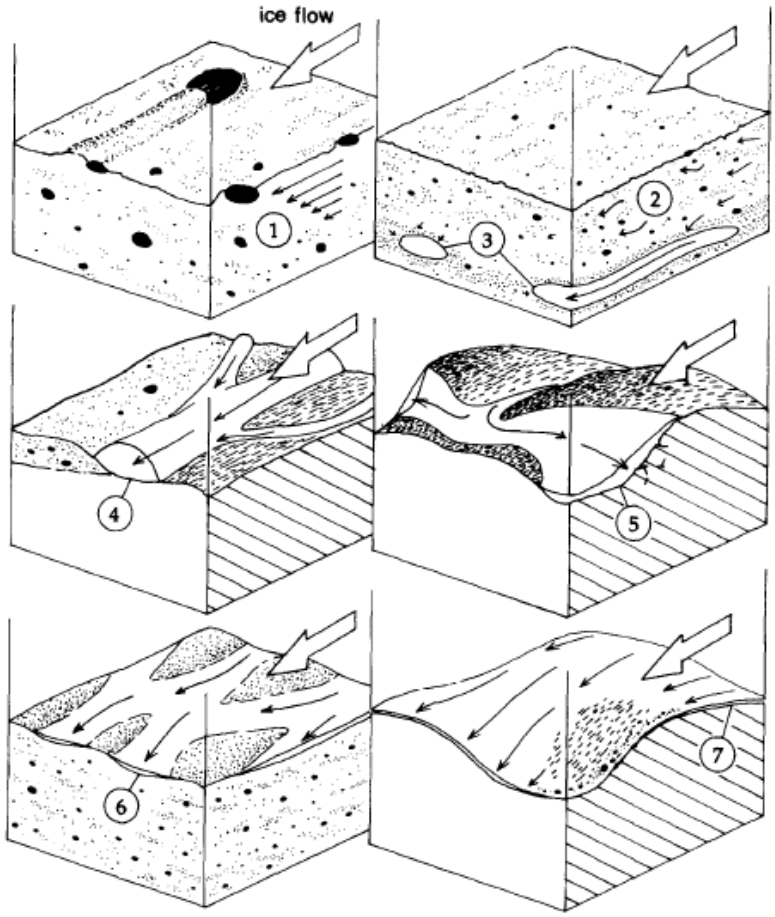

Figure 2.5 – Schematic diagram of the types of subglacial water transport. Including: (1) throughflow; (2) Darcian flow; (3) pipe flow; (4) dendritic channels; (5) linked cavity system; (6) braided canal network; (7) water film at ice-bed interface. From Benn and Evans (1996).

Recently several studies have identified the presence of subglacial lakes in connection with ice streams (e.g. Fricker *et al*., 2007; Bell *et al*., 2007). Subglacial lakes diminish the friction at the ice base and generate thermal energy via the freezing of lake water to the ice base, allowing ice to flow rapidly over them (Kohler, 2007). This may explain the spatial coincidence of subglacial lakes at the onset zones of ice streams and their tributaries, where ice velocity increases (Siegert and Bamber, 2000; Peters *et al*., 2007). The presence of several large subglacial lakes at the onset zone of Recovery Glacier Ice Stream, East Antarctica, led Bell *et al*. (2007) to conclude that they are fundamental to the onset of ice streaming at this location. However, the presence of a subglacial lake is not a pre-requisite for streaming flow and ice streams may initiate or be favoured in a range of environments (e.g. Winsborrow *et al*., 2010). Changes in ice surface elevation have revealed discontinuous and episodic discharge through the subglacial lake systems (Gray *et al*., 2005; Wingham *et al*., 2006; Fricker *et al*., 2007). Yet, despite the importance of subglacial water to ice streams, the presence of water below much of the

stagnant Kamb Ice Stream (West Antarctica) demonstrates that alone, it is not a sufficient condition for ice streaming (Gades *et al*., 2000).

Preservation of subglacial channels in palaeo-ice streams can indicate the type and extent of subglacial drainage and its connection to potential landscape controls. Studies of the subglacial hydrology of palaeo-ice streams have revealed networks of meltwater channels, tunnel valleys, anastomosing channels and large scale S-forms and cavities (e.g. Ó Cofaigh *et al*., 2002; Lowe and Anderson, 2002; 2003; Domack *et al*., 2006; Smith *et al*., 2009; Graham *et al*., 2009). Several studies of Antarctic palaeo-ice streams have found a downstream transition of hydrological features and bedforms, (e.g. Lowe and Anderson, 2002; 2003; Graham *et al*., 2009), whereby erosional hydrological features, such as meltwater channels, S-forms, gouges and cavities, dominate upstream on the crystalline bedrock and drumlins and mega scale glacial lineations dominate downstream on unconsolidated sediments overlying sedimentary bedrock.

Palaeo-ice streams may give a biased view of ice stream subglacial hydrology because only certain hydrological features may have a geomorphological signature, such as meltwater channels or eskers (eskers usually form in Rothlisberger channels, which are cut into the ice sole). In addition these may be eroded, either under the ice or following deglaciation, leaving only fragmentary evidence of ice stream subglacial hydrology. Another consideration is that palaeo-ice stream hydrological features may identify a time trangressive signature of subglacial hydrology and not necessarily a snapshot view of ice stream behaviour (Clark and Walder, 1994). Nonetheless, they have a major advantage over studies of contemporary ice streams because they can show the extent of the subglacial drainage network across a large area, which is not feasible in studies of contemporary ice streams.

Given the importance of the hydrological regime in an ice stream, further studies would be useful to characterise this environment and how it may vary between and within ice streams. The importance of high pore water pressures means that their subglacial hydrological systems have an important role to play in maintaining these conditions across the bed. This and the fact that ice streams may be pre-disposed to certain landscape features, such as in a valley or on soft substrates (e.g. Anandrakrishnan *et al*., 1998; Winsborrow *et al*., 2010) may mean that certain hydrological systems are typical

of ice streams, thus distinguishing them from other subglacial environments. Nonetheless, it is evident that a range of hydrological systems and features may operate below ice streams because ice streams display considerable variation in a range of factors, such as processes, substrate, geometry and their position in the landscape (e.g. Truffer and Echelmeyer, 2003; Winsborrow *et al*., 2010).

2.2.4 Spatial variations

Despite the broad trends in ice stream geomorphology and basal processes outlined above, findings from both contemporary and palaeo-ice streams have indicated that ice stream beds may be spatially heterogeneous at a macroscale, in terms of hydrology, substrate properties and shear stress (e.g. Alley, 1993; Smith, 1997; Wellner *et al*., 2001; Stokes *et al*., 2007; Murray *et al*., 2008). This is significant because conditions at the ice stream bed enable rapid flow and areas of frictional resistance will contribute to the basal shear component of ice stream force balance. The evolution of areas of basal frictional resistance are potentially able to cause dynamic behaviour of an ice stream (Alley, 1993; Stokes *et al*., 2007). The frequency of heterogeneities at ice stream beds is demonstrated by Joughin *et al*. (2004b) and Joughin *et al*. (2006), who, using a glaciological inversion model, found that basal shear stress could vary considerably across ice stream beds and an example of this is shown in Figure 2.6. Given that the inaccessibility of contemporary ice streams limits direct examination of bed properties and conditions to relatively small geographical areas, palaeo-ice streams may provide a useful approach to systematically examine spatial variabilities.

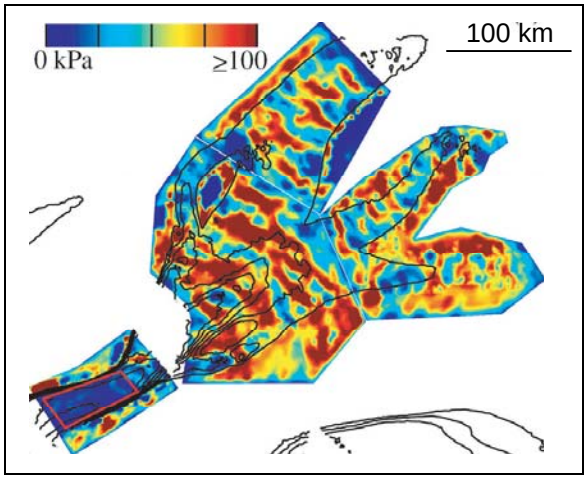

Figure 2.6 – Approximation of basal shear stress for the Slessor Ice Stream, which drains into the Filchner Ice Shelf, West Antarctica. Ice flow direction is from the upper right to the lower left of the image. Localised areas of high basal shear stress (red areas) represent sticky spots. Modified from Joughin *et al*. (2006).

Areas of high basal shear stress represent areas of the bed that offer resistance to ice flow. These areas are termed 'sticky spots' and may occur due to the presence of a topographic high; a till-free area; an area of strong, well drained till; or an area of basal freeze-on (Alley, 1993; Stokes *et al*., 2007). Sticky spots are significant because they contribute to basal shear stress and hence play a role in the force balance of an ice stream (Stokes *et al*., 2007). Additionally, they may change in time and space, and therefore have the potential to cause dynamic ice stream behaviour. Stokes *et al*. (2007) argue that progressive increase in the amount and/or size of till-free or freeze-on sticky spots may lead to ice stream shutdown. Whilst studies of contemporary and palaeo-ice stream beds have identified sticky spots, relatively little is known about their role and particularly their potential impact on ice stream flow and dynamics (Alley, 1993; Stokes *et al*., 2007). Stokes *et al*. (2007) suggest that palaeo-ice streams provide an excellent means to further characterise sticky spots, particularly using the morphometry and orientation of subglacial lineations, which may be expected to divert around a sticky spot and have lower elongation ratios on and around a sticky spot (Stokes *et al*., 2007).

2.2.5 Macroscale conclusions

Macroscale studies of contemporary ice streams have provided an insight into some significant characteristics of ice stream beds (e.g. Clark and Stokes, 2001; Lowe and Anderson, 2003; Joughin *et al*., 2006). Geophysical studies may provide some of the most direct evidence of ice stream basal processes, but they are generally limited to a small proportion of an ice stream bed and can only represent a snapshot in time (e.g. Blankenship *et al*., 1987; Vaughan *et al*., 2003). They have relatively coarse resolutions and only provide an indirect examination of the ice stream bed or substrate. Therefore, other methods are required to characterise the smaller scales at ice stream beds, such as investigation of basal conditions and till via boreholes or investigation of palaeo-ice streams (e.g. Hicock and Fuller, 1995; Engelhardt and Kamb, 1998; Ó Cofaigh and Evans, 2001).

As with geophysical studies of contemporary ice streams, remote sensing studies of palaeo-ice streams are limited by the resolution of the imagery. This is especially significant where studies rely solely on this type of dataset, without any ground truthing to confirm geomorphological interpretations (e.g. De Angelis and Kleman, 2005; Stokes, 2006; Anderson and Fretwell, 2008). Ground truthing may strengthen this type

of investigation, but the considerable size of ice streams means that ground truthing may only be feasible across a small proportion of the ice stream. Remote sensing studies of palaeo-ice stream beds will usually be limited to the macroscale and to investigate an ice stream in greater detail requires a very different set of techniques and practicalities, as described in the following sections.

2.3 Mesoscale characteristics of ice streams

The mesoscale of ice streams refers to a scale of centimetres to tens of metres at the ice stream bed, which broadly corresponds to the field examination of subglacial sediments. In contemporary ice streams, boreholes are the primary means of investigating mesoscale processes at ice stream beds (e.g. Engelhardt and Kamb, 1998; Tulaczyk *et al*., 2001). In palaeo-ice streams subglacial till typically provides evidence for mesoscale processes and characteristics in the former subglacial environment. The investigation of these sediments can provide an additional level of information beyond that which is gained from geomorphological mapping or morphometry.

2.3.1 Subglacial conditions in contemporary ice streams

Geophysical investigations have revealed the presence of a saturated, dilated layer of sediment layer beneath several contemporary ice streams (e.g. Blankenship *et al*., 1986; Smith, 1997; Anandakrishnan, 2003; Vaughan *et al*., 2003) and these findings are corroborated by borehole investigations. Engelhardt *et al*. (1990) drilled boreholes into the Whillans Ice Stream and found high basal water pressures, close to overburden pressures (resulting in low effective pressures). These conditions have implications for ice flow mechanisms and may promote either decoupling and basal sliding; or a reduction in sediment strength causing subglacial deformation. Engelhardt and Kamb (1997) and Kamb (2001) also found low effective pressures below Whillans, Kamb and Bindschadler ice streams from borehole observations. These studies measured till pore water and found evidence for substantial lateral variations, over a scale of 10 to 100 m. Subglacial water was also found to be present at the ice-till interface. Engelhardt and Kamb (1997) reported a canal system, with spacings of 50 to 300 m between canals. The subglacial conditions at this scale may differ from other glacial environments, as slow moving, stable glaciers are unlikely to have high effective pressures across large

areas of their beds. However, such conditions are not necessarily exclusive to ice streams and widespread high pore water pressures may also be found in certain other environments, such as a surging glacier (Benn and Evans, 2010).

Borehole observations provide a key means to observe the basal hydrological conditions of an ice stream. However, the fact that they can only represent the local (meso) scale means that they may not be representative and their application to macroscale subglacial water systems and ice flow rates is uncertain (Tulaczyk, 2006a). Additionally, boreholes perturb the subglacial hydrological system, potentially biasing any observations (Tulaczyk, 2006a).

2.3.2 Subglacial till

Despite some limited evidence for hard bedded ice streams (e.g. Stokes and Clark, 2003b; Roberts and Long, 2005) it is clear that the majority of ice streams have subglacial till distributed across most of their beds (Alley *et al*., 2004). Several studies of contemporary and palaeo-ice streams have reported the presence of unconsolidated sediments at their beds, forming a range of thicknesses from several centimetres to several metres (e.g. Blankenship, 1986; Engelhardt *et al*., 1990; Hicock and Fuller, 1995; Engelhardt and Kamb, 1997; Tulaczyk *et al*., 1998; Dowdeswell *et al*., 2004; Jennings, 2006). The presence of subglacial till is also essential to the flow mechanism of subglacial deformation (see Figure 2.2). Examination of subglacial till at the beds of contemporary and palaeo-ice streams has the potential to reveal many of the characteristics and processes in the ice stream subglacial environment (e.g. Tulaczyk *et al*., 1998; Lian *et al*., 2003; Ó Cofaigh *et al*., 2005). Knowledge of subglacial till mainly comes from studies of palaeo glaciers and studies in the forelands of contemporary glaciers. Comparatively few studies have sampled or observed sediment from below contemporary ice streams and glaciers, because of practical difficulties doing such studies.

Subglacial till typically constitutes a poorly sorted diamicton with a bi- or multimodal particle size distribution, which can be split into a clast and matrix component (Benn and Evans, 2010). The specific properties of a subglacial till may widely vary and are determined by several factors, including: parent material(s), transport history and

depositional environment of the till. Other subglacial sediments may include glaciofluvial or glaciolacustrine deposits that have been deposited subglacially (Eyles and Lazorek, 2007), or glaciotectonites, which were deformed by overriding ice but originally deposited in a different environment (Benn and Evans, 2010).

a. Ice stream subglacial till characteristics

Certain features may be typical of an subglacial ice stream till. Fine-grained till, which facilitates high pore water pressures, thus promoting rapid flow; may be a characteristic of ice stream till (Hicock and Dreimanis, 1992; Lian *et al*., 2003; Alley *et al*., 2004; Jennings, 2006). Some studies have reported homogeneous ice stream tills (Tulaczyk *et al*., 1998; Jennings, 2006). However, variability in till texture has been observed in a palaeo-ice stream bed (Rattas and Piotrowski, 2003), a characteristic that may enable the 'strong well drained till' sticky spots (Stokes *et al*., 2007). Reported common features of ice stream tills from the Laurentide and Cordilleran ice sheets include: far travelled clast provenance, clast morphological evidence for fast flow (e.g. striae), glaciotectonic structures, and preservation of soft sediment clasts (due to rotation) (Hicock and Driemanis, 1992; Lian and Hicock, 2000; Lian *et al*., 2003). However, in contrast sedimentological analyses of subglacial till from the Whillans Ice Stream found that clasts typically lacked morphological evidence for subglacial crushing and abrasion, which was thought to reflect a lack of comminution due to cushioning from the fine-grained matrix and high pore water pressures (Tulaczyk *et al*., 1998).

Various clast fabrics have been argued as being typical of fast flow and/or high strain. Lian *et al*., (2003) report that multimodal and girdle fabrics are typical of fast flow tills in the Cordilleran and Laurentide ice sheets, and weak fabrics have been linked to deformation tills (e.g. Dowdeswell and Sharp, 1986; Hart, 1994). However, laboratory experiments demonstrate that strained clasts develop into strong shear parallel fabrics (e.g. Hooyer and Iverson, 2000). Additionally, investigations of the bed of a palaeo-ice stream in the Baltic region found that relatively strong clast fabrics were typical (Jørgensen and Piotrowski, 2003). Evidently multiple types of fabric signatures may be found below ice streams, and a greater understanding of the mechanisms that determine particle fabric is required to explain the diverse fabrics that have been reported.

Vertical changes in till characteristics have also been reported from palaeo-ice streams (e.g. Ó Cofaigh *et al*., 2005; Christoffersen and Tulaczyk, 2003a) and such sequences may be used to constrain the depth of deformation (Benn and Evans, 1996). A subglacial ice stream till in Marguerite Trough, off the coast of the Antarctic Peninsula revealed a consistent vertical change in till properties. Several investigations found a vertical transition from a 'stiff' deformation till, with high shear strength, into a 'soft' deformation till, with low shear strength (Ó Cofaigh *et al*., 2005; Ó Cofaigh *et al*., 2007; Reinardy *et al*., 2010); which may relate to the spatial distribution of till dilation (Ó Cofaigh *et al*., 2005). This till sequence was also studied at the microscale (Ó Cofaigh *et al*., 2005; Reinardy *et al*., 2011), which is discussed in Section 2.4.2.

Table 2.1 – Summary table of some of the reported mesoscale characteristics from ice stream subglacial tills.

Region	**Ice stream till characteristic**	**Reference**
Laurentide Ice Sheet; West Antarctic Ice Sheet	Fine-grained till	Hicock and Dreimanis, 1992; Lian *et al*., 2003; Alley *et al*., 2004; Jennings, 2006
West Antarctic Ice Sheet	Homogeneous till	Tulaczyk *et al*., 1998; Jennings, 2006
East Baltic ice stream	Variability in till texture	Rattas and Piotrowski, 2003
Cordilleran and Laurentide ice sheets	Far travelled clast provenance	Hicock and Driemanis, 1992; Lian and Hicock, 2000; Lian *et al*., 2003
Cordilleran and Laurentide ice sheets; Antarctic Peninsula	Striations on clasts	Hicock and Driemanis, 1992; Lian and Hicock, 2000; Lian *et al*., 2003; Ó Cofaigh *et al*., 2005
West Antarctic Ice Sheet	Lack of morphological evidence for subglacial crushing and abrasion	Tulaczyk *et al*., 1998
Cordilleran and Laurentide ice sheets	Glaciotectonic structures	Hicock and Driemanis, 1992; Lian and Hicock, 2000; Lian *et al*., 2003
Cordilleran and Laurentide ice sheets	Preservation of soft sediment clasts	Hicock and Driemanis, 1992; Lian and Hicock, 2000; Lian *et al*., 2003
Cordilleran and Laurentide ice sheets	Multimodal and girdle fabrics	Lian *et al*., 2003
Baltic Ice Stream	Strong, flow parallel clast fabrics	Jørgensen and Piotrowski, 2003
Norwegian Channel	Both weak and strong clast fabrics	Stalsberg *et al*., 2003
Marguerite Trough, Antarctic Peninsula	Both high and low shear strengths (according to depth in sediment profile)	Ó Cofaigh *et al*., 2005; Ó Cofaigh *et al*., 2007; Reinardy *et al*., 2010

Table 2.1 summarises the various characteristics have been identified from subglacial ice stream tills and shows clearly that many of these observations contradict each other.

This suggests that despite certain fundamental conditions for ice stream beds, their sediments have a wide range of possible characteristics. However regardless of the variabilities observed, the conditions at ice stream beds are more constrained than subglacial environments as a collective, which include a much wider range of environments. This means that although some variation in till characteristics is evident there may be a range of characteristics typical to ice stream subglacial till. Their characteristics will be dependent on the source materials (e.g. bedrock or other sediment deposits), on the flow mechanism or mechanisms and how these may vary in space and time, as well as the overall history of the deposit. Expected characteristics of an ice stream till at the mesoscale may include: evidence for a high level of deformation in the upper levels of the till, possibly manifest by ductile and brittle deformation structures (Menzies, 2000); evidence for decoupling of the till from the ice, possibly manifest via fluvial deposits and flow structures in the upper levels of the till, with evidence for low strain in underlying sediments (e.g. Piotrowski *et al*., 2006); and evidence for high pore water pressures, which may be manifest via evidence for dilation, water movement (such as hydrofracturing) and a pressure gradient. In some cases characteristics such as these may distinguish an ice stream till from other subglacial tills, however, in many cases characteristics of an ice stream till are very likely to overlap with characteristics seen in other subglacial tills.

b. Inferred flow mechanisms

A small number of studies have utilised the subglacial till in palaeo-ice streams to infer former ice flow mechanisms (e.g. Hicock and Dreimanis, 1992; Rattas and Piotrowski, 2003; Evans *et al*., 2008). Evans *et al*., (2008) found a thickening of basal sediments towards the ice margins of the Central Alberta Ice Stream, which is considered to be evidence of subglacial deformation (see Boulton 1996a, b). They also found thin tills unconformably overlying stratified sediments in ice streams of the Laurentide Ice Sheet, and evidence for extensive subglacial meltwater, which they consider indicative of basal sliding. Rattas and Piotrowski (2003) used sedimentological evidence, including diffusive contacts between sand intraclasts, to infer that subglacial deformation was operating under a palaeo-ice stream in Estonia. They also considered evidence for abundant meltwater at the ice-bed interface as indicative of subglacial sliding, and infer that these mechanisms alternated spatially and temporally, causing stick-slip flow (see Sergienko *et al*., 2009). However, identification of flow mechanisms based on

sediments may not always be straightforward. Potential criteria for certain flow mechanisms may be debated, for example subglacial deformation has been argued by various researchers to result in both weak and strong clast fabrics (e.g. Hart, 1994; Hicock, 1992; Hooyer and Iverson, 2000; Thomason and Iverson, 2006). Furthermore, different researchers may interpret similar features in different ways. This indicates that further work is needed to establish the sediment characteristics that are linked to certain flow mechanisms.

Subglacial till from palaeo-ice streams has also been used to infer mechanisms of ice stream shutdown. Christoffersen and Tulaczyk (2003a) found that areas of the Baltic Sea Ice Stream were characterised by a strong well consolidated till crust overlying a weak, poorly consolidated till. They used a numerical model to demonstrate that this till sequence probably resulted from basal freezing, which may have been triggered by, or accompanied by, shutdown of this ice stream.

c. Till rheology

The rheology of till, which determines its ability to flow and deform, has been an issue of considerable debate (e.g. Boulton, 1986; Kamb, 1991; Tulaczyk *et al*., 2000b). Its importance lies in the fact that it controls the mechanics of soft bedded ice streams (Tulaczyk, 2006a) and as such it is an important parameter in ice stream modelling. Observations from West Antarctic ice streams (Alley *et al*., 1986; Blankenship *et al*., 1986), as well as a set of experiments on Breiðamerkurjökull in Iceland, and associated modelling (Boulton and Hindmarsh, 1987) led to the theory that subglacial till has a viscous rheology and that subglacial deformation was widespread. This caused a ‘paradigm shift’ in the understanding of glaciers and ice streams (Boulton, 1986; Murray, 1997). These findings were reflected in ice stream modelling, whereby a near linear viscous rheology was used to model till (e.g. Alley *et al*., 1987; MacAyeal, 1989), which means that till deformation directly controlled ice velocity in these models. However, later experiment and field studies found subglacial till to better approximate a Coulomb plastic rheology (e.g. Kamb, 1991; Hooke *et al*., 1997; Tulaczyk *et al*., 2000b; Kavanaugh and Clarke, 2006), reflecting soil mechanics experiments. In models that use a Coulomb plastic rheology (e.g. Tulaczyk *et al*., 2000a) once till strength is exceeded, the ice will slide over the till at a rate controlled by areas of resistance (sticky spots) rather than by the till itself (Benn and Evans, 2010).

Despite the evidence for a Coulomb plastic rheology, viscous bed models have accurately predicted ice stream activity (e.g. MacAyeal, 1989; Alley *et al*., 1987). This has led some researchers to consider the possibility that whilst till behaves plastically at a small scale, over large spatial and temporal scales it behaves viscously (Hindmarsh, 1997; Fowler, 2003). This theory is rejected by Tulaczyk (2006b) who demonstrates agreement between (small scale) laboratory experiments and (larger scale) field observations for a Coulomb plastic rheology of till below the Whillans Ice Stream.

2.3.3 Mesoscale conclusions

Mesoscale analysis has provided some significant information on ice stream subglacial properties and till characteristics. Studies have provided insight into the sediments of palaeo-ice streams, but these studies are relatively limited, which is surprising when the considerable spatial extent of ice streams is considered. However, an inherent problem of studying ice stream beds at this scale is whether a borehole or sediment section is representative. This means characterisation at the macroscale and a careful sampling strategy is important. Nonetheless, these types of studies have the potential to reveal flow mechanisms, mesoscale hydrology and other basal processes.

2.4 Microscale sediment processes and features in subglacial till

The microscale of ice stream beds refers to the sediment characteristics that require microscopic examination and processes that are manifest at this scale. This scale is typically less routinely investigated than those of the macro and meso scales at ice stream beds and to date there have been very few studies of the microscale characteristics of ice stream subglacial till. Microscale techniques include micromorphology, scanning electron microscopy and X-ray computed micro tomography. Micromorphology involves processing of sediment into thin sections, which are then examined under plane and cross polarised light, revealing the constituent parts of the sediments and the two dimensional arrangement of particles (e.g. van der Meer, 1993; Menzies, 2000; Phillips, 2006). Scanning electron microscopy provides a useful way to look at the microscale of glacial sediments without time consuming processing (e.g. Mahaney and Kalm, 2000). One of the key ways it has been utilised is to study the surface of sand grains from till (e.g. Krinsley and Takahashi, 1962; Tulacyzk *et al*., 1998; Ó Cofaigh *et al*., 2005). However, this technique only provides

the researcher with a view of the surface morphology of a sediment sample. X-ray computed micro tomography uses x-ray to view sediment samples in three dimensions (Kilfeather and van der Meer, 2008; Tarplee *et al*., 2011). Applying micro tomography to glacial sediments is a relatively new field of research and it has yet to be applied to ice stream sediments.

Thin section micromorphology is the most common technique used to study the microscale of glacial sediments and allows researchers to ascertain the characteristics and history of subglacial sediments (e.g. van der Meer *et al*., 1993; Hart *et al*., 2004; Hiemstra *et al*., 2005). Glacial micromorphology can reveal the stress history of a sediment and potentially evidence for its emplacement (Menzies *et al*., 2010). Whilst diamicts may appear identical at the mesoscale, particularly where only a limited sediment sample can be viewed (e.g. if the sediments have been cored), micromorphology may be able to differentiate different lithofacies and identify elements of the sediment history (Carr, 2004). The technique of micromorphology applied to palaeo or contemporary glacial sediments from fieldwork or via laboratory experiments has provided the majority of our understanding of the microscale characteristics and processes of glacial sediments (e.g. van der Meer, 1993; Menzies, 2000; Khatwa and Tulaczyk, 2001; van der Meer *et al*., 2003; Hiemstra and Rijsdijk, 2003). This thesis will be using the technique of thin section micromorphology because the research literature for microscale investigation of till has been primarily based on thin section analysis (e.g. van der Meer, 1993; Menzies, 2000; Khatwa and Tulaczyk, 2001) and it has yielded significant information into their characteristics and behaviour (e.g. van der Meer, 1993; Larsen *et al*., 2006a).

2.4.1 Micro structures in subglacial till

The application of thin section micromorphology to glacial sediments has revealed a suite of micro structures and fabrics that are common in glacial sediments (e.g. van der Meer, 1993; Menzies, 2000; Figure 2.7). Till viewed in thin section comprises skeleton grains matrix (plasma) and voids. Skeleton grains are particles that can be individually identified (typically coarse silt and larger) and matrix refers to the component within which individual grains cannot be identified (typically < 20µm; Carr, 2004). Voids are typically classified according to their form and may also provide an insight into depositional, deformation and post-depositional processes that have acted upon the

sediment. The range of voids identified in tills may include: fissures or planar voids, vesicles, vughs, packing voids and connected channels and chambers (see Kilfeather and van der Meer, 2008). Micro structures and voids in a glacial sediment may be inherited, actual *in situ* (i.e. a product of the primary deposition or deformation process), postdepositional or in some cases may be sampling/processing artefacts (Menzies, 2000).

Sediment deformation accounts for many of the characteristic glacial micro structures, which typically are common in subglacial till, which indicates that the deformation processes are widespread. However, the deformation depicted in such structures does not necessarily indicate the operation of subglacial deformation as a fast flow mechanism, as to carry overlying ice downstream till requires significant displacement rather than just small scale movements between particles (see Boulton and Hindmarsh, 1987). Deformation as seen at the microscale takes place as a change in bulk shape, primarily along grain boundaries and is manifest as brittle or ductile deformation (e.g. Menzies, 2000; van der Meer *et al*., 2003; Larsen *et al*., 2006a). Brittle deformation is a result of enhanced stress concentrations, causing fracturing and disaggregation along zones of weakness. It may result from a rapid change in confining pressure, relatively high effective pressures and low pore water pressures (Menzies, 2000; Larsen *et al*., 2006a). Common subglacial brittle deformation structures include shears, faults, lineations and crushed grains, as shown in Figure 2.7 (e.g. van der Meer, 1993; Menzies, 2000, Hiemstra and Rijsdijk, 2003). Grain lineations can be defined as a line of at least three grains, orientated end to end or on either side of a line within the matrix (Hiemstra and Rijsdijk, 2003; Menzies *et al*., 2006; 2010). They are often interpreted as a reflection of shearing within a sediment (van der Meer, 1996; Menzies *et al*., 2006).

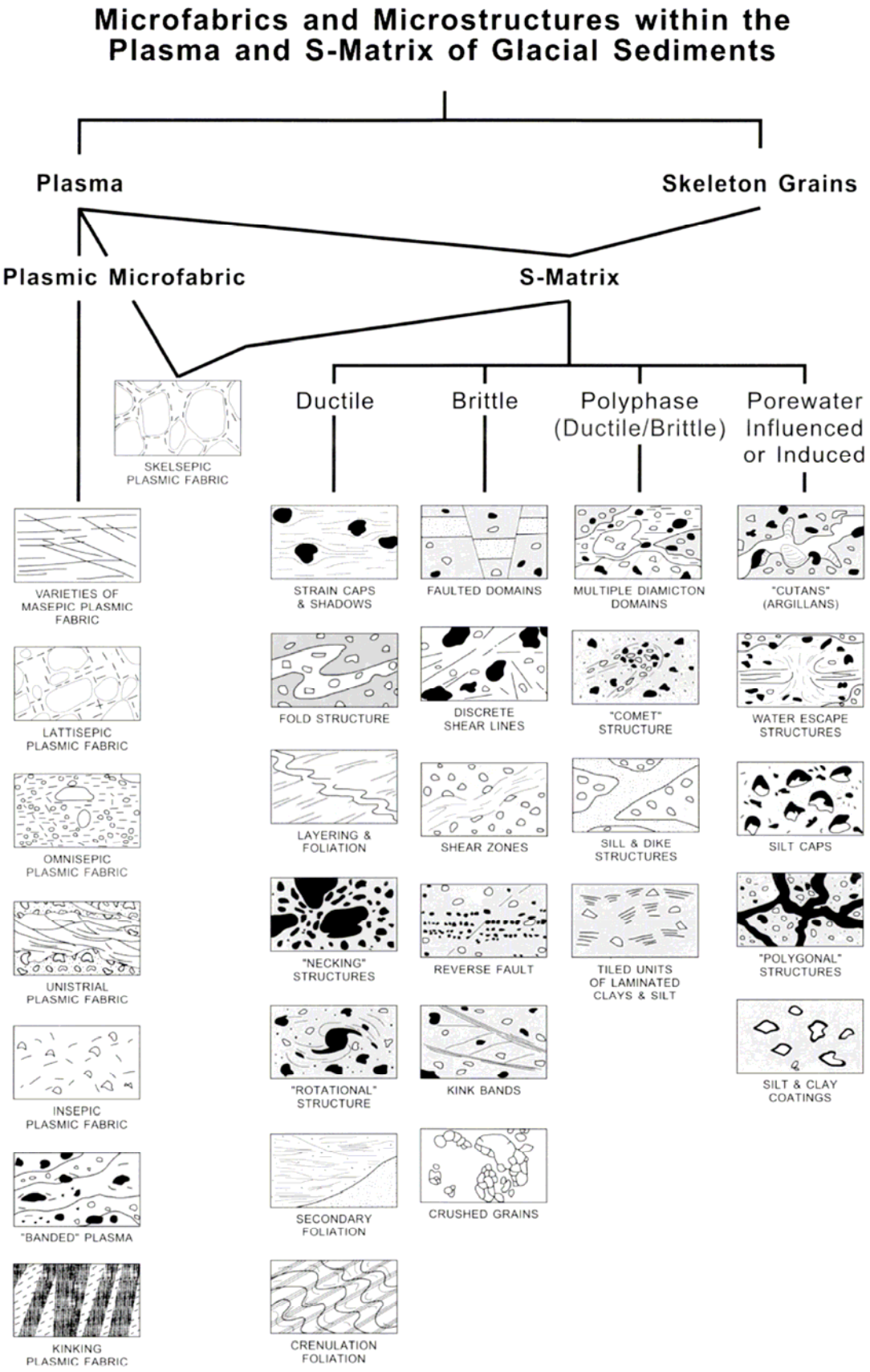

Figure 2.7 – Schematic diagram of some of the key features observed in subglacial tills, including microfabrics and microstructures. From Menzies, 2000 (after van der Meer, 1993). Refer to sections 5.3.4, 5.4.4, 6.3.4 and 6.4.4 for photomicrographs showing real examples of some of these features.

Ductile deformation may result from relatively low stress or confined stress, causing grains and matrix to flow (Menzies, 2000). It is associated with high pore water pressures, high confining pressures and low effective pressures (Menzies, 2000). Common subglacial ductile deformation structures include turbates, folding and intraclasts, as shown in Figure 2.7 (e.g. van der Meer, 1993; Menzies, 2000, Carr, 2004). Turbates, also known as rotation structures, can be defined as circular alignments of grains, with or without a core stone. Grains may be aligned so they are parallel to the edge of the central grain if present, they may also appear to curve out from the structure in a galaxy shape (van der Meer, 1993). These widespread microscale structures are thought to be a reflection of rotational movements within the sediment (van der Meer, 1997). Intraclasts refer to a distinct pocket of sediment or aggregate in a sediment (Kilfeather *et al*., 2010) and may indicate sediment mixing (Menzies, 2000).

A subglacial till may have both brittle and ductile deformation structures. If these different types of structures overprint each other in multiple phases it is referred to as polyphase deformation (Menzies, 2000). Despite categorising these structures into either brittle or ductile, these different types of deformation may be closely related and grain structures can be a result of both rotational and planar movements (Hiemstra and Rijsdijk, 2003).

Other subglacial features include those associated with fluid escape or injection (e.g. Lachniet *et al*., 2001; Phillips *et al*., 2007). Structures formed by particles within the matrix are referred to as plasmic fabric, which is the orientation of clay sized particles that display birefringence in cross polarised light. Common plasmic fabrics include skelsepic (rotational), masepic (planar), and unistrial (planar), and are illustrated in Figure 2.7 (e.g. van der Meer, 1993; Hiemstra and Rijsdijk, 2003; Hart *et al*., 2004; Phillips *et al*., 2007). Skelsepic refers to the plasmic fabric whereby plasma is orientated around skeleton grains and situated parallel to the surface of the skeleton grain (van der Meer, 1993). It is commonly thought to be a reflection of rotation within subglacial till (e.g. Hiemstra and Rijsdijk, 2003; Hart *et al*., 2004) but thin skins of plasmic fabric can also be formed via wetting and drying of a sediment (Dalrymple and Jim, 1984). Masepic is a plasmic fabric whereby domains of plasma are orientated in one overall direction and may be a result of planar, ductile deformation in a sediment (Menzies, 2000; Menzies *et al*., 2006). Unistrial plasmic fabric is a discrete line of high

birefringence, formed by the alignment of clay sized particles along a shear plane and as such it represents brittle deformation (van der Meer, 1993).

Many of the structures described above may also be typical of other sediments such as sediment flow deposits (e.g. Harris, 1998; Menzies and Zaniewski, 2003; Lachniet *et al*., 2001; Phillips, 2006) and neotectonic sediments (Menzies and Taylor, 2003). This highlights the importance of using a range of structures and ideally a range of techniques (e.g. sedimentological logging, clast morphological analysis) to identify the depositional environment and associated processes from micromorphological samples (Menzies, 2000; Lachniet *et al*., 2001; Carr, 2004). Micromorphological structures may also be used to infer the rheological behaviour of subglacial till. Hiemstra and Rijsdijk (2003) conducted uniaxial compression on ceramic clay (a Coulomb plastic material) producing micro structures that are typical of subglacial till. Following this, other studies have interpreted discrete ductile and brittle deformation structures, as well as a Riedel shear geometry as representative of a Coulomb plastic material (Larsen *et al*., 2006a; 2007).

2.4.2 Ice stream micromorphology

Only a handful of studies have investigated the micromorphology of ice stream subglacial till, meaning that understanding of microscale characteristics and processes in ice stream beds is very limited. This is important to address because one of the key fast flow mechanisms, subglacial deformation, is manifest at this scale, although it is not necessarily identifiable from micromorphological data alone (Hiemstra and Rijsdijk, 2003; Menzies *et al*., 2006). The few studies of this have demonstrated that many of the same structures that have been identified in (non-ice stream) subglacial till (e.g. turbates, intraclasts, grain lineations, crushed grains) may also be found within an ice stream subglacial till (Carr *et al*., 2000; Khatwa and Tulaczyk, 2001; Ó Cofaigh *et al*., 2005; Reinardy *et al*., 2011), and no microscale features have been demonstrated to be unique to ice stream till. These studies have demonstrated that the amount of micromorphological structures (such as turbates, lineations, crushed grains) may vary between an ice stream subglacial till and a non-ice stream subglacial till, as well as spatially within a subglacial ice stream till. Khatwa and Tulaczyk (2001) found that a Pleistocene subglacial till (from Norfolk) contained significantly more micromorphological structures than subglacial till from the Whillans Ice Stream. They

consider this contrast to be a result of differences in strain magnitude, parent material heterogeneity and sediment sorting from subglacial water. Reinardy *et al*. (2011) conducted a detailed micromorphological study of palaeo-ice stream bed sediments in Marguerite Trough, off the Antarctica Peninsula. Two till horizons with differing shear strengths were found to have distinct suites of micro structures. They attribute this difference to the preferential formation and preservation of certain structures in the upper and lower horizons, owing to their different deposition and deformation histories.

Table 2.2 – Summary table of some of the reported microscale characteristics from ice stream subglacial tills.

Region	**Ice stream till characteristic**	**Reference**
West Antarctic Ice Sheet	Masepic, bi-masepic and skelsepic plasmic fabric; turbates; fractured grains	Khatwa and Tulaczyk, 2001
Norwegian Channel	Turbates; pressure shadows; crushed grains; intraclasts; water escape structures; grain lineations; skelsepic, lattisepic, masepic and unistrial plasmic fabric	Carr *et al*., 2000
West Antarctic Ice Sheet	Grains display chemical weathering microfeatures, such as etch pits; overprinted by older physical microfeatures, such as fracture planes	Tulaczyk *et al*., 1998
Marguerite Trough, Antarctic Peninsula	Intraclasts; turbates; necking structures; crushed grains; grain alignments; boudins; masepic and unistrial plasmic fabric	Reinardy *et al*., 2011
Marguerite Trough, Antarctic Peninsula	Turbates; grain lineations; masepic and unistrial plasmic fabric; dominantly sub-angular sand sized grains	Ó Cofaigh *et al*., 2005; Ó Cofaigh *et al*., 2007
Norwegian Channel	Grain concentrations displaying deformation; bi-masepic and unistrial plasmic fabric	Stalsberg *et al*., 2003

A micromorphological investigation of the Whillans Ice Stream subglacial till clearly demonstrates the link of some of these common micromorphological features to subglacial deformation and demonstrate that they can form in a weak sub-ice stream till (Khatwa and Tulaczyk, 2001). This same till was found to behave as a Coulomb plastic material (Tulaczyk *et al*., 2000b), signifying that these micromorphological structures can form within a Coulomb plastic material, an inference reinforced by Hiemstra and Rijskdjk (2003). Whilst the formation and preservation of micro structures in ice stream till may result from a range of factors, some researchers have explored the possibility of using micromorphology (structures, fabrics and shears) as an indicator of strain magnitude (e.g. Carr and Rose, 2003; Larsen *et al*., 2006b; Thomason and Iverson, 2006; Hooyer *et al*., 2008), which if reliable would be of considerable value for interpreting palaeo-ice stream sediments.

There have been relatively few studies of the micromorphology of ice stream till and as such there are few studies upon which differences can be highlighted between ice stream tills and other subglacial tills, as outlined in Table 2.2. Evidently similar structures do exist between ice stream tills and other subglacial tills (e.g. Khatwa and Tulaczyk, 2001; Reinardy *et al*., 2011), indicating that the microscale processes that create these structures are universal. As mentioned previously the key factor that differentiates a subglacial ice stream environment to most other subglacial environments is the widespread condition of high pore water pressures. So this may lead to the supposition that certain structures associated with water movement should be expected, for example water escape structures. Moreover high pore water pressures may be associated with dilation of sediments (Alley *et al*., 1986), which may mean that high porosity should be expected of these tills at least in some layers (Iverson *et al*., 1998).

2.4.3 Microscale conclusions

Several studies demonstrate that subglacial till and the properties and processes of the subglacial environment are spatially variable (e.g. Fischer and Clarke, 2001; Piotrowski *et al*., 2004). This means that if micromorphology samples are to be considered representative of a sediment then a careful sampling strategy is needed. Ideally several samples should be taken from a lithofacies and selection should take consideration of mesoscale features (Carr, 2004).

Traditionally micromorphology of glacial sediments has been largely descriptive (e.g. van der Meer, 1993; Menzies, 2000). However, using purely descriptive methods make it difficult to compare between thin sections and groups of thin sections. This led researchers to use semi quantitative measurements by estimating relative abundance of the observed features (e.g. Carr, 1999; van der Meer and Hiemstra 1998; Carr *et al*., 2006; Baroni and Fasano, 2006). More recently researchers have tried to increase accuracy and objectivity by conducting absolute counts of structures across an area of the thin section (e.g. Larsen *et al*., 2007; Reinardy *et al*., 2011). These developments have helped advance the field of micromorphology of glacial sediments. Regarding the study of ice streams, a very small number of studies have investigated the micromorphology of ice stream subglacial till. This is especially striking when compared to numbers of studies that have investigated the geomorphology of ice

streams. Micromorphology has been demonstrated to be a useful tool in the interpretation of subglacial sediments and so has much potential for furthering our understanding of microscale structures and processes at ice stream beds. The technique may be particularly useful for contemporary ice streams or marine palaeo-ice streams where sediments are only accessible via coring.

2.5 The significance of scale in ice stream beds

The above review shows that studies of ice stream beds are not equal between the three scales of analysis. This is also depicted in Table 2.3, which gives a representative selection of studies from contemporary and palaeo-ice stream from these three scales. It shows that investigations are very much skewed to studying the macroscale and whilst some have looked at the mesoscale, very few have looked at the microscale. Specifically, the total numbers of ice streams studied, from this table alone are: 76 ice streams at the macroscale; 21 at the mesoscale; and 3 at the microscale. Some studies have looked at more than one scale of analysis (Table 2.3), but very few have looked at all three scales of analysis. This means that understanding of the connection between the scales is extremely limited.

Table 2.3 – List of studies of contemporary and palaeo-ice streams, organised into sections according to the scale of analysis they examine. This list is not exhaustive and in particular the macroscale studies given are only a representative selection.

Scale	Ice Stream	Technique	Contemporary /palaeo	Reference
Macro	MacAyeal Ice Stream, WAIS	Repeat satellite imagery to determine ice velocity	Contemporary	Bindschadler and Scambos, 1991
	Kamb Ice Stream, WAIS	Geophysical survey	Palaeo (inactive)	Anandakrishnan, 2003
	Marguerite Ice Stream, Marguerite Bay, Antarctic Peninsula	Bathymetric survey	Palaeo	Anderson and Fretwell, 2008
	Whillans Ice Stream, WAIS	Numerical modelling	Contemporary	Beem *et al.*, 2010
	Whillans Ice Stream, WAIS	Geophysical survey	Contemporary	Bell *et al.*, 1998
	Whillans and Kamb ice streams, WAIS	Geophysical survey	Contemporary and palaeo	Bentley *et al.*, 1998
	Whillans Ice Stream, WAIS	Geophysical survey	Contemporary	Blankenship *et al.*, 1986
	M'Clintock Channel Ice Stream	Satellite imagery mapping and analysis	Palaeo	Clark and Stokes, 2001
	Whillans Ice Stream, WAIS	Numerical modelling	Contemporary	Bougamont *et al.*, 2003
	The Minch Ice Stream, Western Scotland	Onshore: Nextmap DEM, aerial photography, field mapping. Offshore: Bathymetry data	Palaeo	Bradwell *et al.*, 2007
	Ice Stream in the Western Bransfield Basin, offshore Antarctic Peninsula	Swath bathymetry and sonar	Palaeo	Canals *et al.*, 2000
	Ice streams in northern Keewatin and the Boothia Peninsula, Nunavat, Canada	Satellite imagery mapping	Palaeo	De Angelis and Kleman, 2005
	Ice streams in Baffin Island and the Foxe Basin, Nunavat, Canada	Satellite imagery mapping	Palaeo	De Angelis and Kleman, 2007
	Vestfjorden and Trænadjupet, Norwegian continental shelf	Geophysical and seismic data	Palaeo	Ottesen *et al.*, 2005b
	Jakobshavns Isbræ, Greenland	Geophysical survey	Contemporary	Clarke and Echelmeyer, 1996
	Filchner and Ronne Ice Streams, WAIS	Numerical modelling using geophysical data, satellite imagery and DEM's	Contemporary	Joughin *et al.*, 2006
	North East Greenland Ice Stream	Satellite radar interferometry and numerical modelling	Contemporary	Joughin *et al.*, 1999
	Two ice streams, Witch Ground Basin, North Sea	Geophysical survey (3D seismic)	Palaeo	Graham *et al.*, 2007
	Rutford Ice Stream, WAIS	Measurement of surface stake movements to determine velocity	Contemporary	Gudmundsson and Jenkins, 2009
	Rutford Ice Stream, WAIS	Geophysical survey	Contemporary	King *et al.*, 2007
	Dubawnt Lake Ice Stream, Northwest Territories, Canada	Geomorphological mapping from satellite imagery and aerial photography	Palaeo	Stokes, 2006
	Ice Stream in the Amundsen Gulf, Nunavat and Northwest Territories, Canada	Geomorphological mapping from satellite imagery DEM's and bathymetric data	Palaeo	Stokes *et al.*, 2006
	Rutford Ice Stream, Evans Ice Stream, Taulis Inlet, Carlson Inlet, WAIS	Geophysical survey and GPS survey	Contemporary	Vaughan *et al.*, 2003
	Whillans Ice Stream, WAIS	Repeat aerial photogrammetry to determine force balance	Contemporary	Whillans and van der Veen, 1997

Scale	Ice Stream	Technique	Contemporary /palaeo	Reference
Macro and Meso	Marguerite Ice Stream, Marguerite Bay, Antarctic Peninsula	Bathymetric survey, sonar data and sedimentological analysis of a series of cores	Palaeo	Dowdeswell *et al.*, 2004
	Whillans Ice Stream, WAIS	Geotechnical tests of subglacial till and numerical modelling of flow mechanisms	Contemporary	Tulaczyk *et al.*, 2000(a, b)
	Central Alberta and High Plains ice streams, Alberta, Canada	Geomorphological mapping regional DEM and aerial photography. Sedimentological analysis of several sites across the region (three from the ice stream beds)	Palaeo	Evans *et al.*, 2008
	Ice streams in Minnesota, USA	Description of geomorphology and sedimentology	Palaeo	Jennings, 2006
	Baltic Ice Stream, Scandinavia	Examination of geomorphology from topographic maps and sedimentological analyses	Palaeo	Jørgensen and Piotrowski, 2003
	Baltic Ice Stream(s), Scandinavia	Examination of clast composition data, directional indicators of ice flow and glaciotectonics	Palaeo	Kjær *et al.*, 2003
	Ice stream in Estonia (East Baltic)	Geomorphological analysis and sedimentology	Palaeo	Rattas and Piotrowski, 2003
	Irish Sea Ice Stream, UK	Examination of geomorphology and sedimentology	Palaeo	Roberts *et al.*, 2007
Meso	Baltic Ice Stream, Scandinavia	Sedimentology and numerical modelling	Palaeo	Christoffersen and Tulaczyk, 2003
	Whillans Ice Stream, WAIS	Measurement of basal sliding using a tethered stake in the ice stream bed via a borehole	Contemporary	Engelhardt and Kamb, 1998
	Irish Sea Ice Stream, Irish Sea, Ireland and Wales.	Stratigraphy and sedimentological analyses	Palaeo	Evans and Ó Cofaigh, 2003
	Postulated areas of ice streaming in Southern Ontario, Canada	Sedimentological analyses	Palaeo	Hicock and Dreimanis, 1992
	Ice stream in British Columbia mainland and Queen Charlotte Islands, British Columbia, Canada	Sedimentological analyses	Palaeo	Hicock and Fuller, 1995
	Possible ice streams in the Cordilleran Ice Sheet, British Columbia, Canada	Sedimentological analyses	Palaeo	Lian and Hicock, 2000
	Ice streams in Lake Ontario and Lake Erie basins, Southern Ontario, Canada	Sedimentological analyses	Palaeo	Lian *et al.*, 2003
	Irish Sea Ice Stream	Sedimentological analyses	Palaeo	Ó Cofaigh and Evans, 2001
Meso and micro	Whillans Ice Stream, WAIS	Sedimentology analyses of subglacial till, including particle morphology using SEM	Contemporary	Tulaczyk *et al.*, 1998
	Ice stream offshore on the NE Antarctic Peninsula	Micromorphology, in addition to examination of acoustic stratigraphy (TOPAS) and sedimentology.	Palaeo	Reinardy *et al.*, 2011
Micro	Norwegian Channel Ice Stream, Norway	Analysis of a borehole core	Palaeo	Carr *et al.*, 2000
	Whillans Ice Stream, WAIS	Micromorphology of 17 thin sections sampled from boreholes from the subglacial sediments	Contemporary	Khatwa and Tulaczyk, 2001
Macro, meso and micro	Several ice streams off the Antarctic Peninsula	Bathymetry, acoustic stratigraphy (TOPAS), sedimentology, x-radiographs, micromorphology	Palaeo	Ó Cofaigh *et al.*, 2007
	Marguerite Ice Stream, Marguerite Bay, Antarctic Peninsula	Bathymetry, acoustic stratigraphy (TOPAS), sedimentology, x-radiographs, micromorphology	Palaeo	Ó Cofaigh *et al.*, 2005
	Norwegian Channel Ice Stream, Norway	Examination of geomorphology, sedimentological analyses, micromorphology	Palaeo	Stalsberg *et al.*, 2003

Subglacial processes are not necessarily restricted to certain scales, they may span multiple scales and/or they may have an affect on other scales. Several large scale ice stream processes appear to be determined by small scale characteristics. For example, till properties such as porosity and permeability may help determine macroscale subglacial hydrology. Given this, changes at certain scales may impact other scales and have a dramatic affect on an ice stream. This is seen in the mechanism of basal freeze-on, which starts at a small scale and scales up, eventually having a dramatic affect on an ice stream and even causing ice stream shutdown (Christoffersen and Tulaczyk, 2003a). This mechanism has been proposed for the currently stagnated Kamb Ice Stream (Vogel *et al*., 2003) and the Baltic Sea Palaeo-Ice Stream (Christoffersen and Tulaczyk, 2003b). Another example is the issue of subglacial till rheology. Despite small scale studies (0.1 to 1 metres) indicating a Coulomb plastic rheology, the applicability of whether this can be scaled up to ice stream wide model (greater than 1 kilometre) is the subject of considerable debate (e.g. Hindmarsh, 1997; Fowler; 2003; Tulaczyk 2006a, b). This indicates that studying multiple scales will bring greater insight into ice stream processes and characteristics than a single scale. Additionally, it may help determine which processes are manifest at which scales and whether certain processes or characteristics can only be identified at certain scales. This could provide significant insight into mechanisms that are typically studied at a specific scale. Investigation of a balance of scales, with integration between them, may provide a means to push the limits of current understanding about ice stream beds.

2.6 Knowledge gaps and research questions

This review has described the main features of ice streams and has outlined the characteristics and processes associated with the three spatial scales investigated in this study. Macroscale studies of contemporary ice streams have demonstrated the presence of a weak, porous, saturated flow layer beneath several Antarctic ice streams (e.g. Blankenship *et al*., 1986; Vaughan *et al*., 2003). These conditions are favourable to the basal flow mechanisms of subglacial sliding and subglacial deformation. Examination of contemporary ice stream beds faces significant challenges and so studying palaeo-ice streams provides an effective means to characterise them (e.g. Stokes and Clark, 2003a; Bradwell *et al*., 2007). Evidence for subglacial hydrological systems, including canals, subglacial lakes, eskers and Nye channels, have been identified from contemporary and

palaeo-ice streams (e.g. Murray *et al*., 2008; Lowe and Anderson, 2003; Domack *et al*., 2006). Observations that subglacial lakes undergo discontinuous and episodic flow, indicates that subglacial hydrology may not always be steady state (e.g. Gray *et al*., 2005; Wingham *et al*., 2006).

Spatial variations in basal properties and flow mechanisms have been identified at ice stream beds as have 'sticky spots', which are regions of the bed that locally retard ice stream flow (e.g. Alley, 1993; Stokes *et al*., 2007). These are significant because they may contribute to up to 50 % of opposing forces to the ice stream driving force (Beem *et al*., 2010). Observations of sticky spots are relatively few, but may provide useful insights into the common types and characteristics of these features (Stokes *et al*., 2007). Elongated subglacial bedforms are ubiquitous at ice stream beds and if elongation ratio is used as a proxy for ice velocity they may provide a useful measure of spatial variations (see Stokes and Clark, 2002; King *et al*., 2007).

Mesoscale studies of contemporary ice streams are typically borehole measurements and such studies have demonstrated that high pore water pressures and low effective pressures are widespread (e.g. Engelhardt *et al*., 1990; Engelhardt and Kamb, 1997). Mesoscale studies of palaeo-ice stream beds usually relate to subglacial till and some characteristics, such as far travelled clast provenance, clast morphological evidence and multimodal and girdle fabrics have been cited as typical of ice stream sediments (Lian *et al*., 2003). However, the widespread nature of these characteristics suggests that they are not diagnostic for ice stream subglacial tills.

Microscale studies of ice stream beds are noticeably fewer than studies at the macro and meso scales (Table 2.3). These studies have demonstrated that many of the micromorphological structures typical to subglacial till are also commonplace in subglacial ice stream till (Carr *et al*., 2000; Khatwa and Tulaczyk, 2001; Reinardy *et al*., 2011). The wide extent of palaeo-ice stream beds means that mesoscale and microscale studies have considerable potential to utilise this archive of information about ice stream subglacial environments.

Whilst the different scales of analysis described are quite disparate, subglacial processes may span multiple scales. Different scales may affect each other, which is particularly

seen where microscale properties and processes affect meso and macro scale processes and behaviour. Integration of these three scales may help bridge these separate scales and increase understanding of ice streams and subglacial processes. These gaps in understanding of ice streams have led to the following research questions:

1. Based on the macroscale characterisation of seven palaeo-ice streams, can any spatial patterns be identified in the subglacial lineations and if so, do these correspond to any landscape variables (in topography, bedrock geology or surficial sediments)?

2. What do the macro, meso and micro scale characteristics of two palaeo-ice streams reveal about their subglacial processes?

3. What are the key findings at each spatial scale and what is the value of studying multiple spatial scales in palaeo-ice streams?

3. Methods

3.1 Introduction

This thesis employs several techniques to allow detailed examination of palaeo-ice stream beds within a multiscale framework, which will address the gaps in understanding of the significance of scale. The techniques used include: geomorphological mapping and analysis using remotely sensed imagery; sedimentological analysis; and micromorphological analysis. These are outlined in Figure 3.1, which outlines the techniques associated with the different spatial scales and the expected outcomes from these.

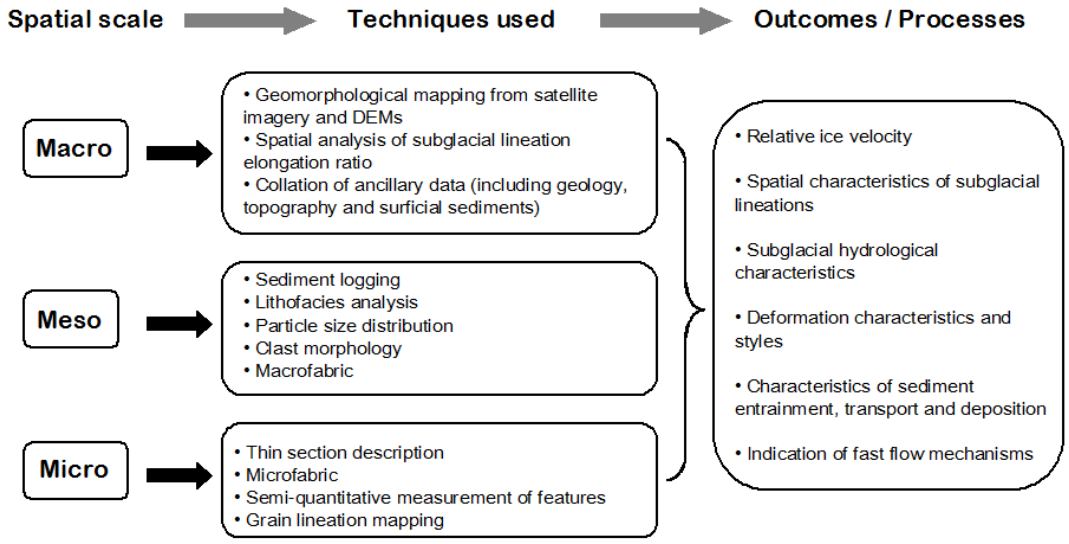

Figure 3.1 – Flow chart showing the key methods used within the multiscale framework, and the expected outcomes and processes that can be inferred from them.

3.1.1 Sampling strategy

Ice streams from the British and Laurentide ice sheets were selected for the investigation. Ice streams were examined from only these two ice sheets in order to reduce the potential number of variables to be considered, as compared to using ice streams from seven different ice sheets. These ice sheets were selected because: previous work has establish the presence of well defined ice streams in these localities (e.g. Stokes and Clark, 2003a; De Angelis and Kleman, 2007; Everest *et al.*, 2005;

Bradwell *et al*., 2007); they could be examined in the field with relative ease and safety; and because of the wide availability of remotely sensed imagery and ancillary data for these areas (Table 3.1). These two ice sheets were quite different, in terms of size, underlying topography and underlying geology. The British Ice Sheet was a relatively small ice sheet, with considerable topographic constraints and was situated on a range of lithologies. The Laurentide Ice Sheet was much larger and comparable in size to the East Antarctic and Greenland ice sheets. The Laurentide Ice Sheet was not topographically constrained across much of its extent and the preservation of superimposed and cross-cutting ice streams indicates that its behaviour has been quite dynamic (Boulton and Clark, 1990). Additionally of note, is that they both reach the mid latitudes and that the Laurentide Ice Sheet has a much greater range of latitudes. This contrasts with modern ice sheets that are located exclusively at high latitudes, which is important to note when comparing between certain Quaternary ice streams and contemporary ice streams.

From these two ice sheets, five palaeo-ice streams were selected for macroscale examination (Chapter 4) and two further ice streams were selected for examination across multiple scales (chapters 5 and 6). Ice streams with a well defined, isochronous signature and well preserved bedforms were selected, in order to isolate and simplify interpretation of ice stream processes as much as possible. Ice streams that fit this criteria were typically deglacial because these types of ice streams usually have minimal geomorphological modification. An isochronous geomorphological signature means that this can be assumed to represent a snapshot of ice stream flow (see Clark, 1999), albeit this is an oversimplification and it is likely that there will be some signature of temporal scale in the landforms and sediments, which was taken into account during interpretation. The ice streams examined at multiple scales were also selected based on the practical considerations of conducting fieldwork and the availability of sediment sections. These ice streams are the Tweed Palaeo-Ice Stream from the British Ice Sheet, and the Central Alberta Palaeo-Ice Stream from the Laurentide Ice Sheet. These two ice streams may be considered typical of their respective ice sheets, in terms of size, geology, dynamics and geomorphological signature.

3.2 Geomorphological analysis

3.2.1 Geomorphological mapping and classification

The geomorphology of the ice streams were mapped using DEMs and/or satellite imagery. British ice streams were mapped primarily with the Nextmap DEM and were cross checked against imagery from Google Maps and Bing Maps. Canadian ice streams were mapped from Thematic Mapper (TM), Enhanced Thematic Mapper Plus (ETM+) and Canadian Digital Elevation Data (CDED). The dataset found to represent the ice stream geomorphology most effectively was used as the primary dataset for mapping, and this was then cross checked against other available datasets. The different spectral bands and spatial resolutions of these remote sensing datasets are shown in Table 3.1. Differing resolutions between the datasets may cause confliction between the level of mapping detail possible in the different ice streams. This was taken into account when comparing results from different datasets.

Table 3.1 – Details of the remote sensing datasets used.

Dataset	Technical details	Horizontal (pixel) resolution	Vertical resolution	Geographical coverage available	Acknowledgement
Nextmap DEM	Radar (interferometry)	5 metres	1 metre	Britain	Intermap technologies, under licence from NERC. Data accessed via NERC Earth Observation Data Centre.
Thematic Mapper	Spectral bands 1 to 7	30 metres for bands 1 to 5 and band 7. 120 metres for band 6.	n/a	Global	Earth science database, Global Land Cover Facility (University of Maryland)
Enhanced Thematic Mapper Plus	Spectral bands 1 to 8	30 metres for bands 1 to 5 and band 7. 60 metres for band 6. 15 metres for band 8.	n/a	Global	Earth science database, Global Land Cover Facility (University of Maryland)
Canadian Digital Elevation Data	Digitised from national topographic maps	11 and 23 metres (dependent on latitude)	1 metre	Canada	Geobase, Canadian Council on Geomatics

Table 3.2 – Morphological classification criteria for mapped glacial landforms and examples.

Landform	Key characteristics	Example
Subglacial lineations	A broad term to describe the range of subglacial bedforms with a drumlinoid or elongate shape, which is orientated parallel to the direction of ice flow (e.g. Kleman and Borgström, 1994; Hart, 1999). They may include: drumlins, MSGL, flutes and crag-and-tails; identification of these individual bedform types was not conducted because the datasets did not provide sufficient information to do so for the majority of landforms. Subglacial lineations were mapped in polygons and as such required a definable outer extent. (Next column: Nextmap image from the Tweed Valley)	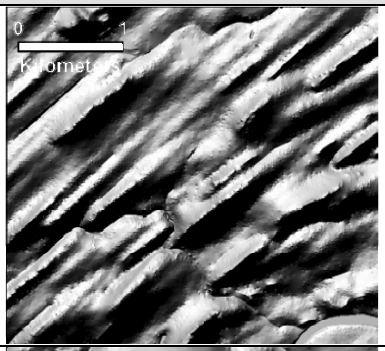
Meltwater channels	Channel that trends independently to the topography (i.e. does not trend directly downhill). May suddenly stop and start and may have variable depths along its length. (N.B. This criteria includes subglacial and lateral meltwater channels) (Sissons, 1961; Sugden *et al*., 1991). (Next column: Nextmap image from the Tweed Valley, meltwater channel is highlighted with a red line)	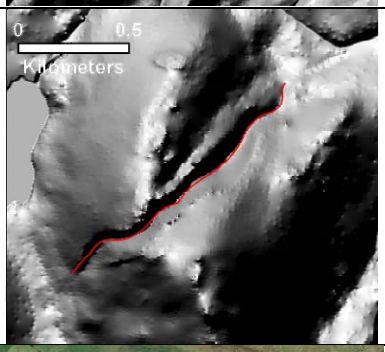
Eskers	Meandering ridge that sits above the land surface. May be associated with meltwater channels. (Warren and Ashley, 1994). (Next column: Aerial photography from the Tweed Valley. Image from Gazetteer for Scotland)	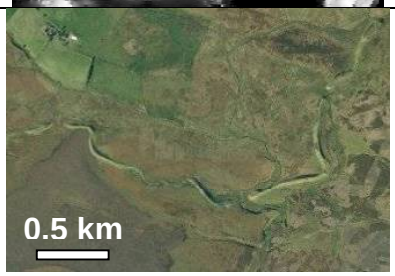
Ribbed moraine	Large ridges, transverse to palaeo ice flow. Display a wide range of features including: arcuate and concave down-ice, anastomosing, arcuate and concave up-ice, hummocky, straight, rectangular and barchonoid (Hättestrand and Kleman 1999; Dunlop and Clark, 2006). (Next column: Image from Dunlop and Clark, 2006)	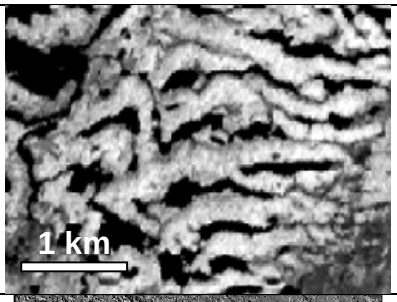
Lateral shear moraine	Moraine ridge(s) located at the lateral extent of a palaeo-ice stream. Typically long and thin. May be curved along its length and composed of several ridges. (Stokes and Clark, 2002b; Ottesen *et al*., 2008). (Next column: Canadian Digital Elevation Data image from Prince of Wales Island, Canada; lateral shear moraine is indicated with red arrows)	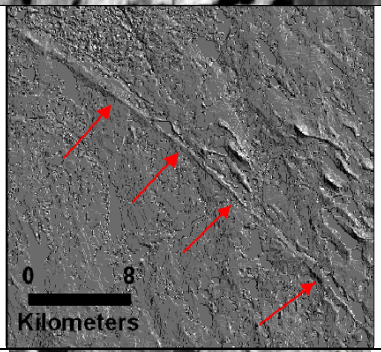
Terminal moraine	Ridge located at the downstream extent of a glacier, which marks its terminal position. Includes glaciotectonic moraines, dump moraines and ablation moraines (Bennett and Glasser, 1996). (Next column: Image of terminal moraine ridges, from Evans *et al*., 1999)	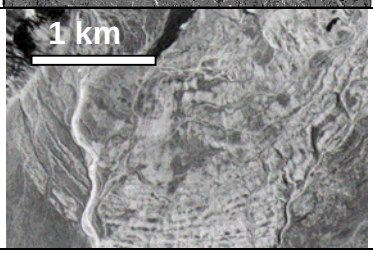

Satellite imagery and DEMs were studied and principally mapped in Erdas Imagine. DEMs were viewed at optimal light elevations and angles, and vertical relief exaggeration, to optimise the clarity of the geomorphology. The visualisation method used (e.g. the orientation of light and vertical exaggeration) can potentially introduce bias to DEM mapping (Smith and Clark, 2005). Therefore, mapping was conducted from a single visualisation (the one considered optimum for highlighting the landform type being mapped) and was regularly checked for accuracy during and after mapping by viewing the dataset in different ways. Satellite imagery was viewed in the band combination that best optimised the clarity of the geomorphology and was crossed checked against other combinations. Geomorphological features were mapped in shapefiles as polygons or polylines. Maps throughout the thesis were created in ArcMap and ArcGlobe (ArcGIS software by ESRI).

Geomorphological mapping was kept as consistent as possible by using established criteria for each of the landform types mapped. These are outlined in Table 3.2. The large areas, numbers of landforms mapped and the inherent variations in these landforms means that there may be an element of subjectivity to landform classification. This was minimised by mapping from a consistent visualisation and resolution and cross-checking against other visualisations and resolutions. Some of the mapping that was done early in the period of research was revisited at a later stage, and in some cases remapped in order to minimise inconsistencies that may have arisen due to changes in the mapping technique of the researcher over time. In the two instances where ice streams were also studied in the field, ground truthing was conducted to confirm some of the key landform interpretations, and to obtain additional information on some of the geomorphological features.

3.2.2 Spatial analysis of subglacial lineations

Subglacial lineations and their characteristics provide a key link to former ice stream flow. Elongation ratio in particular has been identified as a possible indicator of ice velocity (e.g. Hart, 1999; Stokes and Clark, 2002a; Briner, 2007; King *et al*., 2007). Spatial distribution of subglacial lineations may also be of significance and areas where they are highly clustered may bring an insight into the optimal conditions for their formation. Subglacial lineations were analysed to establish the spatial distribution of

elongation ratio, clustering of the subglacial lineations and the relation of these characteristics to certain bed variables.

Elongation ratios of the mapped subglacial lineation polygons were measured using the ArcScript 'Bounding Containers' (Patterson, 2008), which generates a rectangle around each polygon, allowing length, width and thereby elongation ratio to be obtained. The spatial distribution and characteristics of elongation ratios were investigated and visualised in several ways. Spatial autocorrelation (*Morans I*) was conducted in ArcMap, to ascertain whether elongation ratio is organised in a clustered, random or even distribution, across the ice stream beds. This used a fixed distance band of 2 km, a distance that was chosen because for most ice streams the average subglacial lineation would have approximately eight subglacial lineations within this distance of it (''How Spatial Autocorrelation'', 2011). In order to effectively visualise the spatial distribution of elongation ratios they were interpolated. This was conducted using inverse weighted distance interpolation, which is based on the assumption that data points will have similar characteristics to those around them (de Smith *et al*., 2012), a characteristic that was established by the spatial autocorrelation. This analysis was conducted in Quantum GIS. A distance coefficient (the value that controls the extent of the influence of each data point) of 3 was chosen for the analysis, which was based on the visual effectiveness of the output data produced at this value.

Transverse and longitudinal distribution of elongation ratio across the ice stream bed was also specifically investigated. This was done by mapping the ice stream centreline (located from the midpoints between the two lateral margins and maintaining an orientation parallel to the subglacial lineations) in ArcMap and exporting the coordinates of the centreline and the subglacial lineations into Excel. A macro was then used to compare the coordinates for each subglacial lineation to the coordinates of the centreline, determining the distance of each from the centreline (transverse distance) and along the centreline (longitudinal distance). The data was then plotted onto graphs. Subglacial lineations shaded according to elongation ratio were also viewed on a 3D DEM for some ice streams where it provided additional insight into this characteristic.

Clustering of bedforms was determined by creating heatmaps in Quantum GIS, based on the centroids of the subglacial lineations. This analysis generates a raster layer that reflects the spatial distribution of the input point data, with higher values reflecting a closer proximity of points and lower values reflecting a wider distribution of points. The buffer distance parameter (which controls the extent of the influence of each data point) was set to 2 km, consistent with the spatial autocorrelation analysis. The only exception was the Central Alberta Ice Stream, which had subglacial lineations on a considerably larger scale than the other ice streams and so the buffer distance was set to 6 km in order to produce a meaningful heatmap. The 'heat' or degree of clustering generated by a data point will affect the area around it to a distance of 2 km, so if several data points fall within this 2 km radius around a data point it will have a higher value than one which does not. In addition to the presentation of the heatmaps as individual figures, they were also used to identify areas of high clustering for further analysis in relation to bed variables. The range of values in the generated heatmaps (from 0 to 20.6 for the ice streams examined) were used to isolate the areas with the most clustering. This was done by identifying the areas that fell above the chosen threshold value of 10 (and 6 for the Central Alberta Ice Stream) and these areas were isolated and converted into polygon vector files.

The spatial distribution of both elongation ratio and bedform clustering were compared to bed variables including bedrock lithology, bedrock permeability, topography, land curvature and surficial sediments, where such data was available. This was done by overlying this data in maps and each bed variable was displayed with: (a) subglacial lineations shaded according to elongation ratio and (b) subglacial lineation clustering data, shown as contours. Additionally, the defined areas of high bedform clustering (above the values of 10 or 6 in the generated heatmaps), were directly compared to the bed variables. This was done by clipping these areas from the bed variable datasets and calculating the areas of the different variables present therein (e.g. bedrock lithology) and presenting this in bar charts as a percentage of the total area. The areas of the bed variables across the entire ice stream were also calculated and presented in bar charts for comparison. This direct analysis was possible for the lithology, permeability and surficial sediments data, which were all in categories (i.e. vector datasets) but not for the curvature data because this data is comprised of contiguous values in a raster.

Data on bed variables was derived from a range of sources including: the British Geological Survey; the Geological Survey of Canada; the Alberta Geological Survey; NERC Earth Observation Data Centre; Geobase; the Environment Agency; MacDonald *et al*. (2004); and Harrison *et al*. (2008). Curvature of the land surface was determined using DEM surface tools (Jenness, 2012) as an add-in to ArcMap, using the curvature type 'general curvature'. Data for bedrock permeability was constrained by the datasets available and these did not have equivalent categories according to permeability values, so they were broadly categorised descriptively from very high to very low. Table 3.3 presents the basis for these categories from the datasets used and serves to highlight any differences between them. Permeability data was not available for the ice streams in Arctic Canada because of the lack of detailed geology data from these regions.

Table 3.3 – Categories for the bedrock permeability data, derived from MacDonald *et al*. (2004), the Alberta Geological Survey and the Environment Agency. Some discrepancies are evident between the categories due to the differences between the datasets.

Permeability category	**Aquifer productivity rating**		
	Scotland (litres/second)	**England (Environment Agency aquifer designations)**	**Alberta (litres/second)**
Very low	< 0.1	Unproductive	< 0.1
Low	0.1 – 1	Secondary aquifers, Type B	0.1 – 0.4
Moderate	1 – 10	Secondary aquifers, Type A	0.4 – 2 and 2 – 8
High	10 – 20	Principal aquifers	8 – 38
Very high	> 20	-	> 38

3.3 Sedimentology

Sedimentological analyses were conducted at the Tweed and Central Alberta ice streams. Selection of sites for this analysis involved visiting several sites (throughout the Tweed Ice Stream and within the study area of the Central Alberta Ice Stream) and choosing two sites for each ice stream, which were considered to be the most representative of that ice stream (in terms of geomorphology and sediments).

3.3.1 Sediment logging

Detailed sedimentary logging and lithofacies analysis was carried out at each site following the guidelines of Evans and Benn (2004). Vertical sediment logs and 2D section drawings were produced at each site in order to give a comprehensive insight into the architecture and characteristics of the various lithofacies.

Vertical logs (Figure 3.2) and 2D logs include details of lithofacies type, the codes for which are given in Figure 3.3. Additional details that were provided in the logs included: matrix colour (measured with a Munsell Colour Chart); contacts between sediment units; upper particle size; and annotations of any further information considered to be relevant. Particle size indicated in the logs (Figure 3.2) refers to the Wentworth scale (Wentworth, 1922), and includes: clay (0.06 to 3.9 μm); silt (3.9 to 63 μm); sand (0.063 to 2 mm); gravel (2 to 4 mm); pebbles (4 to 64 mm); cobbles (64 to 256 mm); and boulders (256 to 4096 mm). Diamicton codes that were used are explained in Figure 3.3; and symbols for different sediment types were used to give a visual impression of the sediment, a key for these is given in Figure 3.4.

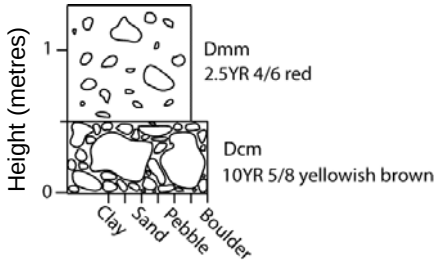

Figure 3.2 – Example of a vertical sediment log. Refer to figures 3.3 and 3.4 for details of the lithofacies codes and symbols.

Code	Description
Diamictons	*Poorly sorted admixture of a wide range of particle sizes*
Dmm	Matrix supported, massive
Dcm	Clast supported, massive
Dcs	Clast supported, stratified
Dms	Matrix supported, stratified
Boulders	*Particles > 256 mm*
BL	Boulder lag or pavement
Gravels	*Particles of 8 to 256 mm*
Gms	Matrix supported, massive
Gm	Clast supported, massive
Gh	Horizontally bedded
Granules	*Particles of 2 to 8 mm*
GRh	Horizontally bedded
GRp	Cross bedded
Sands	*Particles of 0.063 to 2 mm*
Sp	Medium to very coarse and planar cross bedded
St	Medium to very coarse and trough cross bedded
Sm	Massive
Silts and Clays	*Particles of < 0.063 mm*
Fm	Massive
Fp	Intraclast or lens

Figure 3.3 – Lithofacies codes used in sediment logs. Adapted from Benn and Evans (1998) and Evans and Benn (2004), originally developed from Miall, (1978); Eyles *et al*. (1983) and Maizels, (1993).

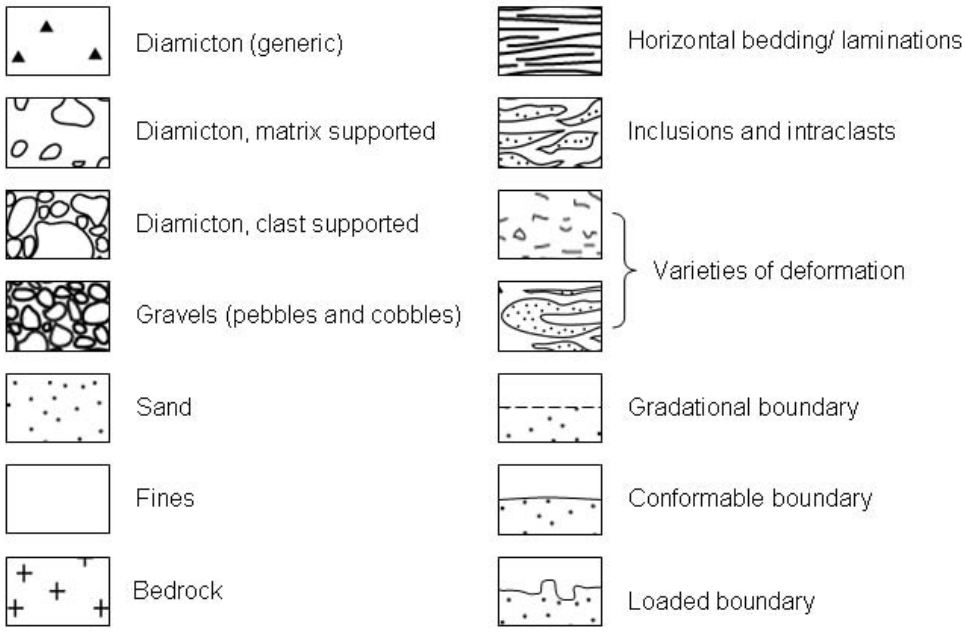

Figure 3.4 – Key to the main lithofacies, sedimentary structures and boundaries between lithofacies from the vertical logs and 2D logs. Adapted from Benn and Evans (1998), and originally developed from Miall, (1978) and Eyles *et al*. (1983)

3.3.2 Particle size distribution

Particle size distribution was measured to help ascertain the processes of sediment transport and deposition (e.g. Boulton, 1978; Haldorsen, 1981; Hoey, 2004) and identify textural variations within and between lithofacies. Bulk samples (of no less than 0.5 kg) were sampled from some of the key lithofacies, from representative points within vertical logs. These were dry sieved according to the method from Gale and Hoare (1991), which involved overnight drying of samples at 105 °C, followed by weighing and gentle disaggregation using a pestle and mortar. Samples were then sieved at increments of 32 mm, 16 mm, 8 mm, 4 mm and 2 mm and the remaining sediment in each sieve was weighed. This allowed the proportion of each size fraction to be obtained in weight.

The particle size distribution of the particles less than 2 mm was calculated using a Coulter Laser Sizer. Approximately 1 g of sediment was taken from each sample and placed in beakers. Organic matter was then removed by adding 5 ml of distilled water and 5 ml 30% hydrogen peroxide. This was left on a hot plate at 80 °C for 3 hours and further hydrogen peroxide was added until the substance stopped fizzing. The sediment was then disaggregated by adding 30 ml of Calgon and shaking overnight on a flask shaker at 300 repetitions per minute. Samples were then decanted into centrifuge tubes and run through the Coulter Laser Sizer. Data were analysed in the grain size analysis program 'GRADISTAT' (Blott and Pye, 2001). Data for the > 2 mm fraction (measurement in weight) and the < 2 mm fraction (measurement in volume) were presented in one diagram based on the assumption that the particles measured by volume all have the same density, which implies that the proportions of different particle sizes in volume is the same as the proportions of different particle sizes in weight (Blott and Pye, 2001).

3.3.3 Clast morphology

Clast morphology was measured to help identify the processes involved in sediment transport, deposition and deformation (Benn, 2004a). This analysis was conducted for key lithofacies, from representative points in vertical logs. Sampling involved random selection of clasts from a limited area. Each clast was then measured for shape and roundness. Clast shape was ascertained by measuring the a, b and c axes, which

represent the long, intermediate and short axes of the clast, respectively. To identify the distribution of clast shapes, results were plotted in a ternary shape diagram, using the Excel spreadsheet (Tri-plot) of Graham and Midgley (2000). This categorises the clast shapes into spheres, discs, rods and any intermediates of these. Additionally, the C_{40} index was calculated for each sample, which is a measure of the percentage of clasts with a-axis to c-axis ratios ≤ 0.4 (Benn and Ballantyne, 1993). As shown, this is the percentage of data-points under the horizontal line in the ternary diagram in Figure 3.5.

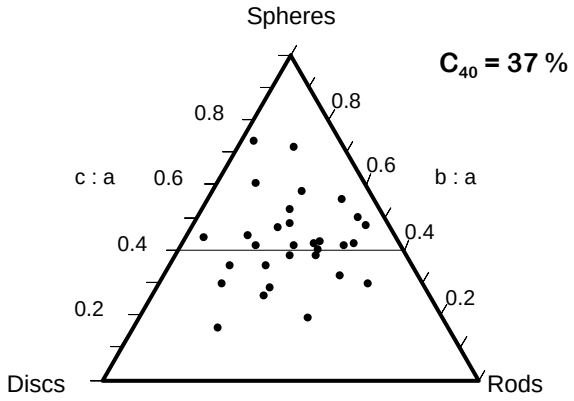

Figure 3.5 –Ternary shape diagram, created in spreadsheet from Graham and Midgley (2000), categories adapted from Sneed and Folk (1958)

Clast roundness was measured by categorising clasts into one of the six classes of visual clast roundness (Figure 3.6) from Benn and Ballantyne (1994), modified from Powers (1953). These six descriptive classes are very-angular, angular, sub-angular, sub-rounded, rounded and well-rounded. The roundness-angularity (RA) index was also measured, which is a measure of the percentage of clasts that are very-angular and sub-angular (Ballantyne and Benn, 1994).

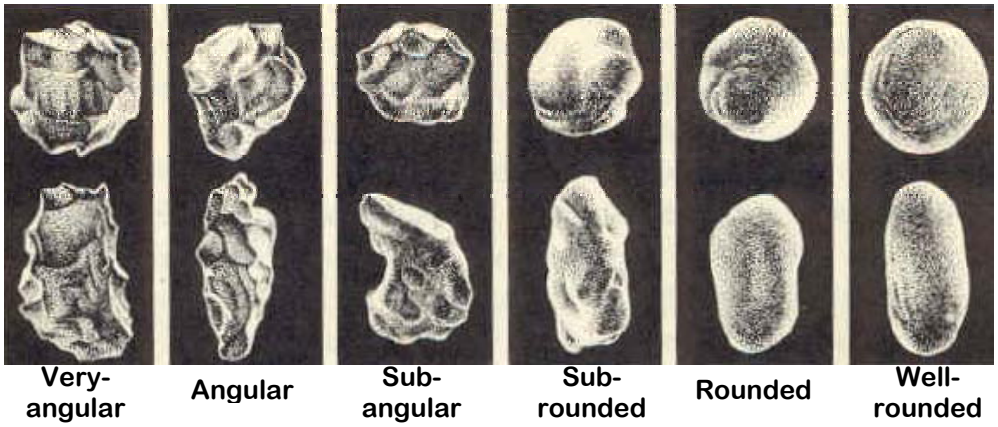

Figure 3.6 – Class roundness categories. Adapted from Dockal (2003), modified from Powers (1953).

Samples usually consisted of 50 clasts, which is the sample size adopted in many field studies using this technique (Benn, 2004a). In some instances when clasts were particularly difficult to remove *in situ* from the sediment, the sample size was dropped to 30 clasts. Clasts of size 35 to 125 mm were sampled, since this size range has been found to produce reliable results (Benn and Ballantyne, 1994; Benn, 2004a).

3.3.4 Clast macrofabric

Particle fabric refers to the orientation of particles in a sediment. This was done for two particle size ranges: macrofabric (8 to 32 mm) and microfabric (0.031 to 8 mm), which were measured from the same locations. Macrofabric was measured in the field, from a limited area (approximately 20 x 20 x 20 cm) in order to minimise the effects of spatial variability. Elongate particles were randomly selected from this area, which had a minimum ratio of 1.5:1 for the a and b axes. This ratio has been found to give a representative fabric in several studies (e.g. Benn, 1995; Millar and Nelson, 2003; Carr and Rose, 2003; Benn, 2004b). These were carefully excavated so the elongation and precise orientation could be established and then the azimuth and the dip of the clast were measured using a compass clinometer. Results were plotted on stereographic plots (Schmidt net, equal area, lower hemisphere plots), which were generated using Rockworks 2006. Eigenvectors and eigenvalues were generated for macrofabric data, also using Rockworks. The eigenvalue method (Mark, 1973) generates three eigenvectors (V_1, V_2, V_3), which indicate clustering direction, and three eigenvalues, (S_1, S_2, S_3) which indicate clustering strength. The principle eigenvector (V_1) is the orientation of maximum clustering in the data and the second and third eigenvectors are orthogonal to this. Eigenvalues represent the distribution of the data and can allow isotropic ($S_1 \sim S_2 \sim S_3$), girdle ($S_1 \sim S_2 > S_3$) and linear cluster ($S_1 \geq S_2, \sim S_3$) distributions to be distinguished. Macrofabric eigenvalues were plotted on ternary fabric shape diagrams, to help identify the differences in fabric shape between the samples. These were plotted using the Excel spreadsheet (Tri-plot) of Graham and Midgley (2000).

3.4 Micromorphology

Micromorphological samples were collected to obtain microfabrics and to characterise the microscopic properties and processes in the sediments. Samples intended for microfabric measurement were collected directly next to macrofabric measurements, to allow a direct comparison between the two. Samples were also collected for lithofacies characterisation, and characterisation of contacts between lithofacies, for which samples were taken from areas that were considered representative.

Kubiena tins (92 x 67 x 45 mm) were used to collect the micromorphological samples. These were placed against the sediment face and carefully pushed into the sediment with the aid of a penknife, enabling an *in situ* sediment sample to be removed. Kubiena tins were labelled with details of the precise orientation of the sample. These were then taken back to the lab, dried, impregnated with resin, cut, mounted onto glass slides and ground to the correct thickness to make thin sections, as detailed in Figure 3.7.

Vertical thin sections (profile view) were produced from all the samples, which are referred to as (a). For many samples microfabric was also measured, and in these cases horizontal thin sections (plan view) were also produced to measure azimuth particle fabric, which are referred to as (b). In some cases secondary vertical thin sections were also produced, which were cut parallel to the mean azimuth fabric and these are referred to as (c). Description of thin sections was done from both (a) and (b) slides, where available.

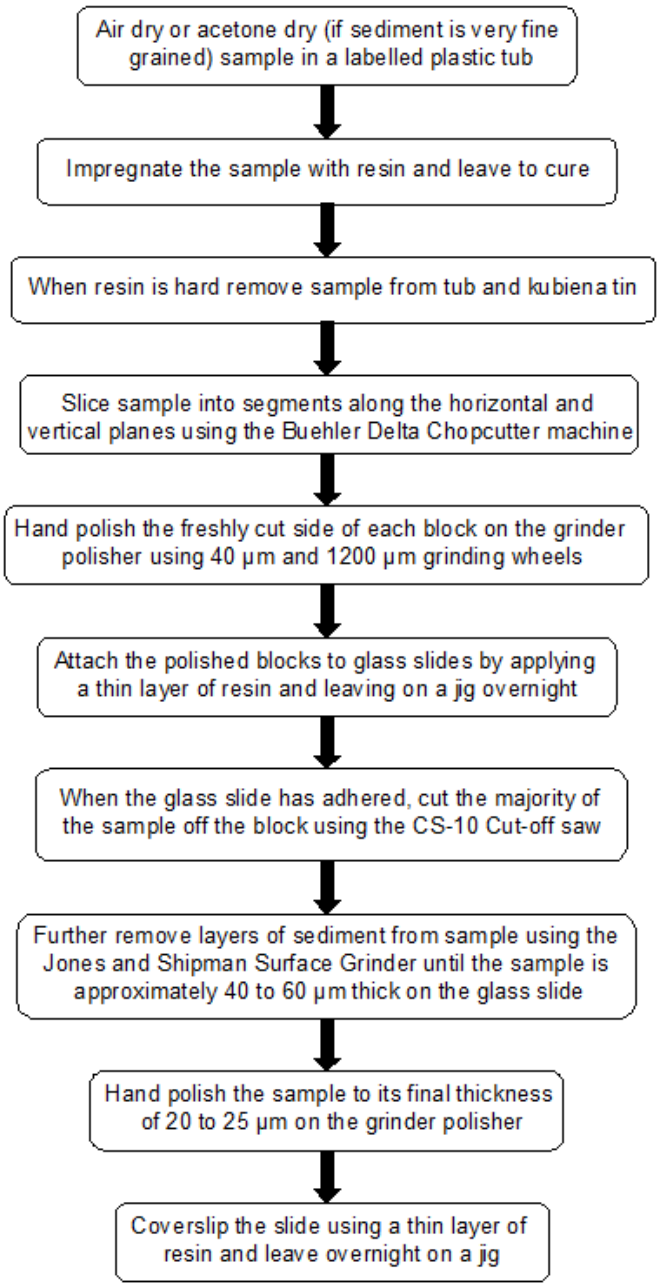

Figure 3.7 – Flow chart of the laboratory procedure for making thin sections, adapted from Carr and Lee (1998).

Thin sections were studied using a Leica microscope at magnifications between 6.2X and 32X. Thin sections from each sample were described following a procedure adapted from Brewer (1976); van der Meer (1987; 1993; 1996) and Carr (2004). The steps for this are outlined in Figure 3.8.

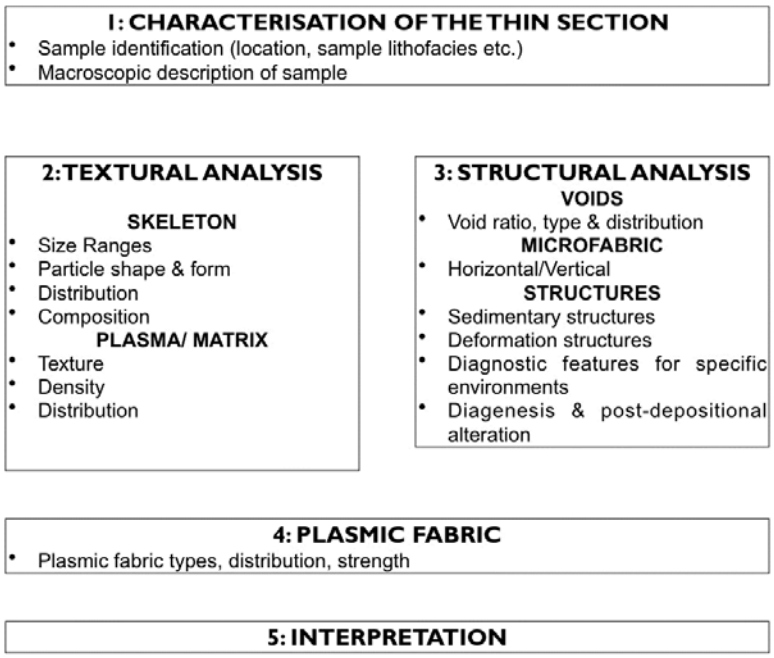

Figure 3.8 – Guideline for the description of thin sections. From Carr 2004; following Brewer (1976); van der Meer (1993; 1996); and Carr (1999).

Sediment texture refers to the skeleton (all visible individual grains) and the matrix (< 20 μm) (Carr, 2004). Structure refers to the voids, any visible fabric or grain and to specific features or structures (Figure 3.9). Plasmic fabric refers to the arrangement of the matrix particles and can be identified under cross-polarised light in the appearance of interference colours (Carr 2004). Interference colours are determined by the birefringence, which is the difference between the maximum and minimum refractive index within a point in the thin section (MacKenzie and Adams, 1994), which is high for orientated plasmic fabric (e.g. skelsepic, masepic). Different plasmic fabric types are shown in Figure 3.9. The microscale features and structures identified are outlined in Figure 3.9 and further description of these and how they may be interpreted is outlined in Section 2.4.1.

Following micromorphological description an interpretation can be made, which is based on previous work including: field studies of palaeo glacial deposits (e.g. van der Meer, 1993; Menzies, 1997; Carr, 1999; Larsen *et al*., 2007; Phillips *et al*., 2007); field studies of contemporary glacial deposits (e.g., Khatwa and Tulaczyk, 2001; Carr, 2001; Larsen *et al*., 2006a); and laboratory experiments (e.g. Evans, 1998; Muller and Schluchter, 2000; Hiemstra and Rijsdijk, 2003; Larsen *et al*., 2006b) in which structures have been linked to specific processes.

Voids

Fissures
Planar voids, may or may not be interconnected

Packing voids
Voids in between loosely packed areas of matrix and/or particles

Vughs
Irregular shaped voids, may have smooth or coarse walls

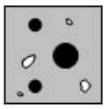

Vesicles
Circular voids

Channels and chambers
Smooth walled planar voids and connected chambers

Sediment mixing

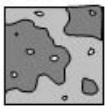

Multiple domains
Two or more zones of different matrix material

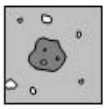

Intraclasts
Individual sediment pebble within a different matrix material. Can be classified into three types (van der Meer, 1993)

Papules
Clumps of that cutan are not *in situ*. Usually in blocky or angular shapes

Water movement

Cutans
Laminations of clay and silt within a discrete area

Grain structures

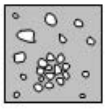

Grain concentrations
A concentration of grains

Turbates
Skeleton grains arranged in arcuate and circular structures (also known as rotation structures). May or may not have a corestone

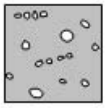

Grain lineations
Grains arranged in linear structures

Haloes
Grain encircled by a matrix material that is different to that surrounding it

Figure 3.9 – Continued overleaf

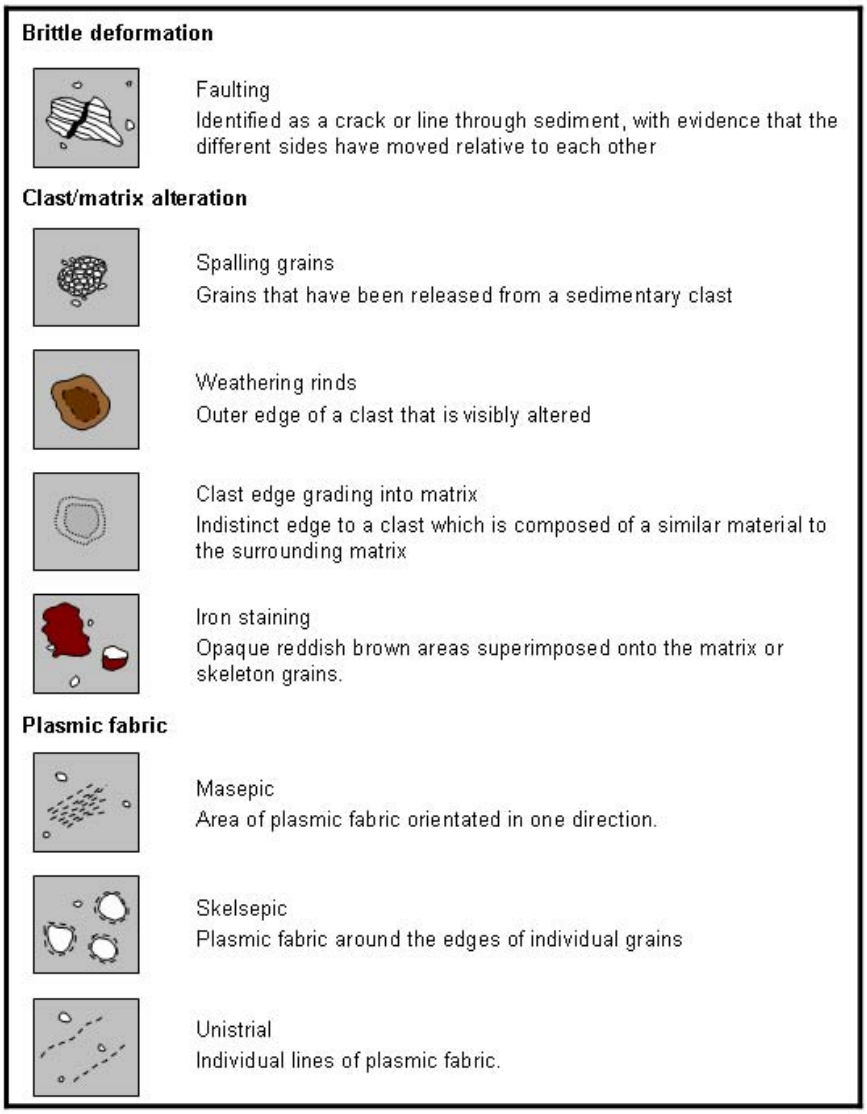

Figure 3.9 – List of the micromorphological structures and features identified in this study, adapted from van der Meer (1993) and Menzies (2000). In the diagrams of the features: voids are black; matrix is grey; particles are white (and are brown and grey in the clast/matrix alteration section); plasmic fabric is depicted by dashed lines; cutans are orange; and iron staining is dark red.

Micromorphology results are presented in tables, descriptions and images. These are mostly qualitative and semi-quantitative. Features are summarised in tables that indicate relative abundance of each feature on a scale of zero to three, which follows the approach of Carr *et al*. (2000; 2001). Images are shown in plane-polarised view, and the orientation is up, unless otherwise stated. Micro structures were also mapped across areas of selected thin sections in order to help identify any associations between different structures and their spatial distributions, similar to the approach of Piotrowski *et al*., (2006).

3.4.1 Microfabric

In this study microfabric refers to the orientation of particles at a microscopic scale (Carr, 2004) and includes particles within the size range 0.031 to 8 mm. Microfabric was measured from horizontal and vertical thin sections. Each thin section was scanned (alongside a scale bar) to a resolution of 9600 dpi, and the scans were imported into ArcMap. The orientations of all the elongate grains (with a minimum ratio of 1.5:1 for the a and b axes) were mapped as polylines into a shapefile. The azimuth and length of each polyline were then generated as attributes using the ArcScripts longest lines (Jenness, 2007) and linear properties (Rathert, 2003). Attributes for each slide were then exported into Excel and the particle lengths were then calibrated. Rose diagrams (Schmidt net, equal area, lower hemisphere, bi-directional plots) and statistics were generated in Rockworks. Statistics generated included mean lineation vector and confidence interval around the mean (95%).

The microfabric method that has been adopted in this study follows the approaches of previous studies of diamict microfabrics using thin sections (e.g. Ostry and Deane, 1963; Chaolou and Zhijiu, 2001; and Carr and Goddard, 2007). The technique involves measurement of 'apparent' fabric and the assumption is that given a sufficiently low particle dip the 2D horizontal particle orientation on the thin section is the same as the true 3D particle orientation. This measurement of a 3D object in 2D is an inherent problem and limitation of this technique and can lead to bias, however, this has never been thoroughly investigated. Three variables affect the 2D microfabric measurement of a grain: (1) particle azimuth; (2) particle dip and (3) particle shape. An azimuth measurement (from a horizontal thin section) of a rod shaped grain that is dipping at a low angle will be accurate, but at a high dip this particle will not be measured. For a rod shaped particle ($a > b, b = c$) the particle azimuth will not be measured if the dip of the particle is greater than 48º (given that the thin section passes through the middle of the particle). If fabric is found to have a steep dip this problem can be addressed by producing a thin section that is parallel to the mean dip from which to measure the azimuth fabric.

Another potential problem may arise from measurement of disc shaped and blade shaped grains. If these particle shapes have a sufficiently steep dip they may be

measured inaccurately along their b-axis, rather than along their a-axis, as shown in the example in Figure 3.10(a and b). The threshold dip at which a particle will be measured inaccurately will depend on its dimensions. The effect of different particle shapes on microfabric measurements is shown in Figure 3.11. A further problem may arise if the thin section passes through the edge or the corner of a grain. As shown in Figure 3.10c, this can lead to an inaccurate azimuth measurement even if the particle has a low dip. This is more of a problem for highly angular particles.

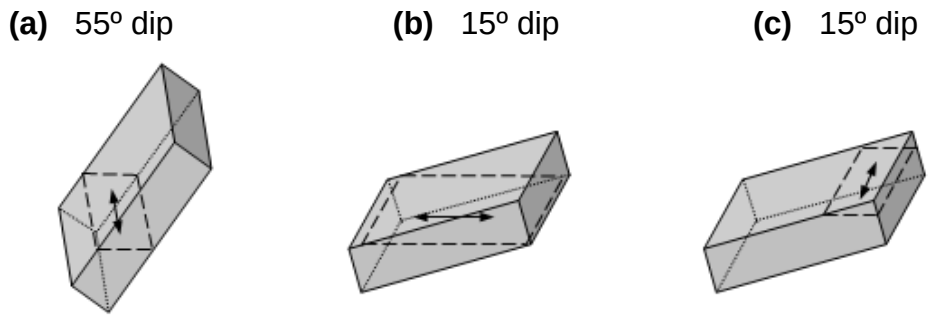

Figure 3.10 – Schematic representation of the measurement of 2D microfabric for a disc/slab shaped particle at: (a) 55º dip; (b) 15º dip; and (c) 15 º dip where the thin section passes through the end of the particle. The dashed rectangles represent the areas that the thin section crosses the particle and the arrows indicate the apparent 2D fabric of the particle.

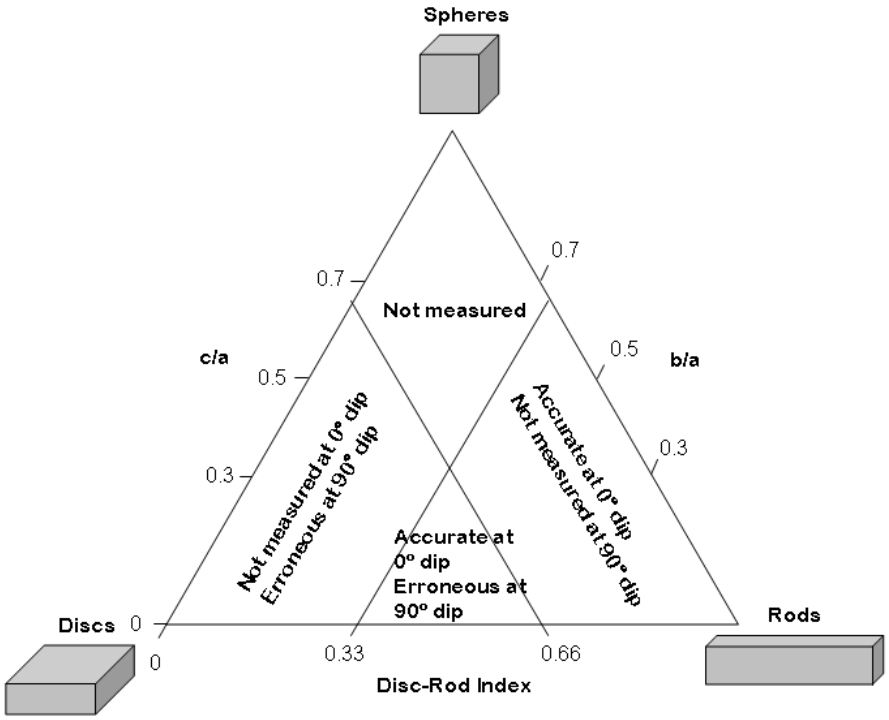

Figure 3.11 – Ternary shape diagram, demonstrating which particle shapes are accurately measured and those that are erroneous for 0° and 90° dips, for microfabric measurements.

Steps were taken in order to minimise the effects of these potential sources of bias. Large sample sizes were used to reduce the probability of erroneous fabrics skewing the data. Dips were measured for some of the samples and in some cases they were measured from vertical thin sections that were cut parallel to the mean azimuth lineation, this allowed the mean dip to be identified and the relative proportions of particle dip, which can highlight bias in the azimuth measurement. Awareness that azimuth fabrics only represent particles dipping at 48º or below and dip fabrics only represent the dips on and around the vertical plane of the thin section. Disc shaped particles may produce erroneous results, but this effect is considered to be minimal. Assessment of particle shape would be of value to ascertain the degree of this bias, however, this was not measured because of the difficulties in obtaining reliable shape measurements for these small grain sizes (Clayton *et al*., 2009).

3.4.2 Grain lineation mapping

Grain lineations are the linear alignments of grains (van der Meer, 1993), as shown schematically in Figure 3.9. An experimental analysis, involving mapping of grain lineations across entire thin sections, was conducted for one of the ice stream case studies (Chapter 5). The definition adhered to with regard to the mapping is that a lineation is comprised of at least three grains, either aligned end to end (Hiemstra and Rijsdjik, 2003) or aligned adjacent to a discrete line within the matrix (see Menzies, 2000; Menzies *et al*., 2006). This gave insights into the extent and spatial distribution of grain lineations, their orientations and associated processes. The technique employed the same approach as the microfabric methodology, mapping from thin sections scanned into ArcMap, which provided an efficient way to map and measure grain lineations. Thin sections were viewed within a frame of approximately 5 mm wide and systematically mapped by moving this frame across the entire thin section. Mapped orientations of the lineations were found to be biased according to the orientation at which the thin sections were mapped, in other words, the lineations mapped differed according to whether the thin section was viewed vertically or on its side. To minimise the effects of this bias the mapping was conducted with the thin section at two orientations, the second of which was orientated 90° from the first position. The orientations of the lineations were then presented in rose diagrams, which provided an

overview of them and allowed comparison to the range of shears found in a Riedel shear system (see Larsen *et al*., 2007).

3.5 Integration of multiscale data

Following the different analyses the results were interpreted at each of the individual scales and then considered together to interpret each ice stream and identify common factors between the ice streams. This is summarised in Figure 3.12. The diagram illustrates that the three scales of analysis were distinct and whilst some data could be directly compared (e.g. the macrofabric and microfabric), the majority of the data had to be analysed and interpreted in its individual scale. Following this process the three scales were then compared and integrated to derive an overall picture of the ice stream and its subglacial processes.

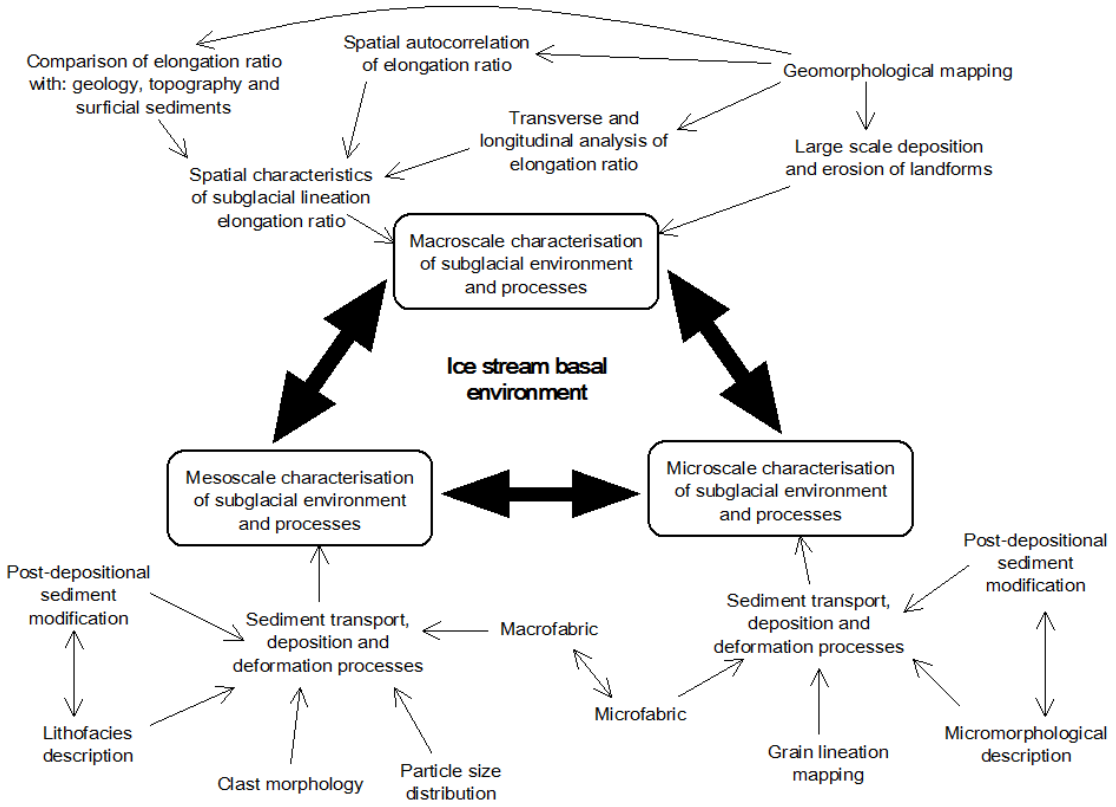

Figure 3.12 – Schematic diagram of the links between, and the integration of, different datasets within the thesis.

Some specific steps were also taken in order to minimise inconsistencies across the different scales and so that comparisons could be made confidently. The macroscale geomorphology provided an overview of the entire ice stream, which was important in order to characterise the ice stream in its entirety as well as possible. To integrate

between the macro and meso scales as effectively as possible the sites chosen for mesoscale investigation were selected from areas with a representative geomorphological signature of the ice stream. However, choice of sites was very limited because there were few suitable sections available in the area. An image of the DEM and geomorphological mapping around each sediment site was also presented alongside the mesoscale analysis in order the characterise the geomorphological context of each site as well as possible. This helped facilitate up and down scaling between the scales and also aided the meso and micro scale interpretations. The microscale analysis was conducted so it could be directly compared to the mesoscale as much as possible, this was done by selecting sampling areas for the micromorphology carefully and from an area that is representative of the lithofacies (Carr, 2004). In addition to this, the samples taken for microfabric were taken from directly behind the location from which the macrofabric was measured.

4. Subglacial lineations and macroscale characteristics of palaeo-ice streams

4.1 Introduction

Contemporary ice streams reveal spatial variations in terms of ice velocity, shear stress, bed properties, and bed processes over a wide range of scales (< 4 km to 100's km) (e.g. Smith, 1997; Vaughan *et al*., 2003; Joughin *et al*., 2004b; 2006; Murray *et al*., 2008). Heterogeneous bed conditions in terms of hydrology and inferred ice flow mechanisms (i.e. deformation vs sliding) have been reported from modern ice streams (Smith, 1997; Vaughan *et al*., 2003; Smith *et al*., 2007; Murray *et al*., 2008). Whilst variation in basal shear stress appears to be a typical characteristic of several west Antarctic ice streams (Joughin *et al*. 2004b; Joughin *et al*. 2006). However, despite the fact that such spatial variations are so common in ice streams, the controls on these are rarely understood. Characterisation and conception of subglacial spatial variations is important to enable understanding and accurate modelling of ice stream flow. Moreover the contribution of bed resistance to the force balance of the ice stream means that any changes therein have the potential to cause dynamic behaviour of an ice stream.

Some variations in shear stress and ice velocity display certain systematic spatial trends across ice streams. Transversely, velocity typically declines quite sharply at the lateral margins of an ice stream and this transition may account for 22 to 35 % of ice stream width (Bindschadler and Scambos, 1991; Echelmeyer *et al*., 1994; Whillans and van der Veen, 1997; Echelmeyer and Harrison, 1999; Joughin *et al*., 2002; Truffer and Echelmeyer, 2003). Longitudinally, velocities are fastest in the central trunk of an ice stream and are slower at the onset zone, tributaries, and terminus (e.g. Alley and Whillans, 1991; Bamber *et al*., 2000; Joughin *et al*., 2002; Clark and Stokes, 2003). Examples of longitudinal and transverse velocity distributions from west Antarctic ice streams are shown in Figure 4.1. The transverse and longitudinal velocity distribution may also vary from the overall trend described, both within and between ice streams (e.g. Bindschadler *et al*., 1996; Joughin *et al*., 2002).

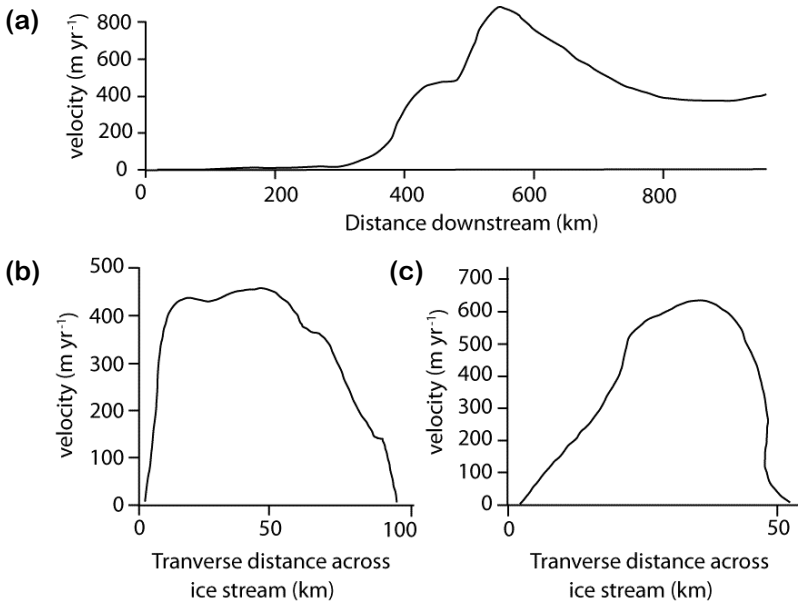

Figure 4.1 – Velocity profiles across ice streams in the West Antarctic Ice Sheet. (a) Longitudinal profile of the Whillans Ice Stream. Adapted from Alley and Whillans (1991); (b) and (c) Transverse profiles of MacAyeal and Bindschadler ice streams, respectively. Adapted from Bindschadler *et al.* (1996). Velocity distribution across these ice streams is also shown in Figure 2.1.

Besides the transverse and longitudinal variations, other sporadic variations in ice velocity may be apparent, whereby localised areas within an ice stream are slower than surrounding ice (Whillans *et al*., 1987; Bindschadler and Scambos, 1991; Bindschadler *et al*., 1996; Joughin *et al*., 1999). These may be described as sticky spots and are usually considered to relate to variability in basal characteristics and/or basal processes (Alley, 1993; MacAyeal *et al*., 1995; Vogel *et al*., 2003; Bougamont *et al*., 2003; Stokes *et al*., 2007). Of the potential bed variables that may cause heterogeneity or sticky spots, some are readily identifiable from palaeo-ice streams, including (i) topography, (ii) surficial sediments and (iii) bedrock geology (e.g. Clark and Stokes, 2001; Ó Cofaigh *et al*., 2002; Phillips *et al*., 2010).

Bed topography (i), is considered to play a role in controlling the location, margins and continuity of flow within an ice stream (e.g. Raymond *et al*., 2001; Andrews and MacLean, 2003; Stokes *et al*., 2007; Winsborrow *et al*., 2010), it may also influence bedform distribution (Raukas and Tavast, 1994). Topographic lows are known to experience greater driving stress and increased basal temperatures (Paterson, 1994), which will affect ice velocity, basal hydrological conditions and even the ice flow mechanism. Conversely topographic highs at the bed of an ice stream may cause drag and deflection of ice around them (Gudmundsson *et al*., 1998; Stokes *et al*., 2007).

Surficial sediments (ii), including the extent, distribution and properties of till at ice stream beds may also play a key role in continuity of flow, ice flow mechanism and hydrological conditions. Till plays a fundamental role in the subglacial deformation ice flow mechanism (Boulton, 1987) and thereby its extent and distribution will directly affect the potential for this flow mechanism to operate. Furthermore, till properties such as texture will affect its permeability and effective porosity, which will affect the water drainage at the bed and hence till variations will create variations in water pressure. This has implications for flow mechanisms, variations therein and the bed hydrological system. Till-free areas have been identified at the beds of contemporary and palaeo-ice streams and linked to increased friction, which is thought to cause localised velocity decreases (Rooney *et al*., 1987; Alley, 1993; Clark and Stokes, 2001).

Bedrock geology (iii) may influence: the location and lateral margins of an ice stream; ice velocity; subglacial lineation type; and subglacial hydrology (e.g. Anandrakrishnan *et al*., 1998; Bell *et al*., 1998; Wellner *et al*., 2001; Ó Cofaigh *et al*., 2002; Lowe and Anderson, 2003; Ottesen *et al*., 2008; Graham *et al*., 2009; Phillips *et al*., 2010). Bedrock lithology will commonly strongly influence the properties of till that overlie it, thereby changes in bedrock lithology may relate to changes in properties of the overlying till (e.g. Rattas and Piotrowski, 2003). In some Antarctic and Norwegian palaeo-ice streams, downstream changes in geology have been linked to changes in bedforms; whereby upstream crystalline bedrock is characterised by short subglacial lineations and meltwater channels; and downstream sedimentary bedrock is characterised by highly elongated subglacial lineations (e.g. Ó Cofaigh *et al*., 2002; Ottesen *et al*., 2008). A significant characteristic of bedrock geology is permeability. This will directly affect the basal hydrological conditions, as shown by Clark and Walder (1994) who found that eskers, indicative of R-channels, are commonly located on crystalline bedrock in North America, whereas few were found on sedimentary bedrock. Rattas and Piotrowski (2003) found that bedrock permeability had a relationship with drumlin size and morphometry and found that smaller, more elongated drumlins were associated with lower permeability bedrock.

Palaeo-ice streams have the advantage of an accessible bed, while their link to processes and characteristics pertaining to ice stream flow, lies in their bedforms (Stokes *et al*., 2007). As discussed in Section 2.2.1a, evidence suggests that subglacial lineation

elongation ratio relates to ice velocity (Hart, 1999; Stokes and Clark, 2002a; Briner, 2007; King *et al*., 2007). If elongation ratio mirrors ice velocity accurately, then a palaeo-ice stream signature would be expected to display a distribution of subglacial lineation elongation ratios similar to that in the idealised pattern in Figure 4.2 (Clark and Stokes, 2003). The distribution of subglacial lineations and their relationship with certain bed variables, including topography, bedrock geology and surficial sediments, may also reveal insights into subglacial conditions and controls. Localised areas of slower flow (sticky spots) may be identifiable from the distribution of subglacial lineations and their elongation ratios.

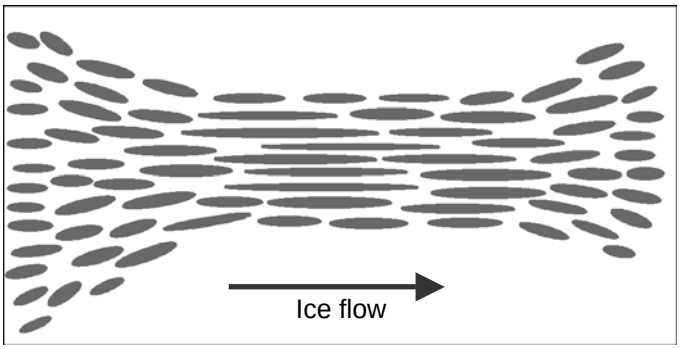

Figure 4.2 – Pattern of subglacial lineation elongation ratios in an idealised palaeo-ice stream signature, based on Clark and Stokes (2003). Convergent subglacial lineations with low elongation ratios characterise the onset zone, highly elongated subglacial lineations characterise the main trunk of the ice stream and divergent lineations with low elongation ratios characterise the terminus for terrestrially terminating ice streams.

This chapter will investigate five palaeo-ice streams in order to study variations in subglacial lineation elongation ratio and clustering, and the relation of these parameters to certain bed variables. This addresses the first research question of the thesis:

1. *Based on the macroscale characterisation of seven palaeo-ice streams*, can any spatial patterns be identified in the subglacial lineations and if so, do these correspond to any landscape variables (in topography, bedrock geology or surficial sediments)?*

* The analysis for two of these palaeo-ice streams is presented in the chapters 5 and 6.

4.1.1 Study sites

As discussed in Section 3.1.1 palaeo-ice streams from the British and Laurentide ice sheets were selected for investigation. Ice streams that had well defined, isochronous bedform signatures were chosen, in order that any geomorphological evidence for ice stream basal processes was preserved as much as possible. The characteristics of the ice streams are given in Table 4.1 and their locations are shown in Figure 4.3.

Table 4.1 – Key characteristics of the ice streams studied in this chapter.

Ice stream	Location	Characteristics
Solway Firth Ice Stream	British Ice Sheet; Solway Firth, NW England	- Previous work has identified the context of this landform set and identified it as representative of ice streaming (Livingstone *et al*., 2008) - Relatively small ice stream (c. 45 km long and 15 km wide) - Continuous set of bedforms - Appearance in numerical ice sheet models as an ice stream (Boulton and Hagdorn, 2006; Hubbard *et al*., 2009)
Forth Ice Stream	British Ice Sheet; Firth of Forth, Midland Valley of Scotland	- Previous work has identified glacial bedforms and streamlining - Relatively large ice stream for the British Ice Sheet (c. 100 km long and 60 km wide) - Bedforms display discontinuities across the ice stream extent - Appearance in numerical ice sheet models as an ice stream (Boulton and Hagdorn, 2006; Hubbard *et al*., 2009)
Crooked Lake Ice Stream	Laurentide Ice Sheet; Prince of Wales Island, Nunavut	- No apparent topographical control on location of ice stream - Identification by previous studies as an ice stream (Dyke *et al*., 1992; Stokes *et al*., 2005; De Angelis and Kleman, 2005) - Some discontinuities in bedforms within the ice stream extent - Ice stream size is approximately 190 km long and 65 km wide
Transition Bay Ice Stream	Laurentide Ice Sheet; Prince of Wales Island, Nunavut	- Identification by previous studies as an ice stream (Dyke and Morris, 1988; Dyke *et al*., 1992; De Angelis and Kleman, 2005; Stokes *et al*., 2005) - Entire ice stream signature is visible - No apparent topographical control on location of ice stream - Relatively small ice stream for the Laurentide ice sheet (c. 80 km long and 45 km wide)
Haldane Ice Stream	Laurentide Ice Sheet; Northwest Territories	- Identification by previous studies as an ice stream (Winsborrow *et al*., 2004) - Entire ice stream signature is visible - Ice stream is situated in valley - Relatively small ice stream for the Laurentide ice sheet (c. 85 km long and 50 km wide)

As shown in Table 3.1 different datasets were used for the mapping of the British ice streams and the Laurentide ice streams. The main imagery used to map the British ice

streams was the Nextmap dataset (5 m horizontal resolution, and 1 m vertical resolution) and the main imagery used to map the Laurentide ice streams was Landsat ETM+ (15 and 30 m horizontal resolution), and this discrepancy is acknowledged.

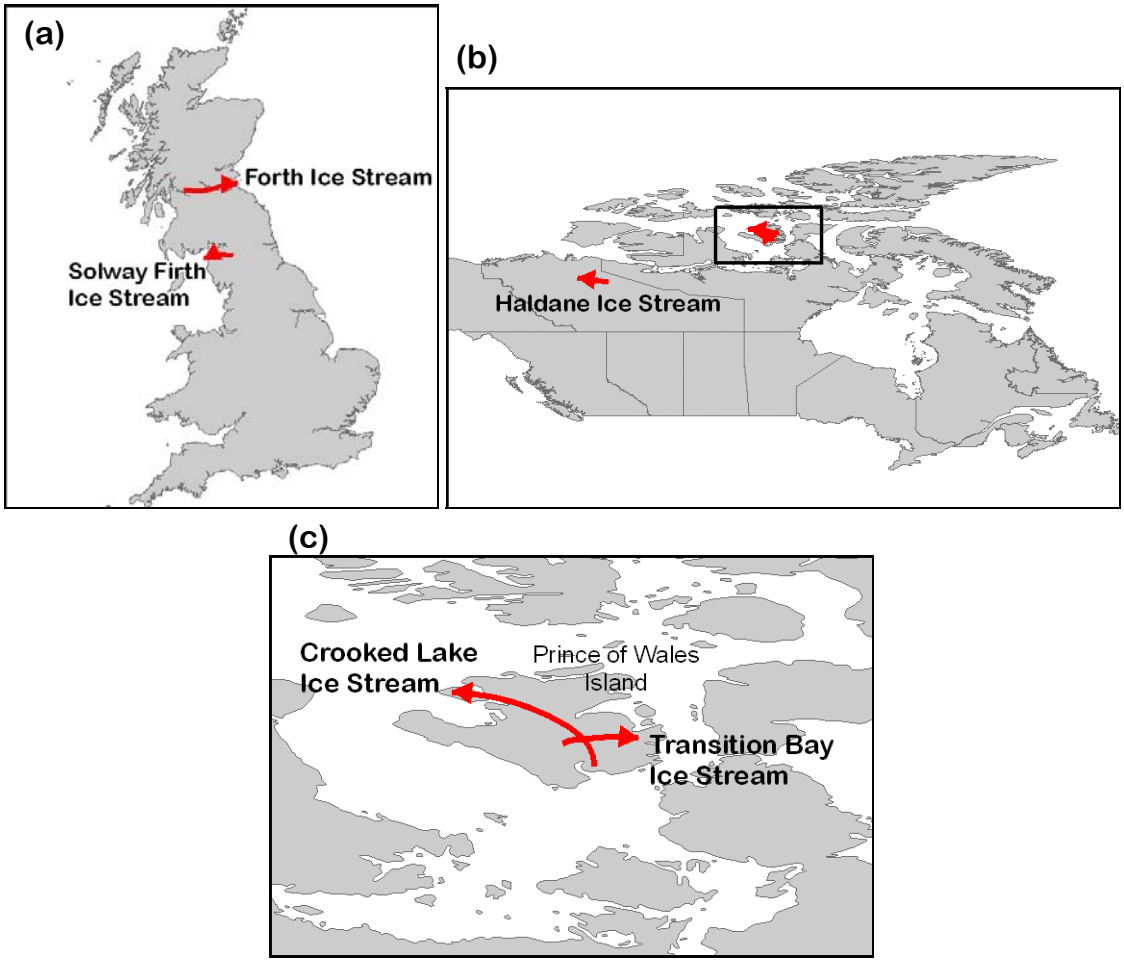

Figure 4.3 – Ice stream locations. (a) Map showing the British Ice Sheet ice streams; (b) Map showing the Laurentide Ice Sheet ice streams. Rectangle shows location of (c); (c) Map of the ice streams on the Prince of Wales Island.

4.2 Solway Firth Ice Stream

4.2.1 Background

The Solway Firth Palaeo-Ice Stream is located in NW England, directly north of the Lake District Mountains, flowing approximately NE to SW, with a curvature along its length (Figure 4.4). Glacial landforms were first reported and studied here by Trotter (1929) and Hollingworth (1931). Livingstone *et al*. (2008) present a geomorphological map for the region, exploring the glacial history and flow dynamics of the area. The Solway Firth Ice Stream is represented by the purple flow-set in Figure 4.4 and it

displays typical geomorphological characteristics of a palaeo-ice stream, including characteristic shape and dimensions, attenuated bedforms and abrupt lateral margins (Stokes and Clark, 1999). The upstream extent of the ice stream is overprinted by a subsequent flow-set, which flows south to north along the Vale of Eden (Figure 4.4; Livingstone *et al*., 2008). This ice stream may have been a tributary of the large Irish Sea Ice Stream (see Ó Cofaigh and Evans, 2001; Hiemstra *et al*., 2006; Roberts *et al*., 2007).

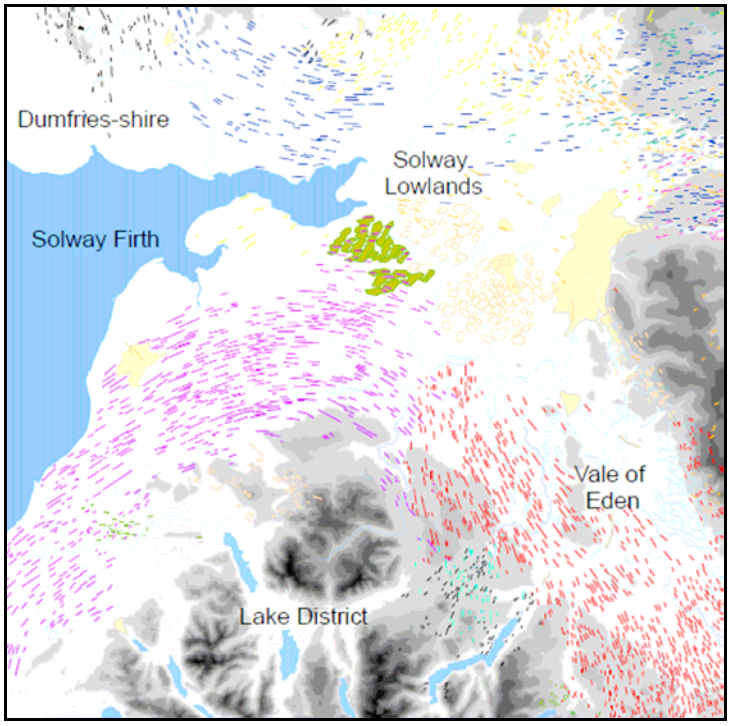

Figure 4.4 - Excerpt from the geomorphological map of Livingstone *et al.* (2008), which demonstrates the basis for the extent of the mapping for this study. Purple lineations constitute the Solway Firth Ice Stream. Lineations relating to other flow-sets in the area are shown in different colours, and an area of ribbed moraine (green) is present in the centre of the map.

4.2.2 Geomorphological mapping

Following the work of Livingstone *et al*. (2008), this ice stream has been remapped in order to obtain polygons for subglacial lineation shape. The flow-sets established by Livingstone *et al*. (2008; Figure 4.4) provided the limits of the isochronous ice stream signature. It should be noted that the ice stream signature appears to be partial, as it is terminates at the coastline and is overprinted by a subsequent flow-set at its upstream end. This is depicted by Figure 4.5b, which indicates the approximate location of the ice stream signature within an idealised ice stream (in this case it is in the upstream corner).

The results of the mapping are shown in Figure 4.5a. Glacial geomorphology associated with this ice stream includes subglacial lineations, meltwater channels and ribbed moraine. Subglacial lineations (n = 683) have a high degree of parallel conformity and range from 0.02 to 1.2 km^2 in area (median area was 0.21 km^2) and 1.5 to 9.4 in elongation ratio (median elongation ratio was 3.6). An area of ribbed moraine is situated at the north lateral margin, overprinted by small subglacial lineations.

4.2.3 Subglacial lineation analysis

To understand the spatial characteristics of the subglacial lineations, they were examined further with regard to distribution of elongation ratios, clustering and in relation to bed variables. The map presented in figures 4.8 and 4.10 demonstrates that clusters of lineations with high elongation ratios are present, especially towards the upstream end of the ice stream. Spatial autocorrelation (Moran's I) was used to test whether the apparent pattern of clustering was statistically significant (see Appendix A for further details of the results of this analysis). This confirmed that the subglacial lineations were clustered according to elongation ratio (critical values are above the 99 % significance level), rather than displaying a random or distributed pattern and this signifies spatial heterogeneity at a relatively large scale across the ice stream bed.

Elongation ratios were interpolated across the ice stream bed to provide a visualisation of this as a continuous surface (Figure 4.6). It is clear from this figure that an area of high elongation ratios dominates the upstream end of the ice stream, apart from the most peripheral areas. Whereas the downstream half of the ice stream has a mix of areas of both high and low elongation ratios and this appears to be randomly distributed. The figure also clearly displays the clustering of elongation ratios.

Transverse and longitudinal distributions of elongation ratio across the ice stream are shown in Figure 4.7. This analysis was conducted to assess if the subglacial lineations conform to the idealised pattern of elongation ratios (Figure 4.2), which is based on the understanding that elongation ratio correlates with ice velocity (e.g. Hart, 1999; Stokes and Clark, 2002a; King *et al*., 2007), and that velocity displays systematic variations across ice streams (Figure 4.1). Figure 4.7 demonstrates that the data has a significant amount of noise. Below average elongation ratios are present across the entire width of

the ice stream, whilst above average elongation ratios are only found in the central regions of the ice stream (Figure 4.7a). A slight asymmetry is also apparent, whereby larger subglacial lineations are preferentially situated in the centre and north side of the ice stream, which is the outside of the bend in the ice stream. As seen in figures 4.6 and 4.7b, the most elongate lineations are concentrated at the upstream end of the ice stream, whilst subglacial lineations with below average elongation ratios are present throughout its length.

The spatial distribution of the subglacial lineations is shown in Figure 4.9, which depicts how clustered these bedforms are across the ice stream. This shows that this parameter is spatially variable and that subglacial lineations are situated in clusters, the most concentrated of which are found towards the central and slightly upstream area of the ice stream. The median elongation ratio of subglacial lineations is higher within the clusters above 10 (as shown in figure 4.9) at 4.4, than the ice stream as a whole, at 3.6.

4.2.4 Topography, bedrock geology and surficial sediments

Characteristics at the bed of an ice stream, including topography, bedrock geology and surficial sediments, may affect several factors, including: the continuity of fast flow; basal hydrology; ice flow mechanism; and subglacial lineation characteristics (e.g. Alley, 1993; Anandrakrishnan *et al*., 1998; Andrews and MacLean, 2003; Stokes *et al*., 2007; Winsborrow *et al*., 2010; Phillips *et al*., 2010). In the Solway Firth Ice Stream, its southern lateral margin is coincident with the rise of the Lake District mountains whereas its northern margin does not coincide with a change in land elevation. At its upstream end there is an increase in land elevation perpendicular to ice stream flow direction, from south to north (Figure 4.8). Here, the most elongate subglacial lineations are typically located in the centre of the ice stream and on the lower, northern side of the ice stream, which reflects the pattern seen in Figure 4.7a. Figure 4.8 also shows that some of the topographic high points have relatively few subglacial lineations. The curvature map shows the range of the land surface across the area, from convex to flat to concave (Figure 4.10). These differences are most pronounced in the upland area to the south of the ice stream, where the mountain tops and ridges are depicted by a convex topography and the intervening valleys are characterised by a concave topography. The actual bed of the ice stream displays some subtle variations in

curvature in isolated areas, but does not appear to be strongly convex or concave. The areas upstream and north of the ice stream are also characterised by a flat topography.

The distribution of surficial sediments across the ice stream is shown in Figure 4.11. Evidently, till is widespread across the ice stream, which is clear from the analysis presented in Figure 4.11c as well as from the maps (Figure 4.11a and b). Whilst a range of surficial sediments are present at the ice stream bed, examination of Figure 4.11a indicates that the subglacial lineations are seldom located on a sediment other than till. Furthermore, Figure 4.11c shows that till is even more common within the most concentrated clusters of subglacial lineations than the ice stream as a whole. Areas free of any surficial sediments become increasing common towards the southern lateral margin of the ice stream and beyond. None of the till-free areas display a deflection of subglacial lineations around them, which would be a possible indicator of a till-free sticky spot (Stokes *et al*., 2007).

The mapped extent of the ice stream is situated almost entirely on sedimentary bedrock and does not encroach onto the igneous bedrock to the south (Figure 4.12). The maps (Figure 4.12a and b) do not show any apparent trends between either elongation ratio or clustering of subglacial lineations according to bedrock lithology. However, analysis presented in Figure 4.12c indicates that the areas of highly clustered subglacial lineations are most commonly underlain by mudstone. Permeability of the bedrock is displayed in Figure 4.13, which shows that the permeability of the area is characterised by several broad bands trending east-west, which range from low to high permeability. The palaeo-ice stream is located across permeabilities from very low to high, the most notable being moderate permeability, which accounts for nearly 50 % of its area (Figure 4.13c). A contrasting pattern is seen in the permeabilities located in the areas of high bedform clustering, which are located on, in order of dominance: low, high and moderate permeabilities. The area of low permeability to the north of the ice stream appears to coincide with the highest elongation ratios (figures 4.13a and 4.7). However, comparison of median elongation ratios on the different permeabilities reveals that it does not vary significantly between them at 3.70 on high permeability bedrock, 3.39 on moderate and 3.76 on low.

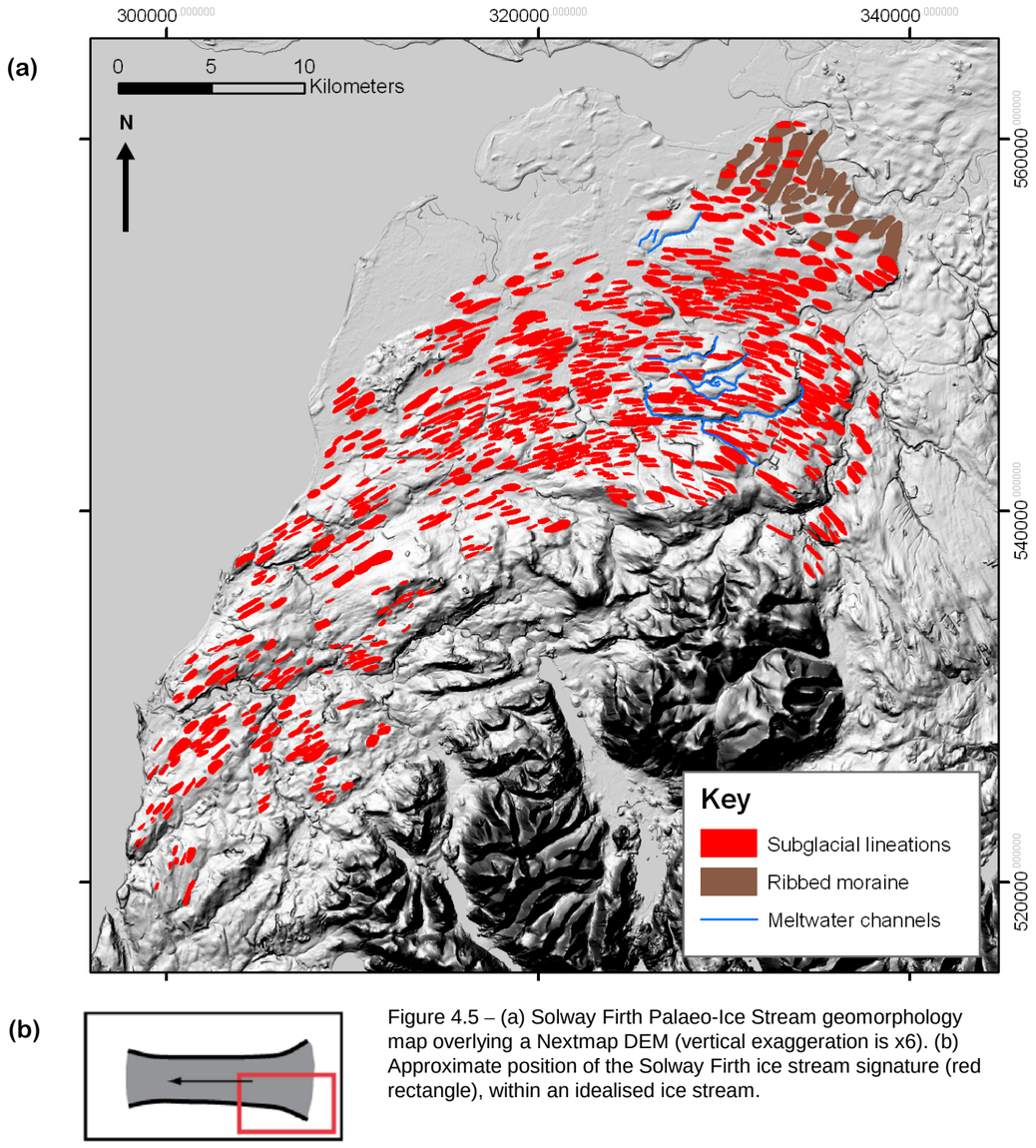

Figure 4.5 – (a) Solway Firth Palaeo-Ice Stream geomorphology map overlying a Nextmap DEM (vertical exaggeration is x6). (b) Approximate position of the Solway Firth ice stream signature (red rectangle), within an idealised ice stream.

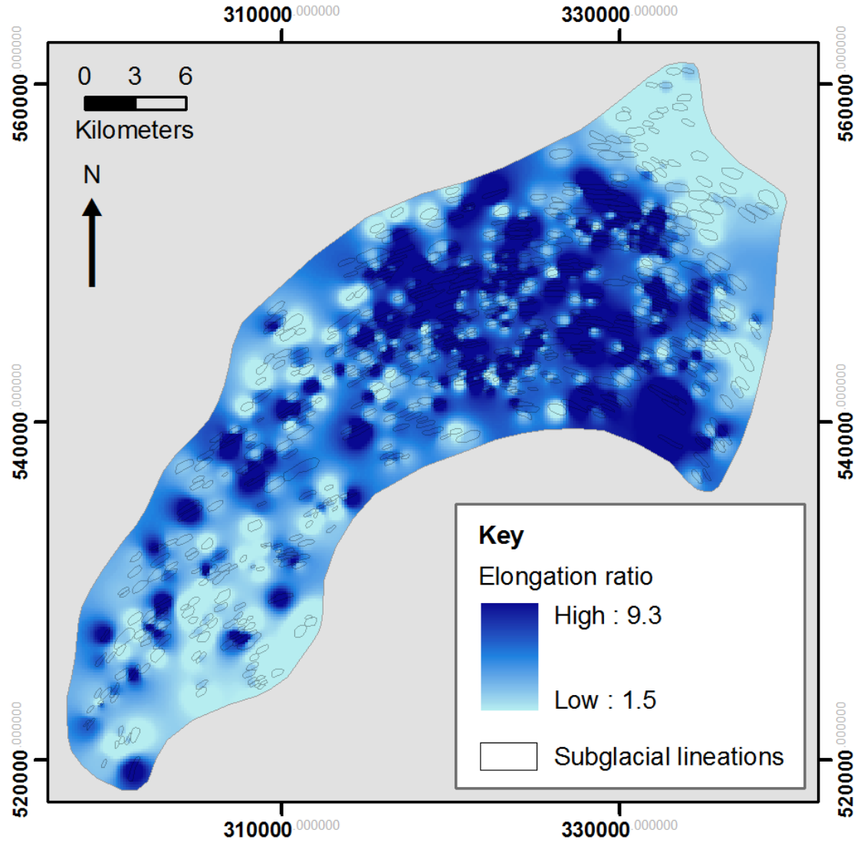

Figure 4.6 – Elongation ratio interpolated across the Solway Firth Palaeo-Ice Stream, which provides a visual impression of the spatial distribution of elongation ratios. The grey background allows the interpolated surface to be shown only to the approximate extent of the ice stream.

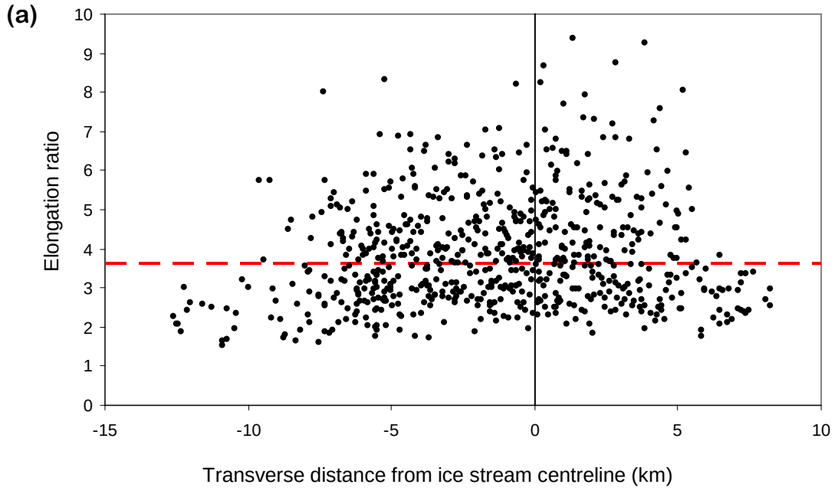

Figure 4.7 - Transverse and longitudinal trends in subglacial lineation elongation ratio. (a) Elongation ratio plotted against distance from the ice stream centreline (black vertical line). Distance from centreline is on the x axis, positive values represent north of the centreline and negative values represent south of the centreline. (b) Elongation ratio plotted against distance along the ice stream, from 0 (upstream) to 70 km (downstream). Median elongation ratio is marked with red dashed lines.

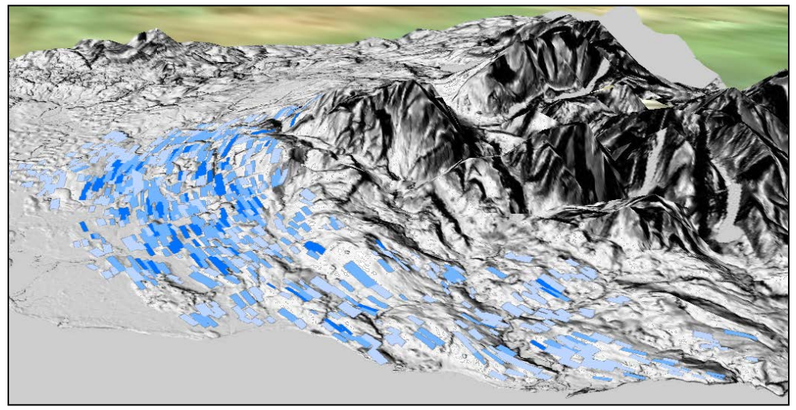

Figure 4.8 - 3D view of the Solway Firth topography, overlain by subglacial lineations that are shaded according to elongation ratio (see key in Figure 4.10). View is to the SE, looking approximately upstream along the ice stream. Nextmap image has a vertical exaggeration of x5.

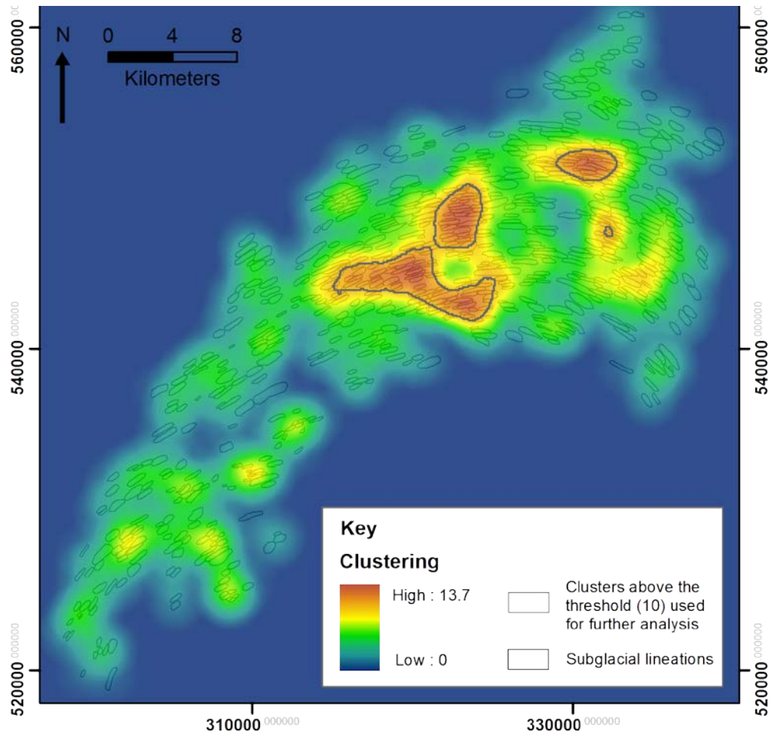

Figure 4.9 – Map depicting the clustering of subglacial lineations across the Solway Firth Palaeo-Ice Stream. Clusters that fall above the value of 10 are outlined, because these are the basis for later analysis. Median elongation ratios from the clusters above 10 is 4.4, which compares to a median value of 3.6 for the entire ice stream.

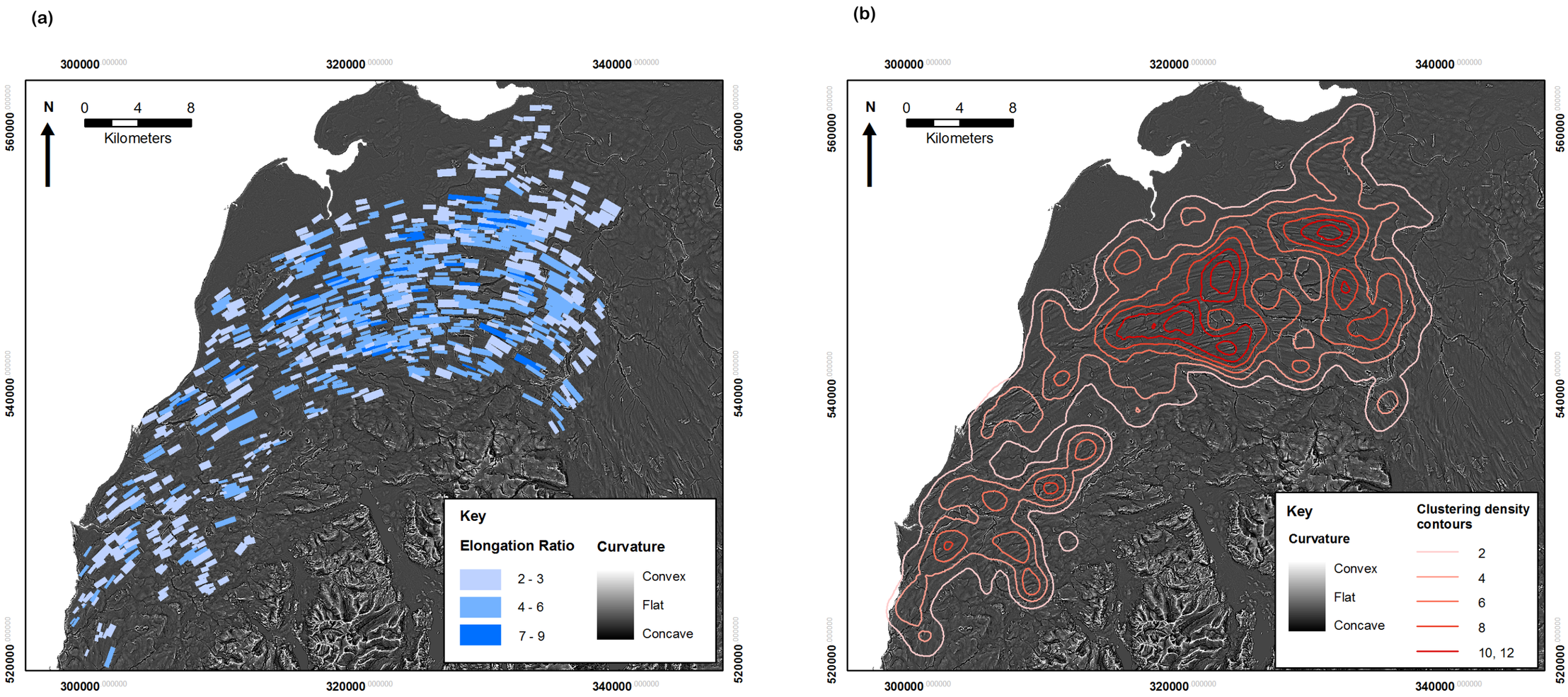

Figure 4.10 – Topography curvature across the Solway Firth Palaeo-Ice Stream. Data derived from Nextmap DEM. (a) Curvature map overlain by subglacial lineations shaded according to elongation ratio. (b) Curvature map overlain by contours of subglacial lineation clustering (derived from the data presented in Figure 4.9).

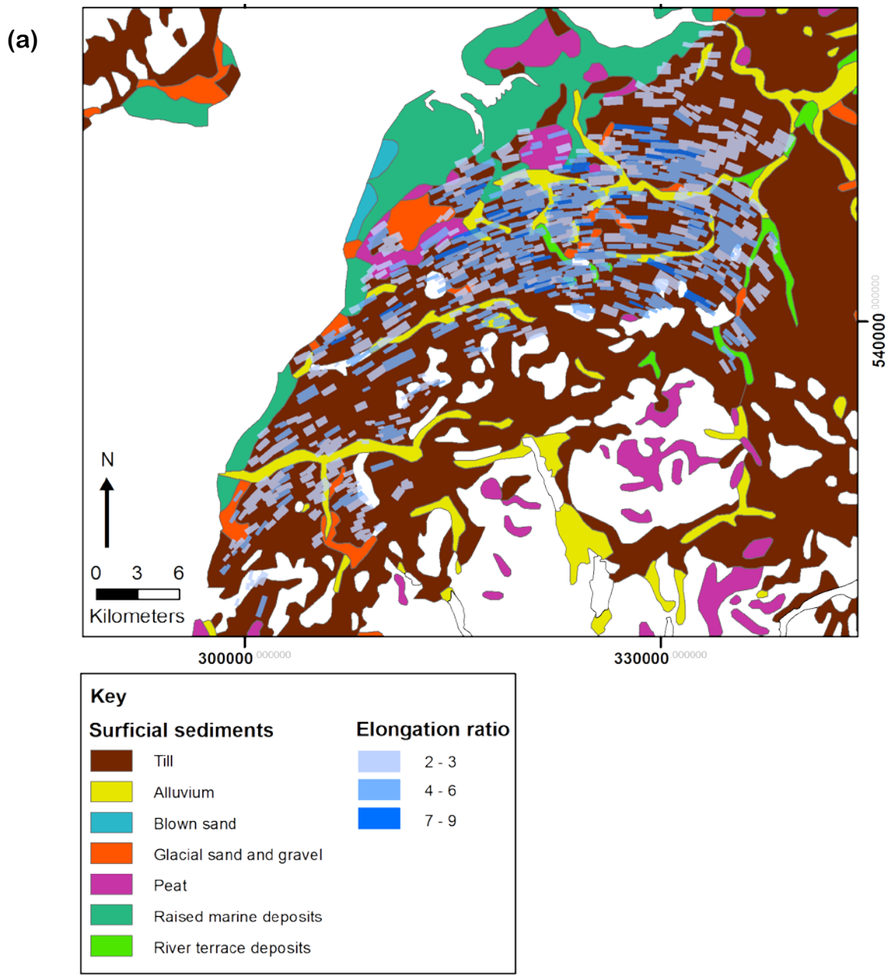

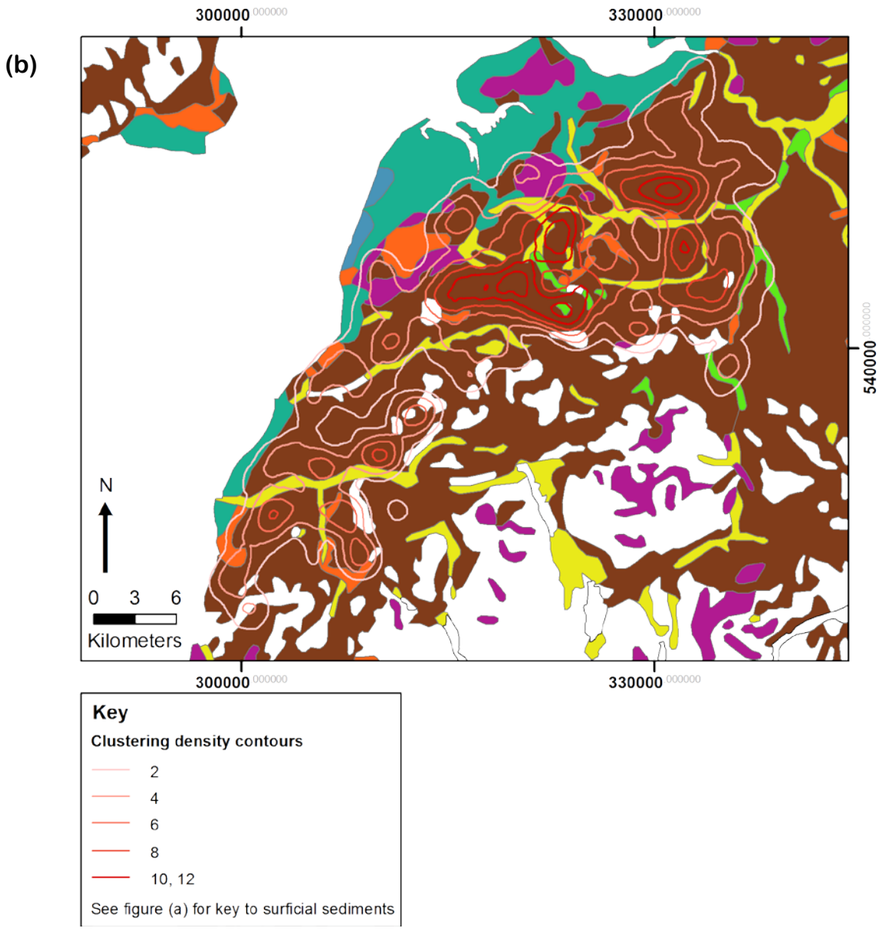

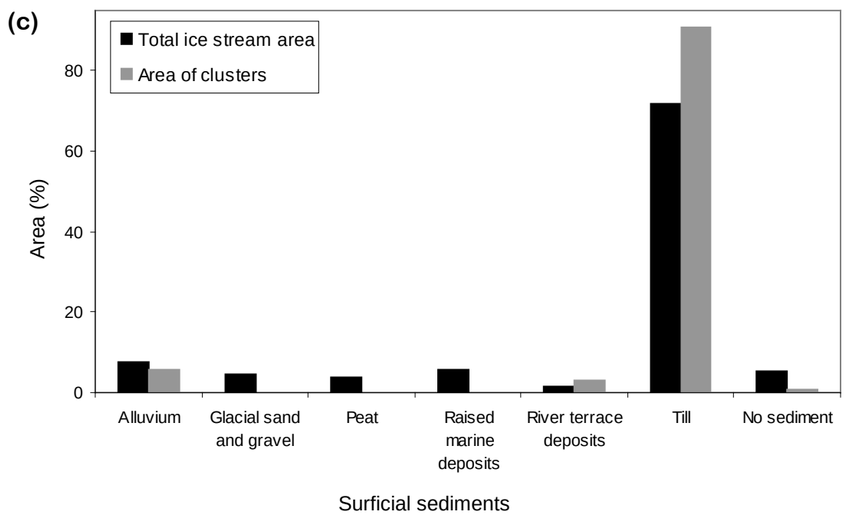

Figure 4.11 – Surficial sediments across the Solway Firth Palaeo-Ice Stream. Quaternary geology data from British Geological Survey (1977). (a) Surficial sediment map overlain by subglacial lineations shaded according to elongation ratio. (b) Surficial sediment map overlain by contours of subglacial lineation clustering (derived from the data presented in Figure 4.9). (c) Bar chart displaying the percentage coverage of surficial sediments across the whole ice stream and within the cluster areas identified in Figure 4.9.

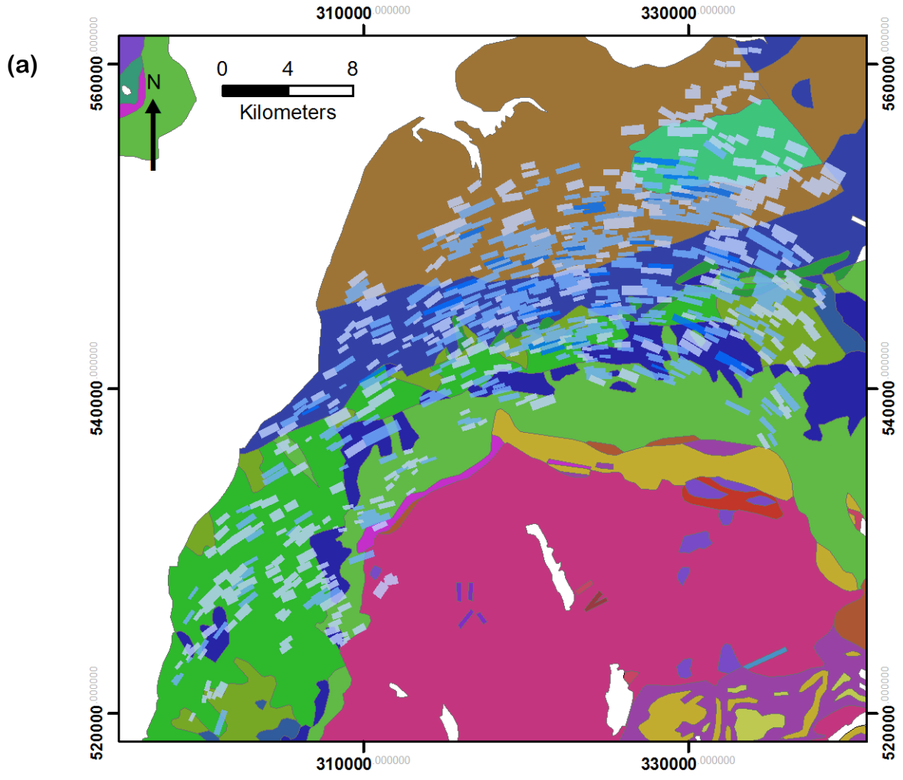

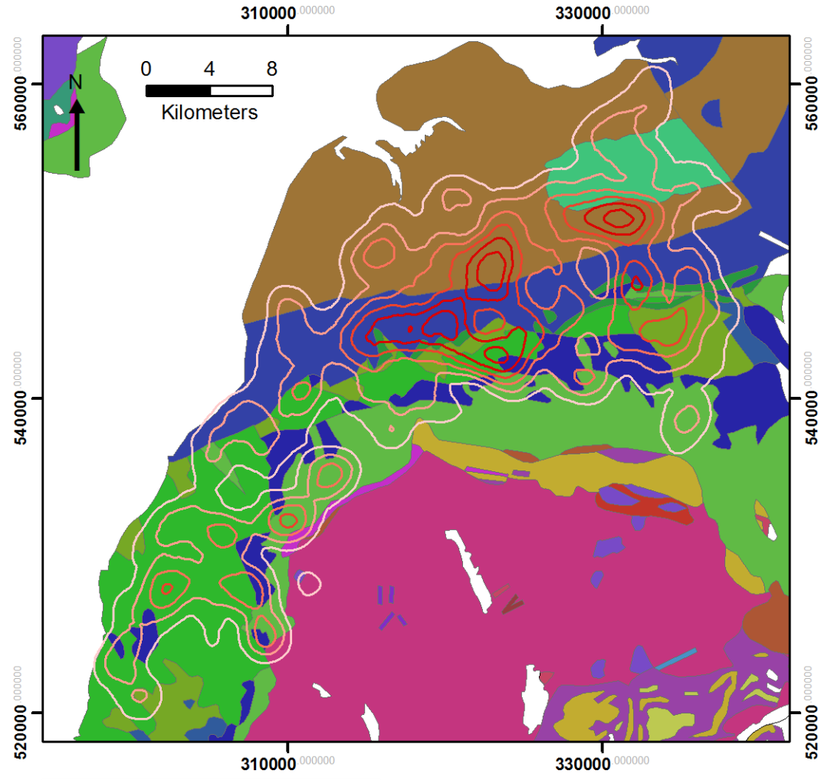

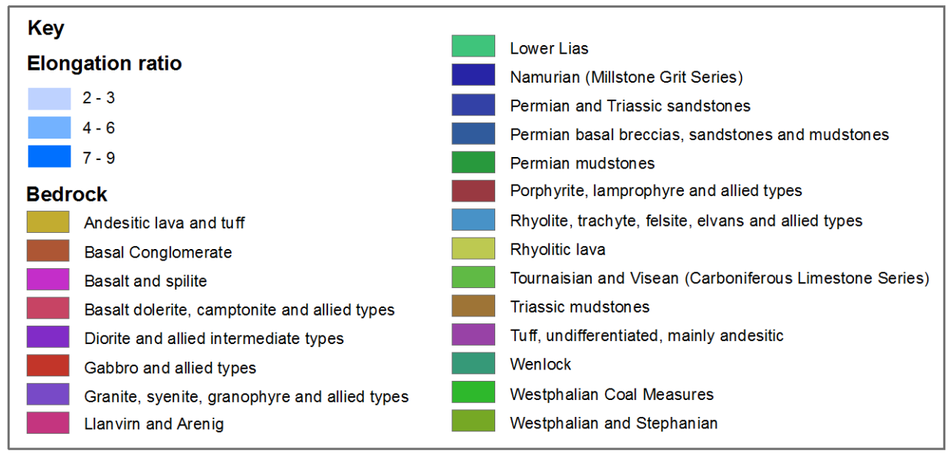

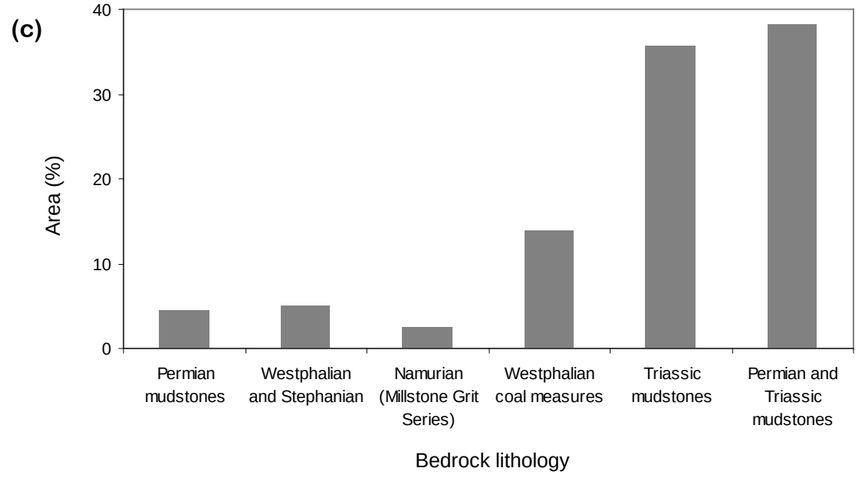

Figure 4.12 – Bedrock lithologies across the Solway Firth Palaeo-Ice Stream. Geology data from British Geological Survey (2007). (a) Bedrock map overlain by subglacial lineations shaded according to elongation ratio. (b) Bedrock map overlain by contours of subglacial lineation clustering (derived from the data presented in Figure 4.9). (c) Bar chart displaying the percentage coverage of bedrock lithologies within the cluster areas identified in Figure 4.9 (the lithologies from the entire ice stream are not shown because they are so numerous).

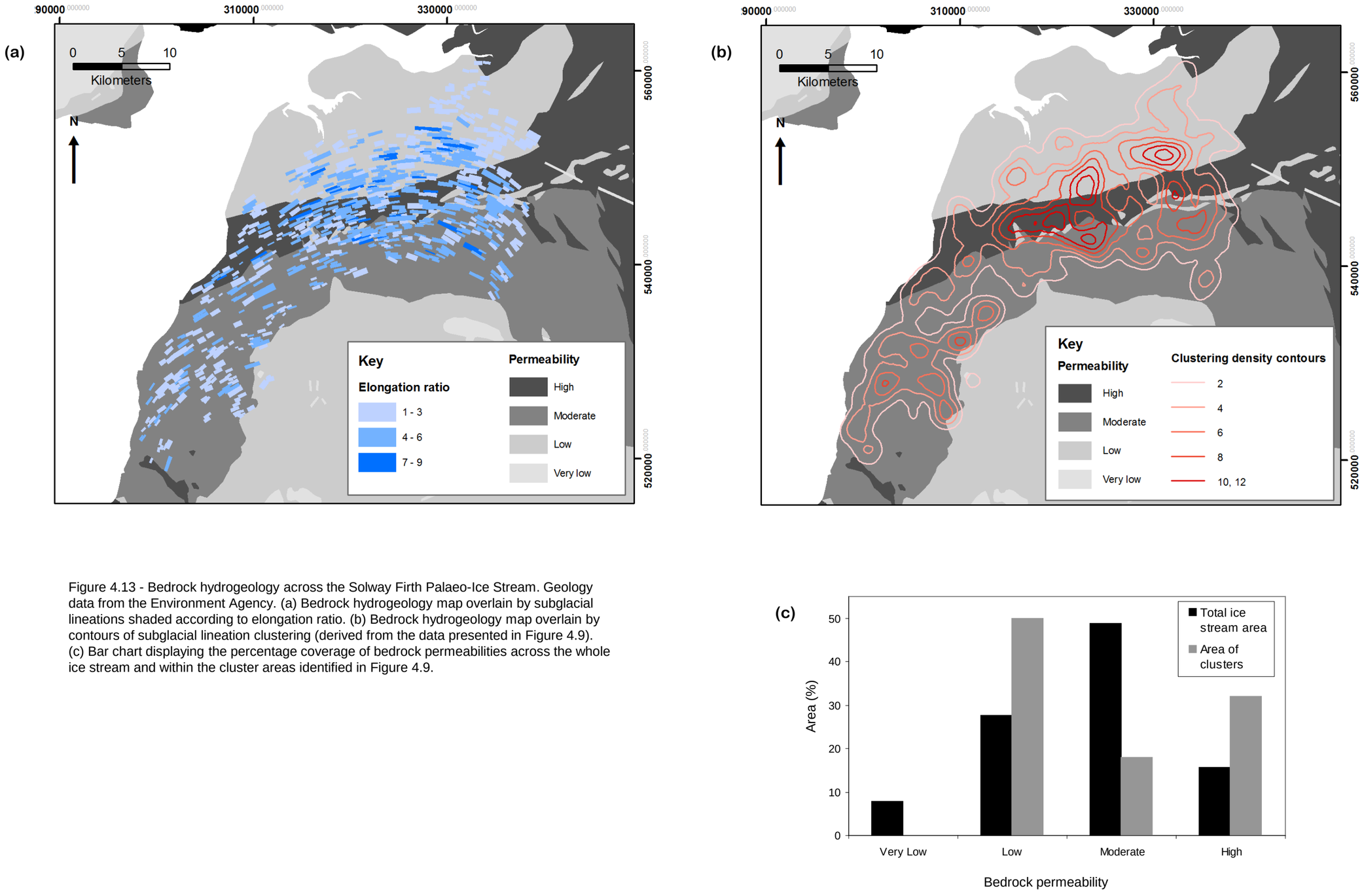

Figure 4.13 - Bedrock hydrogeology across the Solway Firth Palaeo-Ice Stream. Geology data from the Environment Agency. (a) Bedrock hydrogeology map overlain by subglacial lineations shaded according to elongation ratio. (b) Bedrock hydrogeology map overlain by contours of subglacial lineation clustering (derived from the data presented in Figure 4.9). (c) Bar chart displaying the percentage coverage of bedrock permeabilities across the whole ice stream and within the cluster areas identified in Figure 4.9.

4.3 Forth Ice Stream

4.3.1 Background

The Forth Ice Stream occupies a broad area across the Midland Valley of Scotland (Figure 4.3) and drumlins and streamlining of the landscape have long been recognised in this area (e.g. Geikie, 1865; Burke, 1969). Burke (1969) analysed the relief using contours and found a clear streamlining of the landscape from west to east (Figure 4.14).

The ice flow direction in the region during the LGM is west to east from the Clyde Valley to the Firth of Forth (Clark *et al*., 2004; Rose and Smith, 2008; Findlayson, 2010). Mapping of this region has been conducted across several separate areas (e.g. Menzies, 1996; Rose and Smith, 2008) and only recently has the entire area been mapped together (Clark *et al*., 2004; 2009) owing to the availability of the Nextmap DEM dataset. Geomorphological characteristics indicate that the area is a palaeo-ice stream, including characteristic shape and dimensions, convergent flow patterns, and attenuated bedforms (Stokes and Clark, 1999). Additionally, models of the British Ice Sheet have shown ice streaming in this location (Boulton and Hagdorn, 2006; Hubbard *et al*., 2009).

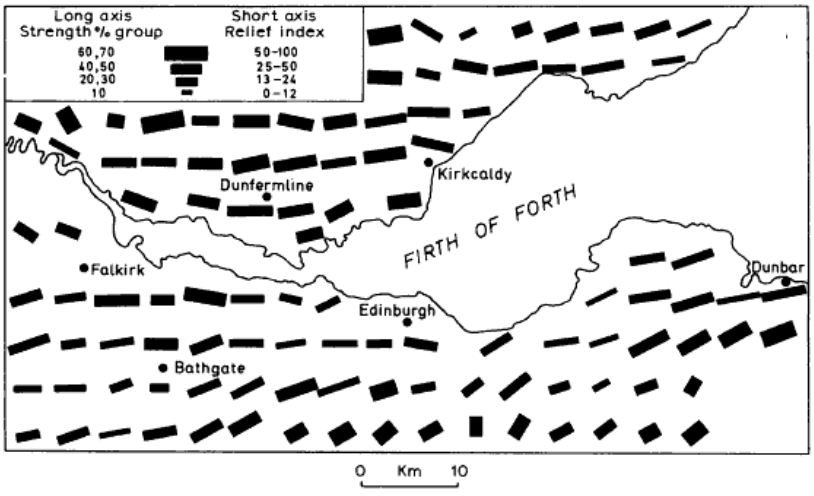

Figure 4.14 – Streamlining of relief around the Firth of Forth. From Burke (1969).

4.3.2 Geomorphological mapping

The geomorphological map in Figure 4.15, shows that the ice stream covers a wide area and has several minor tributaries. Tributaries are located in lowland areas and converge into the main trunk of the ice stream. The subglacial lineations (n = 2445) display a considerable range of sizes, from 0.1 to 5 km in length and from 0.007 to 2.8 km^2 in area. Elongation ratios range from 1.2 to 10.8. Meltwater channels are abundant in this ice stream. They are often located at the sides, tops and lee sides of hills and are frequently orientated parallel or sub-parallel to the ice stream. Meltwater channels range in length from 45 to 6610 m. An extensive network of meltwater channels is present near the southern lateral margin, at the downstream end of the ice stream (Figure 4.15). These are located on the inside of a slight bend in the ice stream. Mapped meltwater channels include subglacial and lateral marginal meltwater channels. A small number of eskers are present at the edges of the ice stream and of upland areas.

4.3.3 Subglacial lineation analysis

The spatial distribution of subglacial lineation elongation ratio is presented in figures 4.16, 4.18 and 4.19. Elongation ratio is low across much of the ice stream, especially in its marginal areas, whilst some clusters of high elongation ratios can be identified towards the centre and downstream end of the ice stream. Interpolation of this variable shows some distinct regions of contrasting elongation ratios and demonstrates that it may change significantly over short distances. Spatial autocorrelation analysis confirms that the subglacial lineations are clustered according to elongation ratio, to a 99 % level of confidence (see Appendix A).

The transverse and longitudinal variations in elongation ratio are presented in Figure 4.18. As is clear from this figure the transverse distribution of subglacial lineations is uneven across the Forth Palaeo-Ice Stream because large central areas of the ice stream bed are under the sea in the Firth of Forth, and the ice stream has some tributary regions. The most elongate subglacial lineations are focussed in the centre of the ice stream, as can be seen in Figure 4.18, although above average elongation ratios are present across the entire width of the ice stream. A slight transverse asymmetry can be seen, whereby a concentration of elongate subglacial lineations is present on the south

side of the ice stream (Figure 4.18). Longitudinally there is a downstream increase in the upper limit of elongation ratios (Figure 4.18b), whilst there are subglacial lineations with above average elongation ratios along the entire length of the ice stream.

The degree and distribution of subglacial lineation clustering is shown in Figure 4.17. Subglacial lineations appear to be present in clusters across the entire ice stream bed and areas of the highest clustering are found in peripheral regions of the ice stream as well as in the centre. Comparing the cluster map (Figure 4.17) and the elongation ratio interpolation map (Figure 4.16) indicates the highest clusters may relate to high elongation ratios, but that areas of high elongation ratios do not always relate to areas of high subglacial lineation clustering.

4.3.4 Topography, bedrock geology and surficial sediments

The ice stream bed topography and its relation to subglacial lineation elongation ratio can be seen in Figure 4.19. The palaeo-ice stream is broadly situated in a large valley, which is punctuated by several upland areas including the Campsie Fells and Lennox Hills, the Pentland Hills and the Lomond Hills (referred to in Figure 4.15). Subglacial lineations are concentrated, and most elongate in the lowland areas of the valley, with relatively few situated on upland areas, suggesting that ice velocities were reduced in these locations. Subglacial lineations also appear to deflect around topographic highs. This is similar to the findings of Hodgson (1994), who documented the deflection of subglacial lineations around a topographic high (c. 640 km^2) in the M'Clintock Channel Palaeo-Ice Stream. This pattern is also seen in the surface features of contemporary ice streams where ice is deflected around topographic obstacles at the bed (e.g. Bindschadler and Scambos, 1991).

The curvature of the Forth Ice Sream bed broadly correlates with the relief, whereby the aforementioned upland areas are typically characterised by a convex topography, alongside corresponding areas of concavity and with minimal flat topography. The more lowland areas of the bed are characterised by a broadly flat topography, with minimal convex or concave areas, and it is on this landscape where the subglacial lineations are typically located.

A range of surficial sediments other than till is present at the ice stream bed, albeit examination of the maps in Figure 4.20 indicate that the majority of subglacial lineations are located on till, but not exclusively. The areas of highly clustered lineations are dominated by till, to a greater proportion than that of the entire ice stream (Figure 4.20c). However, a considerable proportion of the ice stream bed (19 %) does not have any surficial sediments and these areas are most commonly located towards the peripheries of the ice stream and on the upland areas. The largest till-free areas correlate with topographic highs and regions of igneous bedrock. Subglacial lineations situated on areas lacking diamicton or other Quaternary deposits constitute 15 % of the total number of subglacial lineations and they have a median elongation ratio of 3.04. This, interestingly, is higher than those situated on till (85 % of the total population of subglacial lineations), which have a median elongation ratio of 2.93.

The Forth Palaeo-Ice Stream overlies many different bedrock lithologies (Figure 4.21), including both sedimentary (73 % of the total ice stream area) and igneous (27 % of the total ice stream area). Given this wide range of lithologies no correlation is apparent between lithology and subglacial lineations (Figure 4.21a and b). A range of different lithologies, mostly sedimentary but also igneous, underlie the areas with the most highly clustered subglacial lineations (Figure 4.21c).

Compared to lithology, bedrock permeability displays a simpler pattern across the ice stream bed (Figure 4.22). A wide range of permeabilities is present, from very low to very high. The most widespread of these is moderate, which is present across most of the central areas of the ice stream bed. This overall trend contrasts with the permeabilities that underlie the areas of the most highly clustered lineations, which are dominated by high permeabilities and to a lesser extent low, moderate and very low permeabilities (Figure 4.22c). Examination of the map in Figure 4.22b shows that most of these clusters are located outside of the central area of the ice stream, thus explaining the substantial difference between the distribution of permeabilities across the ice stream and that fall within the clusters (Figure 4.22c). Median elongation ratio does not appear to vary significantly on different permeabilities and is 3.05 on very high permeability bedrock, 2.83 on high, 2.91 on moderate, 3.05 on low and 3.00 on very low.

(a)

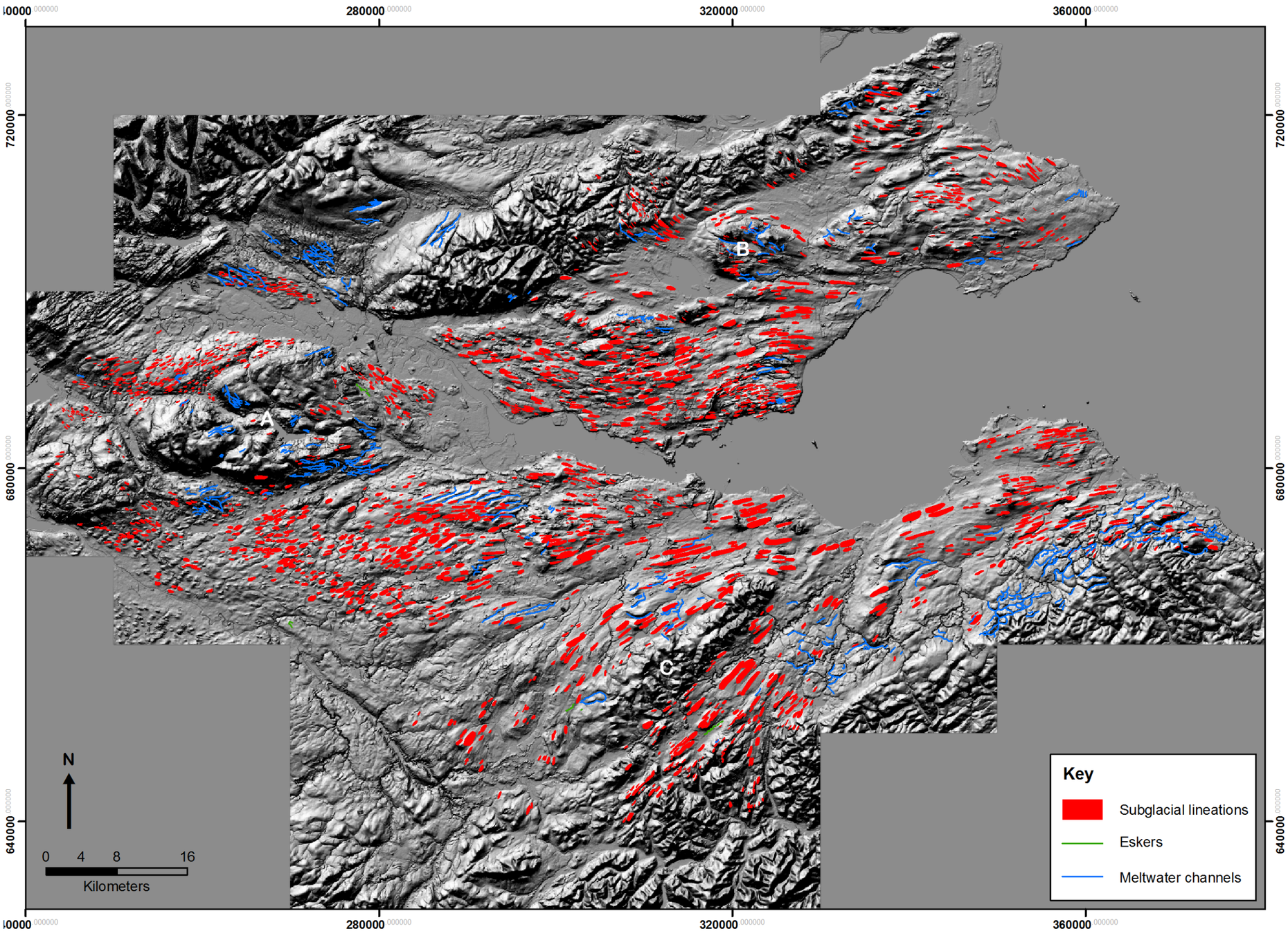

(b)

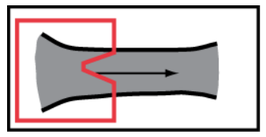

Figure 4.15 - Forth Palaeo-Ice Stream geomorphology map overlying a Nextmap DEM (vertical exaggeration is x6). Upland areas within the ice stream are labelled: A indicates the Campsie Fells and Lennox Hills; B indicates the Lomond Hills; and C indicates the Pentland Hills. (b) Approximate position of the Forth ice stream signature (red rectangle), within an idealised ice stream.

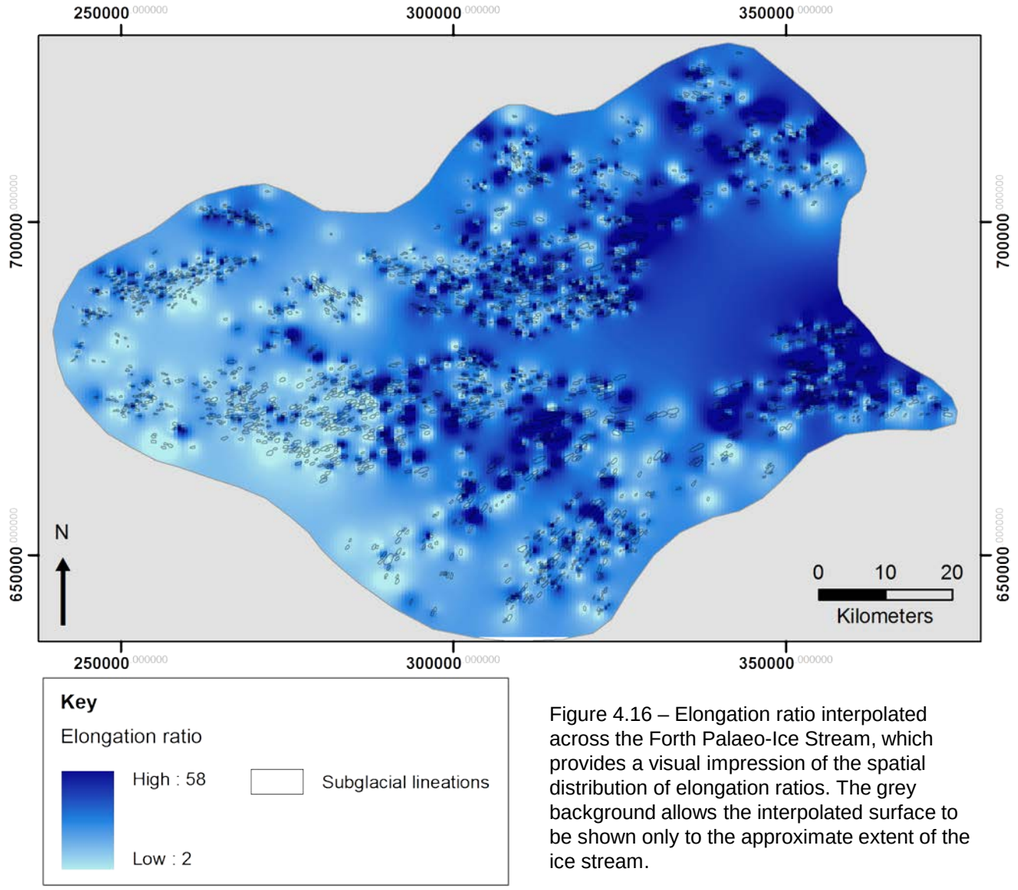

Figure 4.16 – Elongation ratio interpolated across the Forth Palaeo-Ice Stream, which provides a visual impression of the spatial distribution of elongation ratios. The grey background allows the interpolated surface to be shown only to the approximate extent of the ice stream.

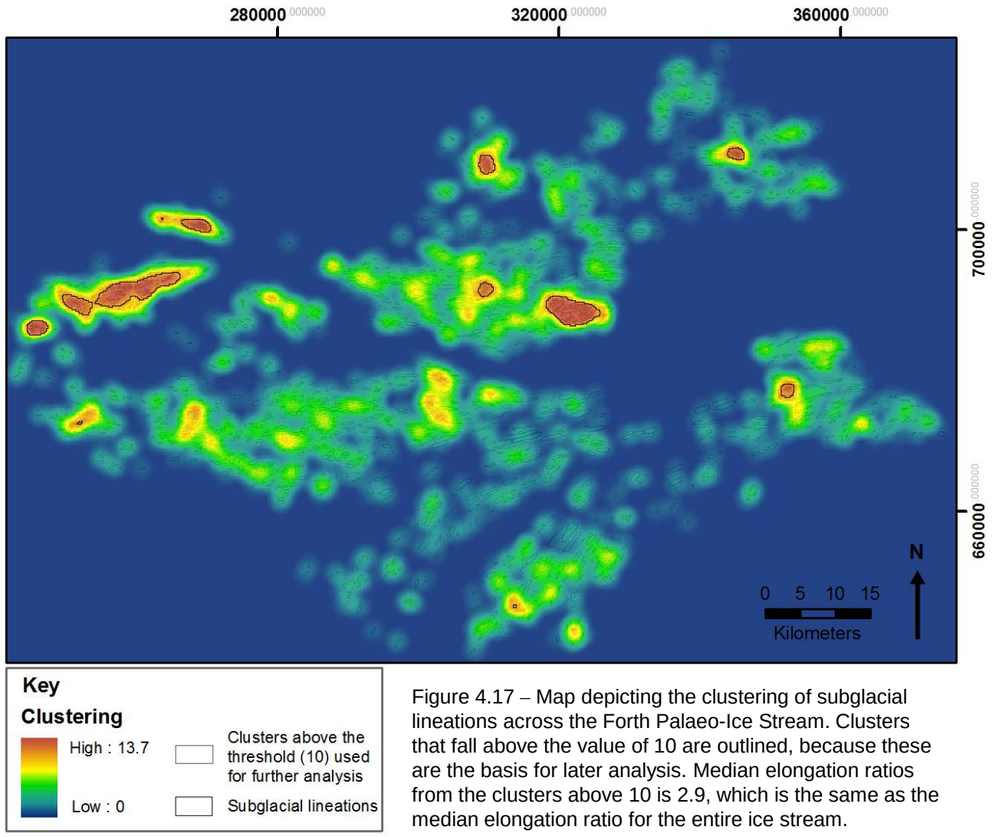

Figure 4.17 – Map depicting the clustering of subglacial lineations across the Forth Palaeo-Ice Stream. Clusters that fall above the value of 10 are outlined, because these are the basis for later analysis. Median elongation ratios from the clusters above 10 is 2.9, which is the same as the median elongation ratio for the entire ice stream.

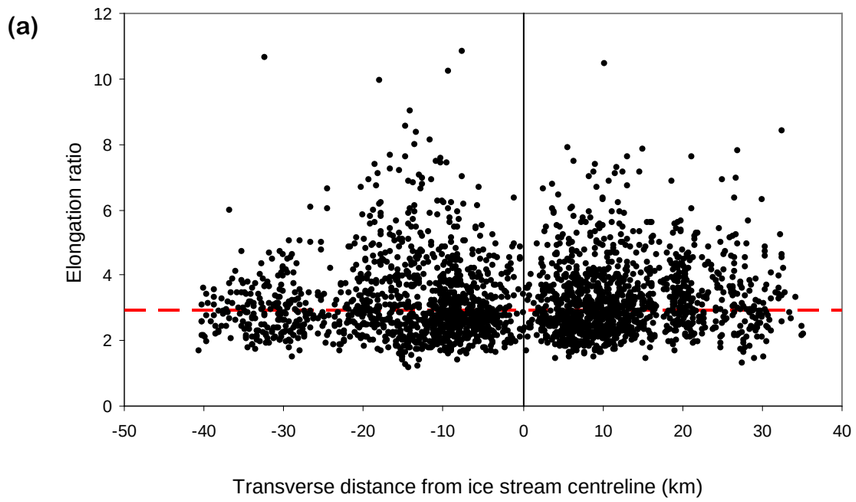

Figure 4.18 – Transverse and longitudinal trends in subglacial lineation elongation ratio. (a) Elongation ratio plotted against distance from the ice stream centreline (black vertical line). Distance from the centreline is on the x axis, positive values represent north of the centreline and negative values represent south of the centreline. (b) Elongation ratio plotted against distance along the ice stream, from 0 (upstream) to 130 km (downstream). Median elongation ratio is marked with red dashed lines.

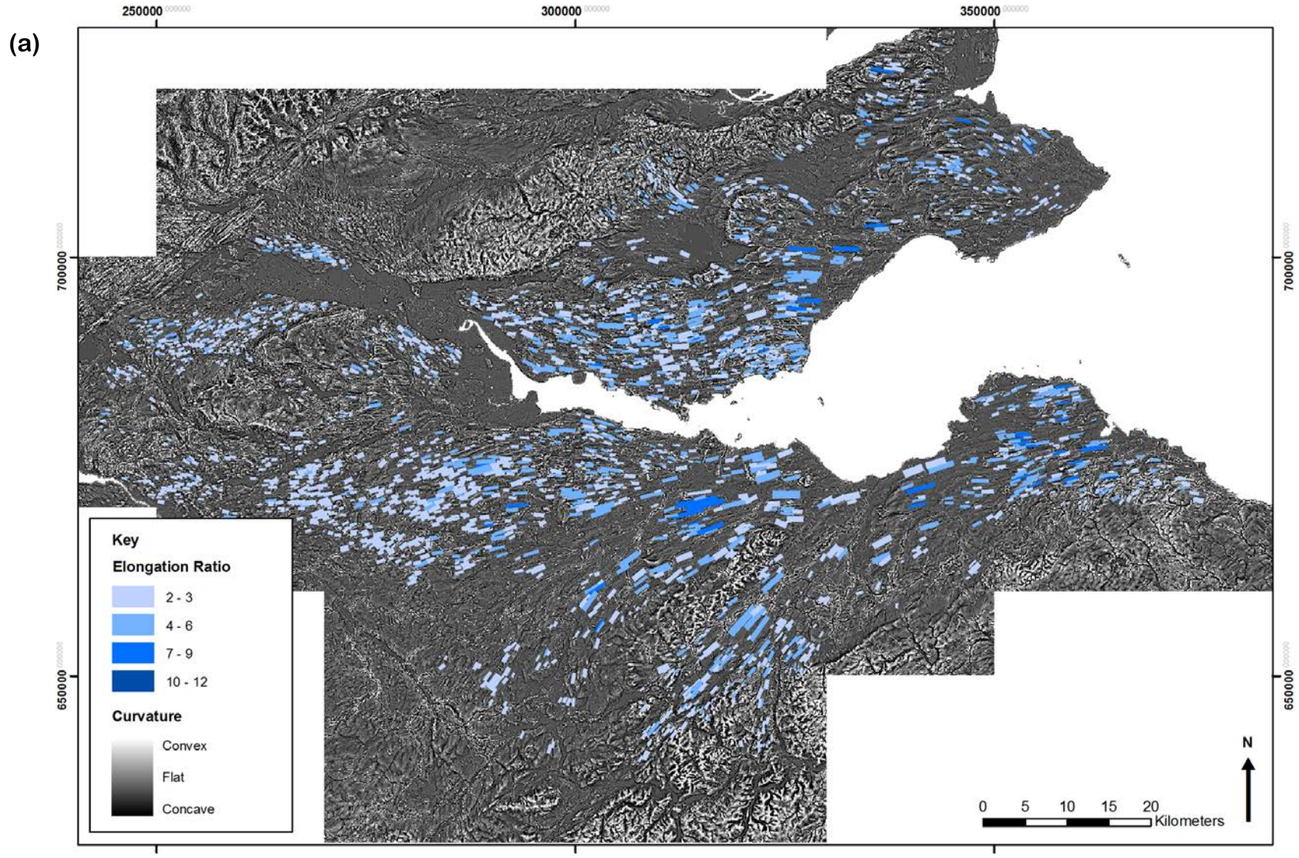

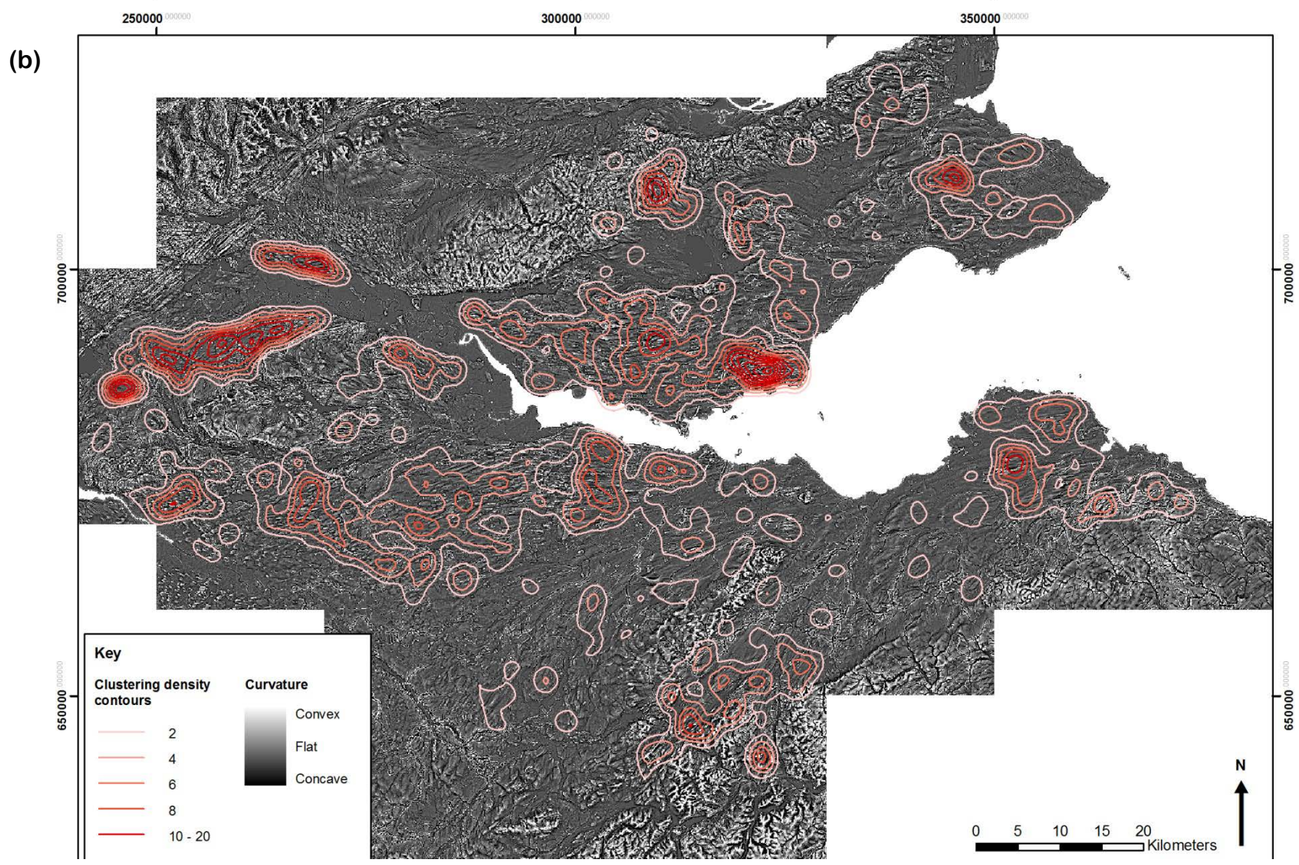

Figure 4.19 –Topography curvature across the Forth Palaeo-Ice Stream. Data derived from a Nextmap DEM. (a) Curvature map overlain by subglacial lineations shaded according to elongation ratio. (b) Curvature map overlain by contours of subglacial lineation clustering (derived from the data presented in Figure 4.17).

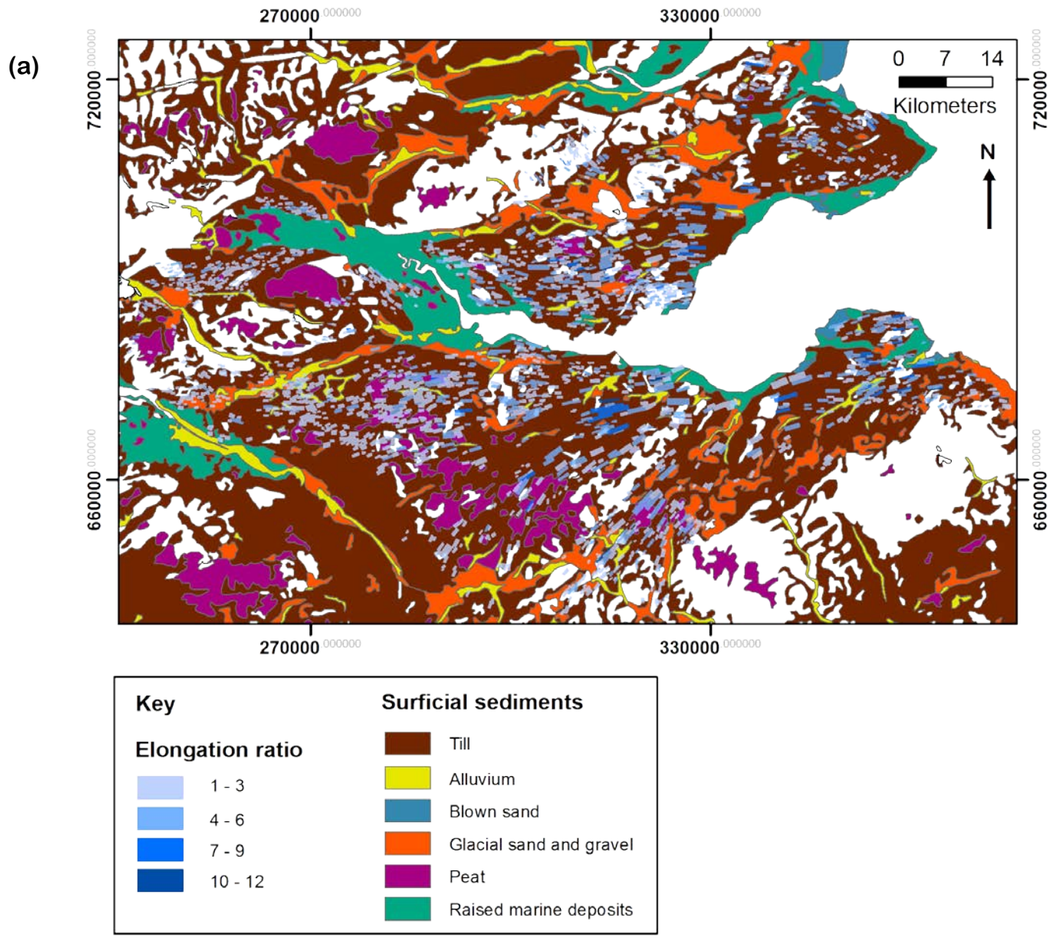

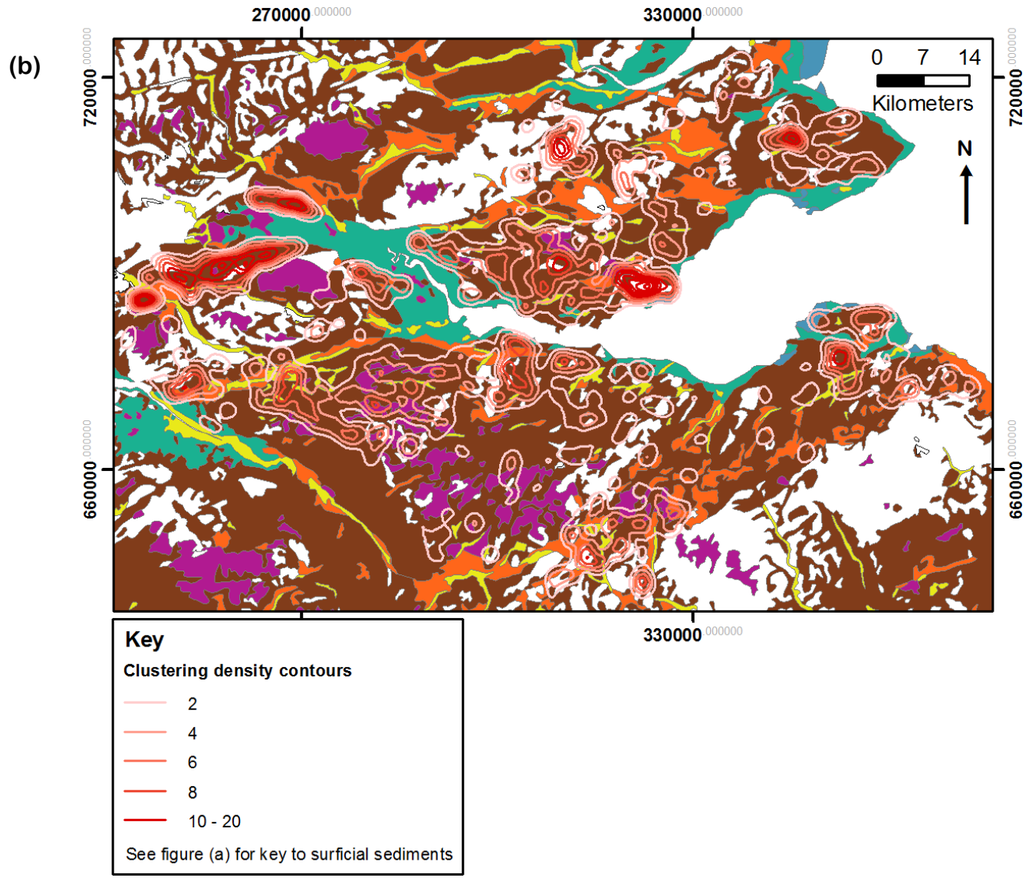

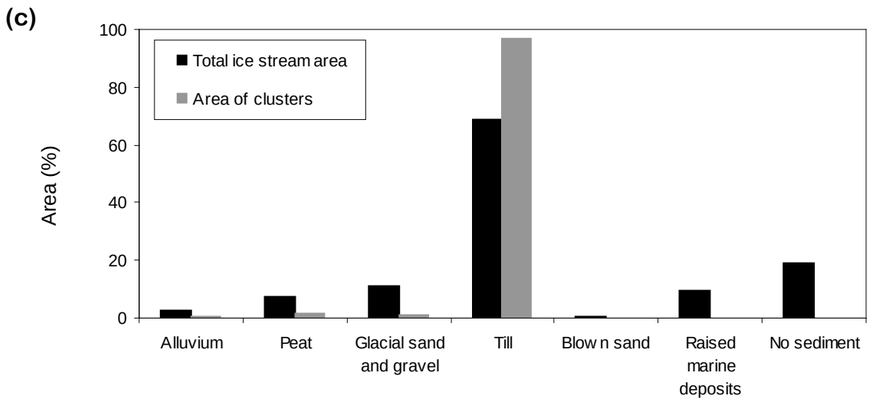

Figure 4.20 – Surficial sediments across the Forth Palaeo-Ice Stream. Quaternary geology data from British Geological Survey (1977). (a) Surficial sediment map overlain by subglacial lineations shaded according to elongation ratio. (b) Surficial sediment map overlain by contours of subglacial lineation clustering (derived from the data presented in Figure 4.17). (c) Bar chart displaying the percentage coverage of surficial sediments across the whole ice stream and across the cluster areas identified in Figure 4.17.

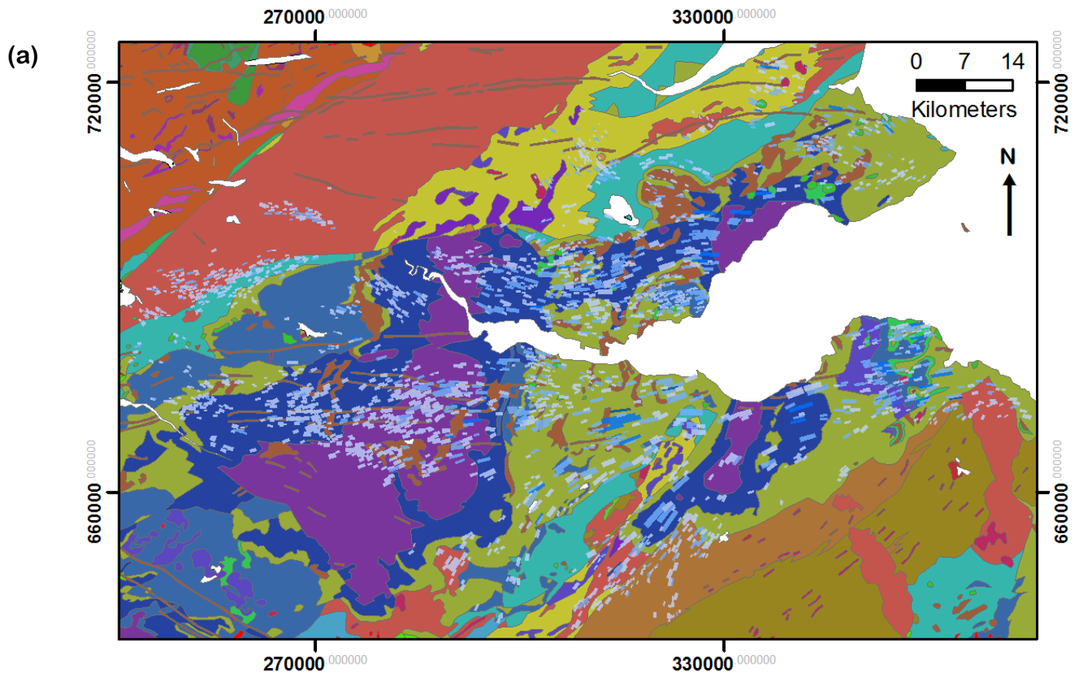

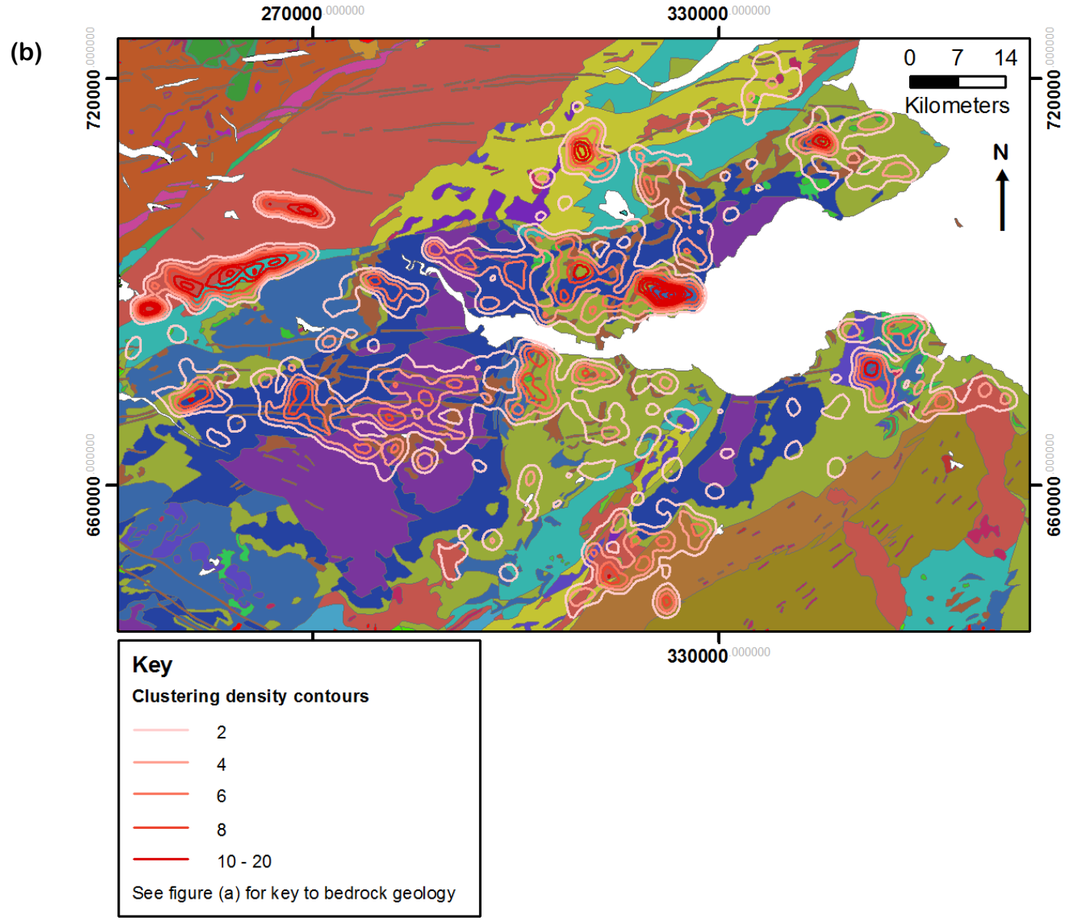

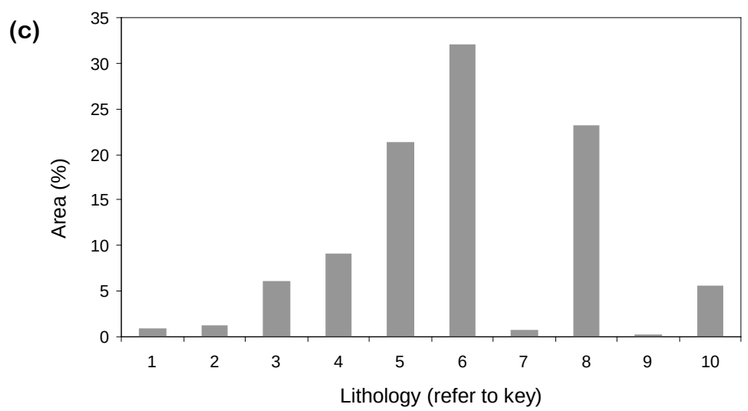

Key	
1	Rhyolite, trachyte, felsite, elvans and allied types
2	Agglomerate in neck
3	Basalt dolerite, camptonite and allied types
4	Tournasian and Visian (Carboniferous Limestone Series)
5	Basalt and spilite
6	Lower Old Red Sandstone, including Downtonian
7	Ryolite, trachyte and allied types
8	Upper Old Red Sandstone
9	Namurian (Millstone Grit Series)
10	Andesitic and basaltic lavas and tuffs

Figure 4.21 – Bedrock lithologies across the Forth Palaeo-Ice Stream. Geology data from British Geological Survey (2007). (a) Bedrock map overlain by subglacial lineations shaded according to elongation ratio. (b) Bedrock map overlain by contours of subglacial lineation clustering (derived from the data presented in Figure 4.17). (c) Bar chart displaying the percentage coverage of bedrock lithologies within the cluster areas identified in Figure 4.17 (the lithologies from the entire ice stream are not shown because they are so numerous).

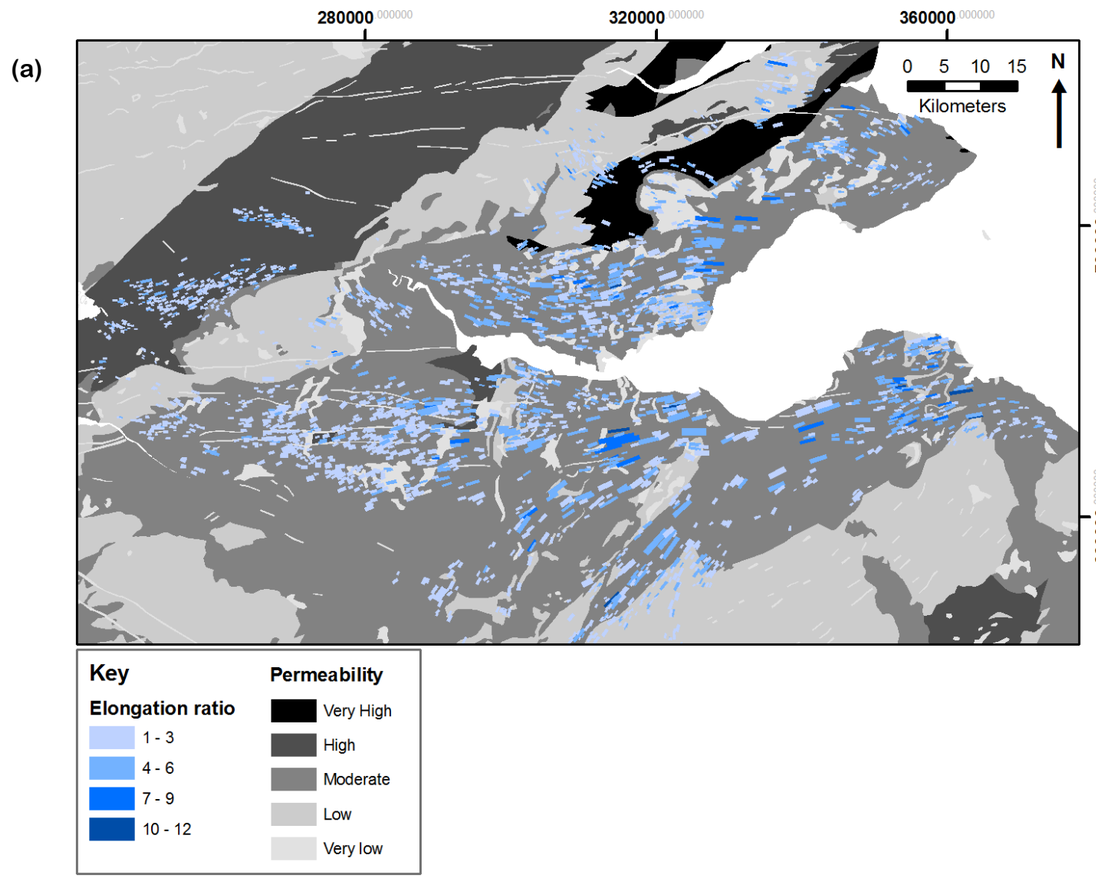

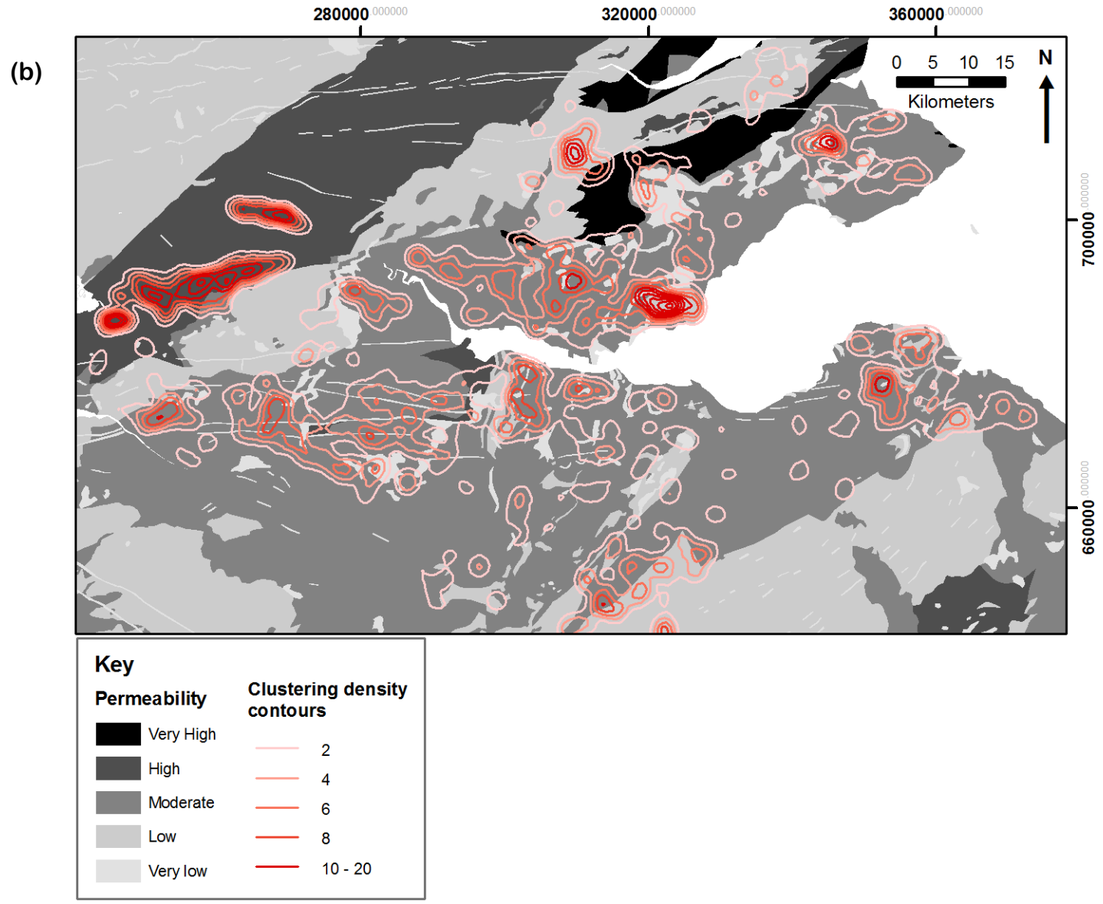

Figure 4.22 - Bedrock hydrogeology across the Forth Palaeo-Ice Stream. Geology data from MacDonald *et al.* (2004). (a) Bedrock hydrogeology map overlain by subglacial lineations shaded according to elongation ratio. (b) Bedrock hydrogeology map overlain by contours of subglacial lineation clustering (derived from the data presented in Figure 4.17). (c) Bar chart displaying the percentage coverage of bedrock permeabilities across the whole ice stream and within the cluster areas identified in Figure 4.17.

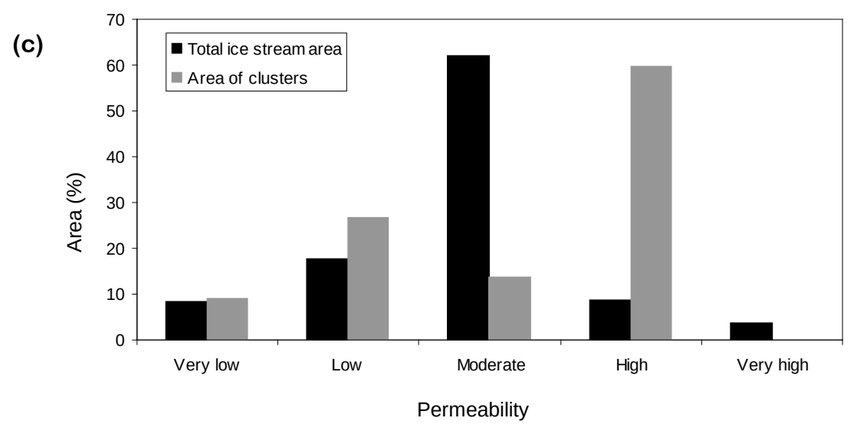

4.4 Crooked Lake Ice Stream

4.4.1 Background

Crooked Lake Ice Stream flowed south to north, with a curvature along its length (of approximately 40º), across Prince of Wales Island, Nunavut, Canada (Figure 4.3). Dyke and Morris (1988) and Dyke *et al*. (1992) have described the geomorphology of this ice stream, which is characterised by a set of asymmetric drumlins with distinct tails, 10 to 30 m high. These are superimposed on top of bedforms from the larger M'Clintock Channel Ice Stream (Clark and Stokes, 2001). However, De Angelis and Kleman (2008) consider the Crooked Lake landform set to represent a generation of the M'Clintock Channel Ice Stream. Nonetheless it represents an isochronous landform set, and De Angelis and Kleman (2005) describe it as a clear example of a pure ice stream. Geomorphological characteristics of a palaeo-ice stream include, characteristic shape and dimensions, highly attenuated bedforms, abrupt lateral margins, and lateral shear moraines (see Stokes and Clark, 1999). De Angelis and Kleman (2005) and De Angelis (2007b) present generalised mapping of this entire region of the Canadian Arctic. This provides a useful starting point for this study and enables landform interpretations to be cross checked. Remapping was necessary in order to analyse elongation ratios and determine the spatial arrangements of bedform patterns.

4.4.2 Geomorphological mapping

Subglacial lineations are absent across some areas of the Crooked Lake Palaeo-Ice Stream and are tightly packed in some areas (Figure 4.23). The 1565 subglacial lineations mapped on this ice stream are typically larger and have a wider range of areas than the other ice streams studied in this chapter. They range from 0.2 to 6.76 km in length (median 1.3 km) and from 0.01 to 7.31 km^2 in area (median 0.38 km^2). Elongation ratio ranges from 1.01 to 16.6, with a median of 3.1. The largest subglacial lineations are concentrated on the west side of the ice stream, on the inside of the bend. The subglacial lineations are modified on the east side of the ice stream, where they are overprinted by the Transition Bay Ice Stream.

At the downstream end of the ice stream, ribbed moraine are present, which extend across a wide area (c. 3160 km^2) as marked in Figure 4.23. Much of the ribbed moraine

are quite irregular and difficult to delineate, so consequently it was not mapped in detail. Dunlop and Clark (2006) document a wide range of characteristics of ribbed moraine, derived from a large sample of over 30,000 landforms. Based on this classification, the ribbed moraine at Crooked Lake has similarities to poorly developed, lumpy, anastomosing and hummocky ribbed moraine.

A discontinuous lateral shear moraine is present on the west lateral margin, downstream from the bend in the ice stream. The network of ridges is 37.5 km long and the individual ridges are up to 12 km long and 1 km wide, with a similar form to those observed in previous studies (e.g. Stokes and Clark, 2002b; Ottesen *et al.*, 2005). The shear moraines display some variations in width and at the northern end there are two or more adjacent moraine ridges. Few meltwater channels were identified, which may be related to the image resolution (30 m on ETM+ as compared to 5 m on Nextmap DEM) or because of the relatively low relief across the ice stream (which often provides the criteria to distinguish meltwater channels from modern channels).

4.4.3 Subglacial lineation analysis

Low elongation ratios (1 to 3) are found across most of the Crooked Lake Palaeo-Ice Stream subglacial lineations (figures 4.25 to 4.27). The highest elongation ratios are generally located on the east lateral margin, on the outside of the bend in the ice stream (Figure 4.26) and this is also seen very clearly in the interpolation (Figure 4.25). Interestingly this contrasts with the trend in subglacial lineation size, whereby the largest subglacial lineations are found on the west margin, on the inside of the bend. As seen in previous ice streams, a degree of clustering can be seen in the elongation ratio, which is confirmed by spatial autocorrelation analysis (see Appendix A).

The asymmetry in subglacial lineation elongation ratio observed in Figure 4.25 is reflected in Figure 4.26a, that whilst fewer subglacial lineations fall on the east side of the ice stream, they have higher elongation ratios than those on the west side. As observed for the Solway and Forth ice streams, there is a slight decrease in elongation ratios at the lateral margins. Longitudinally, there is an uneven distribution of subglacial lineations, as depicted by Figure 4.26b, which is related to the overprinting of the

Transition Bay Ice Stream at its southern end. A slight downstream increase in elongation ratios can be seen in Figure 4.26b.

Clustering of subglacial lineations is shown in Figure 4.24, which gives a visual impression that the bedforms fall into small clusters across the entire ice stream. The highest clustering is seen in several discrete areas towards the downstream end of the ice stream. The upper limit of clustering is fairly low (11.7) and the areas of clustering above 10 are relatively small compared to some of the other ice streams examined. It is notable that the Crooked Lake Palaeo-Ice Stream contains some of the largest subglacial lineations, which means that their centroids (from which the cluster map is generated) will be spaced further apart than smaller subglacial lineations.

4.4.4 Topography and bedrock geology

The topographic context of the ice stream can be seen in Figure 4.27. Prince of Wales Island has low relief and the highest ground is situated in the NE of the island, upon which some subglacial lineations encroach. Figure 4.27a shows that the ice stream appears to be deflected away from the higher, rougher terrain to the east (land elevation ranges from 90 to 170 m above sea level (asl)) and into the flatter west side (land elevation ranges from 50 to 90 m asl) of the island. Subglacial lineations are concentrated on the lowland, west side of the ice stream and very few are located on the higher land on the east side. The lineations on this upland area have below average elongation ratios, despite being on the outside of the bend, which overall has higher elongation ratios. The topographic curvature of the ice stream bed does not display any clear trends, and indicates that the entire area is largely flat, with only some small variations to convexity or concavity. However, it should be noted that the Canadian DEM's are at a relatively low resolution (at 11 to 23 m horizontal resolution and 1 m vertical resolution), compared to the UK DEM's (at 5 m horizontal resolution and 1 m vertical resolution), which may affect the result of processing this data into a curvature map.

The ice stream is underlain entirely by sedimentary bedrock, with a range of lithologies present. Figure 4.28 illustrates the overall spatial variations in terms of bedrock lithology and age. The majority of the ice stream and the areas of high bedform

clustering were located on limestone, dolostone, shale, evaporites, chalk and carbonate reefs from the Silurian and Devonian periods. To the west of this area lies an area with the same lithologies but differentiated by a variation in age. This age difference may correspond to a distinction in permeability and effective porosity due to the greater overburden on the older formation to the west. Interestingly the upper part of the west lateral margin coincides with the boundary between these two domains, a section of the margin that is notable for the presence of an ice stream shear margin moraine.

Due to the remote localities of the Canadian arctic ice streams examined there exists only a rudimentary knowledge and very generalised maps of their bedrock and surficial sediments. As such the degree of analysis that was conducted for the UK ice streams was not possible for these Canadian ice streams, specifically neither surficial sediments nor bedrock permeability were examined due to a lack of this data.

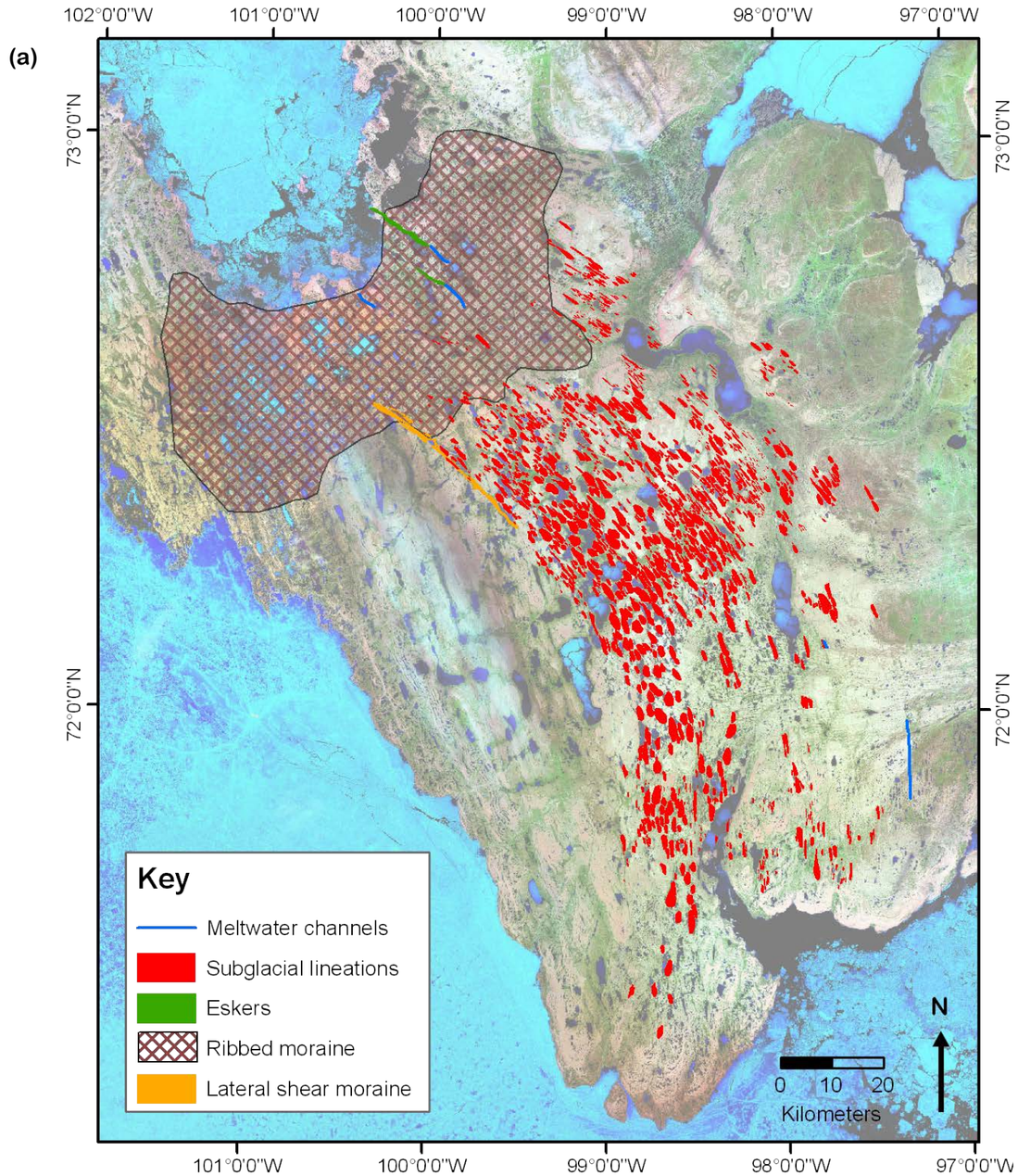

Figure 4.23 – (a) Crooked Lake Palaeo-Ice Stream geomorphology map overlying Landsat ETM+ mosaic (b) Approximate position of the Crooked Lake ice stream signature (red rectangle), within an idealised ice stream.

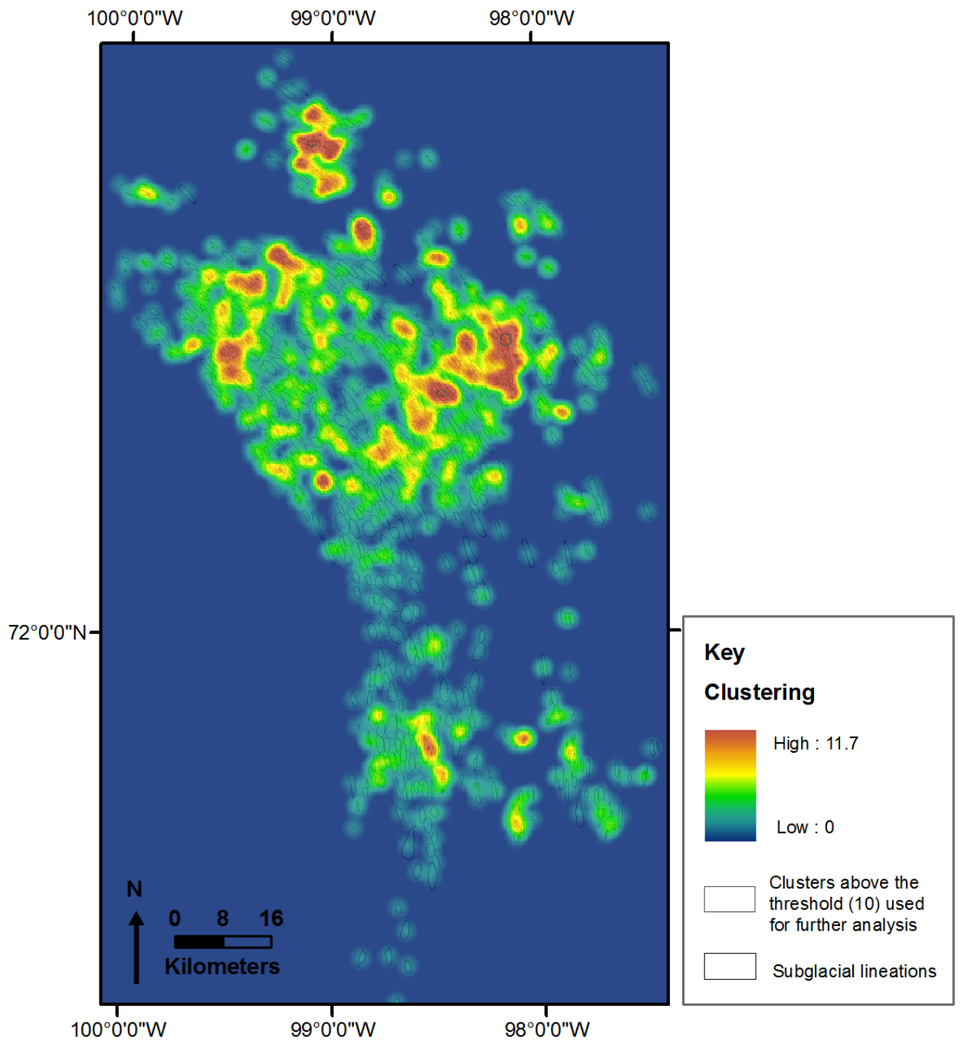

Figure 4.24 – Map depicting the clustering of subglacial lineations across the Crooked Lake Palaeo-Ice Stream. Clusters that fall above the value of 10 are outlined, because these are the basis for later analysis. Median elongation ratios from the clusters above 10 is 3.5, which compares to a median value of 3.1 for the entire ice stream.

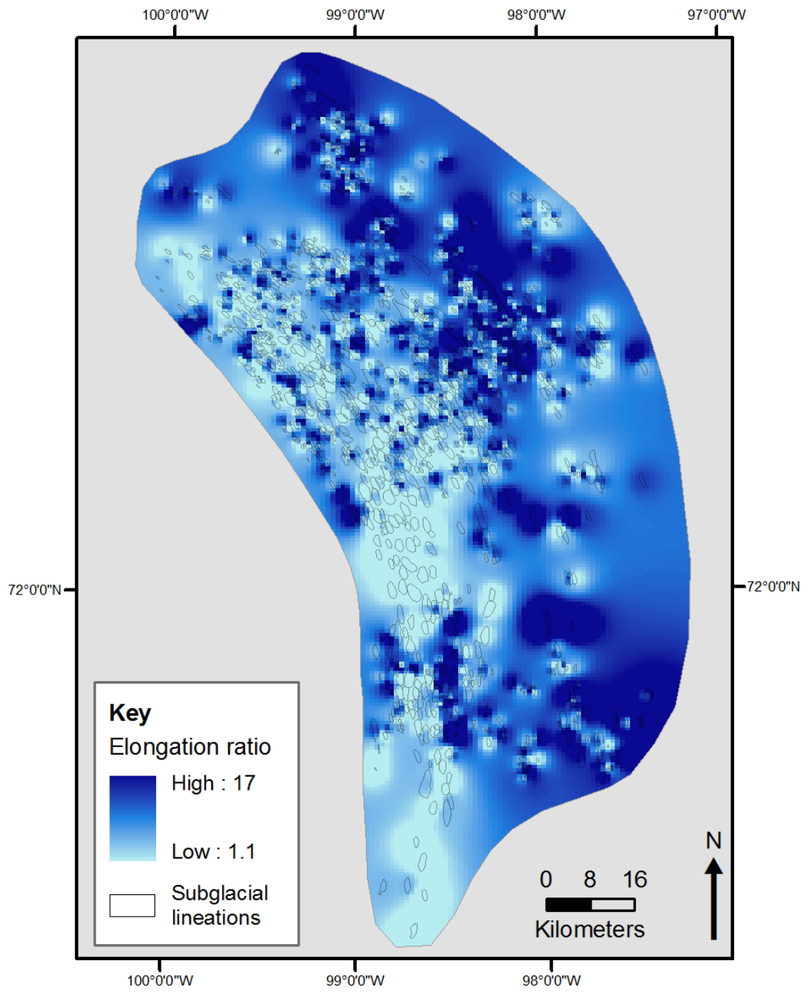

Figure 4.25 – Elongation ratio interpolated across the Crooked Lake Palaeo-Ice Stream, which provides a visual impression of the spatial distribution of elongation ratios. The grey background allows the interpolated surface to be shown only to the approximate extent of the ice stream.

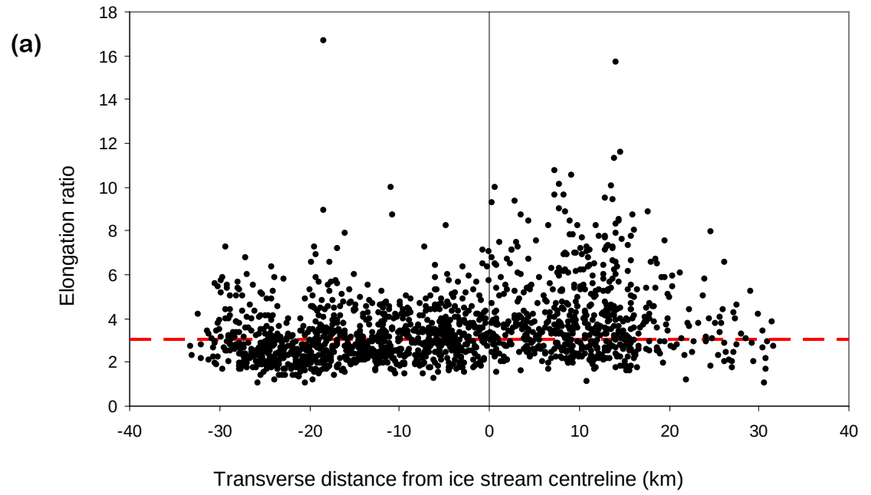

Figure 4.26 – Transverse and longitudinal trends in subglacial lineation elongation ratio. (a) Elongation ratio plotted against distance from the ice stream centreline (black vertical line). Distance from the centreline is on the x axis, positive values represent east of the centreline and negative values represent west of the centreline. (b) Elongation ratio plotted against distance along the ice stream. Distance along the ice stream is on the x axis, from 0 (upstream) to 180 km (downstream). Median elongation ratio is marked with red dashed lines.

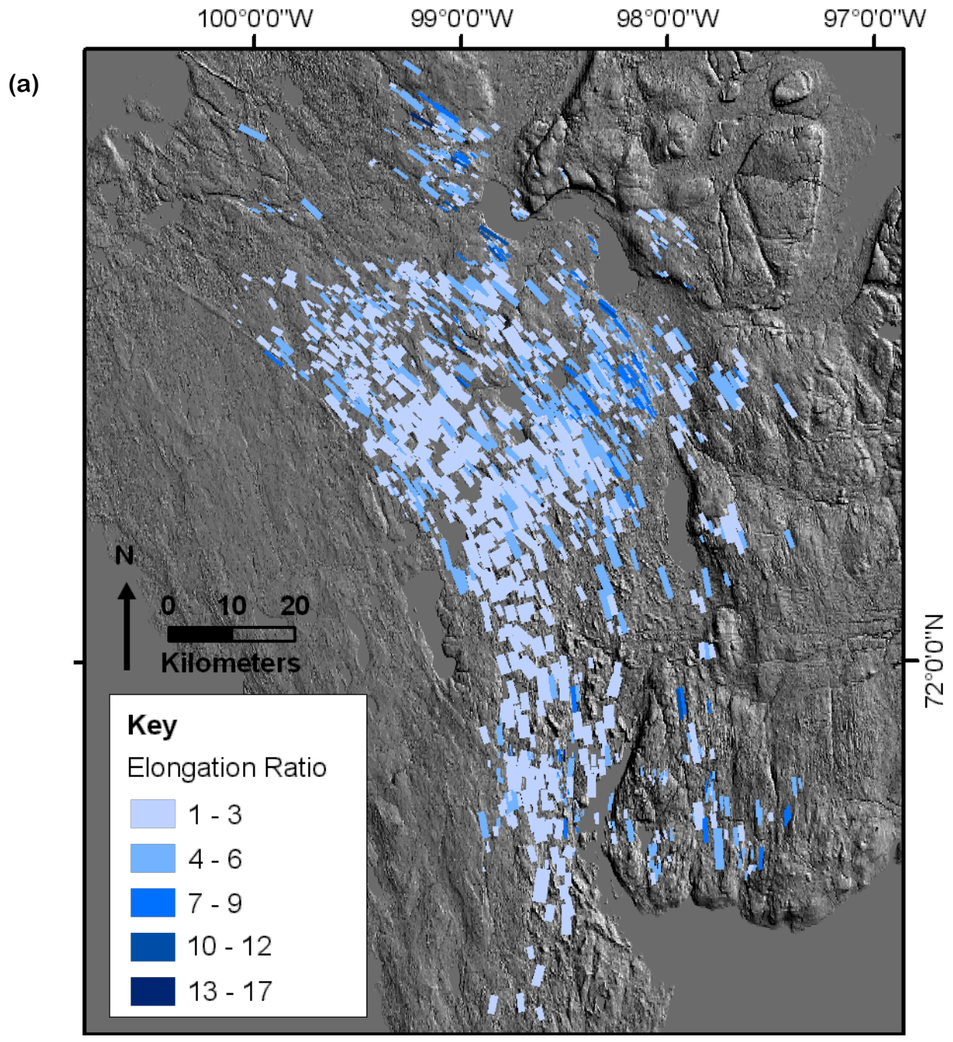

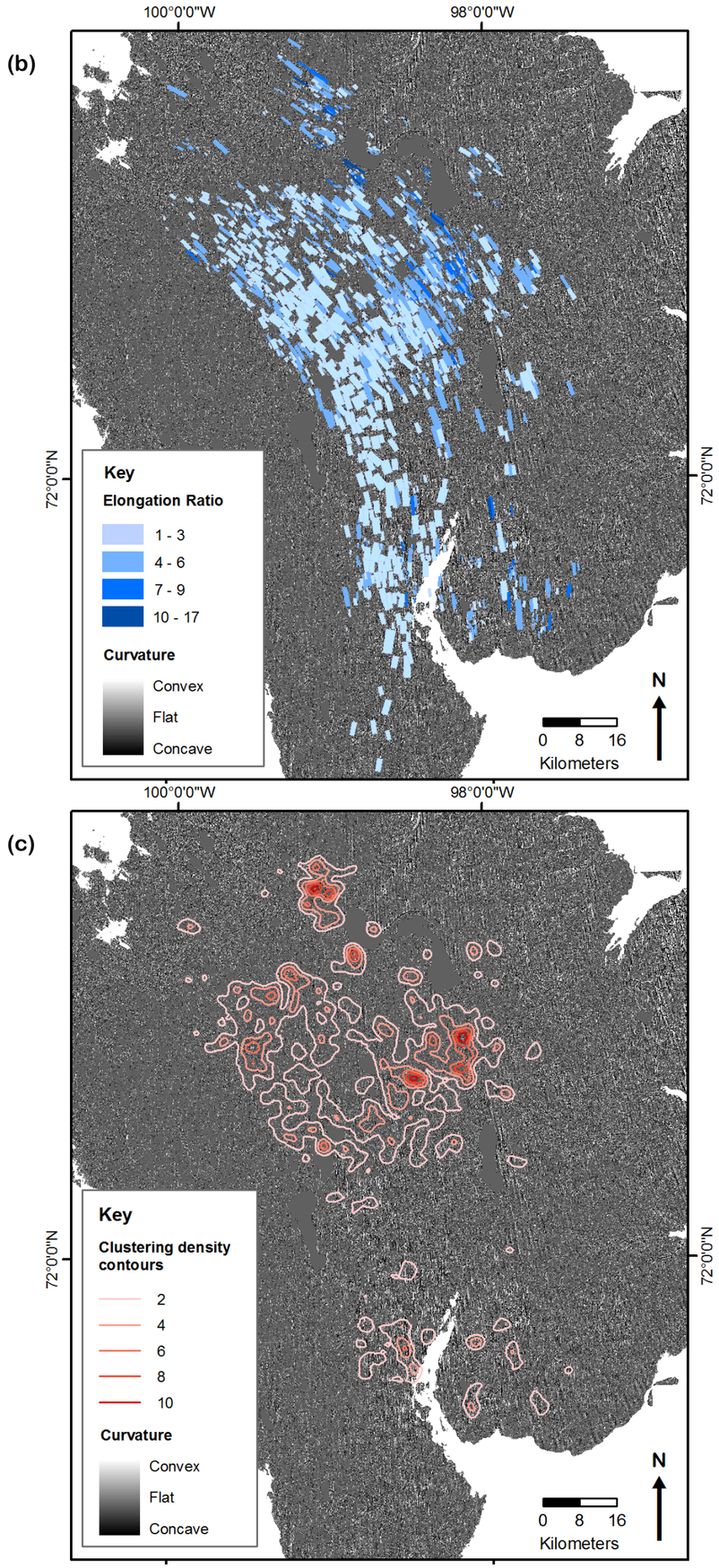

Figure 4.27 – Topography across the Crooked Lake Palaeo-Ice Stream. Data from Canadian Digital Elevation Data. (a) DEM with a vertical exaggeration of x6 overlain by subglacial lineations shaded according to elongation ratio. (b) Curvature map overlain by subglacial lineations shaded according to elongation ratio. (b) Curvature map overlain by contours of subglacial lineation clustering (derived from the data presented in Figure 4.24).

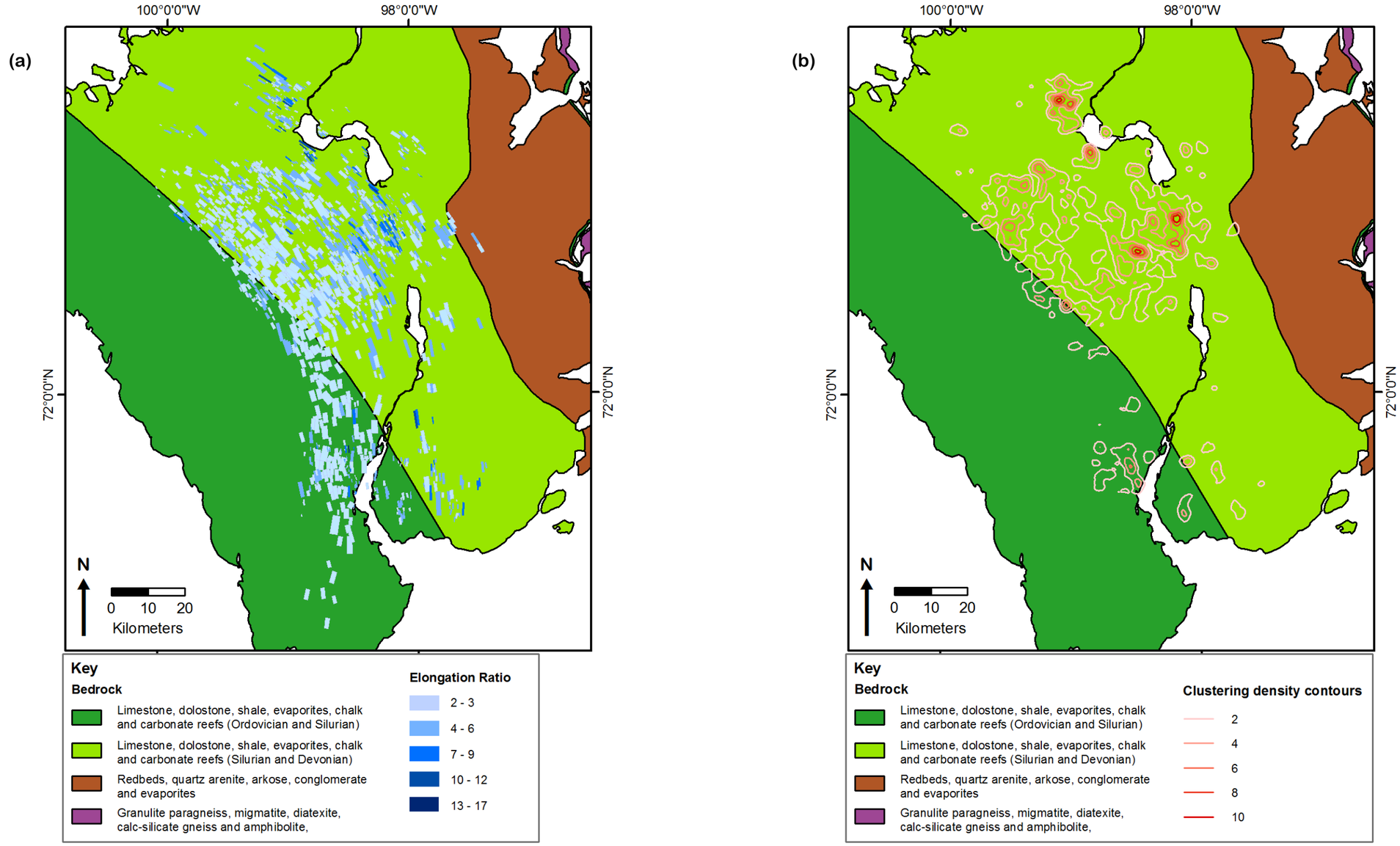

Figure 4.28 – Bedrock lithologies across the Crooked Lake Palaeo-Ice Stream. Geology data from Harrison *et al.* (2008). (a) Bedrock map overlain by subglacial lineations shaded according to elongation ratio. (b) Bedrock map overlain by contours of subglacial lineation clustering (derived from the data presented in Figure 4.24). (c) Bar chart displaying the percentage coverage of bedrock lithologies across the whole ice stream and within the cluster areas identified in Figure 4.24.

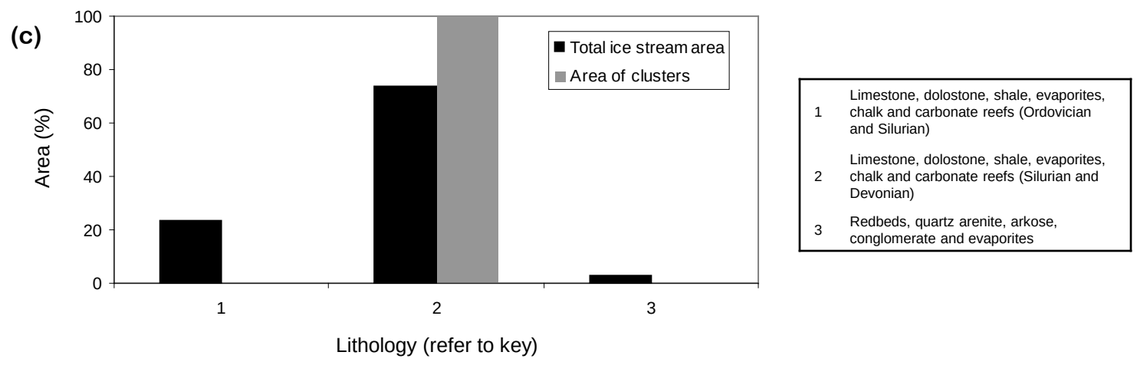

4.5 Transition Bay Ice Stream

4.5.1 Background

Transition Bay Ice Stream flows west to east across Prince of Wales Island (Figure 4.3) and is superimposed at its upstream end onto the Crooked Lake Ice Stream. It comprises a plume of streamlined, light coloured, limestone and dolomite rich till, that overlies dark coloured red clastic sediments (Dyke and Morris, 1988). Satellite imagery and geomorphological mapping (De Angelis and Kleman, 2005) shows drumlins that are highly convergent at the upstream end of the ice stream and end abruptly at the lateral margins of the ice stream. This ice stream is also characterised by a Boothia type dispersal plume (see Dyke and Morris, 1988). Other typical palaeo-ice stream characteristics for this ice stream includes a characteristic shape and dimensions and highly attenuated bedforms (see Stokes and Clark, 1999).

4.5.2 Geomorphological mapping

Most, if not the entire geomorphological signature of this ice stream appears to be preserved on Prince of Wales Island, as evidenced by the convergent onset zone, followed by downstream narrowing into the ice stream trunk (Figure 4.29). The onset zone of the ice stream is located within the limits of the Crooked Lake Ice Stream and many subglacial lineations in this zone are also reworked sediment from the Crooked Lake Ice Stream. Whilst subglacial lineations are abundant at the upstream and downstream ends of the ice stream, there is a c. 15 km stretch in the centre of the ice stream that is relatively devoid of subglacial lineations (Figure 4.29). Subglacial lineations (n = 999) are typically not tightly packed and are relatively evenly spaced. They range from 0.15 to 4.69 km long (median length of 0.6 km) and 0.008 to 2.27 km^2 in area (median area of 0.093 km^2), which is markedly smaller than the Crooked Lake Ice Stream subglacial lineations. Elongation ratios range from 1.1 to 11.4, with a median of 3.

Some limited areas of ribbed moraine are present at the onset zone of the ice stream. Some researchers argue that this landform relates to the transition between warm based and cold based ice, which may be expected at an ice stream onset zone (Dyke *et al*.,

1992; Hättestrand and Kleman, 1999; De Anglelis and Kleman, 2008). Some meltwater channels are present, which are located mid way down the ice stream in the area where few subglacial lineations are present.

4.5.3 Subglacial lineation analysis

The spatial distribution of elongation ratios across the ice stream is shown in figures 4.31, 4.33 and 4.34. Low elongation ratios (between 1 and 3) and some medium elongation ratios (between 4 and 6) dominate the onset zone of the ice stream, whilst the downstream end of the ice stream contains the highest elongation ratios. A pattern of elongation ratio clustering is seen (Figure 4.31), as was the case for the other ice streams examined, and this is confirmed by the spatial autocorrelation analysis (see Appendix A).

Figure 4.33a shows that the highest elongation ratios dominate the centre of the ice stream and decrease towards the lateral margins. Longitudinally (Figure 4.33b) there is an overall increase in elongation ratios downstream, which is also evident from the interpolation (Figure 4.31). In the area of few subglacial lineations mid-way down the ice stream, elongation ratios are notably low. In the first 10 km and the last 10 km of the ice stream, elongation ratios are also low.

4.5.4 Topography and bedrock geology

The bed topography of the Transition Bay Palaeo-Ice Stream appears to have no broad control over ice stream location (e.g. a valley which channels the ice stream), but there are some topographic variations along the length of the ice stream (Figures 4.30 and 4.34). A small hill (marked A in Figure 4.30) can be seen mid way down the ice stream (which rises up to 120 m above the surrounding land), which is characterised by meltwater channels and few subglacial lineations. Downstream of this hill, the subglacial lineations do not reappear for approximately 10 km (Figure 4.30). At the far downstream end of the ice stream, the land rises, corresponding with geological faults (figures 4. 30 and 4.35) and this small upland area has very few subglacial lineations. Topographic curvature of the ice stream bed is displayed in Figure 4.34 and no overall pattern is discernable from this. The majority of the ice stream bed appears to have a flat

curvature, with any deviation from this limited to small speckled areas. As such, no correlation between curvature and subglacial lineation characteristics is seen.

The ice stream overlies sedimentary bedrock comprising a range of lithologies, as indicated in Figure 4.35. The bedrock at the south-western end of the ice stream is characterised by few, small subglacial lineations with low elongation values. However, similar subglacial lineations are also found across the entire onset zone of the ice stream. Areas of highly clustered subglacial lineations are present on all of the bedrock areas identified (Figure 4.35b), but the most highly clustered areas analysed in Figure 4.35c display a preference for the westernmost lithologies of limestone, dolostone, shale, evaporates, chalk and carbonate reefs.

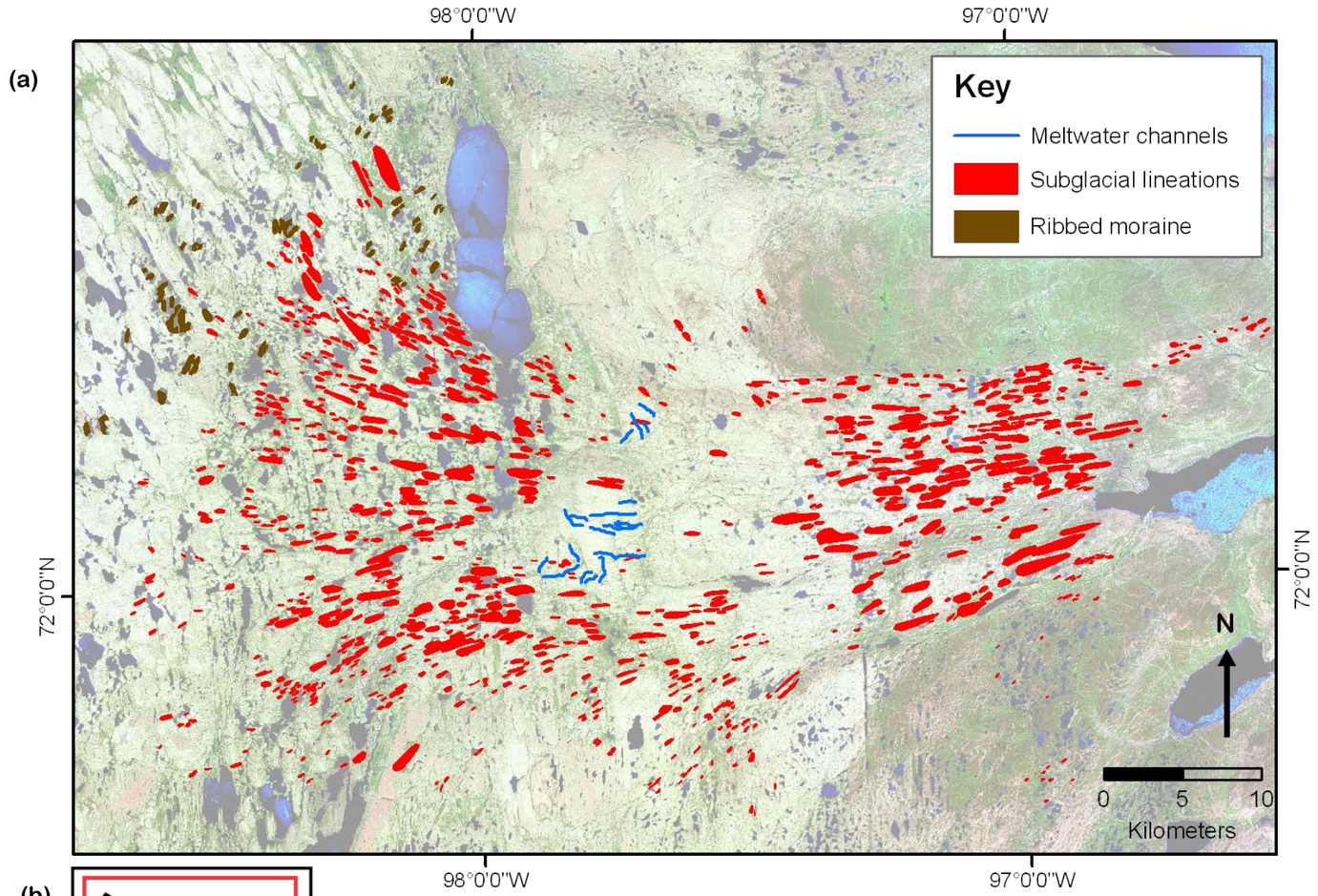

Figure 4.29 – (a) Transition Bay Palaeo-Ice Stream geomorphology map overlying a Landsat ETM+ mosaic (b) Approximate position of the Transition Bay ice stream signature (red rectangle), within an idealised ice stream.

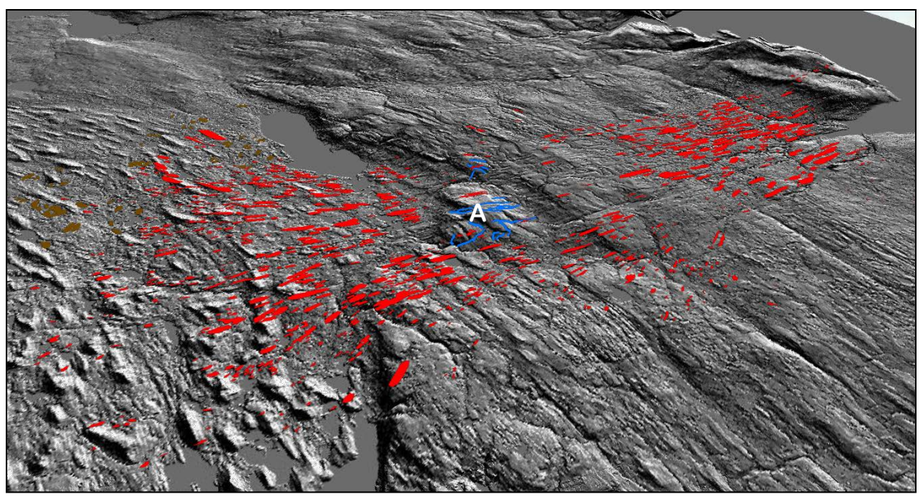

Figure 4.30 – 3D image of the Transition Bay Ice Stream, overlain by geomorphology (see Figure 4.29 for geomorphology key). View is NE across Prince of Wales Island, and the Transition Bay Ice Stream flows from left to right across the image. The small hill referred to in the text is labelled A. DEM is Canadian Digital Elevation Data, and has a vertical exaggeration of x10.

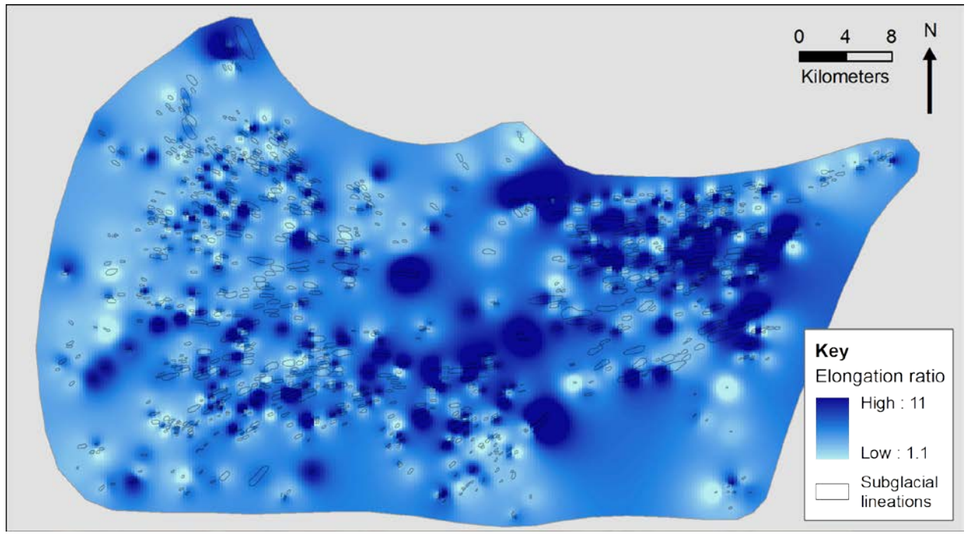

Figure 4.31 – Elongation ratio interpolated across the Transition Bay Palaeo-Ice Stream, which provides a visual impression of the spatial distribution of elongation ratios. The grey background allows the interpolated surface to be shown only to the approximate extent of the ice stream.

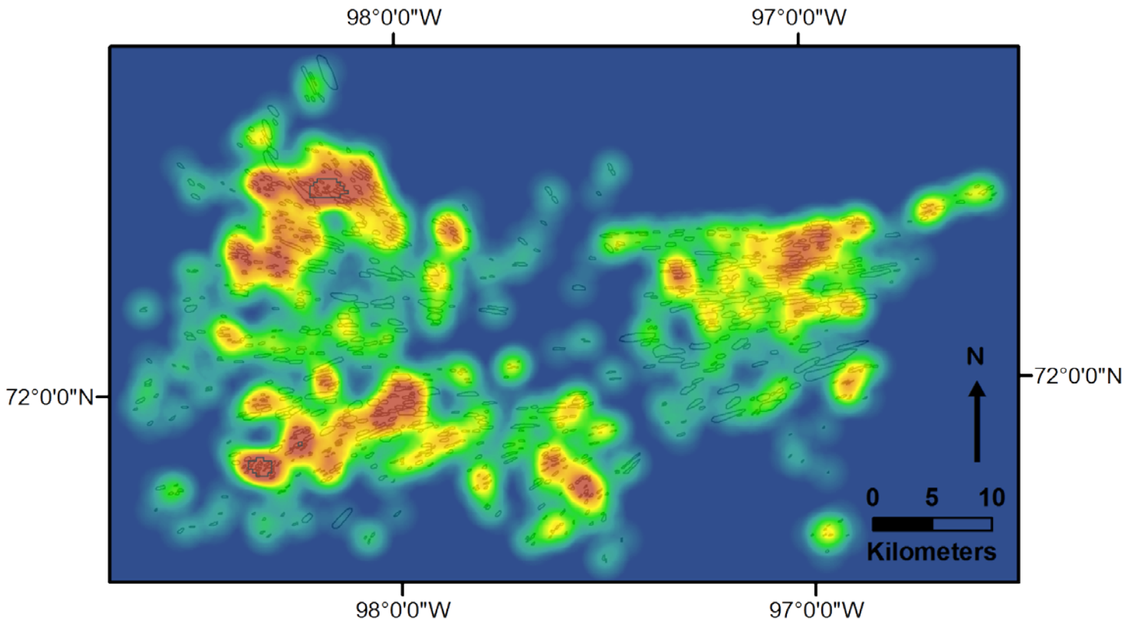

Figure 4.32 – Map depicting the clustering of subglacial lineations across the Transition Bay Palaeo-Ice Stream. Clusters that fall above the value of 10 are outlined, because these are the basis for later analysis. Median elongation ratios from the clusters above 10 is 2.6, which compares to a median value of 3.0 for the entire ice stream.

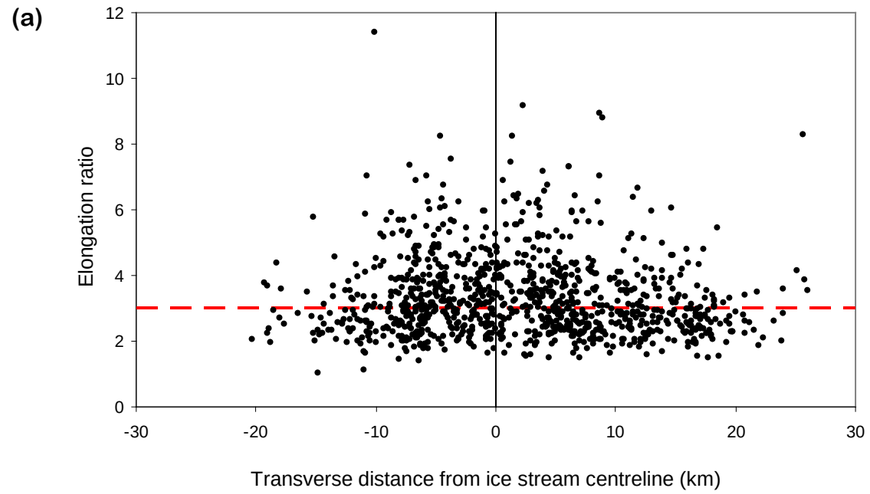

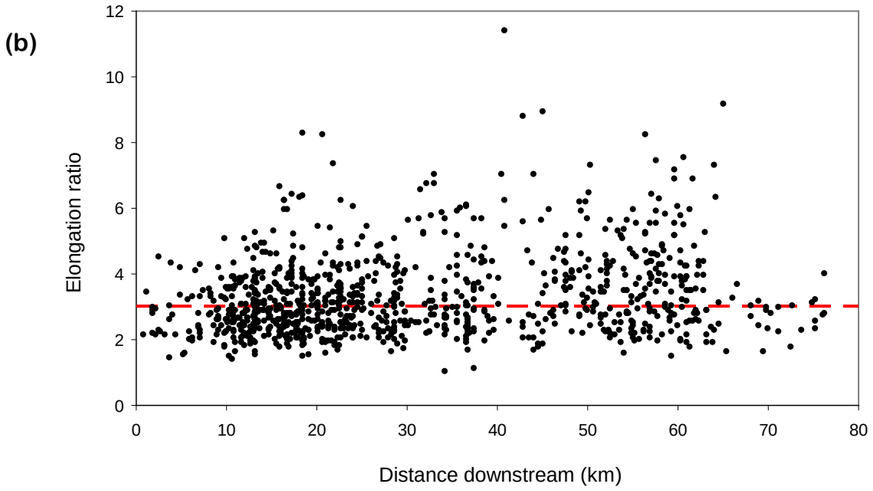

Figure 4.33 – Transverse and longitudinal trends in subglacial lineation elongation ratio. (a) Elongation ratio plotted against distance from the ice stream centreline (black vertical line). Distance from the centreline is on the x axis, positive values represent north of the centreline and negative values represent south of the centreline. (b) Elongation ratio plotted against distance along the ice stream. Distance along the ice stream is on the x axis, from 0 (upstream) to 80 km (downstream). Median elongation ratio is marked with red dashed lines.

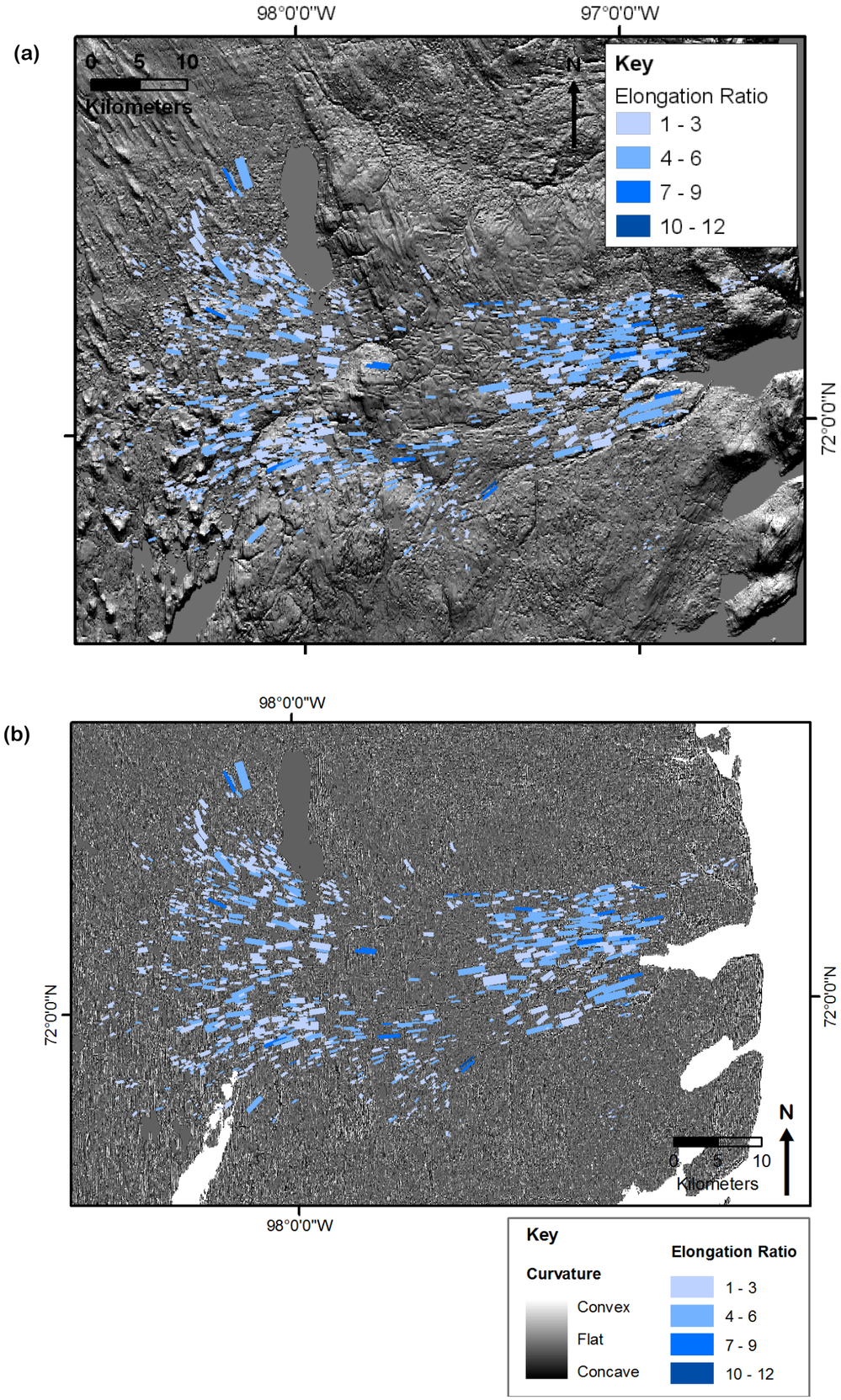

Figure 4.34 – Topography across the Transition Bay Palaeo-Ice Stream. Data from Canadian Digital Elevation Data. (a) DEM with a vertical exaggeration of x6 overlain by subglacial lineations shaded according to elongation ratio. (b) Curvature map overlain by subglacial lineations shaded according to elongation ratio. (b) Curvature map overlain by contours of subglacial lineation clustering (derived from the data presented in Figure 4.32).

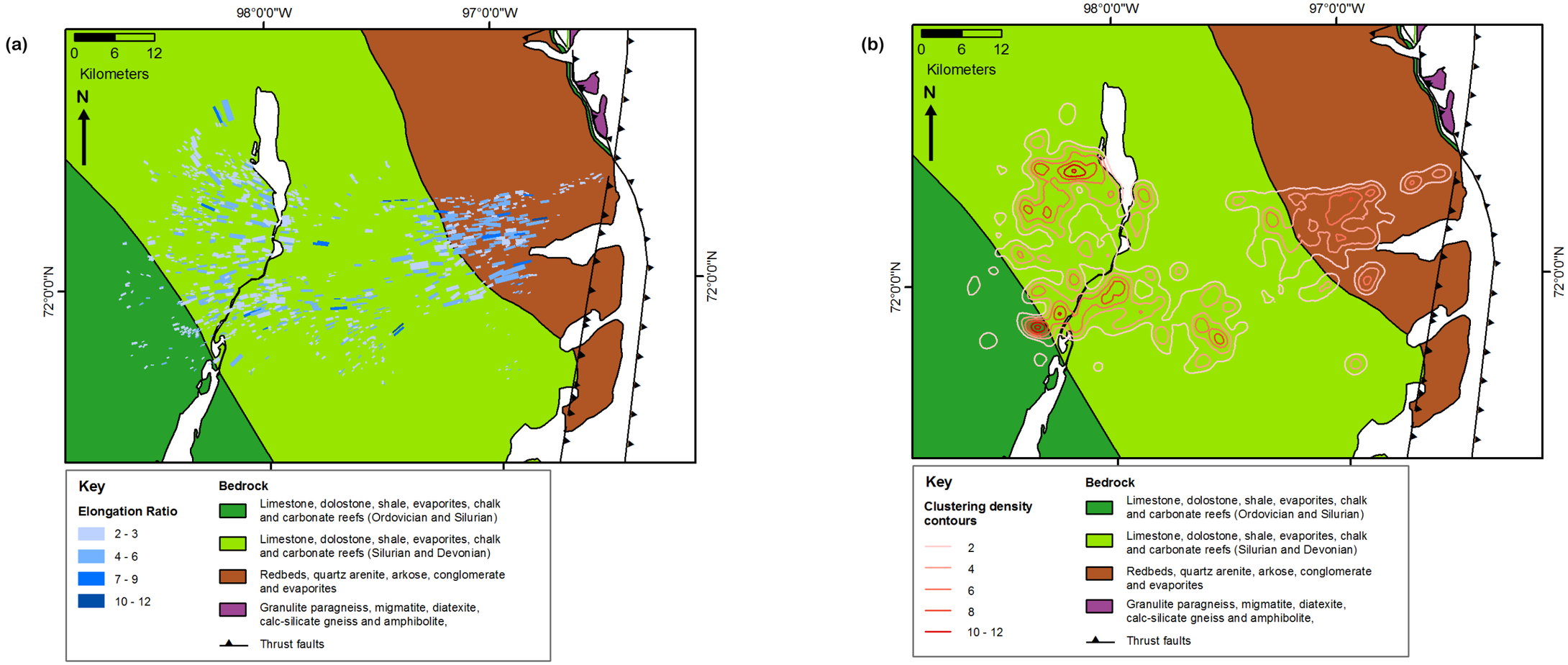

Figure 4.35 – Bedrock lithologies across the Transition Bay Palaeo-Ice Stream. Geology data from Harrison *et al*. (2008). (a) Bedrock map overlain by subglacial lineations shaded according to elongation ratio. (b) Bedrock map overlain by contours of subglacial lineation clustering (derived from the data presented in Figure 4.32). (c) Bar chart displaying the percentage coverage of bedrock lithologies across the whole ice stream and within the cluster areas identified in Figure 4.32.

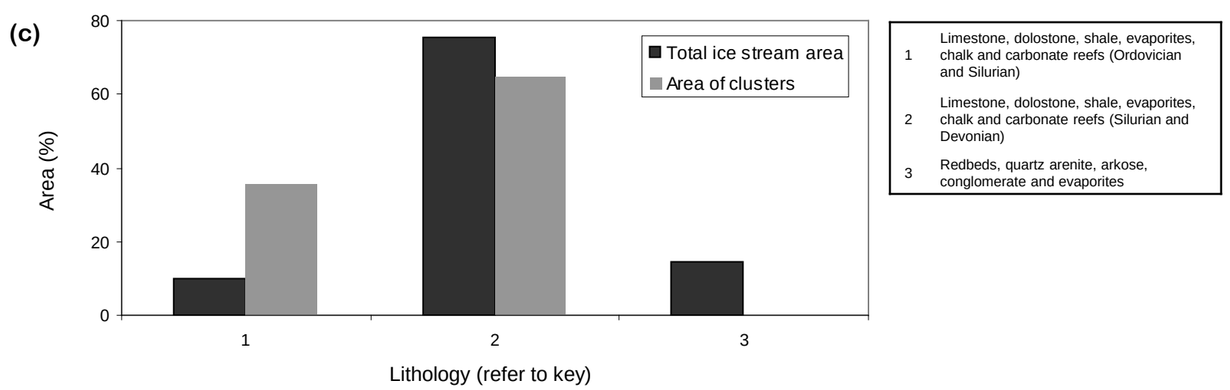

4.6 Haldane Ice Stream

4.6.1 Background

Haldane Ice Stream is located in Northwest Territories, to the north of Great Bear Lake, flowing ESE to WNW (Figure 4.3). It comprises elongate bedforms with high parallel conformity (Winsborrow *et al*., 2004). Other geomorphological characteristics to identify it as an ice stream include: characteristic shape and dimensions, abrupt lateral margins and a lateral shear moraine (see Stokes and Clark, 1999). The timing of this ice stream is thought to relate to ice sheet deglaciation (Winsborrow *et al*., 2004), which was approximately 11.5 ^{14}C ka BP (13.45 cal ka BP) in this area (Dyke *et al*., 2003).

4.6.2 Geomorphological mapping

Figure 4.36 shows that the ice stream has a well preserved, geomorphological signature, with convergent subglacial lineations at the onset zone and parallel, elongate subglacial lineations in the trunk. Subglacial lineations (n = 1458) range from 0.14 to 10.7 km (median 1.2 km long) in length and from 0.01 to 3.14 km^2 in area (median of 0.146 km^2). Elongation ratio ranges from 1.7 to 58 (median of 7.4), which is notably higher than the other ice streams examined in this chapter.

Towards the lateral margins of the ice stream, subglacial lineations transition into areas of smeared, streamlined sediment, which are dissected by streams and this may form small lineations. Meltwater channels are characteristic at the lateral margins, which trend parallel to the slope and typically parallel and sub-parallel to the ice stream. A shear moraine is present at the north lateral margin, located approximately 5 km away from the main concentration of subglacial lineations. This is similar to a lateral shear moraine described by Stokes and Clark (2002b) that had a ‘lateral offset’ of up to 2.8 km outside the ice stream shear margin, which they considered may be a result of margin migration.

A series of large terminal moraines, extending across almost 40 km are present at the end of the ice stream, extending laterally beyond the south lateral margin of the ice stream. The moraine complex is hummocky, fragmented, and cross cut by several

channels. The region outside of the ice stream, which is unmapped, appears to be covered by widespread hummocky terrain.

4.6.3 Subglacial lineation analysis

Haldane Ice Stream is characterised by highly elongate subglacial lineations, which are considerably more elongate than the other palaeo-ice streams examined. Figures 4.38 and 4.41 show that elongation ratio is high across most of the ice stream. Regions of lower elongation ratios are evident at the onset zone, at the lateral margins of the ice stream and in some areas at the downstream end of the ice stream. This gives a pattern similar to the imprint of subglacial lineations across an idealised ice stream (Figure 4.2). Spatial autocorrelation demonstrated that subglacial lineation elongation ratios are clustered, to a significance level of 99 % (see Appendix A). This pattern is apparent in Figure 4.38, which displays the interpolation of elongation ratio across the ice stream.

The transverse distribution of elongation ratios shows a very clear pattern (Figure 4.40a), with very high elongation ratios in the centre of the ice stream, a sharp decrease towards the lateral margins and below average elongation ratios at the outer 10 km of the ice stream. This distribution of elongation ratios is similar to that found by Briner (2007) in the New York drumlin field. Longitudinally, the ice stream displays a clear increase in elongation ratio for the first 50 km of the ice stream, which is followed by an area with few subglacial lineations and a slight drop in elongation ratio (Figure 4.40b).

Subglacial lineations appear to be clustered across most of the ice stream. A large concentration of subglacial lineations is seen in the upstream half of the ice stream and within this a heterogeneous distribution of clustering can be seen. The maximum clustering is located at the upstream end of the ice stream on its southern side, an area that is characterised by small subglacial lineations.

4.6.4 Topography and bedrock geology

Haldane Palaeo-Ice Stream clearly lies within a valley, as shown in figures 4.37 and 4.41. The onset zone of the ice stream is located at the edge of the present day Great Bear Lake and the ice stream flowed up the narrowing valley. Figure 4.37 illustrates the contrast between the smooth ice stream bed and the surrounding hummocky topography. Land elevation rises from the upstream to the downstream end of the ice stream from approximately 200 m asl to 400 m asl. At the downstream end of the ice stream the bed rises sharply, and a hill (marked A in Figure 4.37; 580 m asl and c. 200 km^2) can be seen on the south side of the ice stream. This hill is characterised by a lack of subglacial lineations and a network of meltwater channels. Subglacial lineations are present adjacent to the hill, where the ice stream bed rises more gradually from 200 to 350 m asl, but again these have relatively low elongation ratios compared to the rest of the ice stream. Unlike the topographic obstacles in the Forth Ice Stream, subglacial lineations are not orientated around the hill.

Curvature of the ice stream bed and surrounding area can be seen in Figure 4.41. A distinction can be seen between the relatively flat ice stream bed and the adjacent areas, which are characterised by a convex topography. The rise in elevation at the downstream end of the ice stream labelled ‘A’ in Figure 4.37, which has few subglacial lineations, is also characterised by a markedly more convex topography than the rest of the ice stream bed. The Haldane Ice Stream is underlain entirely by sedimentary bedrock, as shown in Figure 4.42. Most of the ice stream is located on sandstone, siltstone, shale and coal and the areas of high bedform clustering are also entirely located on this geology.

(a)

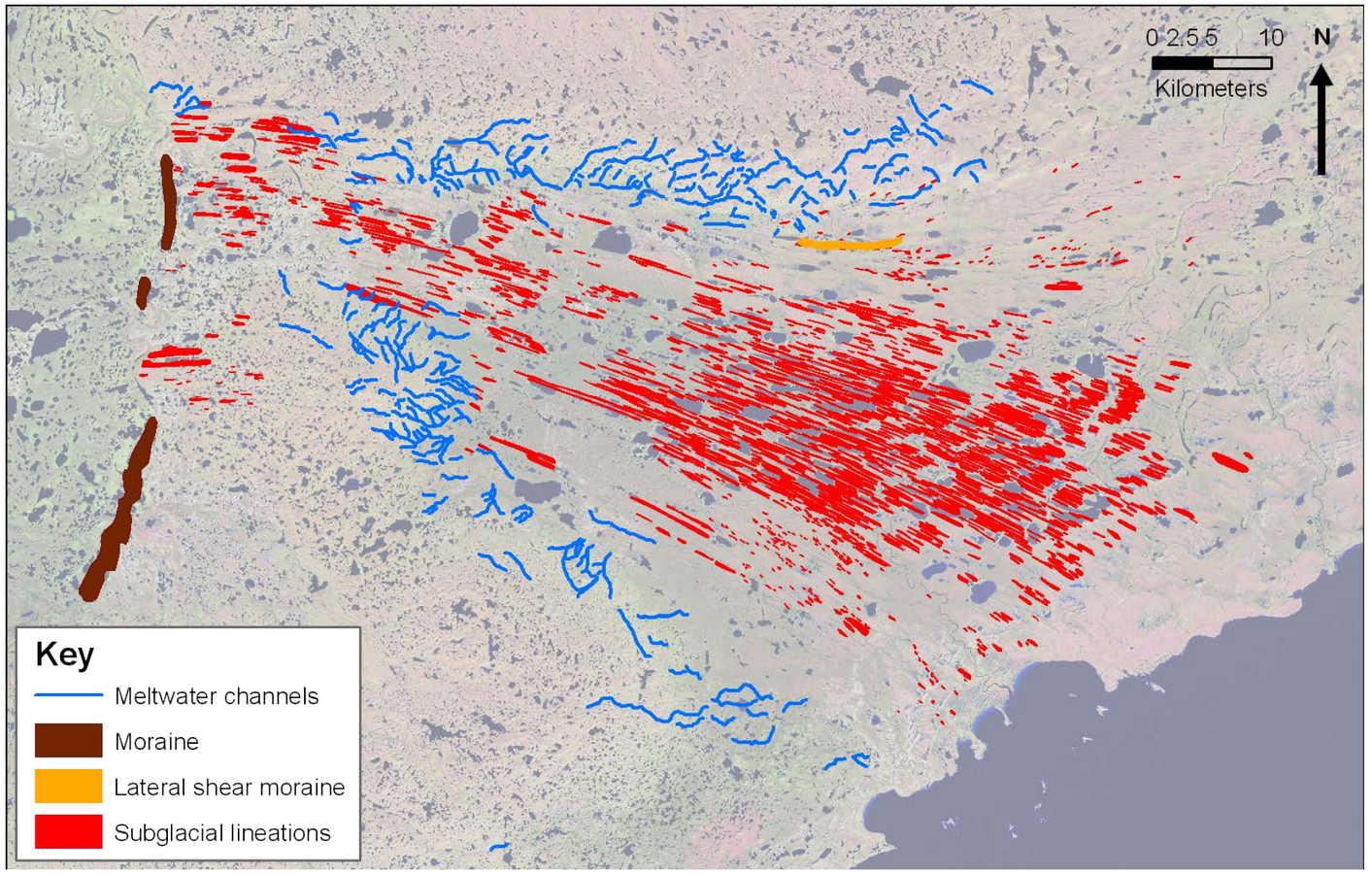

(b)

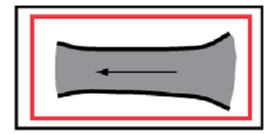

Figure 4.36 – (a) Haldane Palaeo-Ice Stream geomorphology map overlying a Landsat ETM+ mosaic (b) Approximate position of the Haldane ice stream signature (red rectangle), within an idealised ice stream.

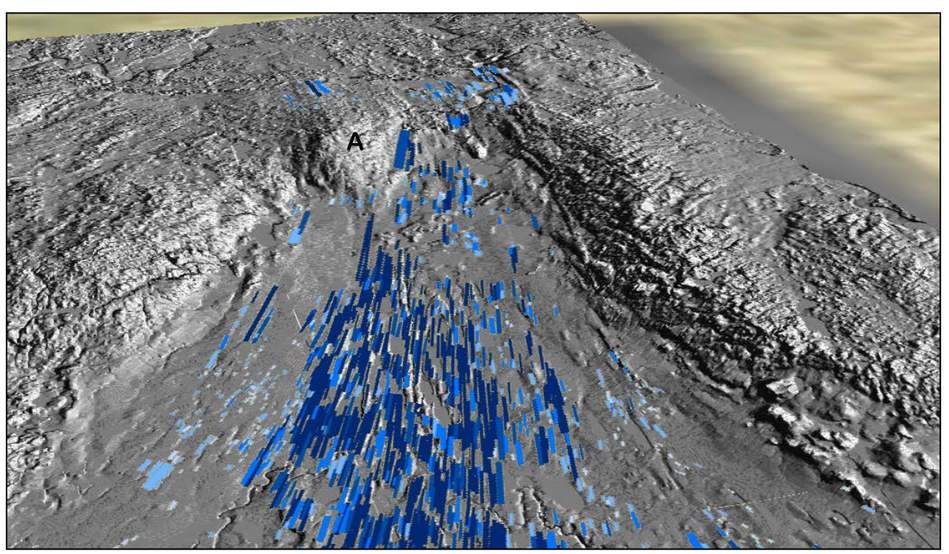

Figure 4.37 – 3D image of the Haldane Ice Stream. View is towards the west, looking downstream. Subglacial lineations are shaded according to elongation ratio (see key in Figure 4.41). The hill (rise in land elevation) referred to in the text is marked A. DEM is Canadian Digital Elevation Data and has a vertical exaggeration x10.

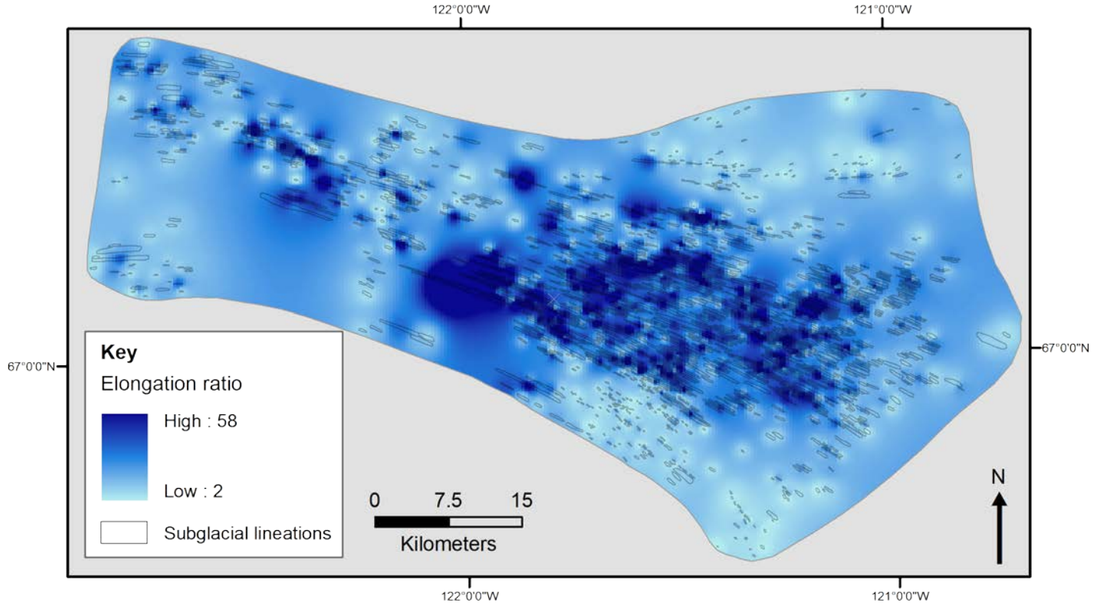

Figure 4.38 – Elongation ratio interpolated across the Haldane Palaeo-Ice Stream, which provides a visual impression of the spatial distribution of elongation ratios. The grey background allows the interpolated surface to be shown only to the approximate extent of the ice stream.

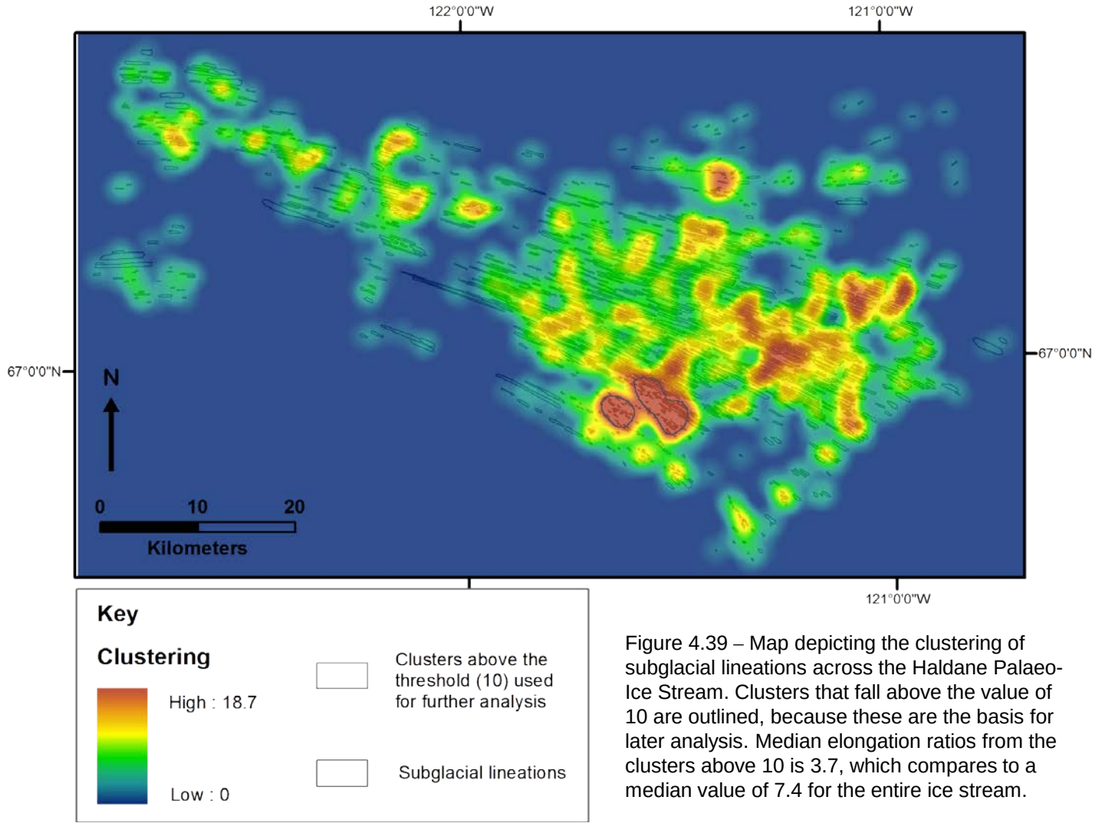

Figure 4.39 – Map depicting the clustering of subglacial lineations across the Haldane Palaeo-Ice Stream. Clusters that fall above the value of 10 are outlined, because these are the basis for later analysis. Median elongation ratios from the clusters above 10 is 3.7, which compares to a median value of 7.4 for the entire ice stream.

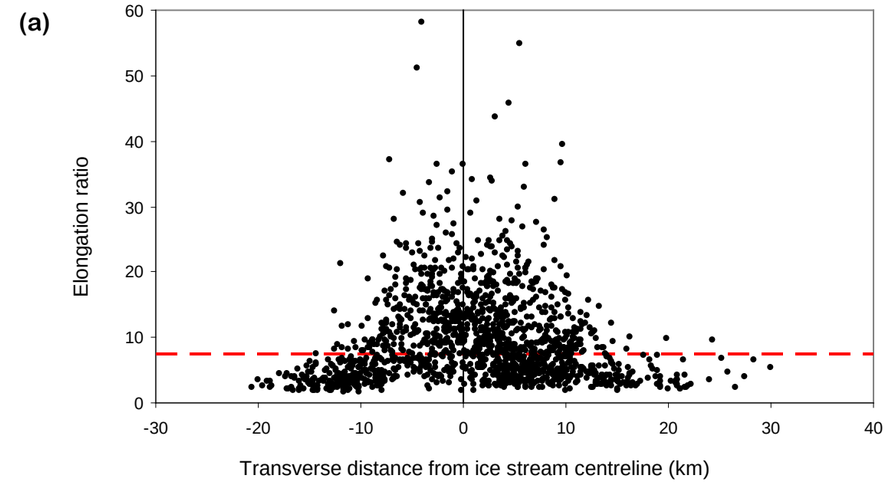

Figure 4.40 – Transverse and longitudinal trends in subglacial lineation elongation ratio. (a) Elongation ratio plotted against distance from the ice stream centreline (black vertical line). Distance from the centreline is on the x axis, positive values represent north of the centreline and negative values represent south of the centreline. (b) Elongation ratio plotted against distance along the ice stream. Distance along the ice stream is on the x axis, from 0 (upstream) to 90 km (downstream). Median elongation ratio is marked with red dashed lines.

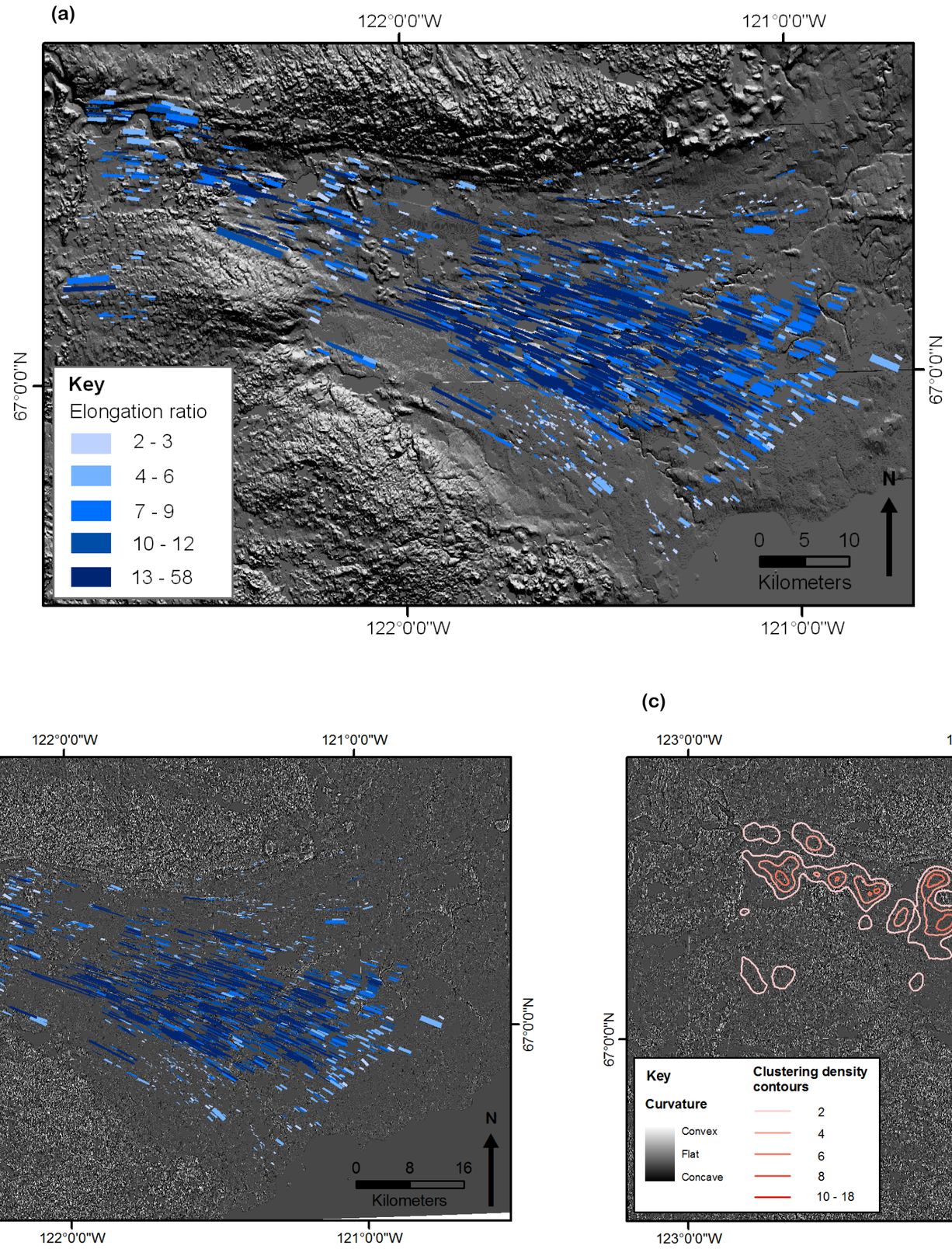

Figure 4.41 – Topography across the Haldane Palaeo-Ice Stream. Data from Canadian Digital Elevation Data. (a) DEM with a vertical exaggeration of x6 overlain by subglacial lineations shaded according to elongation ratio. (b) Curvature map overlain by subglacial lineations shaded according to elongation ratio. (b) Curvature map overlain by contours of subglacial lineation clustering (derived from the data presented in Figure 4.39).

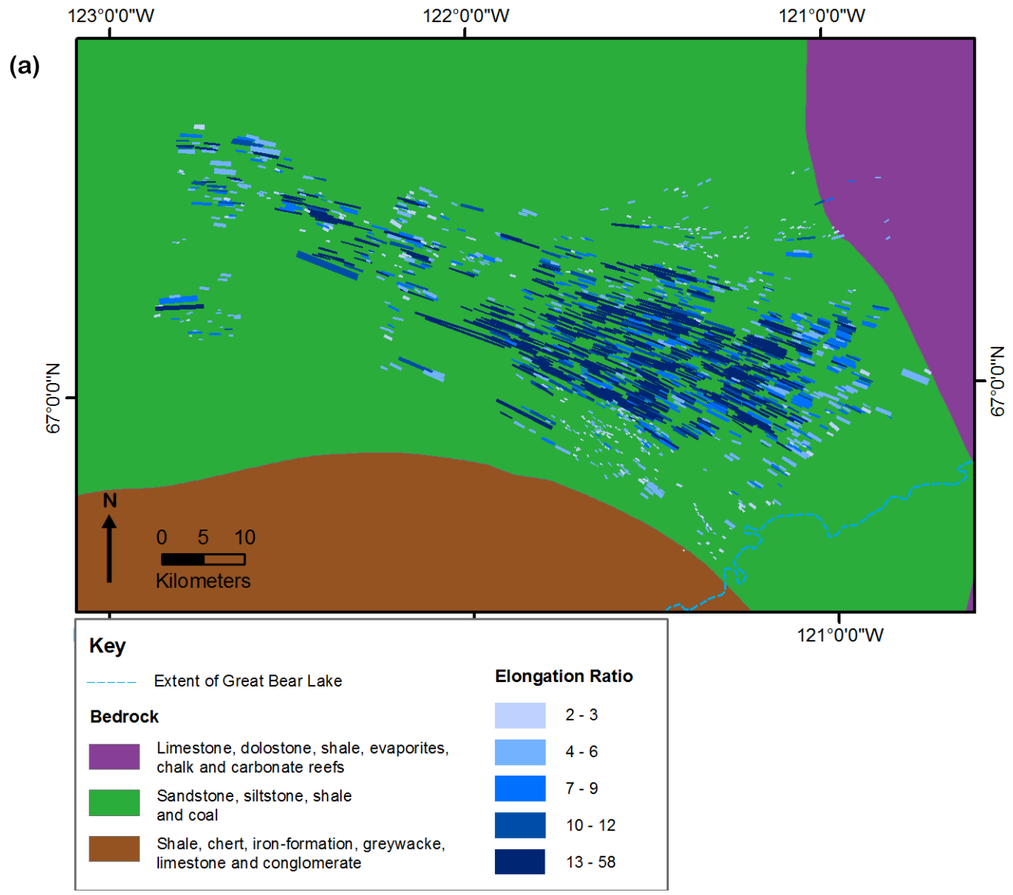

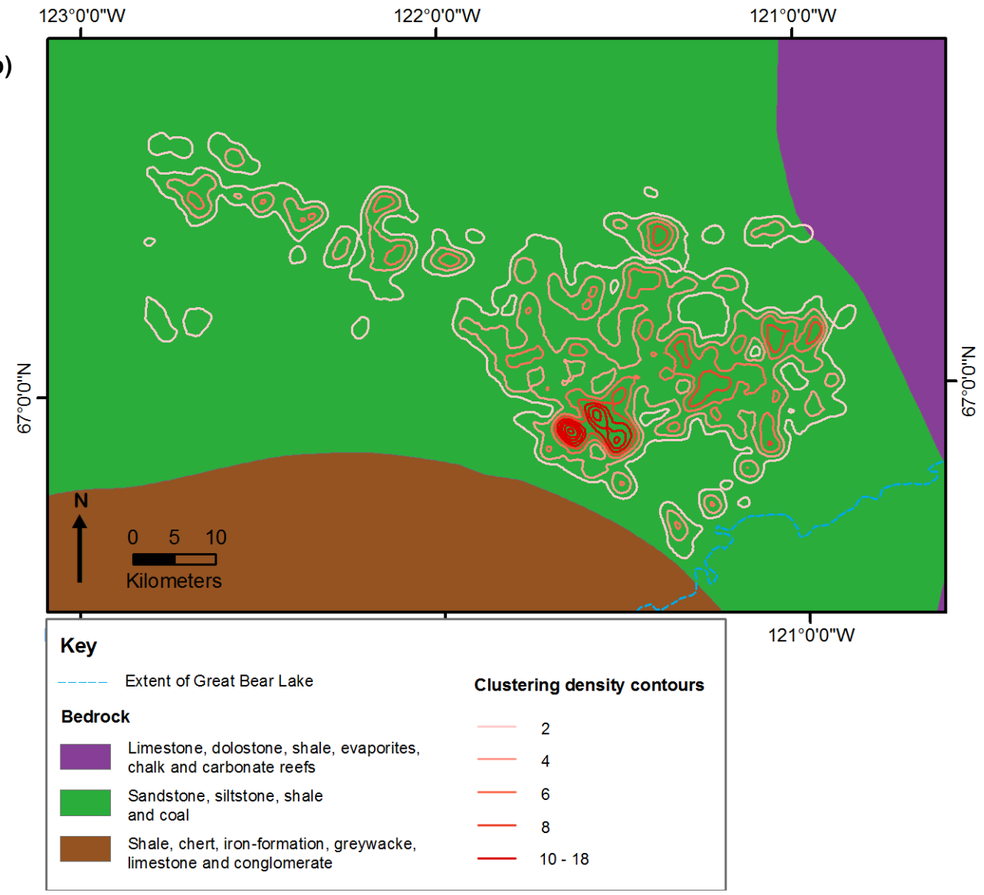

Figure 4.42 – Bedrock lithologies across the Haldane Palaeo-Ice Stream. Geology data from Harrison *et al*. (2008). (a) Bedrock map overlain by subglacial lineations shaded according to elongation ratio. (b) Bedrock map overlain by contours of subglacial lineation clustering (derived from the data presented in Figure 4.39). (c) Bar chart displaying the percentage coverage of bedrock lithologies across the whole ice stream and within the cluster areas identified in Figure 4.39.

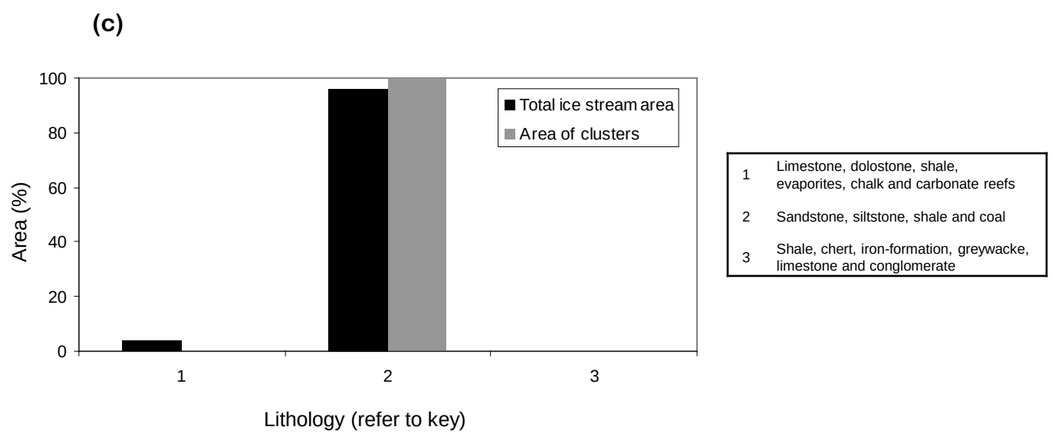

4.7 Interpretation

Geomorphological mapping of the ice streams presented in this chapter provides the context for examination of the subglacial lineations. The following interpretation examines subglacial lineations in depth, whilst other landforms are not discussed in detail, because they are typically sparse and cannot always be explicitly linked to ice streaming.

4.7.1 Spatial characteristics of subglacial lineation elongation ratio

Transverse analysis of subglacial lineations revealed that a high proportion of above average elongation ratios was typically found towards the centre of the ice streams, similar to the patterns observed by Stokes and Clark (2002a) and Briner (2007). This pattern is difficult to directly compare with transverse distributions of contemporary ice stream velocities because elongation ratios represent discrete data-points and their range is quite considerable. This means that running averages of transverse elongation ratio are quite variable, as shown in Figure 4.43 (a and b). However, maximum elongation ratio gives a smoother curve, which is more comparable to contemporary ice stream velocities (figures 4.1 and 4.43), but this is determined by very few data-points and as such may be subject to anomalies. If the maximum elongation ratio is taken to be a proxy for ice velocity, the transition zone from fast flow to slow flow at the lateral margins ranges from 22 to 62 % of total ice stream width for the examined ice streams. This compares to the more restricted range of 22 to 35 % for studied contemporary ice streams (Bindschadler and Scambos, 1991; Echelmeyer *et al*., 1994; Whillans and van der Veen, 1997; Echelmeyer and Harrison, 1999; Joughin *et al*., 2002; Truffer and Echelmeyer, 2003). An additional consideration, is that the transverse patterns of elongation ratio represent the entire length of the ice stream, which is useful to ensure a large number of data-points, but any longitudinal variations may dilute the transverse pattern. Nonetheless, there is evidently a link between the drop in maximum elongation ratio at the lateral margins of the examined palaeo-ice streams and the drop in velocity observed in contemporary ice streams, which strongly suggests that the distribution of ice velocity was responsible for this pattern.

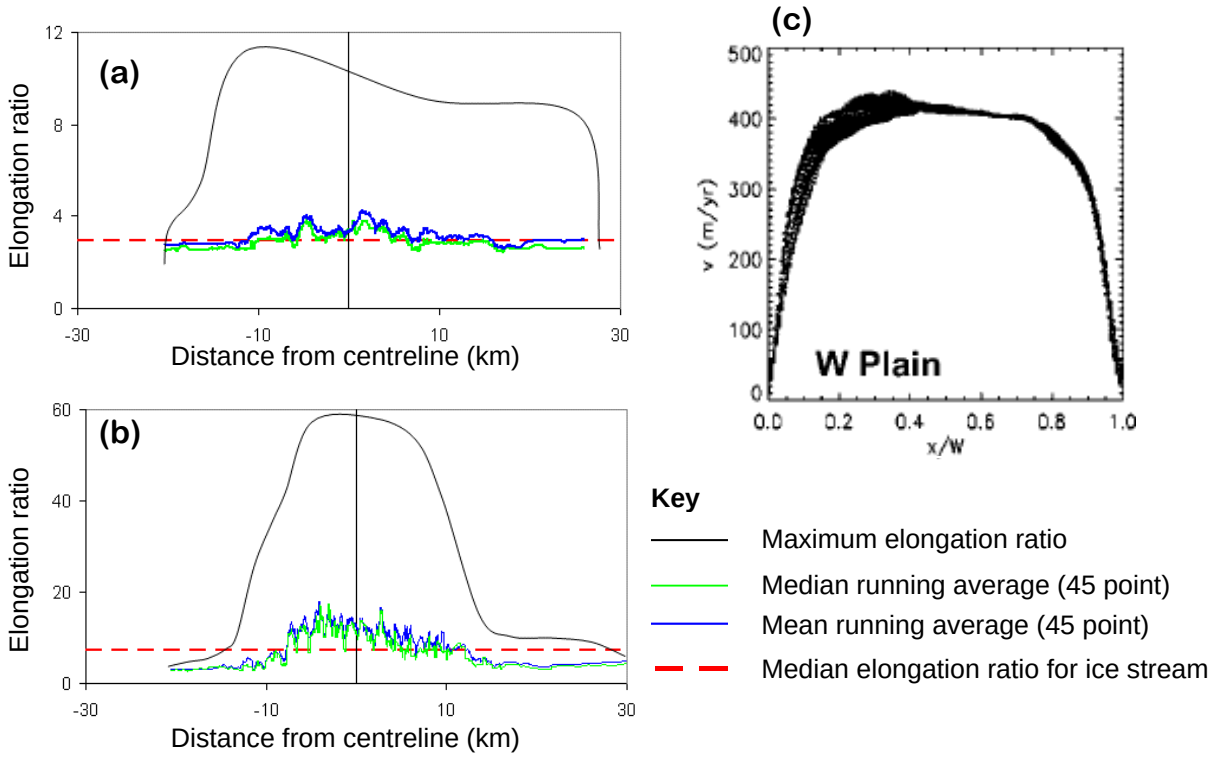

Figure 4.43 – Transverse distribution of average and maximum elongation ratio across (a) Transition Bay and (b) Haldane ice streams. (c) A typical transverse velocity transect across the main trunk of Whillans Ice Stream (from Joughin *et al*., 2002).

Longitudinal analyses from all the ice streams reveal that no overall trend is discernable, since both a downstream increase and a downstream decrease in maximum elongation ratio is seen. This may be because some of the ice stream signatures are only partial and in some cases they end at the coast, as illustrated in the figures depicting the assumed position of the ice streams (figures 4.5b, 4.15b, 4.23b, 4.29b, 4.36b). Additionally, many of the ice streams have areas with few subglacial lineations and this may affect the overall longitudinal trends. Transition Bay and Haldane ice streams have the most complete ice stream signatures, and these ice streams display an increase in elongation ratio at the ice stream onset (c. the first 10 km) and a decrease at the terminus (c. the last 10 km). This reflects the expected signature of ice streaming (Figure 4.2) and observations of the velocity distributions of contemporary ice streams, therefore is probably a reflection of the distribution of ice velocity.

Clustering of subglacial lineation elongation ratio was identified across all of the ice streams examined (Appendix A) and this can be effectively visualised in the interpolation maps (figures 4.6, 4.16, 4.25, 4.31 and 4.38). This observation indicates that the variable(s) controlling elongation ratio is uneven across the ice stream bed, and

varies over areas of sufficient size to contain several subglacial lineations. This pattern may be a result of variations in ice velocity, which would be consistent with studies of contemporary ice streams that indicate spatial variations in velocity (e.g. Whillans *et al*., 1987; Bindschadler and Scambos, 1991; Bindschadler *et al*., 1996; Joughin *et al*., 1999). Alternatively or additionally, clustering of elongation ratios may reflect variations in substrate strain rate or properties (e.g. Rattas and Piotrowski, 2003) or variations in basal conditions (e.g. Murray *et al*., 2008).

Another observation was the widespread presence of low elongation ratios, which was clear across the entire widths and lengths of all the ice streams examined, indicating that low elongation ratios are present even in regions of high ice velocity. This observation demonstrates that the distribution of elongation ratios across an ice stream bed is more complex than indicated in Figure 4.2. Velocity variations on a scale that would be manifest between adjacent subglacial lineations are not apparent in contemporary ice streams (e.g. Joughin *et al*., 2006). Therefore, it is evident that individual subglacial lineations do not necessarily reflect ice velocity, albeit a population of subglacial lineations may do. This indicates that average elongation ratio may not be the best indicator of ice velocity because this will be skewed by the pervasive presence of low elongation ratios, as also seen in Figure 4.43.

This finding may reflect the ongoing appearance of subglacial lineations over time within an ice stream, which then progressively elongate (i.e. a population of subglacial lineations do not form instantaneously). This explanation demands a formation mechanism for these bedforms that involves their initiation at a single point, followed by elongation under a sufficiently high ice velocity and flow duration (see Clark, 1993; Stokes and Clark, 2002a). This mechanism is consistent with the appearance of a drumlin at the bed of the Rutford Ice Stream, within a time span of seven years (Smith *et al*., 2007). Alternatively, the presence of subglacial lineations with low elongation ratios may represent variability in substrate strain rates, but the considerable variability of adjacent subglacial lineations found in all of the ice streams suggests that this is unlikely and no evidence for this is seen in the substrate and bedrock maps. Or this characteristic may reflect localised variability in ice stream processes, such as basal hydrology or bed decoupling. This may be possible and variations in hydrology and flow mechanism have been observed in contemporary ice streams over scales of several

kilometres (e.g. Smith, 1997; Vaughan *et al*., 2003; Murray *et al*., 2008). If correct this would imply that hydrological variability was pervasive across all of the ice streams examined. Despite the various possibilities, multiple factors probably contributed to the observed variabilities in elongation ratio in terms of both clustering and ubiquity of low elongation ratios. This is because it is apparent that neither the bed, nor ice velocity, nor basal processes are uniform across an ice stream; as indicated by this investigation and previous studies (e.g. Whillans *et al*., 1987; Bindschadler and Scambos, 1991; Joughin *et al*., 2006; Murray et al., 2008).

4.7.2 Spatial distribution and clustering of subglacial lineations

Heatmaps (figures 4.9, 4.17, 4.24, 4.32, 4.39) displaying the spatial distribution of subglacial lineations gave a useful insight into how these bedforms are distributed. All of the ice streams display considerable spatial variability in subglacial lineation density and appear clustered. The spatial variability appeared to be at a scale larger than the variations seen in elongation ratio, which is evident from comparing the heatmaps with the elongation ratio interpolation maps. The highest clustering of subglacial lineations appeared in different areas of the ice stream across all those examined, suggesting that different zones of the ice stream have equal chance of containing highly clustered subglacial lineations. This and the fact that highly clustered lineations are located right at the lateral margins of the Transition Bay Palaeo-Ice Stream (Figure 4.32) suggests that clustering of lineations is not affected by ice velocity variations within the ice stream.

Clusters of subglacial lineations may be seen as an area in which the conditions are most favourable to the formation of these bedforms. Comparing the maps of bedform clustering with those of elongation ratio revealed largely dissimilarities between these two characteristics and whilst at least one area with both high clustering and high elongation ratio can be identified in most of the ice streams, typically these areas do not match up. Additionally, comparing the median elongation ratio of subglacial lineations in the clusters over 10, with those from the entire ice stream did not show a consistent relationship and for some ice streams (e.g. Solway) median elongation ratio was higher within the clusters than the entire ice stream and for some (e.g. Haldane) median elongation ratio was lower in the clusters. This suggests that the areas in which

subglacial lineations most favourably occur are not the same as the areas in which these bedforms most favourably elongate. Following on from this it would be expected that subglacial lineation occurrence and density is determined by a different variable or variables than subglacial lineation elongation ratio.

The issue of bedform size has the potential to introduce bias and so should be considered when examining clustering. The significant of this is because analysis is based on how clustered the *centroids* of the subglacial lineations are and as such smaller subglacial lineations are more likely to appear clustered than larger subglacial lineations, because no consideration is taken of the areal extent of the bedform (Menzies, 1979). Typically bedform size is similar within an ice stream and greater differences are seen between ice streams, thus indicating that absolute clustering values should not be compared between ice streams. However, an exception to this is seen in the Crooked Lake Palaeo-Ice Stream in which large subglacial lineations are seen on the east side of the ice stream and considerably smaller subglacial lineations are seen on its west side. As such the pattern of clustering in this ice stream should be interpreted with caution.

4.7.3 Topography, bedrock geology and surficial sediments

Variations in topography, surficial sediments and bedrock geology were investigated in order to establish if these factors display any correlation with variations in subglacial lineations, and to see if any potential sticky spots can be identified. Topographic variations were found at all of the ice streams studied and some of these appeared to correlate with heterogeneities in subglacial lineations. The bed of the Forth Ice Stream has several upland areas including the Campsie Fells, Pentland Hills and Lomond Hills (Figure 4.15). These are characterised by few, if any, subglacial lineations and a deflection of subglacial lineations around them, which suggests that ice flow was retarded on and around these areas and that they acted as sticky spots. In Transition Bay and Haldane ice streams, increases in land elevation are seen midway down their lengths (figures 4.30 and 4.37). These are accompanied by decreases in the abundance of subglacial lineations, decreases in elongation ratios and increases in the abundance of meltwater channels, as compared to surrounding areas. Therefore, these localities could well represent topographic sticky spots (see Stokes *et al*., 2007). Assuming meltwater

channels at the Haldane and Transition Bay ice streams are subglacial rather than deglacial, this suggests that ice velocity slowed where bed elevation increased and that subglacial meltwater may have cut channels into the bed, carrying water up and over the topographic obstacle. Excessive meltwater may be generated from frictional heating at the bed, which may have a knock on effect on lubrication, thereby decreasing resistance. Further investigation would be useful to understand these processes and feedback mechanisms.

Curvature of the land surface (figures 4.10, 4.19, 4.27, 4.34 and 4.41) typically displayed a flat ice stream bed, which contrasted with some of the adjacent upland areas that displayed more convex topographies. The observed flat ice stream beds probably relates to the association between topography and ice stream location, which has been well documented (e.g. Payne, 1999; Winsborrow *et al*., 2010). Topographic high points in the Forth and Haldane ice streams appear more convex than the rest of the ice stream bed and hence it is a possibility that this convex topography may be a contributory factor to the lack of subglacial lineations in these localities. However, the widespread flat ice stream beds clearly cannot explain the majority of the observed variations in subglacial lineations.

Some variations in surficial sediments were apparent on the Solway and Forth ice streams. Till was the most common surficial sediment and for both of these ice streams the most clustered subglacial lineations were located in areas with a high till coverage (figures 4.11c and 4.20c). This correlation reinforces the understanding that till has an important role to play in formation of subglacial lineations (e.g. Boulton, 1987; Stokes *et al*., 2011) and indicates that subglacial lineations are more likely to form and cluster in areas of high till continuity. The large upland areas on the Forth Palaeo-Ice Stream (discussed above) are characterised by discontinuous till and this may well have contributed to the retardation of ice flow in these areas. Other, smaller till-free areas on the Solway and Forth ice streams typically did not coincide with a lack of subglacial lineations, a decrease in elongation ratio, or a deflection of subglacial lineations. This suggests these areas did not form till-free sticky spots. The presence of elongated subglacial lineations in these localities demonstrates that rapid flow continued over the areas that lacked till, and hence subglacial sliding may have operated in these areas.

Sedimentary bedrock was found at the beds of all of the ice streams and only the Forth ice stream had areas of igneous bedrock at its bed. In the upstream region of this ice stream, there are large regions of igneous bedrock, which have very few subglacial lineations and adjacent subglacial lineations clearly deflect around these areas, suggesting that they were persistent sticky spots. However, these areas also coincided with upland areas and discontinuous till cover (the Campsie, Pentland and Lomond hills; Figure 4.15), so it is uncertain whether one or a combination of these factors contributed to the slowing of ice flow in these areas. The range of lithologies at the beds of all the ice streams and in the areas of high bedform clustering means that this variable is difficult to assess and as such no clear correlations can be identified.

Bedrock permeability was examined for the Solway and Forth ice streams (figures 4.13 and 4.22) and this showed that both are characterised primarily by moderate permeabilities. Despite this, the areas of highly clustered subglacial lineations were mostly underlain by high and low permeabilities. Therefore, no clear trend between this variable and subglacial lineations emerges, although later analysis for the Tweed and Central Alberta ice streams may shed further light on this characteristic.

In summary, spatial variations in subglacial lineations were evident in terms of clustering and elongation ratio. Examination of these variations against bed variables revealed some trends, including low bedform clustering on topographic high points on the ice stream bed and a tendency for high bedform clustering to be located on continuous till cover. No clear trends were evident based on bedrock lithology and permeability.

4.8 Summary and concluding remarks

In this chapter, macroscale analysis has provided an overview of the geomorphology of five palaeo-ice streams and allowed detailed examination of subglacial lineations. All of the five ice streams examined displayed clear spatial variabilities in elongation ratio. Spatial autocorrelation established that a clustered pattern of elongation ratio was present in all of the ice streams examined, suggesting that this characteristic may be related to variability in basal processes, basal conditions and/or ice velocity across these

ice streams. Analysis of the transverse and longitudinal distribution of elongation ratio revealed some similarities to the idealised pattern of subglacial lineations (Figure 4.2), but these were usually subtle and sometimes not apparent at all. From this, the most common finding was that transversely, the highest elongation ratios were found towards the centre of the ice stream and so maximum elongation ratio dropped at the lateral margins. Also of note was that low elongation ratios were found throughout, even in areas of expected relative fast flow. This demonstrates the limitations of elongation ratio as a proxy for ice velocity. If ice velocity is assumed to be the main factor affecting elongation ratio, then the ubiquity of low elongation ratios, may reflect point initiation of subglacial lineations and staggered growth. If a population of lineations emerge gradually and progressively elongate over time if subject to sufficiently high velocities, then the population would be expected to have a considerable range of elongation ratios. Other possible explanations were considered for the observed spatial variabilities in elongation ratio, including the spatial variability of basal hydrology and flow mechanisms, which may also contribute. Comparison of transverse distribution of elongation ratio to the transverse distribution of velocity in contemporary ice streams indicates that maximum elongation ratio, rather than average elongation ratio is the most comparable.

Analysis of subglacial lineation distribution demonstrated that these bedforms are spread unevenly across all of the ice streams examined and display a clustered pattern. Clustering of subglacial lineations did not appear to be systematic and they did not display a preference for any one area of the ice stream. This suggests that this characteristic is unaffected by velocity variations within the ice stream.

A range of bed variables were examined and compared against subglacial lineations for each ice stream (where available). Topography was identified as a key characteristic affecting subglacial lineation distribution. All of the topographic obstacles on the ice stream beds coincided with relatively few subglacial lineations and low elongation ratios. Subglacial lineations downstream of obstacles were also relatively few and had low elongation ratios. Variability in surficial sediments was evident at the ice stream beds examined, but till was clearly the most widespread. In the areas of highly clustered subglacial lineations till was even more prevalent, indicating that its continuity is a contributory factor in the occurrence of dense subglacial lineations. Sedimentary

bedrock was widespread across all of the ice streams. However, more detailed examination of bedrock lithology revealed that it was particularly diverse across the ice stream beds and so very few trends between this variable and subglacial lineations could be identified. Examination of bedrock permeability revealed that moderate permeabilities were most common on the two ice streams where this data was available, but the analysis of this for areas of high bedform clustering did not reveal a clear trend. The Forth Palaeo-Ice Stream was notable for certain areas that had few subglacial lineations with low elongation ratios and a deflection of subglacial lineations around them. These areas were all upland areas with igneous bedrock and discontinuous till cover and so it is possible that a combination of factors caused them to be sticky spots within the ice stream.

5. The Tweed Ice Stream

5.1 Introduction

Our understanding of ice streams has been traditionally based on three broad scales of investigation, for both contemporary (e.g. Engelhardt and Kamb, 1997; Tulaczyk *et al*., 1998; Gades *et al*., 2000) and palaeo-ice streams (e.g. Clark and Stokes, 2001; Sejrup *et al*., 2003; Graham *et al*., 2009). Few studies have integrated different scales of analysis, which could be a significant limitation to our understanding of them. This chapter presents an investigation of the Tweed Ice Stream, in order to gain a comprehensive insight into ice stream processes using three spatial scales of analysis. This provides the first ice stream multiscale case study for the thesis, primarily addressing research question 2, and also research question 3, which is examined further in Chapter 7. Research question 2 is repeated as follows:

2. *What do the macro, meso and micro scale characteristics of two palaeo-ice streams reveal about their subglacial processes?*

The Tweed Palaeo-Ice Stream is located in the Tweed Valley, situated between the Lammermuir Hills and the Cheviot Hills, in the Borders region of Scotland (Figure 5.1). Most of the Tweed Valley is mantled by Devensian till, and it is underlain by Silurian (sandstone, siltstone and mudstone), Old Red Sandstone, Basaltic and Carboniferous (mudstones and siltstones) bedrock (British Geological Survey, 2007). The glacial imprint on the landscape is very apparent in the swarm of subglacial lineations that cover the valley. The Tweed Ice Stream drained the Southern Uplands, flowing NE, then curving round to the SE, towards the present day coastline (Figure 5.1). This chapter investigates the geomorphology across the ice stream; and the sedimentology and micromorphology at two sites: Blinkbonny Quarry and Newton Quarry, as shown in Figure 5.1.

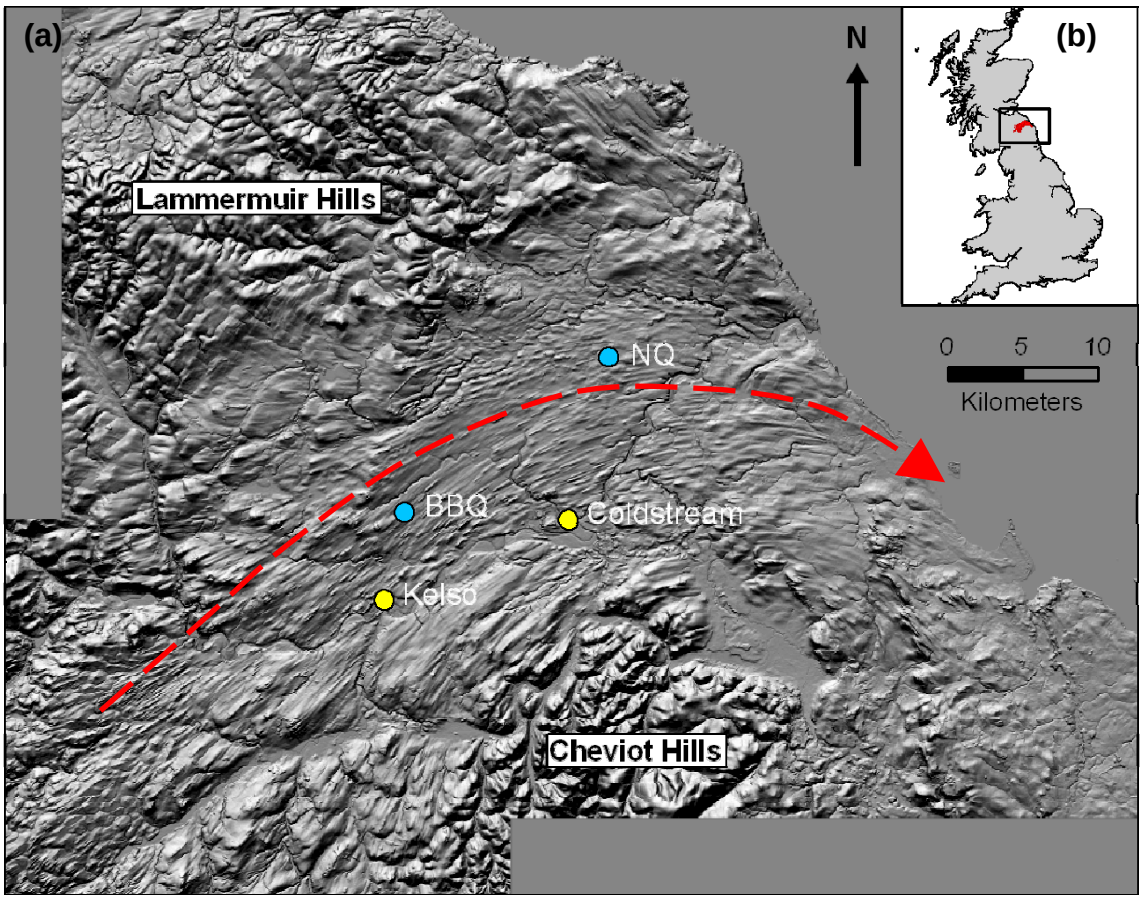

Figure 5.1 – (a) Nextmap DEM (vertical exaggeration is x4) of the Tweed Valley and surrounding area. The direction of the ice stream is marked with a red arrow, the flanking upland areas (the Lammermuir and Cheviot hills) are labelled, as are the towns of Kelso and Coldstream. The two study sites are labelled BBQ (Blinkbonny Quarry) and NQ (Newton Quarry). (b) Location map of the Tweed Palaeo-Ice Stream.

5.1.1 Previous research

Streaming of Quaternary ice through the Tweed Valley was noted by Kendall and Muff (1901) and Clapperton (1970a). Following this, Everest *et al*. (2005) identified several characteristics of the Tweed Valley glacial signature (including characteristic shape and dimensions, sharp lateral margins, elongated bedforms and evidence of deformed till), which led them to conclude that it is a palaeo-ice stream track (see Stokes and Clark, 1999).

The drumlin swarm in the Tweed Valley was mapped by Clapperton (1970a) (Figure 5.2) and later studied by Kerr (1978). Kerr (1978) observed that the most elongate drumlins are found in the centre and south side of the valley, and that there is a slight decrease in drumlin elongation downstream. He also measured clast macrofabrics in several drumlins and found that fabrics were typically orientated parallel with the

drumlin, and tended to point outwards (away from the drumlin) at the stoss end and inwards (into the drumlin) at the lee end. Kerr also noted that many of the drumlins had rocky outcrops on top and hypothesised that many of them could be rock cored.

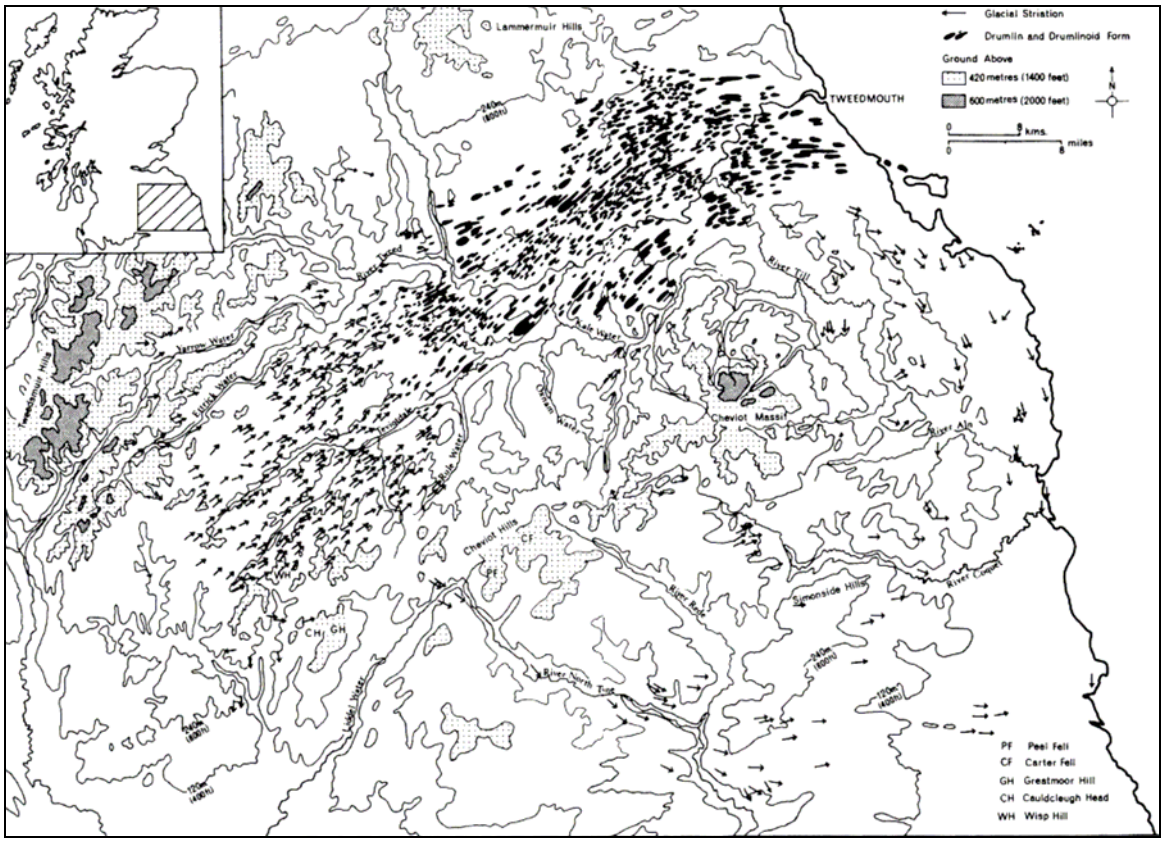

Figure 5.2 – Clapperton's (1970a) original mapping of drumlins (black polygons) and striations (arrows), in the Tweed Valley.

Meltwater channels are extensive in parts of the Cheviots and have been studied by several authors (Kendall and Muff, 1901; Common, 1954; Derbyshire, 1961; Price, 1960; Clapperton, 1968; 1970b). They are common below 300 m asl and are typically orientated east or south (Derbyshire, 1961). Most authors infer the channels to be subglacial and associated with ice sheet stagnation.

Till in the Tweed Valley has been studied extensively by Kerr (1978), particularly along a pipeline trench that runs obliquely across the valley (Figure 5.4). He described characteristic till profiles, which are associated with three different bedrock geologies, and these are shown and described in Figure 5.3. Stone counts across the valley (Kerr, 1978) showed that Silurian clasts, which originate from a wide area of Silurian sedimentary bedrock at the upstream end of the valley, are concentrated in the centre of the valley, suggestive of a Boothia type erratic train (see Dyke, 1988). Kerr identified erratic paths from several igneous intrusions and outcrops that are situated upstream in

the valley (Figure 5.4). The orientations of these are consistent with drumlin orientations, suggesting that till deposition and drumlin formation were contemporaneous.

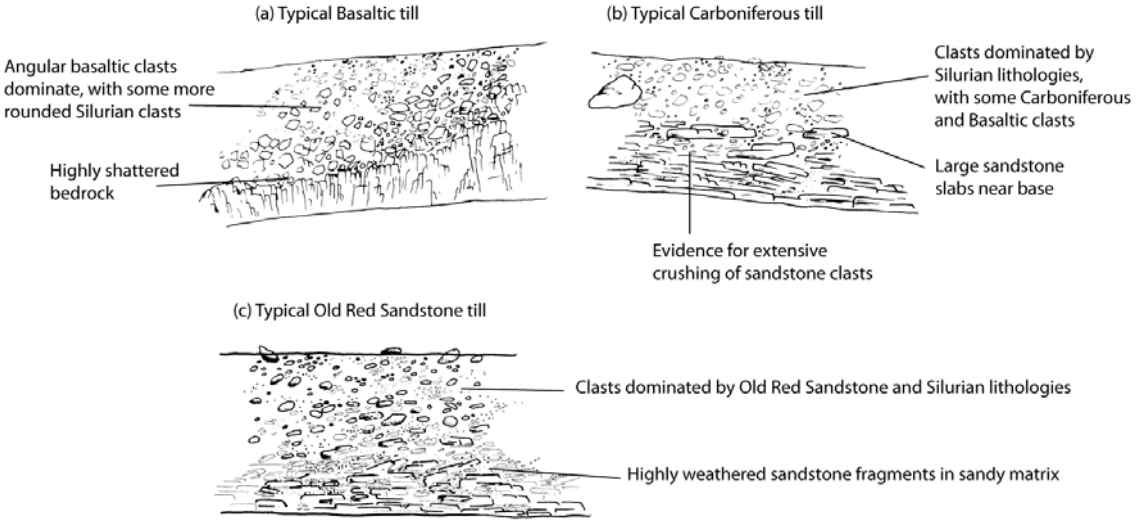

Figure 5.3 – Typical till profiles from the Tweed Valley, adapted from Kerr (1978). (a) Till overlying Basaltic bedrock, which is typically shallow (< 1 m deep) and dominated by angular local bedrock clasts. (b) Till overlying Carboniferous bedrock, which typically contains well rounded Silurian (approximately 80%) and Carboniferous (up to 30%) clasts; (c) Till overlying Old Red Sandstone bedrock, which was typically dominated by Old Red Sandstone (especially in shallow tills) and Silurian clasts.

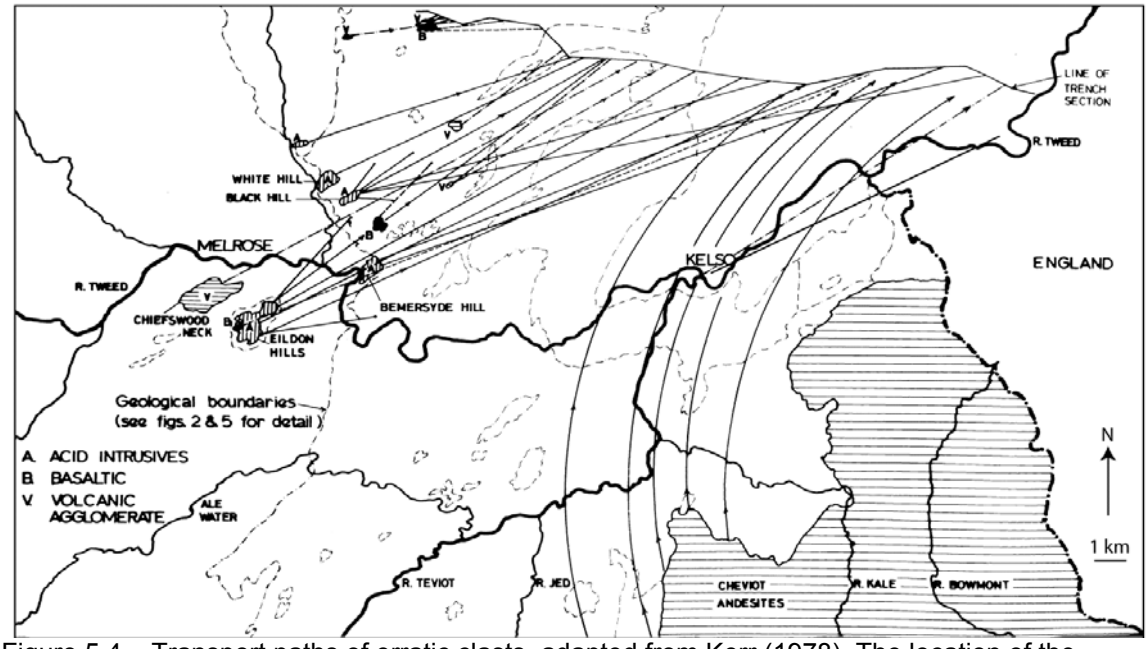

Figure 5.4 – Transport paths of erratic clasts, adapted from Kerr (1978). The location of the pipeline trench runs across the top of the image and it was from this that Kerr conducted many of his analyses.

Fluvioglacial deposits have been found in the Tweed Valley by Gregory (1915), Derbyshire (1961) and Kerr (1978). Kerr (1978) identified surface and sub-surface fluvioglacial deposits, which typically consisted of crudely stratified gravels and sands.

Previous research on the glacial geomorphology and sedimentology in the Tweed Valley provides a useful starting point for this study. It provides clear evidence that there was an ice stream in this location and provides insights into some of the glacial landforms, deposits and processes, which will provide an important context. The unique contribution of this study is to understand processes at the ice stream bed, at three spatial scales of analysis. The results and interpretation of each are presented in turn, followed by an overall interpretation and summary.

5.2 Geomorphology

Geomorphology of the Tweed Valley was mapped using a Nextmap DEM, alongside satellite imagery (including Google Maps, Bing Maps and Gazetteer for Scotland) and ground truthing. Mapping is presented in Figure 5.5 and more detailed descriptions of the landforms are given in the subsequent sections. The subglacial lineations are looked at in further detail and compared to bed variables including topography, surficial sediments, bedrock lithology and bedrock permeability.

(a)

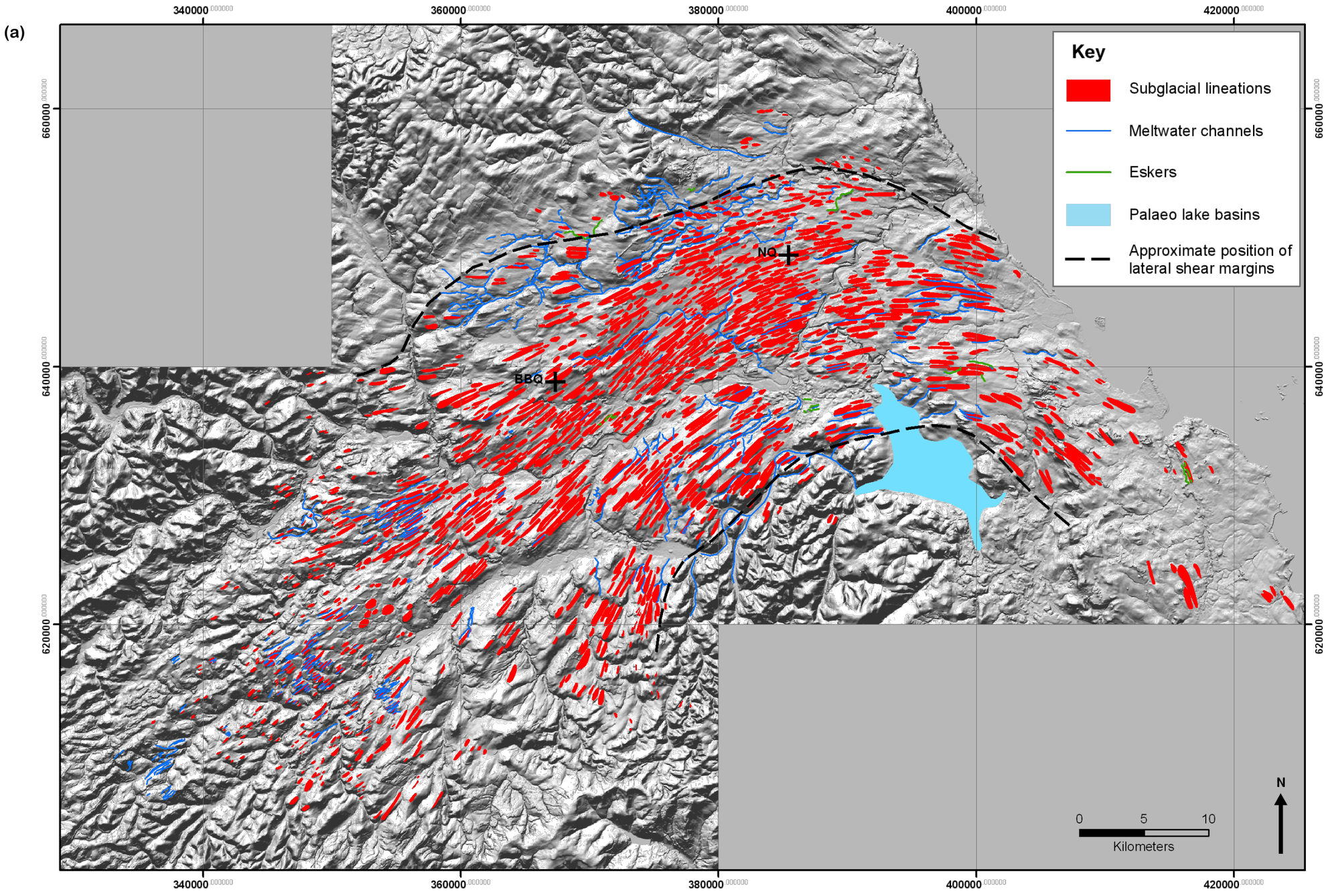

(b)

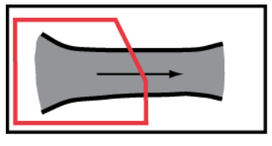

Figure 5.5 – (a) Tweed Palaeo-Ice Stream geomorphology map overlying a Nextmap DEM (vertical exaggeration is x4). (b) Approximate position of the Tweed ice stream signature (red rectangle), within an idealised ice stream.

5.2.1 Subglacial lineations

The subglacial lineations in the Tweed Palaeo-Ice Stream form a coherent flow-set, with a high degree of localised parallel conformity and a large bend (Figure 5.5). Subglacial lineations are convergent at the upstream end of the ice stream and at some areas along the lateral margins. They are highly concentrated at the centre of the flow-set and smaller and sparser at the upstream end of the ice stream. The 1575 subglacial lineations mapped across the ice stream range from 0.008 to 1.7 km^2 in area (median of 0.18 km^2) and from 1.3 to 14.5 in elongation ratio (median of 3.6), which is similar to the ranges of areas and elongation ratios of the ice streams presented in Chapter 4.

Spatial characteristics of subglacial lineation elongation ratio are presented in figures 5.6 and 5.12. Typically, elongation ratios are highest towards the centre of the ice stream, whilst the peripheries of the ice stream typically have lower elongation ratios. Clusters of high and low elongation ratios can be seen in Figure 5.6. This is confirmed by spatial autocorrelation analysis, which identifies clustering of elongation ratios to a confidence level of 99 % (Appendix A).

The transverse and longitudinal distributions of subglacial lineation elongation ratio are presented in Figure 5.8. Transversely across the ice stream, the highest elongation ratios are concentrated in the centre and they are also higher on the north side of the ice stream, which corresponds to the outside of the bend. Longitudinally, elongation ratios peak midway down the ice stream (30 to 60 km downstream). A sharp increase in the upper limit of elongation ratios can be seen at the upstream end of the ice stream (0 to 10 km downstream), and a gradual decrease in this upper limit is evident at the downstream end of the ice stream (60 to 110 km downstream), which is similar to the expected pattern of elongation ratios across an idealised palaeo-ice stream (Figure 4.2).

Clusters of subglacial lineations can be seen across the ice stream bed (Figure 5.7). This figure shows that these bedforms are closely spaced across many of the central regions of the ice stream and also at its far upstream end.

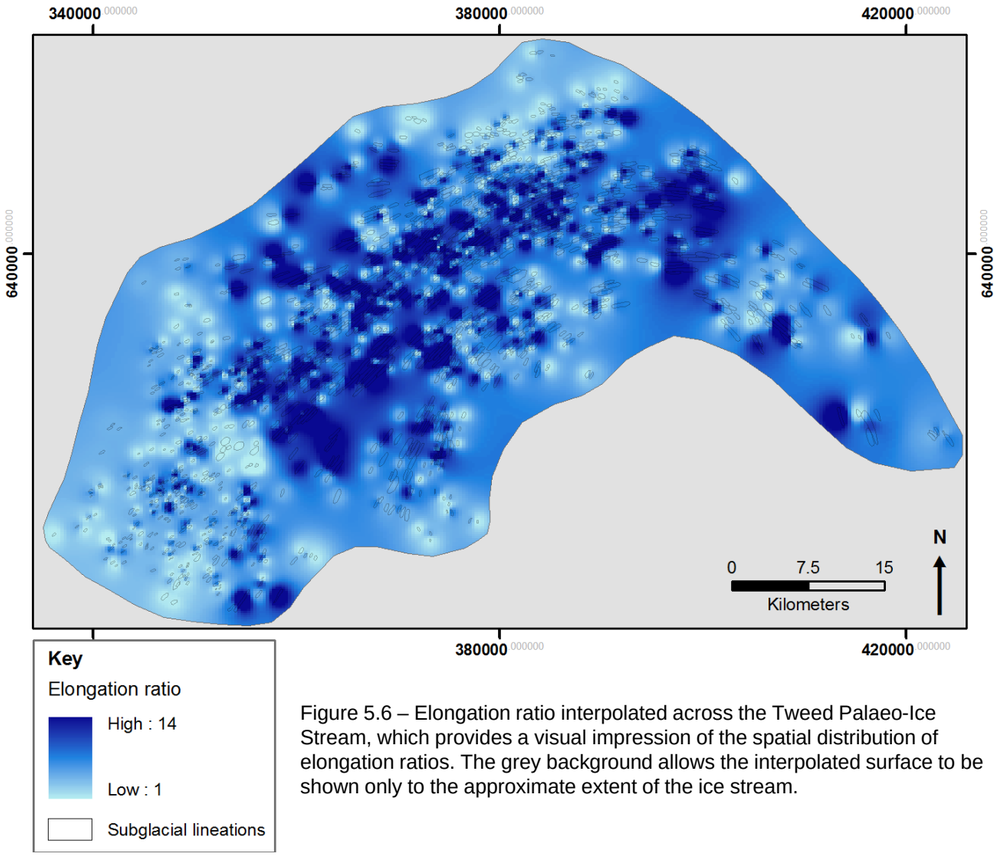

Figure 5.6 – Elongation ratio interpolated across the Tweed Palaeo-Ice Stream, which provides a visual impression of the spatial distribution of elongation ratios. The grey background allows the interpolated surface to be shown only to the approximate extent of the ice stream.

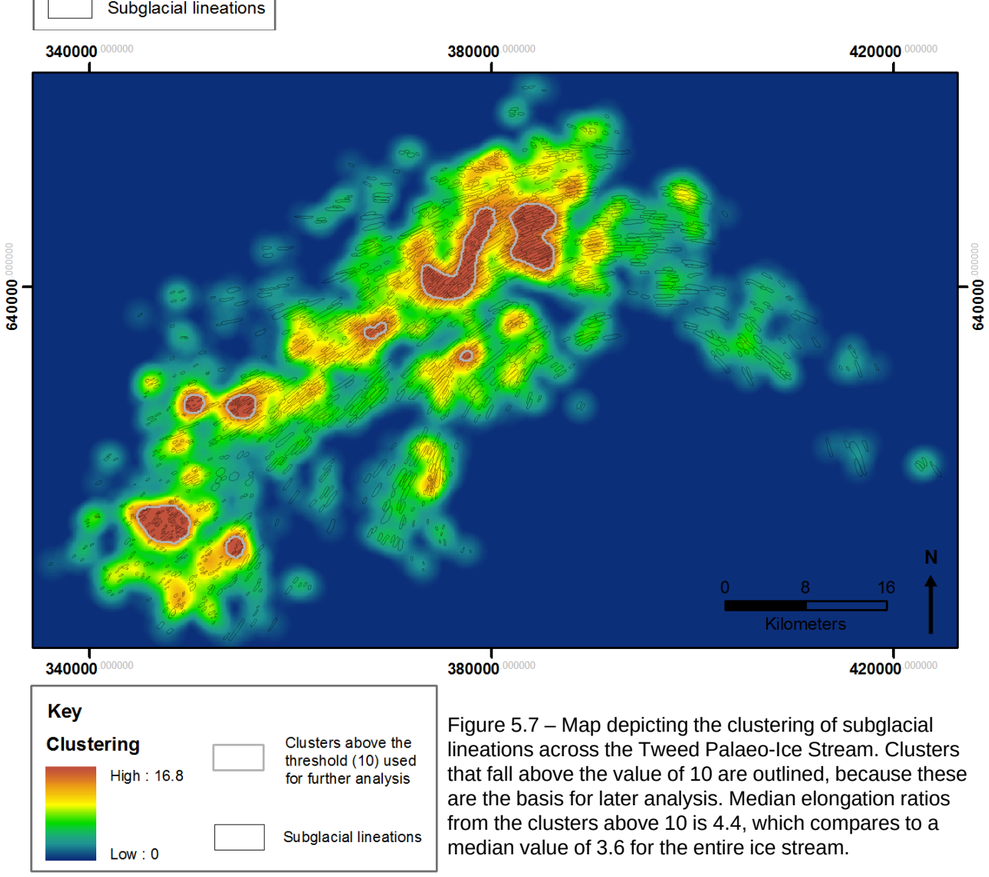

Figure 5.7 – Map depicting the clustering of subglacial lineations across the Tweed Palaeo-Ice Stream. Clusters that fall above the value of 10 are outlined, because these are the basis for later analysis. Median elongation ratios from the clusters above 10 is 4.4, which compares to a median value of 3.6 for the entire ice stream.

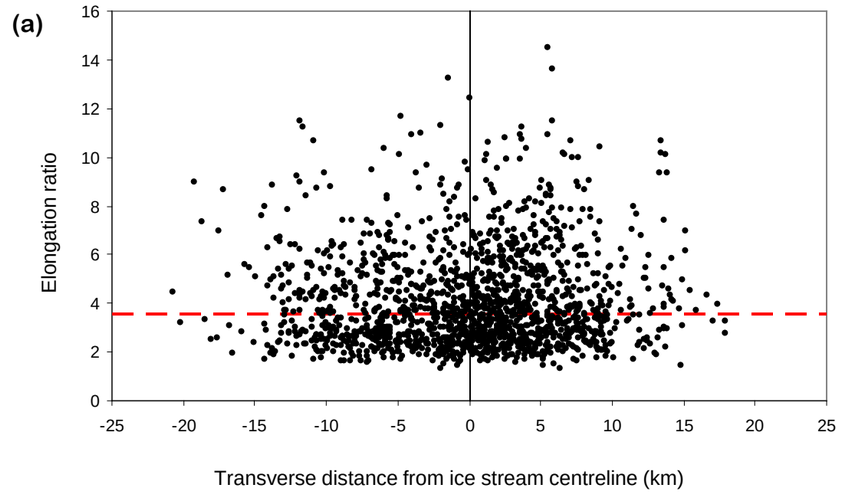

Figure 5.8 – Transverse and longitudinal trends in subglacial lineation elongation ratio. (a) Elongation ratio plotted against distance from the ice stream centreline (black vertical line). Distance from centreline is on the x axis, positive values represent north of the centreline and negative values represent south of the centreline. (b) Elongation ratio plotted against distance along the ice stream. Median elongation ratio is marked with red dashed lines.

5.2.2 Meltwater features

Meltwater channels are widespread across the Tweed Valley (Figure 5.5) and are particularly common at the lateral margins and the upstream end of the ice stream. Many channels are parallel or sub-parallel to the former ice stream trajectory, a trend observed in other palaeo-ice streams (e.g. Lowe and Anderson, 2003). Meltwater channels in certain regions of the ice stream can be grouped together according to their characteristics. These include: valley-side meltwater channels, upstream meltwater channels (i.e. located in the upstream region of the ice stream) and a large meltwater channel at the southern side of the valley.

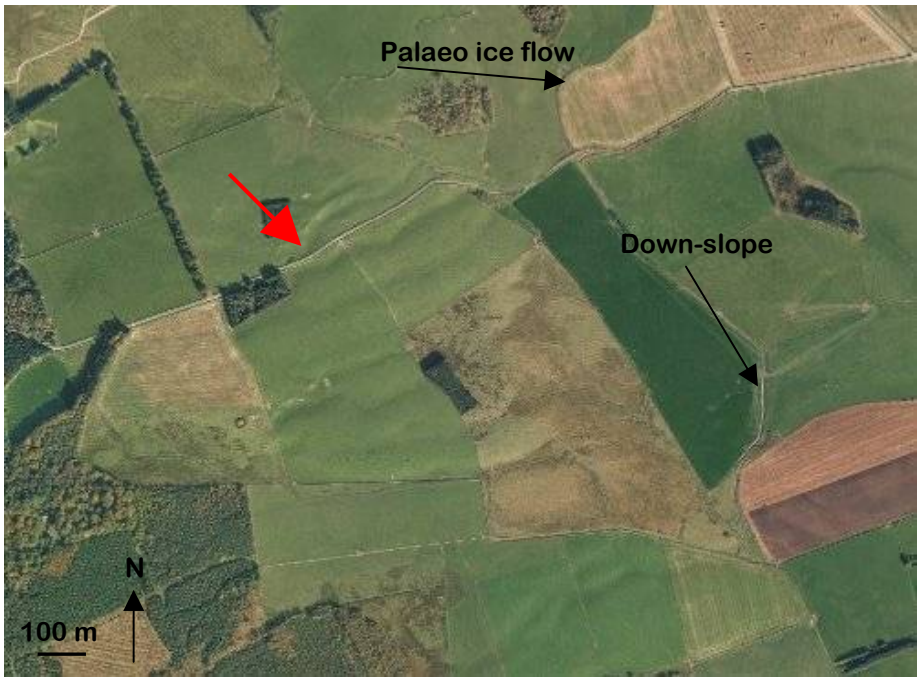

Figure 5.9 - Meltwater channels near the northern margin of the ice stream (361000 650000/NT6150). One of the several meltwater channels present is indicated with a red arrow. Channels trend approximately east to west, with abrupt starts and stops. Image is an aerial photo from Gazetteer for Scotland.

A large population of meltwater channels are cut into the valley sides, towards the lateral extent of the subglacial lineation flow-set. Channels typically traverse the slope and are parallel or sub-parallel to the ice stream trajectory (e.g. Figure 5.9). Channels range from 10 to 20 m wide, 0.2 to 5 km long and 1 to 8 m deep and usually have relatively steep sides. Some connectivity between channels is evident, but many channels are isolated. The size and form of the channel may vary along its length and some channels terminate at topographic depressions. Small meanders can be seen in many channels, as shown in Figure 5.9. Comparison with surficial geology and bedrock permeability maps shows that these channels spatially coincide with areas of both till and glaciofluvial deposits, and are situated on moderate and high bedrock permeabilities (British Geological Survey, 1977; Figure 5.16d). Where the valley side channels are near subglacial lineations they are usually located around them and in-between them. In very few cases the meltwater channels can be seen to cross-cut the subglacial lineations.

Meltwater channels at the upstream end of the ice stream typically occur in clusters, parallel and sub-parallel to each other and the direction of ice streaming (Figure 5.5). They are typically associated with subglacial lineations, where they may be located in-between them. Notably they do not cross cut any subglacial lineations. Often they appear in dense networks of channels, which are relatively straight and of similar length (ranging from 100 to 900 m) (Figure 5.10). These channels appear to be deeper (approximately 5 to 30 m deep) and considerably more defined in the landscape than the valley-side channels. Many are located on the crests and stoss sides of hills (e.g. Figure 5.10). Some of these channels route over the top of these hills and correspondingly have undulating long profiles, which is a key characteristic of subglacial meltwater channels (Sissons, 1960). Comparison with surficial geology maps reveals that many of these channels are located on bedrock or discontinuous till. They are predominantly situated on Silurian bedrock (Gala and Hawick groups), which comprise thin to medium bedded siltstones, mudstones and sandstones (Figure 5.15). In some cases, the extent of a cluster of meltwater channels coincides with a lithological boundary between Silurian bedrock and the coarser grained Old Red Sandstone (Stratheden and Inverclyde groups), which corresponds to a change in bedrock permeability (Figure 5.16d).

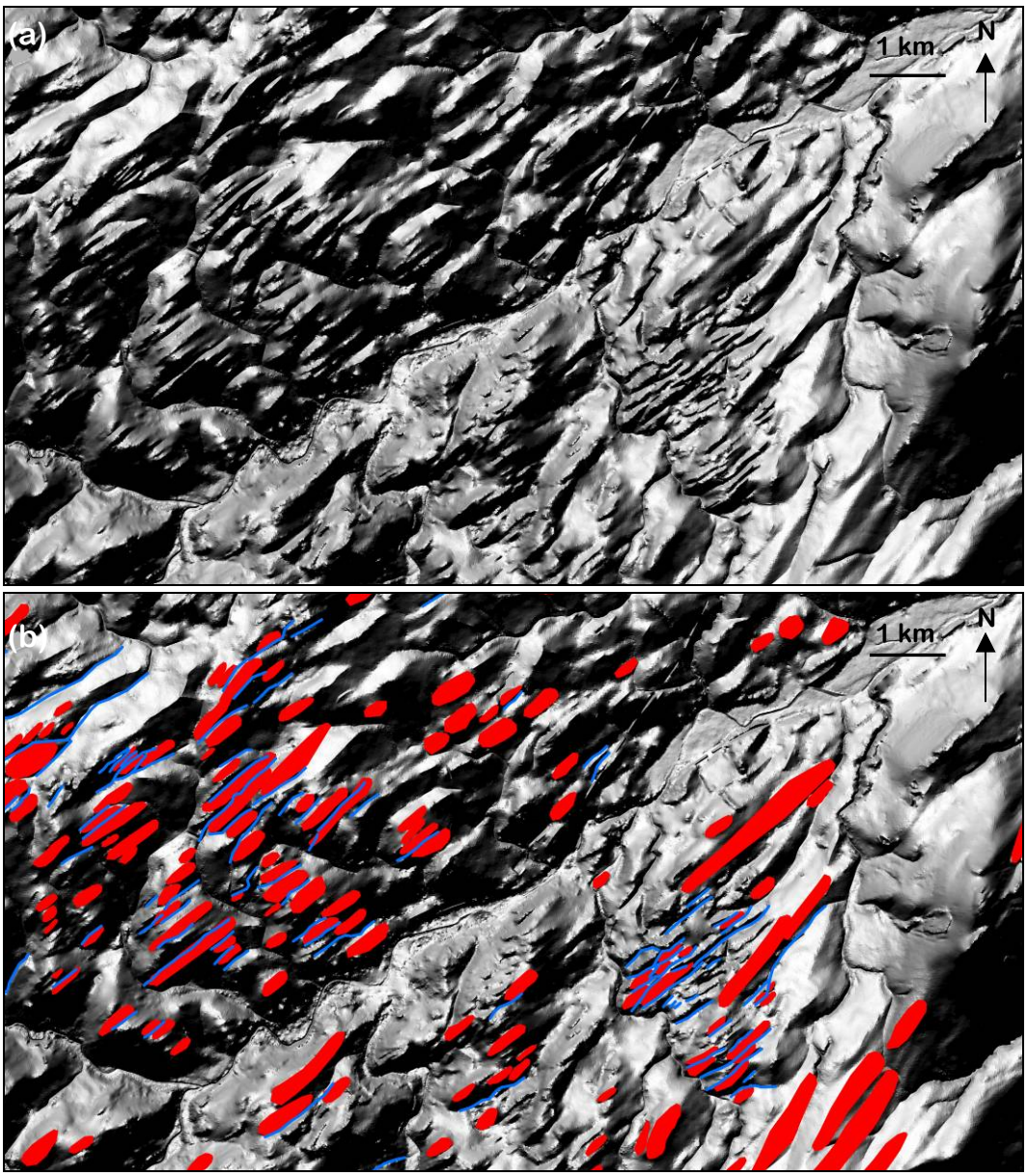

Figure 5.10 – Meltwater channels that are characteristic of the upstream end of the ice stream (345000,615000/NT4515). (a) Unannotated DEM of upstream meltwater channels; (b) DEM and geomorphological mapping, red polygons are drumlins and blue lines are meltwater channels. Note the clustering of the meltwater channels and that many are situated on the crests and stoss sides of small hills. Nextmap DEM has a vertical exaggeration of x20.

On the southern side of the Tweed Valley is a large meltwater channel and associated tributaries, (figures 5.5 and 5.11), which coincide with the lateral extent of the ice stream. Figure 5.11 illustrates the marked difference between the streamlined terrain north of this channel and non-streamlined terrain south of the channel. The channel is 300 to 800 m wide, up to 23 km long, and on average 70 m deep, and has certain characteristic features of a subglacial meltwater channel, including steep sides, an undulating long profile (Figure 5.11c) and a range of sizes and forms within the same connected system (Sissons, 1960; Bennett and Glasser, 1996). It is situated on the Cheviot Volcanic Formation, which is comprised primarily of andesitic lava. The area around the channel is characterised by a lack of surficial sediments (Figure 5.14), apart from the Quaternary deposits at the channel base, which include alluvium and glaciofluvial sands and gravels (British Geological Survey, 1977). This demonstrates that the channel is not cut into Quaternary sediments and instead is presumably cut into bedrock.

This large channel terminates in a large, flat, low-lying (30 to 40 m asl) basin, which is shown in figures 5.5 and 5.13. Previous work has established that this was a palaeo lake basin, interpreted as a former ice dammed lake that developed during deglaciation (Clapperton, 1970a; Evans *et al*., 2005). The lake basin is situated on the inside edge of the bend in the ice stream, and appears to straddle the ice stream lateral margin.

Few eskers were identified in the Tweed Valley (Figure 5.5). They are located individually or in small clusters, typically near the valley sides. They range from 0.6 to 2 km in length, 30 to 200 m in width and 5 to 35 m in height. One of the eskers is linked to a meltwater channel, whereby it continues directly downstream from the end of the channel.

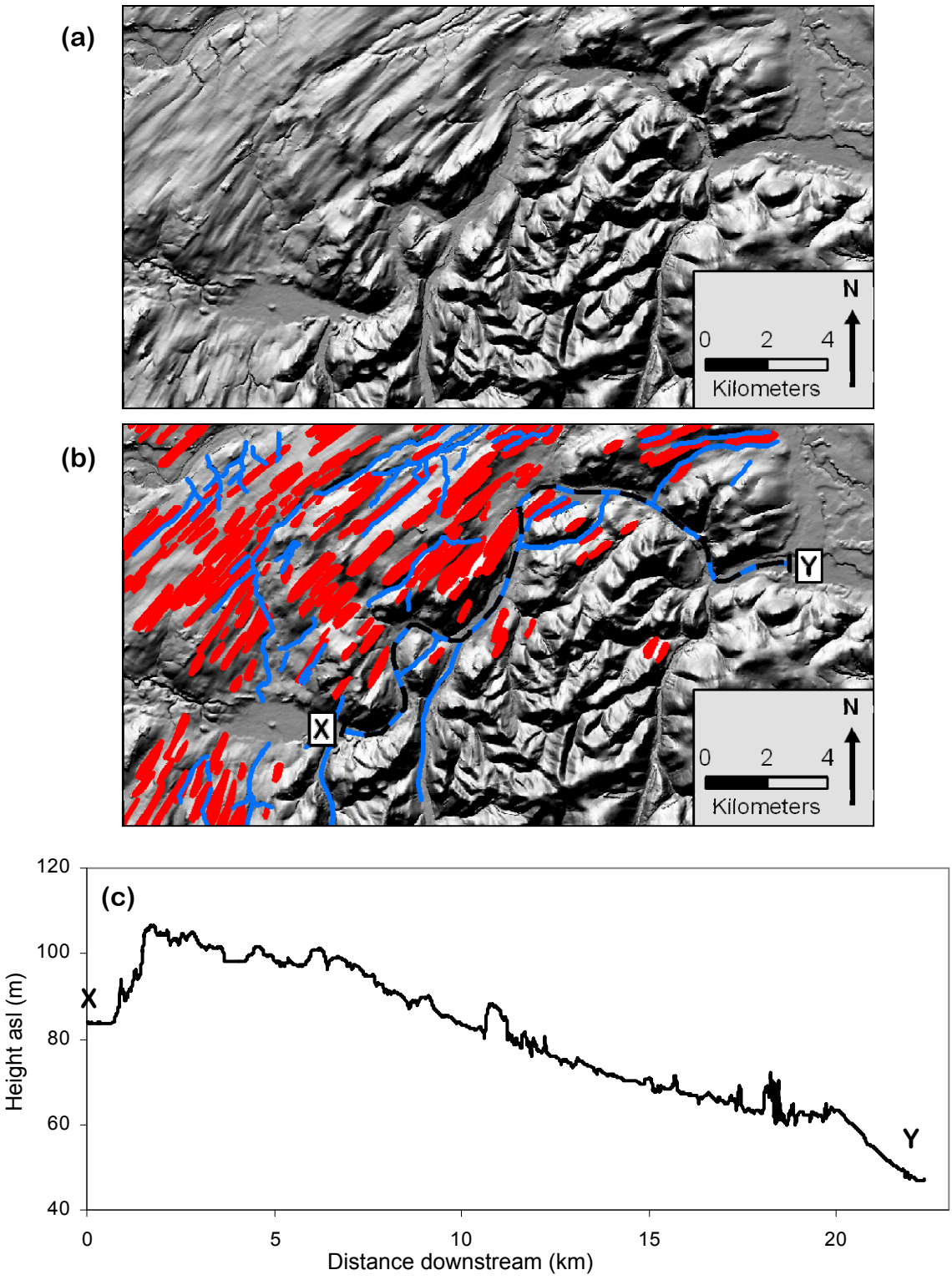

Figure 5.11 – Large meltwater channel at the southern lateral margin of the ice stream. Channels trend from bottom left to the top right of the map. (a) Unannotated Nextmap DEM of the area; (b) Nextmap DEM overlain with geomorphological mapping, red polygons are subglacial lineations and blue lines are meltwater channels. Black dashed line (X to Y) marks the position of the channel long profile shown in (c). (c) Long profile of the main channel, X to Y. Nextmap DEM has a vertical exaggeration of x20.

5.2.3 Topography, surficial sediments and bedrock geology

Potential controls on the ice stream geomorphology were examined, including topography, till continuity and bedrock geology; all of which may play a role in ice flow variability as well as bedform formation, location and extent (e.g. Clark and Walder, 1994; Bell *et al*., 1998; Rattas and Piotrowski, 2003; Stokes *et al*., 2007; Winsborrow *et al*., 2010; Phillips *et al*., 2010).

Topographically, the Tweed Palaeo-Ice Stream is situated in a valley. But the ice stream extent was not wholly contained within it, because at the southern lateral margin of the ice stream, the bedforms clearly encroach onto the flanks of the Cheviots, which are higher than the adjacent valley by approximately 150 m. Smaller scale topographic variations can be seen at the valley floor. The upstream end of the ice stream is relatively rough (range of relief between 140 and 350 m asl is typical) and characterised by small hills, which contrasts with the flat and smooth topography seen at the downstream end of the ice stream (range of relief between 40 and 100 m asl is typical) (Figure 5.13). Topographic curvature shows that the bed of the ice stream is largely flat, with some small variability across most of the bed except the far upstream end of the ice stream (Figure 5.12). This upstream area has a slightly rougher topography than the rest of the ice stream bed (Figure 5.13) and this is also seen in the curvature, in a greater range of values between convexity and concavity. Topographic curvature also displays variability at the southern lateral margin of the ice stream where the land surface rises towards the Cheviots.

The surficial geology map of the Tweed Valley (Figure 5.14) shows that till is widespread across the valley, which contrasts with adjacent upland areas that are relatively till-free. Figure 5.14c shows that till is even more prevalent in the clusters above 10 (see Figure 5.7), which is the same trend that was seen in the Solway and Forth ice streams (Chapter 4). Some till-free areas can be seen in the valley, which range from 0.2 to 45 km^2 in area. They do not appear to correlate with a lack of, or a divergence of subglacial lineations, which is similar to the observations at the Solway Ice Stream (Section 4.2).

Examination of bedrock lithology (Figure 5.15) reveals that the ice stream is located across a range of lithologies and several of these are present across significant areas of the bed. Most of the ice stream is underlain by sedimentary bedrock, apart from a strip of basalt and spilite that crosses the centre of the ice stream. The continuity and elongation ratio of subglacial lineations do not appear to be significantly affected by this strip of igneous bedrock. The subglacial lineations overlying the Llandovery bedrock at the upstream end of the ice stream appear to be significantly smaller and less elongated than other areas of the ice stream. These bedforms also appear to be highly clustered here, and this clustering drops directly downstream on the Old Red Sandstone. The bedrock underlying the high clustered areas of subglacial lineations is also shown in Figure 5.15c, which indicates that Carboniferous Limestone is the most prominent followed by Llandovery bedrock.

Bedrock permeability is presented in Figure 5.16, which shows that a range of permeabilities are present across the ice stream bed, the most common of which are moderate and low permeabilities. The areas of high bedform clustering display a clear preference for moderate and low permeabilities (Figure 5.16c). The Llandovery bedrock at the upstream end of the ice stream has a low permeability, which contrasts with the downstream Old Red Sandstone that has a high permeability. As noted this transition appears to coincide with a change in subglacial lineation size, elongation ratio and clustering. Furthermore, Figure 5.16d shows that the upstream meltwater channels (described in Section 5.2.2) are preferentially located on the low permeability Llandovery bedrock and do not encroach onto the highly permeable Old Red Sandstone. The large meltwater channel at the southern lateral extent of the ice stream displays a similar pattern as it is located on low permeability bedrock and at each end, its termini coincide with boundaries to high and moderate permeability bedrock. At these points the channel opens up into basins (see figures 5.5 and 5.15). However, across the ice stream bed as a whole the meltwater channels are located on permeabilities from low to high and do not appear to display a preference for any one of these. Figure 5.16d does show that the meltwater channels on different permeabilities and in different areas of the ice stream have different characteristics.

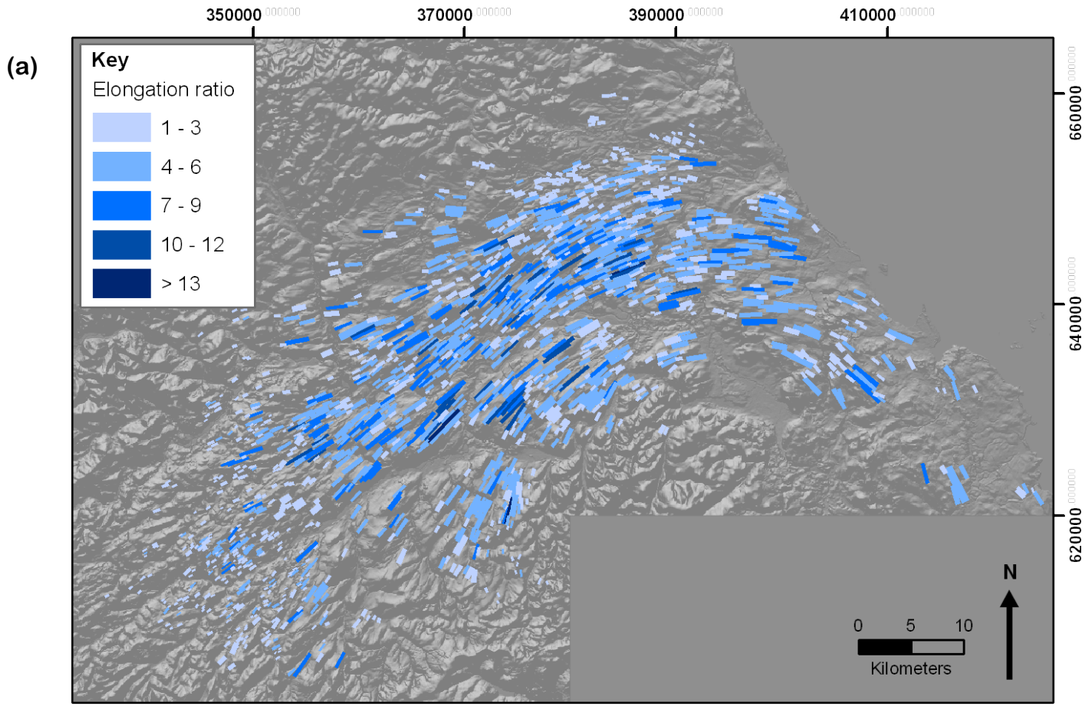

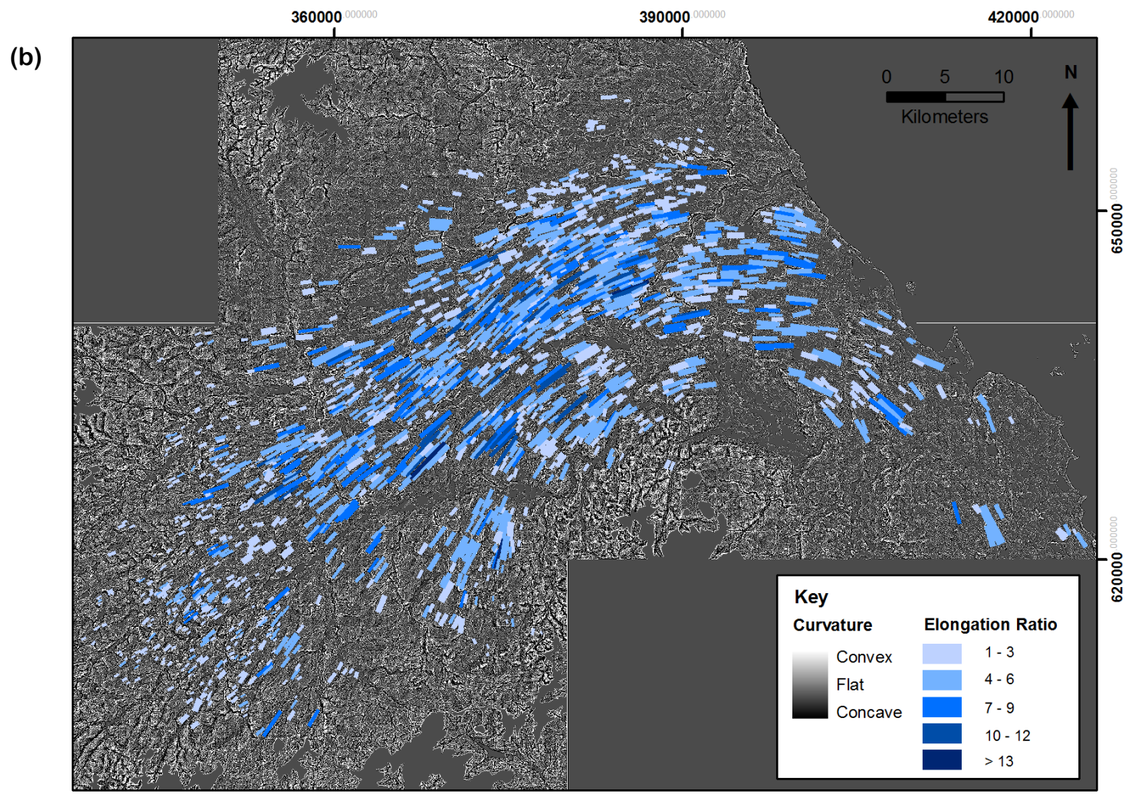

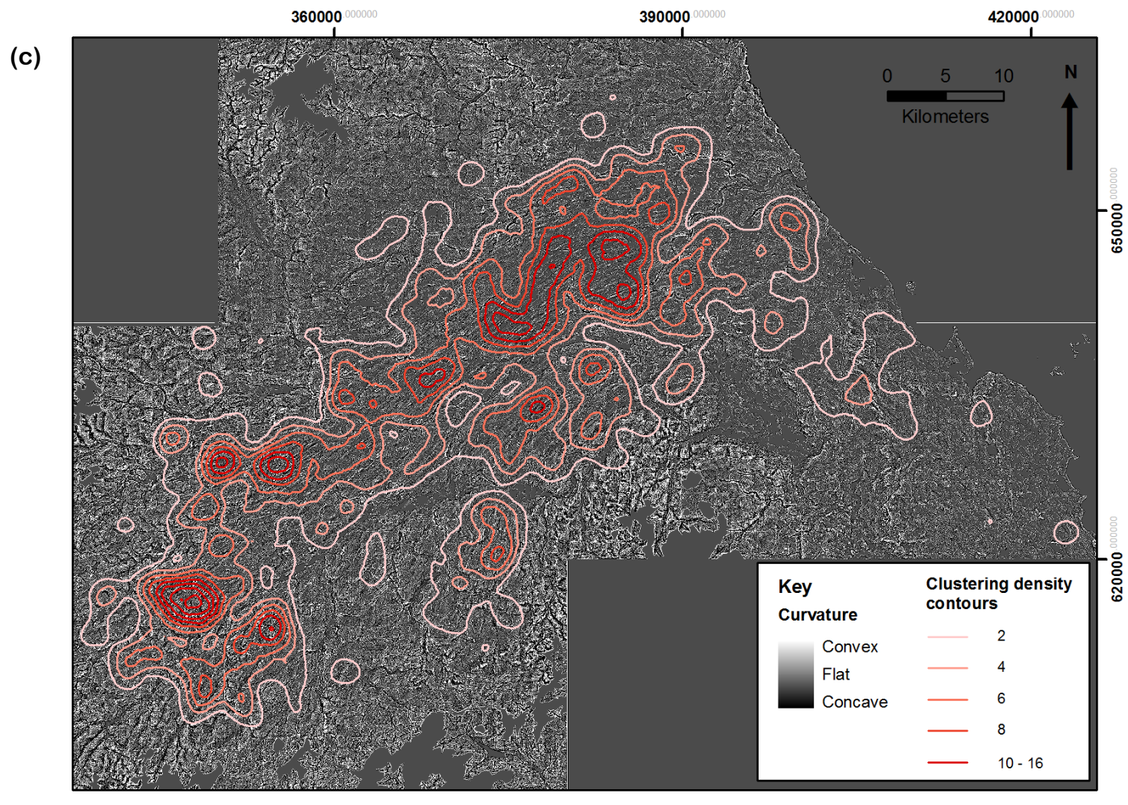

Figure 5.12 – Topography across the Tweed Palaeo-Ice Stream. Data derived from Nextmap DEM. (a) DEM with a vertical exaggeration of x4 overlain by subglacial lineations shaded according to elongation ratio. (b) Curvature map overlain by subglacial lineations shaded according to elongation ratio. (b) Curvature map overlain by contours of subglacial lineation clustering (derived from the data presented in Figure 5.7).

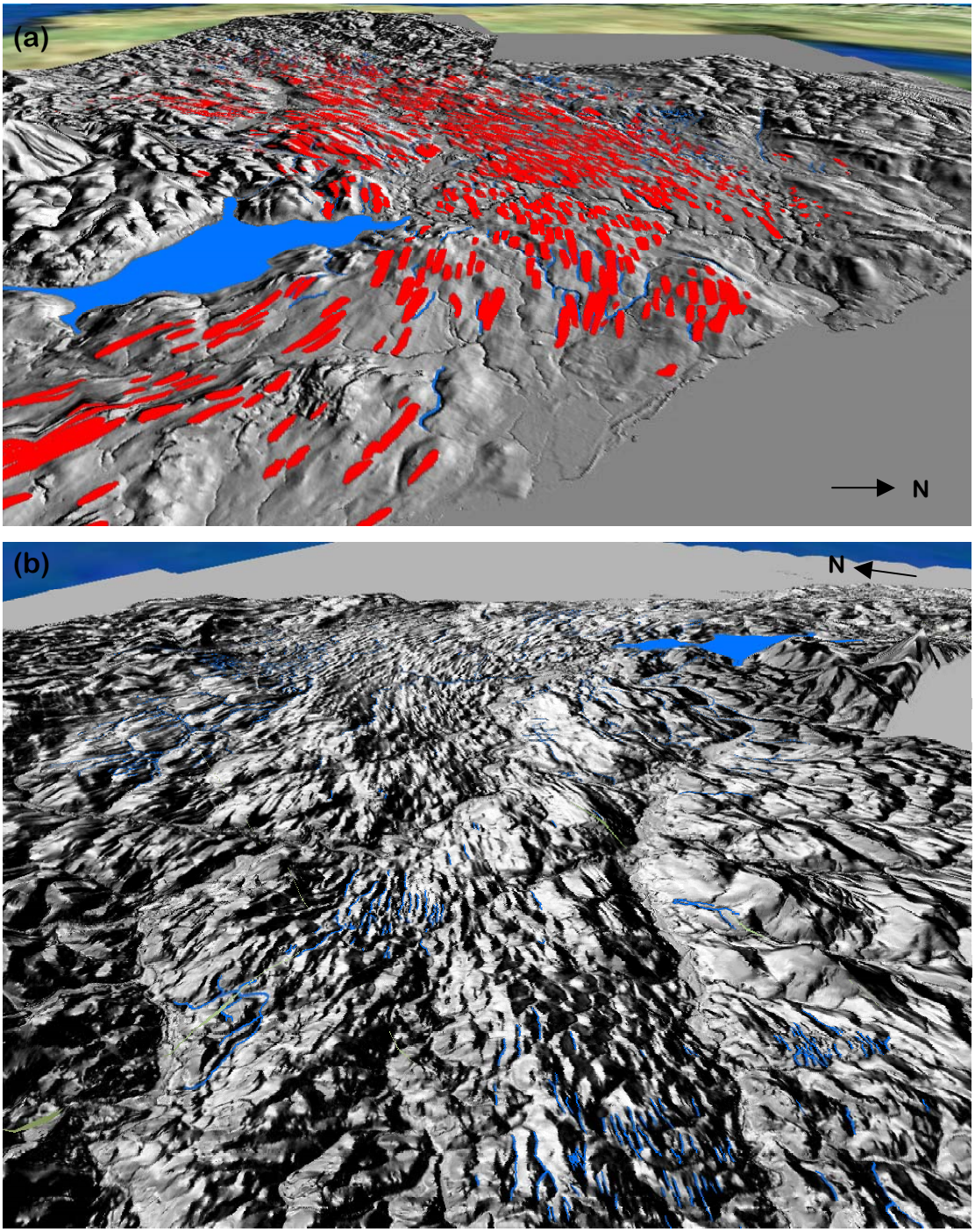

Figure 5.13 – 3D DEM images of the Tweed Palaeo-Ice Stream. (a) Offshore view looking upstream along the ice stream (grey foreground is the sea); and (b) View from the upstream end of the ice stream looking downstream (grey and blue in the background is the sea). Subglacial lineations are red polygons, meltwater channels are blue lines and the palaeo lake basin is a blue polygon. Subglacial lineations are not shown in image (b) in order to show the land surface more clearly. Nextmap DEMs have vertical exaggerations of x5.

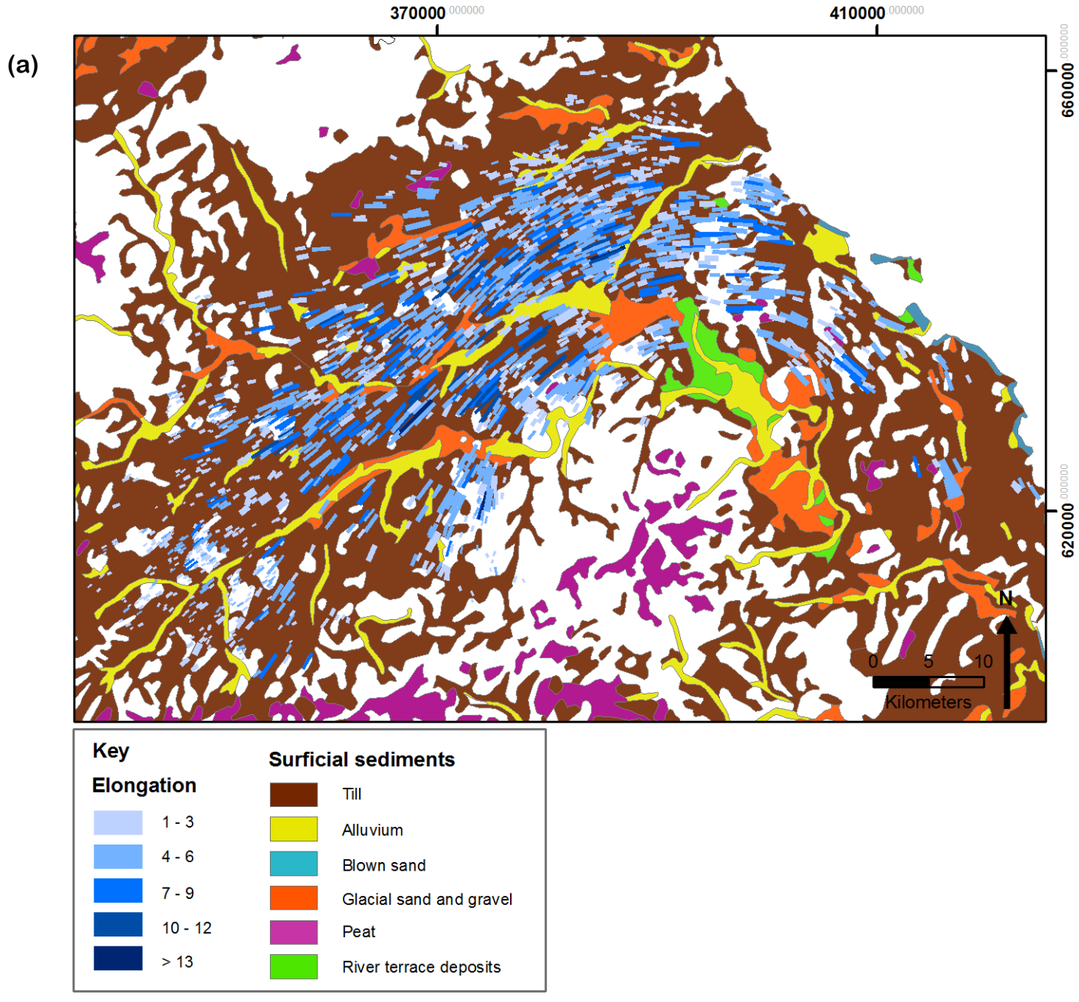

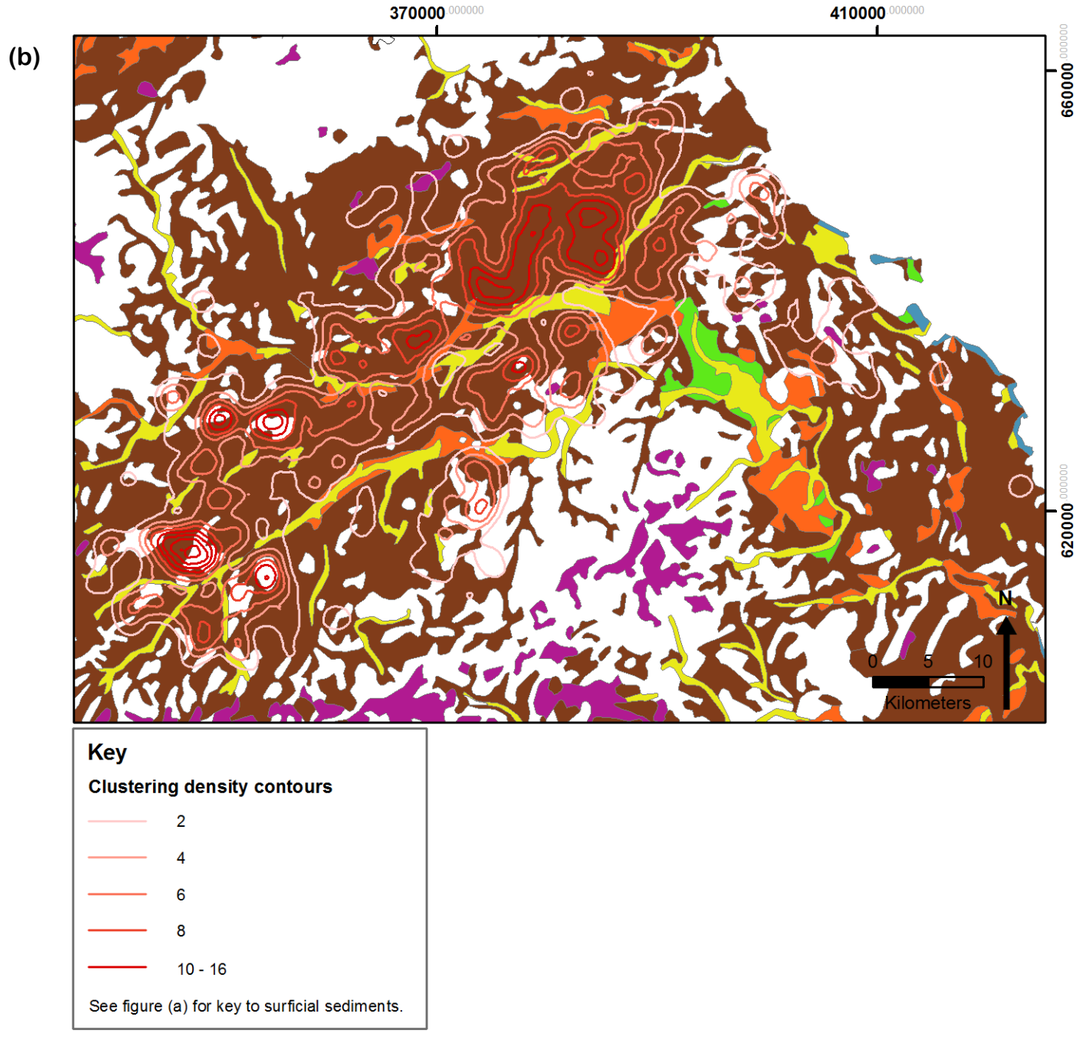

Figure 5.14 – Surficial sediments across the Tweed Palaeo-Ice Stream. Quaternary geology data from British Geological Survey (1977). (a) Surficial sediment map overlain by subglacial lineations shaded according to elongation ratio. (b) Surficial sediment map overlain by contours of subglacial lineation clustering (derived from the data presented in Figure 5.7). (c) Bar chart displaying the percentage coverage of surficial sediments across the whole ice stream and within the cluster areas identified in Figure 5.7.

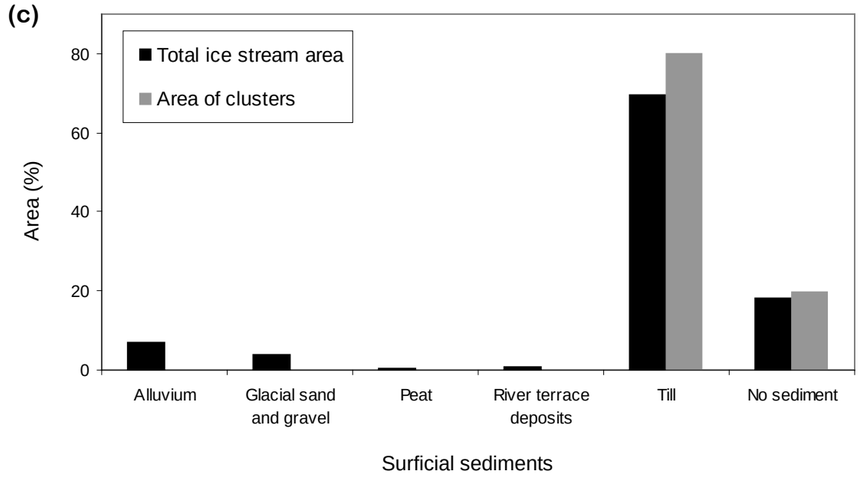

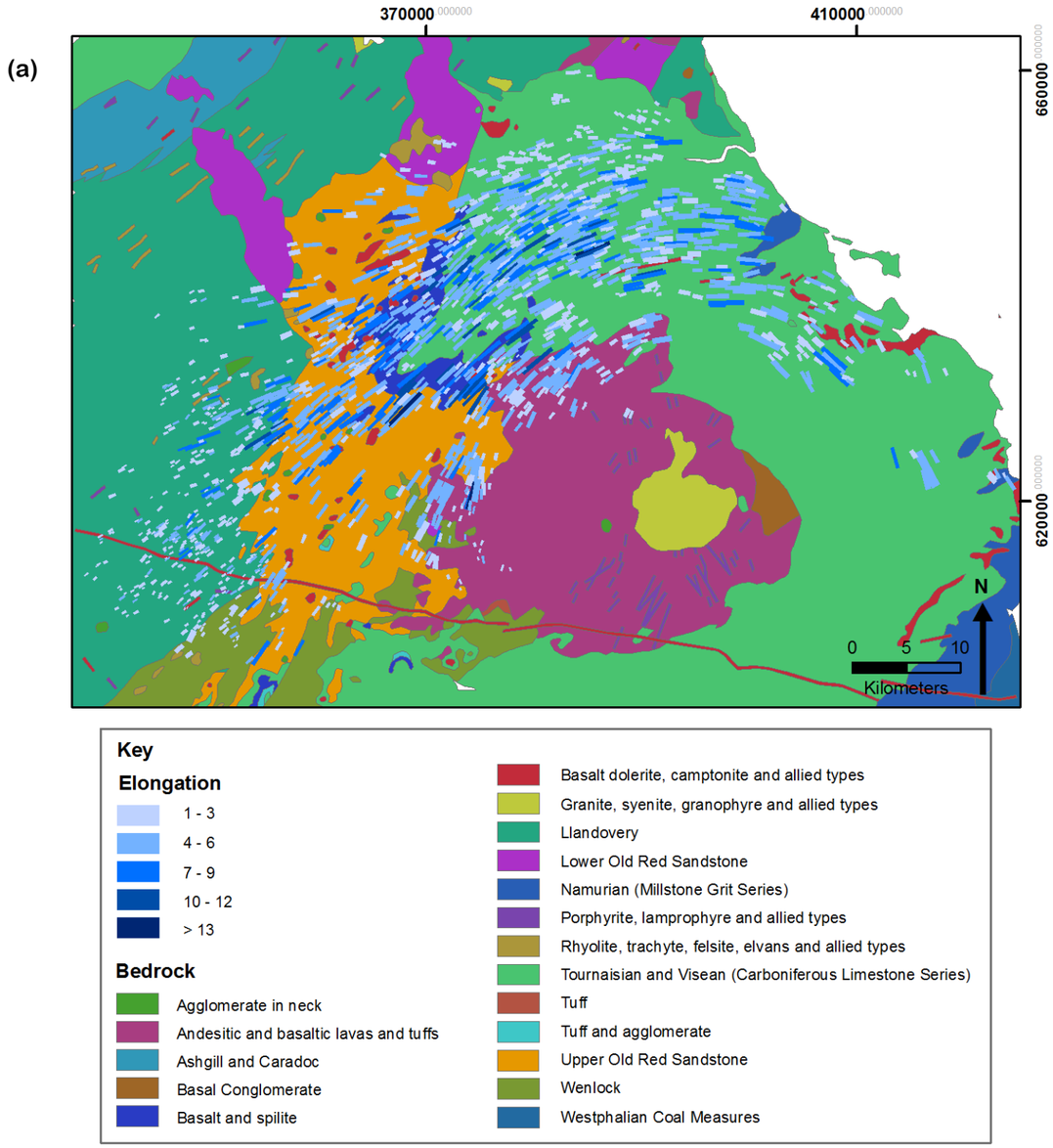

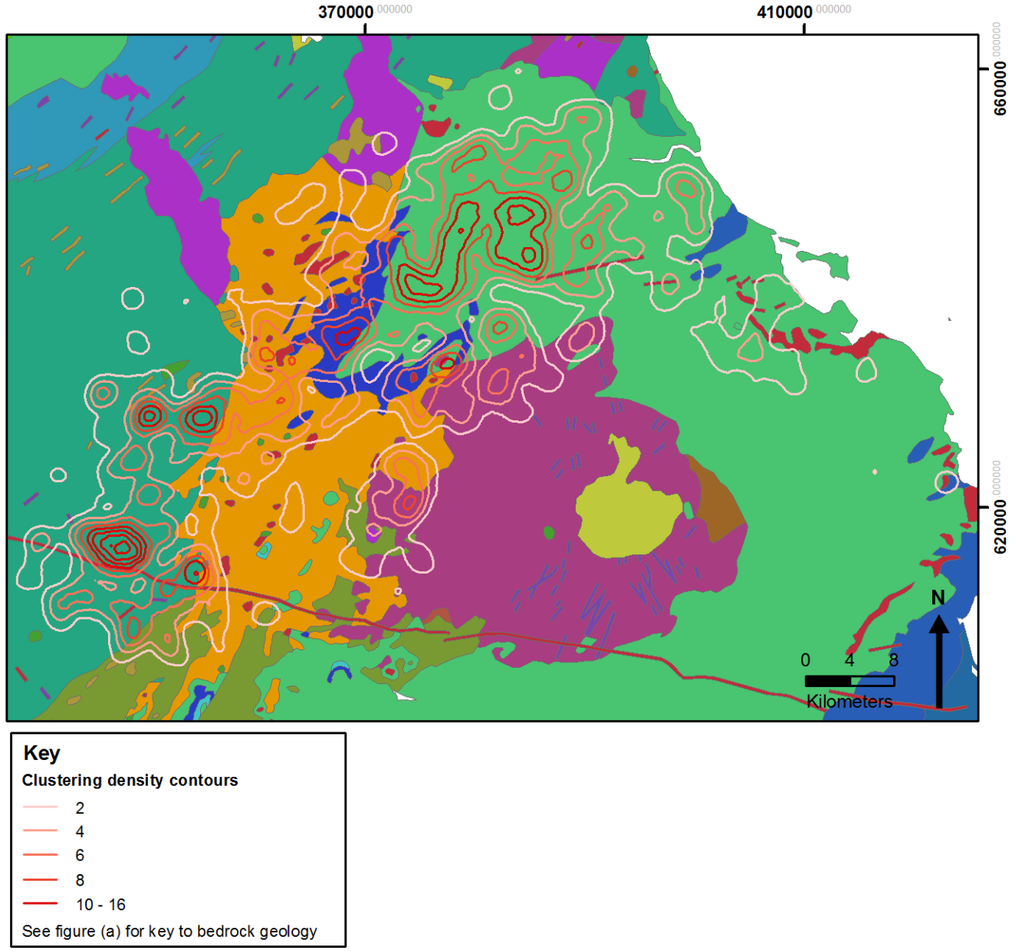

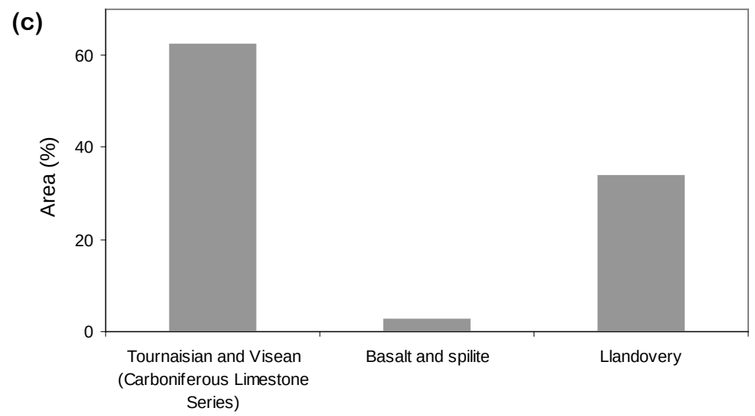

Figure 5.15 – Bedrock lithologies across the Tweed Palaeo-Ice Stream. Geology data from British Geological Survey (2007). (a) Bedrock map overlain by subglacial lineations shaded according to elongation ratio. (b) Bedrock map overlain by contours of subglacial lineation clustering (derived from the data presented in Figure 5.7). (c) Bar chart displaying the percentage coverage of bedrock lithologies within the cluster areas identified in Figure 5.7 (the lithologies from the entire ice stream are not shown because they are so numerous).

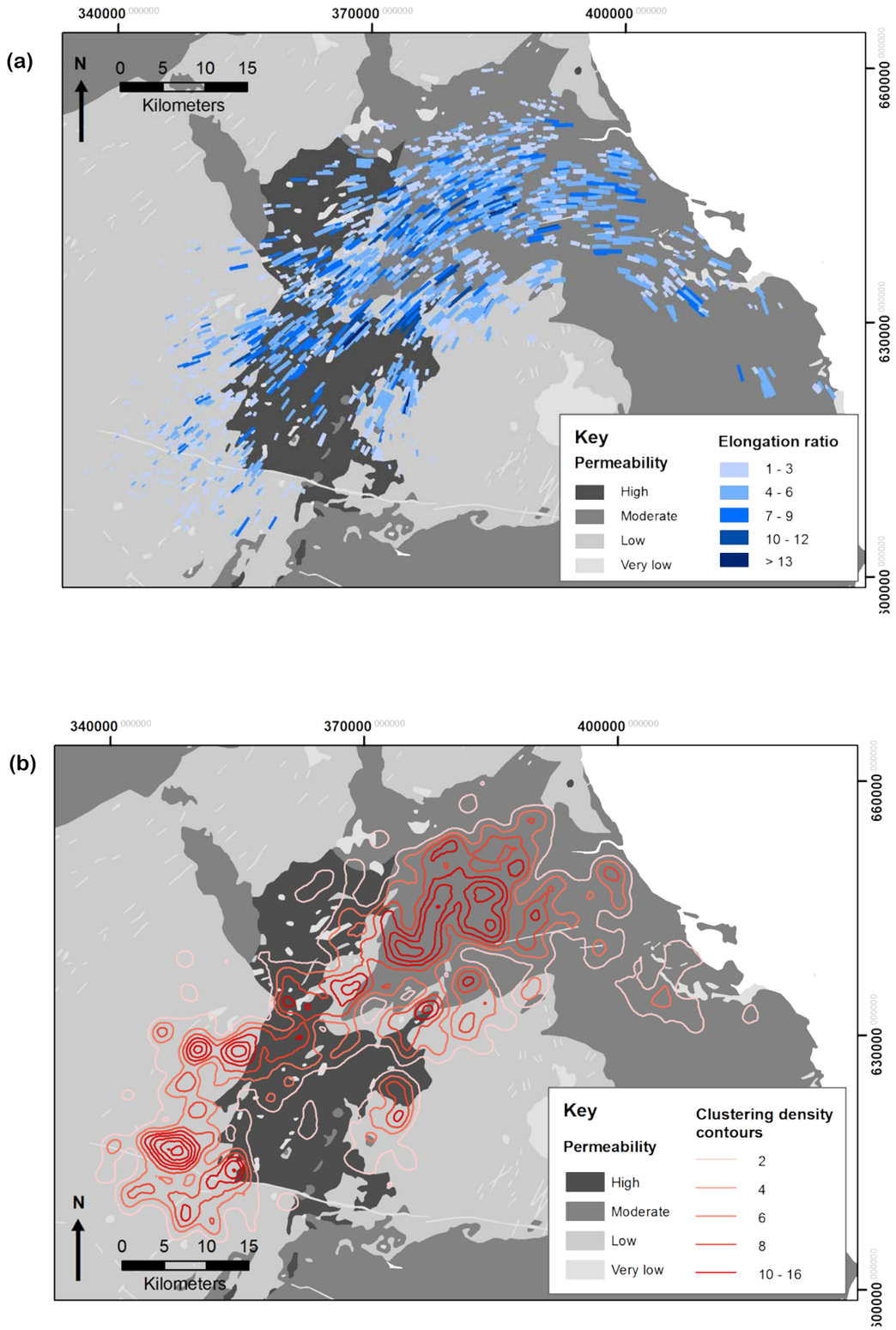

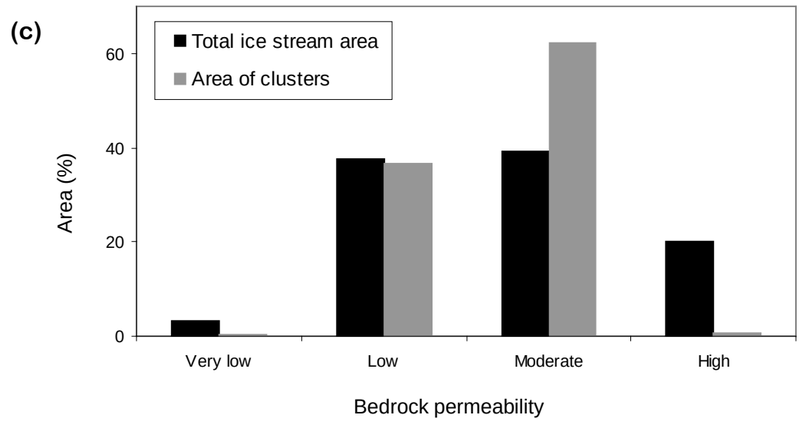

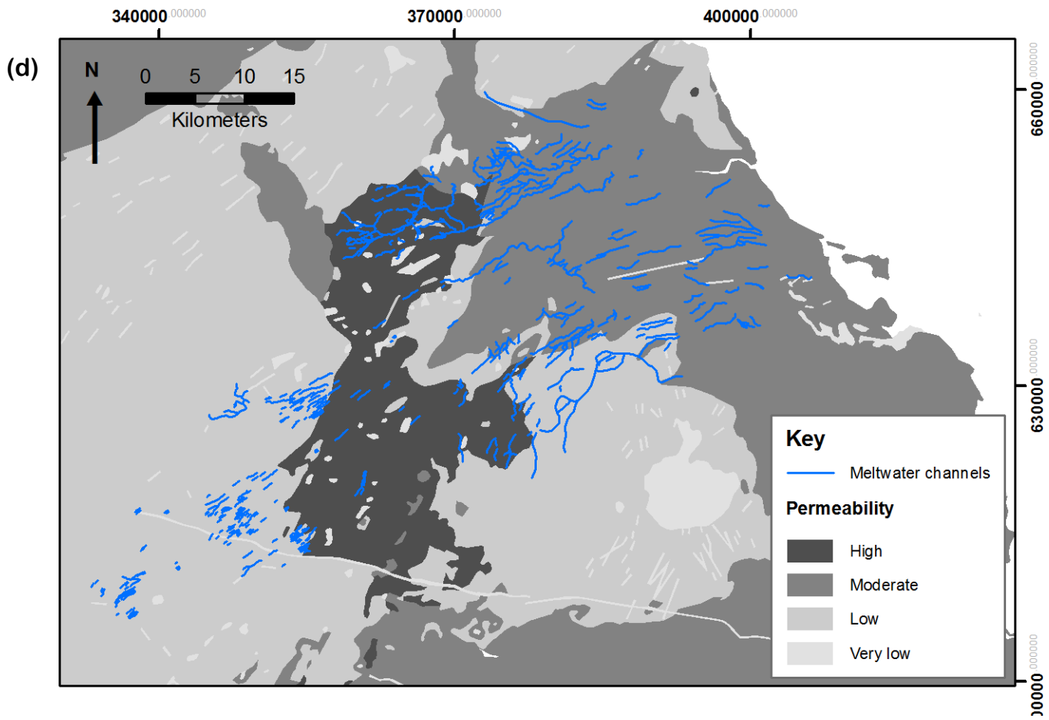

Figure 5.16 - Bedrock hydrogeology across the Tweed Palaeo-Ice Stream. Geology data from the Environment Agency. (a) Bedrock hydrogeology map overlain by subglacial lineations shaded according to elongation ratio. (b) Bedrock hydrogeology map overlain by contours of subglacial lineation clustering (derived from the data presented in Figure 5.7). (c) Bar chart displaying the percentage coverage of bedrock permeabilities across the whole ice stream and within the cluster areas identified in Figure 5.7. (d) Bedrock hydrogeology map overlain by meltwater channels.

5.2.4 Macroscale interpretation

a. Subglacial lineations

An isochronous swarm of subglacial lineations depict the Tweed Palaeo-Ice Stream (Figure 5.5). Convergence of subglacial lineations in the upstream end of the valley signifies the ice stream onset zone. However, they fail to diverge at the downstream end of the valley, suggesting that the ice stream did not terminate within the mapped area and instead may have continued into the present day offshore area. Furthermore, the distinct bend in the subglacial lineations suggests that the ice stream may have been deflected to the south, which was probably due to North Sea ice that flowed approximately north to south here (e.g. Eyles *et al*., 1994; Boulton and Hagdorn, 2006).

Subglacial lineation analyses revealed similar trends to those observed in the ice streams examined in Chapter 4. The transverse pattern of maximum elongation ratio decreases towards the lateral margins, which is consistent with the velocity decreases observed at the lateral margins of contemporary ice streams (Echelmeyer *et al*., 1994; Echelmeyer and Harrison, 1999). Longitudinally, the upper 10 km of the ice stream is characterised by small subglacial lineations with low elongation ratios, suggesting that ice velocity was lowest in this onset zone area, analogous to observations of contemporary ice streams (e.g. Joughin *et al*., 2001; Joughin and Tulaczyk, 2002). Some of the observations noted in Chapter 4, relating to elongation ratio clustering and low elongation ratios throughout the ice stream bed, were also found in the Tweed Palaeo-Ice Stream. These characteristics may have multiple explanations as outlined in Section 4.7.1, but they demonstrate that spatial variability was common at the ice stream bed.

Subglacial lineations are clustered in the central areas of the ice stream (Figure 5.7), which reflects the pattern of high elongation ratios here. However, high clustering is also apparent in the upstream areas of the ice stream, in which subglacial lineations are typically small with low elongation ratios. This reflects the observation in Chapter 4 that clustering of these bedforms is unaffected by velocity variations within the ice stream.

Comparison of subglacial lineations with potential controls on bedform elongation (bedrock geology, till continuity and topography) reveals some subtle correlations. Topography has a broad control on ice stream location, as evident from its valley location, but at a smaller scale there is no evidence for any topographic sticky spots. Topographic curvature is largely flat across the ice stream bed, which matches observations from the ice streams presented in Chapter 4. This characteristic is more convex and more variable towards the lateral margins and upstream ends of the ice stream. Interestingly, the upstream end of the ice stream contains highly clustered lineations, which would suggest that such variations in curvature do not reduce the occurrence or clustering of subglacial lineations.

Subglacial lineations are clearly located mainly on till and the areas of highest clustering in particular are characterised by continuous till (Figure 5.14) as was noted for the Solway and Forth ice streams. This relationship is unsurprising given the close association between till and subglacial lineations (e.g. Stokes *et al*., 2011). Till-free areas in the Tweed Valley both do and do not contain subglacial lineations (Figure 5.14). Assuming present day till distribution reflects till distribution during ice streaming, this suggests that till-free areas may act as sticky spots, but they do not always create sticky spots. The presence of high elongation ratios within till-free areas demonstrates that basal sliding rather than subglacial deformation (which requires deformable sediments) operated here to maintain rapid flow.

A subtle trend is apparent between bedrock geology and elongation ratio, whereby average elongation ratio is slightly higher on impermeable igneous bedrock. This reflects the findings from the Forth Ice Stream (Section 4.3.4) and a similar trend observed by Rattas and Piotrowski (2003) on an east Baltic palaeo-ice stream. However, this trend may instead reflect longitudinal changes in ice velocity, since the bedrock geology changes in the longitudinal direction, or the trend could be a function of both these variables. High clustering of subglacial lineations were characterised by moderate and low bedrock permeabilities, which reflected the distribution of bedrock permeability across the whole ice stream. Substrate permeabilities reported from other ice streams indicates that this may be typical (e.g. Hicock and Dreimanis, 1992; Tulaczyk *et al*., 1998). Bedrock permeability also has implications for the hydrological system of a glacier (Clark and Walder, 1994). Clustering of subglacial lineations

according to elongation ratio, does not appear to display any strong correlations with any of the bed variables examined. This suggests that a glaciological control, or a bed control that is not evident, is responsible for the spatial variations manifest in the subglacial lineations.

b. Meltwater features

Tweed Valley meltwater channels can be broadly grouped into three main types according to their position in the valley and their characteristics: (i) valley-side meltwater channels; (ii) upstream meltwater channels; and (iii) large meltwater channel(s) on the southern side of the valley.

(i) Valley-side or lateral meltwater channels have characteristics of both subglacial and ice marginal (lateral) meltwater channels (see Greenwood *et al*., 2007). Whilst the origins of individual channels within this network probably vary, the presence of marginal meltwater channels suggests that many relate to deglaciation and hence these channels cannot be considered as representative of ice stream subglacial processes.

(ii) Upstream meltwater channels cut across topographic highs and are eroded into bedrock, indicating that they are subglacial Nye channels (see Benn and Evans, 2010). They signify the movement of subglacial meltwater generally parallel to ice flow, and their discontinuity and poor connectivity attests to the concurrent operation of other types of subglacial drainage. They are found in close proximity to and in-between subglacial lineations, which suggests that these landforms formed contemporaneously.

The clustered nature of the channels suggests that their formation was only facilitated in certain areas. This may be attributed partially or entirely to bedrock variations (Figure 5.15). The channels are only located on Gala and Hawick groups, which have a low permeability, and not on the adjacent (downstream) Old Red Sandstone, which has a high permeability (MacDonald *et al*., 2004; Figure 5.16d). Subglacial channels form at the ice stream bed where the underlying sediment and/or bedrock is incapable of maintaining water discharge via Darcian flow (Boulton and Hindmarsh, 1987). Given this, it seems likely that the lower permeability of the Gala and Hawick groups could not maintain throughflow of subglacial meltwater, so this water was forced to the ice-

bed interface where it formed channels. The reason for the clustering of channels within these lithologies may relate to internal variations in hydraulic conductivity.

Whilst the spatial distribution of bedrock lithology and permeability appears to play a role in the distribution of these channels, they are located exclusively in the ice stream onset zone, suggesting that this may also be a factor. Studies of contemporary ice streams have noted that subglacial meltwater is abundant in onset zones and this is considered important for velocity increases here (Gray *et al*., 2005; Peters *et al*., 2007; Winberry *et al*., 2007). Furthermore, several studies have also reported the presence of meltwater channels from the onsets of palaeo-ice streams (e.g. Shipp and Anderson, 1997; Ó Cofaigh *et al*., 2002; Ó Cofaigh *et al*., 2005; Bradwell, 2005; Wellner *et al*., 2006; Anderson and Fretwell, 2008; Graham *et al*., 2009; Passchier *et al.*, 2010), indicating that the hydrological conditions in onset zones may be conducive to formation of meltwater channels. This suggests that the formation of these channels in this location was facilitated by the conditions at the ice stream onset zone, in addition to the presence of the underlying impermeable bedrock.

(iii) A large subglacial meltwater channel and associated tributaries is situated at the former lateral margin of the ice stream (Figure 5.11). Subglacial lineations depict this area of the southern lateral margin as particularly abrupt (Figure 5.5), indicating that it may have been relatively static. Modelling experiments indicate that ice stream lateral margins are inherently unstable on a morphological uniform bed (Jacobson and Raymond, 1998), indicating that an external control is required to enable a lateral margin to remain static. As no topographic or geological features coincide with the Tweed Ice Stream lateral margin in this location, it is possible that the large meltwater channel maintained the location and stability of the lateral margin. This may have involved meltwater evacuation from the ice stream bed, preventing encroachment of this water outside of the ice stream; in addition to the evacuation of excessive meltwater generated at the lateral margin, which may otherwise cause outward migration of the lateral margin (Jacobson and Raymond, 1998).

Conversely the location of the lateral shear margin may have facilitated formation of this large channel. Friction at a lateral margin between the ice stream and adjacent slow moving ice creates focussed shear and heat, generating meltwater (Jacobson and

Raymond, 1998; Schoof, 2004), which may have facilitated formation and growth of the channel here. Whilst the spatial association of this large channel and the ice stream lateral margin could be coincidental, the uniqueness of the channel and static margin within this ice stream means that it seems likely that they are linked via one of these two possibilities, if not both (i.e. the margin position formed the channel here and then the channel contributed to fixing the margin in place).

The locality of the channel on igneous bedrock (Figure 5.15) is also significant. It is situated on low permeability, igneous bedrock and it terminates at the boundaries with high and moderate permeability, sedimentary bedrock (Figure 5.16; MacDonald *et al*., 2004). This demonstrates that subglacial meltwater could not be discharged through the igneous bedrock and so was channelised at the ice-bed interface (Boulton and Hindmarsh, 1987).

c. Palaeo lake basin

The large palaeo lake basin indicated in Figure 5.5 (known as Milfield basin), is thought to have held an ice dammed lake during deglaciation (Clapperton, 1970a). Evidence for this is seen in deltas, eskers, meltwater channels, kame tarraces and a thick layer of laminated clays (Gunn, 1895; Clapperton, 1970a). Geomorphological mapping in this study has revealed that several meltwater channels relating to the ice stream begin and terminate in this basin, all of which have an up-down long profile, indicating that they are subglacial. Most notable is the large channel at the ice stream lateral margin, discussed in the previous section. The association of subglacial meltwater channels with this basin suggests that it may have also contained a lake during ice streaming, in addition to a lake during deglaciation. The Cheviots are thought to have been glaciated during the last glacial maximum (Clapperton, 1970a), which means that if a lake was present at this time it would have been subglacial, rather than ice dammed and proglacial, which may have been expected if the Cheviots were ice free. This hypothesis is supported by the low level of the basin compared to the surrounding land (150 to 220 m below) and the considerable depth of the basin, which reaches close to sea level below the sediment infill (Gunn, 1895). Therefore, the basin may have been situated below the ice hydraulic head, a parameter that is controlled by the ice surface topography and bed topography (Benn and Evans, 2010). The location of the basin, at

the ice stream margin and close to the Cheviots, also fits with recent observations that subglacial lakes below ice streams are commonly associated with regions of high basal traction (Sergienko and Hulbe, 2011). However, further investigation, such as numerical modelling or examination of its sedimentology, is required to test the hypothesis that a subglacial lake was present at this location.

5.3 Blinkbonny Quarry

5.3.1 Site Background

Blinkbonny Quarry is located at NT 674 388 (367400, 638800), at a central location within the Tweed Palaeo-Ice Stream (figures 5.1 and 5.5). It is situated at the stoss end of a subglacial lineation (Figure 5.17), which is a rock cored drumlin, capped with a thin (c. 0.5 to 2 m) layer of Devensian till. The drumlin is 1800 m long, 240 m wide, 20 m high and orientated at 48°. It is situated directly next to a slightly larger drumlin (Figure 5.17), and the lateral change from one drumlin to the next is marked by a break in slope, which becomes less pronounced towards the lee end of the drumlin.

Blinkbonny Quarry comprises a main quarry and a second adjacent pit that was being excavated during 2008. This second pit (approximately 100 m by 100 m) is the location of the sediment sections in this study. The quarry is located on the Kelso Volcanic Formation, which consists of effusive alkali olivine-basalts that are associated with tuffs or with volcaniclastic sandstone (British Geological Survey, 2007). At the top of the basalt bedrock is a weathering mantle containing corestones. The weathering mantle appears to be a ferrallitic (lateritic) saprolite, which forms on iron rich volcanic and ultramafic metamorphic rocks (Mignon and Lidmar-Bergström, 2001), as a result of chemical weathering.

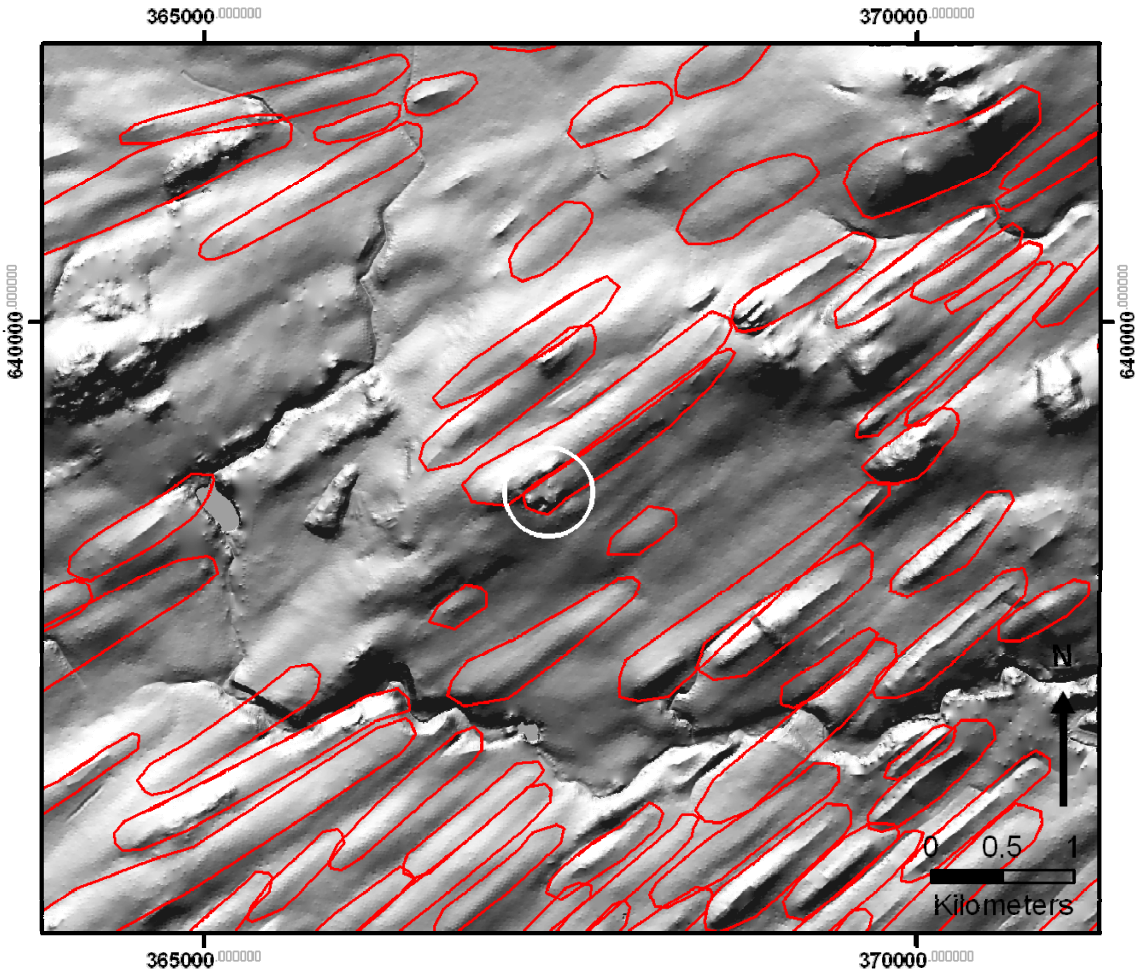

Figure 5.17 – DEM of Blinkbonny Quarry and the surrounding area. The location of the quarry is indicated with a white circle. Ice flow is from lower left to upper right of the image. Nextmap DEM has a vertical exaggeration of x4.

5.3.2 Mesoscale sedimentology

The sediments at Blinkbonny Quarry were recorded in several vertical and section logs (figures 5.19 and 5.20). Locations of the logs (which were selected to be representative of the sediments in the pit) are given in Figure 5.18. The majority of sections are located parallel or perpendicular to the long axis of the drumlin. The observed sediment profile was broadly similar throughout Blinkbonny Quarry and three lithofacies were identified (figures 5.19 and 5.20).

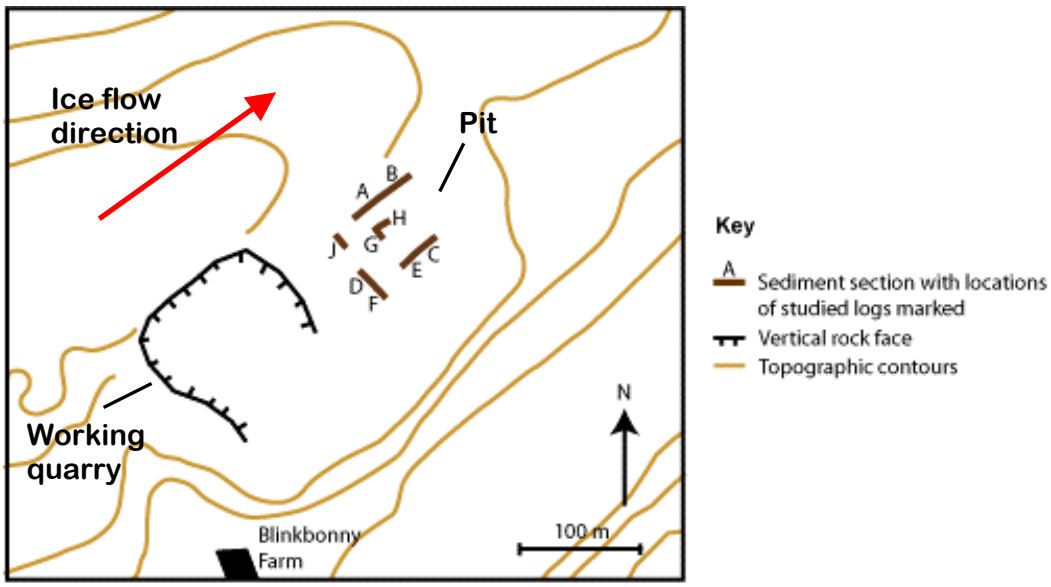

Figure 5.18 – Map of Blinkbonny Quarry and the locations of the sediment sections. Topographic contours (10 m intervals) are from Ordnance Survey data (Ordnance Survey).

At the base of many sediment profiles in the quarry is Lithofacies 1 (LF1), which is a fissile, altered bedrock, up to 2 m thick where visible (Figure 5.19). This is evident where bedrock is exposed at the base of sediment face, where it is typically weathered and brecciated. Fissures in LF1 are packed with silty sand (Figure 5.22b), within which fine laminations, aligned parallel to the fissure walls, can be identified. A sample from one fissure shows it contains particles from clay size to medium sand size (see Appendix B for further details).

Folding and faulting is also common in the upper 1 to 2 m of bedrock, as found in Section D (Figure 5.19) and sections G and H (figures 5.20 and 5.22c). Measurement of faults at Section G, indicates that the trend of the fold axis is 345°, which is relatively close to perpendicular from the drumlin orientation (within 27°) and the plunge is 35°. Striations were also observed on some bedrock outcrops.

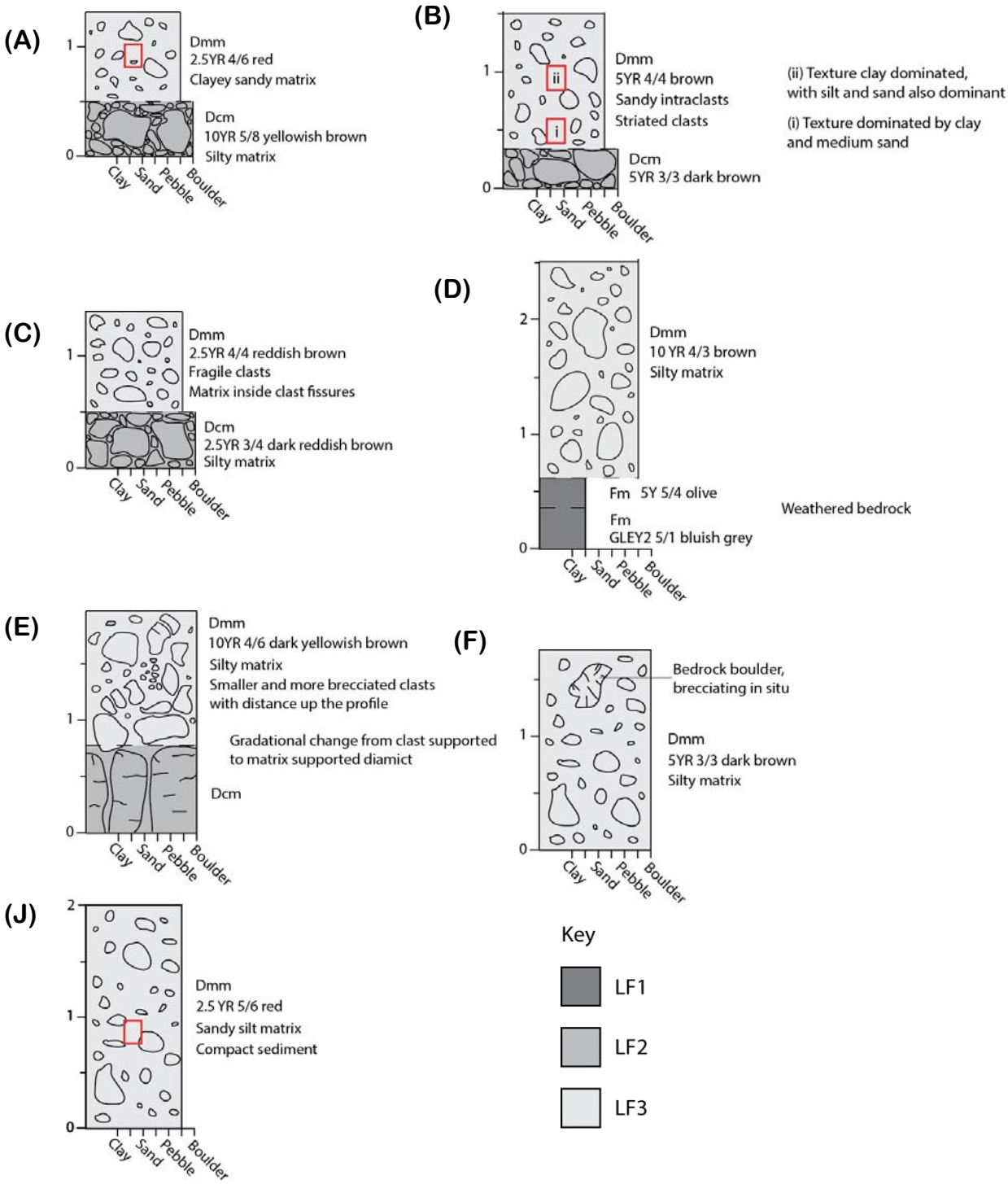

Figure 5.19 – Vertical sediment logs from Blinkbonny Quarry. Different shades of grey represent different lithofacies and these are indicated in the key. Locations of kubiena tin samples are shown with red rectangles. For key please see figures 3.3 and 3.4, pages 41-42.

Lithofacies 2 (LF2) is a clast-supported diamicton, 0.35 to 1.6 m thick where seen. It comprises cobbles, boulders and bedrock rafts in a sandy silt matrix (e.g. Sections A, B and C; figures 5.19 and 5.22a). LF2 contains subangular and angular clasts, and shears can also be identified within it (Figure 5.20). The boundary between LF1 and LF2 is gradational and sometimes loaded.

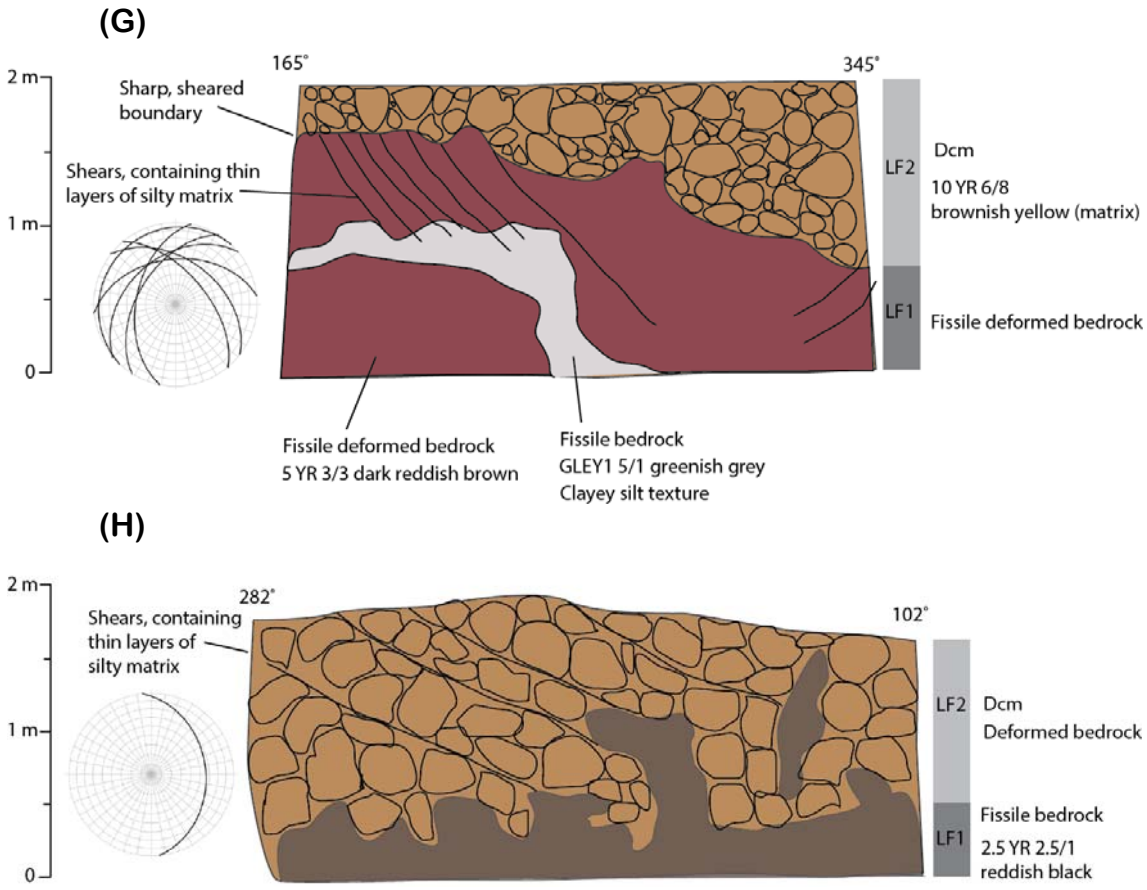

Figure 5.20 – 2D section logs for sediment profiles G and H. The right hand column indicates lithofacies type. Great circles for the strikes and dips of the shears are shown in the stereographic plots to the left of the section diagrams.

Lithofacies 3 (LF3) is a matrix-supported diamicton. This lithofacies is present in most of the sediment profiles (e.g. Sections A, B, C, D, E, F and J; figures 5.19 and 5.22a). It is a compact sediment, up to 2 m thick and comprises a multimodal particle size distribution, with particles from clay to boulder sized (see Appendix B for details of the particle size distribution). Multimodal particle size distributions may reflect progressive particle size reduction via crushing and abrasion (Boulton, 1978; Haldorsen, 1981). Clasts are typically slightly spherical in shape and sub-rounded, which is indicative of abrasion and active clast transport (Figure 5.21). C_{40} indices are relatively low, suggesting that clast travel distances were long and clast crushing and fracturing was significant (Evans *et al*., 1998). In this lithofacies, clasts are notably weak compared to equivalent clasts from the underlying bedrock. They are embedded in the diamicton in a coherent form, yet on removal they disintegrate and lose their integrity. Small bedrock rafts were identified in this lithofacies, up to c. 0.7 m in size. Flame structures were also

identified in this lithofacies (Figure 5.22d), which point in the downstream direction of the drumlin. LF2 has a gradational contact with LF3.

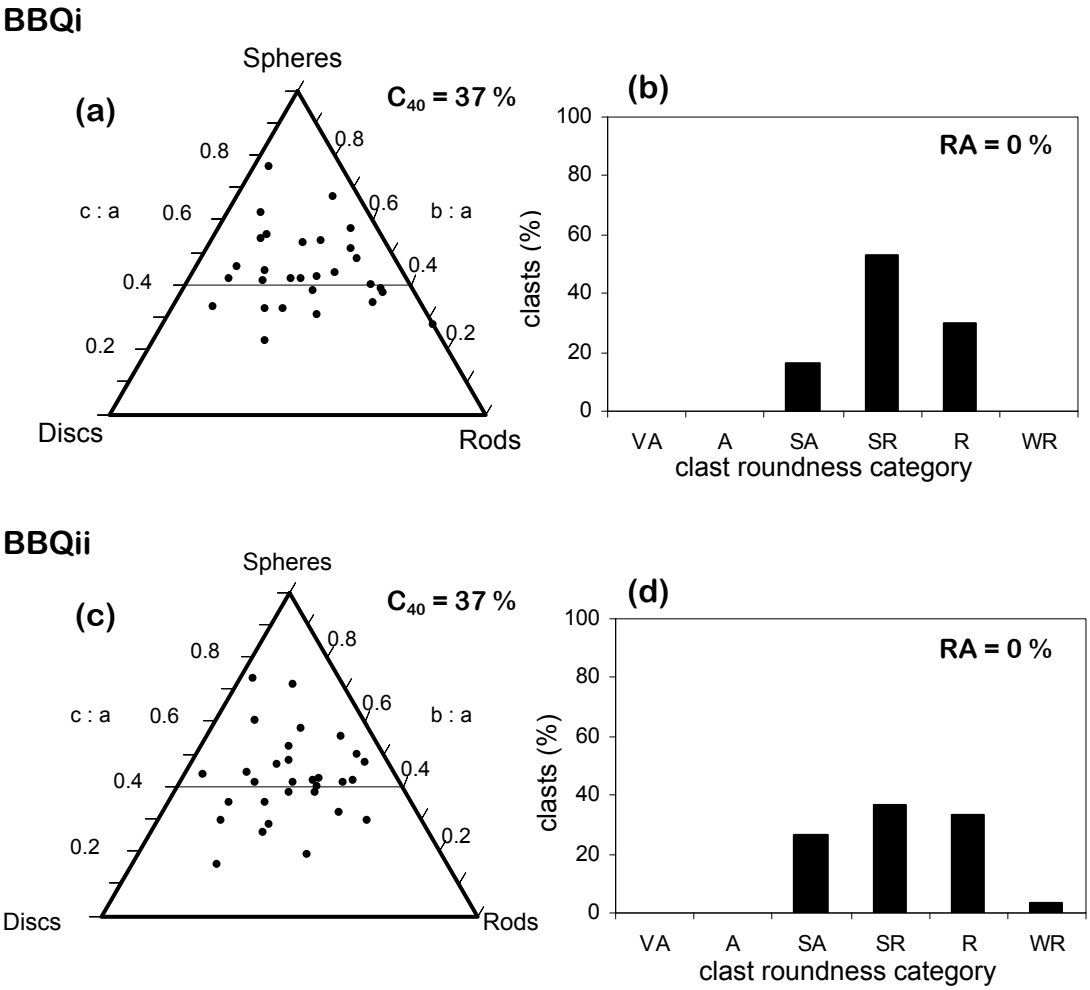

Figure 5.21 – Blinkbonny Quarry clast morphology. (a) Clast shape for BBQi, sampled from LF3, 0.5 m up Section B (n = 30). (b) Clast roundness for BBQi, sampled from LF3, 0.5 m up Section B (n = 30). (c) Clast shape for BBQii, sampled from LF3, 0.9 m up Section B (n = 30). (d) Clast roundness for BBQii, sampled from LF3, 0.9 m up Section B (n = 30). Clast roundness categories are as follows; VA = very-angular, A = angular, SA = sub-angular, SR = sub-rounded, R = rounded, WR = well-rounded.

The three lithofacies share some characteristics and have gradational contacts, hence forming a continuum rather than distinct sedimentary units. With distance up the profile there are certain notable changes: the bedrock becomes increasingly disturbed, losing its original structure; the proportion of matrix increases; clasts become fewer; and clasts have a wider range of morphologies and generally become more rounded.

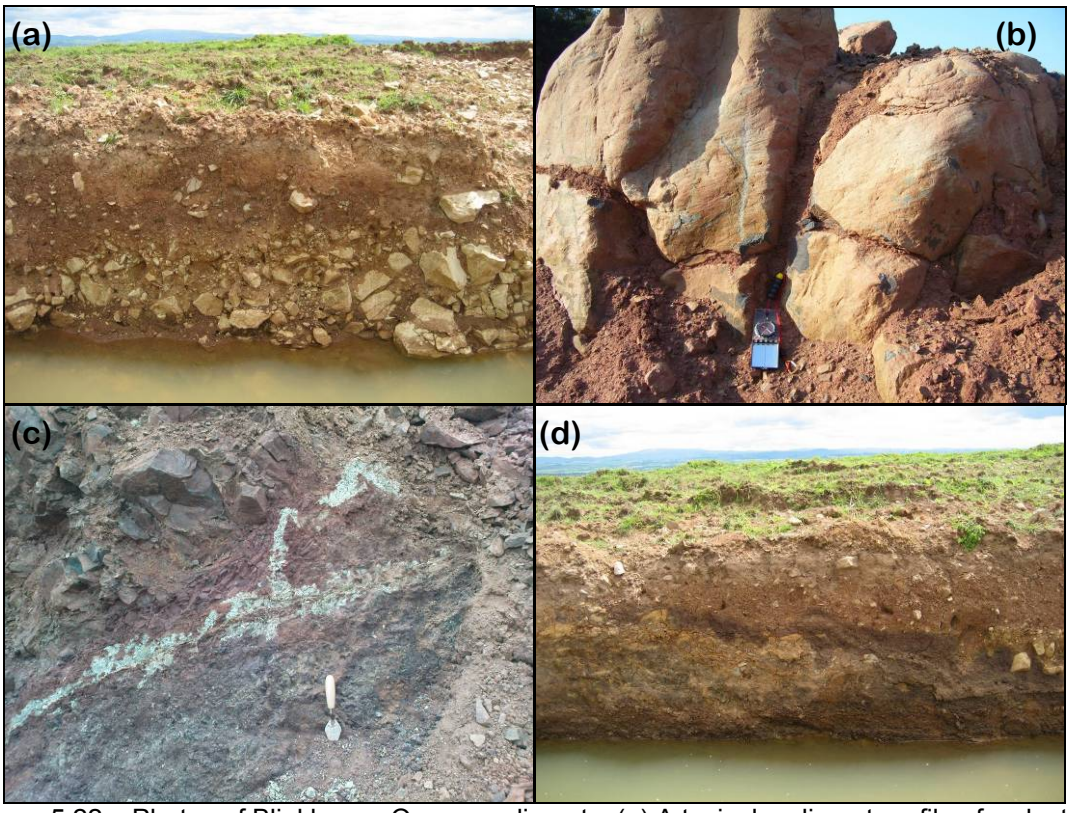

Figure 5.22 – Photos of Blinkbonny Quarry sediments. (a) A typical sediment profile of a clast-supported diamicton (LF2) containing large local bedrock boulders, which is overlain by a matrix-supported diamicton (LF3) (profile height is 1.2 m). (b) Striated bedrock containing fissures that are filled with densely packed sediment, the texture of which is dominated by sand and clay. (c) Section G, which comprises folded and faulted fissile bedrock (LF1) (trowel length is 23.5 cm). (d) Matrix-supported diamicton with some layering and flame structures, which point downstream (LF3) (profile height is 1.2 m).

Macrofabric (particles 8 to 32 mm in length) was measured from LF3 at sections B and J (which were selected for their representative sediment profiles and thick units of LF3) (Figure 5.23). The clast macrofabrics from Section B (at 50 cm and 90 cm) are characterised by an arc of shallowly dipping clasts, transverse to the orientation of the drumlin (Figure 5.23). Since the land slopes down to the SE here (away from the drumlin crest), the clasts dip *into* the drumlin. The clast macrofabric from BBQJ is more clustered and is orientated approximately parallel to the orientation of the drumlin, dipping upstream. The macrofabric eigenvalues depict the strength and shape of the fabric sample and Figure 5.23c indicates that all of the fabrics measured are linearly clustered, but not strongly so, as they are situated fairly centrally in the ternary diagram.

(a)

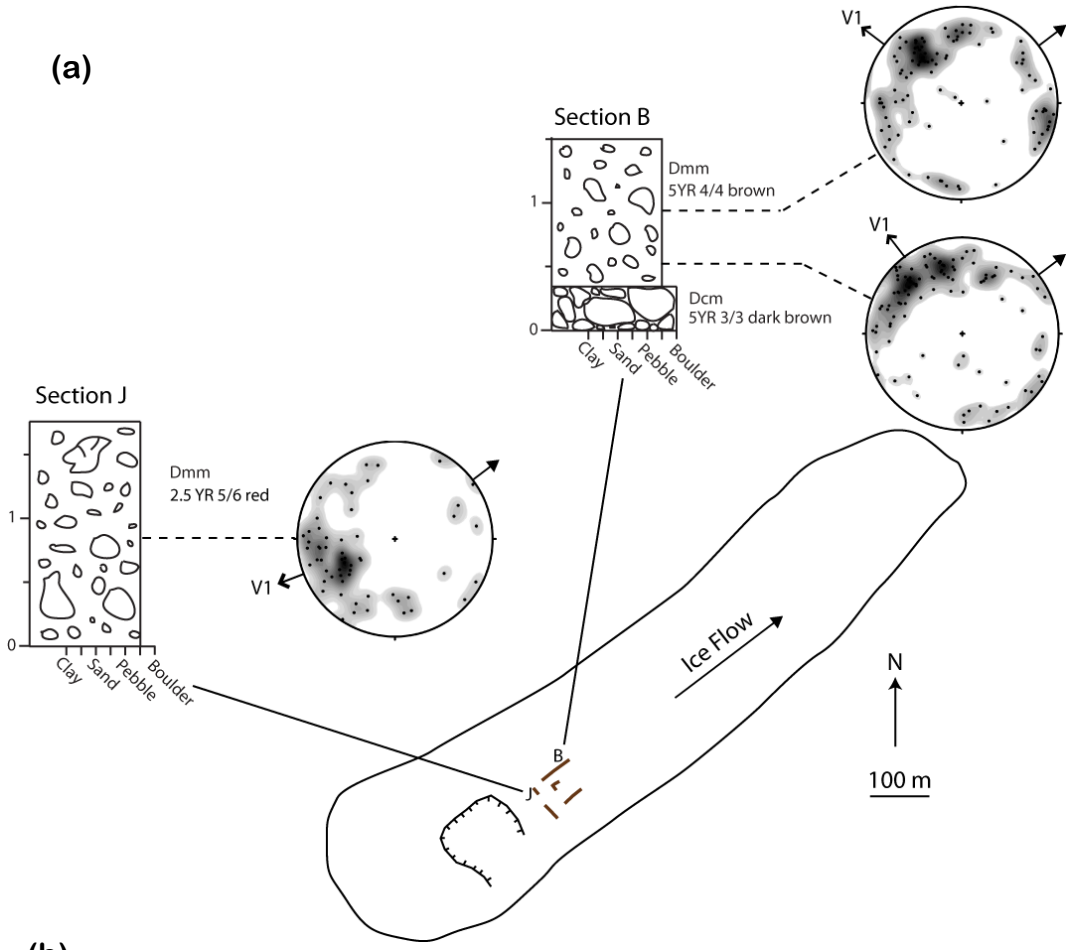

(b)

Sample	Mean Vector	Mean Dip	Eigenvalue	Clustering
BBQi	322.5°	22.1°	0.607 (S_1) >> 0.272 (S_2) ~ 0.121 (S_3)	Linear
BBQii	307.3°	26.3°	0.549 (S_1) >> 0.319 (S_2) ~ 0.132 (S_3)	Linear
BBQJ	249.4°	28.7°	0.638 (S_1) >> 0.247 (S_2) ~ 0.116 (S_3)	Linear

(c)

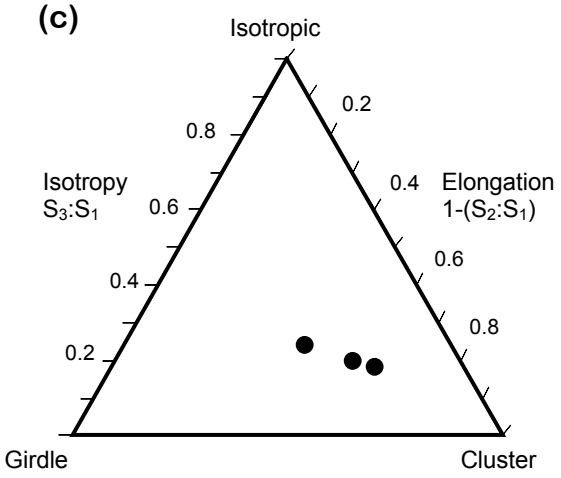

Figure 5.23 – Macrofabric from LF3. (a) Blinkbonny drumlin and quarry shown with the vertical sediment logs and the macrofabrics that were measured from these. Open arrows show the principle eigenvector azimuth, labelled V1; and solid arrows indicate direction of former ice flow. Both fabrics from Section B (n = 100) have transverse fabrics and the fabric from Section J (n = 60) has a parallel clustered fabric. (b) Eigenvalues for the macrofabric measurements. (c) Ternary diagram displaying fabric shape.

5.3.3 Mesoscale interpretation

The sediments at Blinkbonny Quarry form part of the drumlinised surface, suggesting that they are contemporaneous to drumlin formation and hence to ice streaming. At the base of the sediment profiles is deformed bedrock (LF1), which is folded and faulted in the same direction as the drumlin. This, along with the presence of striations, indicates that the unit is a glaciotectonite. LF1 is overlain by a clast-supported diamicton (LF2), which retains characteristics of the bedrock and has evidence for deformation, indicating that it is also a glaciotectonite. LF2 is considerably more brecciated than LF1, suggesting that it was subject to greater stress. Clasts are typically angular or sub-angular, indicating that abrasion and rotation was minimal in LF2. A fine-grained diamicton is present within fissures in the glaciotectonite units, suggesting that the overlying matrix-supported diamicton had been injected downwards into the fissures. These characteristics indicate that LF1 and LF2 can be defined as penetrative Type A glaciotectonites (see Benn and Evans, 1996). The locality of the matrix-supported diamict, LF3, comprising part of a subglacial lineation within a flow-set, in addition to evidence for abrasion, bedrock rafting, ductile deformation and shear, indicates that is a subglacial traction till (see Evans *et al*., 2006a). The sediment profiles clearly demonstrate a vertical increase in deformation from base to top, as evident from the loss of bedrock structure, increasing range of clast roundness and an increasing input of foreign clasts. This is consistent with models of subglacial till deformation, which depict an accelerating increase in deformation with distance up a vertical till profile (e.g. Alley 1991; van der Meer, 1993). The fragile clasts within the till at the top of the profile are likely to have weakened after they were emplaced in the till because if they had weathered prior to this it is likely they would have completely disintegrated in the subglacial environment.

Concentrations of laminated, fine-grained till within bedrock fissures, indicate that the subglacial environment was highly pressurised and subject to frequent, high magnitude fluctuations in pore water pressure, causing till injection down the sediment profile (Evans *et al*., 1998). This process may have weakened the underlying bedrock and suggests that detachment of bedrock rafts was facilitated via the injection of pressurised water (Evans *et al*., 1998), rather than other possible processes such as basal freeze-on

(e.g. Aber, 1988). There is evidence for brecciation of rafts, indicating that abrasion and crushing processes operated, and that rafting processes contributed to till development here (see Hiemstra *et al*., 2007).

The macrofabrics do not give a clear pattern of clast orientation because they are both parallel and transverse to palaeo ice flow. Collectively the fabrics do not appreciably conform to fabric patterns observed by previous researchers, such as orientations around the flanks of the drumlin (e.g. Andrews and King, 1968; Kerr, 1978; Krüger and Thompsen, 1984), or strong flow parallel fabrics (e.g. Hooyer and Iverson, 2000; Piotrowski *et al*., 2001; Thomason and Iverson, 2006; Iverson *et al*., 2008). The fabric S_1 eigenvalues fall within the lower end of the scale of S_1 values reported for other till fabrics (Figure 5.23; e.g. Evenson, 1971; Stanford and Mickleson, 1985; Carr and Goddard, 2007). This suggests that the fabrics are relatively weak and in some studies this has been considered to be indicative of high strain (e.g. Hicock, 1992; Hart, 1994; Hicock *et al*., 1996; Hart, 1997). However, this argument is based on the assumption of a viscous till rheology, which is brought into question in light of recent experimental studies that have found subglacial till to have a Coulomb plastic rheology (e.g. Tulaczyk *et al*., 2000a).

Transverse fabrics are not considered typical for subglacial tills (e.g. Hooyer and Iverson, 2000; Larsen and Piotrowski, 2003) but they have been reported from some studies (e.g. Kerr, 1978; Hicock and Dreimanis, 1992; Carr and Rose, 2003). Compressive flow has been associated with transverse fabrics, based on the theory that in the longitudinal position a particle will experience a velocity gradient along its length and thereby it is unstable and likely to reposition into a transverse position (Stanford and Mickleson, 1985). Compressive flow may take place near glacier termini in situations such as the transition from warm based ice to cold based ice or rapid glacier advances (Benn and Evans, 2010) and thus is not likely to be associated with a flat bed. However, the rise in bed topography at the stoss end of a drumlin may cause localised compressive flow. The Blinkbonny fabric samples are situated slightly downstream of the crest of the drumlin at its stoss end (Figure 5.18), so it is feasible that compressive flow may have affected clast fabric in this locality, although it is unclear why this would vary spatially between sections B and J. Seemingly instead of a process to account for transverse clast orientations the process primarily needs to account for the spatial

variability within the clasts. A possible explanation for this is that fluctuating pore water pressures, as evidenced by the laminated sediments in the fissures, may have caused variable pressure gradients within a dilated, fluidised sediment, in which clasts are mobile and able to respond to local variations in flow (see Benn, 1995; Evans *et al*., 2006a).

Another consideration is that the sediments may have been subject to postglacial influences. Frost action can affect clast fabric particularly at shallow depths and may cause a clustered fabric to weaken and increase clast dip (Benedict, 1976; Millar and Nelson, 2001). Clasts that dip into the drumlin is unusual as if fabrics are transverse to ice flow they are instead likely to be dipping parallel to the drumlin surface whereby they may roll (Andrews and King, 1968). Movement of clasts via frost action could explain this because whilst these environments commonly produce clasts orientated downslope, they also may develop oblique orientations as clasts move towards the direction of (downslope) movement (Benedict, 1976). However, Kerr (1978) also recorded weak and transverse fabrics in the Tweed Valley from over 25 fabric samples. These were sampled from greater depths (2 to 2.5 m below the ground surface) than those in this study (0.5 to 1.2 m below the ground surface) and so are less likely to be subject to the potential influence of ground surface frost, which would indicate that these types of fabrics are instead a reflection of the subglacial signature. Furthermore, fabrics with weak, transverse and variable fabric signatures have been reported from other subglacial tills (e.g. Hicock, 1992; Stalsberg *et al*., 2003; Carr and Goddard, 2007). Given this and the fact that there is no other clear evidence for postglacial processes it seems that the most favourable interpretation is that the fabrics represent a subglacial signature. The formation of such fabrics in this environment may relate to the variable pore water pressures, but further investigation is necessary to establish the precise mechanisms.

5.3.4 Micromorphology

Four micromorphology samples were collected from LF3, details of which are given in Table 5.1. This allowed the study of microscopic features in the sediment and measurement of the microfabrics. Samples were not collected from the clast rich LF1 and LF2. A scan of sample BBQi is given in Figure 5.24. This shows the vertical (a)

slide and the horizontal (b) slide, which were examined for each sample. This sample shows the overall texture and structure that is typical of this lithofacies. It is characterised by small to medium sized (c. 1 to 10 mm) igneous and sedimentary clasts and abundant quartz grains, within a red-brown matrix.

Table 5.1 – Details of the micromorphology samples collected from Blinkbonny Quarry. Locations of samples are also indicated in Figure 5.19.

Sample	Sample location	Orientation to subglacial lineation	Lithofacies	Why sampled?
BBQi	Section B, 0.5 m up profile	Parallel	3	Characterisation of lithofacies and microfabric
BBQii	Section B, 0.8 m up profile	Parallel	3	Characterisation of lithofacies and microfabric
BBQA	Section A, 0.8 m up profile	Parallel	3	Characterisation of lithofacies
BBQJ	Section J, 0.9 m up profile	Transverse	3	Characterisation of lithofacies and microfabric

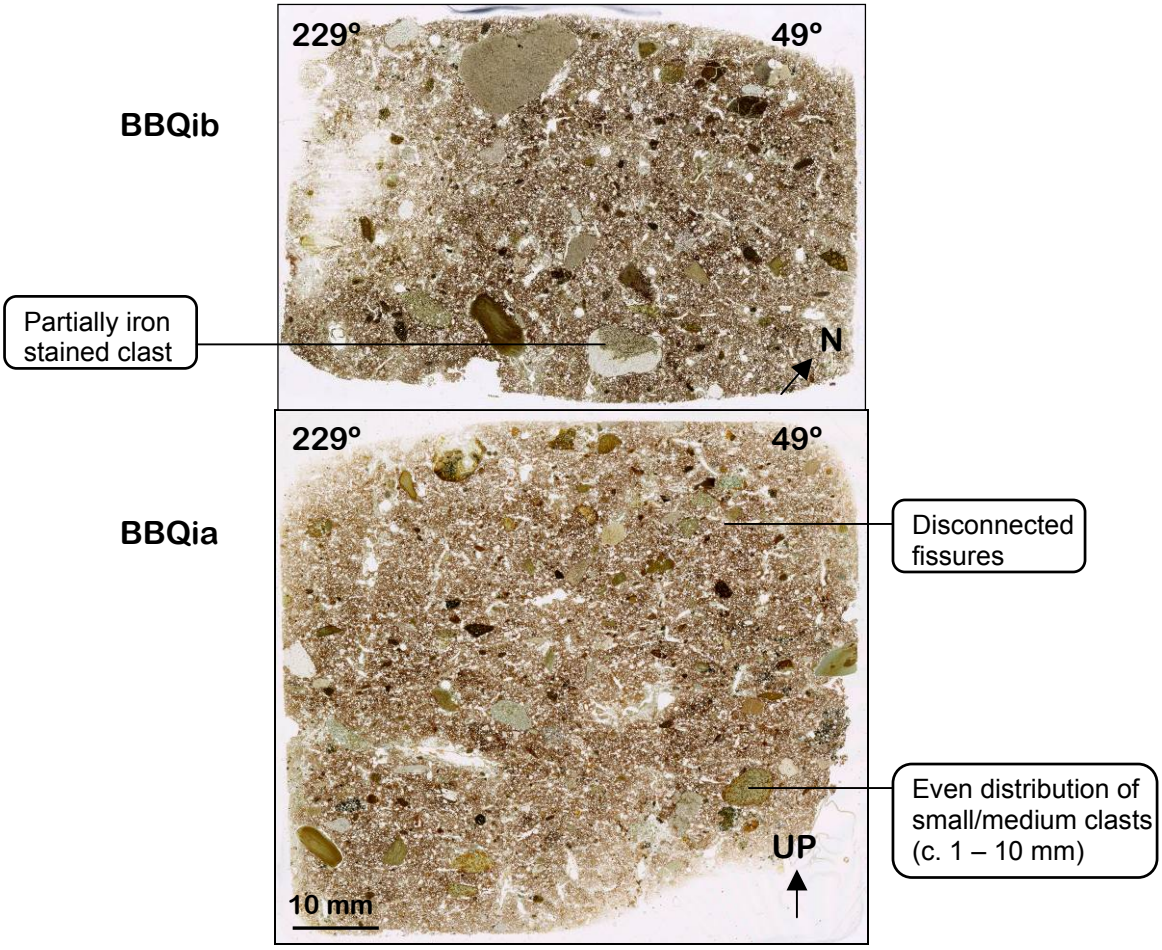

Figure 5.24 – Scans of BBQib (plan view) and BBQia (profile view) with annotations of some of the key features that can be seen at this scale. The orientations of the thin sections are displayed, BBQia is orientated parallel with the orientation of the drumlin.

Table 5.2 – Summary table of the micromorphological features from the Blinkbonny Quarry samples. The relative abundance of each feature for each sample is given in a 1 to 3 scale; 3 (●●●) = very abundant, 2 (●●) = present in two or more locations in the sample; 1 (●) = present in a single location in the sample; 0 (-) = not present.

	Voids		Sediment mixing			Water movement	Grain structures			Clast/matrix alteration			Plasmic fabric		
	Fissures	Vughs	Multiple domains	Intraclasts	Papules	Cutans	Grain concentrations	Turbates	Grain lineations	Spalling grains	Clast weathering rinds	Iron staining	Masepic	Skelsepic	Unistrial
BBQi	●●	●●●	●	●	●	●●●	-	●●	●●●	-	●●	●●●	●●	●●●	●
BBQii	●●	●●	●●	●	●	●●●	●●	●●●	●●●	●●●	●●●	●●	●●●	●●●	●
BBQA	●●●	●●●	●	●	●●	●●●	●●	●●●	●●●	●●	●	●●	●●	●●●	●●
BBQJ	●●●	●●●	●	-	-	●●●	-	●●	●●●	●●	●	●●●	●●●	●●●	-

An overview of the structures identified in each sample is given in Table 5.2, followed by descriptions and images of the most common features. Definitions of the micromorphological features described are given in the glossary (Figure 3.9, pages 48-49). More detailed micromorphological descriptions for each sample are given in Appendix C.

a. Voids

Voids may provide an insight into modern and past porosity and permeability of sediments, as well as highlighting certain processes such as biological activity (Kilfeather and van der Meer, 2008). They may also form during laboratory drying, which can highlight pre-existing weaknesses in a sediment (Carr, 2004). In the Blinkbonny Quarry samples, voids (particularly fissures and vughs) are found throughout all of the thin sections. Fissures are typically disconnected and range in length from c. 0.5 to 30 mm. Some fissures have smooth edges and rounded ends (Figure 5.25a) and some are angular with rough edges. The smooth-walled fissures are often associated with cutans, which demonstrate that they formed *in situ* rather than as a consequence of sample collection or laboratory drying. None of the fissures observed reveal any obvious overall pattern in the sediment, such as a marble bed structure (see van der Meer, 1993).

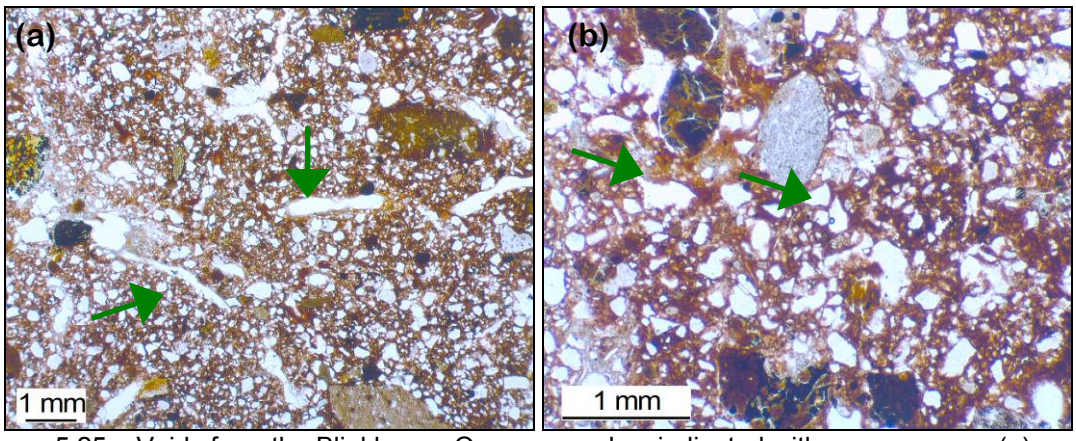

Figure 5.25 – Voids from the Blinkbonny Quarry samples, indicated with green arrows. (a) Typical, smooth walled fissures from BBQib; (b) Vughs from BBQib.

Vughs are usually small (c. 0.3 to 2 mm), ovate to irregular in shape with rounded edges (Figure 5.25b). They can be associated with cutans, where they occur in lines or groups within an area of cutans. Many small, near-circular voids are present, especially in plan view (b) slides and these are often associated with grey cutans.

b. Cutans

Cutans are abundant in all of the Blinkbonny Quarry samples. Cutans (also known as argillans) are deposits of clay or sometimes silt, which typically form by illuviation of fines down a soil or sediment profile, where they form skins that may line voids or coat grains (Kemp, 2007). They can indicate mobilisation of fine sediment and movement of water. Cutans are commonly associated with pedological processes (e.g. Kemp, 2007), but have also been linked to periglacial (van Vliet-Lanoë, 1998) and subglacial processes (Menzies, 2000; van der Meer *et al.*, 2003).

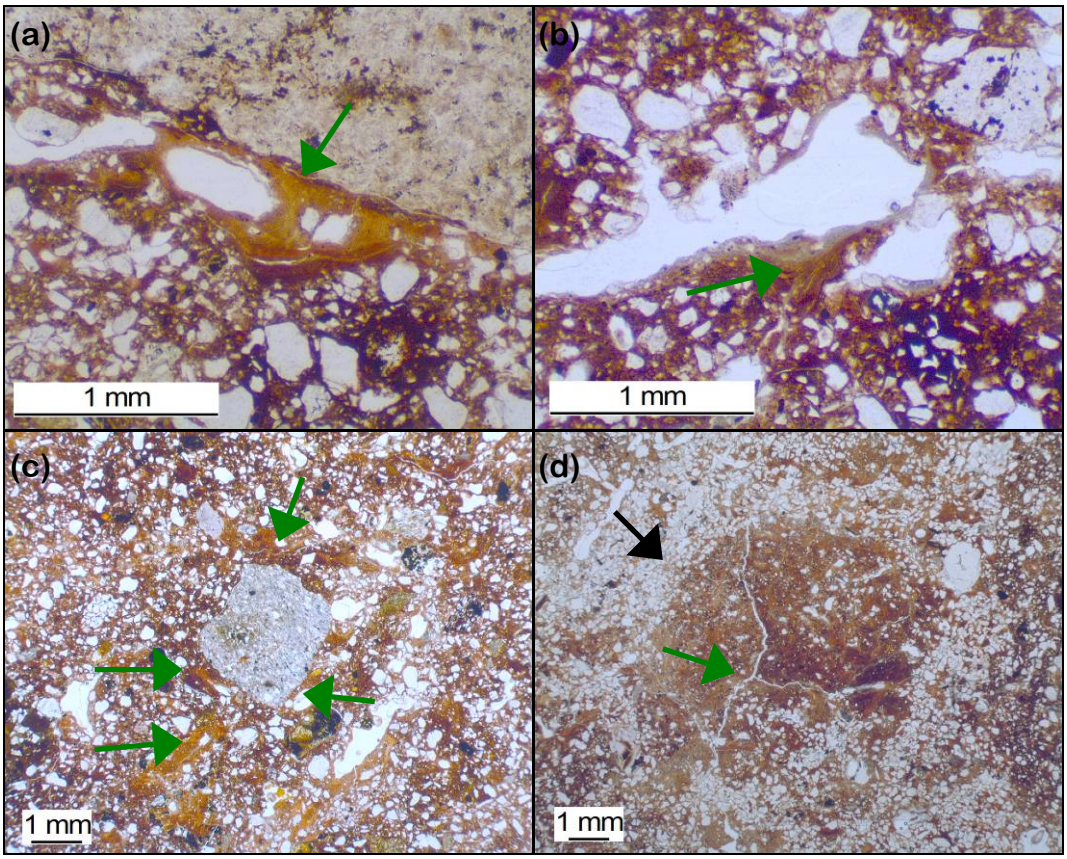

Figure 5.26 – Cutans from Blinkbonny Quarry. Cutans are marked with green arrows. (a) A typical void cutan from BBQAa in plane polarised light. (b) An orange cutan grading into a grey cutan from BBQia. (c) Cutans radiating out from a clast in BBQA. (d) Rounded area of cutans surrounded by a concentrated ring of quartz grains (indicated with a black arrow) from BBQAa.

Two different cutan types were identified: (a) orange clay cutans (the dominant type), which are characterised by strong orange birefringence, laminations and iron staining; and (b) light grey, silty clay cutans, with a grainy yellow birefringence. These two cutan types are sometimes present together, wherein the coarser grained grey cutan is superimposed upon the fine-grained orange cutan (e.g. Figure 5.26b). The texture of the cutans relates to the size of particles mobilised and translocated. Fine-grained, clay

cutans are the most typical, whereas silt within cutans is more unusual and has been linked to agricultural activity (Courty *et al*., 1989; Kemp, 2007).

The more common orange cutans include void cutans (cutans that line voids, e.g. figures 5.26a and 5.26b), grain cutans (cutans deposited on top of grains, which were rare), discrete areas of cutans in the matrix (e.g. figures 5.26c and 5.26d) or as areas of pervasive cutans surrounding quartz grains (i.e. within a grain concentration; figures 5.27a and 5.27b). Laminations can be seen in some of the orange cutans (e.g. Figure 5.26a), particularly in the void cutans, and a general coarsening upwards can be observed in many of them. The grey cutans are typically void cutans.

Cutans range in size from approximately 0.2 to 5 mm in diameter and pervasive cutans may cover even larger areas. Orange cutans that are incorporated within the matrix and not associated with a void or grain may show evidence of deformation. This deformation is relatively subtle, in which birefringence appears disturbed and cutans appear fragmented, the latter are referred to as papules (see Tarnocai and Smith, 1989). In BBQAa there is a large circular area of deformed orange cutans, which is surrounded by a circular ring of densely packed quartz grains, with no apparent orientation (Figure 5.26d). These cutans consist of many clumps of cutans, rather than a large cutan filling the entire area.

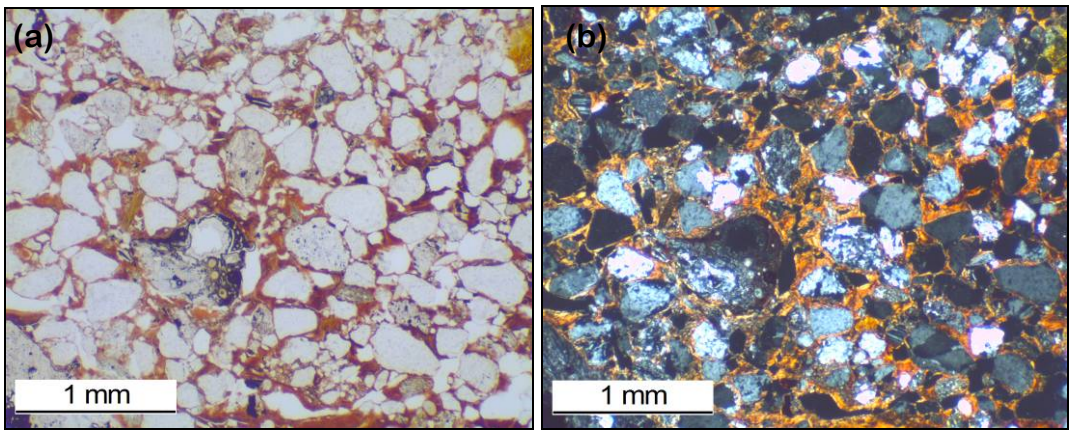

Figure 5.27 – Cutans from Blinkbonny Quarry. Cutans are indicated with green arrows. (a) Quartz grains surrounded by a cutan matrix, from BBQJ. (b) Previous image in cross polarised light. Cutans are highly birefringent.

Orange cutans are sometimes associated with grain concentrations and clasts. They may be located along the edge of or within a grain concentration. Where they are associated with clasts they may be directly below or above the clast and in some cases the cutans radiate out from the clast as shown in Figure 5.26c.

Differences in the type and abundance of orange cutans between different samples are apparent, demonstrating that they are spatially variable over metre scales. BBQA cutans are light to dark orange, often laminated and usually associated with voids or clasts and have a bright orange birefringence. BBQJ is packed with cutans that are distributed throughout the matrix (Figure 5.27) in addition to discrete areas of cutans in voids. BBQi and BBQii cutans are less abundant than those in BBQA and BBQJ.

c. Turbates

Turbates are common structures in tills and other diamictons, where they indicate clast rotation and ductile deformation (van der Meer, 1993; Menzies, 2000). Turbates are present in all of the Blinkbonny Quarry samples. Many are associated with a corestone, whereby particles are aligned around a larger clast (Figure 5.28). Some turbates do not have a corestone and these are typically smaller (Figure 5.28). Some of the alignments pinch out or trail off at the edge of the clast and they often do not extend around the whole clast.

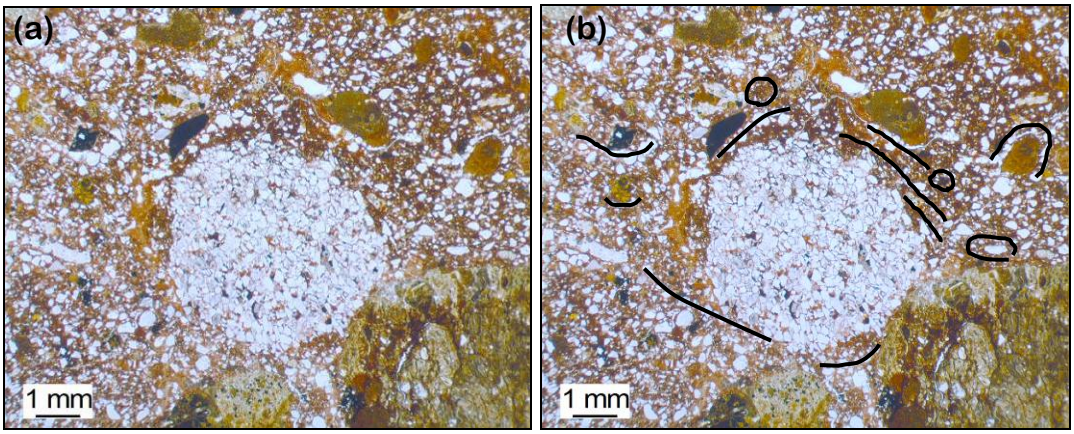

Figure 5.28 – Turbates from Blinkbonny Quarry. (a) Unannotated and (b) annotated image of a large turbate with a corestone and several smaller turbates with and without corestones (marked with black lines). Also note the orange cutans around the structure.

d. Grain lineations

Grain lineations are abundant in all of the Blinkbonny Quarry samples (Figure 5.29). They can indicate the type and direction of strain (e.g. Hiemstra and Rijsdijk, 2003; Larsen *et al*., 2007) and are considered to represent shear planes within diamicts (Larsen *et al*., 2007). Mapped lineation types include both; (a) alignments of skeleton grains; and (b), discrete lines bounded by grains on either side (which may also be highlighted by iron staining along the line). However, the distinction of these two types is not

always clear. These lineations were mapped across selected thin sections, revealing an extensive network of lineations, many of which cross-cut each other (figures 5.29 and 5.33). Of the lineations mapped, some could be connected and traced across the width of the slide (up to 55 mm). Orientations of the lineations are presented in rose diagrams in Figure 5.30, alongside a diagram illustrating common Riedel shears, for comparison. The mapped grain lineations are presented in Appendix C.2.

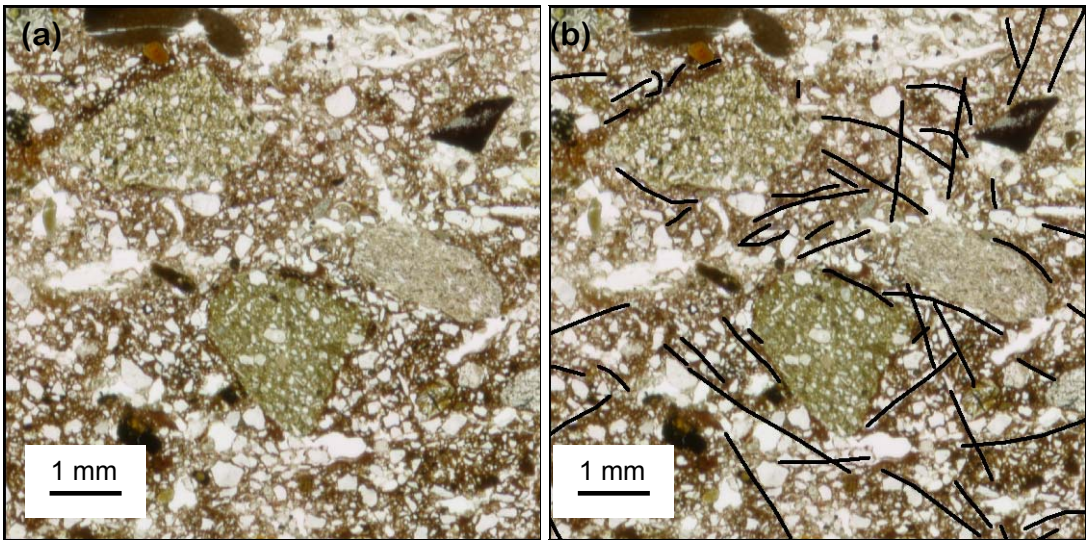

Figure 5.29 – Grain lineations, marked in black, from BBQi.

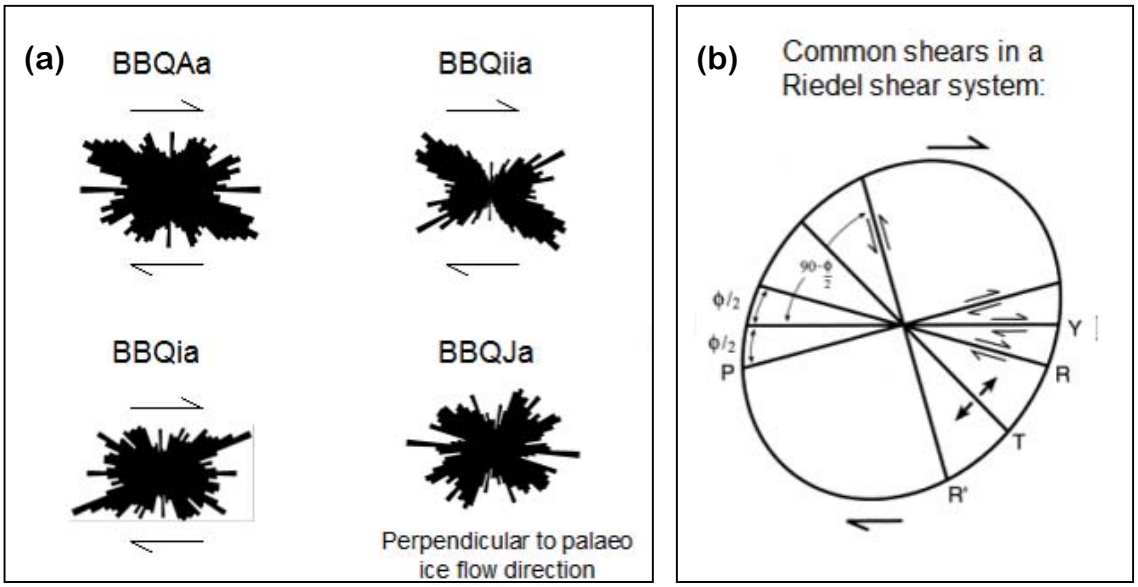

Figure 5.30 – (a) Rose diagrams of grain lineation orientations from vertical thin sections. Relative sense of shear is indicated with arrows. (For BBQAa n = 2590; for BBQiia n = 1489; for BBQia n = 3061; and for BBQJa n = 1387). (b) A schematic diagram of the common shears within a Riedel shear system (φ = the angle of internal friction), modified from Davis *et al*. (2000).

e. Disintegrating grains

Weathering features, including weathering rinds and spalling grains, are evident on some of the clasts in the Blinkbonny Quarry samples. Spalling grains refer to the removal of grains from clasts, which take place via erosional processes such as abrasion (Hooke and Iverson, 1995). Weathering rinds are formed by chemical alteration of the outer edge of clasts and they can form within a soil or sediment profile (Gordon and Dorn, 2004). Weathering rinds can be seen on several lithologies, including sandstones, mudstones and igneous clasts (Figure 5.31).

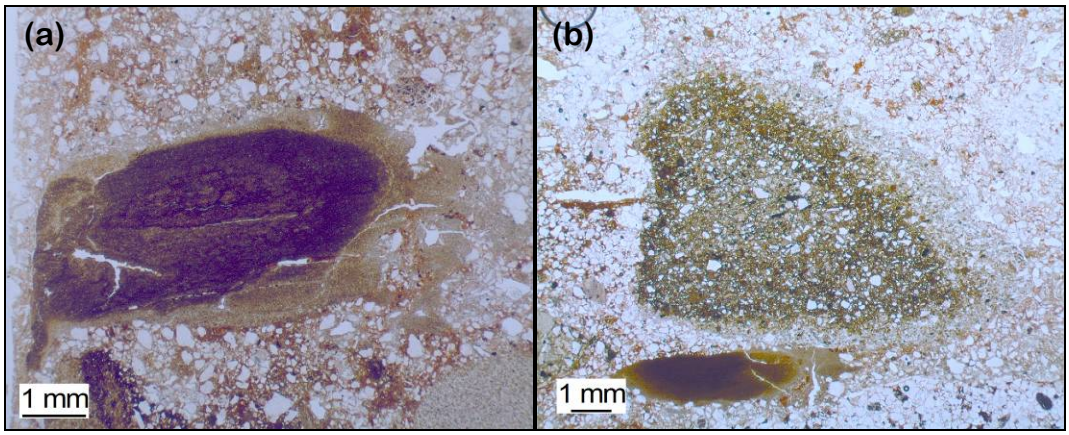

Figure 5.31 – Disintegrating grains from Blinkbonny Quarry. (a) Mudstone with a weathering rind, from BBQii (typical of BBQii). (b) Greywacke clast (above) and mudstone clast (below), both of which have weathering rinds, from BBQiia.

f. Plasmic fabric

Plasmic fabric refers to the orientation of clay particles seen within a thin section and it may indicate processes such as shear strain, wetting and drying, and shrink and swell (e.g. Dalrymple and Jim, 1984; van der Meer, 1993; Menzies, 2000). Plasmic fabrics are abundant in the matrix and cutans of all the Blinkbonny Quarry samples. Plasmic fabric can be masked by iron staining, which may have caused it to be under-represented in some thin sections. Skelsepic plasmic fabric is common (Figure 5.32) and is present in vertical and horizontal thin sections and in different types of matrix (i.e. multiple domains). Skelsepic plasmic fabric may form by processes such as wetting and drying (Dalrymple and Jim, 1984) and in the subglacial environment it can form via particle rotation (e.g. van der Meer, 1993; Hiemstra and Rijsdijk, 2003). Masepic plasmic fabric is pervasive within cutans, where it is parallel to any laminations and to the void edge (where present). This reflects the deposition of clay particles with a preferential

alignment within cutans. Masepic plasmic fabric is also found in some localised areas of matrix.

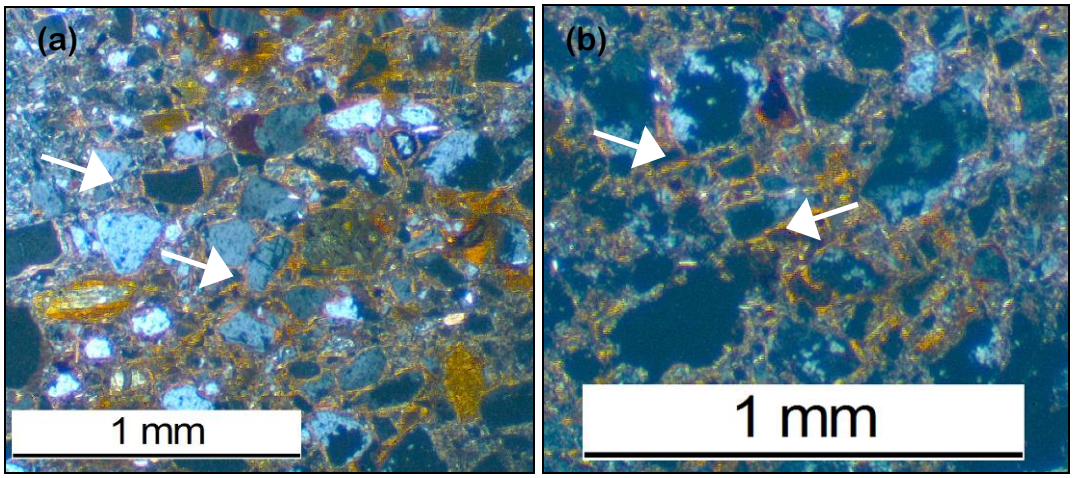

Figure 5.32 – Plasmic fabric from Blinkbonny Quarry, marked with white arrows. (a) and (b) Skelsepic plasmic fabric in BBQia in cross polarised light.

g. Associations between microstructures

The association between some of the key microscale features from LF3 in Blinkbonny Quarry was examined for one thin section that was representative of this lithofacies. This analysis involved mapping out the most common structures and is presented in Figure 5.33, which demonstrates how widespread these common features were. This figure illustrates a dense network of grain lineations that appear chaotic, but as shown in Figure 5.30a collectively these features reveal a pattern and have dominant orientations. The lineations frequently overprint each other and in some areas appear to have an overriding orientation, which may relate to Riedel shear orientations (Figure 5.30b). The lineations also appear to relate to some of the clasts, for example, grain lineations form an arc around the clast labelled ‘1’, which extends around the clast and continues to the right of it, in the direction of former ice flow. Grain lineations can also be observed trending around some of the other clasts and in particular the clast labelled ‘2’, which is also notable for the lack of grain lineations and other features in the zones on each side of the clast. Clast ‘3’ also has many grain lineations associated with it and many lineations are orientated from upper left to the lower right around this clast. The area to its lower left is characterised by several lineations and elongate clasts, all trending left to right and many funnelling down in between clasts 1 and 3. The area to the upper left of clast 3 is notable for its lack of structures.

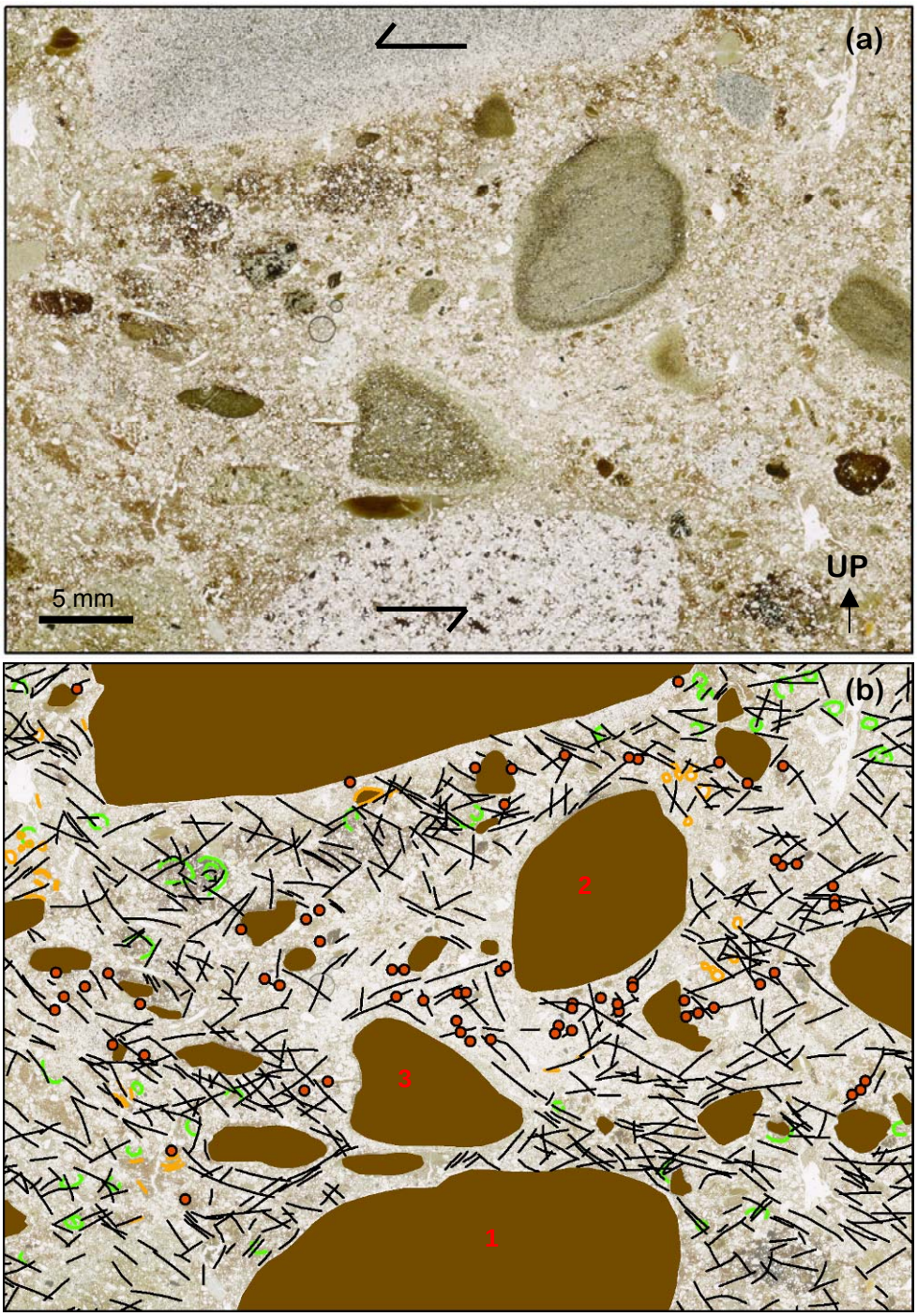

Figure 5.33 - Twinned images of thin section BBQii. An unannotated, high resolution scan of the thin section in normal light conditions, is shown in (a) and a view of annotated features overlying the faded image is shown in (b). Relative sense of shear is indicated with arrows and numbers are referred to in the text. The plasmic fabric indicated is not visible in (a) but has been identified under the microscope in cross polarised light; it is shown schematically in (b), with circles for skelsepic plasmic fabric and lines of plasmic fabric indicating the overall direction of any masepic plasmic fabric.

Figure 5.33 illustrates the widespread nature of the cutans, albeit they are not distributed evenly across the image and some appear in small clusters. Cutans frequently appear in close association with grain lineations and in some cases these features appear to lay directly on top of each other. Plasmic fabric and turbates are both less prolific than grain lineations and cutans. They are usually close to the abundant grain lineations and only rarely display cross cutting relationships with them. For many of the cross-cutting features it is not clear which features are superimposed and which are underlying, however, upon examination of some of the turbates it appears that the lineations may be superimposed on top of them.

h. Microfabric

Microfabric (particle size 0.031 to 8 mm) was measured in horizontal (b) slides (to obtain particle azimuth) from BBQi, BBQii and BBQJ and in a vertical slide (c) (to obtain particle dip) from BBQii (which is parallel to the mean microfabric azimuth). Microfabric can indicate direction and degree of sediment strain (Hooyer and Iverson, 2000; Thomason and Iverson, 2006).

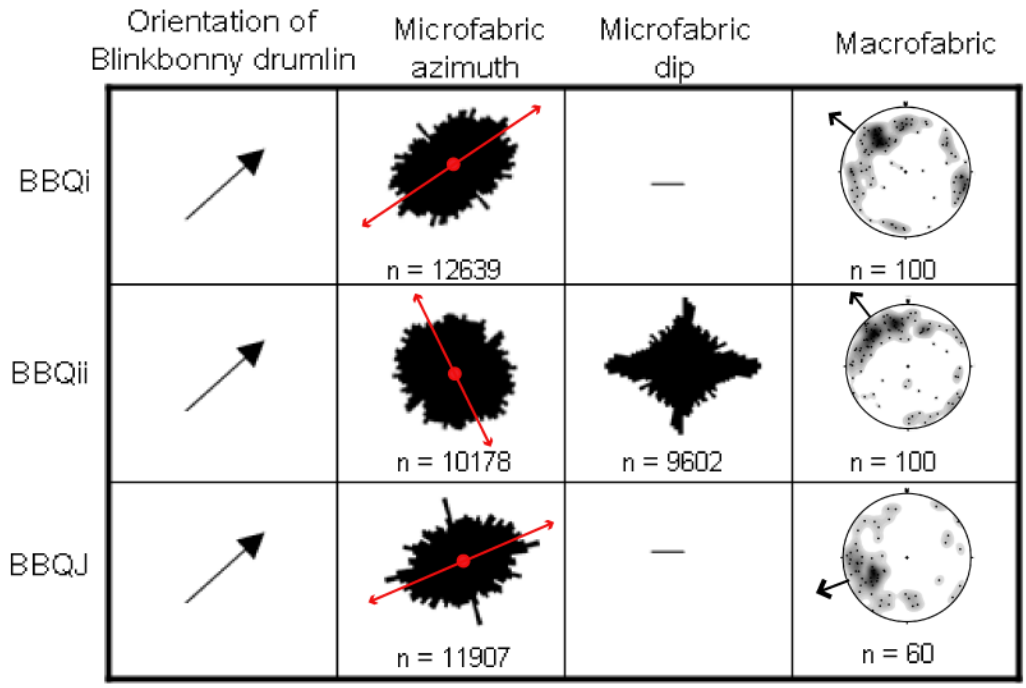

Figure 5.34 – Microfabric rose diagrams of azimuth (vector mean is indicated by a red arrow) and dip. The orientation of the Blinkbonny Quarry drumlin and the macrofabric (principle eigenvector azimuth is indicated with an arrow) is also shown for comparison. BBQii dip was measured along the mean microfabric azimuth.

BBQi microfabric displays a clear orientation at 41º – 221º, it is parallel to the orientation of the drumlin and transverse to the macrofabric orientation (Figure 5.34). BBQii microfabric has a more rounded rose diagram with an average orientation of 144º – 324º, it is transverse to the orientation of the drumlin and parallel to the macrofabric orientation. BBQii microfabric dip has a distinctly shaped rose diagram, with large vertical and horizontal peaks as well as particles in all directions. BBQJ microfabric has an ovate shaped rose diagram with a clear orientation at 66º – 244º, parallel to the macrofabric and the drumlin orientation. All microfabric azimuth rose diagrams have a small transverse peak, which can be seen in each. Confidence intervals for microfabric azimuth are given in Appendix C.3.

5.3.5 Microscale interpretation

The microscale structures identified in LF3, such as turbates, grain lineations and skelsepic plasmic fabric, indicate that the processes of deformation, shear and rotation took place (e.g. van der Meer, 1993; Menzies, 2000). This indicates that the diamict has been subject to the processes associated with shear, which would be expected in certain environments such as subglacially or a sediment flow (e.g. Menzies, 2000; Lachniet *et al*., 2001; Phillips, 2006). However, together with the macro and meso scale evidence, particularly the clear geomorphological evidence for the situation of the site on a drumlin, these observations support the interpretation that this lithofacies is a subglacial traction till. Ductile deformation and sediment mixing is evident from several features including multiple domains, turbates, intraclasts and papules (Tarnocai and Smith, 1989; van der Meer, 1993; Menzies, 2000; van der Meer *et al*., 2003). Turbates and skelsepic plasmic fabric demonstrate that rotation was commonplace within the till (see van der Meer, 1993; Hiemstra and Rijsdijk, 2003).

Evidence for brittle shear in the samples is evident from grain lineations, faulting and unistrial plasmic fabric. Grain lineations were pervasive throughout most of the thin sections (figures 5.30 and 5.33 and Appendix C.2). The vast majority of the mapped lineations were lines within the matrix, that were delineated by grains, and in places highlighted by iron staining, which are thought to represent discrete shear lines (Menzies, 2000; Larsen *et al*., 2007). They depict inhomogeneous deformation of the

sediment and their widespread presence suggests that localised stress concentrations and/or heterogeneities in the sediment were commonplace (White *et al*., 1980).

The microscale features shown in Figure 5.33 give a sense of the former movement and strain in the sediment and associations within and between the features may bring some insight into the processes that formed them. The orientation of the grain lineations around clast '1' appear to point in the direction of shear, which is an occurrence that is well established for porphyroclasts in the field of metamorphic geology (Passchier and Simpson, 1986). The structure is essentially a large turbate structure, which is frequently linked to clast rotation (e.g. van der Meer, 1993; Menzies, 2000; Phillips, 2006). Furthermore, whilst grain lineations are commonly thought of as brittle deformation, turbates are associated with ductile deformation (van der Meer, 1997; Menzies, 2000) and so this combination illustrates how brittle and ductile deformation may take place concurrently at different scales (Menzies, 2000). This association and the close association of grain lineations and turbates elsewhere in Figure 5.33, indicate that these features formed under similar processes within the same environment. The clear evidence for ductile and brittle microstructures in close association suggests that polyphase deformation was typical (see Menzies, 2000), indicating that that the conditions were dynamic. The identified superimposition of shears on top of turbates, suggests that high pore water pressures and ductile deformation were succeeded by low pore water pressures and brittle deformation. It is unclear whether this relates to certain events of the ice stream, such as fast flow followed by retreat and dewatering of sediments, or if it just represents the changeable conditions in the subglacial environment. However, it is evident that ductile and brittle deformation both served to form structures indicative of rotation and shear, indicating that both deformation types operated under simple shear. The preservation of turbates that underlie grain lineations demonstrates that at least in some cases brittle shearing is manifest in very small displacements and/or rotation of grains

Grain lineations are present around clast '2', Figure 5.33, but are lacking in the areas each side of the clast. These may represent pressure shadows, whereby the matrix deforms around the top and base of the clast and in this case concentrated along the shears, whilst the areas either side of the clast are shielded from the deformation (van der Meer, 1993; Menzies, 2000; Barker, 2004). This observation adds to the evidence that ductile deformation was taking place subglacially at the micro scale. Interestingly

this trend is also seen in the cutans, which are lacking from the pressure shadow areas, but are present in other surrounding areas. This could be a result of the favoured deposition of cutans in the areas of higher deformation, maybe because of differences in sediment properties such as dilation. The lineations and clasts around and to the left of clast '3' depict a sense of movement from upper left to lower right. The area lacking in structures on the upper left of clast '3' may represent a pressure shadow, which would fit with the propagation of shear from upper left to lower right.

Whilst overall the mapped grain lineations appear chaotic (figures 5.29 and 5.33), further examination reveals that they display several preferred orientations, which may be indicative of a Riedel shear system. Common Riedel shears, including R, R´, P, Y and T can be identified in the results (Figure 5.30). The strongest peaks are typically in the synthetic (dipping downstream) shears, which is consistent with the findings of Larsen *et al*. (2007) for microshears in a subglacial till. Shearing was extensive and complex, and this may be a result of high strain (Thomason and Iverson, 2006) and/or high water content (Arch *et al*., 1988).

Orange and grey cutans were abundant throughout the thin sections. These two types of cutan differ in colour, texture and location in association with voids and particles; suggesting that they have different depositional origins. The grey cutans are superimposed onto the orange cutans, indicating that the grey cutans are younger and that two phases of cutan deposition took place in the sediment. Cutans are usually considered to be pedogenic features, which form via the gradual accumulation of translocated clay, typically in interglacial climates (Kemp, 2007). This may be the origin of the younger, undisturbed grey cutans, which appear to be *in situ*, inside of voids. The silty texture suggests that they may reflect agricultural activity, which can occur via the translocation of silts and clays from slaked surfaces to form agricutans (Courty *et al*., 1989; Kemp, 2007).

The orange cutans display evidence of deformation and brecciation (papules) demonstrating that they were disturbed after deposition, and hence have a more complex history than the grey cutans. Whether the origin of these cutans is pedogenic, periglacial or subglacial, their explanation must account for their disturbance, which may have occurred during or after deposition. Possible explanations include a pedogenic origin followed by a period of disturbance such as periglacial activity or

mass movement. However, there is no evidence at the site for periglacial activity or mass movement. Furthermore, the position of the cutans were below the reported extent of soil illuviation in the area, at a depth of 71 cm (Ragg, 1960), albeit this may not necessarily be accurate for the locality of the quarry. A pedogenic origin is also inconsistent with the spatial variability (vertically and laterally) of the orange cutans, because pedogenic illuviation would be expected to decrease with depth. A periglacial origin for the cutans would explain their disturbance. However, as noted, there is no evidence for periglacial activity at the site, although the area would have been subject to temperatures conducive to this, during the Loch Lomond Stadial (Ballantyne and Harris, 1994). The final possible explanation for the cutans, a glacial origin, would explain their disturbance and is consistent with the abundant evidence for glacial activity. It is also consistent with the fact that the cutans are closely associated with certain deformation structures, such as turbates (figures 5.26c, 5.28 and 5.33). Given these observations and the lack of evidence for other mechanisms that would explain the cutan disturbance, a subglacial origin for the orange cutans may be the most likely explanation. This implies that sufficiently high pore water pressures were present within the subglacial environment in order to separate the clay particles (van der Meer, pers comm.), and that the voids in which the cutans are situated, were formed subglacially and may reflect subglacial drainage in the form of Darcian flow (Figure 2.5). This evidence is among very few reported examples of subglacial cutans (e.g. Kilfeather, 2004) and as such may help inform future micromorphological studies on the interpretations of cutans within glacial sediments.

5.4 Newton Quarry

5.4.1 Site background

Newton Quarry (also known as Swinton Quarry) is located at NT 864 485 (386400, 648500), near the centre of the Tweed Palaeo-Ice Stream, approximately 20 km downstream of Blinkbonny Quarry (figures 5.1 and 5.5). Newton Quarry is situated on a small drumlin, which is 645 m long, 245 m wide, 10 m high and orientated at 72°. The quarry is situated at the stoss end of the drumlin, on its crest (Figure 5.35). The geomorphology surrounding Newton Quarry is characterised by elongate subglacial lineations (Figure 5.35). They appear more subdued than those surrounding Blinkbonny

Quarry, which may be a result of different underlying lithologies with differing degrees of resistance. Newton Quarry is situated on the Ballagan Formation, which formed during the early Carboniferous, and comprises thinly bedded grey mudstones and siltstones, with some ferroan dolomite (cementstones), gypsum bands and sandstones (British Geological Survey, 2007).

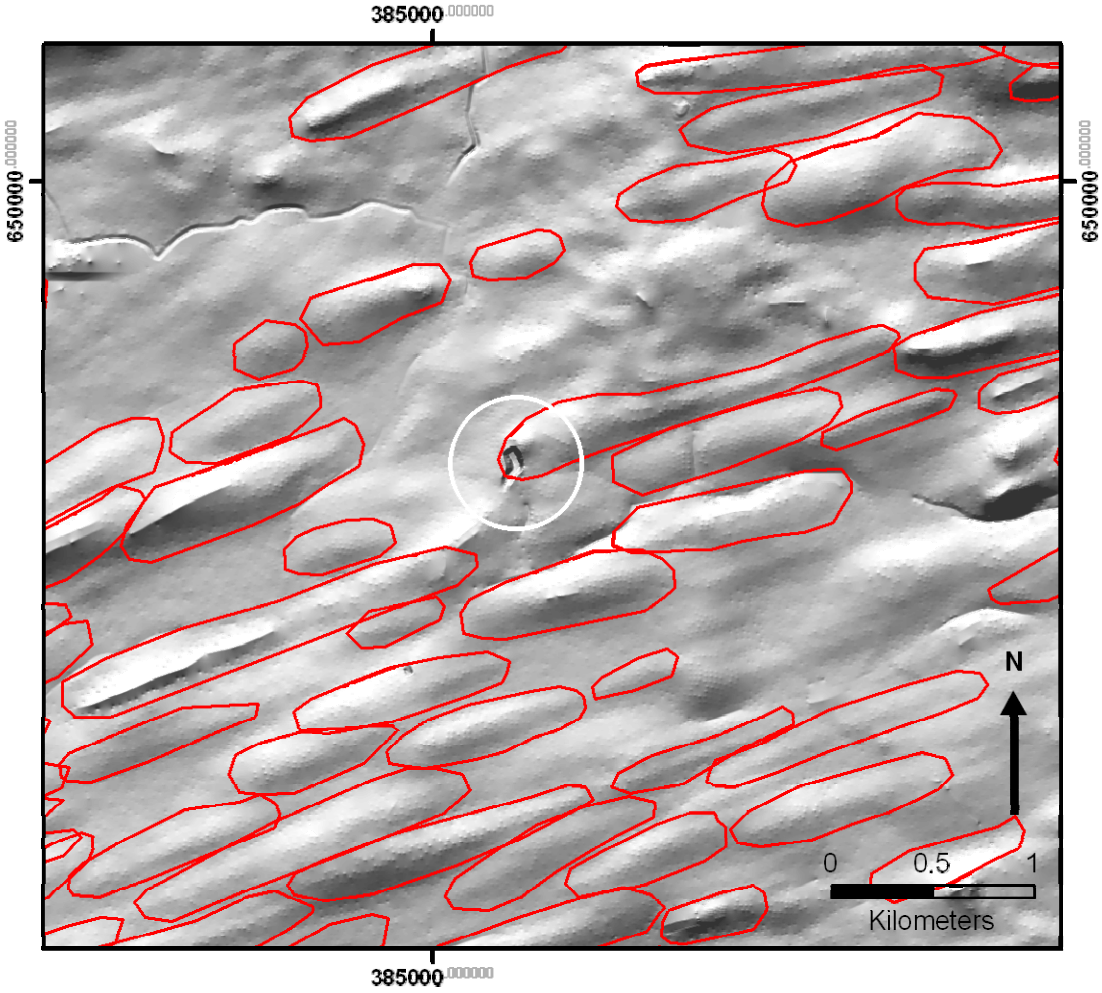

Figure 5.35 – DEM of Newton Quarry and the surrounding area. Subglacial lineations are outlined in red and the quarry is indicated with a white circle. Nextmap DEM has a vertical exaggeration of x4.

5.4.2 Mesoscale sedimentology

Exposed Quaternary sediments overlie bedrock in several sections at Newton Quarry. The sediments are characterised in vertical and 2D section logs, the locations of which are given in Figure 5.36. Sections B and C are approximately parallel to palaeo ice flow; A, G and H are perpendicular to palaeo ice flow; and D is oblique to palaeo ice flow. Five lithofacies were found at Newton Quarry, described as follows.

At the base of many of the sections is Lithofacies 1 (LF1), which overlies the sandstone bedrock. LF1 is a fissile mudstone bedrock, containing some sandstone rafts and layers and is 1 to 4 m thick where seen (figures 5.37 and 5.39c). The fissile structure that is apparent at the base of this lithofacies gradually declines with distance up the profile. Towards the top of the lithofacies there is also evidence for disturbance of the pre-existing structure and minor deformation.

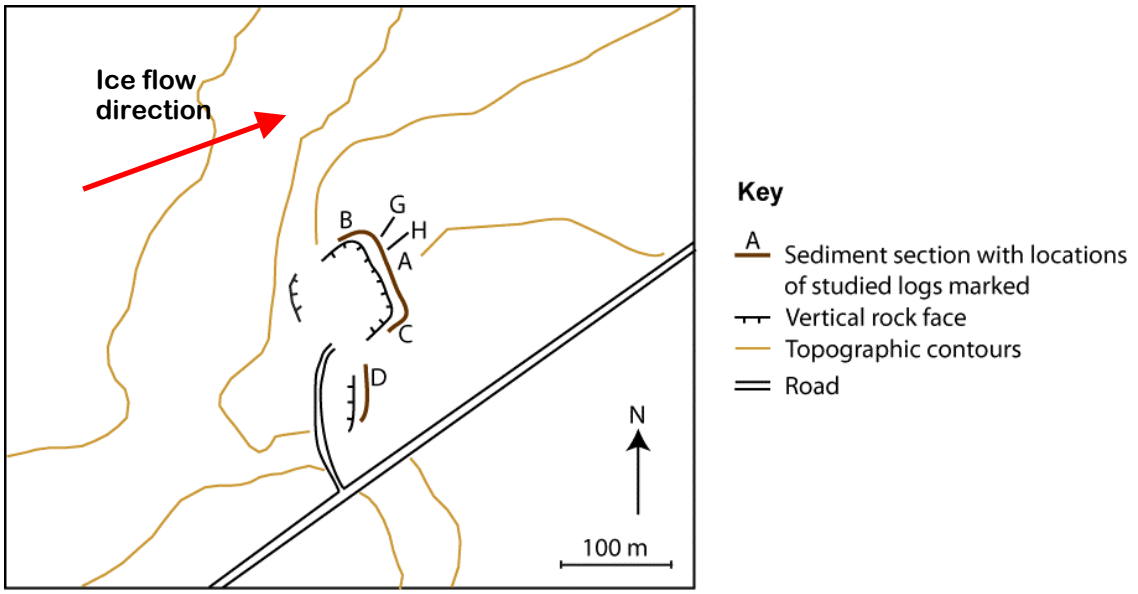

Figure 5.36 – Map of Newton Quarry showing the locations of the main sediment sections (A, B, C and D) and additional sections (G and H). Topographic contours (10 m intervals) are from Ordnance Survey data (Ordnance Survey).

Lithofacies 2 (LF2) is a clayey, matrix-supported diamicton (Figure 5.37), which is present at sections A and C (Figure 5.37). This lithofacies is dominated by a fine-grained matrix very similar in texture to the underlying LF1. It contains very few gravel sized clasts of a different lithology. Particle size distribution data shows that it is dominated by clay and silt sized particles, with some sand and gravel, the proportion of which increases with distance up the lithofacies (Appendix B). It is dominated by brecciated, fissile bedrock, clasts of which completely disintegrate when removed from the sediment. There are also several sandstone bedrock rafts present (up to 60 cm thick). There is a gradational contact between LF1 and LF2 and an upwards trend of increasing deformation and loss of bedrock structure.

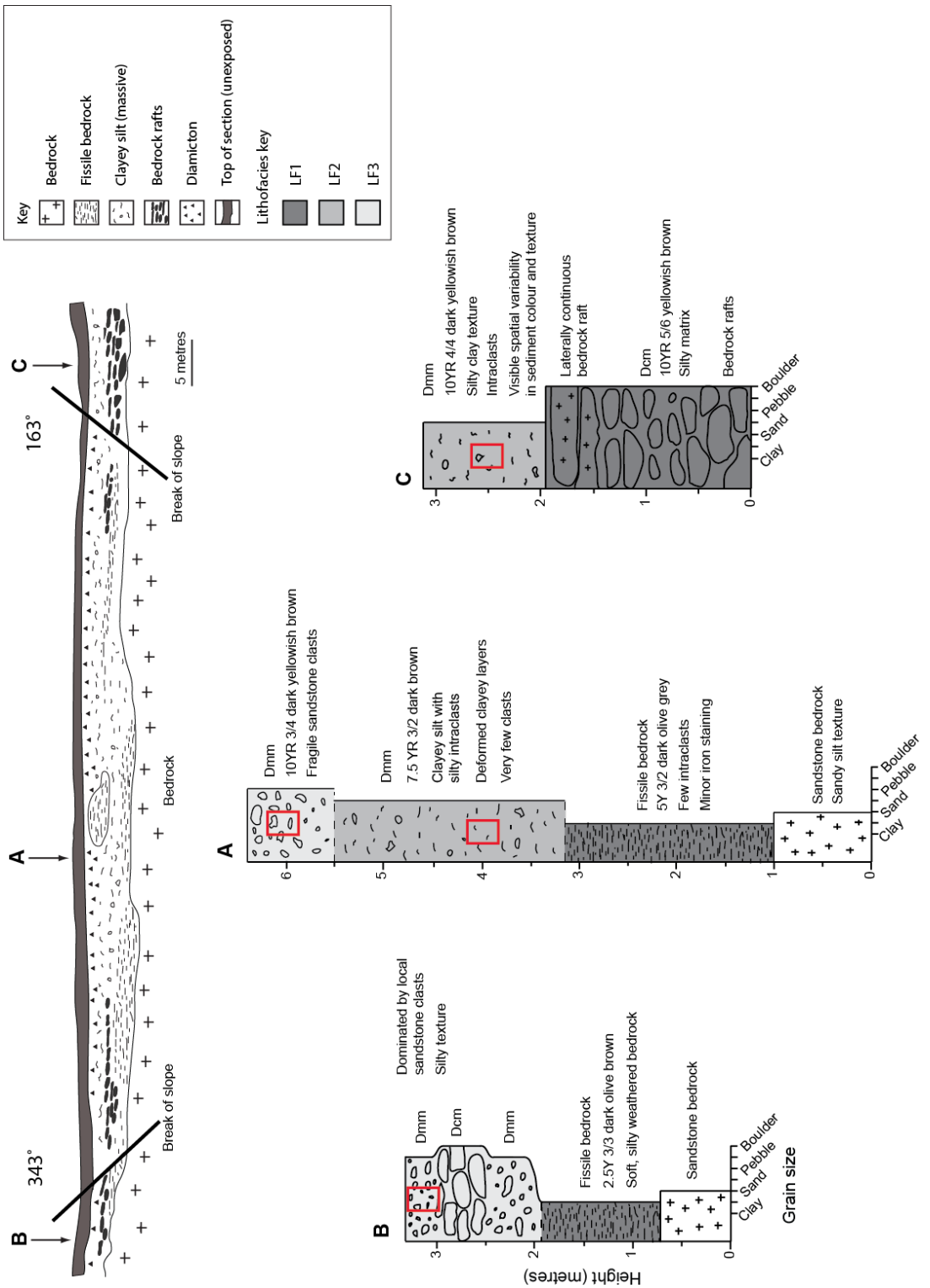

Figure 5.37 – Section drawing of the main sediment section at Newton Quarry and vertical logs for profiles A, B and C. Locations of the logs are given in Figure 5.36. Note that the side sediment faces on which section B and C are situated are both perpendicular to the central face. Locations of kubiena tin samples are shown with red rectangles in the vertical logs. LF1 is dark grey, LF2 medium grey and LF3 is light grey.

Lithofacies 3 (LF3) is a matrix-supported diamicton (Figure 5.37), which is considerably more clast rich than LF2. This diamicton caps the sequence at sections A, and B. It contains a range of clast lithologies, including many local sandstone clasts. Particle size distribution data demonstrates that this lithofacies contains clay size to gravel size particles. It has a coarser matrix than LF2 and a greater proportion of gravel sized clasts (see Appendix B). Clast morphology demonstrates that clasts from this lithofacies trend towards a spherical shape, rather than a disc or rod shape and they are typically sub-angular and sub-rounded, indicative of abrasion processes (Figure 5.38). This lithofacies is compact and as observed at Blinkbonny Quarry, the majority of clasts disintegrate very easily upon removal, which contrasts with the strong, coherent clasts that can be obtained from the underlying sandstone bedrock.

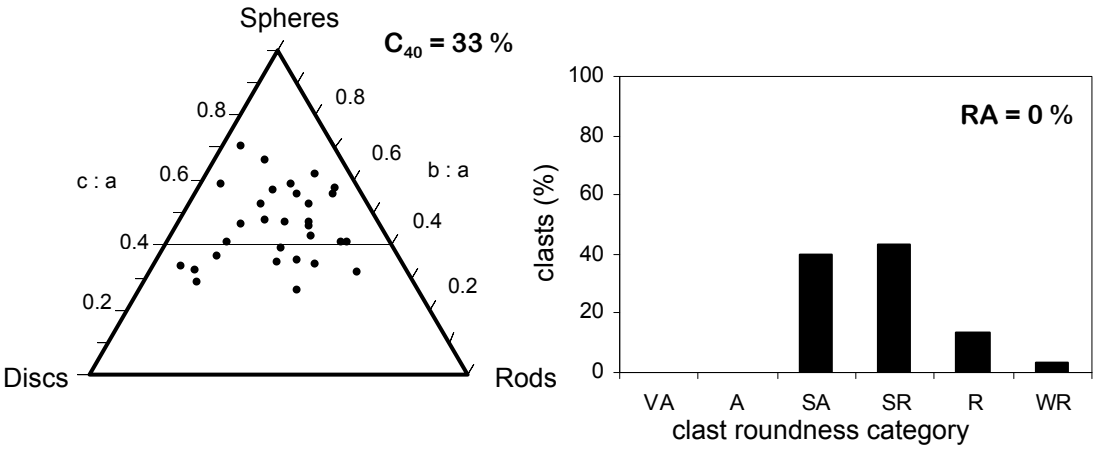

Figure 5.38 – Newton Quarry clast morphology. (a) Clast shape for NQA; sampled from 6 m up Section A (n = 30). (b) Clast roundness for NQA; sampled from 6 m up Section A (n = 30). Clast roundness categories are as follows; VA = very-angular, A = angular, SA = sub-angular, SR = sub-rounded, R = rounded, WR = well-rounded.

Lithofacies 4 (LF4), a reddish, matrix-supported diamicton, is dominant in Section D (figures 5.39d and 5.37). It reaches up to 2.5 m thick and overlies undeformed fissile bedrock. It is spatially variable in texture and colour, as depicted in Figure 5.40. Inclusions of a grey diamicton, sandy intraclasts and clast concentrations are present within it. Particle size distribution shows that it is dominated by clay and silt sized particles, with little sand and a very small quantity of gravel sized clasts (see Appendix B).

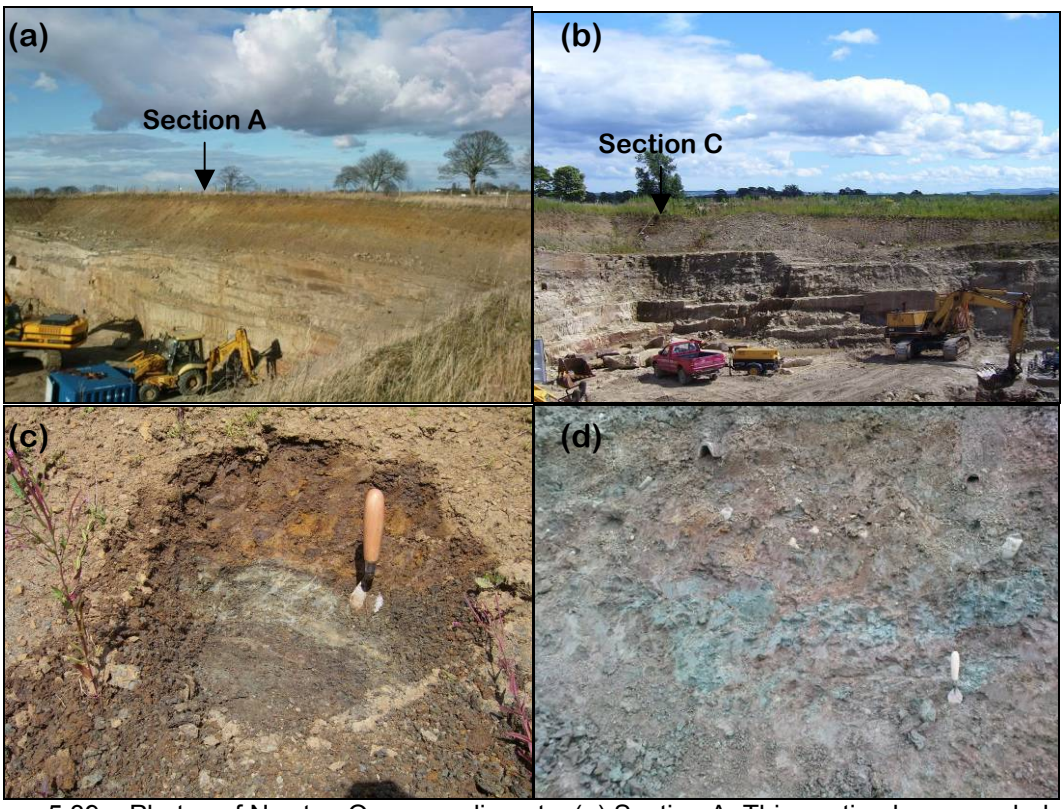

Figure 5.39 – Photos of Newton Quarry sediments. (a) Section A. This section has a graded surface and overlies sandstone bedrock. Note the spatial variability of the sediments, which is depicted by colour changes. (b) Section C. This section is situated in the corner of the quarry on the north facing sediment face, the section pinches out to the right hand side of the image (to the west). (c) Fissile bedrock layers from Section A (trowel length is 23.5 cm). Note the disturbance of the light grey layers and the orange iron staining. (d) Diamict melange (LF3) from Section D, which depicts the spatial variabilities in colour and texture in this section (trowel length is 23.5 cm).

Lithofacies 5 (LF5) is situated at the northern end of Section D, overlying Lithofacies 4 (Figure 5.40). LF5 is a grey, fissile, matrix-supported diamicton, up to 1 m thick. It has a sharp, angled contact with the underlying lithofacies, dipping to the east.

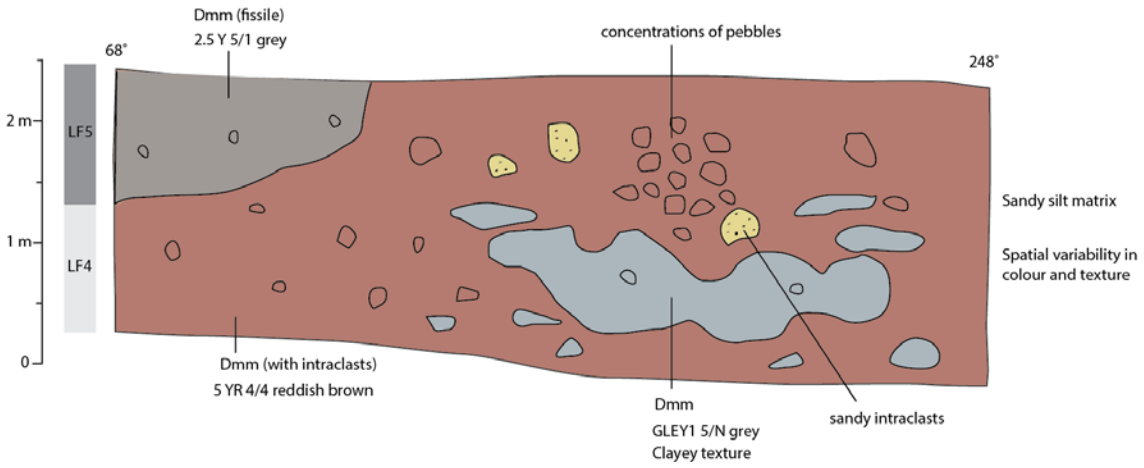

Figure 5.40 – 2D log of Section D. LF4 is marked with light grey and LF5 is marked with dark grey, in the left hand column.

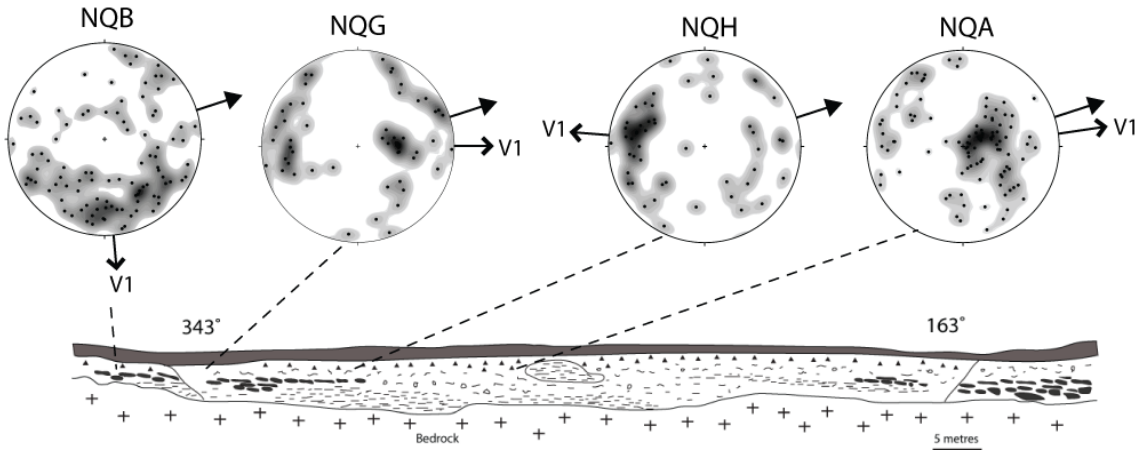

Figure 5.41 – Macrofabrics from LF3, from sections NQB, NQG, NQH and NQA. Closed arrows indicate the orientation of the subglacial lineation and open arrows, labelled V1, indicate the principle eigenvector azimuths. Macrofabric sample sizes are as follows: NQB (n = 100); NQG (n = 50); NQH (n = 50); and NQA (n = 100).

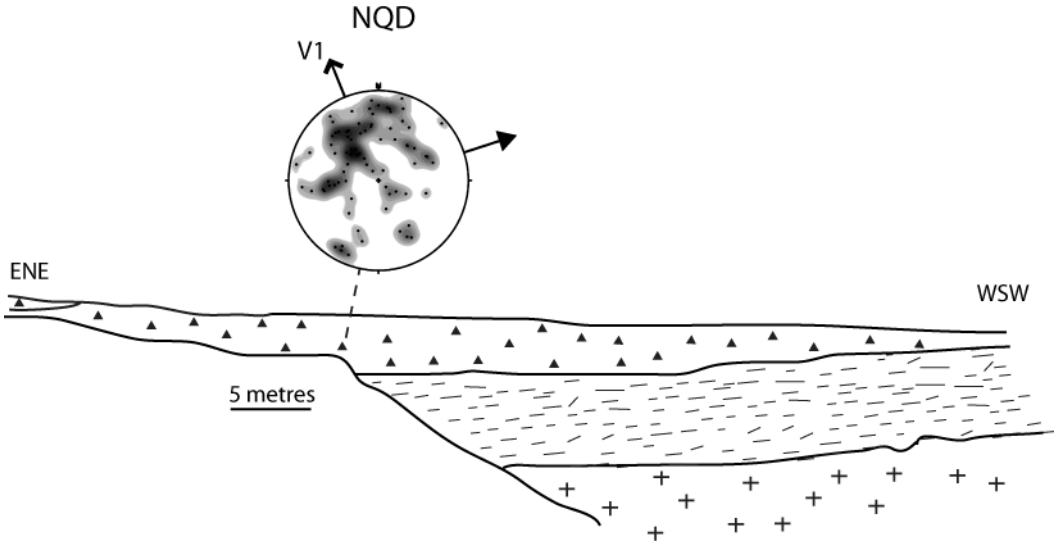

Figure 5.42 – Macrofabric from LF4, section NQD (n = 80). The closed arrow indicates the orientation of the subglacial lineation and the open arrow, labelled V1, indicates the principle eigenvector azimuth.

Macrofabric was measured from LF3 at sections A, B, G and H and from LF4 at Section D (figures 5.41 and 5.42). NQA macrofabric is weakly clustered, orientated parallel to the drumlin and steeply dipping downstream. It is notable that this fabric was sampled from close to a large clast, which became evident as the sediment was excavated to measure the fabric. NQG and NQH macrofabrics have a range of orientations, but have overall orientations similar to that of the drumlin and their eigenvalues indicate that they are both linearly clustered. They both have shallow dips (Figure 5.43) in the downstream and upstream directions, respectively. In NQB, clasts are orientated transverse to the orientation of the drumlin in a isotropic or girdle shaped fabric. Clasts have a medium/low dip to the south. NQD has a weak linear clustering of clasts orientated transverse to the subglacial lineation. It has a medium dip to the north.

The ternary diagram in Figure 5.43 shows that the fabrics all have a broadly similar shape and are weakly clustered, apart from NQB, which has a more isotropic fabric. Based on the suggestion of Dowdeswell and Sharpe (1986) the S_1 value <0.5 and S_3 value >0.17 at NQB indicates a random distribution of clast orientation.

(a)

Sample	Lithofacies	Mean vector	Mean dip	Eigenvalue	Clustering
NQA	LF3	98.5°	66.2°	0.551 (S_1) >> 0.279 (S_2) ~ 0.17 (S_3)	Linear
NQB	LF3	175.1°	31.4°	0.46 (S_1) ~ 0.338 (S_2) >> 0.202 (S_3)	Isotropic
NQD	LF4	338°	50.3°	0.541 (S_1) >> 0.269 (S_2) ~ 0.19 (S_3)	Linear
NQG	LF3	89.9°	9.6°	0.501 (S_1) >> 0.258 (S_2) ~ 0.24 (S_3)	Linear
NQH	LF3	274.5°	18.1°	0.534 (S_1) >> 0.258 (S_2) ~ 0.208 (S_3)	Linear

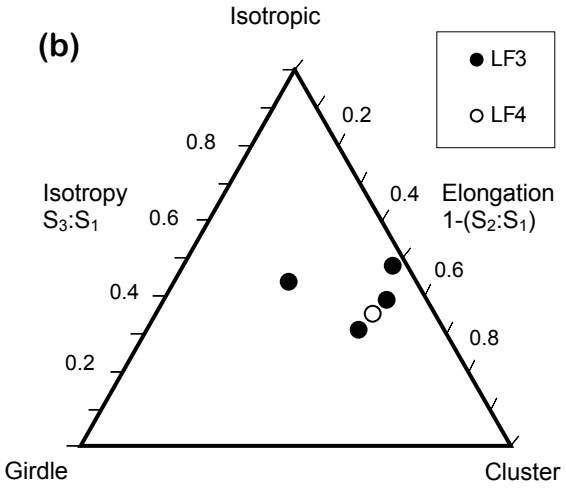

Figure 5.43 – Macrofabric eigenvalues and fabric shape. (a) Table of eigenvalues for the Newton Quarry samples. (b) Ternary diagram displaying fabric shape for the samples.

5.4.3 Mesoscale interpretation

As found at Blinkbonny Quarry, the sediments at Newton Quarry form part of the drumlinised surface of the ice stream bed, suggesting that they are contemporaneous with drumlin formation. Fissile bedrock (LF1), present at the base of the sequence here, contains some sandstone rafts and layers, and some limited evidence for deformation, indicating that this lithofacies is a glaciotectonite. This is overlain by LF2, which is similar in texture and derived from the same fissile bedrock. However, it is heavily deformed and predominantly lacks the fissile structure of the bedrock, indicating that it

is also a glaciotectonite, but with a higher level of strain than LF1. Layers of fissile siltstone and more competent sandstones can be identified within this lithofacies, which comprise bedrock rafts and boudins, and may reflect bedrock rafting. LF3 lies at the top of the sequence and is interpreted as a subglacial traction till based on its locality on top of a drumlin and its characteristics, including a multimodal particle size distribution and abraded clasts. Strain shows a clear vertical increase through the sequence of lithofacies and is highest in the subglacial traction till at the top of the sequence. At Section D a greater degree of spatial variability is evident and the increase in strain up the sediment profile is less clear. The diamictons that characterise LF4 and LF5 are both interpreted as subglacial traction tills. The high spatial variability in LF4 in terms of texture and colour suggests that it is a till melange.

Despite some spatial variabilities observed, the mesoscale results show that a vertical sequence of lithofacies of glaciotectonites overlain by a subglacial traction till, is typical for both of the quarries examined. This indicates that the processes of sediment formation and distribution of strain was similar for both sites. Moreover, Kerr (1978) found similar sediment profiles (Figure 5.3) across a large area of the Tweed Valley, suggesting that this profile of subglacial sediments may be typical for the Tweed Palaeo-Ice Stream.

Macrofabric displayed considerable spatial heterogeneity, in terms of variations in clast orientation. Nearly all of the macrofabrics were weakly clustered and most were parallel, or nearly parallel, to palaeo ice flow and few transverse to palaeo ice flow. This inconsistency and combination of parallel, transverse and oblique fabric orientations is similar to that observed at Blinkbonny Quarry and also shares characteristics of the fabrics reported by Kerr (1978) for other areas of the Tweed Valley. The anomalously high dip of NQA may be explained by the fact that it was situated close to a large clast behind which the fabric was being excavated. This may have affected the clasts directly adjacent because they may lie in a pressure shadow area and thus would not have been subject to the same shear stress as clasts elsewhere.

As was seen at Blinkbonny Quarry the fabrics are relatively weak, shown by their low S_1 values that range from 0.46 to 0.551. This is not entirely outside of the range of fabric strengths reported for subglacial tills (e.g. Hicock, 1992; Carr and Goddard,

2007) but it is considerably lower than many fabric strengths reported in the field and from experiments suggesting that it may be atypical and that another process besides simple shear was affecting the clasts (e.g. Hooyer and Iverson, 2000; Piotrowski *et al*., 2001; Larsen and Piotrowski, 2003; Iverson *et al*., 2008). The Newton Quarry site is situated directly on the stoss side of the drumlin (figures 5.35 and 5.36) and the rise in bed topography at the front of the drumlin by approximately 20 metres may have been sufficient to cause compressive flow here. However, only one clustered fabric is orientated transversely and most are orientated near-parallel to the drumlins, so an interpretation that compressive flow caused this transverse fabric is unconvincing, since it would be expected to affect the whole area.

The sediments sampled for macrofabric may have also been subject to postglacial influences, namely frost heave and gelifluction. Frost heave disturbs the particles of sediment near the surface (Harris, 2007) and can cause relatively weak, steeply dipping clast fabrics (Millar and Nelson, 2001). Gelifluction occurs when ice rich sediments thaw to produce a saturated, easily deformed sediment mass (Harris, 2007) and can cause clast fabrics strongly orientated downslope (Ballantyne and Harris, 1994). This could explain the transverse NQB fabric, which is weakly orientated downslope with the sloping sediment surface here, but this explanation does not account for the transverse fabric at NQD. Given this and without clear evidence elsewhere for postglacial processes such as these, this interpretation is not compelling. In light of reports of other weak and variable subglacial fabrics, including nearby within the Tweed Valley (e.g. Kerr, 1978; Hicock, 1992; Stalsberg *et al*., 2003; Carr and Goddard, 2007), they can be tentatively considered to be a reflection of subglacial processes. As was suggested at Blinkbonny Quarry, the possibility that high, variable pore water pressures and dilation of the sediment (see Benn, 1995; Evans *et al*., 2006a) could cause the clasts to behave differently than they do under simple shear alone.

5.4.4 Micromorphology

Four micromorphology samples were collected from LF2 and LF3 in Newton Quarry, details of which are given in Table 5.3.

Table 5.3 – Details of the micromorphology samples collected from Newton Quarry. Locations of samples are also indicated in Figure 5.37.

Sample	Sample location	Orientation to subglacial lineation	Lithofacies	Why sampled?
NQA	Section A, 6 m up profile	Transverse	3	Characterisation of lithofacies and microfabric
NQB	Section B, 3.1 m up profile	Parallel	3	Characterisation of lithofacies and microfabric
NQAxi	Section A, 4 m up profile	Transverse	2	Characterisation of lithofacies
NQC	Section C, 2.5 m up profile	Parallel	2	Characterisation of lithofacies and microfabric

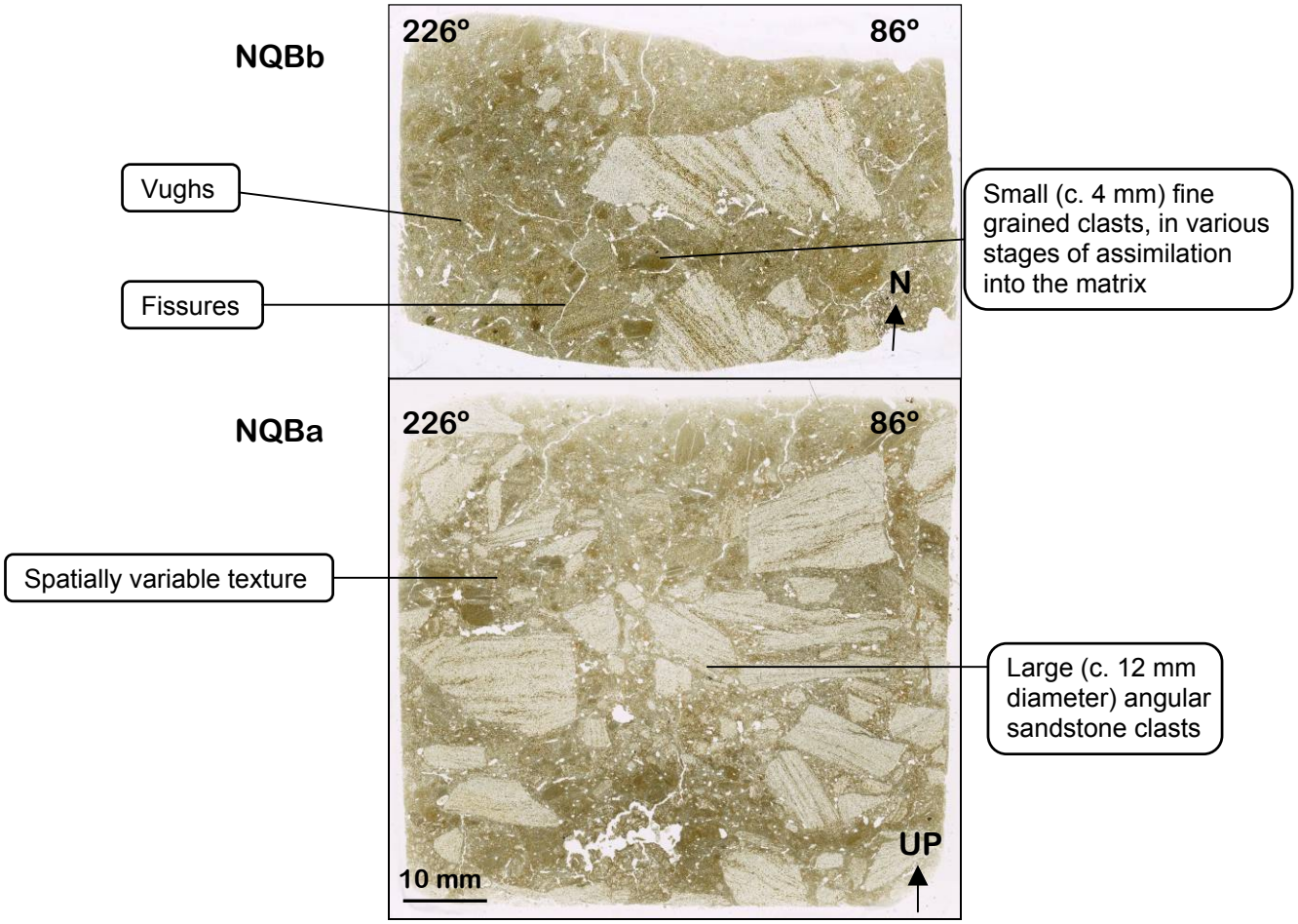

Figure 5.44 – Scans of NQBb (plan view) and NQBa (profile view), with annotations of some of the key features that can be seen at this scale. The orientations of the thin sections are displayed. NQBa is approximately parallel with the orientation of the drumlin.

Scans of thin sections from NQB (LF3) and NQC (LF2) are shown in figures 5.44 and 5.45. They show the overall texture and structure that characterises each lithofacies. NQB is dominated by local sandstone clasts. Skeleton grains are highly concentrated and are dominated by grains derived from the larger clasts, including quartz, mica and biotite. NQC has a finer texture than NQB. NQC is characterised by mudstone clasts in a fine-grained matrix, with localised areas of grain concentrations. The abundant local mudstone clasts in LF2 are very similar in appearance and texture to the matrix and in many clasts have indistinct edges where they grade into the matrix.

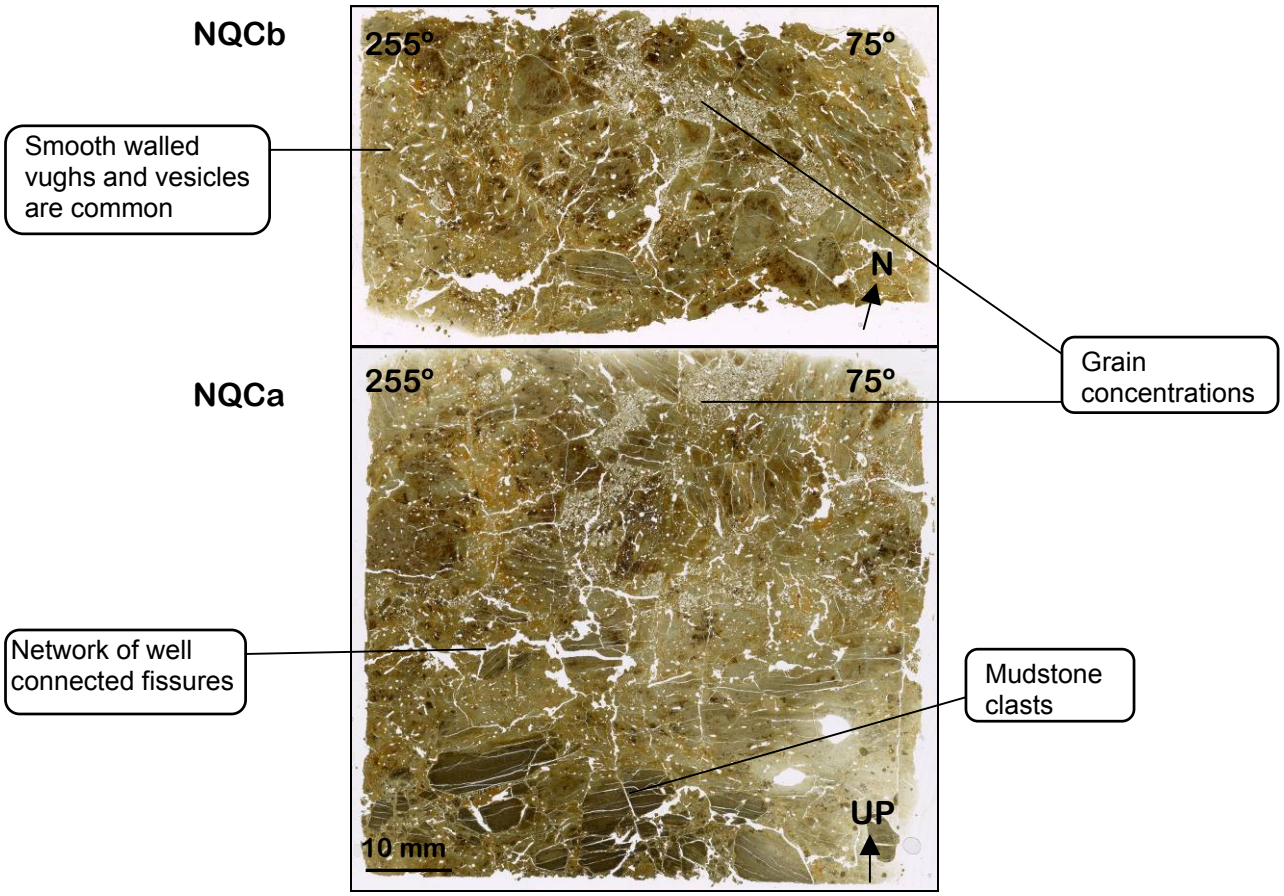

Figure 5.45 – Scans of NQCb (plan view) and NQCa (profile view) with annotations of some of the key features that can be seen at this scale. The orientations of the thin sections are displayed. NQCa is approximately parallel to the orientation of the drumlin.

An overview of the micromorphology is given in Table 5.4 followed by descriptions and images of the most significant features. Definitions of the micromorphological features described are given in the glossary (Figure 3.9, pages 48-49). More detailed micromorphological descriptions for each sample are given in Appendix C.1.

Table 5.4 – Summary table of the micromorphological features from the Newton Quarry samples. The relative abundance of each feature for each sample is given in a 1 to 3 scale; 3 (●●●) = very abundant, 2 (●●) = present in two or more locations in the sample; 1 (●) = present in a single location in the sample; 0 (-) = not present.

	Voids			Sediment mixing		Water movement	Grain structures			Brittle deformation	Clast/matrix alteration				Plasmic fabric		
	Fissures	Vesicles	Vughs	Multiple domains	Intraclasts	Cutans	Grain concentrations	Turbates	Grain lineations	Faulting	Spalling grains	Clast weathering rinds	Clast edge grading into matrix	Iron staining	Masepic	Skelsepic	Unistral
NQB	● ● ●	●	● ● ●	● ●	● ●	● ●	● ●	● ● ●	● ●	-	● ●	-	● ● ●	-	● ● ●	● ●	●
NQA	● ● ●	● ●	● ●	● ● ●	● ●	● ● ●	● ● ●	● ● ●	● ● ●	-	● ●	-	● ● ●	-	● ● ●	● ● ●	●
NQAxi	● ● ●	● ●	● ● ●	● ●	● ●	● ● ●	● ● ●	●	●	●	●	●	● ●	●	● ●	-	-
NQC	● ●	● ●	● ● ●	● ●	-	● ● ●	● ●	●	● ●	● ●	-	-	● ●	● ●	● ● ●	● ●	-

a. Voids

Smooth walled voids are abundant throughout all of the samples, including circular vesicles and more elongate or irregular shaped vughs (Figure 5.46). They are principally found in the fine-grained areas within the thin sections. They are typically small (approximately 0.2 to 0.4 mm in diameter) and often associated with clasts (Figure 5.46b). Vesicles in diamict are typically associated with the formation of bubbles in saturated sediment (e.g. Liquefaction) (Bertran and Texier, 1999), but they can also form in sediment underlying melting snow (van der Meer *et al*., 2010).

Fissures are also common. They range from dominant features across the entire thin section to small features concentrated in the fine-grained areas, which may be parallel or sub-parallel to pre-existing laminations (Figure 5.45). Some short isolated fissures may have smooth walls, similar in appearance to the smooth walled vesicles and vughs.

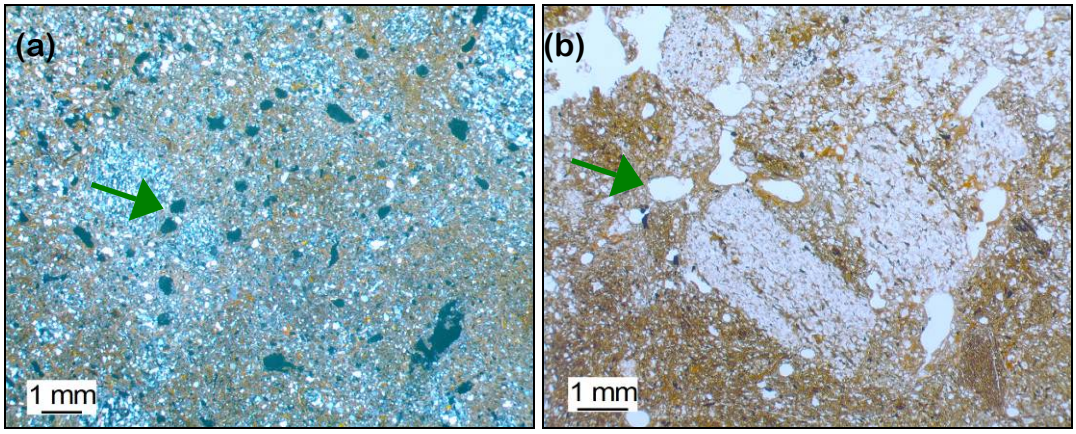

Figure 5.46 – Voids within the Newton Quarry samples, indicated with green arrows. (a) Smooth walled vughs and vesicles from NQAa (LF3) (image is in cross polarised light, therefore the voids are black). (b) Smooth walled vughs from NQAa (LF3), arcing around a clast.

b. Cutans

Cutans are present throughout all of the Newton Quarry samples. The majority are orange and range from pale to dark orange. They display strong birefringence and some are laminated. Cutans are usually present inside or around voids (Figure 5.47a) in discrete, elongate zones or at the edges of large clasts. Orange cutans are particularly abundant in LF2 (NQAxi and NQC), where they are common in-between mudstone clasts (Figure 5.47b). Grey cutans are present in NQB, where they form thin coatings inside rounded vughs and vesicles.

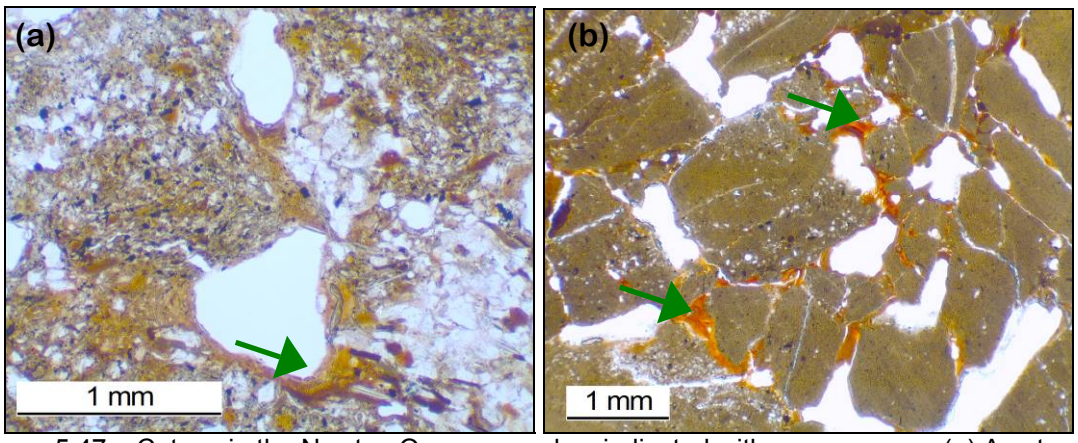

Figure 5.47 – Cutans in the Newton Quarry samples, indicated with green arrows. (a) A cutan lining the inside of a void in NQBa (LF3). (b) Cutans within voids from NQAxib (LF2).

c. Grain concentrations

Grain concentrations are present in most of the Newton Quarry samples. They are particularly apparent in the fine-grained LF2 (NQC and NQAxi) (e.g. Figure 5.45). In NQB (LF3), concentrations of grains are found in-between the large, tightly packed skeleton grains. The grain concentration in Figure 5.48 appears to be an intraclast, with some evidence for rotation.

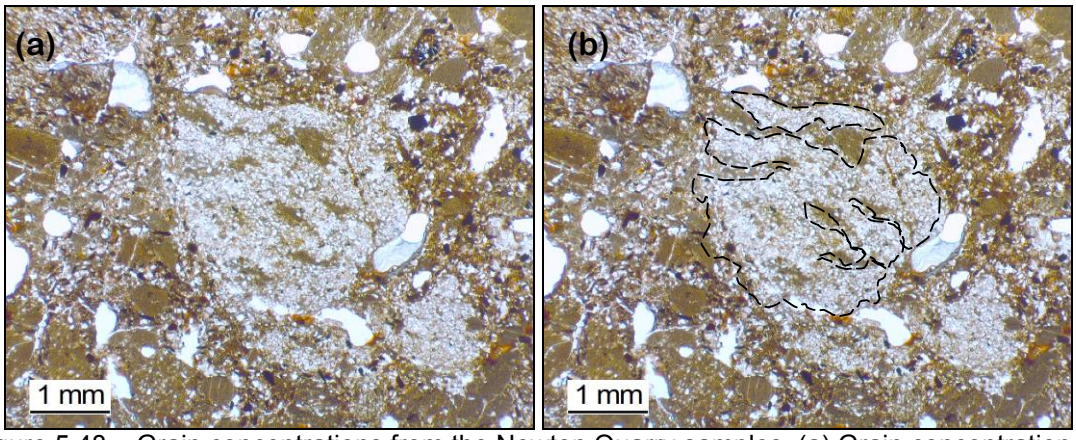

Figure 5.48 – Grain concentrations from the Newton Quarry samples. (a) Grain concentration forming a complex wavy intraclast structure in NQAxia (LF2). (b) The previous image with the structure outlined with a dashed black line.

d. Turbates

Turbates are present in all the Newton Quarry samples and are most abundant in NQA and NQB (LF3). Abundant elongate mica grains make these structures particularly apparent. Alignments of grains around the edges of the larger skeleton grains are common (Figure 5.49) and some turbates can be seen around circular voids.

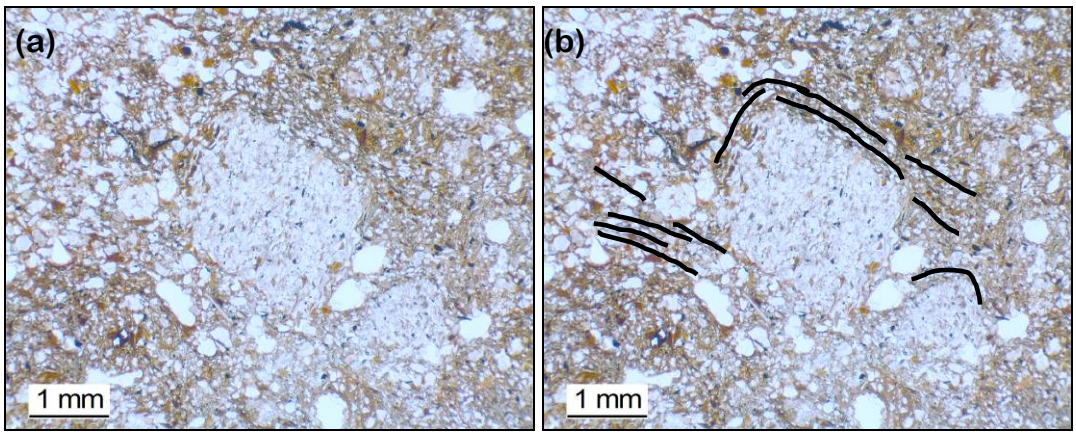

Figure 5.49 – Turbate around a sandstone clast from NQAa, (a) unannotated and (b) annotated.

e. Grain lineations

Grain lineations are present in all the Newton Quarry samples, particularly in LF3 (NQA and NQB), examples of these are shown in figures 5.50 and 5.53. Grain lineations include both alignments of grains and grains aligned along one or both sides of a line in the matrix. Grain lineations were mapped across all of NQAa and NQAc (Appendix C.2). Grain lineations are typically shorter than those from Blinkbonny Quarry. They were orientated in all directions and pervasive, but some areas of the samples contained higher concentrations of lineations, and this appeared to have some correlation with spatial variations in texture across the samples. Some lineations could be linked up and traced a considerable way across the thin sections (up to 25 mm in length). The orientations of the lineations are shown in Figure 5.51. As noted for grain lineations from Blinkbonny Quarry, rose diagrams of lineation orientation have several peaks and these are typically more steeply dipping than those from Blinkbonny Quarry.

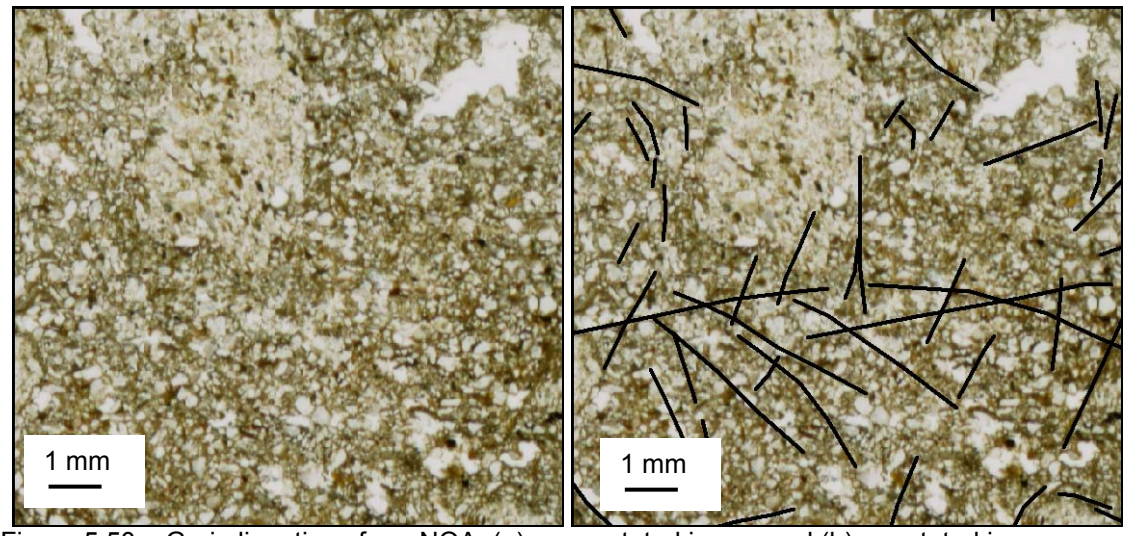

Figure 5.50 – Grain lineations from NQA. (a) unannotated image and (b) annotated image, black lines are grain lineations.

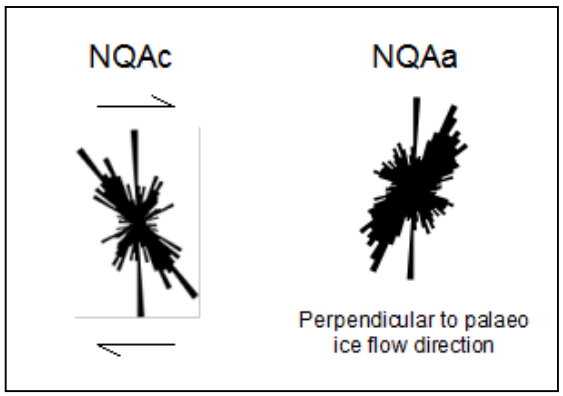

Figure 5.51 - Rose diagrams of grain lineation orientations from vertical thin sections. Relative sense of shear is indicated with arrows, where applicable. (For NQAc n = 538; and for NQAa n = 2274).

f. Plasmic fabric

Masepic and skelsepic plasmic fabric is present within the Newton Quarry samples (Figure 5.52). Plasmic fabric is subtle in thin sections from LF3 (NQA and NQB) because of the high concentrations of small skeleton grains and lack of fine-grained matrix. Plasmic fabric is more apparent in the fine-grained samples from LF2 (NQAxi and NQC), as shown in Figure 5.52 (c and d).

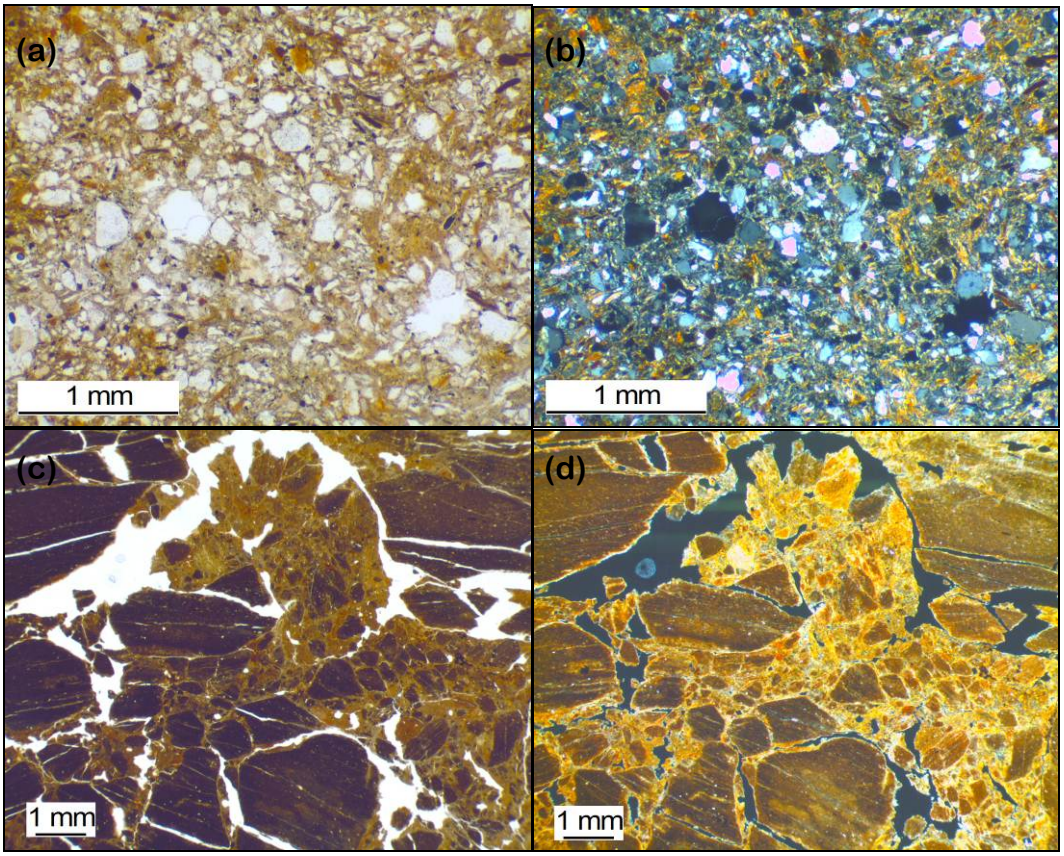

Figure 5.52 – Newton Quarry plasmic fabrics. (a) Grains and matrix in NQAa (LF3). (b) Cross polarised view of previous image. Grainy skelsepic plasmic fabric. (b) Mudstone clasts and matrix in NQCa (LF2). (d) Cross polarised view of the previous image. Skelsepic and masepic plasmic fabric in the matrix.

g. Associations between microstructures

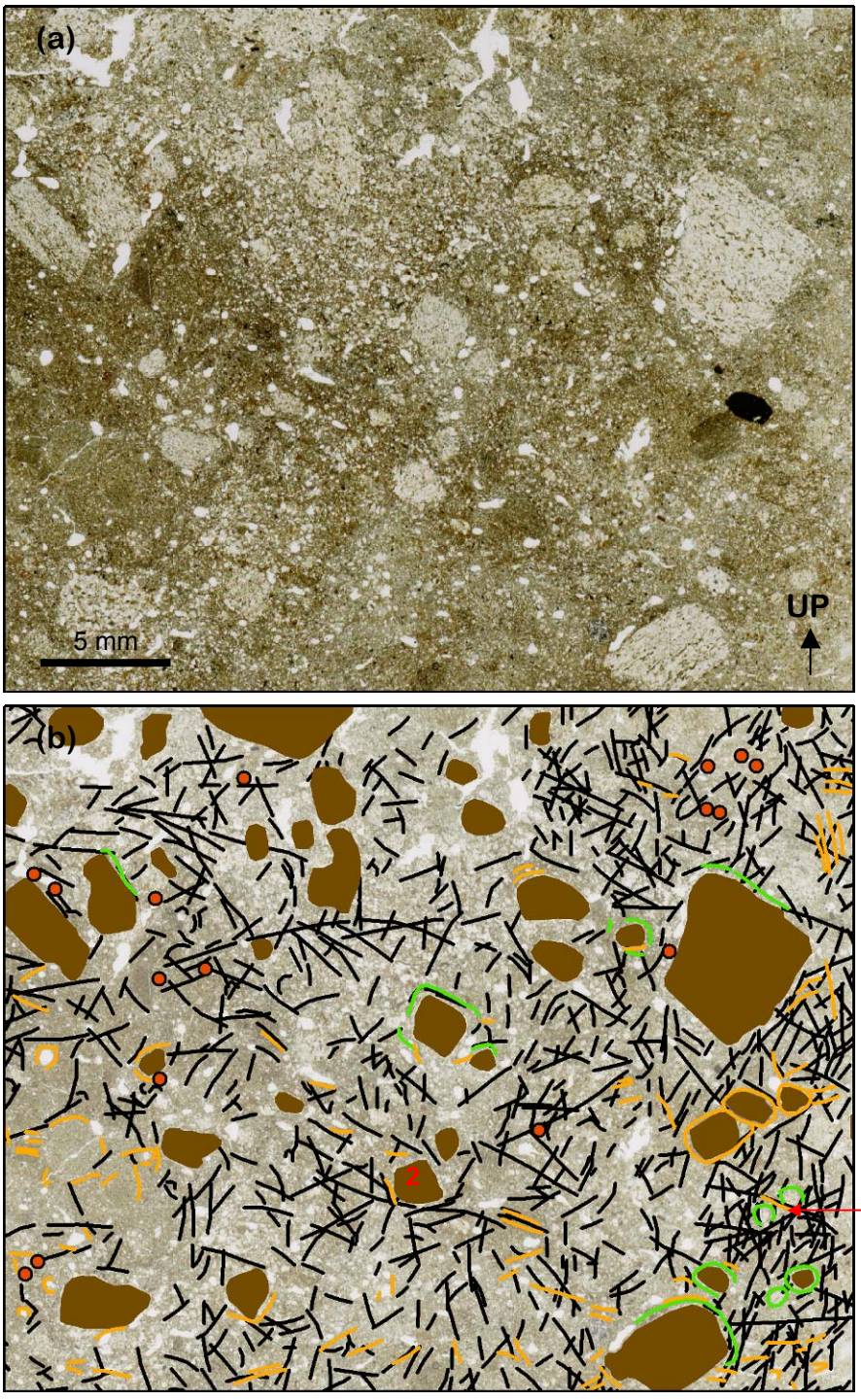

Figure 5.53 - Twinned images of thin section NQA (LF3). An unannotated, high resolution scan of the thin section in normal light conditions, is shown in (a) and a view of annotated features overlying the faded image is shown in (b). The thin section has an orientation perpendicular to the direction of former ice flow. Numbers are referred to in the text. The plasmic fabric indicated is not visible in (a) but has been identified under the microscope in cross polarised light; it is shown schematically in (b), with circles for skelsepic plasmic fabric and lines of plasmic fabric indicating the overall direction of any masepic plasmic fabric.

Associations between some of the most common features identified in LF3 are presented in Figure 5.53. This figures illustrates how widespread the mapped features are, particularly the grain lineations. Grain lineations display a range of orientations and some patterns can be identified, such as grain lineations that are situated end to end, or those within an area that share a common orientation. Several key modes of orientation can be identified and these are also shown in the rose diagram in Figure 5.51. The high angles of the measured grain lineations depicted in Figure 5.51 can also be identified in the image in Figure 5.53. The horizontal and sub-horizontal grain lineations are notably longer than the grain lineations that have a vertical or near vertical orientation. Another noticeable trend is the higher concentration of grain lineations on the right side of the image. The grain lineations also may frequently seen orientated around clasts, forming a similar structure to turbates. Clast '2' for example, has lineations and plasmic fabric orientated around it in a turbate like structure. This structure is also situated right in the middle of several grain lineations that trend from upper left to lower right of the image.

Plasmic fabric is common and in some areas it cross cuts the grain lineations, although it is usually unclear which feature is superimposed and which is underlying. Turbates are associated with skelsepic plasmic fabric in some instances and are also frequently seen close to grain lineations. Two turbates labelled '1' in Figure 5.53 are surrounded by a dense network of grain lineations, which are orientated parallel to the edges of the turbates. Cutans appear to be less abundant then in Blinkbonny Quarry (see Figure 5.33) and are concentrated in small areas containing several cutans. They are also all closely associated with grain lineations.

h. Microfabric

Microfabric was measured from samples NQA, NQB (LF3) and NQC (LF2), from the same location as the macrofabric measurements (macrofabric could not be taken at NQC due to the lack of competent gravel sized clasts). In NQA microfabric azimuth is parallel to the subglacial lineation, whereas NQB and NQC are oblique to and perpendicular to the subglacial lineation, respectively (Figure 5.54). Microfabric azimuth for NQA and NQB are consistent with the macrofabrics. Microfabric dips are orientated in all directions, many with peaks in the horizontal and vertical positions.

Interestingly, the rose diagrams display quite different orientations to those for the grain lineations. Confidence intervals for microfabric azimuth are given in Appendix C.3.

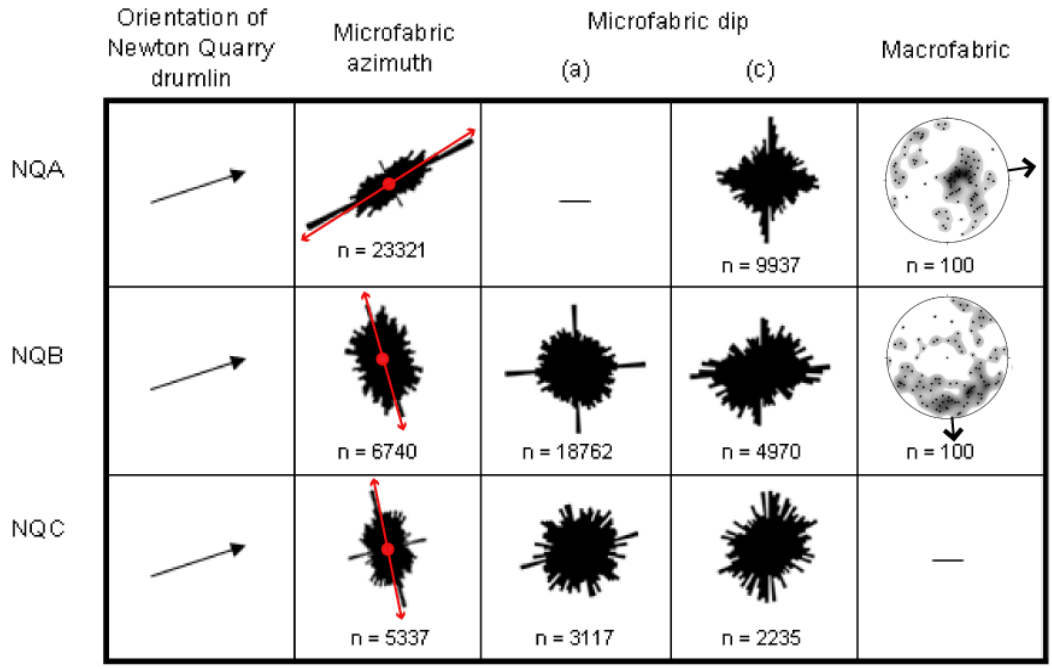

Figure 5.54 – Microfabric rose diagrams of azimuth (vector mean is indicated by a red arrow) and dip. The orientation of the Newton Quarry drumlin and the macrofabric is also shown for comparison. Dip (a) was measured approximately perpendicular to the mean azimuth and dip (c) was measured approximately parallel to the mean azimuth.

5.4.5 Microscale interpretation

Micromorphological structures in LF3, such as turbates, grain lineations and skelsepic plasmic fabric, are similar to observed suites of micro structures in subglacial tills (e.g. van der Meer, 1993; Carr, 2001; Larsen *et al*., 2006a). Therefore, they corroborate the interpretation that LF3 is a subglacial traction till. Investigation of the microscale also confirms that a bedrock structure in LF2 exists and it displays evidence for ductile and brittle deformation, and therefore, confirms the mesoscale interpretation that this lithofacies is a glaciotectonite. Ductile deformation and sediment mixing is apparent from several features, including multiple domains, turbates, intraclasts and papules (Tarnocai and Smith, 1989; van der Meer, 1993; Menzies, 2000; van der Meer, 2003). Turbates, skelsepic plasmic fabric and a rotated intraclast (Figure 5.48) demonstrate that rotation was operating in the subglacial traction till and in the glaciotectonite (see van der Meer, 1993; Hiemstra and Rijsdijk, 2003).

Sand concentrations are present in the fine-grained glaciotectonite, indicating that sand has been incorporated into this lithofacies. This may have been via mixing and comminution processes within the glaciotectonite. However, measurement of the orientations of these grains indicates that the majority are vertical or sub-vertical, which suggests that the sand was liquefied and flowing in response to a pressure gradient. Given that the likely source of water would have been down the profile from the ice bed, this sand was probably injected downwards from the overlying subglacial traction till. This would imply that LF2 is a penetrative, Type A glaciotectonite (see Benn and Evans, 1996).

Evidence for brittle shear in the samples is evident from grain lineations, faulting and unistrial plasmic fabric (see van der Meer, 1993; Menzies, 2000; Larsen *et al*., 2007). The majority of the mapped grain lineations are lines within the matrix, delineated by grains, which are thought to represent discrete shear lines (Menzies, 2000; Larsen *et al*., 2007). Some grain lineations are situated end to end and these may be up to several centimetres long, which may reflect shears that propagated through the sediment (Figure 5.53). The extent of these features indicates that brittle shear was pervasive and overlapping shears indicate that this was ongoing over a period of time. The extent and amount of the shears may support the inference of Thomason and Iverson (2006), who consider that slip along shears accommodated the most strain within the subglacial sediments sheared in their experiments. Furthermore, the grain lineations in Figure 5.53 with a near horizontal orientation are noticeably longer than those with a more vertical orientation. This indicates that most of the displacement took pace in the horizontal direction, which is what would be expected in a subglacial environment.

The lineations display similarities to the expected pattern of shears in a Riedel shear zone (Figure 5.30) and their extent and complexity probably relates to high strain and/or high water contents (Arch *et al*., 1988; Thomason and Iverson, 2006). The higher average angle of shears at Newton Quarry, compared to Blinkbonny Quarry (see figure 5.30 and 5.51), may be a result of different till textures, because the angle of R and R´ shears are dependent on the internal angle of friction of the sediment (Davis *et al*., 2000). Microfabric dip orientations are very different to shear orientations, which is seen at both sites, suggesting that these different fabric elements of the sediment are unrelated and may take place via different processes. This contrasts with Thomason and

Iverson (2006), who infer that particle orientations may result from the orientation of shears in a deformed diamict.

Some associations between the mapped features in Figure 5.53 can be identified. Turbates are commonly associated with grain lineations, particularly those labelled ‘1’ in Figure 5.53. These turbates are surrounded by a dense network of grain lineations, which are orientated consistently with the edges of the turbates, indicating that these features were closely related, a conclusion that matches the interpretations of Hiemstra and Rijsdijk (2003). In this case when deformation was triggered here the initial development of one or more of the structures may have had a knock on effect on the surrounding sediment, creating this suite of deformation structures in close proximity to each other. Clast ‘2’ in Figure 5.53 is also within a turbate like structure, depicted by grain lineations and plasmic fabric that arcs around it. This clast in the centre of an area of grain lineations all trending from upper left to lower right of the image and this suggests that shear was propagated in this direction and may have also activated rotation around the clast. These grain lineations have a curvature to them, which also contributes to the interpretation that there was also a ductile element to the deformation.

Grain lineations appear to be highly concentrated on the right side of the image shown in Figure 5.53, which suggests that strain was higher here, possibly a result of differences in texture or differences in absolute stress. Whilst texture appears heterogeneous in Figure 5.53, there is not a clear difference between sediment on the right and left sides of the image, which would suggest that the apparent strain variation relates to spatial variations in stress imparted on the sediment. A spatial variation such as this may be a result of heterogeneity in the surrounding sediment that focuses a higher level of stress in some areas more than others.

Ductile and brittle deformation, for which evidence is abundant at Newton Quarry, are associated with different sediment conditions (Menzies, 2000). Ductile deformation is typically associated with high pore water pressures and/or low stress, whereas brittle deformation is typically associated with low pore water pressures and/or high stress (Menzies, 2000). Whilst there is overprinting of different structures, there is no clear evidence for superimposition of one of these deformation styles on top of the other, suggesting that they operated concurrently or that there was alternation between them.

This may have been a consequence of rapidly changing conditions (Menzies, 2000), such as fluctuating pore water pressures.

Mean vectors are typically similar between the microfabric and its respective macrofabric, however, they are not necessarily orientated with palaeo ice flow direction. This is similar to the pattern seen at Blinkbonny Quarry and suggests that the same directional processes operated on the micro particles (0.031 to 8 mm) as the larger particles (8 to 32 mm). Dip microfabric rose diagrams for both Newton and Blinkbonny quarries typically have a rounded shape, with some vertical and horizontal peaks. This contrasts with lab experiments that found shear strain to cause low particle dips (Thomason and Iverson, 2006). This discrepancy may be because this study measured a wider range of grain sizes than Thomason and Iverson (2006), in particular smaller particles including fine sand and coarse silt that made up a considerable proportion of the sample. The relevance of this lies in the fact that grain size is known to have an effect on fabric strength and potentially even orientation (Kjær and Kruger, 1998; Carr and Rose, 2003; Thomason and Iverson, 2006; Carr and Goddard, 2007). Or the particles could have been subject to another process, notably frost action, which may cause very steep dips, but this does not explain the full range of dips measured (e.g. Harris, 1990). Thus the particles are interpreted as having a subglacial origin. Considering this with respect to proposed particle rotation mechanisms, then the dip fabrics are inconsistent with the expected pattern for March rotation (March, 1932) and are more similar to the expected pattern for Jeffery rotation (Jeffery, 1922). However, neither of these mechanisms can fully explain the observed fabrics and indicates that further work would be desirable to better understand the observations.

Orange and grey cutans, with the same characteristics as those found at Blinkbonny Quarry, were also common at Newton Quarry, which suggests that the processes responsible for these cutan types were widespread in the Tweed Valley. The orange cutans were found up to 200 cm below the ground surface at Newton Quarry, significantly deeper than the grey cutans (found up to 20 cm below the ground surface). This suggests that the orange cutans either formed over a longer period of time than the grey cutans, or that they formed via different processes. As was noted for Blinkbonny Quarry, the lack of evidence for periglacial activity or another process that may have disturbed the cutans indicates that a subglacial origin is the simplest explanation.

Whatever their origin, their presence in voids suggests that the voids may form part of the primary porosity of the sediment. Given this, it can be speculated that these voids were previously water filled, indicating that the sediment was dilated.

5.5 Tweed Ice Stream interpretation and conclusions

Following analysis of the datasets pertaining to each individual scale separately, they can now be examined together. Three key themes that emerge from the findings are discussed in the following sections, which include: deformation, hydrology and fast flow mechanisms of the ice stream.

5.5.1 Deformation

The precise mechanisms of subglacial lineation formation are not known, but if a simplistic assumption is made, that they initiate at a point and progressively elongate with time (see Clark, 1993; Stokes and Clark, 2002a), then elongation ratio can be considered to be an indicator of strain. This would indicate that strain was pervasive across the bed of the Tweed Ice Stream and that strain was variable, as manifest in the clustered pattern of subglacial lineation elongation ratio. Some of the examined variables (topography, bedrock geology and surficial sediments) display some subtle correlations with elongation ratio, but for the most part the observed variability appears to be random.

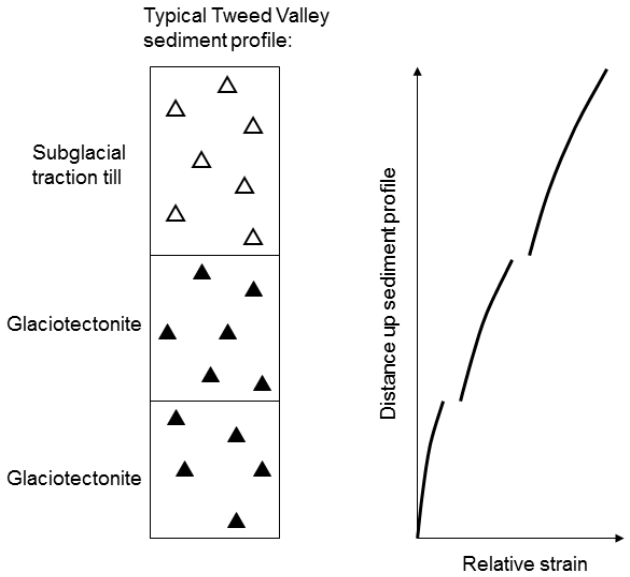

Figure 5.55 – Schematic diagram of the distribution of strain throughout a typical sediment profile in the Tweed Palaeo-Ice Stream.

Sediment profiles at both quarries demonstrate a vertical increase in deformation from the base to the top of the profile, as evident from: the loss of bedrock structure; increasing range of clast roundness; increasing input of non-local clasts; and increasing range and extent of microscale deformation structures. These vertical changes take place within and between the different lithofacies. The schematic diagram of this vertical distribution of strain, based on the findings of this study, is depicted in Figure 5.55. Within this framework, further spatial heterogeneities in texture and structure are evident at the meso and micro scales, particularly in the subglacial traction till. This demonstrates that whilst the subglacial traction till displays the most strain, deformation is not wholly pervasive through this unit and that mixing is incomplete. Both quarries also revealed evidence for extensive microscale deformation, in the upper parts of the sediment profiles, contributing to inferences from the macro and meso scales that the sediment had been subject to considerable deformation.

5.5.2 Hydrology

Macroscale evidence for ice stream basal hydrology reveals that subglacial meltwater was discharged via channels in the ice stream onset zone and at the southern lateral margin. These areas were characterised by low bedrock permeabilities (Figure 5.16) and this is thought to have been a key factor in the development of Nye channels in these areas of the ice stream. There was no evidence for subglacial meltwater channels across the majority of the ice stream bed, suggesting that a different mechanism of subglacial meltwater discharge operated. However, a channelised system may have existed here, but the geomorphic signature may not have been preserved, may be too small to resolve within the dataset used for mapping or may not fall within the criteria for identification of subglacial channels.

Within the sediments, several lines of evidence from both quarries indicate that pore water pressures were high and variable. At Blinkbonny Quarry the process of till injection into fissures requires high pore water pressures, and the presence of laminations indicates that this varied temporally. Possible evidence for till injection and liquefaction is also seen at the microscale at Newton Quarry. Abundant microscale ductile deformation structures suggest pore water pressures were high, and their presence alongside brittle deformation structures may reflect rapidly changing conditions such as variable pore water pressures (see Menzies, 2000). The presence of

subglacial cutans also demonstrates that pore water pressure was high enough to mobilise the clay particles that they are composed of. This strong evidence for high pore water pressures is consistent with studies of contemporary ice streams, which have found high water pressures at ice stream beds (e.g. Engelhardt *et al*., 1990; Engelhardt and Kamb, 1997). And the strong evidence for variability of pore water pressures supports recent studies from ice streams (Smith *et al*., 2007), contemporary glaciers (Fischer and Clarke, 2001) and theoretical models (Piotrowski *et al*., 2004) that subglacial hydrological conditions may vary in time and space.

5.5.3 Fast flow mechanisms

For rapid ice stream flow subglacial deformation and/or subglacial sliding must operate, and these mechanisms are dependent on the bed hydrological conditions. So the strong evidence for high pore water pressures in the Tweed Valley is consistent with this requirement. Another key process identified, deformation, was manifest at all of the spatial scales and the widespread extent of elongated subglacial lineations may indicate that it was prevalent across the ice stream. Sediment deformation displayed a vertical distribution of strain that was common throughout the sites examined (Figure 5.55) and similar sediment profiles reported by Kerr (1978) suggests that this vertical strain distribution is widespread within the Tweed Valley. This profile is similar to theoretical models of vertical strain distribution within subglacially deformed sediment (Alley, 1989; van der Meer *et al*., 2003), suggesting that subglacial deformation was a major fast flow mechanism for the ice stream. Further evidence may be in the widespread cutans that are thought to have formed subglacially, because they demonstrate the existence of high primary sediment porosity in. This may be symptomatic of sediment dilation, which is considered to be indicative of pervasive sediment deformation (e.g. Alley *et al*., 1986; Murray and Dowdeswell, 1992; Smith, 1997; Vaughan *et al*., 2003).

The mechanism of subglacial sliding may have also contributed to fast flow in the ice stream. In particular, this mechanism may have operated around the southern lateral extent of the ice stream, where till cover is absent or patchy (Figure 5.14), but elongated subglacial lineations demonstrate that flow was rapid. This area is characterised by impermeable igneous bedrock (Figure 5.15), which may have allowed only minimal drainage of water from the bed, promoting the high pore water pressures that are necessary for basal sliding.

6. The Central Alberta Ice Stream

6.1 Introduction

This chapter presents a study of the geomorphology, sedimentology and micromorphology of the Central Alberta Ice Stream. This will allow the ice stream bed to be characterised and its subglacial processes identified and compared to the Tweed Ice Stream. This answers the second research question and the third research question (which is discussed in Chapter 7) of the thesis. The second research question is repeated below:

2. *What do the macro, meso and micro scale characteristics of two palaeo-ice streams reveal about their subglacial processes?*

The Central Alberta Palaeo-Ice Stream is located in Alberta, Canada, in the south west corner of the former Laurentide Ice Sheet (figures 6.1 and 6.2), where it flowed north to south. It was an ice stream of considerable size, at approximately 830 km long and up to 150 km wide. Its narrow trunk and lobate terminus is typical for ice streams at the southern extent of the Laurentide Ice Sheet (Jennings, 2006). Its topographic and geological setting is also typical of the southern Laurentide ice streams (e.g. Jennings, 2006; Ross *et al.*, 2009). This area of Alberta is characterised by relatively flat prairie lands and is underlain by sedimentary rocks including Cretaceous shales, sandstones, mudstone and siltstone. Most of the study area and the examined sediment exposures are underlain by the Bearpaw Formation, which has a marine origin and comprises dark grey, blocky shale and silty shale; greenish glauconitic and grey clayey sandstone; thin concretionary ironstone; and bentonitic beds (Hamilton *et al.*, 1999).

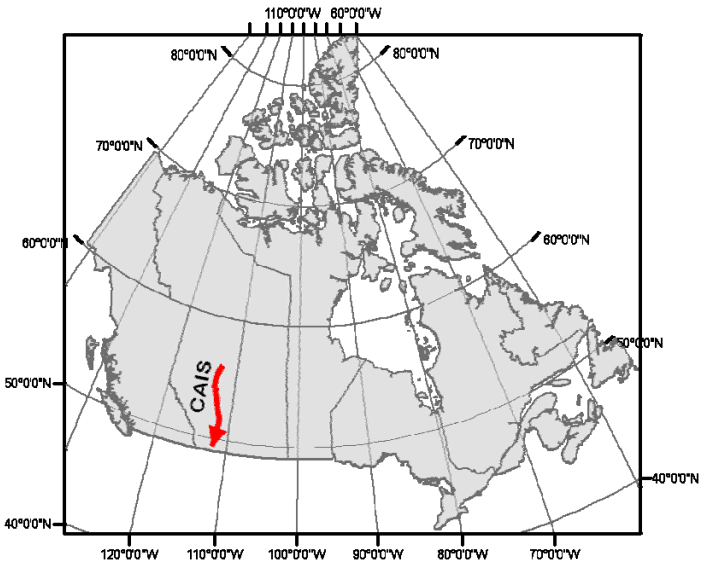

Figure 6.1 – Location map of the Central Alberta Ice Stream in Canada.

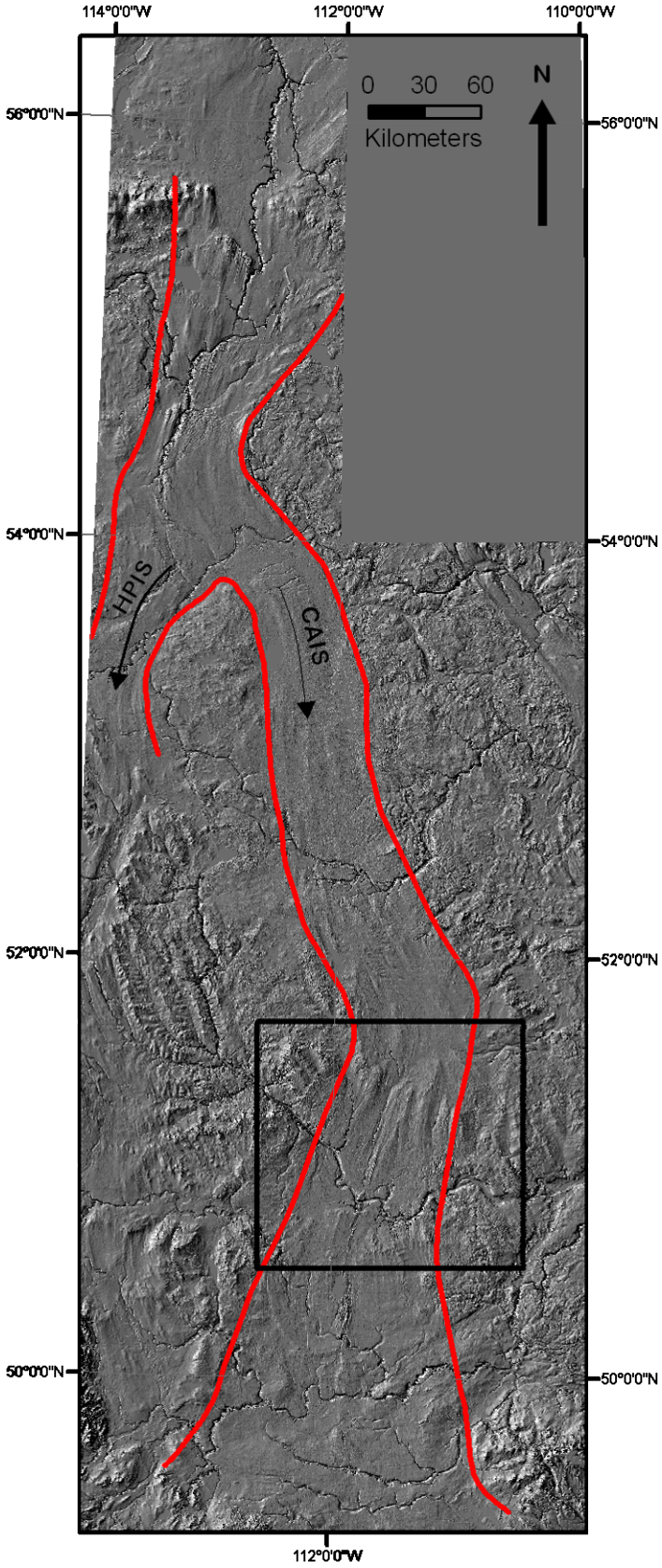

Figure 6.2 – Location and extent of the Central Alberta Ice Stream (CAIS) on a Canadian Digital Elevation Data DEM (vertical exaggeration of x6). The upstream end of the adjacent High Plains Ice Stream (HPIS) is also indicated. Note the streamlined terrain of the ice stream that contrasts with the adjacent hummocky terrain. The black rectangle shows the study area for the investigation (Figure 6.6), which was selected on the basis of availability of sediment exposures and a clear geomorphological signature, as discussed in the text.

6.1.1 Previous research

The Quaternary geology of Alberta has been studied and mapped by several researchers (e.g. Stalker, 1977; Shetsen, 1987; 1990; Munro and Shaw, 1997; Evans and Campbell, 1992; 1995; Evans *et al*., 2008). There is uncertainty as to the number of glaciations that have affected southern Alberta. Some evidence suggests that only one glaciation reached Alberta and Montana to the south, which was during the Late Wisconsin (e.g. Liverman *et al*., 1989; Young *et al*., 1994; Fullerton *et al*., 2004), whilst some stratigraphical evidence indicates that an earlier glaciation, or even multiple earlier glaciations, may have also reached southern Alberta (e.g. Stalker, 1983; Evans and Campbell, 1992; 1995). The Cordilleran Ice Sheet also extended into western Alberta, from the Rockies, where it coalesced with the Laurentide Ice Sheet and was deflected to the south, as documented by the Foothills erratic train (see Stalker, 1956; Jackson *et al*., 1997).

Research into the geomorphology and Quaternary geology in southern Alberta has enabled the identification of former ice flow patterns (Prest *et al*., 1968; Shetsen, 1987; 1990). Recently, Evans *et al*. (2008) identified that the fast flow corridors in Alberta, which are depicted by landforms, represent palaeo ice streams. These streamlined paths are characterised by elongate landforms, giant flutings, drumlins, scoured bedrock, major meltwater channels and ice flow transverse ridges (Rains *et al*., 1993; Evans *et al*., 2008). Among evidence for multiple fast flow events, two key ice streams were identified by Evans *et al*. (2008): the Central Alberta Ice Stream in eastern Alberta, and the High Plains Ice Stream to the west (Figure 6.2). The timing of these ice streams are poorly constrained, but a moraine assemblage in southern Alberta (known as the Lethbridge moraine), which is associated with the Central Alberta Ice Stream, is thought to relate to a regional ice sheet readvance at 14 000 ^{14}C yr BP (Evans *et al*., 2008).

Surficial sediments on the Central Alberta Palaeo-Ice Stream are typically thin (Figure 6.3; Shetsen, 1987; Rains *et al*., 1993; Evans *et al*., 2008). Till displays a downstream thickening towards the terminal extent of the ice stream (Shetsen, 1987; 1990; Evans *et al*., 2008) and is thicker outside of the ice stream, as shown in Figure 6.3. These are characteristics predicted by the subglacial deformation models of Boulton (1996a, b).

Till also increases in thickness downstream of preglacial valleys, possibly because they act as sediment sources (Evans *et al*., 2008). The areas surrounding the ice streams are characterised by hummocky terrain and thick till (up to 25 m thick) (Shetsen, 1987; 1990; Rains *et al*., 1993; Eyles *et al*., 1999; Evans *et al*., 2008). Figure 6.3 shows that lacustrine deposits are widespread in southern Alberta, which are thought to relate mainly to proglacial and ice dammed lakes that formed during deglaciation (Evans, 1994). These palaeo lakes are often associated with meltwater channels or spillways (Shetsen, 1987; 1990; Evans *et al*., 2006b).

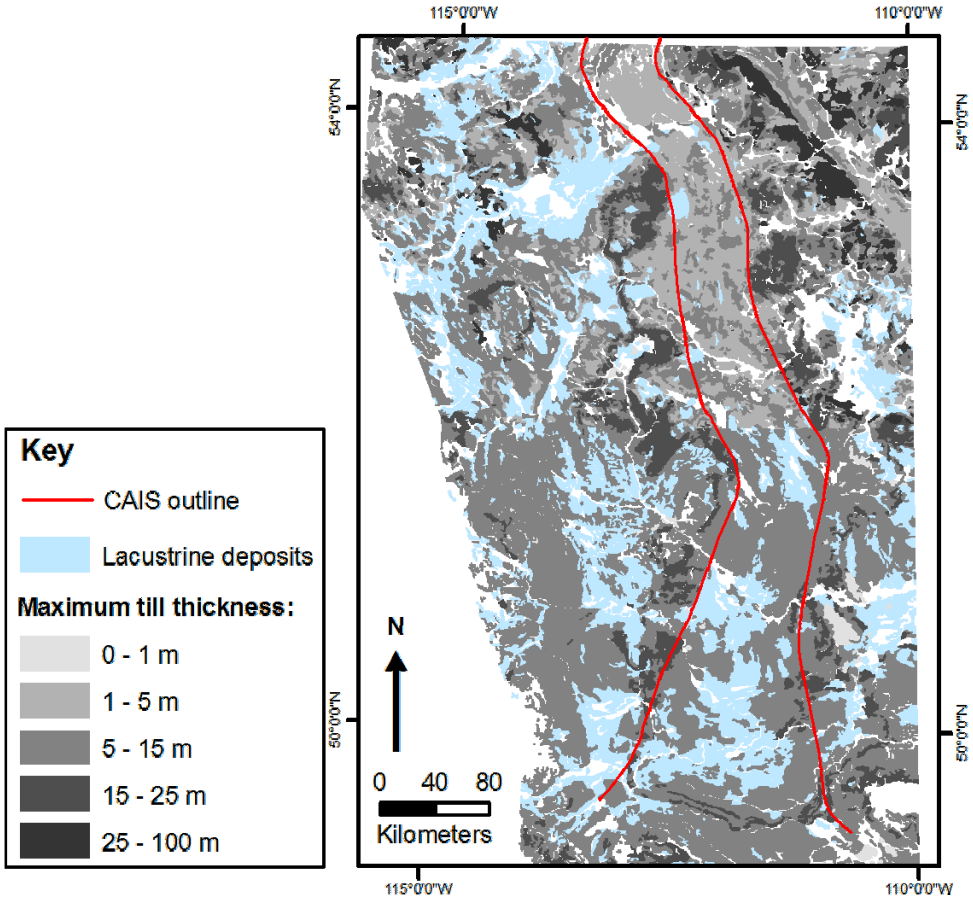

Figure 6.3 – Distribution of till and lacustrine deposits on and around the Central Alberta Palaeo-Ice Stream. Till is shaded according to its maximum thickness. Data from Shetsen (2002).

An alternative view on the proposed Albertan palaeo-ice streams and other glacial landforms and sediments in the region is upheld by Rains *et al*. (1993), Munro and Shaw (1997), Shaw (2002; 2009) and Beaney and Shaw (2000), among others. They consider subglacial megafloods to have formed much of the geomorphology and sedimentology observed in Alberta, including the streamlined flow paths (e.g. Shaw and Freschauf, 1973; Munro and Shaw, 1997; Munro-Stasuik and Shaw, 2002). However, there are several compelling arguments against the subglacial megaflood theory, which

point out that there is a lack of modern analogues for subglacial megafloods and a number of inherent problems with the theory (Clarke *et al*., 2005; Benn and Evans, 2006; Evans *et al*., 2006b). Of these, Clarke *et al*. (2005) argue that the key failing to the subglacial megaflood theory is the unviability of storage and catastrophic release of huge volumes of water from an ice sheet. In Alberta, investigation of landforms and sediments by several authors (e.g. Evans *et al*., 1999; Evans *et al*., 2006b; Evans *et al*., 2008) have demonstrated that the evidence cited by advocates of the megaflood theory (e.g. Munro and Shaw, 1997; Munro-Stasiuk and Shaw, 2002; Munro-Stasiuk, 2003) may also be explained by glacial and proglacial processes and arguably are more easily explained by this. One such line of evidence is that the lacustrine sediments considered to have been deposited subglacially by Munro-Stasiuk (2000; 2003), could equally have been deposited in a proglacial ice dammed lake (Evans *et al*., 2006b). Furthermore, Evans *et al*., (2008) argue that the streamlined terrain corridors in Alberta are analogous to many other palaeo ice streams and have many of the diagnostic characteristics of palaeo ice streams, including characteristic shape and dimensions, convergent flow patterns, highly elongated bedforms and sharp lateral margins (see Stokes and Clark, 1999).

Previous studies provide an overview of the geomorphology of the Central Alberta Ice Stream (e.g. Shetsen, 1987; 1990; Rains *et al*., 1993; Evans *et al*., 2008) and some insight into its sedimentology (e.g. Evans *et al*., 2008). Given the detail and extent of existing geomorphological data (Shetsen, 1987; 1990; Evans *et al*., 2008), this study has focussed on a limited area for geomorphological mapping, which was chosen to encompass the sites examined for sedimentology and micromorphology. This area was selected on the basis that suitable sediment exposures are otherwise rare on the ice stream bed (Evans pers comm.) and at least one sediment site was known to exist in this area (Evans *et al*., 2008; Figure 6.4). In addition to geomorphological mapping of this limited area, subglacial lineation mapping and analysis was conducted across the entire ice stream. Interpretation of the macroscale includes the results of this study and a discussion of inferences made from the data of Shetsen, (1987; 1990) and Evans *et al*. (2008).

6.2 Geomorphology

6.2.1 Background

Geomorphological mapping of the ice stream and surrounding region conducted by Evans *et al*. (2008) is presented in Figure 6.4 and some of that compiled by Shetsen (1987; 1990) is presented in Figure 6.5. Subglacial lineations, including drumlins and flutes are present in irregular clusters across the bed of the Central Alberta Ice Stream (Shetsen, 1987; 1990; Evans *et al*., 2008; Figure 6.4). These landforms are typically poorly developed and often concentrated on the lee side of transverse ridges (Evans *et al*., 2008). Notably, a succession of highly elongate subglacial lineations lies at the centre of the ice stream bed, within the main study area for this investigation (figures 6.2 and 6.4). Based on geomorphology and sedimentology, Evans (1996) interprets this network of subglacial lineations to be subglacial streamlining of an esker network. Given its relationship with other, undisturbed geomorphology, including thrust moraines and another esker network, Evans *et al*. (2008) consider that this streamlining occurred during a substantial readvance of the ice stream. However, the lineations are interpreted very differently by Rains *et al*. (1993), who interpret them to be a reflection of scouring from a subglacial megaflood event. This interpretation is dismissed by Evans *et al*. (1999; 2006b; 2008) based on the consistency of the ice stream geomorphology and sedimentology with modern glacier and ice stream analogues.

Meltwater channels and eskers at the ice stream bed have been mapped by Shetsen (1987; 1990) and Evans *et al*. (2008), and document drainage both parallel and transverse to the ice stream. Evans *et al*. (2008) assigns the groups of west-east trending channels (Figure 6.4) that cross-cut the subglacial lineations, to a subglacial origin. These are thought to relate to subglacial encroachment of water from adjacent proglacial lakes (Evans *et al*., 2008). The many meltwater channels and eskers that trend parallel to ice streaming (Shetsen, 1987; 1990), have not been assigned a specific origin (i.e. subglacial, proglacial or ice marginal) and as such cannot be interpreted as indicators of subglacial processes.

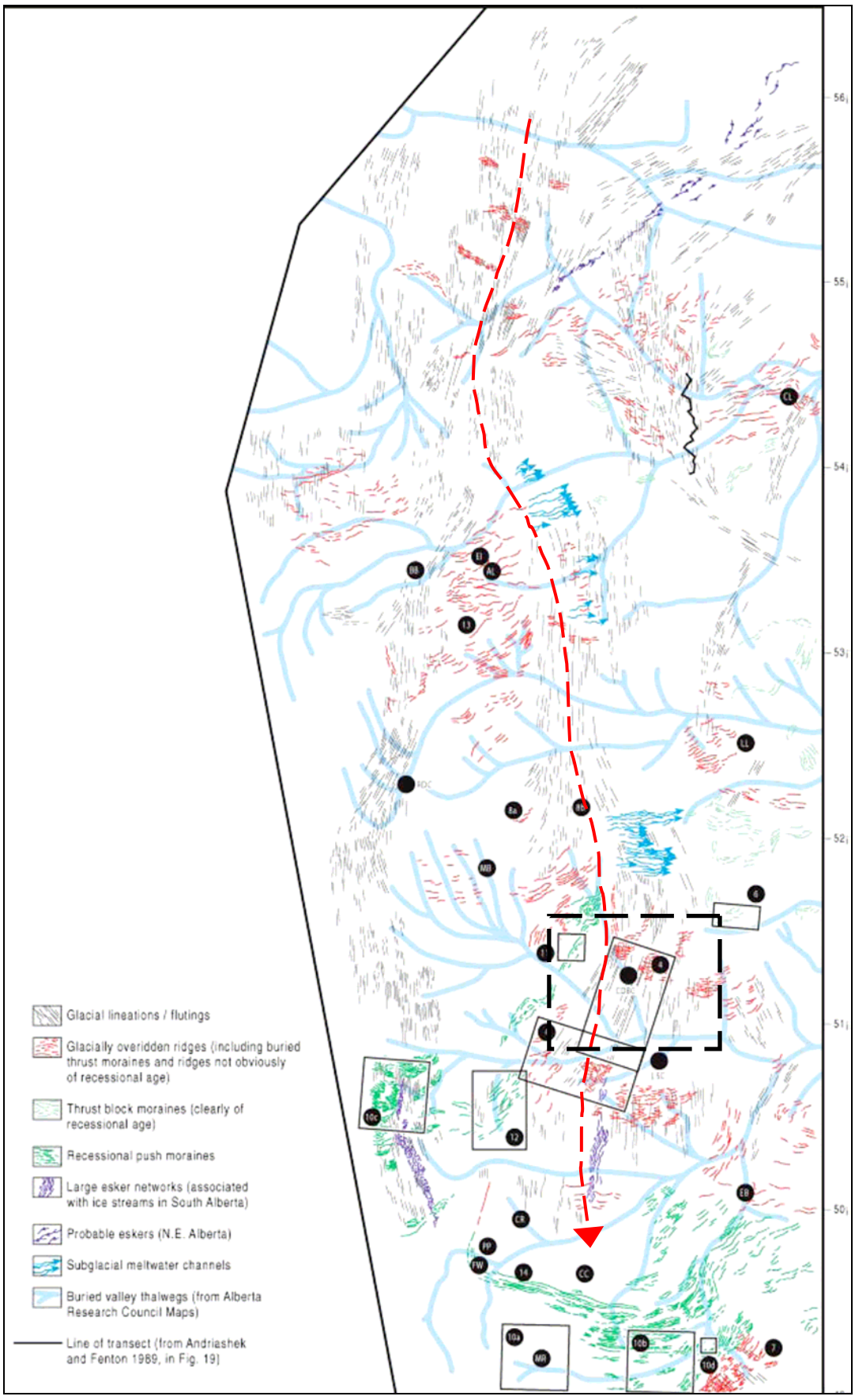

Figure 6.4 – Evans *et al*., (2008) geomorphological map of the Central Alberta Ice Stream and surrounding area. The ice stream track is highlighted with a red dashed line. The approximate extent of the geomorphological mapping study area for this study is indicated with a black dashed box.

Hummocky terrain is common at the south western margins of the Laurentide Ice Sheet and is typically thought to be associated with ice stagnation, although its precise origins are debated (e.g. Eyles *et al*., 1999; Jennings, 2006; Ross *et al*., 2009). It is most common in the areas outside of the ice streams and at their termini (e.g. Eyles *et al*., 1999; Jennings, 2006; Ross *et al*., 2009), although Figure 6.5 shows that it is also present on the bed of the ice stream. This landform assemblage has a range of characteristics, including forms such as transverse and longitudinal ridges, depressions, moraine plateaux, circular rim ridges ('doughnuts') and corrugated moraine ('humdrums') (Stalker, 1960; Munro and Shaw, 1997; Eyles *et al*., 1999). Munro and Shaw (1997) interpret this extensive landform as erosional in origin, based on the existence of truncation surfaces. However, Evans *et al*. (2006b) argue that these truncation surfaces are not located on top of the hummocks, thus contradicting the argument for an erosional origin for hummocky terrain development here. Eyles *et al*. (1999) note a downstream transition from chaotic landforms into weakly orientated hummocks and, based on the work of Stalker (1960), they invoke a mechanism of 'pressing' of dead ice blocks into soft till and bedrock to explain the landforms.

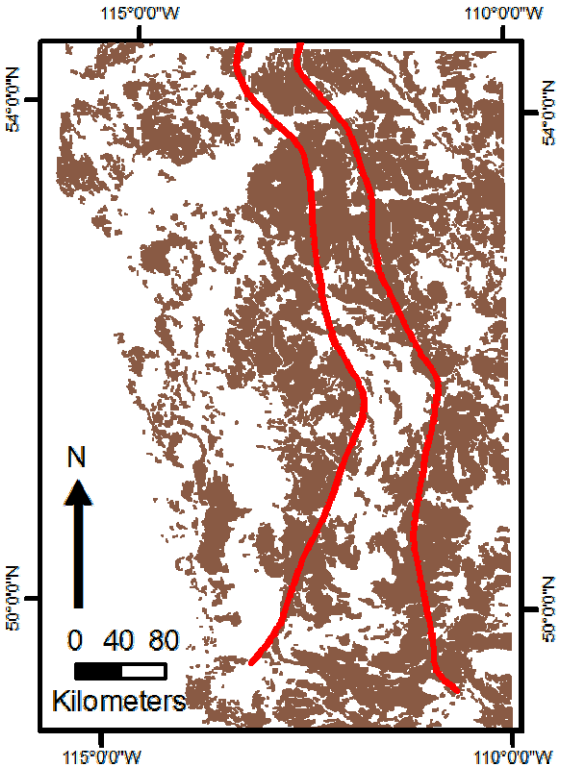

Figure 6.5 – Hummocky moraine (shaded brown) extent on and around the Central Alberta Ice Stream (outlined in red). Data from Shetsen (2002).

Moraines in and around the ice stream include minor ridges, which are often present in a succession; and larger ridges, which make up the large moraine complex at the southern limit of the ice stream (the Lethbridge moraine) (Shetsen, 1987; 1990; Evans *et al*., 2008). Evans *et al*. (2008) consider the large moraine ridges that are transverse to ice flow to be thrust block moraines, or composite ridges and hill-hole pairs. Based on sedimentological evidence indicating that these landforms cross-cut sedimentary and bedrock structures, Evans *et al*. (2008) interpreted that their construction was proglacial and a reflection of ice recession.

6.2.2 Geomorphological mapping of study area

As mentioned previously, the study area selected for mapping and sedimentological analysis was selected based on the knowledge that sediment exposures are rare on the ice stream bed, but are known to exist in this area (Evans pers comm.). Geomorphological mapping of the study area was based on a regional Canadian Digital Elevation Data (CDED) DEM, with a spatial resolution of between 11 and 23 m and a vertical resolution of 1 m. Landforms were very rarely apparent in available satellite imagery of the area, so this dataset was not used. The mapping identified several glacial landforms, including subglacial lineations, meltwater channels, hummocky terrain and moraine ridges (Figure 6.6). These are similar to the geomorphological maps of Shetsen (1987) and Evans *et al*., (2008), although some minor differences exist. The mapping shows that the ice stream bed is relatively smooth and characterised by few, large subglacial lineations, which are concentrated in the centre of the ice stream. This was also apparent when visiting this area, which appeared very flat and no subglacial lineations could be discerned. The scarcity of subglacial lineations contrasts with the ice streams examined in chapters 4 and 5. This also meant that the ice stream lateral margins could not be defined by the extent of the subglacial lineations, and instead are delineated by the extent of the smooth, streamlined topography.

Meltwater channels are most common at the edges and outside of the ice stream, which may be related to the higher relief in these areas, because this can enable identification of meltwater channels that run against the topography. Hummocky terrain is typical at the lateral margins and outside of the ice stream bed. The characteristics of the hummocky terrain (such as hummock size, shape, orientation and connectivity) display

some spatial variability, but the landforms form a continuum and do not display any abrupt changes in character. The two sites where sediments were examined are within the smooth, streamlined area of the ice stream bed and are not situated directly on any of the mapped landforms (Figure 6.6).

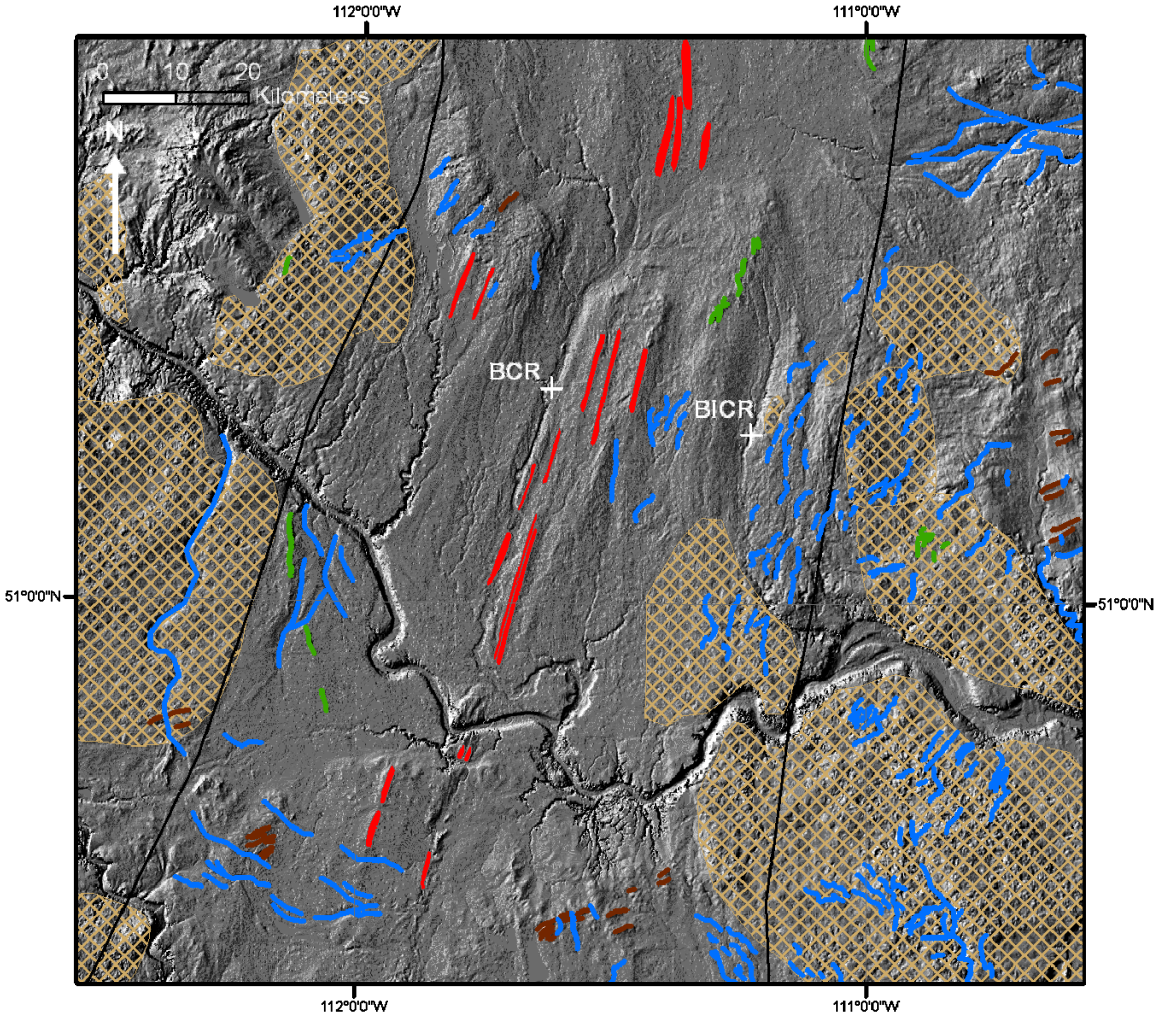

Figure 6.6 – Geomorphological mapping within the study area. Sediment sites are marked BCR (Berry Creek Reservoir) and BICR (Blood Indian Creek Reservoir). Mapping overlies a CDED DEM, with a vertical exaggeration of x6.

6.2.3 Subglacial lineation mapping and analysis

The discontinuity of the subglacial lineations evident in Figure 6.6, is also seen in the ice stream wide mapping of this landform (Figure 6.7). These landforms are most abundant at the upstream end of the ice stream, where they are often present in clusters (Figure 6.8), and downstream of topographic ridges. Vast areas of the ice stream bed lack subglacial lineations. These areas often appear streamlined (see Figure 6.7), but could not be delineated into individual subglacial lineations. This may be affected by the lower resolution of the DEM compared to that used for the palaeo ice streams from the British Ice Sheet. Elongation ratios range from 1.1 to 19.6, with a median of 3.2, which is not dissimilar to the ice streams examined in previous chapters. Subglacial lineation areas range from 0.19 to 57.76 km^2, with a median of 1.67 km^2, which is considerably larger than those found in the ice streams in previous chapters. Clustering of subglacial lineations is evident in Figure 6.8 and spatial autocorrelation reveals that they are also clustered according to elongation ratio, to a 99 % confidence level (see Appendix A).

The transverse distribution of elongation ratios reveals they are high around the central region of the ice stream and maximum elongation ratio very clearly drops towards the lateral margins (Figure 6.13a), which is similar to the idealised signature of elongation ratios (Figure 4.2). This trend is probably mostly derived from the upstream end of the ice stream where the majority of subglacial lineations are located. No clear longitudinal trend is apparent, which may be due to the lack of subglacial lineations along vast areas of the ice stream length (Figure 6.9b). The spatial distribution of elongation ratios is also depicted in the interpolation (Figure 6.10), which shows some variation in elongation ratio along the length of the ice stream.

The DEM (Figure 6.7) reveals that the ice stream bed is flat, whereas surrounding areas have slightly higher and more variable relief. Investigation of topographic curvature shows that the entire area has a flat curvature and reveals little else because of the lack of spatial variability (Figure 6.11).

Data on surficial sediments was only available for central and southern Alberta (Shetsen, 2002). Figure 6.12a reveals that glacial and lacustrine deposits are the most prominent across the entire area. The analysis clearly shows that glacial deposits,

namely till, is by far the most widespread surficial sediment on the ice stream bed (Figure 6.12c) and most of the subglacial lineations appear to be situated on it (Figure 6.12a). However, a wide range of surficial sediments are present across the entire area. As the areas of high lineation clustering were located in northern Alberta, analysis of the surficial sediments of the clusters was not possible.

The ice stream is underlain entirely by sedimentary bedrock and crosses several different formations, as indicated in Figure 6.13. These comprise very similar lithologies, in particular shales, sandstone, siltstone, mudstone and ironstone.
As Figure 6.13c shows, no one geological formation is dominant for the ice stream bed as a whole. However, the upstream clusters of subglacial lineations clearly are mostly located on the Labiche Formation (Klp), which comprise shales and ironstone partings (Hamilton *et al*., 1999). Besides this, no clear trends between the subglacial lineations and bedrock geology are evident. Examination of Figure 6.13a shows that the most elongate lineations appear to be situated on the Belly River Group and Bearpaw Formation.

Examination of bedrock permeability across the ice stream reveals that moderate and low permeabilities are dominant across the ice stream as a whole. This trend is also reflected in the permeabilities that are present in the clusters. The subglacial lineations are situated on both moderate and low permeabilities and do not appear to show a clear preference for either, nor does elongation ratio appear to display any correlation with permeability.

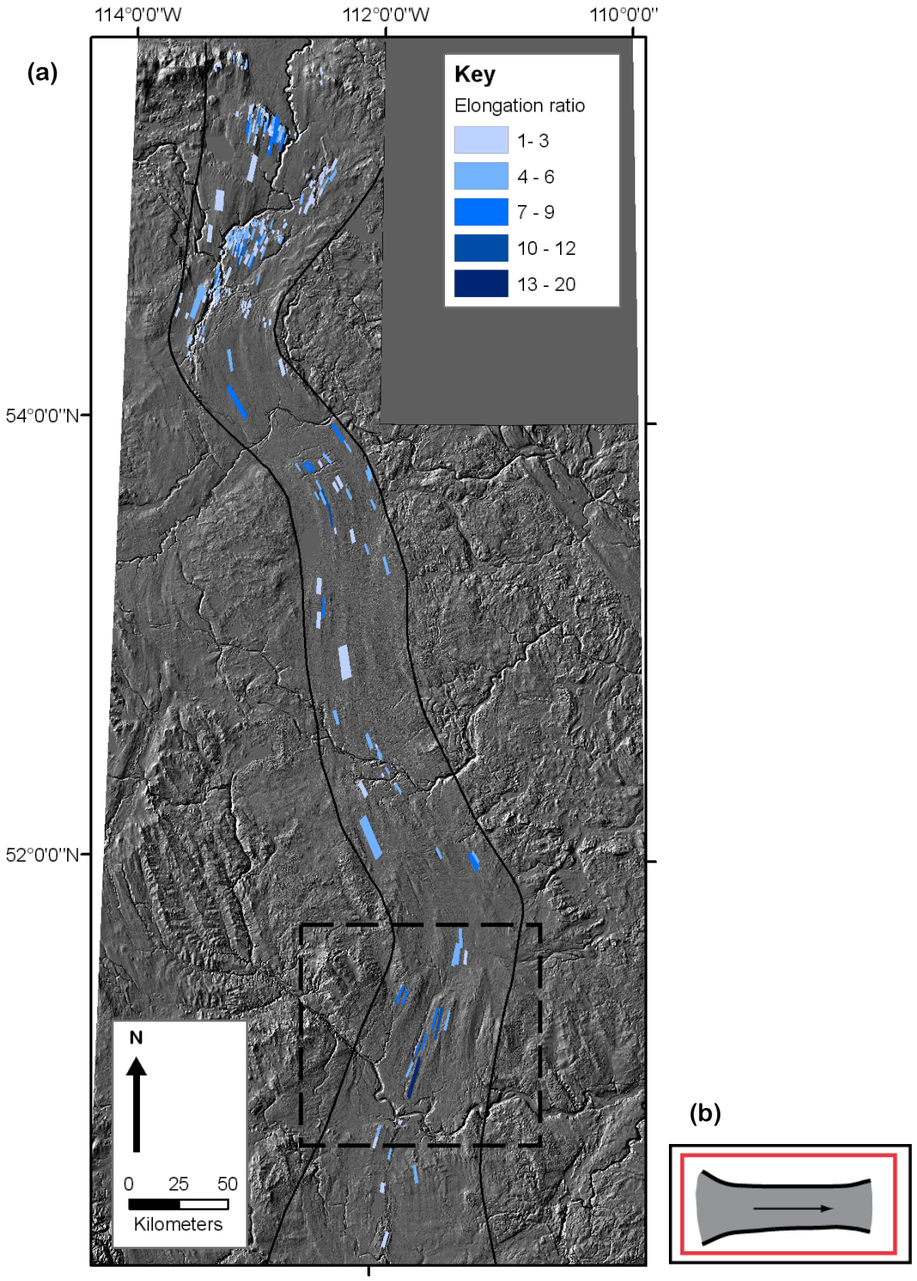

Figure 6.7 – (a) Spatial distribution of subglacial lineation elongation ratio across the Central Alberta Palaeo-Ice Stream. Subglacial lineations are shaded according to elongation ratio. Location of the study area is shown with a black dashed box. Background is a CDED DEM, with a vertical exaggeration of x6. (b) Approximate position of the Central Alberta ice stream signature (red rectangle), within an idealised ice stream.

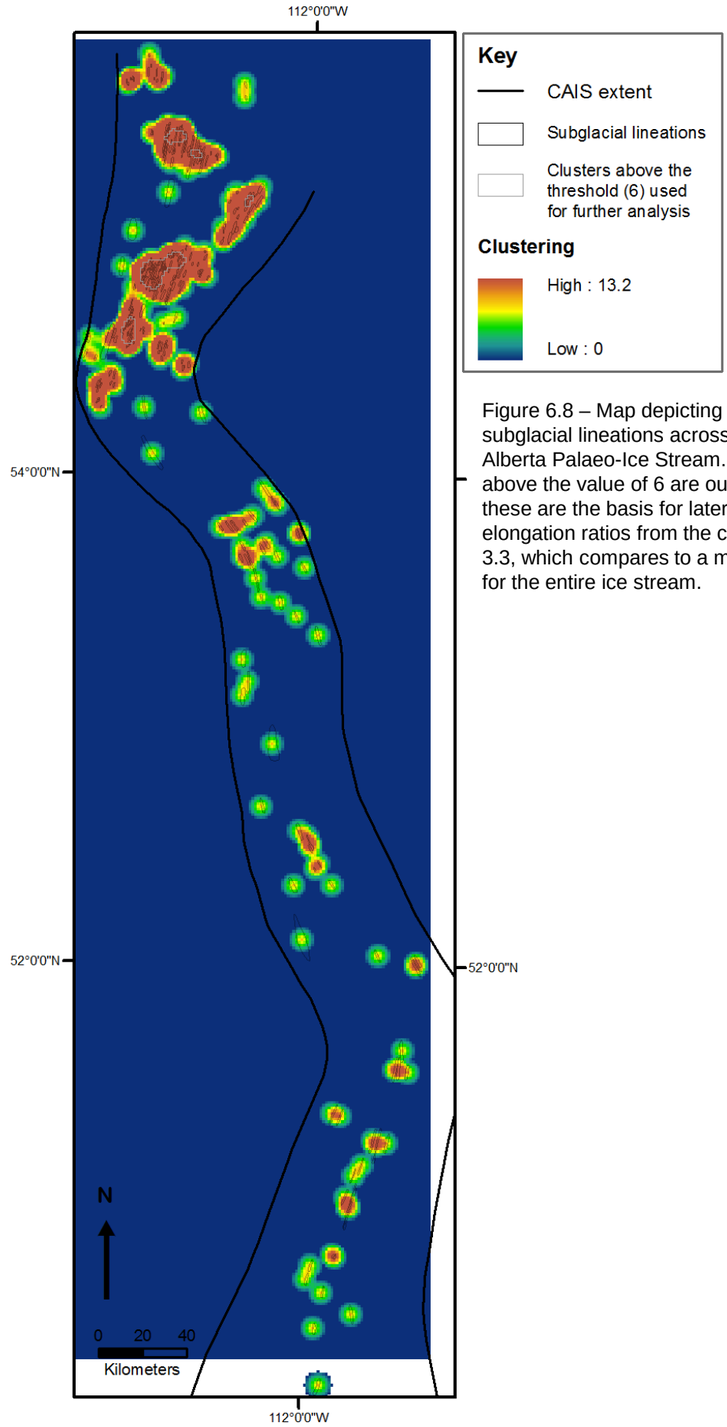

Figure 6.8 – Map depicting the clustering of subglacial lineations across the Central Alberta Palaeo-Ice Stream. Clusters that fall above the value of 6 are outlined, because these are the basis for later analysis. Median elongation ratios from the clusters above 6 is 3.3, which compares to a median value of 3.2 for the entire ice stream.

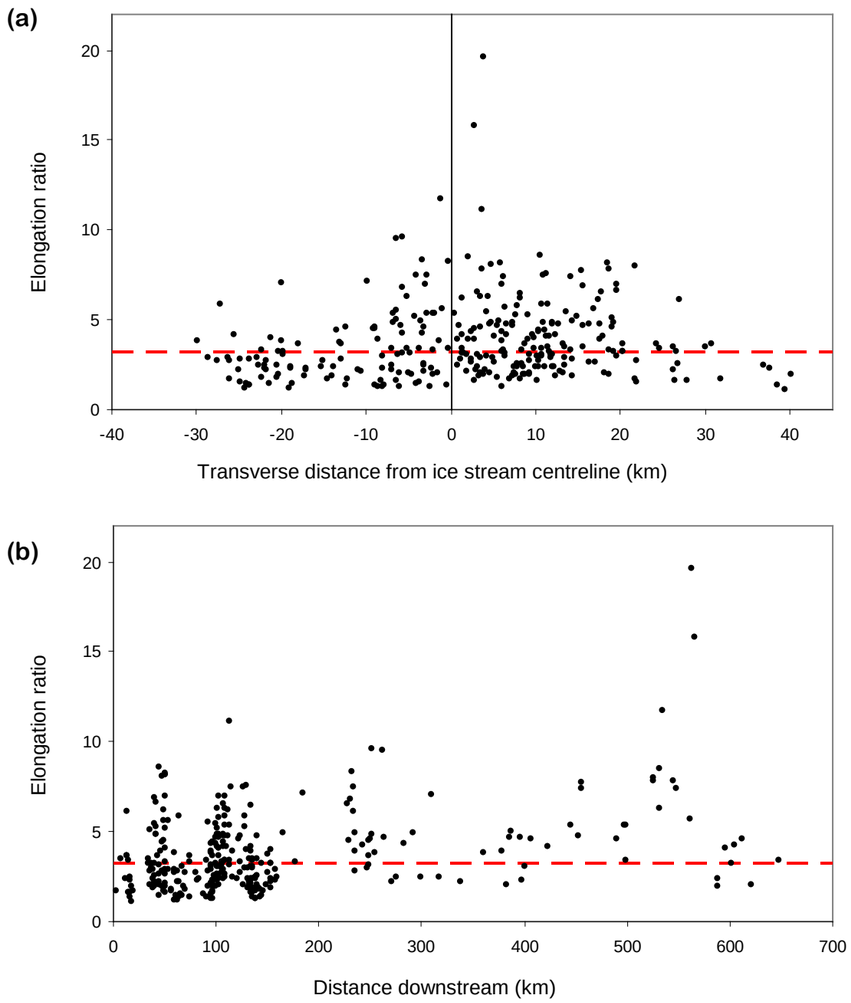

Figure 6.9 – Transverse and longitudinal trends in subglacial lineation elongation ratio. (a) Elongation ratio plotted against distance from the ice stream centreline (black vertical line). Distance from the centreline is on the x axis, positive values represent east of the centreline and negative values represent west of the centreline. (b) Elongation ratio plotted against distance along the ice stream. Distance along the ice stream is on the x axis, from 0 (upstream) to 700 km (downstream). Median elongation ratio is marked with red dashed lines.

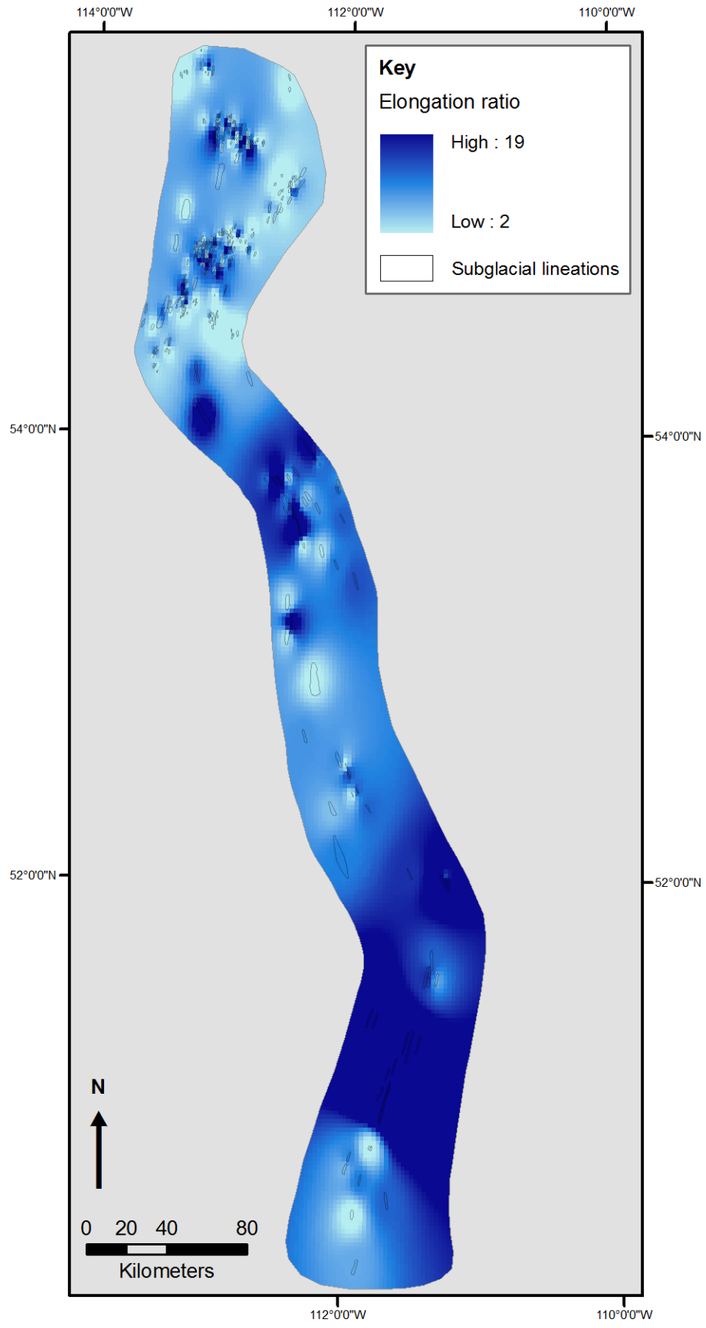

Figure 6.10 – Elongation ratio interpolated across the Central Alberta Palaeo-Ice Stream, which provides a visual impression of the spatial distribution of elongation ratios. The grey background allows the interpolated surface to be shown only to the approximate extent of the ice stream.

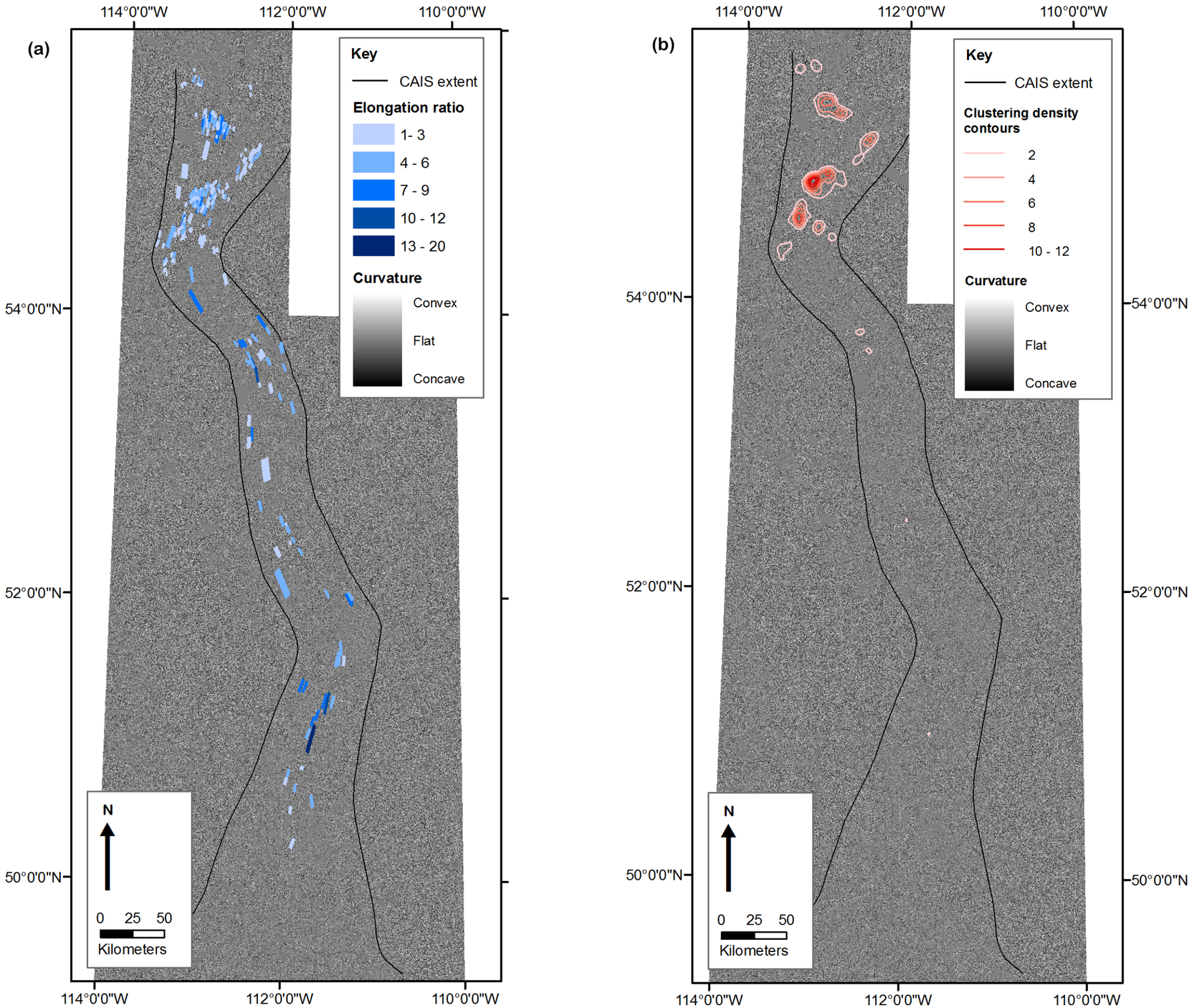

Figure 6.11 – Topography curvature across the Central Alberta Palaeo-Ice Stream. Data derived from Canadian Digital Elevation DEM. (a) Curvature map overlain by subglacial lineations shaded according to elongation ratio. (b) Curvature map overlain by contours of subglacial lineation clustering (derived from the data presented in Figure 6.8).

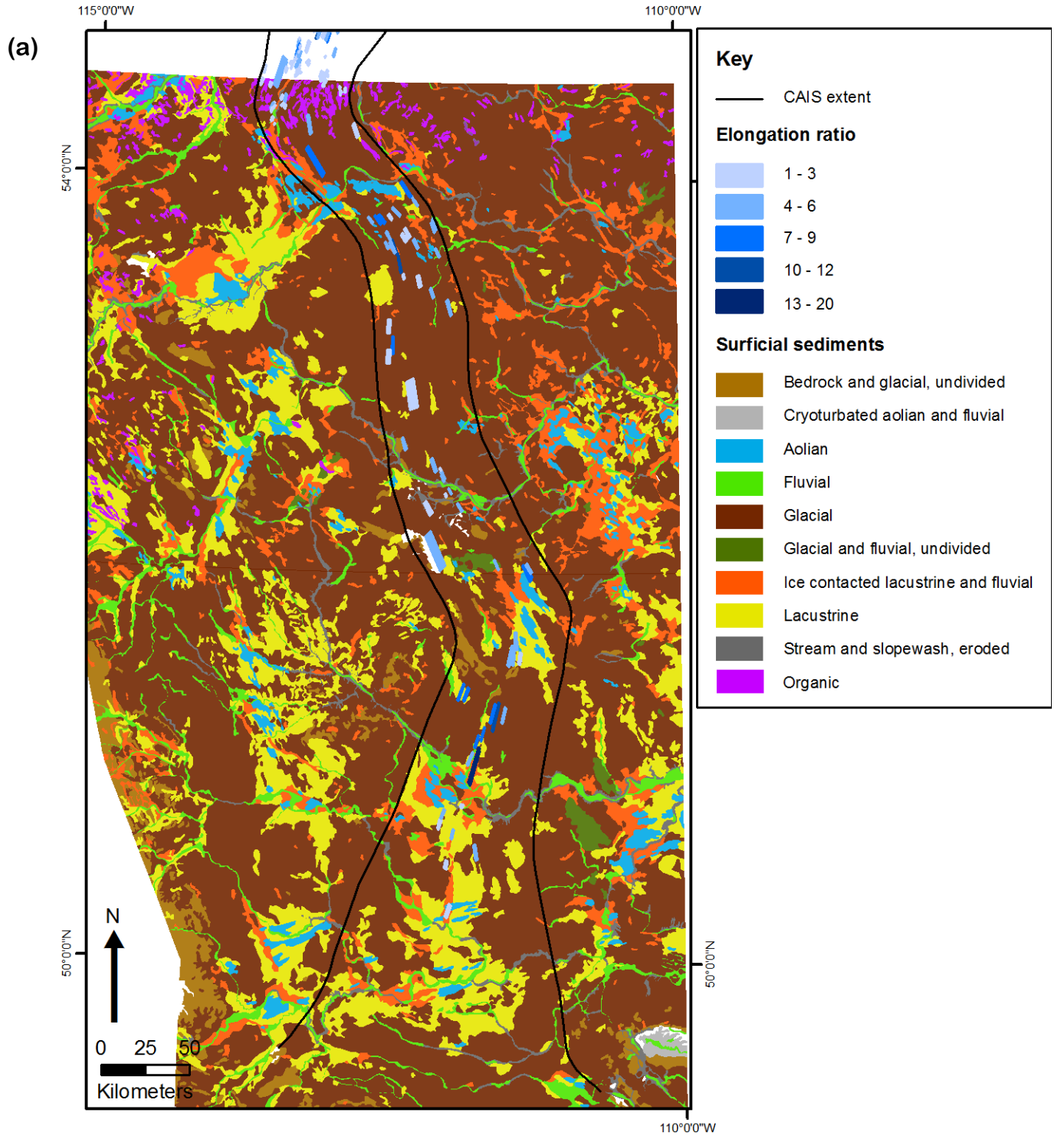

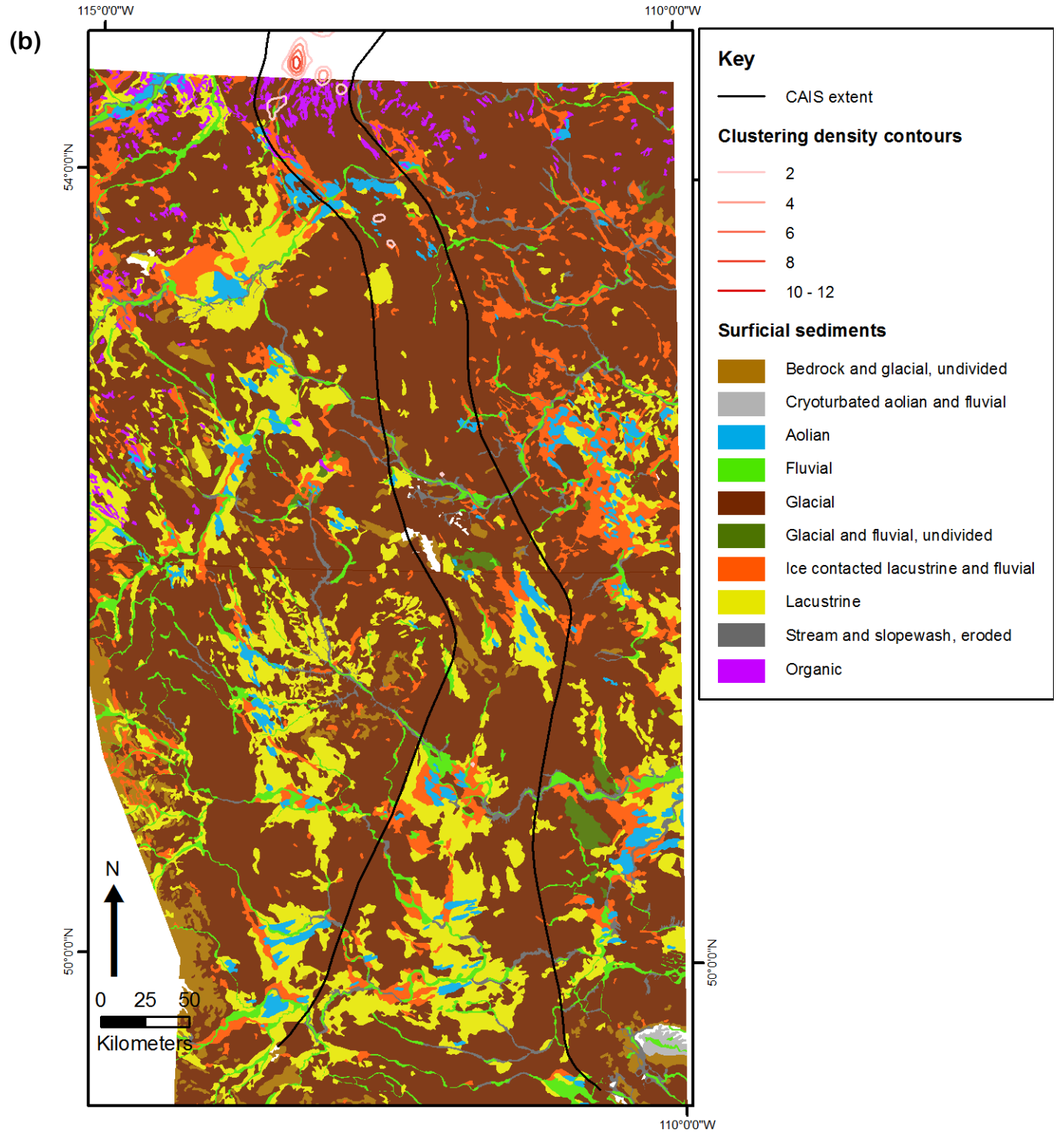

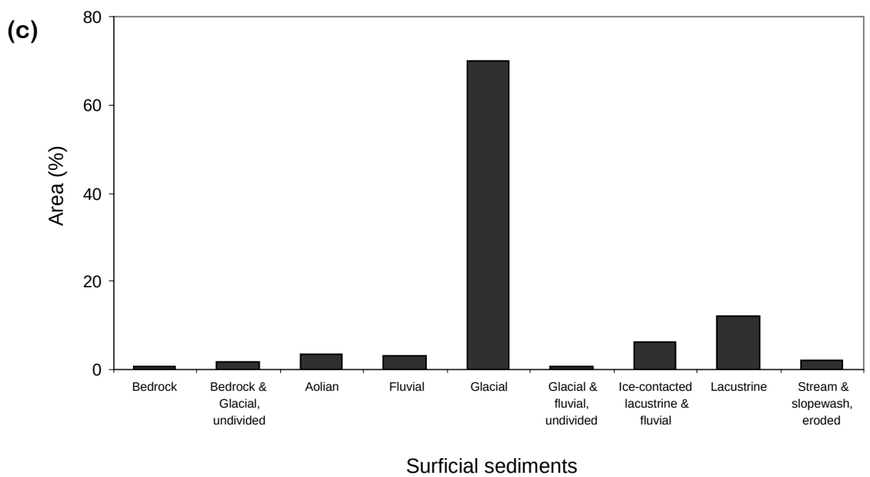

Figure 6.12 – Surficial sediments across the central and southern areas of the Central Alberta Palaeo-Ice Stream. Quaternary geology data from Shetsen (2002). (a) Surficial sediment map overlain by subglacial lineations shaded according to elongation ratio. (b) Surficial sediment map overlain by contours of subglacial lineation clustering (derived from the data presented in Figure 6.8). (c) Bar chart displaying the percentage coverage of surficial sediments across the whole ice stream.

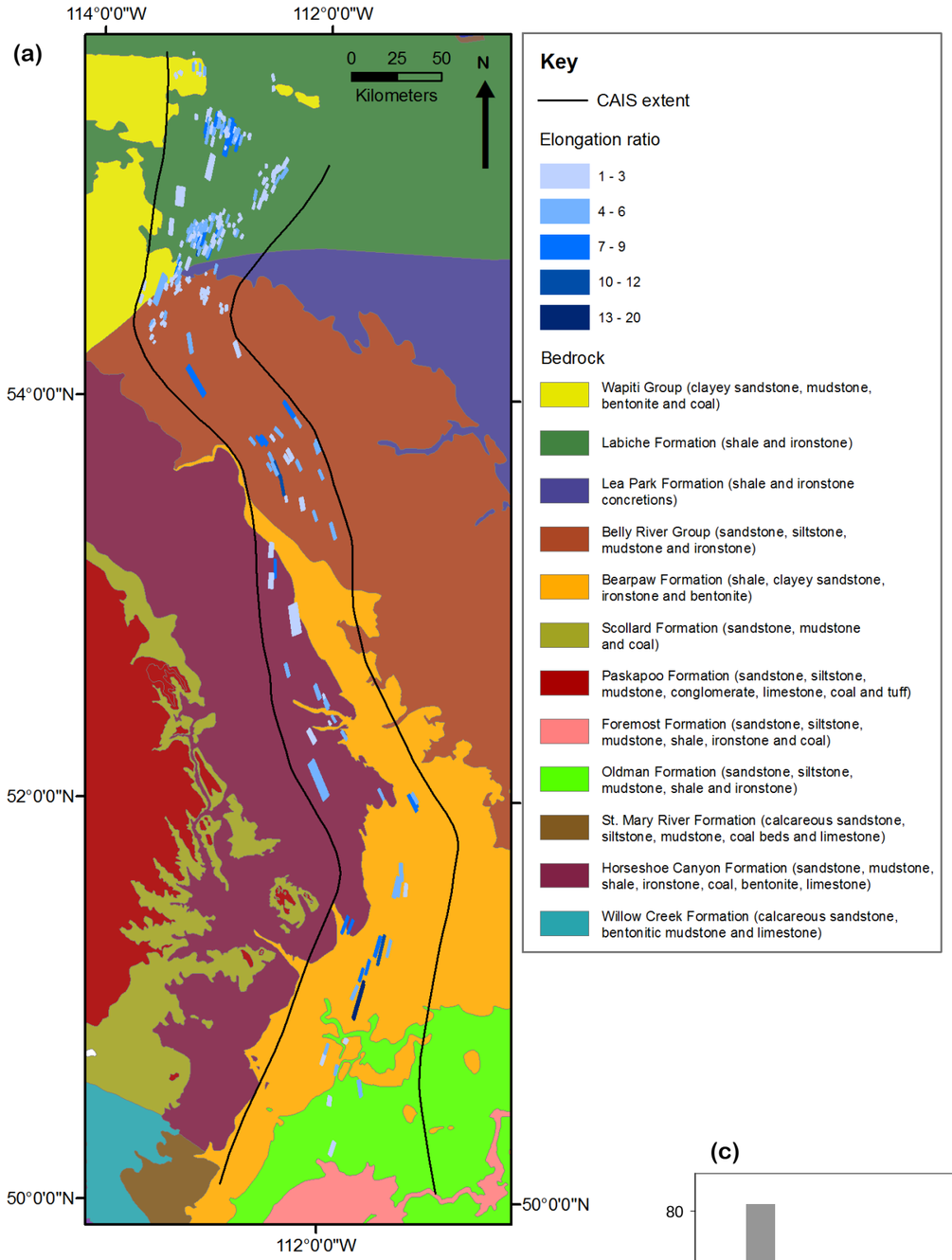

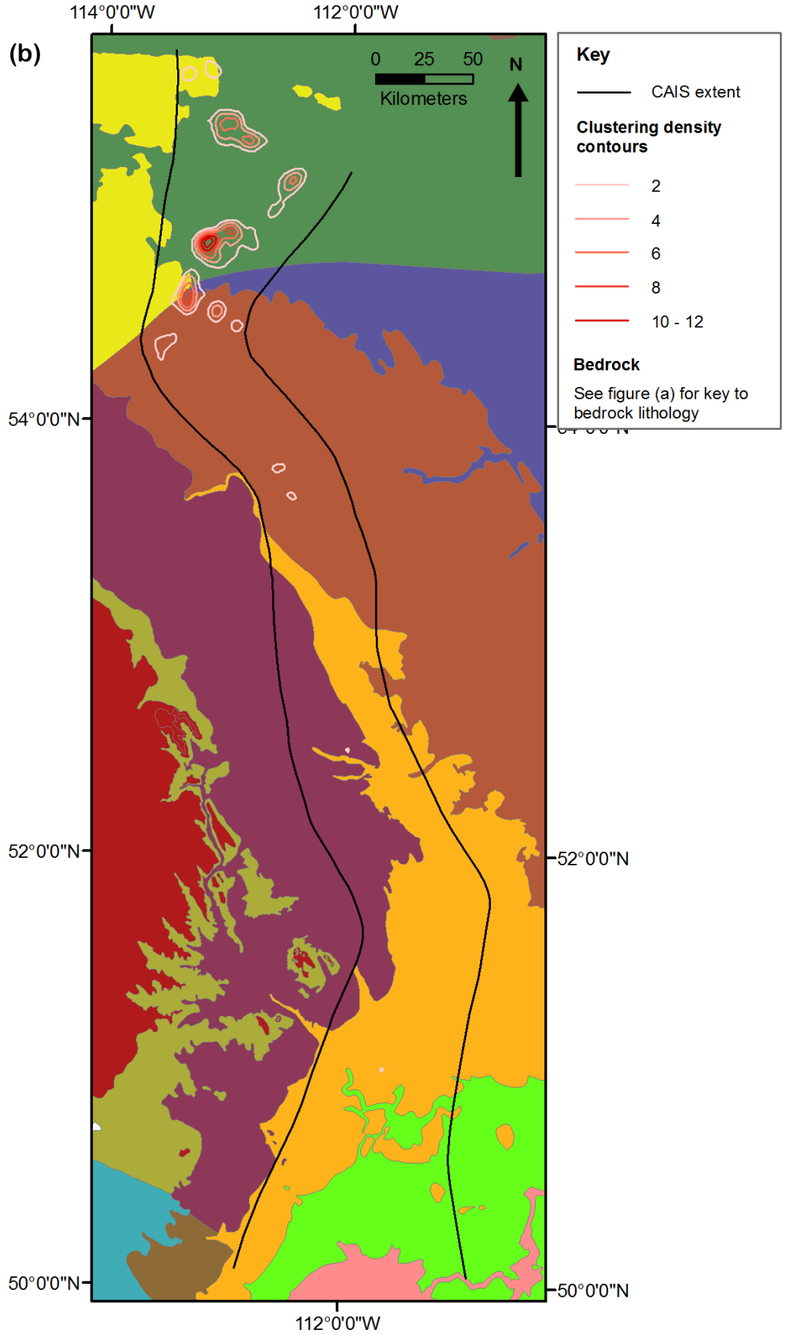

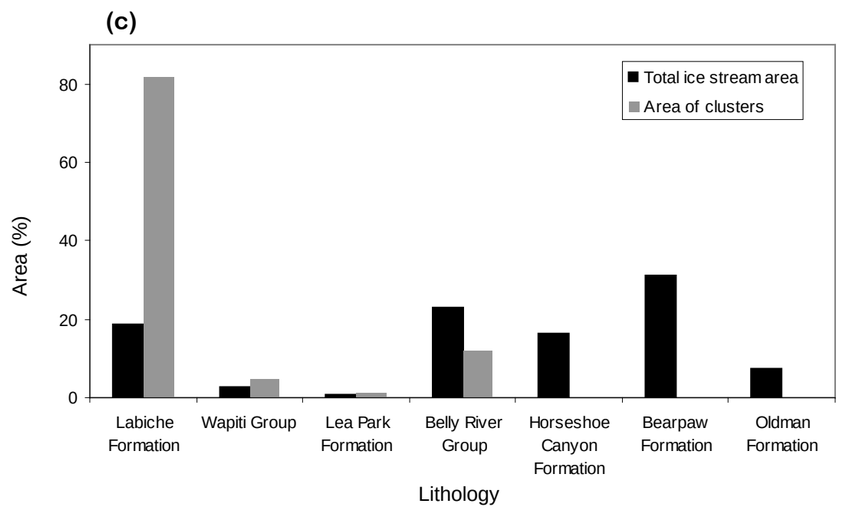

Figure 6.13 – Bedrock lithologies across the Central Alberta Palaeo-Ice Stream. Geology data from Alberta Geological Survey (2009). (a) Bedrock map overlain by subglacial lineations shaded according to elongation ratio. (b) Bedrock map overlain by contours of subglacial lineation clustering (derived from the data presented in Figure 6.8). (c) Bar chart displaying the percentage coverage of bedrock lithologies across the entire ice stream area and within the cluster areas identified in Figure 6.8.

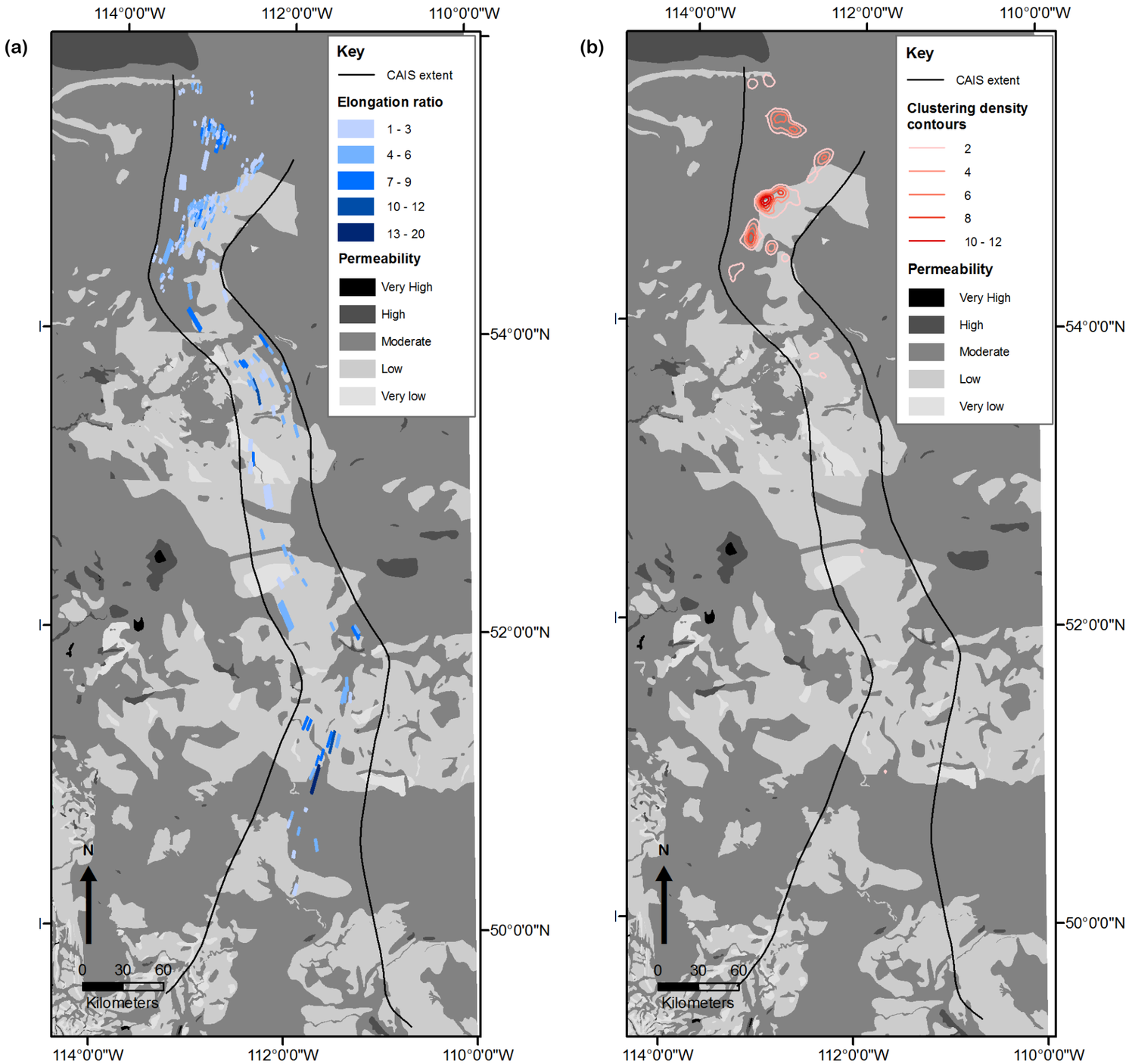

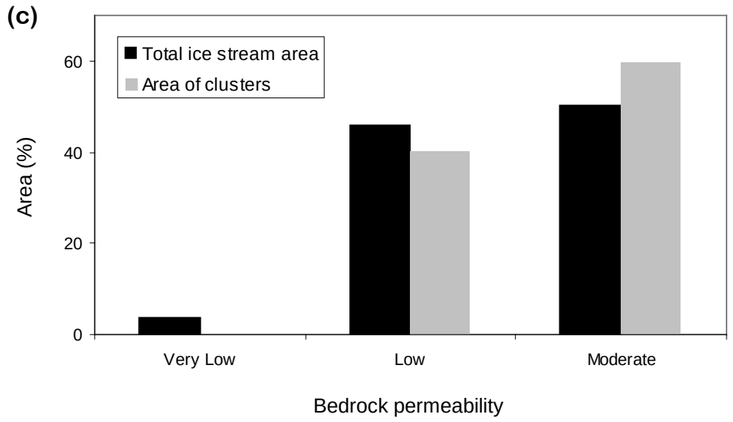

Figure 6.14 - Bedrock hydrogeology across the Central Alberta Palaeo-Ice Stream. Geology data from Alberta Geological Survey (2009). (a) Bedrock hydrogeology map overlain by subglacial lineations shaded according to elongation ratio. (b) Bedrock hydrogeology map overlain by contours of subglacial lineation clustering (derived from the data presented in Figure 6.8). (c) Bar chart displaying the percentage coverage of bedrock permeabilities across the whole ice stream and within the cluster areas identified in Figure 6.8.

6.2.4 Macroscale interpretation

Despite being the largest ice stream examined in this investigation, the Central Alberta Ice Stream has the smallest number of subglacial lineations. The presence of large scale streamlining, identified in other areas of the bed (Figure 6.7), indicate that the lack of subglacial lineations is not a result of them having been eroded postglacially. It indicates that the processes and conditions conducive to the formation of subglacial lineations were only present in certain areas of the bed. Subglacial lineations are commonly located downstream of topographic ridges (Evans *et al*., 2008). The lee side of a topographic high may provide a low pressure area that may be conducive to the sediment deposition, similar to the processes conducive to flute formation (see Benn, 1994). Whilst some of the lineations, at the downstream end of the ice stream, are thought to reflect streamlining of a former esker sequence (Evans, 1996). This highlights a relationship between pre-existing undulations at the ice stream bed and subglacial lineations, which possibly explains why they are only found in certain areas of the otherwise flat ice stream bed.

Of the few subglacial lineations present, these display a degree of clustering (Figure 6.8) particularly at the northern end of the ice stream. Assessment of bed variables show that the clustering does not appear to reflect the spatial characteristics of the bed variables examined here (figures 6.11 to 6.14). Topographic curvature reveals very little, and shows the entire area as flat, which is probably because the area has very low relief. The surficial sediments on the ice stream bed are mostly till, which is probably mostly subglacial, and fluvial or lacustrine deposits, which were likely associated with deglacial processes (see Evans, 1994). Unsurprisingly till is the most widespread sediment across the ice stream bed and the majority of subglacial lineations and other evident streamlining of the bed is situated on till.

Investigation of bedrock lithology reveals the ice stream is situated across several bedrock formations, all comprised of sedimentary bedrock (Figure 6.13). Assessment of the highly clustered subglacial lineations reveals they are preferentially located on the Labiche Formation. This formation consists of the lithologies shale and ironstone, which are more fine-grained than the range of lithologies in other areas of the ice stream bed and this may help explain why subglacial lineations are more abundant here than in

any other areas of the ice stream bed. Bedrock permeability is dominantly moderate and low across the ice stream bed (Figure 6.14), which is similar to trends seen in the ice stream examined in Chapters 4 and 5 as well as reports from modern ice streams (e.g. Tulaczyk *et al*., 1998). Whilst this characteristic varied spatially across the ice stream bed, visually this does not appear to correlate with the occurrence or elongation ratio of the subglacial lineations, indicating that it did not significantly affect subglacial lineation growth.

The rarity of subglacial lineations arguably could be a result of a limited time period for their formation, but the high elongation ratios of those that are present suggest otherwise (assuming that they progressively elongate over time). Furthermore, the downstream thickening of till (Shetsen, 1987; 1990) also suggests that the time period (or periods) for ice streaming was considerable. The rarity of subglacial lineations may reflect certain processes that operated at the bed of this ice stream; or properties of the substrate. Comparison of the underlying bedrock geology to ice streams examined in previous chapters, indicates that many of them are also characterised by fine-grained sedimentary bedrock. Therefore, whilst this does not rule out differences in the substrate between different ice streams as an explanation, it possibly hints that the basal processes may instead be the more likely explanation for the observed bedform assemblage.

The low amplitude streamlining and smooth topography is dissimilar to the mapped subglacial lineations in this ice stream and those mapped in chapters 4 and 5, because they do not represent discrete landforms and instead appear as an undulating character of the land surface. These features may reflect different processes to the well defined subglacial lineations seen in previous chapters; and this reinforces the idea that this ice stream was characterised by a bed environment that was different to those of the other palaeo-ice streams examined. However, the observed streamlining is similar to regions of fast flow elsewhere within the Laurentide Ice Sheet (e.g. Shaw and Freshauf, 1973; Evans *et al*., 2008; Ross *et al*., 2009).

Other landforms in the study area include: meltwater channels, eskers, hummocky terrain and moraine ridges, none of which can be explicitly attributed to ice streaming processes. On the ice stream bed (outside of the study area), west-east trending subglacial channels are considered by Evans *et al*. (2008) to relate to movements of ice

dammed lake water (Figure 6.4). They consider that the existence of abundant subglacial water may have promoted basal sliding. Moraine ridges within the study area (Figure 6.6) are typically transverse or slightly oblique to the direction of ice streaming. This corresponds to the interpretation of Evans *et al*. (2008), that minor moraine ridges across the ice stream bed represent active ice recession. Hummocky terrain mapped in the study area is consistent with previous observations that this landform is concentrated in the interstream or interlobate areas between palaeo-ice streams. Meltwater channels within this area do not cross-cut the hummocky terrain and they have similar directional trends to it, indicating that either they formed contemporaneously, or the hummocky terrain influenced the formation of the meltwater channels. If the hummocky terrain is assumed to reflect deglacial processes (e.g. Eyles *et al*., 1999), then this indicates that these meltwater channels were also deglacial. Examination of the mapping of Shetsen (1987; 1990; Figure 6.3) suggests that hummocky moraine forms on relatively thick till.

6.3 Berry Creek Reservoir

6.3.1 Site background

Berry Creek Reservoir, which formed in 1948, lies within the centre of the Central Alberta Palaeo-Ice Stream (N 51 15’ 55’’ W 111 37’ 48’’). Underlying bedrock in the area is the Bearpaw Formation, which is composed primarily of shales. Berry Creek and its reservoir is situated in a large deglacial spillway, which runs parallel to palaeo-ice streaming and probably reflected output of deglacial lakes (Shetsen, 1987; Evans *et al*., 2006b). To the west and downstream of the reservoir are several highly elongate subglacial lineations (figures 6.6 and 6.20), interpreted by Evans (1996) to be a glacially overridden esker, based on an examination of their geomorphology and sedimentology. Figure 6.20 shows the topography in the immediate area around the reservoir, which shows the lateral extent of the spillway valley (approximately 9 km wide).

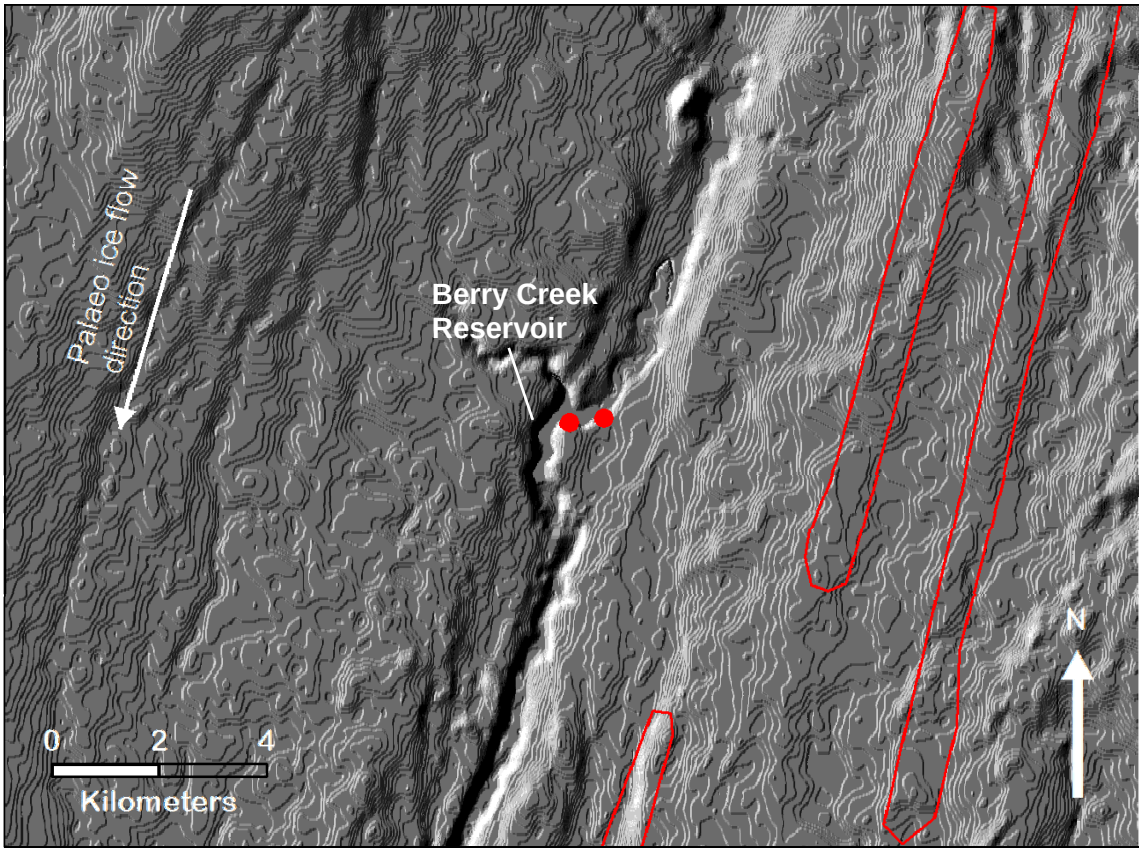

Figure 6.20 – Berry Creek Reservoir and surrounding area. Locations of the examined sediment sections are marked with red dots and subglacial lineations are outlined in red. DEM is Canadian Digital Elevation Data, with a vertical exaggeration of x6.

Shetsen (1987) records the Quaternary sediments of this area as draped moraine, with localised areas of fluvial deposits within the spillway channel. At the reservoir itself, a vertical sediment log comprising 2 m of diamict with sand layers and lenses is reported by Evans *et al*. (2008) and interpreted as a subglacial till.

6.3.2 Mesoscale sedimentology

Several exposures were identified at Berry Creek Reservoir, comprising both bedrock and Quaternary sediments. This is consistent with Shetsen (1987), who reports thin and discontinuous sediment cover in the area. Two sections (Figure 6.21) were chosen to examine in detail, selection being based on the degree of Quaternary sediments exposed and accessibility.

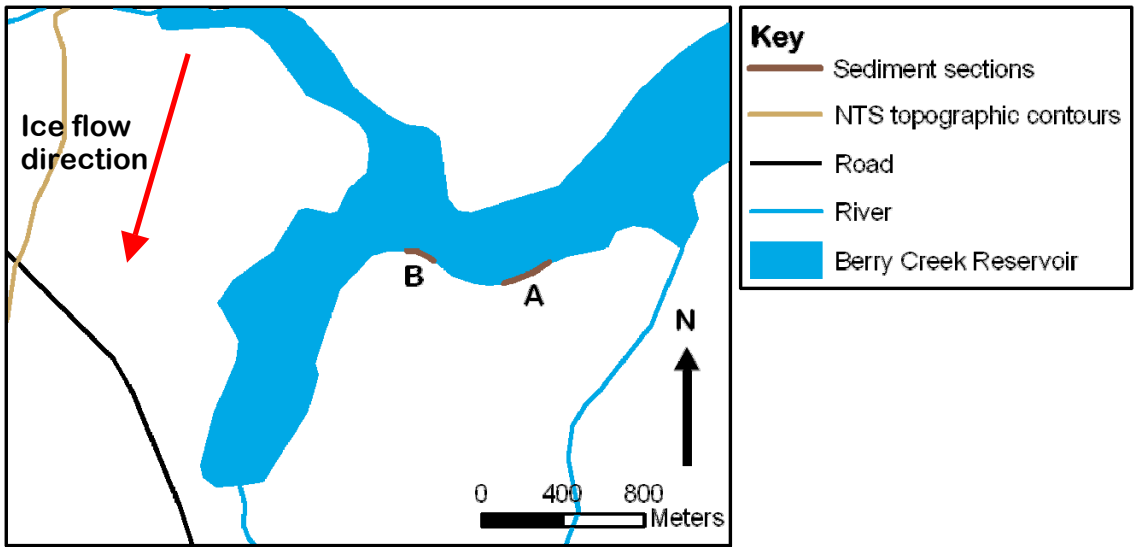

Figure 6.21 – Map of the examined sediment sections at Berry Creek Reservoir. Section A is oblique to palaeo-ice streaming and Section B is transverse to palaeo-ice streaming. Map data from the National Topographic Database (Natural Resources Canada).

The larger section, Section A, is represented by a section log and a vertical log (figures 6.22 and 6.23), which depict a sediment melange. In the architecture of Section A (Figure 6.22), an anticline of diamict can be seen at the north end of the section (5 to 15 m) and the downstream end of the section is characterised by unturned bedding of sorted sediments and diamict (55 to 65 m). Throughout the section large and small deformed intraclasts are present, up to several metres in diameter. This indicates that the entire section has undergone large scale deformation. Section B is represented by a vertical log (Figure 6.25), which depicts a vertical succession of sediments that is representative of the entire 28 m long section. Five lithofacies were identified across the two sections.

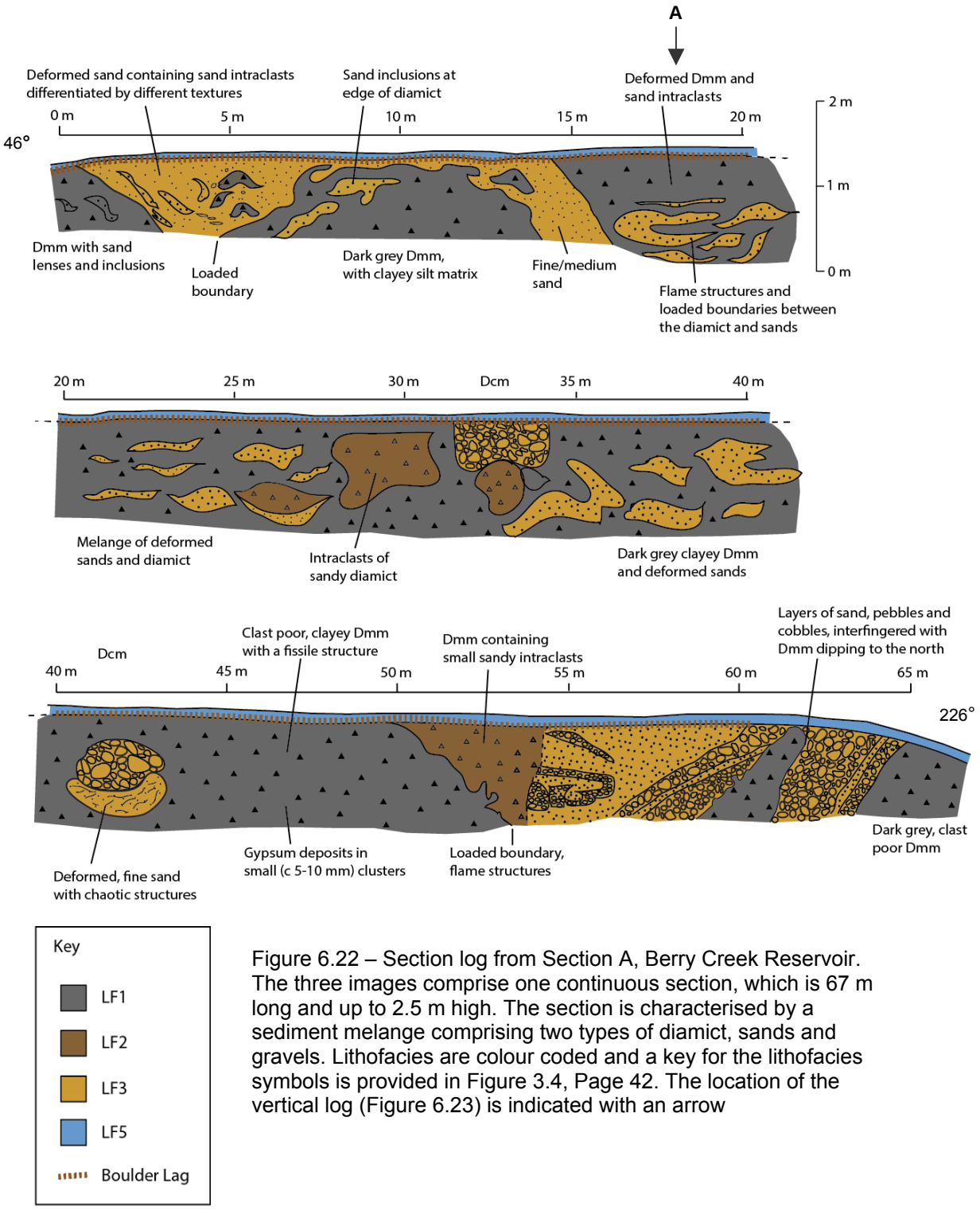

Figure 6.22 – Section log from Section A, Berry Creek Reservoir. The three images comprise one continuous section, which is 67 m long and up to 2.5 m high. The section is characterised by a sediment melange comprising two types of diamict, sands and gravels. Lithofacies are colour coded and a key for the lithofacies symbols is provided in Figure 3.4, Page 42. The location of the vertical log (Figure 6.23) is indicated with an arrow

Lithofacies 1 (LF1) is the most common lithofacies within Section A and comprises a dark grey, clayey diamict. Digging at the base of the section revealed that it overlies bedrock. Clasts are typically resistant igneous and metamorphic lithologies, which clearly are far travelled, considering that Alberta is almost entirely sedimentary bedrock, apart from a small area of metamorphic and intrusive igneous rock in its NE corner (Wheeler *et al.*, 1996). Carbonate deposits are frequently seen as a thin layer at the base of clasts (see Figure 6.28). A boulder lag is present at the top of this lithofacies

and along most of Section A (figures 6.22 and 6.23). Macrofabric from LF1 (figures 6.23 and 6.27) shows a weakly clustered orientation of clasts, and a mean clast orientation sub-parallel to palaeo-ice streaming and dipping upstream. This fabric pattern has some similarities with those observed in lab experiments, which have found that sheared clasts within a till develop shear parallel fabrics that dip slightly upstream (e.g. Hooyer and Iverson, 2000). However, the evident dissimilarity is that the fabric is considerably weaker, as is shown clearly by how centrally the LF1 fabric is situated in the ternary diagram in Figure 6.27. LF1 is characterised by several loaded boundaries, with both LF2 (50 – 54 m, Figure 6.22), and LF3 (5 – 14 m and 59 – 61 m, Figure 6.22).

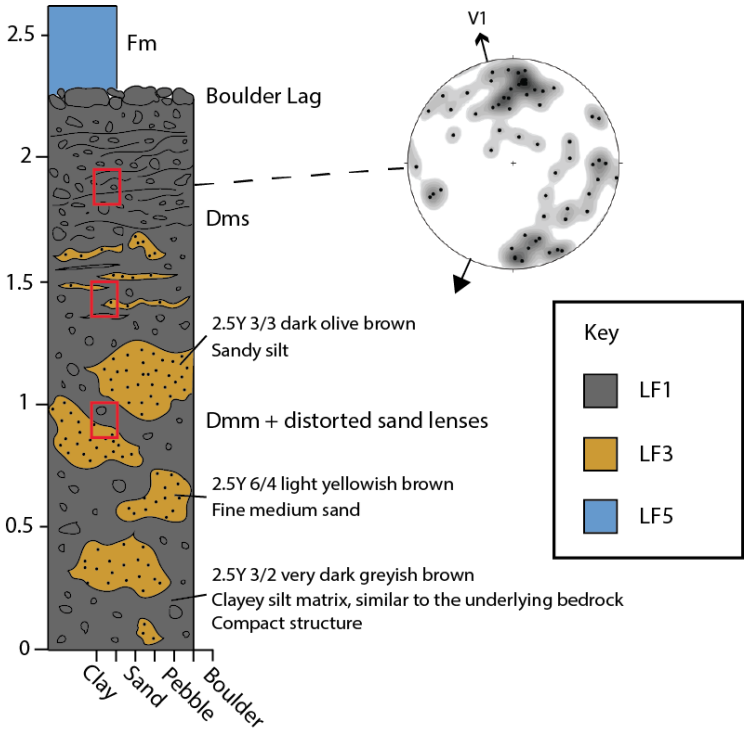

Figure 6.23 – Vertical section log for Section A, Berry Creek Reservoir (located at 18 m on Figure 6.22). Stereonet shows the macrofabric results, in which the open arrow (labelled V1) indicates the principal azimuth eigenvector and the closed arrow indicates the direction of palaeo-ice flow. Micromorphology sample locations are indicated with red rectangles.

Lithofacies 2 (LF2) is a light brown, sandy diamict, which is found in localised areas within Section A. It overlies LF1 at 50 m along Section A (Figure 6.22), where a loaded boundary can be seen between these two lithofacies. A loaded boundary demonstrates the existence of a density difference between two sediment types and commonly takes place where a sediment of higher bulk density overlies a sediment of lower bulk density (Owen, 2003). This results in a range of load structures, which reflects the attempt to reverse this density difference (Owen, 2003). Loading typically takes place during or shortly after sediment deposition (Owen, 1996). LF2 is also present as large intraclasts

(1 to 3 m in diameter) within LF1 as well as smaller intraclasts and attenuated layers in some localities within LF1. Clasts within LF2 are far travelled, resistant lithologies, commonly with carbonate deposits at their base.

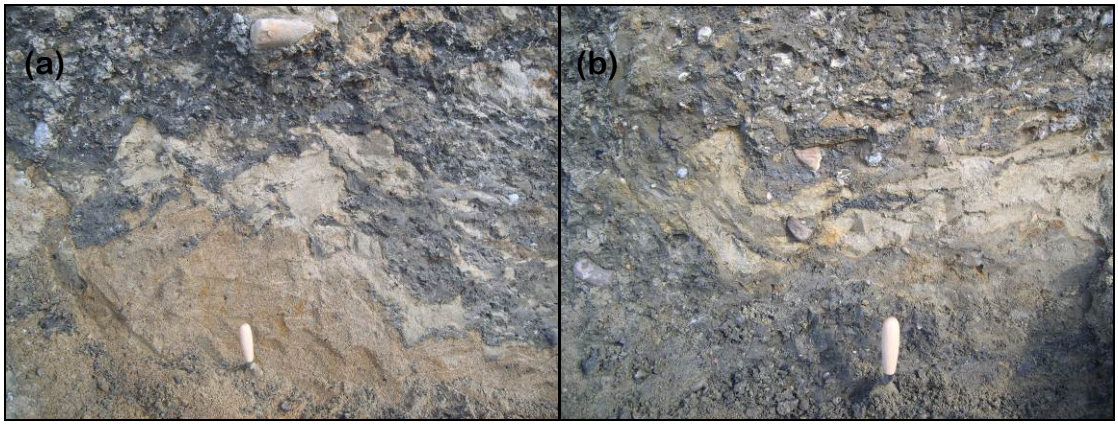

Figure 6.24 – (a) and (b) Images of deformed sand intraclasts (LF3) within the clayey diamict (LF1) at Section A, Berry Creek Reservoir. Note the different textures of sand and the deformed shapes of the intraclasts.

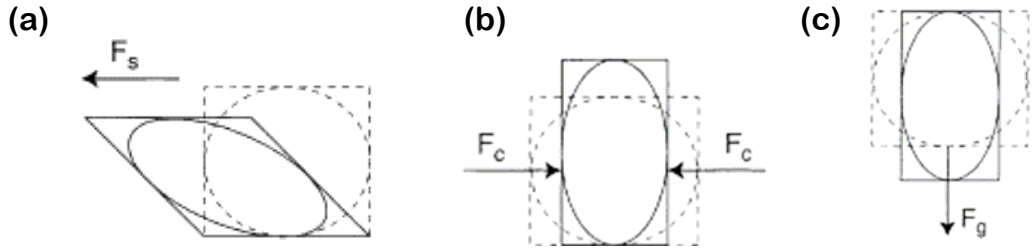

Figure 6.25 – Strain ellipses that represent different styles of deformation: (a) pure shear; (b) compressional deformation; and (c) vertical deformation. From McCarroll and Rijsdijk (2003).

Lithofacies 3 (LF3) comprises deformed sands and gravels. At the north end of the section (0 to 15 m in Figure 6.6) sands overlie LF1 on a loaded, deformed boundary. The sands are typically massive and display no internal stratification, but sand intraclasts of different textures can be identified within it. Intraclasts of LF1 are present within LF3. At the south end of Section A (54 to 65 m along the section) LF3 is the dominant lithofacies. Bedding here is upturned and appears in places randomly orientated; it also interfingers with LF1.

Throughout most of Section A, sand intraclasts and some gravel intraclasts are present within LF1. These sand intraclasts have a range of shapes (Figure 6.24) and are often attenuated, undulating and may have tails extending out from them. These intraclasts often appear elongate in a horizontal direction, with an imbricated orientation and may

have tails extending out horizontally from the main body of the intraclast, as shown in Figure 6.24. This morphology is indicative of simple shear via ductile deformation, as demonstrated by the strain ellipse (Figure 6.25a), which can result from subglacial shear or shear via sediment flow (McCarroll and Rijsdijk, 2003). A few sand intraclasts contain heavily deformed stratification. Some of the apparently massive sand intraclasts contain diagonal lines, possibly reflecting shears or faults. Gravel intraclasts within LF1 typically have more rounded and compact shapes than the sand intraclasts (Figure 6.22).

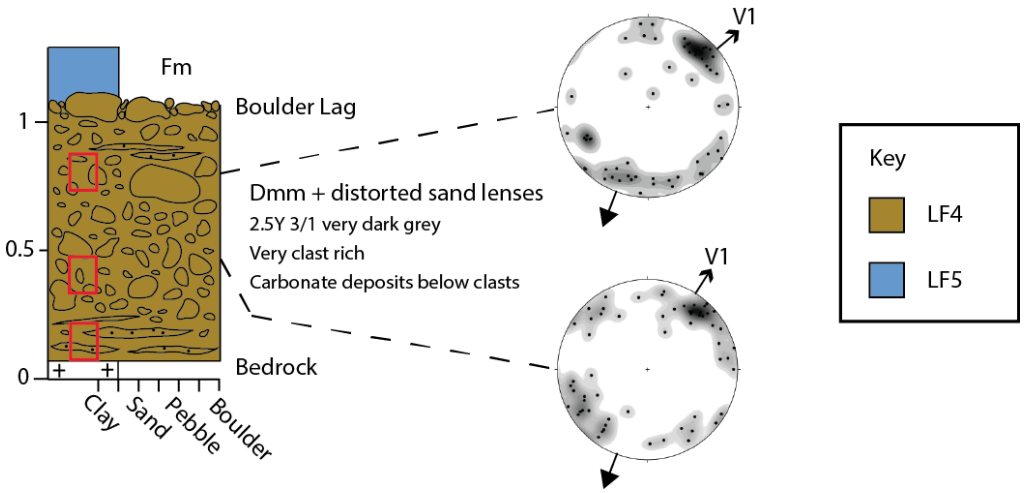

Figure 6.26 – Vertical log of Section B, Berry Creek Reservoir. Stereonets show the macrofabric results, in which the open arrows (labelled V1) indicate principal azimuth eigenvector and the closed arrows indicate the direction of palaeo-ice flow. Micromorphology sample locations are indicated with red rectangles.

Lithofacies 4 (LF4) is a clast rich diamict, containing sand layers and lenses (figures 6.26 and 6.28). LF4 is present along the 28 m length of this section and is approximately 1 m thick. Clasts include far travelled resistant lithologies and carbonate deposits are common at their base (Figure 6.28). Clasts are typically spherical in shape and are most commonly sub-rounded, but a wide range of roundnesses are present (Figure 6.28). C_{40} indices are relatively low, suggesting that clast travel distances were long and clast crushing and fracturing was significant (Evans *et al.*, 1998). Particle size distribution of LF4 is polymodal, with a dominance of clay, and fine gravel size to very coarse gravel size grain categories (Appendix B). Bimodal or polymodal particle size distributions in subglacial sediments are thought to reflect progressive particle size reduction via crushing and abrasion (Boulton, 1978; Haldorsen, 1981).

(a)

Sample	Lithofacies	Mean vector	Mean dip	Eigenvalues	Clustering
BCRA	LF1	346.6°	13.5°	0.511 (S_1) >> 0.32 (S_2) ~ 0.169 (S_3)	Linear
BCRB40	LF4	49.1°	0.5°	0.581 (S_1) >> 0.311 (S_2) ~ 0.108 (S_3)	Linear
BCRB80	LF4	32.7°	3.5°	0.612 (S_1) >> 0.27 (S_2) ~ 0.118 (S_3)	Linear

(b)

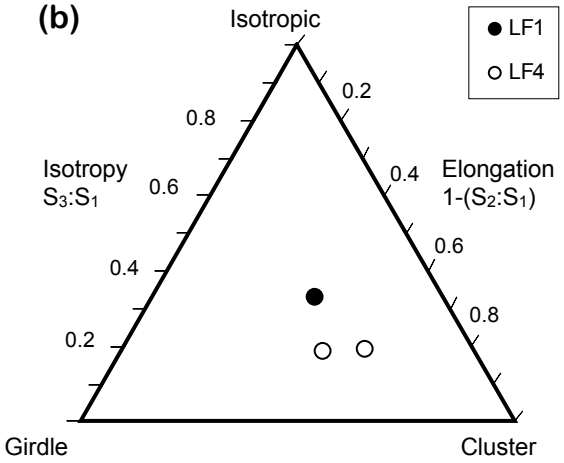

Figure 6.27 – Macrofabric eigenvalues and fabric shape. (a) Table of eigenvalues for the Berry Creek Reservoir samples. (b) Ternary diagram displaying fabric shape for the samples.

Figure 6.28 – Image of Section B (LF4 and LF5), Berry Creek Reservoir. The green arrow indicates a typical white/grey carbonate deposit, which is located at the base of a clast.

Macrofabric in LF4 is weakly clustered and orientated parallel to palaeo-ice streaming, dipping primarily upstream (figures 6.26 and 6.27). At the top of LF4 is a boulder lag, which is present along the entire sediment face here. At 25 to 30 cm thick, the boulder lag is thicker than that seen at Section A and this correlates with the more clast rich sediments at Section B than at Section A. Carbonate deposits are present at the base of many of the clasts in the main body of the diamict and in the boulder lag, an example of this is shown in Figure 6.28. Lithofacies 5 (LF5) is a well sorted layer of silt, up to 50 cm thick. It is present at the top of sections A and B, where it overlies the boulder lag (figures 6.22, 6.26 and 6.28).

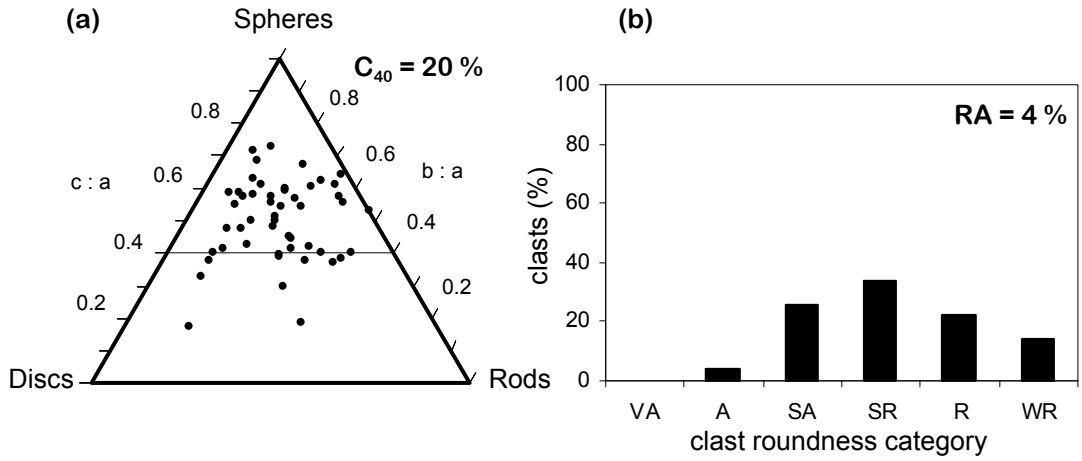

Figure 6.29 – Berry Creek Reservoir, LF4 clast morphology. (a) Clast shape for BCRB; sampled from 60 cm up vertical log (n = 50). (b) Clast roundedness for BCRB; sampled from 60 cm up vertical log (n = 50). Clast roundedness categories are as follows; VA = very-angular, A = angular, SA = sub-angular, SR = sub-rounded, R = rounded, WR = well-rounded.

6.3.3 Mesoscale interpretation

Both sections at Berry Creek Reservoir comprise part of the streamlined surface of the ice stream bed, indicating that at least their uppermost lithofacies were moulded, and also potentially deposited, by ice streaming.

a. Section A

The different lithofacies at Section A, including two types of diamict, sands and gravels, have different depositional origins and were probably deposited at different times. The overall structure of these lithofacies form a melange and clear structural elements can be identified within this, including an anticline and upturned bedding, which document considerable deformation. Abundant intraclasts with distinctive attenuated and

imbricated shapes, indicate the process of simple shear and also suggest that strain was low (Figure 6.25). Given the lack of evidence for sediment flow deposits or a palaeo slope, it is likely that this shear was subglacial (Figure 6.25a; see McCarroll and Rijsdijk, 2003). This indicates that, during or subsequent to deposition of the different sediments, they comprised a subglacial traction zone (see Evans *et al*., 2006a).

The process of loading is seen at the contacts between several of the lithofacies in Section A and appears to have been a significant process here. Load induced structures within glacigenic sediments are not necessarily produced under glacial conditions (Aber and Ber, 2007). This process can take place if there is an increase in stress on a sediment deposit, such as loading by glacier ice, a thick layer of sediment, or a lake; or it can take place if there is a decrease in sediment strength, such as liquefaction triggered by an earthquake (Owen, 2003). Of these possibilities, there is no evidence for the former existence of a thick overlying sediment load or a lake, and whilst it is possible that a drop in sediment strength caused loading, the extensive suite of glacial structures at the site suggest that glacial loading was the mechanism responsible.

An alternative explanation for the complex deformation structures seen may be relict permafrost. Cryosolic soils are present in Northern Alberta and relict crysols have been reported from more southern environments (Soils of Canada). Cryoturbations may originate from gravitational loading in thawing soil and requires liquefaction and a reversed density gradient (Vandenberghe, 2007). This process can form periglacial involutions including flame structures, ball and pillow structures, injection structures and amorphous deformations (French, 2007). However, the ground surface around Berry Creek Reservoir does not reveal any evidence for permafrost such as patterned ground, which typically accompanies cryoturbation (Washburn, 1980). Furthermore, the permafrost thaw explanation does not account for the evidence for shear, because the area around the site is very flat. The imbrication of many of the structures in question are consistent with the direction of palaeo ice flow, thus providing persuasive evidence that the loading was glaciotectonic.

Loading may explain some of the complex structures observed in Section A. A large gravel intraclast in the section (Figure 6.30; 42 m along Section A, Figure 6.22) has a vertical elongate shape, indicative of either vertical or compressional deformation

(Figure 6.25b and c). The shape of the intraclast resembles a teardrop, which is a typical shape for pseudonodules (an intraclast that forms via sinking due to loading) (Rijsdijk, 2001; Owen, 2003). Teardrop shaped pseudonodules may form during sinking, as a result of a higher proportion of loading at the centre of the intraclast (Rijsdijk, 2001), which would explain the upturned ends of the sand layer that underlies the gravels (Figure 6.30). The upturned ends in the sand layer cannot be explained by compression, which, assuming that this layer was horizontal before deformation, would be expected to produce a short, thick, flat layer. Additionally of note is that the intraclast is imbricated slightly downstream, consistent with the direction of palaeo-ice streaming, which is further evidence that loading took place subglacially.

Figure 6.30 – Gravel and sand intraclast (LF2) within LF1, which is indicative of a teardrop shaped pseudonodule (Rijsdijk, 2001; Owen 2003). The sands at the intraclast base display pervasive deformation of the internal stratification. The upturned ends of this sand layer is consistent with increased loading in the centre of the intraclast during sinking (see Rijsdijk, 2001). Image is approximately 2.3 m wide.

A finger of till within upturned, bedded gravels can be seen at the end of the Section A (Figure 6.31; 60 m along the section, Figure 6.22). The vertical, slightly imbricated morphology of this structure suggests that it is a result of either: vertical and shear deformation; or compressional deformation (Figure 6.25). Vertical and shear deformation may have resulted from loading, whereby a diapir of till is intruded up into the gravels and dragged in the same direction as palaeo-ice flow. Compressional deformation, in a glacier forefield location for example, may have caused thrusting of the tills and gravels into an upturned position. The lack of surface expression of these features is easily reconciled with the loading explanation, but less easily with a proglacial, compressional explanation. It would be possible, however, if following compression and thrusting these features were overridden by ice and the surface

streamlined. Despite this possibility, the evidence for large scale loading structures in the rest of the section indicates that loading is a simpler and more likely explanation. Furthermore, at a smaller scale certain features in the structure suggest that loading was taking place, including a loaded boundary on the north side of the structure and individual particles of gravel that have sunk into the till (figures 6.22 and 6.31); a phenomena that was noted by Rijsdijk (2001) in loaded sands and gravels overlying diamict, in Traeth y Mwnt, Wales.

Figure 6.31 – (a) Annotated and (b) unannotated image of a possible till diapir, which is intruded into gravels and sands. Note the load structures (including load casts and diapirs) on its left (north) side and the occasional individual gravel clasts that have dropped into the till. The structure is imbricated in a direction consistent with palaeo-ice flow, which is approximately left to right. Image is approximately 1.8 m wide.

The process of loading has implications for sediment rheology because loading requires the lower, less dense sediment (i.e. LF1) to be viscous (Rijsdijk, 2001). Within sediments, viscous behaviour may result from temporary fluid behaviour, which in granular materials may be via liquefaction or fluidisation (Rijsdijk, 2001). The types of load structures observed indicates that the style of loading deformation was granular or ductile (see Rijsdijk, 2001). The viscous behaviour of the sediment may explain the especially weak fabric observed in LF1 (Figure 6.27) if the line of argument is followed that considers weak fabrics to develop in viscously deforming sediment (see Hicock, 1992; Hart, 1994; Hicock *et al*., 1996; Hart, 1997).

Lithofacies 1 fabric has a parallel orientation with former ice flow, which is consistent with field and lab studies of subglacial fabric (e.g. Hooyer and Iverson, 2000; Larsen and Piotrowski, 2003). However, the fabric is very weakly clustered, with a similar fabric strength to those reported from the Tweed Palaeo-Ice Stream (Chapter 5). This is not consistent with laboratory experiments that have shown that under moderate to high

shear strains fabric becomes strongly clustered (Hooyer and Iverson, 2000). This would suggest that the sediment was either under very low shear strains or was subject to another process. The loading processes may provide an explanation for this, as some studies have argued that weak fabric may develop under high strains in viscously deforming sediments (e.g. Hicock, 1992; Hart, 1997). However, the preservation of structures and intraclasts in the sediments does suggest that strain was low, which may also provide the explanation for weak macrofabrics.

The sand intraclasts within LF1 (LF3) may have been deposited concurrently with deposition of the LF1 till, as sand lenses or layers; or they may have been incorporated into LF1 during deformation and mixing, via subglacial shear and loading. The intraclasts clearly display evidence for deformation, but their preservation and the heterogeneity of the melange suggests that deformation was not pervasive. Pervasive subglacial deformation would be expected to produce a relatively homogenised till and is not conducive to the preservation of intraclasts that have sharp contacts with surrounding sediment (Weertman, 1968; Hooyer and Iverson, 2000). However, intraclast preservation in a subglacially deforming till may be possible in specific conditions, such as if they were frozen during deformation or if they were located in the lee of boulders (Menzies, 1990; Waller *et al*., 2009; Waller *et al*., 2011). The possibility that intraclasts were frozen is unlikely because the process of loading demonstrates that the lower lithofacies (LF1) was under high pore water pressures and viscous, indicating that it was unfrozen during loading processes. Nor is there any evidence that the widespread intraclasts were confined to the lee side of boulders. Therefore, this evidence suggests that pervasive subglacial deformation did not take place and strain was low at this locality.

Geomorphology indicates that the sediment melange at Section A, comprising three lithofacies, was moulded by ice streaming. The relative positions of these lithofacies indicates that LF1 was deposited first, followed by LF2, then LF3. It is unlikely that the two till lithofacies (LF1 and LF2), which have distinct characteristics in terms of colour and texture, were deposited within a single period of ice streaming. They suggest that there were at least two glacial advances here, which is consistent with other stratigraphic evidence in the area (e.g. Stalker, 1983; Evans and Campbell, 1992; 1995). LF1 may relate to a prior glacial advance and LF2 may have been deposited by the ice

stream, which would imply that the overlying sands and gravels (LF3) were also deposited below the ice stream. In this case LF3 may reflect subglacial water movement and may also relate to the streamlined esker system, which is inferred to exist directly downstream of Berry Creek Reservoir (Evans, 1996). Alternatively, all of these lithofacies may have been deposited prior to ice streaming and were subsequently overridden and streamlined by the ice stream. However, given the downstream position of the site within the ice stream it seems unlikely that ice streaming would not deposit any sediment here.

b. Section B

At Section B a thin layer of diamict (LF4) caps the bedrock (Figure 6.26). The locality of this diamict within the streamlined geomorphology of the ice stream, in addition to macrofabrics, sand layers and lenses and clast morphology suggests that this deposit is a subglacial traction till. Clast morphology indicates that this till is well developed. Fabric is orientated in the direction of former ice flow, which is consistent with many other field and laboratory studies of subglacial till (e.g. Hooyer and Iverson, 2000; Larsen and Piotrowski, 2003). However, fabric is very weak compared such studies as indicated by the low S_1 values, which are at the very lower end of the reported range of values for subglacial till (e.g. Hicock, 1992; Carr and Goddard, 2007). Laboratory experiments have shown that strong fabrics develop under moderate to high shear strains and thus it follows that the fabric observed was either under very low shear strains or was subject to another process, such a paraglacial influences (Benedict, 1976; Millar and Nelson, 2001). LF4 is quite different in texture to the tills in Section A and is considerably more granular and coarser grained, which is unusual for an ice stream till, which are typically fine-grained (e.g. Tulaczyk, 1999; Alley *et al*., 2004; Jennings, 2006). The differences in lithofacies and processes between sections A and B attests to considerable variation in processes and conditions at the ice stream bed, over distances of less than 500 m.

c. Boulder pavement

The presence of a boulder pavement, observed near the top of all the sediment sections at Berry Creek Reservoir indicates that the processes for its formation took place across the entire site. Whilst there may be different types of boulder pavement (e.g. Eyles, 1988; Hicock, 1991; Boulton, 1996; Jørgensen and Piotrowski, 2003), several

characteristics suggest that this boulder pavement formed via the post-depositional winnowing of fines from the land surface (see Eyles, 1988). These include: the situation of the boulder pavement directly overlying glaciogenic sediments (rather than within glaciogenic sediments for example); the similar appearance and composition of clasts in the boulder pavement to those in the underlying sediments; the greater thickness of the boulder lag on top of the more clast rich sediments; and the lack of structures around clasts to suggest an alternative origin (for example clast ploughing). The winnowing of fines may have occurred via wind or water erosion following deglaciation. The location of the site within a former proglacial spillway (Shetsen, 1987), indicates that meltwater flow down this route was considerable and as such it seems likely that winnowing was due to water. This interpretation is similar to that of Evans (1991), regarding a thick gravel lag overlying a till in Dinosaur Provincial Park (approximately 60 km south of Berry Creek Reservoir), which was also in the path of a former spillway.

6.3.4 Micromorphology

Six micromorphology samples were collected from lithofacies 1, 3 and 4 (Table 6.1), allowing the study of microscopic features and measurement of microfabric.

Table 6.1 – Details of the micromorphology samples collected from Berry Creek Reservoir. Locations of samples are also indicated in figures 6.23 and 6.26.

Sample	Where?	Orientation to palaeo ice flow	Lithofacies	Why sampled?
BCRa95	Section A, 0.95 m up profile	Oblique (30 ° from parallel)	1 and 3	Characterisation of lithofacies
BCRa145	Section A, 1.45 m up profile	Oblique (30 ° from parallel)	1	Characterisation of lithofacies
BCRa180	Section A, 1.8 m up profile	Oblique (30 ° from parallel)	1	Characterisation of lithofacies and microfabric
BCRb10	Section B, 0.1 m up profile	Transverse	4	Characterisation of lithofacies
BCRb40	Section B, 0.4 m up profile	Transverse	4	Characterisation of lithofacies and microfabric
BCRb80	Section B, 0.8 m up profile	Transverse	4	Characterisation of lithofacies and microfabric

Thin sections sampled from LF1 are shown in figures 6.32 and 6.33, which show its fine-grained and spatially variable nature. LF1 is characterised by small to medium sized (0.2 – 10.6 mm) skeleton grains, including local and far travelled lithologies. Small grains (> 0.3 mm) are typically rounded and well-rounded, whilst larger grains (< 0.3 mm) are typically sub-angular and sub-rounded. The different structures of the two thin sections shown in figures 6.32 and 6.33 (which are 45 cm apart) demonstrate the spatial variability of LF1.

A thin section through a sand intraclast (LF3), is shown in Figure 6.23. It shows the typical composition of the intraclast, which is clast-supported skeleton grains and no matrix. The contact between the intraclast and the adjacent diamict is sharp and there is some evidence of limited mixing between the two, such as a finger of diamict within the intraclast.

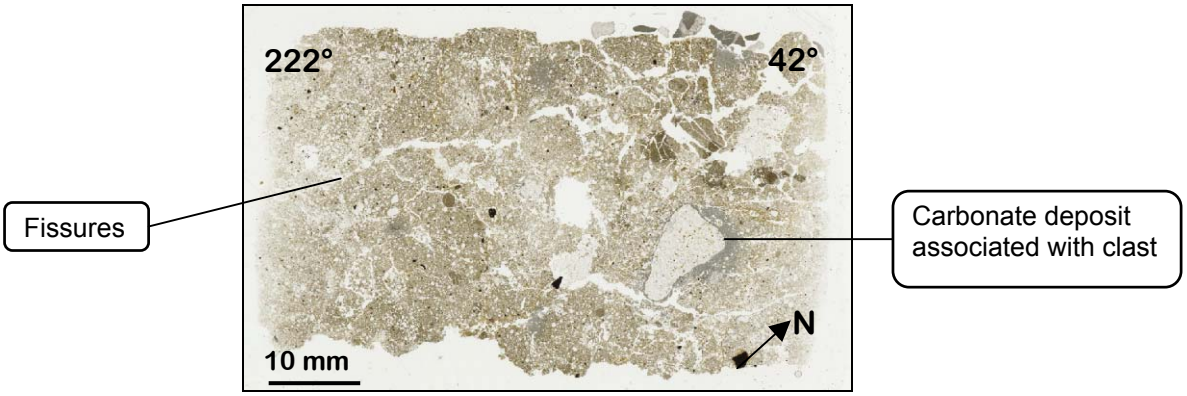

Figure 6.32 - Scan of BCRA180b (LF1), displaying some of the key features that can be seen at this scale.

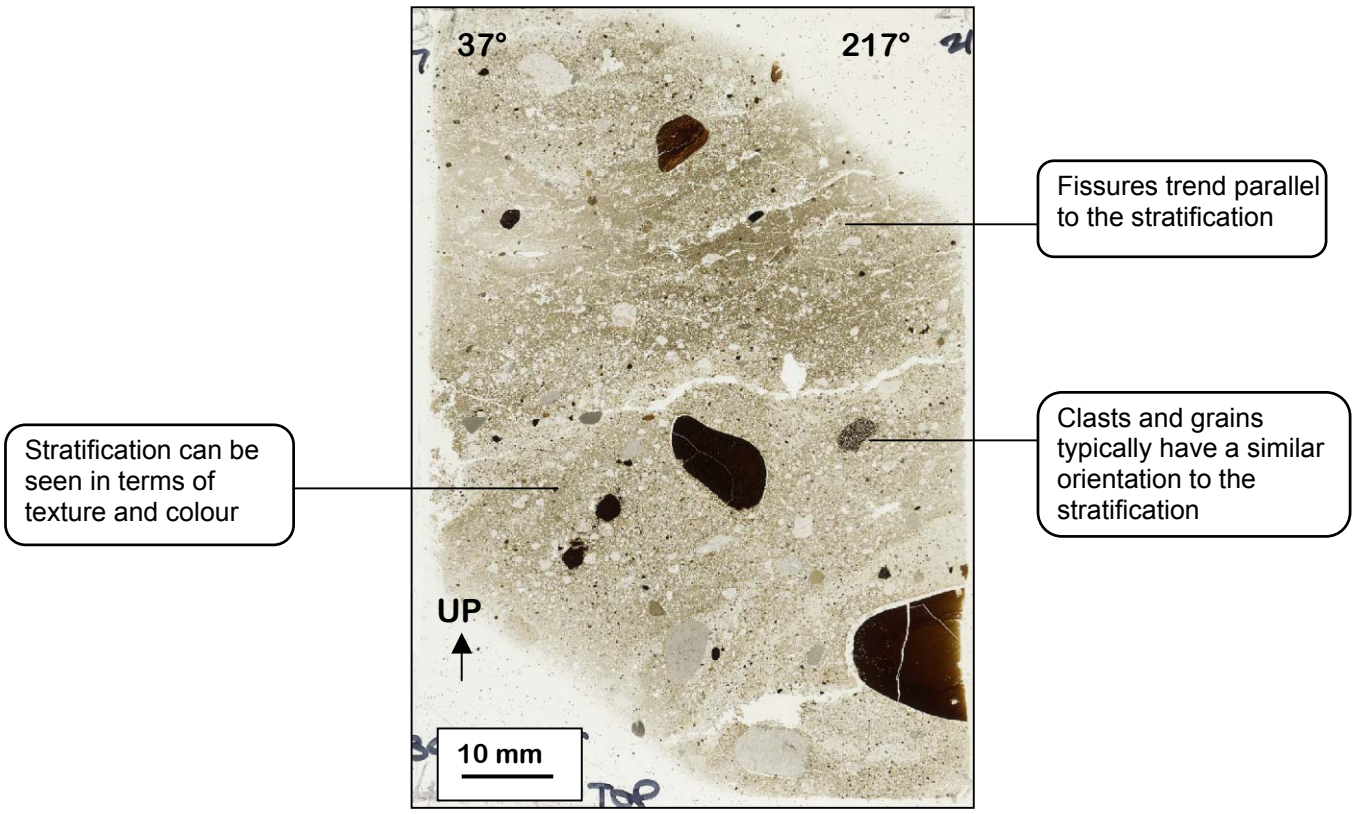

Figure 6.33 - Scan of BCRA145Top (LF1), displaying some of the key features that can be seen at this scale.

A thin section from LF4, illustrating the typical texture and structure of this lithofacies, is shown in Figure 6.35. This lithofacies has a coarse texture, with large skeleton grains (0.04 to 18mm), little matrix and abundant packing voids.

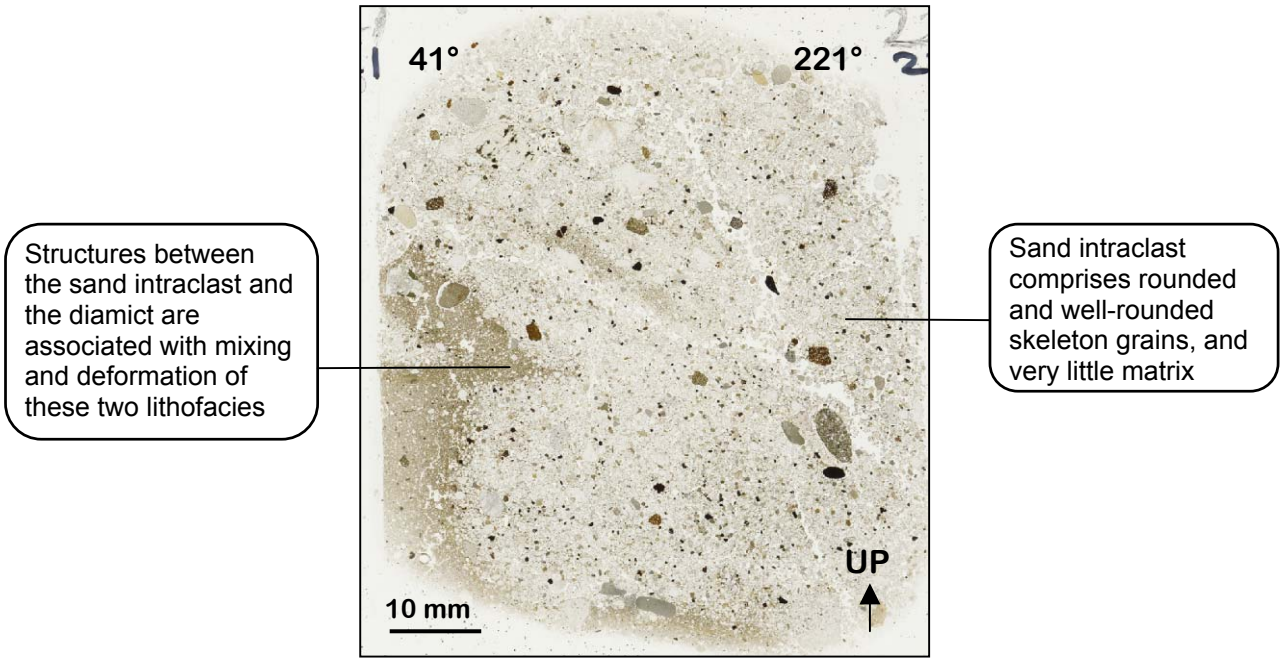

Figure 6.34 – Scan of BCRA95Base, displaying some of the key features that can be seen at this scale. This thin section displays a sand intraclast (LF3) and diamict (LF1).

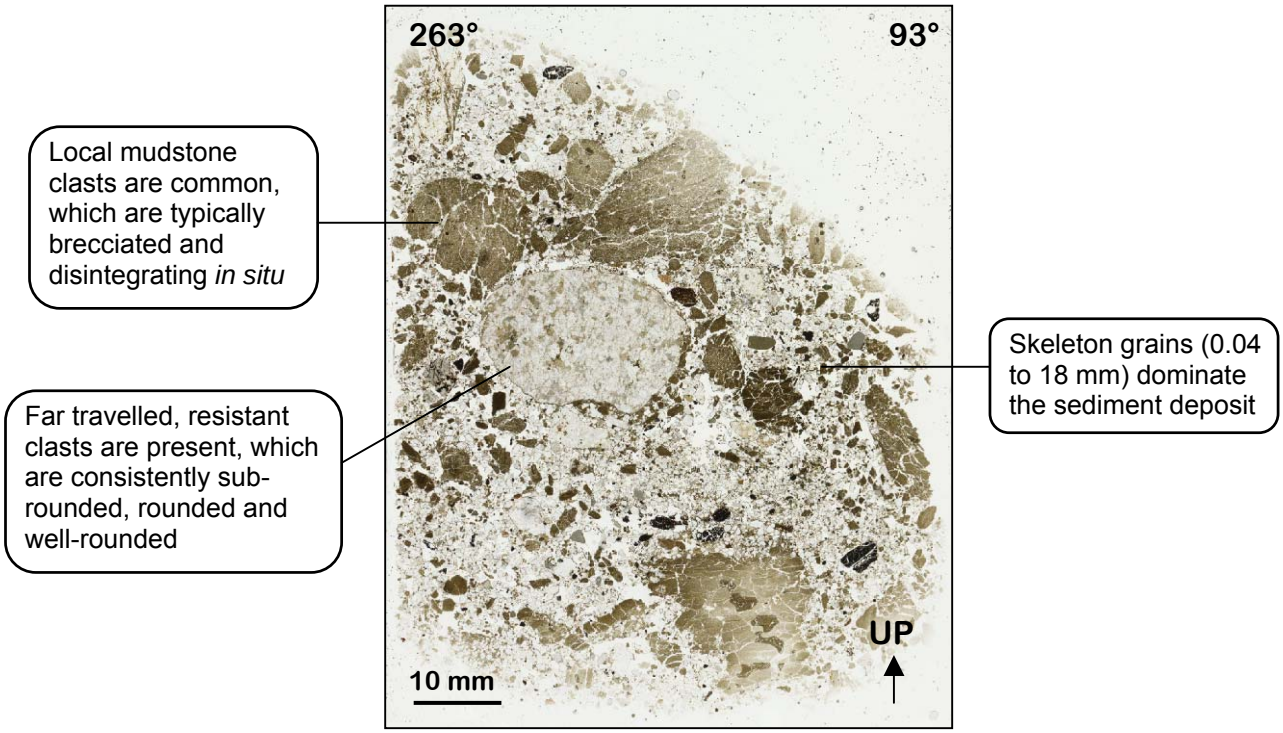

Figure 6.35 – Scan of sample BCRb10 (LF4), displaying some of the key features that can be seen at this scale.

An overview of the micromorphological structures identified in Berry Creek Reservoir is given in Table 6.2, followed by descriptions and images of the some of the key features. Definitions of the micromorphological features described are given in the glossary (Figure 3.9, pages 48-49) and more detailed micromorphological descriptions for each sample are given in Appendix C.

Table 6.2 - Summary table of the micromorphological features from Berry Creek Reservoir. The relative abundance of each feature for each sample is given in a 1 to 3 scale; 3 (●●●) = very abundant, 2 (●●) = present in two or more locations in the sample; 1 (●) = present in a single location in the sample; 0 (-) = not present.

	Voids			Sediment mixing		Grain structures			Clast/matrix alteration							Biological	Plasmic fabric		
	Fissures	Vughs	Packing voids	Multiple domains	Intraclasts	Grain concentrations	Turbates	Grain lineations	Spalling grains	Clast brecciation	Clast edge grading into matrix	Clast weathering rinds	Gypsum	Carbonate deposits	Iron staining	Organic matter	Masepic	Skelsepic	Unistrial
BCRa95	●●	●●	●●●	●●●	-	-	●	●●	-	●	-	-	-	-	-	-	●●	●●●	-
BCRa145	●●●	●●	-	●●●	●●	●●●	●●●	●●●	-	-	-	-	●	-	●	-	●●●	●●●	-
BCRa180	●●●	●●	●●	-	-	●●	●	●●	-	-	-	-	●●	●●●	●	●	●●●	●●●	-
BCRb10	●●	-	●●●	-	-	-	-	-	-	●●	●●	-	-	●●	-	-	●●	●●	●
BCRb40	●●	-	●●●	-	-	-	-	-	●●	●●	●	●	-	●●●	-	-	●●●	●●	-
BCRb80	●●●	●●	●●●	-	●●	-	-	-	●●●	●●●	●●	-	-	●●●	-	-	●●●	●●●	-

a. Voids

Fissures, vughs and packing voids are all prevalent in the Berry Creek Reservoir samples. Lithofacies 3 and 4 are skeleton grain rich and matrix poor, meaning that packing voids are pervasive throughout, as shown in figures 6.36b, 6.34 and 6.35. Several of the fissures contain gypsum or carbonate, which indicates that they were real features in the sediment and not artefacts of sampling or processing.

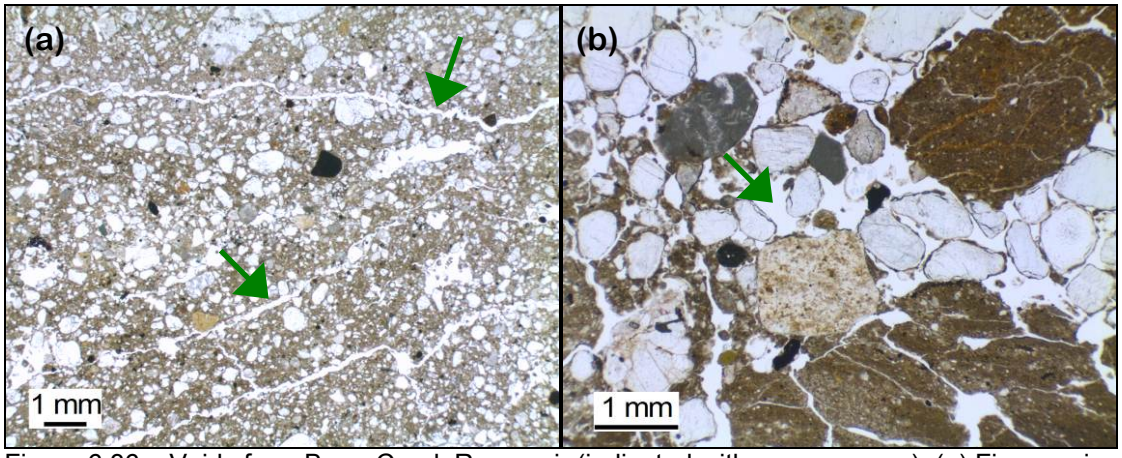

Figure 6.36 – Voids from Berry Creek Reservoir (indicated with green arrows). (a) Fissures in BCRA145 (LF1). (b) Packing voids from BCRB80 (LF4).

b. Grain structures

Grain structures, including turbates, grain lineations and grain concentrations are evident in LF1, and examples of these are given in Figure 6.37. Grain structures can indicate the manifestation of strain within a sediment. For example, turbates indicate rotational movements of particles due to shear (e.g. van der Meer, 1993; Hiemstra and Rijsdijk, 2003) and lineations indicate slip and reorientation of particles along a shear plane (e.g. Hiemstra and Rijsdijk, 2003; Larsen *et al*., 2004). Within LF3 and LF4, grain structures are not apparent because of the clast-supported nature of the sediment at the microscale, which means the typical identification of these structures, as arrangements of grains within matrix, is not possible.

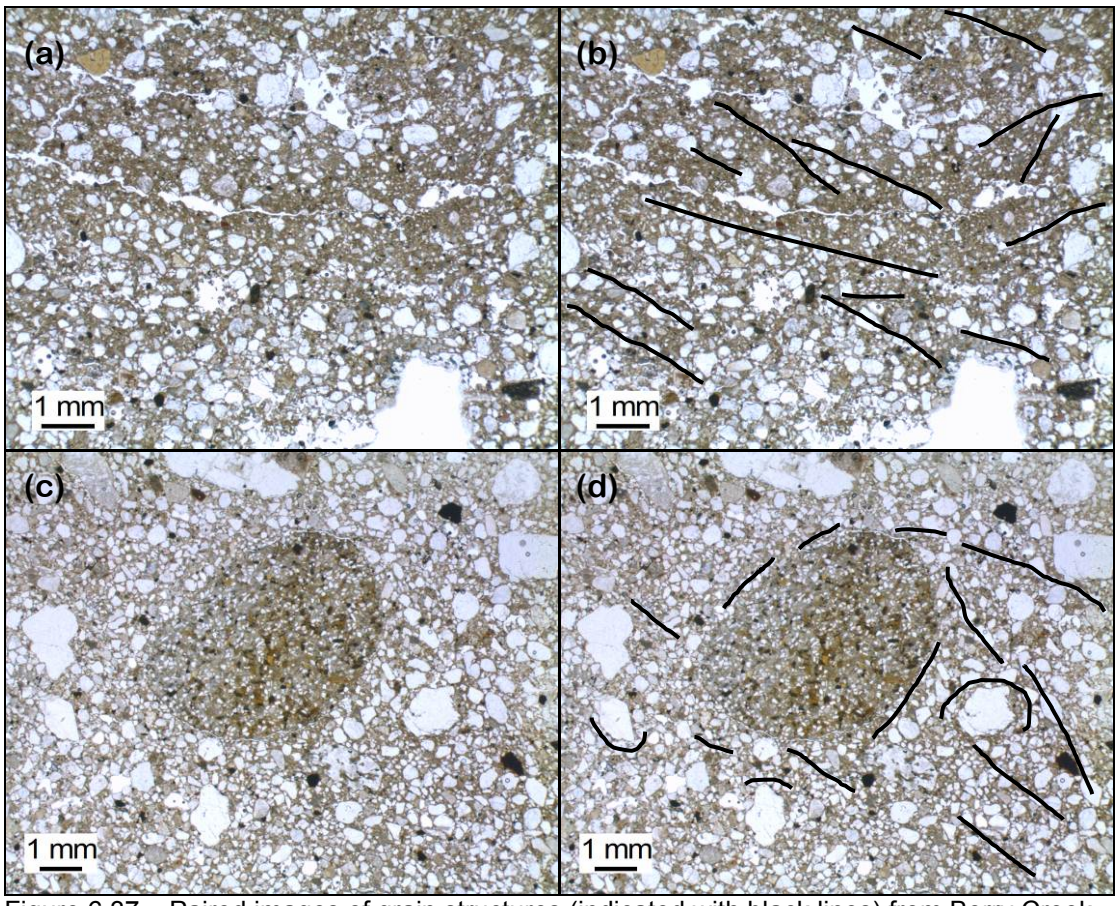

Figure 6.37 – Paired images of grain structures (indicated with black lines) from Berry Creek Reservoir. (a) and (b) Grain lineations from BCRA145Top (LF1). Note the similarity of the orientation of the lineations to the orientation of the fissures. (c) and (d) Turbate with corestone from BCRA145Base (LF1).

c. Clast alteration

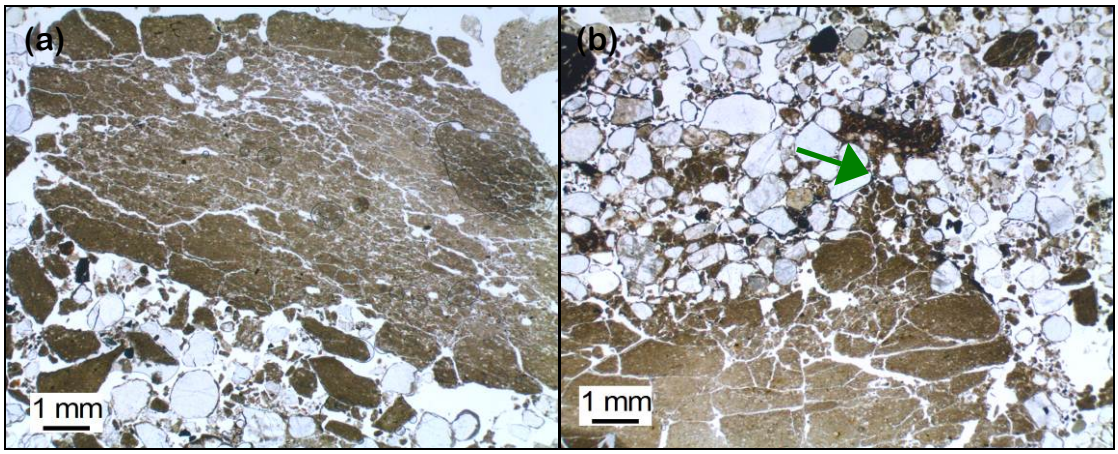

Figure 6.38 – Clast alteration in Berry Creek Reservoir. (a) Mudstone clast brecciation and spalling grains from BCRB40a (LF4). (b) Mudstone clast brecciation and assimilation into the surrounding material in BCRB10 (LF4).

Alteration of clasts, including spalling grains, clast brecciation (Figure 6.38), clast edge grading into matrix, and weathering rinds, is abundant within LF4. These structures

reflect physical and chemical disintegration of clasts (e.g. Haldorsen, 1981; Hooke and Iverson, 1995; Gordon and Dorn, 2004). Clast brecciation and spalling grains are abundant in the local mudstone clasts, as seen in figures 6.35 and 6.38. The larger of the mudstone clasts (approximately 6 to 22 mm in diameter) are typically rounded, sub-rounded and sub-angular, and brecciation is pervasive throughout. The smaller mudstone clasts (< 6 mm) are typically sub-angular and sub-rounded and do not display brecciation. Some of these particles appear to have spalled off the larger mudstone clasts. Clast edge grading into matrix is seen where the mudstone clasts do not have a defined boundary and rather have an amorphous shape with areas extending out into areas of matrix. No clast alteration features are seen on the far travelled, resistant clasts.

d. Plasmic fabric

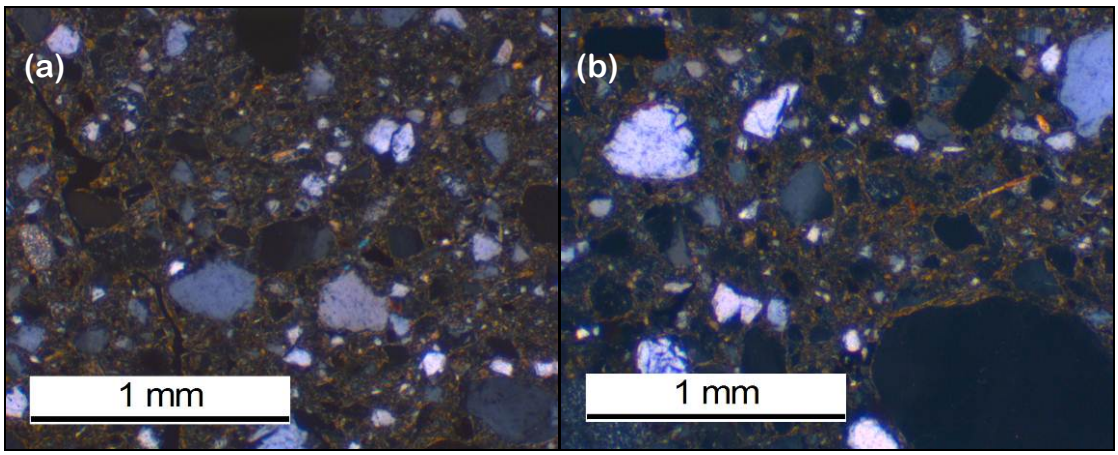

Figure 6.39 – Plasmic fabric from Berry Creek Reservoir. (a) Skelsepic plasmic fabric from BCRA95Base (LF1). (b) Skelsepic and masepic plasmic fabric from BCRA95Base (LF1).

Plasmic fabric, most commonly skelsepic and masepic, was found in all of the lithofacies examined at the microscale from Berry Creek Reservoir. Skelsepic plasmic fabric in LF1 is characterised by relatively thick skins around skeleton grains and is typically pervasive (figures 6.39 and 6.40). This skelsepic plasmic fabric contrasts with that seen in matrix poor LF3 and LF4. In these lithofacies, skelsepic plasmic fabric is typically confined to a very thin layer of matrix, which has adhered to the skeleton grains. Thick skins of skelsepic plasmic fabric may result from rotational movement of grains, such as those in subglacially sheared sediment (Hiemstra and Rijsdijk, 2003), whereas thin skins of skelsepic plasmic fabric can be attributed to other processes including differential compaction of sediment, or wetting and drying (Dalrymple and Jim, 1984; Hiemstra and Rijsdijk, 2003). Notably, plasmic fabric was apparent despite the presence of carbonates in the sediments (see van der Meer, 1993), this may be

because the carbonates are concentrated only in discrete areas. Nonetheless the presence of carbonates may have masked plasmic fabric in some areas of the thin sections.

e. Associations between microstructures

The distribution of the most common micromorphological features observed and any spatial relationships between them are shown in Figure 6.40. This figure displays BCRa145, which is considered representative of LF1 at Section A. Some sub-horizontal stratification and textural variations can be seen across the thin section, which relates to the stratification seen at the mesoscale (Figure 6.23). The difference between these layers is reflected in some of the mapped features, particularly the plasmic fabric, which is strong and widespread at the top half of the image, whereas is only very weakly developed in the lower half. Masepic plasmic fabric is orientated in a horizontal and sub-horizontal direction in the upper half of the image. The plasmic fabric also appears to be concentrated in certain localities rather than distributed evenly across the whole area.

Grain lineations are extensive across all of the areas comprised of grains and matrix, whilst they are rare in the grain rich, matrix poor sediment layer that forms a band across the centre of the image. The fissure running through this layer is also notable as it reflects the orientation of stratification and is confined to this coarse grained, matrix poor layer. In the central lower part of the image many of the grain lineations are orientated at relatively steep angles, pointing upwards, and some of the clasts also display this pattern. The dominant orientation of the grain lineations in this area is from the lower left to the upper right of the image. The turbates identified are usually situated adjacent to grain lineations, but in a few cases are cross cut by grain lineations. Plasmic fabric is usually seen in close association with grain lineations but the plasmic fabric orientation often cross cuts grain lineations obliquely.

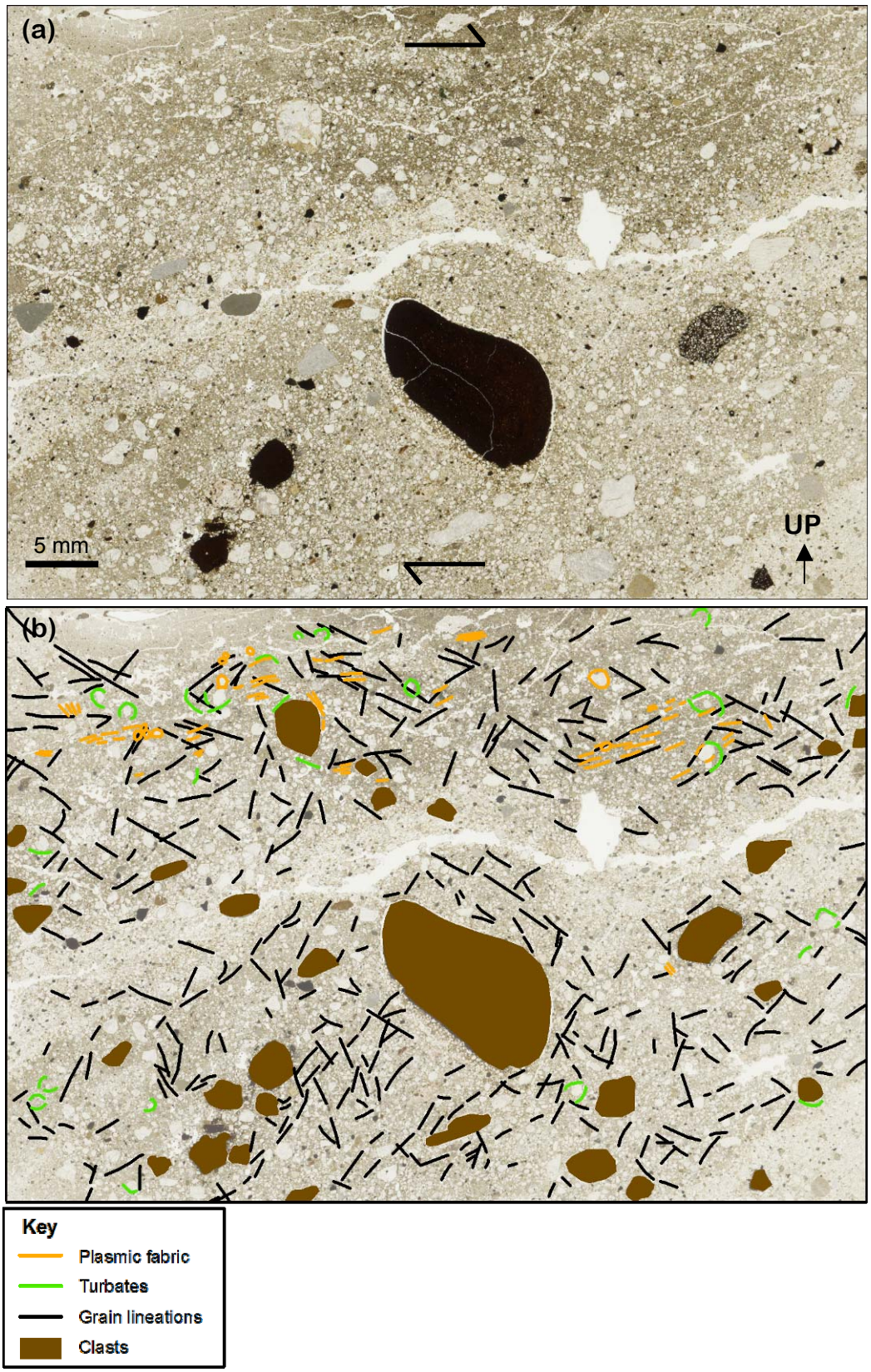

Figure 6.40 – Twinned images of thin section BCRa145 (LF1). An unannotated, high resolution scan of the thin section in normal light conditions, is shown in (a) and a view of annotated features overlying the faded image is shown in (b). Relative sense of shear is indicated with arrows and numbers are referred to in the text. The plasmic fabric indicated is not visible in (a) but has been identified under the microscope in cross polarised light; it is shown schematically in (b), with circles for skelsepic plasmic fabric and lines of plasmic fabric indicating the overall direction of any masepic plasmic fabric.

f. Microfabric

Microfabric was measured in horizontal (b) slides (to obtain particle azimuth) from BCRA180 and BCRB40 (Figure 6.41). The microfabric results show that the particles in both samples have clear preferred orientations and display elliptically shaped rose diagrams. They are orientated transverse and oblique to palaeo-ice streaming and oblique to the equivalent macrofabric, which contrasts with laboratory experiments that show sand sized particles in till orientate parallel to the direction of shear (Thomason and Iverson, 2006). The confidence interval for microfabric azimuth is very small for BCRA180 (3.2°) and larger for BCRB40 (24.8°), which has a considerably lower sample size (Appendix C.3).

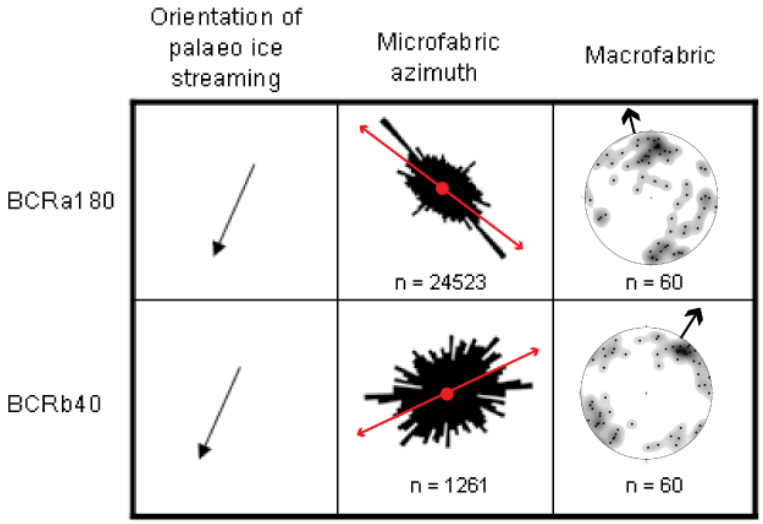

Figure 6.41 – Microfabric rose diagrams of particle azimuth (vector mean is indicated by a red arrow), alongside macrofabric stereonets (vector mean is shown with an arrow) and the orientation of palaeo-ice streaming for comparison.

6.3.5 Microscale interpretation

a. Section A

In LF1 there is considerable evidence for microscale deformation. Ductile deformation structures are common, including multiple domains, intraclasts, deformed laminations, turbates, haloes and skelsepic and masepic plasmic fabric. Brittle deformation structures are also common, including grain lineations and unistrial plasmic fabric. This suite of structures is consistent with what would be expected in a subglacial till (e.g. van der Meer, 1993; Hiemstra and Rijsdijk, 2003). Some cross cutting relationships between ductile and brittle deformation structures was apparent (Figure 6.40), whereby grain

lineations appeared to cross cut turbates and plasmic fabric. This suggests that ductile deformation was followed by brittle deformation, possibly due to changing conditions in the subglacial environment. which is indicative of polyphase deformation and variable pore water pressures (Menzies, 2000). Or these relationships may reflect an event such as glacier retreat, in which dewatering of the sediments caused brittle shear.

Some spatial associations are apparent between microscale features within LF1 from examination of the mapped features in Figure 6.40. The lack of plasmic fabric present in the lower half of the image may reflect a lack of clay sized particles in this layer compared to the upper half of the image. The plasmic fabric in the upper half of the image is orientated sub-horizontally, dipping slightly to the left, whilst the lower half of the image is characterised by grain lineations with a much steeper dominant orientation also dipping to the left. This suggests that shear was propagated here from upper right to lower left but the strain response was different between the layers.

Where plasmic fabric is seen in Figure 6.40 it appears to have orientations both parallel and oblique to grain lineations, which suggests that in some cases these features were a response to the same stress environment but in some instances they were not. This may be because different levels of stress are manifest differently between clay particles and skeleton grains. The close association between turbates and grain lineations implies that these features may form via related processes under the same stress environment (Hiemstra and Rijsdijk, 2003). The apparent structure in the lower centre of Figure 6.40, where grain lineations and clasts appear to be pointing upwards suggests a vertical shear direction. The location of this structure is below a sand layer that is slightly bowed upwards at this point, which suggests that this structure may be a result of water escape (e.g. Menzies, 2000). This interpretation fits with mesoscale loading structures and the evidence for the presence of a density gradient between layers.

The sand intraclast examined (LF3) contains very few microscale deformation structures because of its matrix poor nature. Skelsepic plasmic fabric, which in some cases is linked to subglacial shear, cannot be attributed to this here, because of its very thin skins. The confinement of skelsepic plasmic fabric to a very thin matrix layer surrounded by packing voids, indicates that a wetting-drying origin may be more likely (see Dalrymple and Jim, 1984). However, the overall architecture of the LF3 intraclast

(Figure 6.34) does display evidence for deformation, such as the finger of till within it, which reflects mesoscale observations of intraclast deformation.

b. Section B

Microscale examination of LF4 indicates that it is matrix poor and dominated by both far travelled, resistant clasts and soft, local mudstone clasts. This reveals that the presence of the mudstone clasts are widespread, a fact that could not easily be established at the mesoscale, because on field examination these clasts are difficult to differentiate from matrix material. Furthermore, the micromorphology reveals that in fact matrix is negligible here. This misleading impression of the lithofacies is also seen in the particle size data, which show a considerable proportion of fines. In all probability this reflects the broken down constituents of the abundant mudstone clasts, and hence does not reflect the true proportion of matrix. The lack of matrix in the till and preservation of the soft mudstone clasts suggests that this till is immature and has not been subject to significant crushing, fracturing and abrasive wear (Croot and Sims, 1996). This would also fit with the low macro and micro fabrics measured here based on the understanding that weak fabrics in a shearing environment may reflect low strains (Hooyer and Iverson, 2000). Conversely, clast morphology indicates that abrasion was significant, but this is considered to reflect the resistant lithologies, which were preferentially sampled due to the fact that the fragile mudstone clasts were typically indistinguishable from matrix material. The evidence for abrasion on the resistant lithologies probably reflects successive periods of reworking.

Micromorphological examination demonstrates that LF4 contains very little evidence of ductile or brittle deformation. It showed mudstone clasts to be in the process of disintegration, primarily via brecciation, which may be a result of abrasion or brittle deformation. The reported plasmic fabrics may not reveal ductile deformation, because the masepic plasmic fabric was typically identified in the brecciating mudstone clasts, in which it was likely to be a pre-existing fabric from the bedrock; and the skelsepic plasmic fabric was present within very thin layers around the clasts, which is likely to be a product of wetting and drying rather than rotation of clasts within till matrix (Dalrymple and Jim, 1984; Hiemstra and Rijsdijk, 2003). Packing voids are pervasive throughout LF4, indicating that this sediment has relatively high porosity, a

characteristic that is considered to be typical of tills that have been subject to relatively low amounts of deformation and rotation (Kilfeather and van der Meer, 2008). Alternatively, the high porosity apparent from the thin sections may be a sampling and/or processing artefact caused by the loose, clast rich nature of the till, although the presence of secondary carbonates at the base of the clasts within the thin sections demonstrates that the sediment samples did remain *in situ*, at least to an extent.

To summarise, the immature nature of the till and the evidence for low strain at the microscale suggests that rates of deformation were low and that the transport distance of this deposit as a whole was also low. If this sediment was deposited under streaming ice flow, it is likely that fast flow did not take place via pervasive subglacial deformation. Alternatively, the till may have been deposited during a late stage of glaciation, allowing only small amounts of stress to be imparted onto the deposit.

6.4 Blood Indian Creek Reservoir

6.4.1 Site background

Blood Indian Creek is situated in a shallow valley, which is approximately 8 km wide, situated 28 km to the east of Berry Creek (figures 6.6 and 6.42). It runs approximately north to south, parallel to the direction of palaeo-ice streaming. Shetsen (1987) mapped it as a minor meltwater channel, and the surrounding Quaternary sediments as draped moraine (up to 5 m thick) and stagnation moraine on undulating topography. The area surrounding Blood Indian Creek Reservoir is typically very flat. However, a small area of hummocky moraine to the east of the reservoir is seen in Figure 6.42. There are also several meltwater channels in the vicinity, running approximately parallel to Blood Indian Creek. The river was dammed in 1965, forming the reservoir, which created several sections at its shores, of bedrock (Bearpaw Formation) and Quaternary sediments.

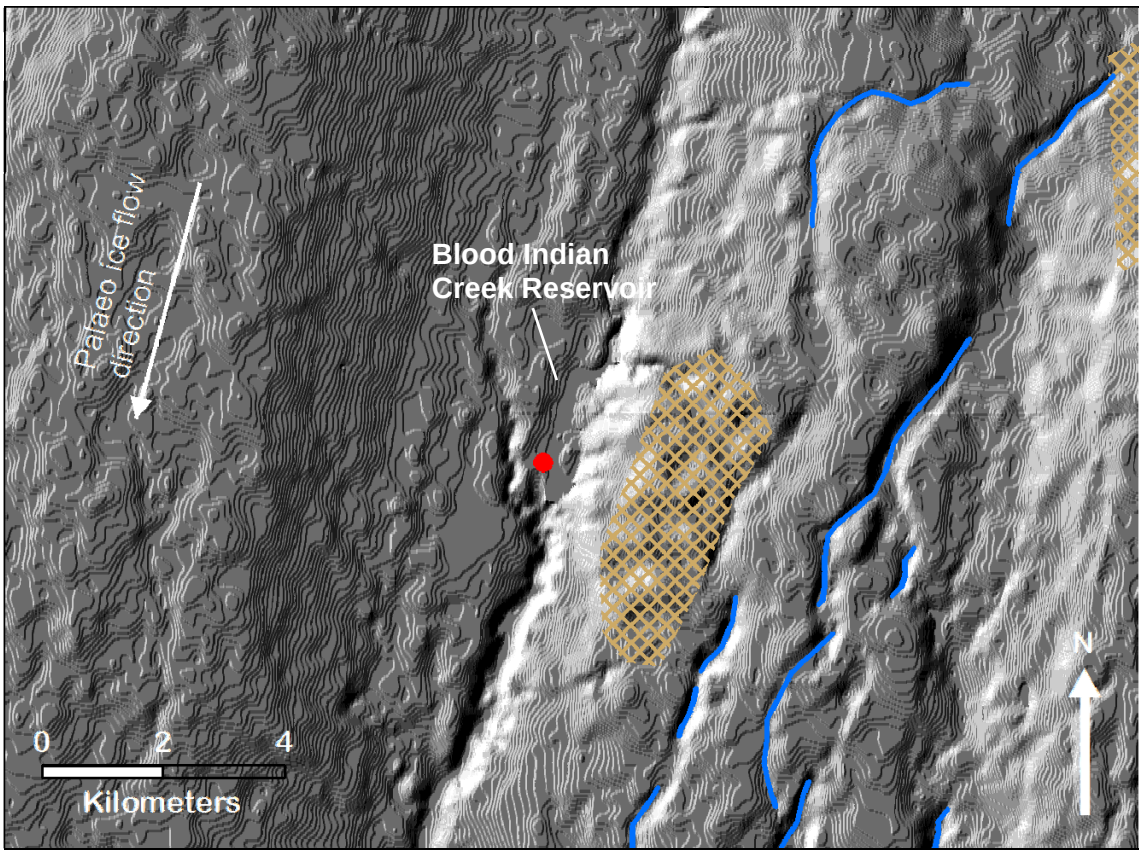

Figure 6.42 – Blood Indian Creek Reservoir and the surrounding area. The location of the studied sections is marked with a red dot. Meltwater channels are blue and hummocky terrain is light brown cross hatch. DEM is Canadian Digital Elevation Data, with a vertical exaggeration of x6.

6.4.2 Mesoscale sedimentology

The sediments from a 73 m long section at the south end of Blood Indian Creek Reservoir were examined in detail. This section was selected because it was the largest of the few accessible sediment exposures around the reservoir. The sediments are presented in four vertical logs (Figure 6.44) and the locations of these are shown in the site map in Figure 6.43. The sediment logs depict two lithofacies.

Lithofacies 1 (LF1) is found at the base of the entire section, therefore it is seen in all the vertical logs. It is a dark grey, clayey, clast poor diamicton containing an abundance of small clusters of gypsum crystals, present throughout the lithofacies. The gypsum clusters are typically aligned in horizontal or sub-horizontal layers (dipping to the north), as shown in Figure 6.46a and b. The diamicton also contains sand intraclasts, channel fills, discontinuous sand and silt layers, and stringers. Several of these are slightly deformed, such as the channel fill shown in Figure 6.36b. Channel fills within a subglacial till are indicative of temporary subglacial meltwater pathways, and hence

temporal variability within the subglacial traction layer (Evans *et al*., 2006a). Several fine grained, sorted layers can be identified within, and at the top of this lithofacies. These layers all dip to the north, which is upstream in terms of palaeo-ice flow.

The diamicton has a similar colour and texture to the underlying Bearpaw Formation. LF1 has a polymodal particle size distribution (Appendix B). Clasts are typically blocky in shape and the C_{40} index is relatively low, characteristics that are associated with considerable clast abrasion (Figure 6.47). The two macrofabrics measured in LF1 (Figure 6.44) are both sub-parallel to the direction of palaeo ice streaming, but oblique to each other, and one dips upstream and one dips downstream. These fabrics are also very weak and the fabric BICRc10 has a more isotropic than clustered shape (Figure 6.45).

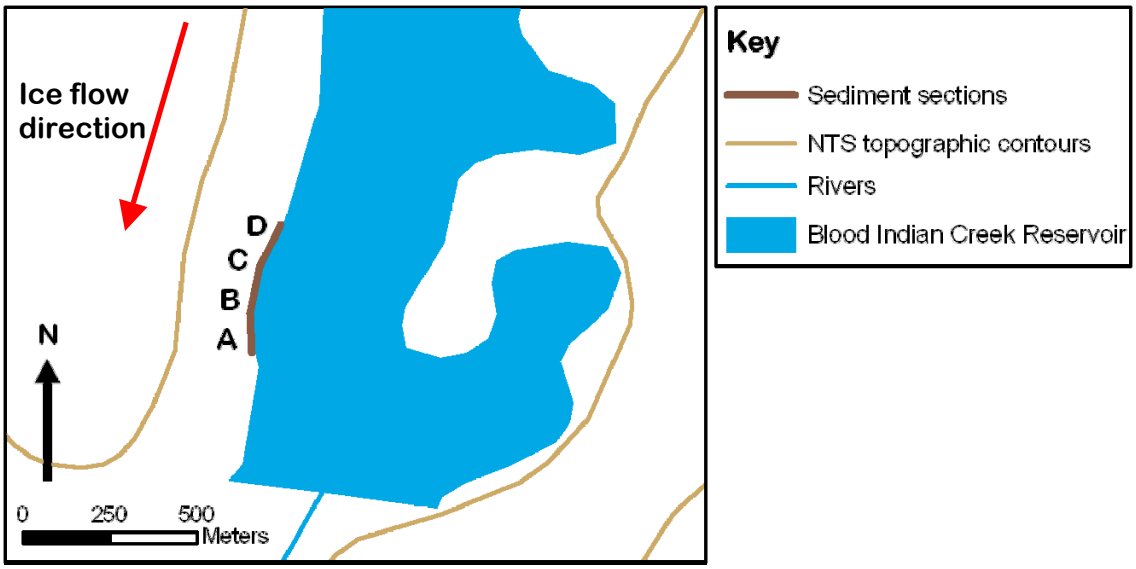

Figure 6.43 - Site map of Blood Indian Creek Reservoir, which shows the locations of the studied sediment sections. Map data from the National Topographic Database (Natural Resources Canada).

Lithofacies 2 (LF2) is a sandy diamicton, containing some deformed sand lenses and characterised by spatial variability in terms of clast concentration and texture. LF2 has a polymodal particle size distribution (Appendix B.1) and slightly higher C_{40} and RA indices than found in LF1. Figure 6.44 shows that clast macrofabric orientations are oblique and sub-parallel to palaeo-ice streaming, and dip downstream. Figure 6.45 shows that fabric strength is relatively low, which is similar to LF1 and fabrics measured at Berry Creek Reservoir.

LF2 is not present at the south end of the section (log A) and is situated on top of LF1 in a wedge shape that increases in thickness to the north of the section. Thus the boundary between the lithofacies dips towards the north, the same as the fine grained layers identified in LF1. LF2 overlies LF1 on a loaded boundary, characterised by simple load casts, diapirs and flame structures, which range from 0.5 cm to 90 cm high (Figure 6.46c, e and f). A large flame structure is present at the north end of the section (Figure 6.46e and f), which is orientated in a downstream direction, consistent with the orientation of ice streaming.

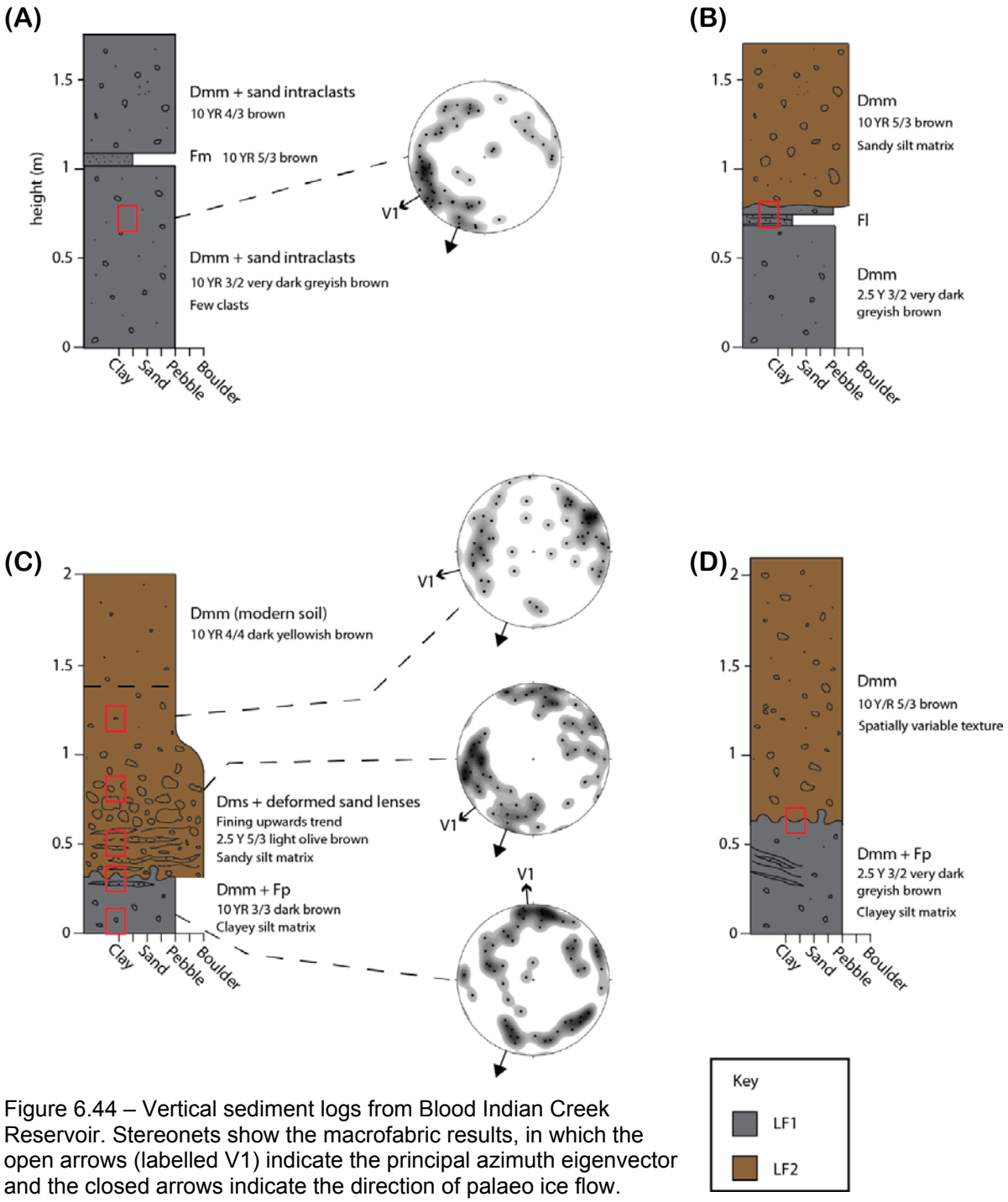

Figure 6.44 – Vertical sediment logs from Blood Indian Creek Reservoir. Stereonets show the macrofabric results, in which the open arrows (labelled V1) indicate the principal azimuth eigenvector and the closed arrows indicate the direction of palaeo ice flow. Micromorphology sample locations are indicated with red rectangles. Different lithofacies are highlighted by different colours and a key for the lithofacies symbols are given in figures 3.3 and 3.4, pages 41-42.

(a)

Sample	Litho-facies	Mean vector	Mean dip	Eigenvalue	Clustering
BICRA	LF1	238.8°	16.1°	0.556 (S_1) >> 0.302 (S_2) ~ 0.143 (S_3)	Linear
BICRC10	LF1	355.9°	6.8°	0.455 (S_1) >> 0.333 (S_2) ~ 0.212 (S_3)	Isotropic
BICRC80	LF2	230.4°	5.2°	0.522 (S_1) >> 0.309 (S_2) ~ 0.17 (S_3)	Linear
BICRC120	LF2	75.7°	2.2°	0.549 (S_1) >> 0.288 (S_2) ~ 0.163 (S_3)	Linear

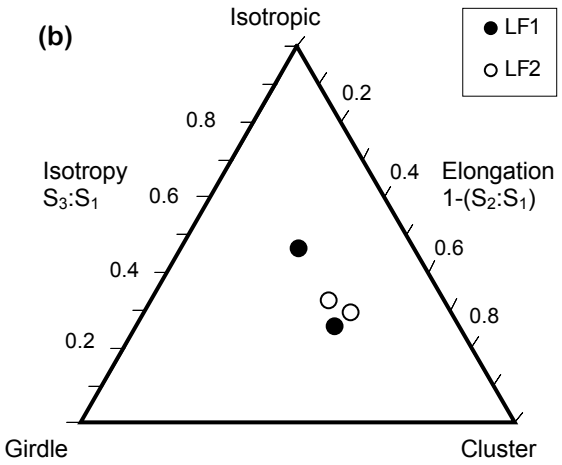

Figure 6.45 – Macrofabric eigenvalues and fabric shape. (a) Table of eigenvalues for the Blood Indian Creek Reservoir samples. (b) Ternary diagram displaying fabric shape for the samples.

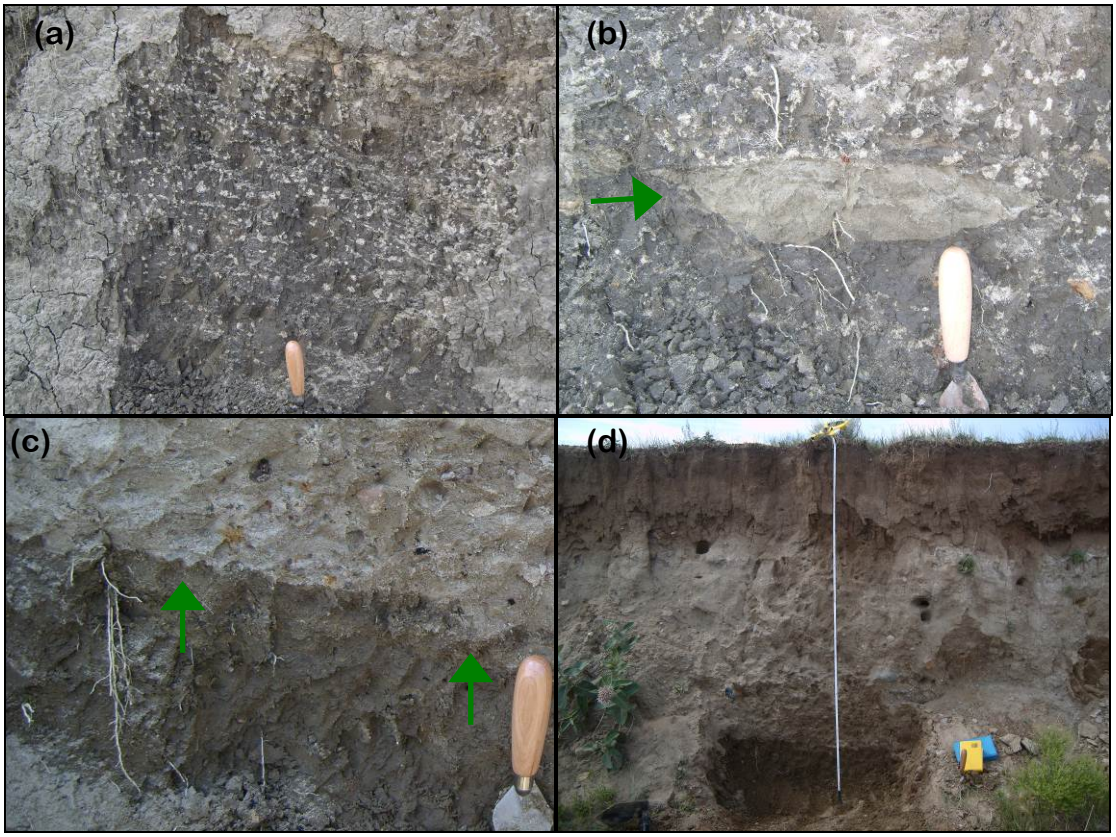

Figure 6.46 – continued overleaf.

Figure 6.46 – Images of sediments at Blood Indian Creek Reservoir. (a) Alignments of gypsum clusters in LF1. (b) Channel fill in LF1. Note the characteristic flat top and concave-up base (Benn and Evans, 2010) and slight deformation at its boundary, which is indicated with a green arrow. (c) Loaded boundary between LF1 and LF2. The green arrows indicate examples of load casts. (d) The succession of sediments at Section C (2 m high). Trowel length is 23.5 cm. (e) Unannotated and (f) annotated images of the loaded boundary and large flame structure at Section D (2.1 m high). Boundary between LF1 and LF2 is highlighted with a black dashed line in (f).

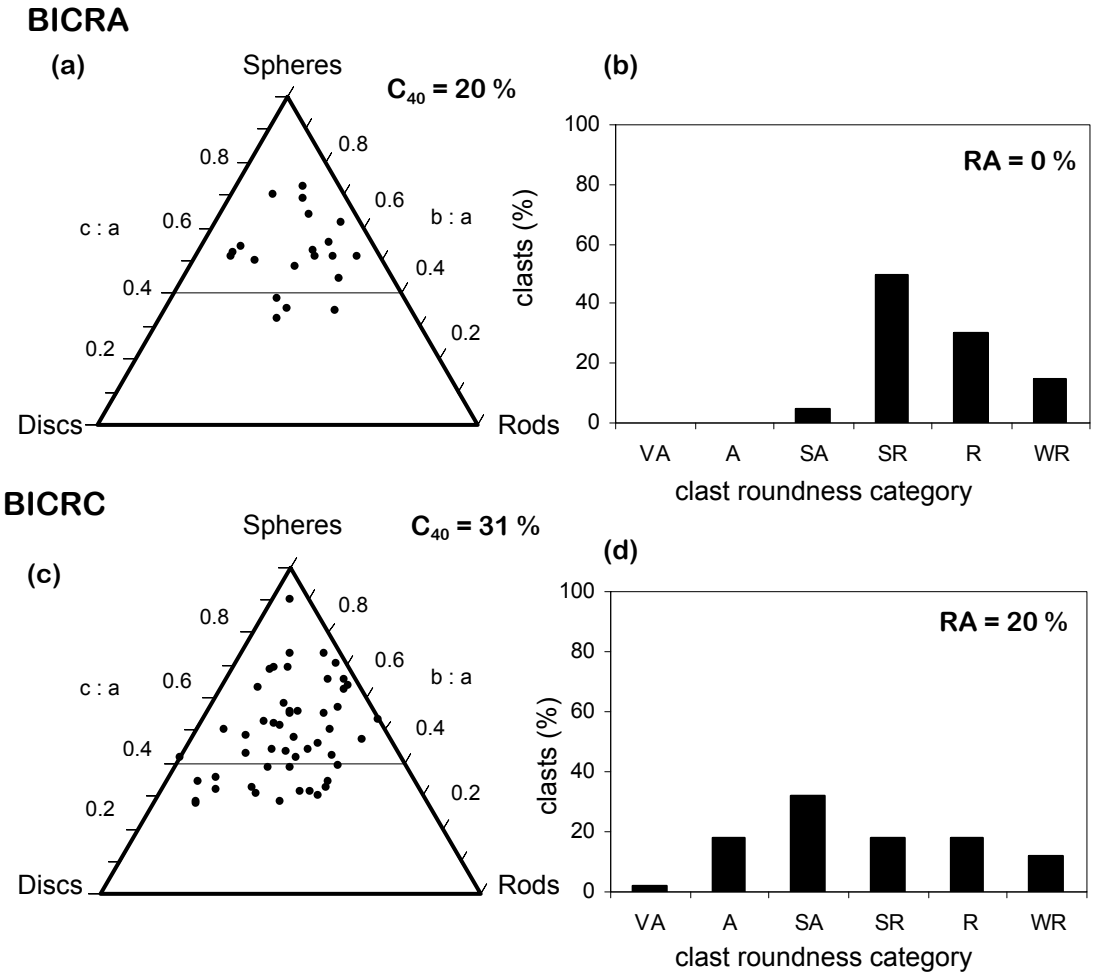

Figure 6.47 – Blood Indian Creek Reservoir clast morphology. (a) Clast shape for BICRA (LF1); sampled from 0.7 m up the profile, (n = 20). (b) Clast roundedness for BICRA (LF1); sampled from 0.7 m up the profile (n = 20). (c) Clast shape for BICRC (LF2); sampled from 0.8 m up the profile (n = 50). (d) Clast roundedness for BICRC (LF2); sampled from 0.8 m up the profile (n = 50). Clast roundedness categories are as follows; VA = very-angular, A = angular, SA = sub-angular, SR = sub-rounded, R = rounded, WR = well-rounded.

6.4.3 Mesoscale interpretation

Whilst there are no subglacial lineations near Blood Indian Creek Reservoir, it is located within the streamlined ice stream bed, suggesting that the diamicts at the reservoir may be subglacial tills. A loaded boundary separates the two diamicts at this site, and the most obvious explanation for this is glaciotectonic loading. There is no evidence for loading due to an increase in overlying stress such as a lake or sediment layer, however a viable alternative possibility is that the structures were formed by permafrost as it may have been present in the area postglacially. Cryoturbation load structures, such as flame structures and ball and pillow structures, can form in thawing permafrost via liquefaction and a reversed density gradient (Vandenberghe, 2007; French, 2007). However, there is no clear evidence for relict permafrost, for example patterned ground, which typically accompanies cryoturbation (Washburn, 1980). Whereas flame structures are orientated in the same direction as palaeo-ice streaming suggesting that the deformation was glaciotectonic. This in addition to the suite of structures documenting subglacial processes indicates that the most likely explanation is glaciotectonic loading. However, it is acknowledged that the possibility that another process is responsible cannot be ruled out.

Both lithofacies have a polymodal particle size range, evidence for considerable clast abrasion, deformed sand and silt lenses and layers and some macrofabrics that are parallel to palaeo-ice streaming, which are characteristics consistent with a subglacial origin. These tills are distinct in texture and colour, suggesting that they were deposited in different environments or different glacial advances. Evidence for two glacial advances in the region, is consistent with the findings at Berry Creek Reservoir and other stratigraphical evidence in the area (e.g. Stalker, 1983; Evans and Campbell, 1992; 1995). Alternatively, deposition of the tills may have differed; one of the lithofacies may be a result of melt-out, for example from debris rich basal ice (e.g. Lawson, 1979). This would explain the sorted sediment layers and lenses and subsequent or concurrent overriding by ice would explain the observed deformation structures. However, the widespread occurrence of subglacial traction tills compared to melt-out tills (Evans *et al*., 2006a) would suggest that a subglacial depositional origin is more likely.

The similarity of LF1 to the underlying Bearpaw Formation suggests that erosion of local bedrock provided some or most of the source material for this till. Channel fills

(Figure 6.47b) and layers and lenses of fine, sorted sediment typically show some evidence for deformation, but their preservation indicates that deformation was either not pervasive or not persistent here. If this till was deposited subglacially, their presence indicates that subglacial processes (i.e. till deposition and hydrology) varied in space and time, which is consistent with the concept of a subglacial mosaic of subglacial processes and forms (Menzies, 1989; Piotrowski and Kraus, 1997; van der Meer *et al*., 2003; Piotrowski, 2004).

LF2 contains some obvious spatial variabilities in clast texture. Section C in particular is dominated by an area of clast rich, matrix poor till that contrasts with surrounding sediment, as indicated by field examination and the particle size data, which may reflect variable conditions of sediment deposition. The profile appears to be located in a large load cast, containing vertically deformed sand layers and lenses at its base, possibly reflecting sinking of LF2 into LF1. This sinking may have been facilitated by the coarse-grained, higher density sediments here.

The weak nature of the macrofabrics from both LF1 and LF2 is similar to observations at Berry Creek Reservoir and the Tweed Palaeo-Ice Stream. However, they are unusual compared to some other studies of subglacial tills, particularly laboratory experiments that have demonstrated a clear link between high fabric strength and moderate to high shear strains (e.g. Hooyer and Iverson, 2000). The loading processes that took place, either glaciotectonically or from permafrost, are associated with vertical shear (Figure 6.25c) as well as a viscous rheology (Rijsdijk, 2001), which may provide an explanation as weak fabrics have been linked to viscous deformation (e.g. Hart, 1994; Hicock *et al*., 1996). However, preservation of structures such as channel fills, suggests that shear strains were low and as such the weak fabrics are probably a reflection of this.

Certain parameters were measured at the mesoscale for all sediment sites, some of which required the use of sample sizes. These included particle size distribution, clast morphology and clast fabric. Evaluation of these results from chapters 5 and 6 provides an insight into how representative they were. Particle size distribution (Appendix B) reveals a range of sediments that typically had a high proportion of fines and in some cases the largest particle sizes are poorly represented. Many of the sediments sampled contained particles above 4 mm and as depicted in Appendix B had multimodal

distributions. This indicates that they ideally required larger sample sizes than the > 0.5 kg that was used, in order to accurately represent the larger particles and to produce reliable results of the multimodal distributions (see Hoey, 2004). There was no indication that clast morphology was not representative and it displayed clear differences between different lithofacies, which suggests that it was sufficient for this purpose. However, whilst the typical sample size used of 50 clasts is considered sufficient for measurement of clast morphology (Benn, 2004a), using this parameter as a means to evaluate spatial variations within a lithofacies may benefit from larger sample sizes in order to discern subtle differences with greater confidence. Clast macrofabric sampling appeared to be sufficient for purpose and the sample sizes used were within the range (50 to 100) considered acceptable in terms of statistical variance (Ringrose and Benn, 1997). However, the lack of a strong preferred orientation for some of the macrofabrics and the spatial variability observed between some of the samples indicates that larger sample sizes and more samples would have been valuable in terms of data reliability and interpretation.

6.4.4 Micromorphology

Eight micromorphology samples were taken from Blood Indian Creek Reservoir, from lithofacies 1 and 2. Locations of these samples are given in Figure 6.44 and details are given in Table 6.3.

Table 6.3 – Details of the micromorphology samples collected from Blood Indian Creek Reservoir. Locations of samples are also indicated in Figure 6.44.

Sample	Where?	Orientation to palaeo ice flow	Lithofacies	Why sampled?
BICRa	Section A, 0.7 m up profile	Parallel	1	Characterisation of lithofacies and microfabric
BICRb	Section B, 0.7 m up profile	Parallel	1 and 2	Characterisation of lithofacies and the contact between them
BICRc10	Section C, 0.1 m up profile	Parallel	1	Characterisation of lithofacies and microfabric
BICRc30	Section C, 0.3 m up profile	Parallel	1 and 2	Characterisation of contact between lithofacies
BICRc50	Section C, 0.5 m up profile	Parallel	2	Characterisation of lithofacies and variations therein
BICRc80	Section C, 0.8 m up profile	Parallel	2	Characterisation of lithofacies and variations therein, and microfabric
BICRc120	Section C, 1.2 m up profile	Parallel	2	Characterisation of lithofacies and variations therein, and microfabric
BICRd	Section D, 0.63 m up profile	Parallel	1 and 2	Characterisation of contact between lithofacies (loaded boundary)

At the microscale LF1 appears to be a fine-grained diamict, with particles greater than 0.5 mm typically sub-rounded, and particles smaller than 0.5 mm typically angular (Figure 6.48). Different lithologies can be identified, including resistant metamorphic and igneous lithologies, and rounded mudstone clasts. Multiple domains can be seen within some of the thin sections from LF1.

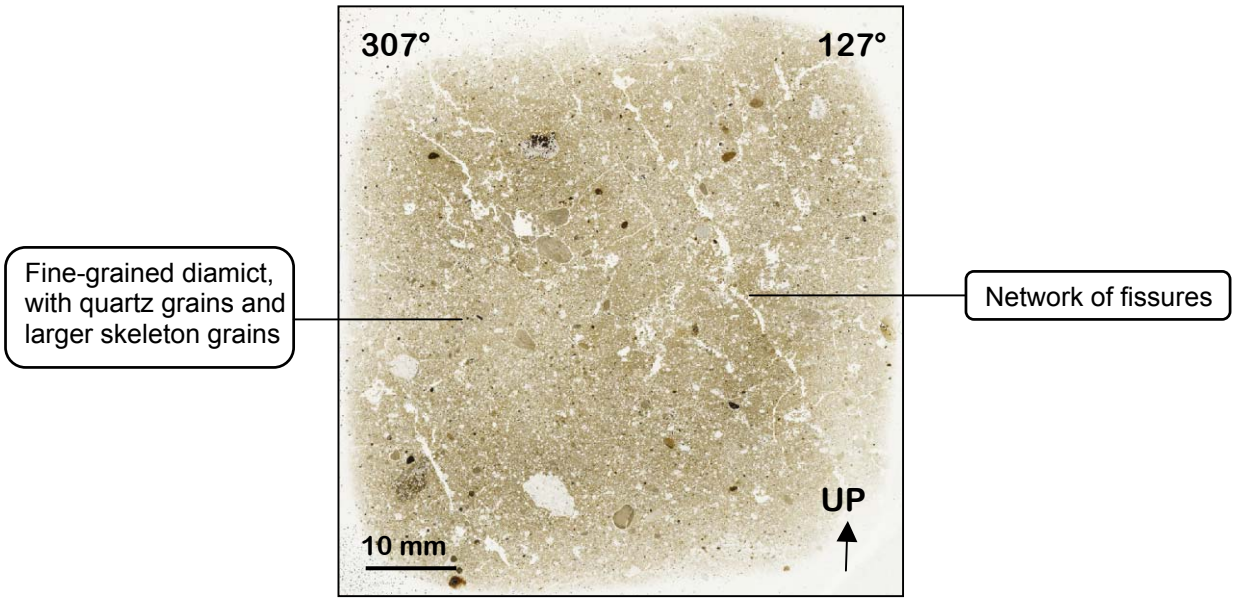

Figure 6.48 - Scan of BICRC10a (LF1), displaying some of the key features that can be seen at this scale.

LF2 is typically coarser at the microscale than LF1. At Section C, LF2 is very grain rich and is typified by high concentrations of skeleton grains and very little matrix. In other areas micromorphology samples show that this lithofacies has more matrix, but poor quality of the thin sections mean that the overall structure and micromorphological features can be difficult to identify.

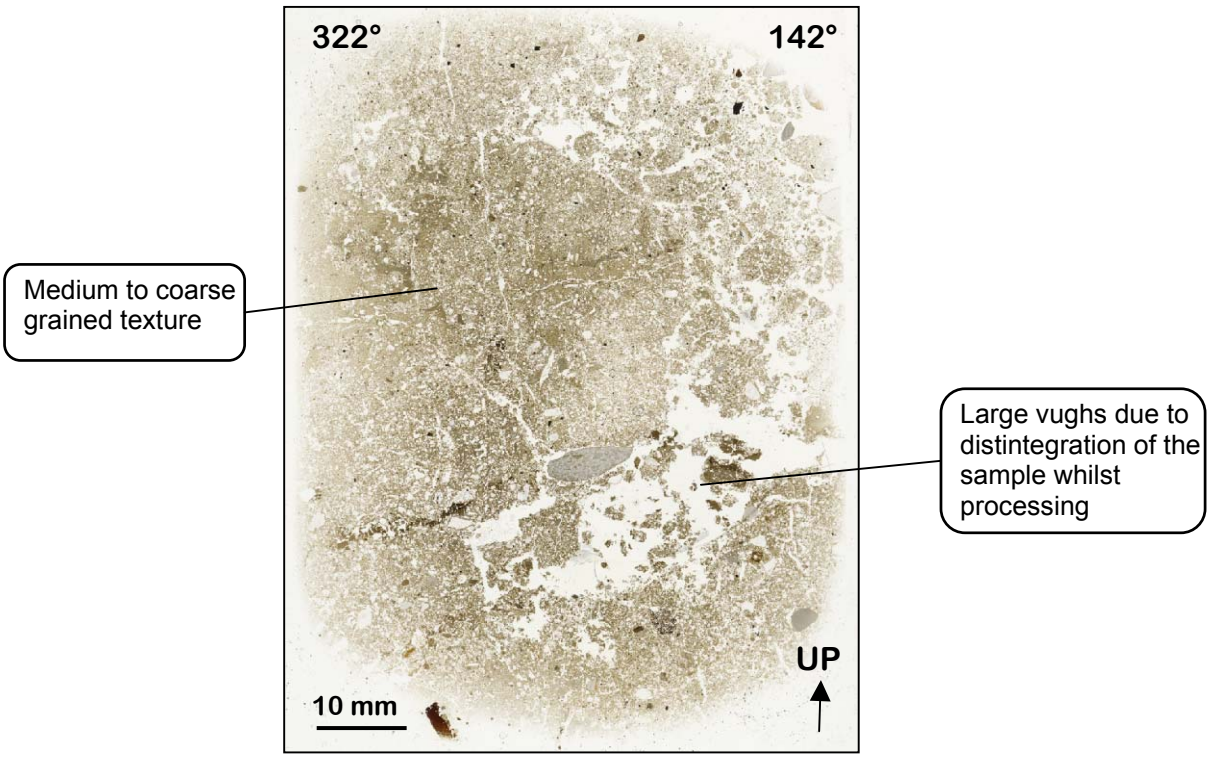

Figure 6.49 – Scan of BICRBTop (LF2), displaying some of the key features that can be seen at this scale.

Micromorphological structures from the samples are summarised in Table 6.4, which is followed by descriptions and images of some of the key structures. Detailed descriptions of each micromorphological sample are given in Appendix C.1.

Table 6.4 - Summary table of the micromorphological features from Blood Indian Creek Reservoir. The relative abundance of each feature for each sample is given in a 1 to 3 scale; 3 (●●●) = very abundant, 2 (●●) = present in two or more locations in the sample; 1 (●) = present in a single location in the sample; 0 (-) = not present.

	Voids				Sediment mixing		Water movement	Grain structures				Clast/matrix alteration				Biological	Plasmic fabric		
	Fissures	Vughs	Vesicles	Packing voids	Channels and chambers	Multiple domains	Intraclasts	Haloes	Laminations	Grain concentrations	Turbates	Grain lineations	Crushed quartz	Spalling grains	Clast brecciation	Gypsum	Carbonate deposits	Iron staining	Burrows/bioturbation	Organic matter	Masepic	Skelsepic	Unistrial
BICRa	●●●	●●	-	-	-	●●●	●●●	-	-	●●	-	-	-	-	-	●●●	-	-	-	-	●●	●●	-
BICRb	●●●	●●●	●●●	-	●●●	●●●	●●	●●●	●●	-	●●	●	●	-	-	-	●●●	-	●●●	●●	●●	●●●	●
BICRc10	●●●	●●	-	-	-	-	●●●	-	-	●	●●●	●●●	-	-	-	-	●●	●	-	-	●●●	●●●	-
BICRc30	●●	●●	-	●●	-	●●●	●●●	-	-	●●	●	●	-	-	-	-	●●●	-	-	●	●●	●●●	-
BICRc50	●	●●	-	●●●	-	-	-	-	-	-	-	-	-	-	●●	-	-	-	-	-	-	●●	-
BICRc80	●●	●●	-	●●●	-	●	●	-	-	-	-	-	-	●●	-	-	●●	-	-	-	-	●●	-
BICRc120	●●	●●●	●●	●●	-	●●	-	-	-	-	●●	●●●	-	-	-	●●	●●	-	-	●	-	●●	-
BICRd	●●	●●●	-	●●	-	●●●	●●●	-	-	-	●●	●	-	-	-	●●●	-	-	-	-	●●	●●●	●●

a. Voids

Several types of void are present, including fissures, vughs, packing voids, vesicles, and channels and chambers. Secondary deposits of gypsum within some of the fissures demonstrate that these voids are real features in the sediment rather than artefacts of sampling or processing (Figure 6.56). Packing voids are characteristic of LF2, particularly at Section C and only minor amounts of fine matrix material are present in these sediments, as indicated in Figure 6.50. Channels and chambers are abundant in BICRB and these features relate to biological activity in the sediment such as roots and burrowing animals.

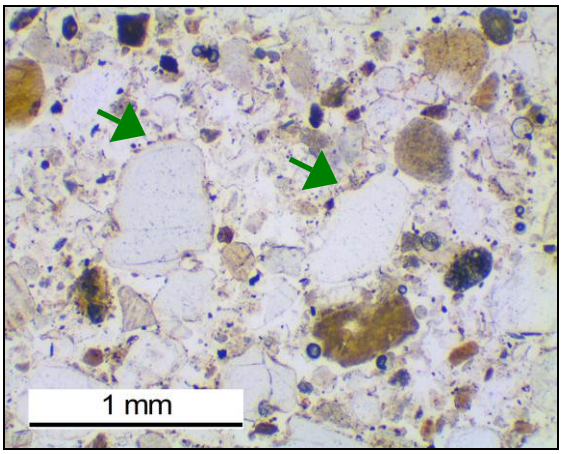

Figure 6.50 – Typical composition of LF2 at Section C (from BICRC50). Skeleton grains and packing voids dominate the sediment. Small amounts of matrix are present, seen here on top of the larger skeleton grains (indicated by the green arrows).

b. Multiple domains

Multiple domains are present in some of the samples and in some cases correspond to different lithofacies within a thin section (e.g. BICRC30). At BICRA clear multiple domains are identified within LF1, which comprise a grain rich domain and two diamict domains (Figure 6.51a). These domains do not correspond to any features identified at the mesoscale upon collection of this sample, but may reflect heterogeneities such as sand lenses and layers. The multiple domains in BICRC30 correspond to LF1 and LF2, between which the loaded boundary appears sharp, with minimal mixing, as shown in Figure 6.51b. Multiple domains are considered to be indicative of sediment mixing and in some cases polyphase deformation (Menzies, 2000).

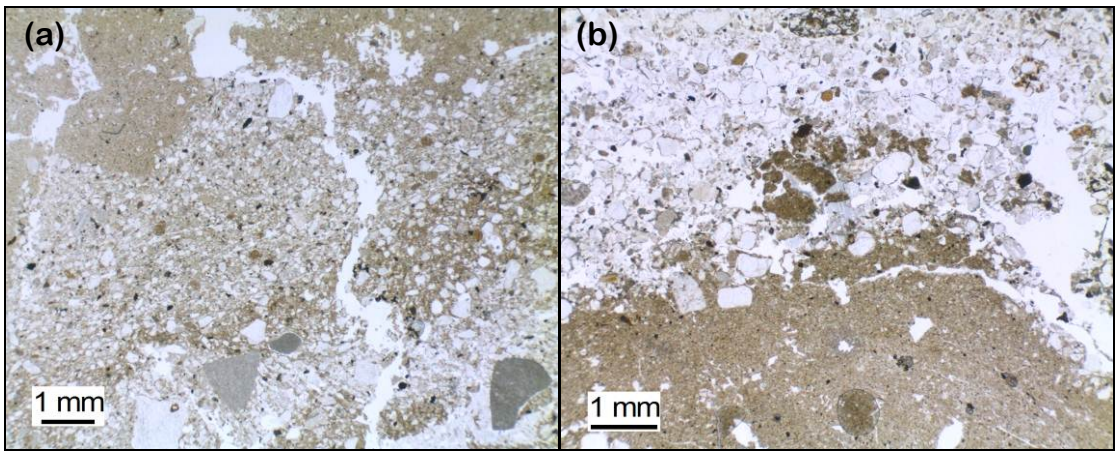

Figure 6.51 – Multiple domains from Blood Indian Creek Reservoir. (a) Multiple domains in LF1 (from BICRAa). (b) Loaded contact between LF1 and LF2 from BICRC30. Note the sharp boundary and the intraclast of LF1 in LF2.

c. Intraclasts

Intraclasts were found in several of the samples, and an example of one is given in Figure 6.52. Intraclasts show heterogeneities in a diamict and indicate sediment mixing and their form may indicate rotation (van der Meer, 1993).

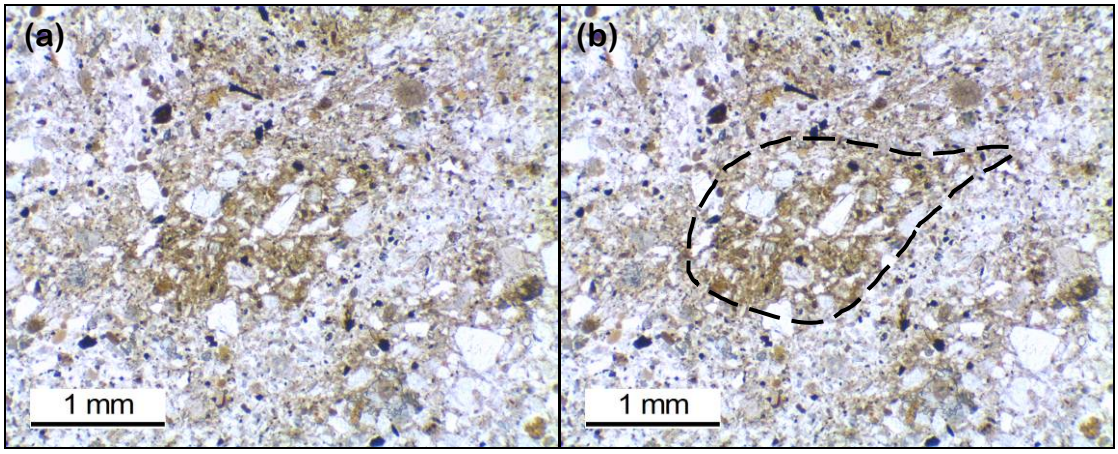

Figure 6.52 – (a) and (b) Paired images of intraclast in LF1, from BICRAa.

d. Haloes

Haloes were identified only in sample BICRb, where they were common near the base of the upper diamict domain (LF2) at the boundary with the underlying LF1. As Figure 6.53 shows, they comprise a clast with an encircling casing of fine-grained sediment that is distinct to the surrounding sediment. Particles with haloes were typically 0.4 – 2 mm in diameter and the haloes were typically 0.05 - 0.2 mm wide. The orientations of the particles within the haloes are parallel to the clast edge.

Haloes (sometimes referred to as grain coatings) have been identified in subglacial tills, melt out tills, subaqueous debris flows and subaerial mass flow deposits, where they are typically attributed to particle rotation (Bertran, 1993; Lachniet *et al*., 1999; 2001; Kilfeather *et al*., 2010; van der Meer *et al*., 2010).

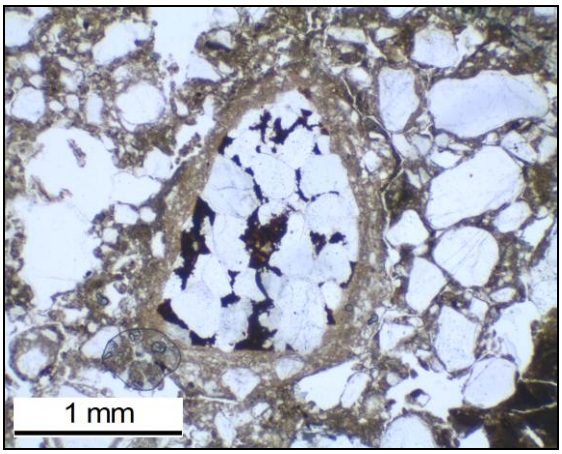

Figure 6.53 – A haloe from BICRBTop.

e. Grain structures

Grain structures, including turbates and grain lineations, were identified in samples where there was a sufficient amount of matrix to enable their identification. Turbates typically have corestones, as shown in the example in Figure 6.54.

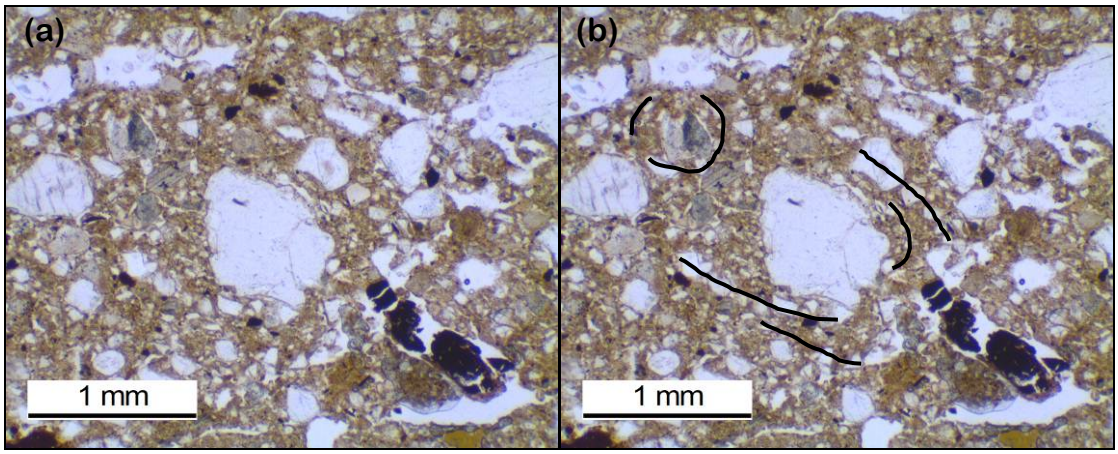

Figure 6.54 – (a) and (b) Paired images of turbates with corestones in LF1 (from BICRBBase).

An example of grain lineations are shown in figures 6.55 and 6.58. In Figure 6.55 they have two main orientations that cross-cut each other (this is sometimes referred to as multiple-directional lineations; e.g. Menzies *et al*., 2006; Larsen *et al*., 2007). Grain lineations and the clarity of them, were spatially variable within and between thin sections.

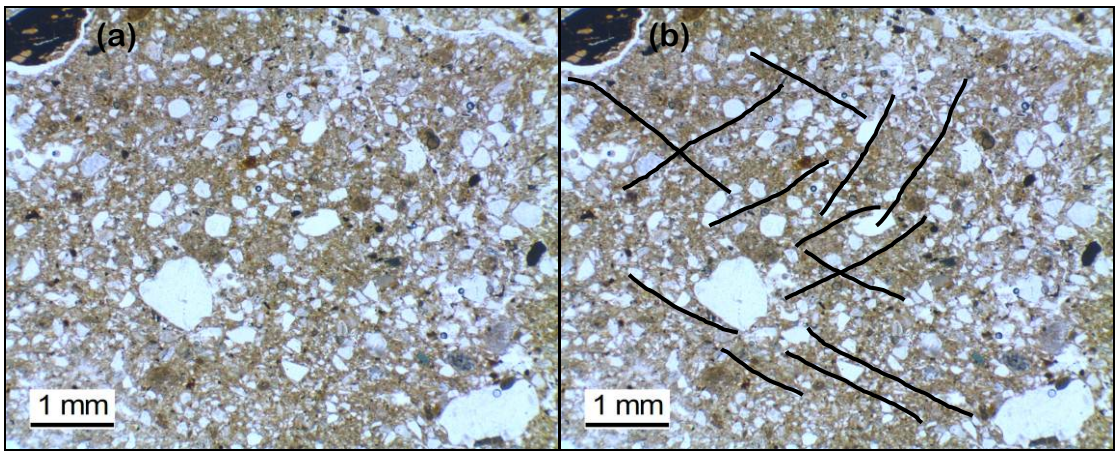

Figure 6.55 – (a) and (b) Paired images of grain lineations in LF1 (from BICRC10).

f. Superimposed Deposits

Carbonate and gypsum deposits were both identified at the mesoscale at Blood Indian Creek Reservoir, which revealed certain characteristics, such as carbonate deposited at the base of clasts and gypsum deposits in clusters that are horizontally aligned. At the microscale, the suspected classifications of these deposits as carbonate and gypsum were confirmed, and the superimposition of these features on top of the primary sediment structure was apparent.

Micromorphology shows that carbonates are present in areas of the sediment matrix, typically below clasts (Figure 6.56a) or associated with clasts (Figure 6.56b) or sometimes in discrete areas of the matrix. As birefringence is not seen where carbonates are present (van der Meer, 1993), the presence of plasmic fabric throughout the samples attests to the fact that carbonate was not pervasive throughout the entire sediment matrix. Carbonate deposits on the undersides of clasts typically form as secondary accumulations, through illuviation of percolating water charged with calcium and bicarbonate, and typically form in arid or semi-arid climates (Blank and Fosberg, 1990).

Gypsum deposits are present as clusters of gypsum crystals within voids, particularly fissures. The crystals display characteristic lenticular shapes, in addition to more rounded and amorphous shapes and display the characteristic black and white colours under cross polarised light (Figure 6.56c and d). Gypsum can form as a secondary deposit, typically in arid or semi-arid climates (Porta and Herrero, 1990). Their presence as clusters within voids indicates that they formed post-depositionally.

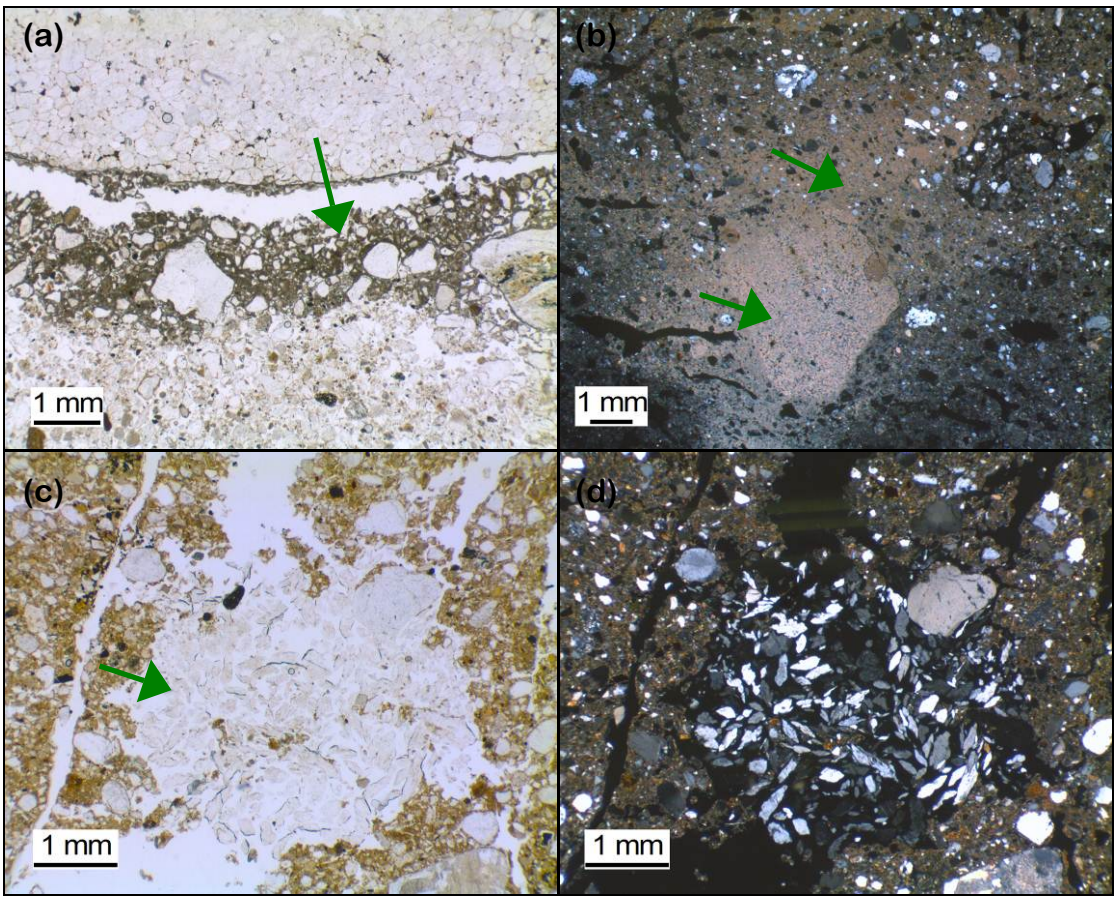

Figure 6.56 – Superimposed deposits at Blood Indian Creek Reservoir. (a) A carbonate deposit below a sandstone clast (from BICRC80a). (b) Carbonate within the matrix surrounding a carbonate rich clast (from BICRC80a). Image is seen in cross polarised light. (c) Cluster of gypsum crystals in a fissure (from BICRAa). (d) The same image as (c), in cross polarised light.

g. Plasmic fabric

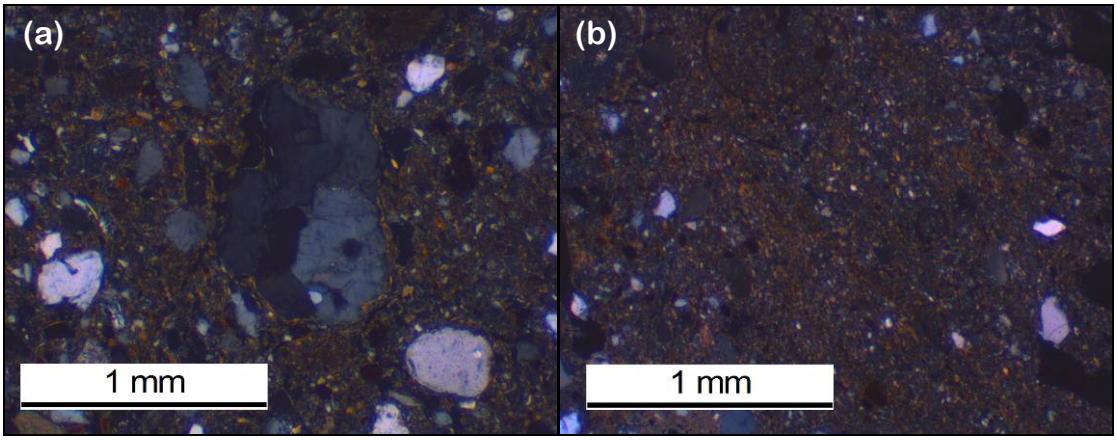

Figure 6.57 – Plasmic fabric from Blood Indian Creek Reservoir. (a) Skelsepic plasmic fabric in LF1 (from BICRC10). (b) Masepic plasmic fabric in LF1 (from BICRC30).

Skelsepic and masepic plasmic fabric is common throughout the samples (figures 6.57 and 6.58). Skelsepic plasmic fabric is present as relatively thick skins around grains within matrix rich sediments (e.g. samples BICRA and BICRC10), whereas in matrix poor sediments only a thin layer of matrix may coat grains and hence the skelsepic

plasmic fabric forms only thin skins (e.g. samples BICRC50 and BICRC80). Masepic plasmic fabric was common in the matrix rich sediments, where it typically occurred in close association with skelsepic plasmic fabric.

h. Associations between microstructures

Associations between microscale features in LF1 are indicated in Figure 6.58. The mapped features in this figure are abundant and closely spaced across most of the image and are only lacking in the areas with several vughs, which may reflect disturbance of the sediment. The most common feature is the grain lineations. Groups of grain lineations appear to have several distinctive modes of orientation, some of which can be broadly matched to the Riedel shear geometry (Figure 5.30b). Some lineations also appear to align with the orientations of the larger skeleton grains, such as the top right corner of the image where lineations and grains are aligned from upper left to lower right. Many, quite long grain lineations are also orientated from the upper left to lower right of the image and some of the fissures also share this orientation.

The central clast in the image, labelled ‘1’, appears to have partially disintegrated on its upper right (Figure 6.58a). The area of disintegration appears to be bounded by grain lineations on either side, which are orientated in the same direction as the clast and some of these are slightly curved. The area that is disintegrating is separated from the rest of the clast by a fissure, which is orientated upper left to lower right. The disintegrating part of the clast appears to be very slightly displaced from the rest of it, down and to the right, along the fissure. Grain lineations and plasmic fabric are widespread and overprint each other, however, turbates are usually orientated consistently with them, for example around the turbate labelled ‘2’. Whilst several lineations appear to extend out from this turbate, in an upper left to lower right orientation, indicating that they may be related. Turbates and plasmic fabric are both seen in close association with the widespread grain lineations.

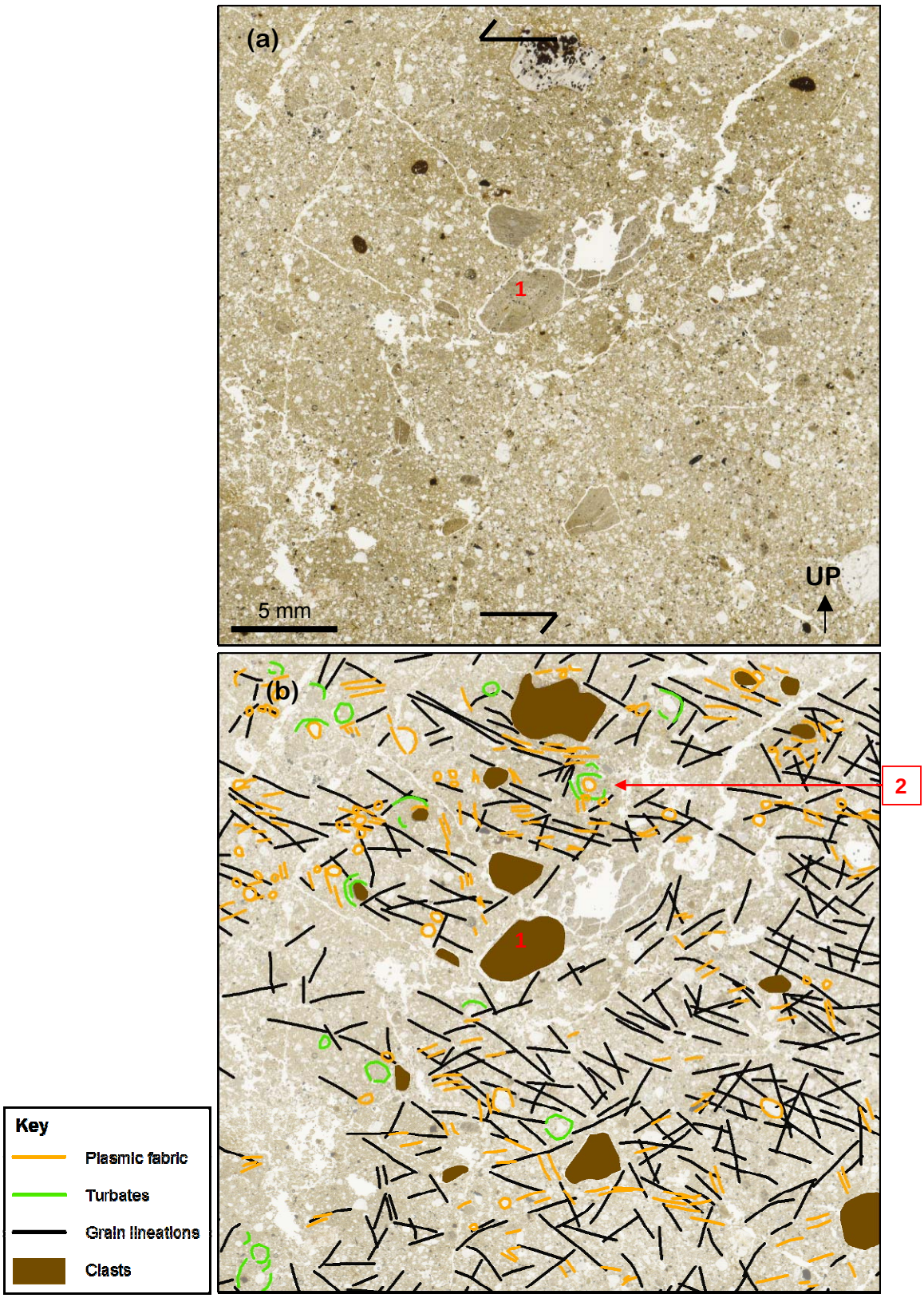

Figure 6.58 - Twinned images of thin sections (LF1). An unannotated, high resolution scan of the thin section in normal light conditions, is shown in (a) and a view of annotated features overlying the faded image is shown in (b). Relative sense of shear is indicated with arrows and numbers are referred to in the text. The plasmic fabric indicated is not visible in (a) but has been identified under the microscope in cross polarised light; it is shown schematically in (b), with circles for skelsepic plasmic fabric and lines of plasmic fabric indicating the overall direction of any masepic plasmic fabric.

i. Microfabric

Microfabric was measured in horizontal (b) slides (to obtain particle azimuth) from BICRA, BICRC10, BICRC80 and BICRC120 (Figure 6.59). Three of these samples display elliptically shaped rose diagrams with a clear preferred alignment of grains, which is parallel to palaeo-ice streaming, but divergent (to varying amounts) from the mean macrofabric orientation. The other microfabric (BICRA) has a rounded rose diagram with two peak alignments, one of which is similar to the mean macrofabric orientation. Confidence intervals for microfabric azimuth are given in Appendix C.3.

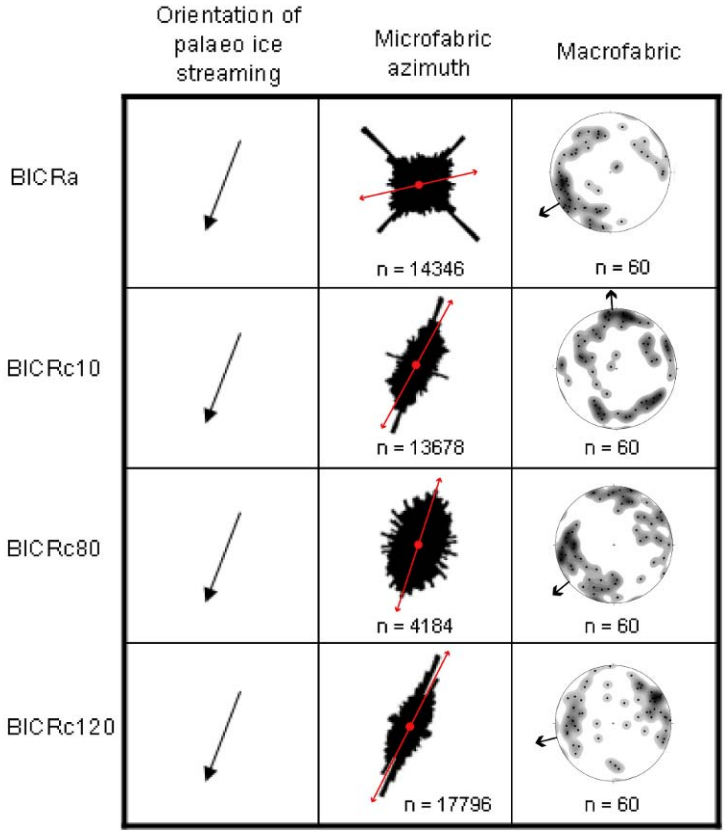

Figure 6.59 – Microfabric rose diagrams of particle azimuth (vector mean is indicated by a red arrow) alongside macrofabric stereonets (principal eigenvector is shown with an arrow) and the orientation of palaeo ice streaming for comparison.

6.4.5 Microscale interpretation

a. Lithofacies 1

Microscale deformation structures in LF1 include those indicative of ductile deformation (multiple domains, intraclasts, deformed laminations, turbates and masepic and skelsepic plasmic fabric) and those indicative of brittle deformation (grain lineations and unistrial plasmic fabric). Both types of structures were abundant in this lithofacies and there is also evidence that they were closely associated and in some cases they overprinted each other (Figure 6.58). This points to polyphase deformation and may indicate that conditions varied temporally in terms of porewater pressure and effective stress (Menzies, 2000).

Associations between microscale features are examined in Figure 6.58, which shows how closely situated and widespread grain lineations, turbates and plasmic fabric are. Collectively these features represent both ductile and brittle deformation, which may have been separated in time, indicating polyphase deformation (Menzies, 2000). The groups of grain lineations with similar orientations across considerable areas of the thin section as well as fissures with the same orientation (Figure 6.58), indicates that the sediment responded to shear in an overall direction across certain areas. The association between grain lineations and a partially disintegrated clast labelled ‘1’ in Figure 6.58, suggests that these features may relate, whereby strain in the direction of the grain lineations may have contributed to the breakdown of the clast on this side. The lineations below the disintegrating area are slightly curved around it suggesting that the sediment may have been deforming ductiley as well as in a brittle manner. Furthermore, a fissure propagates diagonally out from this area, which may indicate that this was a plane of weakness in the sediment relating to the primary sediment structure (see Carr, 2004; Kilfeather and van der Meer, 2008). Together the lineations, disintegrating clast and the fissure strongly suggest that strain was focussed along this plane.

The spatial coincidence of turbates adjacent to grain lineations, such as the one labelled ‘2’ in Figure 6.58, illustrates a relationship between these features. Lineations propagate directly out from the turbate, in the direction of upper left to lower right, indicating that the shear across the whole area is also related to the turbate, suggesting that these

features formed contemporaneously. This demonstrates that brittle and ductile deformation was closely related, which is similar to observations in the Tweed Ice Stream and consistent with the findings of Hiemstra and Rijsdijk (2003).

LF1 contains an abundance of gypsum clusters, which owing to their localisation within voids, are considered to be a secondary accumulation in the sediment. The arrangement of these gypsum clusters in layers and within fissures indicates that they are preferentially located in pre-existing voids and weaknesses in the sediment (Figure 6.47a and b). They are pervasive throughout LF1, rather than just on the section face surface, indicating that they reflect a primary structure in the till rather than a secondary structure on the section face, such as desiccation. The layering of the gypsum clusters, which dip slightly to the north, suggest that this structure is till fissility.

Fissility is a common structure observed in subglacial tills (e.g. Benn, 1994; Lian *et al*., 2003; Hiemstra *et al*., 2007) and may reflect minor shear planes (Evans *et al*., 2006a). Fissile partings are considered to represent failure under shear strains higher than those required to allow the development of structures such as turbates and lineations (Kilfeather and van der Meer, 2008), which gives an indication of the relative degree of strain in LF1. They are also likely to have provided pathways for subsurface water through subglacial till (Kilfeather and van der Meer, 2008).

b. Lithofacies 2

Microscale examination of LF2 at Section C shows that it has very little matrix and is dominated by sand sized grains. This may reflect a localised winnowing of fines, either subglacially or after deglaciation, which may be due to a preferential throughflow of meltwater here, such as via pipe flow (Figure 2.5; Benn and Evans, 1996). If the fines were winnowed away before or during loading this may have increased the density of this area and contributed to the formation of the large load cast here.

In LF2, microstructures reveal evidence for ductile deformation (multiple domains, intraclasts, turbates, skelsepic plasmic fabric, and haloes); brittle deformation (grain lineations); and abrasion (spalling grains and clast brecciation). The relative amounts of ductile and brittle structures implies that ductile deformation was dominant, suggesting

that porewater content was high (Menzies, 2000), which is consistent with the process of loading.

Haloes were identified in a single location, at the lower boundary of LF2. Their limited extent suggests that conditions for their formation were quite specific. Rotation is considered to be a key process for haloe formation (Lachniet *et al*., 1999; Kilfeather *et al*., 2010; van der Meer *et al*., 2010), but this process is not limited to this location, as indicated by the widespread occurrence of other structures that form via this process, such as turbates. However, haloes also require accumulation of sediment around the grain, which may require favourable conditions of sediment cohesion and water content (Lachniet *et al*., 1999; Kilfeather *et al*., 2010; van der Meer *et al*., 2010). These features may have formed when LF2 was deposited on top of LF1, or during the subsequent subglacial shear and loading.

Microfabric seen at both sites and multiple lithofacies in the Central Alberta Ice Stream revealed azimuth orientations slightly oblique to but broadly similar to the respective macrofabric. Given the weak nature of the macrofabrics larger sample sizes may have revealed greater consistency between the macro and micro fabrics. Microfabrics typically revealed a strong preferred azimuth and a clear shape of the rose diagram, which was usually ellipsoid. Furthermore, Figure 6.39 clearly shows that most of the microfabrics are strongly consistent with the direction of palaeo ice streaming, which brings confidence to the interpretation that these fabrics reflect subglacial processes.

In summary, microscale characteristics of both tills at Blood Indian Creek Reservoir are indicative of subglacial deposition or deformation, in support of the mesoscale interpretation. These include ductile and brittle deformation structures and micro fabrics parallel to ice streaming.

6.5 Central Alberta Ice Stream interpretation and conclusions

Following interpretation of each of the scales separately, they are now discussed together and this is centred around three key themes, as follows.

6.5.1 Deformation

Evidence for deformation within the subglacial traction layer included: intraclast shapes; loaded, deformed boundaries between certain lithofacies; and microscale deformation structures throughout most lithofacies. However, despite this and the elongation ratios depicting a high ice velocity, several lines of evidence suggest that strain was relatively low. For example, the preservation of the fragile intraclasts and the spatial heterogeneities of lithofacies, demonstrate that deformation was not sufficient to homogenise the sediments within the subglacial traction layer. Also, the immature till at Berry Creek Reservoir (LF4), contained virtually no microscale deformation structures and very soft clasts were preserved in this lithofacies.

These observations build up a picture of the ice stream; that despite macroscale streamlining and the formation of bedforms with high elongation ratios, this rapid flow had a minimal effect on underlying sediments. This implies that effective pressures were sufficiently low to prevent rapid ice velocities from causing significant deformation or mixing in the subglacial traction layer.

6.5.2 Hydrology

Macroscale analysis revealed relatively limited information about ice stream hydrology. Groups of subglacial meltwater channels mid way down the ice stream are orientated transverse to ice streaming, were mapped by Evans *et al*. (2008) (Figure 6.4). These channels cross-cut streamlining at the ice stream bed and are thought to relate to water release from a deglacial lake (Evans *et al*., 2008), so they may relate to an event or series of events after ice streaming ceased. An esker system at the downstream end of the ice stream (Figure 6.4; Evans *et al*., 2008), indicates that meltwater was transported downstream in the centre of the ice stream here, in a system of Rothlisberger channels. Other than these examples, very little subglacial water movement is evident at the

macroscale, which suggests that meso and micro scales may have been more important pathways for subglacial hydrology.

At the mesoscale, evidence for subglacial water movement included channel fills and layers of fine sediment within the tills. These deposits may relate to canals and water films respectively (see Figure 2.5). Sorted sediments within the sediment melange at Section A, Berry Creek Reservoir, may have been deposited subglacially. This would imply that meltwater was routed along here and was of sufficiently high energy to transport cobble sized clasts. The process of loading, which was evident at both of the examined sites, implies that water pressures were high and that the till behaved as a viscous fluid within the subglacial environment. Ductile deformation structures at the microscale also depict an environment with high pore water pressures and overprinting between ductile and brittle deformation structures suggests that pore water pressures varied temporally. Therefore, despite some macro and meso scale evidence for evacuation of subglacial water from the bed, subglacial drainage was not efficient enough to prevent the build up of high pore water pressures. Packing voids, characteristic of some of the studied lithofacies, are not linked to a specific hydrological condition, but it can be speculated that they were water filled and dilated during ice streaming. The evidence for high pore water pressures is consistent with the inference, based on low levels of deformation, that effective pressures were low at the ice stream bed.

6.5.3 Fast flow mechanisms

Key findings at the Central Alberta Ice Stream include the widespread evidence for low strain as well as high and variable pore water pressures. Studies of contemporary ice streams have documented that high pore water pressures are commonplace at ice stream beds and are necessary for basal sliding and subglacial deformation (Blankenship *et al*., 1987; Kamb, 1991; 2001; Engelhardt and Kamb, 1997; Anandakrishnan *et al*., 1998). Therefore, the evidence for these conditions in the Central Alberta Ice Stream is consistent with the implication that one or both of these mechanisms operated in the ice stream.

The widespread, multiscale evidence for low strain suggests that subglacial deformation as a flow mechanism was not pervasive, laterally or vertically. It is possible that subglacial deformation operated as a fast flow mechanism in the uppermost centimetres of the sediment, but no evidence for this is seen. Furthermore, the preservation of lithofacies such as the immature till (LF4) at Berry Creek Reservoir suggests that the ice was decoupled from its bed, thereby preventing sediment deformation. Decoupling goes hand in hand with the fast flow mechanism of basal sliding (Kjær *et al*., 2006) and hence this was likely to have been the dominant flow mechanism in these localities. As these sites appear to be representative of the ice stream bed (in terms of bedrock lithology, topography and association with geomorphological features), it could be inferred that basal sliding was a key mechanism throughout the ice stream. The inference of basal sliding as an important flow mechanism, is consistent with the interpretation of Evans *et al*. (2008), who consider basal sliding to have been significant, based on the line of evidence that till cover is thin and that there was considerable subglacial meltwater in certain areas of the ice stream. Subglacial sliding as a key mechanism in this ice stream would also fit with the lack of subglacial lineations across the bed, since the ice would have been decoupled from the bed preventing interaction between the two (Stokes and Clark, 2002). This argument is further strengthened by the fact that the conditions conducive to subglacial lineation formation, namely soft sedimentary bedrock and abundant subglacial sediment, are present across vast areas of the ice stream bed (figures 6.12 and 6.13) and yet subglacial lineations are lacking.

Despite the apparently logical explanation that subglacial deformation was minimal and sliding was widespread, it is difficult to reconcile with the downstream thickening of tills observed on this ice stream (Shetsen, 1987; 1990). This is because this characteristic is considered to be a result of subglacial deformation (Boulton, 1996 a, b). It may be explained by a previous glaciation across the area being responsible for this distribution of till (see Evans, 1994). Or it may indicate that both flow mechanisms of deformation and sliding coexisted in the ice stream within the duration of its operation, spatial and/or temporally. Examination of additional sites at meso and micro scales would be crucial to ascertain the spatial (and potentially temporal) extents of the fast flow mechanisms.

7. Discussion

This thesis has presented an investigation of seven palaeo-ice streams, using up to three spatial scales of analysis. These address the main aim of the thesis, to identify ice stream subglacial processes from palaeo-ice streams and to assess the value of multiple spatial scales of analysis. The main outcomes of the thesis are discussed in the following sections, which outline, in turn, how each research question (Page 43) is addressed. These include: (7.1) characteristics and spatial variability at the ice stream bed; (7.2) ice stream basal processes, which primarily summarises the processes identified from the ice streams studied at all three spatial scales; and (7.3) the relevance of spatial scale and examination of each of the three spatial scales of analysis. The last of these issues is examined in the most detail because it has not yet been considered in any of the results chapters.

7.1 Characteristics and spatial variability at the ice stream bed

7.1.1 Subglacial lineation elongation

At the macroscale of palaeo-ice streams, subglacial lineations provide the principal link to subglacial processes. Whilst the formation mechanisms of these bedforms are uncertain, they can reveal spatial heterogeneities at the ice stream bed, which may link to observed and inferred variability in ice streams (e.g. Smith, 1997; Vaughan *et al*., 2003; Joughin *et al*., 2004; 2006; Murray *et al*., 2008). In the ice streams examined in this investigation, several characteristics of the spatial distribution of elongation ratio were found, which are shown schematically in Figure 7.1. These include: a decrease in maximum elongation ratio towards the ice stream lateral margins; clustering of subglacial lineations according to elongation ratio; and the presence of low elongation ratios throughout the ice stream. In addition to these observations, some links were observed between topography and subglacial lineation concentration and elongation ratio, leading to the inference that some of the ice streams had topography sticky spots.

The observed variabilities in elongation ratio distribution within the ice streams, may be attributed to several different factors, which are discussed in the following paragraphs. Elongation ratio has been clearly linked to ice velocity (e.g. Hart, 1999; Stokes and

Clark, 2002a; Briner *et al*., 2007; King *et al*., 2007) and this readily explains the observed decreases in elongation ratios towards the ice stream margins, because similar transverse trends in velocity are also seen in contemporary ice streams (e.g. figures 4.1 and 4.31; Bindschadler *et al*., 1996; Whillans and van der Veen, 1997). However, as noted in Section 4.7.1 the transverse distribution of average elongation ratio bears little similarity to the transverse velocity transects from modern ice streams, which is because of the abundance of subglacial lineations with low elongation ratios. As such, the maximum elongation ratio appears to represent ice velocity more realistically, but its precision is uncertain, because it relies on very few data-points. The fact that all the subglacial lineations do not display high elongation ratios may be because these bedforms initiate over time under an ice stream (e.g. Murray *et al*., 2008), and they then progressively elongate (e.g. Stokes and Clark, 2002a). The observed clustering of subglacial lineations (Figure 7.1) demonstrates that some control is acting upon these features and that this varies across the bed, over a spatial scale larger than individual subglacial lineations. In some instances this clustering could be related to the investigated bed variables, such as topography or bedrock permeability. However, much of the clustering could not be related to these, suggesting that either changes in velocity resulted from another variable, or that the trends in elongation ratio result from another factor.

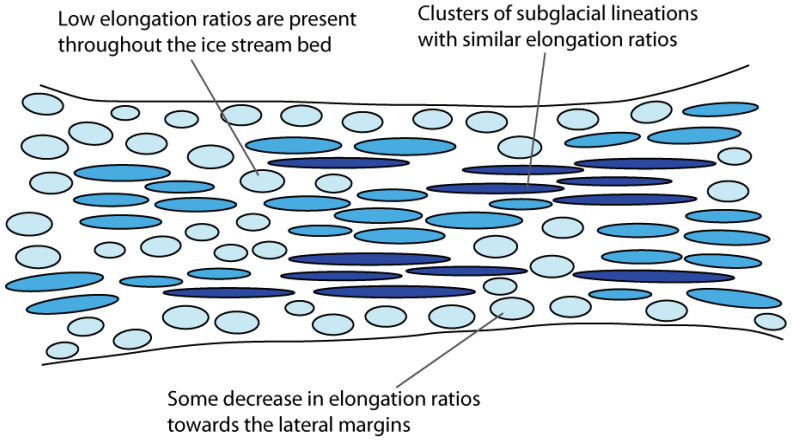

Figure 7.1 – Typical characteristics of subglacial lineation elongation ratios across a palaeo-ice stream.

Substrate strain rate may also affect elongation ratio. If subglacial lineations are assumed to initiate at a point and progressively elongate, then in addition to ice velocity (i.e. the shear stress) the strain rate of the substrate will also determine elongation ratio. Variations in substrate strain rate may relate to differences in underlying geology, and

notably geology appeared to affect elongation ratio in two of the ice streams examined. However, most of the lithological changes across the ice stream beds did not appear to significantly affect elongation ratio. Furthermore, the unusual assemblage of subglacial lineations and streamlining at the Central Alberta Ice Stream does not appear to be a result of its substrate characteristics, because its underlying geology is similar to some of the other ice streams examined. So whilst geology may be a factor affecting sediment strain rate, these observations suggest that it is not the most important factor.

Another important factor to consider is the degree of coupling of the ice to its bed, which will affect the degree of stress that the ice imparts onto the substrate, irrespective of its velocity. Therefore, given that spatial variability in ice-bed coupling has been identified under contemporary ice streams (e.g. Smith, 1997; Vaughan *et al*., 2003; Murray *et al*., 2008) this may also be a viable explanation and further investigation to establish the characteristics and scales in which this may occur, would be valuable. In summary, whilst ice velocity is clearly related to elongation ratio, it is unlikely that it accounts for all of the variability observed and several factors probably contribute to the observed trends.

However, because the formation mechanisms of subglacial lineations are uncertain, these inferences can only be hypothetical. If for instance, subglacial lineations were formed via erosion, then their elongation ratios cannot be considered as indicators of strain. Understanding their formation processes is vital to furthering our interpretations of the macroscale of ice streams. In pursuit of this, the schematic model in Figure 7.1 provides a useful guide for future investigations and a means for testing hypotheses of subglacial lineation formation.

7.1.2 Subglacial lineation clustering and bed characteristics

Analysis of the spatial distribution subglacial lineations allowed any clusters to be identified. Whilst this did have a minor bias as a result of bedform size (see Section 4.7.2) it identified areas of clustering in all of the ice streams. This analysis revealed that subglacial lineations were always spatial distributed in a clustered way and that this clustering did not display a preference for any one area of the ice stream. The degree and extent of the clustering indicated that it was a primary characteristic relating to

subglacial lineation formation below the ice stream, rather then just a result of postglacial modification, which may be focussed in certain areas more than others. The clustered areas were located in some instances up against the ice stream lateral margins (e.g. Figure 4.32), which suggests that velocity variations within the ice stream did not affect this characteristic. They also did not bear much relation to the patterns of elongation ratios identified across the ice streams. Comparison of median elongation ratio between the areas of high bedform clustering and across the ice stream as a whole did not reveal a significant pattern, as for some ice streams elongation was higher in the clusters and for some elongation was higher in the ice stream as a whole. The highest clustering in the ice streams did appear to display certain preferences for bed variables, as outlined in Table 7.1. The most common bed variables in the clusters were: till, fine grained sedimentary bedrock with a moderate permeability, low relief and a flat topographic curvature. This indicates that these conditions provide the most favourable environment for subglacial lineation formation at an ice stream bed.

Table 7.1 – Table outlining the most common of the bed variables for each ice stream, including the ice stream as a whole (*entire ice stream*) and the area of the highest subglacial lineation clustering (*clusters*).

Ice Stream	**Surficial sediments**		**Bedrock lithology**		**Bedrock permeability**	
	Entire ice stream	***Clusters***	***Entire ice stream***	***Clusters***	***Entire ice stream***	***Clusters***
Solway	Till	Till	Mudstone	Mudstone	Moderate	Low
Forth	Till	Till	Limestone	Sandstone	Moderate	High
Crooked Lake	-	-	Limestone, dolostone, shale, evaporites, chalk and carbonate reefs	Limestone, dolostone, shale, evaporites, chalk and carbonate reefs	-	-
Transition Bay	-	-	Limestone, dolostone, shale, evaporites, chalk and carbonate reefs	Limestone, dolostone, shale, evaporites, chalk and carbonate reefs	-	-
Haldane	-	-	Sandstone, siltstone, shale and coal	Sandstone, siltstone, shale and coal	-	-
Tweed	Till	Till	Limestone	Limestone	Moderate	Moderate
Central Alberta Ice Stream	Till	-	Shale, clayey sandstone, ironstone and bentonite	Shale and ironstone	Moderate	Moderate

Whilst a flat ice stream bed is typical in areas where subglacial lineations are clustered, a correlation was found between rises in bedrock topography and a drop in subglacial lineation density and in elongation ratios. This trend also continued downstream of obstacles. In the Forth Ice Stream such areas were also characterised by a deflection of subglacial lineations around them. Therefore, these topographic obstacles at the bed appear to have acted as sticky spots. Some of the topographic obstacles were also characterised by meltwater channels, which if subglacial, indicates an association between resistance at the bed and increased melting. This process may create a positive feedback mechanism enabling flow continuity in such localities.

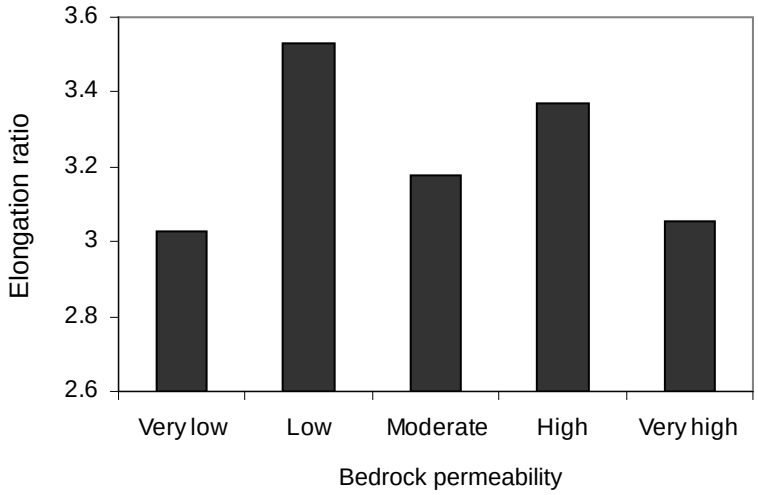

Figure 7.2 – Median subglacial lineation elongation ratio on each of the bedrock permeability categories, from all of the ice streams where this data was available (Solway, Forth, Tweed and Central Alberta ice streams).

Another bed variable that may have an effect on subglacial lineations is bedrock permeability. In the Tweed Ice Stream a relationship was identified in the upstream end of the ice stream, whereby bedrock permeability appeared to correlate with bedform elongation, size and clustering, as well as with the occurrence of subglacial channels. The subglacial lineations were smaller, less elongated and more clustered on bedrock of low permeability compared to an adjacent area of high permeability bedrock (Figure 5.16). Short, straight, clustered subglacial meltwater channels were also common on this same area of low permeability bedrock and virtually absent on the adjacent area of high permeability bedrock. Comparison of elongation ratio and bedrock permeability across all of the ice streams where this was examined is presented in Figure 7.2. This depicts a contrasting pattern because it shows that highest elongation ratios were found on bedrock with a low permeability, which is broadly similar to the findings of Rattas and

Piotrowski (2003), who found lower permeability bedrock to be characterised by more elongated subglacial lineations. The discrepancy suggests that whilst spatial variations in subglacial lineations may correlate with substrate variations this relationship can be quite localised and evidently is also dependent on other factors. Interestingly the subglacial lineations on the moderate permeability bedrock did not have the most elongate lineations (Figure 7.2), despite the fact that it was the most widespread. However, the permeability data may have some discrepancies between ice streams and the range of median elongation ratios across all of the categories is relatively narrow, and consequently this data can only be considered indicative.

The most common variables found across the entire ice stream bed were the same as those found in the areas of high bedform clustering (Table 7.1). These were: widespread till, fine grained sedimentary bedrock with a moderate permeability, low relief and a flat topographic curvature, indicating that these characteristics provide favourable conditions for ice streaming. Some of these identified characteristics are similar to findings from studies of contemporary and palaeo ice streams, which include identification of: fine grained sedimentary bedrock (e.g. Anandrakrishnan *et al*., 1998; Winsborrow *et al*., 2010); presence of subglacial till (e.g. Blankenship *et al*., 1986; Hicock *et al*., 1989; Alley *et al*., 2004; Tulaczyk *et al*., 1998); and a flat (smooth) bed (Siegert *et al*., 2004; Rippin *et al*., 2006; Bingham and Siegert, 2007). Examination of the DEM's and topographic curvature demonstrated that all of the ice streams were characterised by a flat smooth bed. This was particularly notable when compared to the surrounding terrain, which was characteristically rougher and had a wider range of curvature values.

The finding that the ice streams examined were located preferentially on a moderate permeability may be one of the most useful findings as this has not been reported by many other studies (e.g. Rattas and Piotrowski, 2003) and this characteristic plays an important role in subglacial hydrology. These similarities to other studies bring further confidence that these characteristics are among the most favourable for ice streaming. Although it is noted that not all ice streams may conform to these characteristics, for example Roberts and Long (2005) report subglacial bedforms from a hard bedded, till free area of Jakobshavn isbrae. Some or all of these characteristics may have also helped determine the ice stream location, and a (soft) bed of till, sedimentary bedrock

and a flat (smooth) bed are among several identified controlling factors determining ice stream location by Winsborrow *et al*. (2010).

7.1.3 Spatial variability at the meso and micro scales

Spatial variability was not specifically investigated at the meso and micro scales, but the results revealed that heterogeneities were also commonplace at these scales. Variability was apparent in terms of sediment properties, both laterally and with depth. This was most evident at the Central Alberta Ice Stream, which was characterised by multiple lithofacies within a melange of sediments and lateral variations in lithofacies, across distances of several metres. This type of heterogeneity is not uncommon for subglacial sediments and means that sediment strain and sediment response to pore water pressures would have varied spatially (Evans *et al*., 2006a). These substrate characteristics may be associated with observed variabilities in hydrology seen at this scale (e.g. Fischer and Clarke, 2001; Smith *et al*., 2007; Murray *et al*., 2008).

Several lines of evidence suggest that pore water pressures were variable in the palaeo-ice streams studied, as discussed in sections 5.5.2 and 6.5.2. For example, the presence of dense, laminated till within bedrock fissures at Blinkbonny Quarry (Section 5.3.3), suggests that high pore water pressures enabled till to fluidise and followed the pressure gradient downwards to inject into bedrock fissures. And the presence of laminations suggests that these conditions took place multiple times, which indicates that pore water pressures varied temporally. Given that subglacial deformation and subglacial sliding are dependent on specific pore water pressures, this suggests that the flow mechanisms may also have varied in time and space. This assertion is consistent with some other findings from glaciers and ice streams (e.g. Fischer and Clarke, 2001; Murray *et al*., 2008), and theories that spatial and temporal variability is inherent within the subglacial environment (e.g. Piotroswki and Kraus, 1997; van der Meer *et al*., 2003; Evans *et al*., 2006a). The meso and micro scale variability in pore water pressures, may impact the macroscale and could potentially affect larger scale variabilities at the ice stream bed. Further work may be required to reconcile the heterogeneities at the different scales and this may be useful to help elucidate the extent and variability of fast flow mechanisms and hydrology, and their resultant sediments and geomorphology.

7.2 Ice stream subglacial processes

The ice stream bed plays a critical role in facilitating ice stream operation, because specific conditions and processes in this environment enable rapid ice flow (Alley, *et al*., 2004). The subglacial processes at the ice stream bed could be identified somewhat from macroscale analysis, however, this scale of analysis is limited by: what this type of data can reveal, and the restricted understanding of subglacial lineations and other bedforms. For the Tweed and Central Alberta ice streams, the multiscale approach allowed considerably more information on ice stream subglacial processes to be obtained. These are discussed in detail in sections 5.5 and 6.5 and are summarised in the schematic diagrams in figures 7.3 and 7.4. These figures illustrate the different suite of characteristics and processes identified at these two ice streams, which is manifest in the different relative importance of the fast flow mechanisms. Processes and conditions common to both ice streams include: deformation, albeit the degree of this differs between the ice streams; and pore water pressures, which were found to be high and variable in both ice streams. The evidence for deformation at the different scales allowed interpretation of potential ice flow mechanisms that operated in each. Based on the evidence for the extent and spatial distribution of deformation, subglacial deformation was identified as a key and potentially dominant process in the Tweed Ice Stream and subglacial sliding was identified as a key process at the sites examined in the Central Alberta Ice Stream.

Evidently, deformation signatures can vary considerably between different ice streams, as can the primary fast flow mechanism. The results highlight that pervasive deformation does not necessarily go hand in hand with ice streaming (e.g. Alley, 1991; Stokes and Clark, 1999), an assertion that is reflected in some other studies (e.g. Ó Cofaigh and Evans, 2001; Evans *et al*., 2008). This indicates that pervasive till deformation is not applicable as a criterion for the identification of palaeo-ice streams (see Stokes and Clark, 1999).

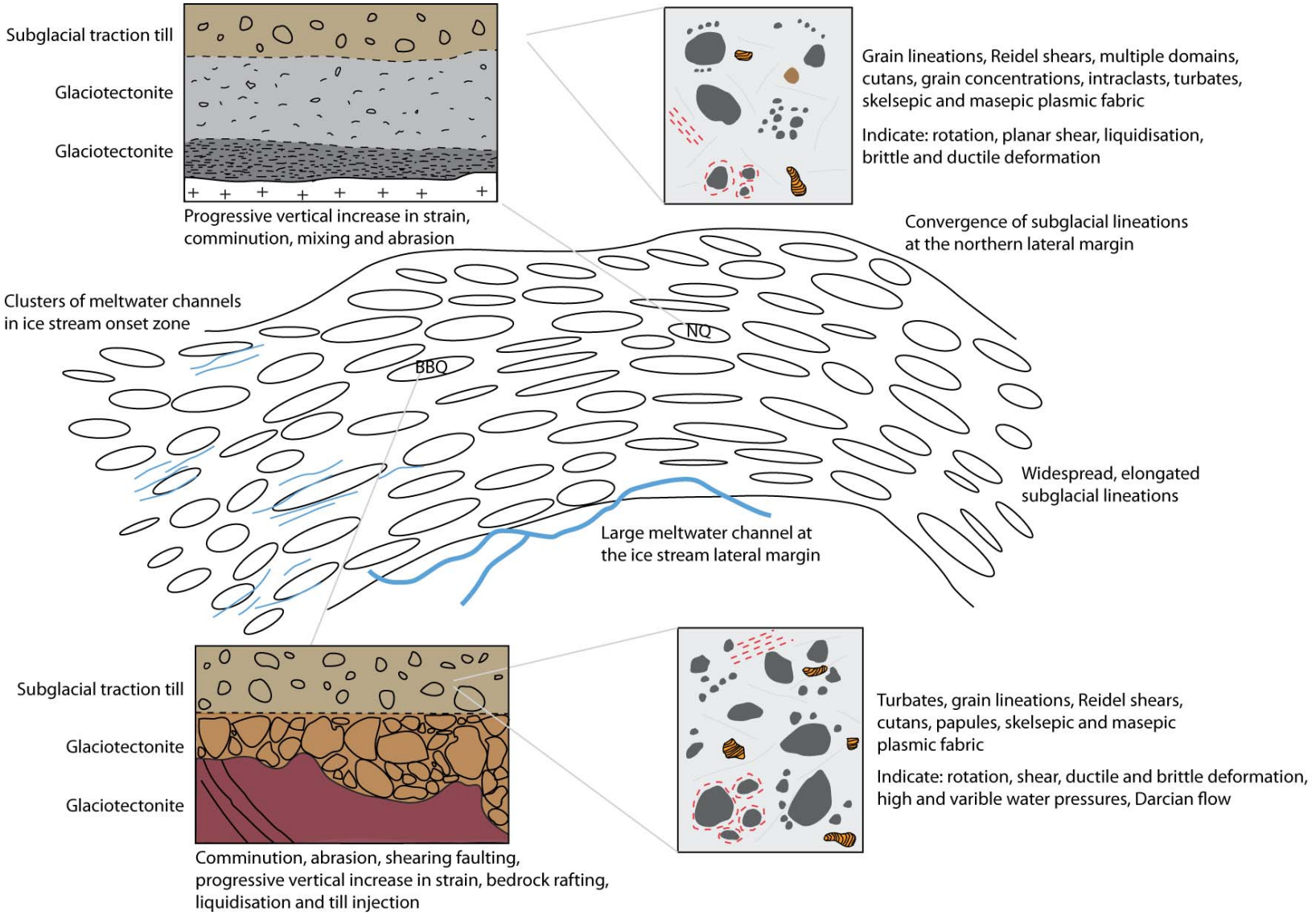

Figure 7.3 – Schematic diagram depicting the some of the key basal processes of the Tweed Ice Stream, which is thought to be dominated by subglacial deformation, as manifest in the geomorphology, sedimentology and micromorphology.

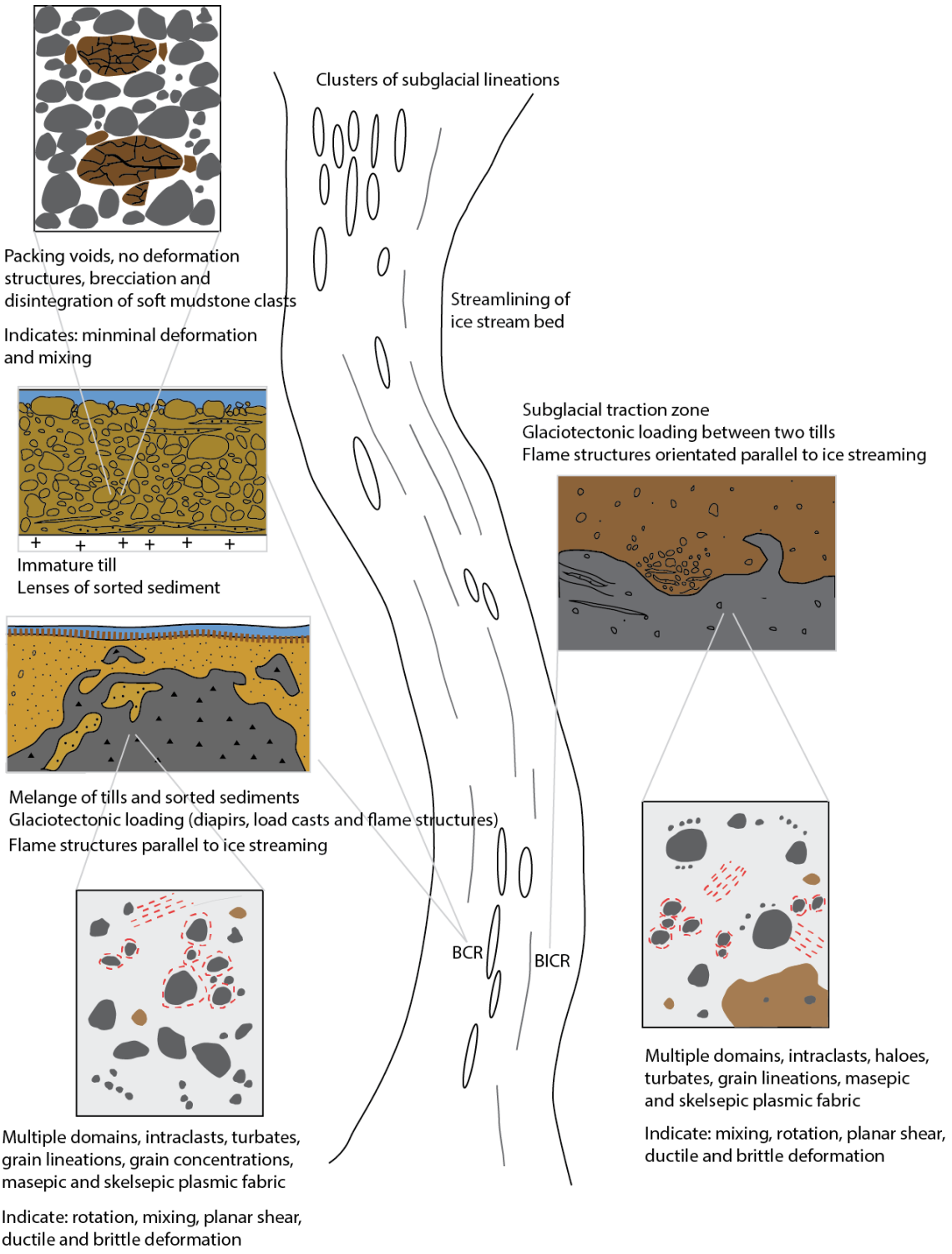

Figure 7.4 – Schematic diagram depicting the some of the key basal processes of the Central Alberta Ice Stream, as manifest in the geomorphology, sedimentology and micromorphology. Subglacial sliding dominates the two sites examined and possibly also wider areas across the ice stream.

Strong evidence for high pore water pressures at both ice streams support research from contemporary ice streams that identify high pore water pressures as common at ice stream beds and a necessary condition for fast flow (e.g. Blankenship *et al.*, 1987;

Kamb, 1991; 2001; Engelhardt and Kamb, 1997; Anandakrishnan *et al*., 1998). The ubiquity of high pore water pressures at ice stream beds, along with the substantive evidence for them in the Tweed and Central Alberta ice streams, suggests that they may provide an additional criterion for the identification of palaeo-ice streams (see Stokes and Clark, 1999). This may be of particular value when macroscale evidence is limited or inaccessible. Although it should be noted that high pore water pressures are not unique to ice streams and they may be found in other glacial and non-glacial environments (e.g. Harris *et al*., 2008; Iverson *et al*., 2007; Iverson *et al*., 2010). Therefore, similar to the other criteria for palaeo-ice stream identification (see Stokes and Clark, 1999), this characteristic alone does not provide a diagnostic indicator of palaeo-ice streaming and should only be used in combination with other criteria.

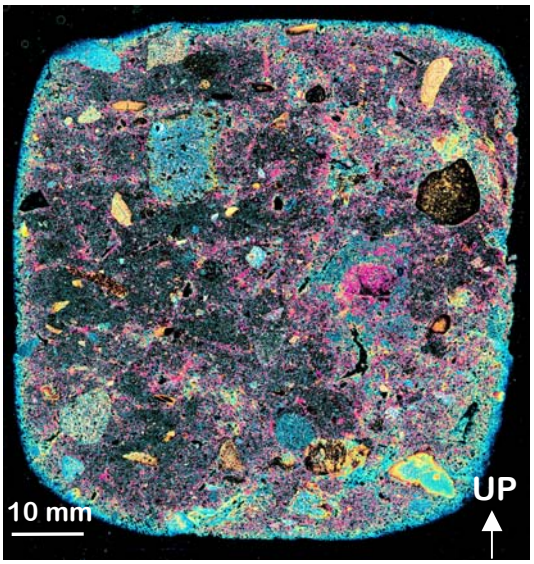

Figure 7.5 – False colour image of thin section BBQAa, from Blinkbonny Quarry. Orange cutans appear pink.

One of the indicators of high pore water pressures was the presence of cutans in the Tweed Valley, interpreted as subglacial in origin (sections 5.3.5 and 5.4.5). If this inference is correct it has significant implications for subglacial hydrology and what information can be obtained about this. The voids and areas that the cutans fill reflect primary porosity of the sediment and so could reveal insights into the pathways of subglacial water. They may also reflect areas of dilation, and the distribution of this within a sediment. The degree of dilation can indicate deformation processes, and above 35-40 % is considered indicative of subglacial deformation (e.g. Alley *et al*., 1986; Murray and Dowdeswell, 1992; Smith, 1997; Vaughan *et al*., 2003). The false colour image of BBQA in Figure 7.5 shows the extent of cutans in this thin section. If the

extent of the cutans is above 35 %, which visually they appear to be, then this suggests that the sediment was undergoing subglacial deformation. This is consistent with the other lines of evidence for the ice flow mechanism here (Section 5.5.3). The cutans are distributed unevenly and are pervasive in some areas and not in others, possibly suggesting that dilation was unevenly distributed, whilst their concentration along lines may reflect routing of subglacial water. Whilst the link between subglacial cutans and dilation is only made tentatively here and is complicated because the sediment reflects a cumulation of subglacial and postglacial processes; further investigation of this may be of value. This potentially could allow significant insights into the microscale processes of dilation and subglacial deformation, and their spatial distribution.

7.3 Spatial scales of analysis

Comparison between the different scales of analysis was one of the key focuses of the study. As outlined in the Methods (Section 3.5) certain steps were taken to enable direct comparisons between scales, such as ensuring that sample locations were representative and characterising these carefully. Comparison between macro and meso scales was limited by the sediment site location, because for both ice streams there were very few options for selecting these sites. This meant that there was a possibility that these sites were not entirely representative of the ice stream bed and hence there was a potential for bias. In the Tweed Palaeo-Ice Stream both sites were quarries situated on the top/stoss end of a drumlin and in the Central Alberta Palaeo-Ice Stream both sites were situated at the edges of reservoirs. So despite that fact that all of the sites were situated within geomorphology that was typical of the ice stream bed there remains some potential for bias. This was particularly the case for the Tweed Palaeo-Ice Stream because the stoss side of a drumlin may experience different subglacial conditions than other parts of a drumlin. However, the comparison of mesoscale findings to the sedimentology data of Kerr (1972), who measured fabrics from various localities on several drumlins, confirmed that many of the sedimentology characteristics were in fact typical for the area. Selection of sites at the microscale was much easier and this is usually only limited in situations where coarse or loose sediments prevent micromorphology samples from being obtained, which was not a problem for this study. This meant that the microscale data was as representative as possible, although it was of course subject to the same possible bias as the mesoscale data.

Table 7.2 – Summary table of the key evidence and subglacial processes inferred from this, from the Tweed Ice Stream. Table is split up into the three spatial scales of analysis.

Scale	Evidence	Inferred subglacial processes and conditions
Macro	Elongated subglacial lineations	High palaeo ice velocity
	Subglacial lineation elongation ratios increase at the upstream end of the ice stream and decrease towards the lateral margins	Increase in ice velocity at onset zone and decrease in ice velocity at margins
	Subglacial lineations are present throughout the ice stream bed (and some spatial variability in elongation ratios is evident)	Strain is generally continuous across the ice stream bed (with some variability)
	Meltwater channels cut into bedrock and sediment, and cross-cutting the topography in the ice stream onset zone	Channelisation of subglacial meltwater into poorly connected Nye channels in the ice stream onset zone
	Large subglacial meltwater channel at the southern ice stream lateral margin	Channelisation and considerable discharge of subglacial water at the southern lateral shear margin. The channel may have contributed to maintaining the location of the ice stream lateral margin
Meso	Decreasing bedrock structure and increasing evidence for mixing with vertical distance up sediment profiles	Increasing deformation with vertical distance up sediment profile, consistent with models of subglacial till deformation signature (Alley, 1989; van der Meer, 2003)
	Subglacial traction tills and glaciotectonites reach a depth of up to 3 metres below ground surface	Extent of deformation up to 3 metres below ground surface
	Concentrations of fine-grained, laminated till within fissures in the glaciotectonites at Blinkbonny Quarry	High and fluctuating water pressures causing till injection down into the glaciotectonites
	Spatial variations in till texture and properties within individual lithofacies	Incomplete mixing of sediment, even in the uppermost till layers
	Presence of bedrock rafts in upper till layers	Bedrock rafting
Micro	Turbates, skelsepic plasmic fabric and multiple domains	Pervasive ductile deformation of subglacial traction tills (Blinkbonny and Newton quarries) and glaciotectonite (Newton Quarry)
	Discrete shears (lineations), faulting and unistrial plasmic fabric	Pervasive brittle deformation of subglacial traction tills (Blinkbonny and Newton quarries) and glaciotectonite (Newton Quarry)
	Multiple domains and intraclasts	A degree of sediment mixing (Blinkbonny and Newton quarries)
	Grain concentration in NQC	High and fluctuating water pressures causing fluidisation and till injection
	Increasing deformation structures and disruption of bedrock structure with vertical distance up sediment profile	Increasing deformation with vertical distance up sediment profile, consistent with models of subglacial till deformation signature (Alley, 1989; van der Meer, 2003)
	Extensive, spatially variable subglacial clay cutans	High water pressures separating clay particles and dilated till (spatially variable)

Table 7.3 – Summary table of the key evidence and subglacial processes inferred from this, from the Central Alberta Ice Stream. Table is split up into the three spatial scales of analysis.

Scale	Evidence	Inferred subglacial processes and conditions
Macro	Elongated subglacial lineations and streamlined bed	High palaeo ice velocity
	Subglacial lineations are sparse across much of the ice stream. The typically are present in clusters, where they may have high elongation ratios	Strain discontinuity and spatial variations in subglacial processes
	Decrease in elongation ratios towards the ice stream lateral margins	Decrease in ice velocity towards the lateral margins
	Streamlining of former esker complex into highly elongated subglacial lineations (Evans, 1996)	Subglacial streamlining of pre-existing sediments
	Hummocky moraine outside of ice streams, which contrasts with the streamlined ice stream bed	Marked difference between geomorphological processes within the ice stream and those outside the ice stream. This may relate to deglaciation (Eyles *et al*., 1999)
Meso	Existence of soft sediment intraclasts, channel fills and multiple lithofacies in the subglacial traction layer.	Relatively low strain
	Sediments are visibly deformed, but they are heterogeneous and mixing is incomplete, indicating that pervasive deformation did not take place	Fast ice flow mechanism either subglacial sliding or very thin layer of deformation at the top of the sediment sequence
	Channel fills in LF1 at Blood Indian Creek Reservoir	Export of subglacial meltwater via canals 20 to 30 cm wide
	Loaded boundaries, large scale diapirs, pseudonodules and flame structures. Orientation of these structures consistent with palaeo ice flow direction. Absence of other evidence to explain loading	Glaciotectonic loading and ductile deformation at Section A at Berry Creek Reservoir and at Blood Indian Creek Reservoir. This indicates that pore water pressures were high and the till behaved as a viscous material
Micro	Matrix poor lithofacies and preservation of local mudrock clasts at Section B, Berry Creek Reservoir (LF4). Lack of brittle and ductile deformation structures. Presence of packing voids, which indicate high porosity.	Low strain and formation of an immature till
	Intraclasts, turbates, deformed laminations, haloes, skelsepic and masepic plasmic fabric	Ductile deformation at Berry Creek Reservoir (LF1) and at Blood Indian Creek Reservoir (LF1 and LF2)
	Grain lineations, unistrial plasmic fabric and clast brecciation	Brittle deformation at Berry Creek Reservoir, (LF1) and at Blood Indian Creek Reservoir (LF1 and LF2)

Use of the three spatial scales of analysis allows an assessment to be made of how the different scales relate to each other in terms of subglacial processes. Tables 7.2 and 7.3 summarise the inferred subglacial processes at each spatial scale of analysis, for the Tweed and Central Alberta ice streams respectively. Processes other than subglacial are not included in the tables because this is not the main focus of the thesis, but it should

be noted that other processes require investigation in order to accurately reconstruct the history of a landscape or sediment.

Tables 7.2 and 7.3 show that some processes are identified at more than one spatial scale. Deformation is the only characteristic to be identified at all scales and is manifest in different ways at each scale. In these two case studies the examination of deformation was critical to the interpretations of likely fast flow mechanisms. Some processes were observed at two of the three scales, such as high pore water pressures, which were found at the meso and micro scales. Additionally, some of the inferred processes are not the same, but have clear similarities between the different scales, such as bedrock rafting identified at the mesoscale and sediment mixing identified at the microscale, in the Tweed Ice Stream (Table 7.2). The microscale often supplements the mesoscale with useful and even crucial information for the interpretation of lithofacies, for example the glaciotectonite at Newton Quarry appears massive at the mesoscale and analysis of the microscale is necessary to confirm the existence of some of the original bedrock structure. Finally, a few of the inferred processes were only identified at a single scale, such as high palaeo ice velocities inferred from elongated subglacial lineations at the macroscale in both of the investigated ice streams. In terms of direct comparison between the three scales, meso and micro scales compare more readily than the macroscale compares to the meso and micro scales. This is probably because the macroscale is focussed on examination of geomorphology whereas meso and micro scales are focussed on examination of sediments.

Many similarities exist between the processes identified at different spatial scales in tables 7.2 and 7.3. However, use of each scale in certain ways may lead to slightly differing or even contradictory results between different scales of analysis, indicating that scale should be considered when selecting a method. For example, ice flow direction is identified from the macroscale via subglacial lineations, but macro and micro fabrics (at the meso and micro scale) may also be used to infer ice flow direction (e.g. West and Donner, 1956; Ham and Mickleson, 1994; Hooyer and Iverson, 2000; Larsen and Piotrowski, 2003; Thomason and Iverson, 2006). In both the Tweed and Central Alberta ice streams macro and micro fabrics are not consistently orientated parallel with palaeo ice flow and, as such, should not be used to infer ice flow direction. This assertion is consistent with the findings of some other field studies of particle fabric (e.g. Carr and Rose, 2003; Carr and Goddard, 2007). Another example is in the

analysis of Section B at Berry Creek Reservoir, which, if studied only at the mesoscale may led to the interpretation that it is a well developed till, based on the evidence for considerable clast abrasion and strong, flow parallel macrofabrics. However, microscale analysis revealed widespread packing voids and soft mudstone clasts, indicating that the till is in fact immature. This demonstrates the value of a multiscale approach and that care should be taken when basing interpretations on a single scale.

7.3.1 The value of each spatial scale of analysis

Common sense tells us that a multi-methodological approach, over a range of spatial scales, is likely to reveal more about a palaeo-ice stream than an investigation restricted to methods associated with a single scale of analysis. However, each of the methods employed in this study require time and specific expertise and as such analysis of all three spatial scales of analysis may not always be practical. This section identifies the advantages and disadvantages of each spatial scale and the most relevant characteristics and processes that may be identified at them, which are summarised in Table 7.4. Recommended avenues for future work are also discussed. This table provides an indication of what results or interpretations may be achieved from each scale, based on the findings of this thesis and supported by previous work (discussed in the following paragraphs). Further work may reveal additional points to add.

As indicated in Table 7.4, macroscale ice stream characteristics can provide a range of information, some of which can only be identified at this scale. Elongated subglacial lineations are widespread and maybe even ubiquitous in palaeo-ice streams and can provide information about relative ice velocity (and potentially strain) and its distribution across the ice stream bed. Where evidence is available, the macroscale may also provide information about processes such as basal hydrology or large scale sediment organisation (into bedforms such as moraines). Limitations to macroscale analysis of palaeo-ice streams are manifest when landforms cannot be explicitly associated with ice streaming and where landforms are few, due to their lack of preservation or because they are not within the resolution of the imagery dataset. The advantages of a macroscale approach is the wide geographical coverage, and this is frequently across an entire ice stream or a suite of ice streams. Also, where imagery is already available, macroscale analysis does not require fieldwork.

Table 7.4 – Table of the key findings from palaeo-ice streams that may be achieved from each of the spatial scales of analysis employed in this study (^ most important scale in which to identify the indicated characteristic; * all scales are ideally required to infer the indicated characteristic).

Ice stream characteristic:	**At what scale can each characteristic be examined:**		
	Macro?	**Meso?**	**Micro?**
Palaeo-ice stream identification	Yes^ - Based on the criteria of Stokes and Clark (1999)	Yes - Based on evidence for high pore water pressures (in combination with other criteria)	Yes - Based on evidence for high pore water pressures (in combination with other criteria)
Ice flow velocity	Yes - Subglacial lineation elongation ratio can indicate relative ice flow velocity and spatial variations therein	No	No
Ice flow orientation	Yes^ - Based on subglacial lineation orientations	Yes - Based on clast fabric (in some instances)	Yes - Based on microfabric (in some instances)
Hydrological system	Yes - Glacial geomorphology, such as meltwater channels, eskers and palaeo lakes, which can be assigned a subglacial origin (this evidence is often quite spatially restricted)	Yes – Fluvial sediments within subglacial tills, e.g. channel fills	Yes – Can reveal information about pore water pressures and Darcian flow
Strain and its spatial variability	Yes - Spatial distribution of subglacial lineation elongation ratio (assuming subglacial lineations initiate at a point and progressively elongate with high ice velocities over time)	Yes^ - Indicated by the type and architecture of lithofacies and structures	Yes - Indicated by analysis of microscale deformation structures and their associations with each other
Ductile/brittle deformation	No	Yes - In certain structures and sediment types, where evidence is available	Yes^ - Based on type and relative amounts of deformation structures (Menzies, 2000)
Sediment rheology	No	Yes - Where evidence is available, for example if there is indication of glaciotectonic loading	Yes - Where evidence is available, certain types and distributions of structures may indicate this
Pore water pressures	No	Yes - Several possible lines of evidence. These are expected to be high and possibly also variable in palaeo-ice streams	Yes - Several possible lines of evidence. These are expected to be high and possibly also variable in palaeo ice streams
Sediment formation and transport	Yes - Large scale sediment transport and deposition across the ice stream bed	Yes - Sediment transport and till formation mechanisms	Yes - Microscale evidence for sediment transport and till formation mechanisms
Fast flow mechanism	Yes* - Extent and distribution of deformation and other possible lines of evidence may indicate likely flow mechanism(s)	Yes* - Extent and distribution of deformation and other possible lines of evidence may indicate likely flow mechanism(s)	Yes* - Extent and distribution of deformation and other possible lines of evidence may indicate likely flow mechanism(s)

As a considerable amount of research has been done on the macroscale analysis of palaeo-ice streams (e.g. Stokes and Clark, 2001, De Angelis and Kleman, 2005; Graham *et al*., 2009), future work of this scale may be most useful if combined with other scales of analysis or with other types of analysis, such as modelling (e.g. Hindmarsh and Stokes, 2008). Despite considerable attention, subglacial lineations are not fully understood and their formation mechanism(s) remains controversial (e.g. Boulton, 1987; Shaw *et al*., 1989; Hindmarsh, 1998; Boulton *et al*., 2001; Shaw, 2002; Clark *et al*., 2009), which holds back interpretations of palaeo-ice stream basal environments. When the formation mechanisms of subglacial lineations are better constrained, they may be used to infer subglacial processes with a greater degree of certainty.

Mesoscale analysis can reveal a range of information about ice stream processes, as depicted in Table 7.4. This analysis will benefit from investigation of multiple locations within an ice stream, so that interpretations about the ice stream as a whole are more reliable. A drawback of this analysis is that exposures of sediment are usually limited and so investigation at this scale may be biased towards locations where exposures are available. This potential bias can be minimised by investigating the macroscale at and around the site, so that the geomorphological context of the site is known. This aids interpretation and helps establish the likely origins of certain sedimentological features. For example, the interpretation of the boulder pavement at Berry Creek Reservoir was aided by the knowledge that the site is located in a former spillway.

Mesoscale analysis can reveal significant characteristics about deformation, including its lateral and vertical extent, magnitude and spatial variability; as has been done by this study and many previous studies (e.g. Piotrowski and Kraus, 1997; Evans *et al*., 1998; Hart, 2007). It can also provide a range of information about the sediment origin and formation, such as orientation and provenance of the sediment particles, strength and variability of pore water pressures and glaciotectonics (e.g. Hicock and Fuller, 1995; Lian and Hicock, 2000; Hiemstra *et al*., 2006; Lee and Phillips, 2008). Identification of fast flow mechanisms is typically centred on mesoscale analysis, and this is the scale at which certain criteria, such as clast fabrics, homogenised till and existence of fine sediment layers within till, have been identified as indicative of certain mechanisms (e.g. Hart, 1995; Piotrowski and Tulaczyk, 1999). In this study macro and micro scale

analyses also provided valuable information to add to the interpretation of flow mechanisms.

Further investigation of mesoscale sediments and associated processes may reveal additional insights into possible indicators of the different flow mechanisms. Examination of this alongside models of different flow mechanisms or processes (e.g. Piotrowski and Tulaczyk, 1999) could be an insightful avenue for future research. Tying down criteria for the different fast flow mechanisms would enable the flow mechanisms within different palaeo-ice streams to be identified, which would help understanding of the relative importance of the different flow mechanisms and how they relate to other ice stream characteristics. This would aid the understanding and modelling of contemporary ice streams.

This study has highlighted the fact that palaeo-ice stream sediments may vary considerably between and within ice streams. This apparent diversity of ice stream sediments would benefit from further investigation, ideally across multiple sites and across multiple palaeo-ice streams and placed within the geomorphological (macroscale) context. This would aid further characterisation of ice stream sediments and mesoscale subglacial processes and may help identify the characteristic geomorphological and sedimentological signatures associated with certain fast flow mechanisms.

The microscale can provide highly detailed information about the constituents and structure of glacial sediments. It allows the different types of deformation to be identified (i.e. brittle or ductile), which may indicate relative pore water pressures (Menzies, 2000). Features at this scale may also indicate the degree of sediment mixing, transportation history of constituent particles and the lithofacies as a whole, and small scale water movement (e.g. van der Meer, 1993; Menzies, 2000). The obvious disadvantage of microscale analysis is that it has a very limited spatial coverage, which may be problematic if the lithofacies is spatially variable. So it is important to select sampling locations with care to ensure that the lithofacies or a structure that is being sampled is a representative as possible (Carr, 2004). This will require some basic meso and macro scale analysis to establish information such as lithofacies type and extent, and ice flow direction, information that will also aid microscale interpretation. Where

some or all of this information is unavailable, interpretations should be made more tentatively.

The interpretation that different flow mechanisms operated at the sediment sites on the two ice streams examined provides an opportunity to compare whether amount of microscale structures can indicate relative strain. Overall analysis of the relative amounts of microstructures (tables 5.2, 5.4, 6.2 and 6.4) does appear to suggest that microstructures are generally more abundant in the Tweed Palaeo-Ice Stream than the Central Alberta Palaeo-Ice Stream. However, more careful examination reveals that the matrix rich till lithofacies in the Central Alberta Ice Stream did contain high amounts of microstructures, which indicates that these structures can be locally abundant despite low overall strain. Additionally, comparison of the areas mapped to identify associations between structures revealed the abundance and interlinked nature of some of the key microstructures at both ice streams (figures 5.33, 5.53, 6.40 and 6.58). Conversely, certain lithofacies from both ice streams, such as those dominated by skeleton grains, contained very few microstructures. Therefore, this study indicates that inherent sediment characteristics, particularly texture, may be one of the most important factors controlling the amount of microstructures that form, whereas the degree of strain could be less significant in many situations.

Given the limited attention the microscale has received in the context of ice streams, further work in this area may be particularly rewarding. Examination at this scale is of great value in identifying the detail of subglacial sediments and, as has been demonstrated, it can strengthen mesoscale interpretations. Future studies investigating this scale may benefit from direct comparison with non-ice streaming sediments (e.g. Khatwa and Tulaczyk, 2001), in order to help further elucidate the processes that are common in ice streaming (such as high pore water pressures). Further experimental work to elucidate the processes responsible for microscale structures would also be of value. These approaches may help establish whether any such characteristics could be used as criteria for identification of ice streaming, which would be useful where macroscale datasets are limited. Mapping of grain lineations using GIS in chapters 5 and 6, demonstrated the potential for quantification and detailed analysis of microscale structures. This work contributes to a range of methodological developments that have been recently made in the micromorphology of glacial sediments (e.g. Larsen *et al.*,

2007; Kalvans and Saks, 2008; Linch, 2010; Phillips *et al*., 2011). Further application of some of these techniques to palaeo-ice streams may allow considerable advancement in our understanding of the structures and processes at this scale.

In summary, the different spatial scales of analysis provide different types of information about a palaeo-ice stream. Findings may overlap between different scales, thus provide valuable internal checks for the analyses, allowing a more robust analysis to be carried out. Equally, findings at a single scale of analysis are less reliable, and may even lead to erroneous interpretations. Whilst for the investigation of some characteristics, such as relative ice flow velocity, a certain scale is critical. In contemporary ice streams a different set of techniques are used, but the potential inferences made by this study, regarding each scale of analysis may still be applicable. Future studies of palaeo-ice streams are advised to focus on meso and micro scales of analysis, whilst placing investigations within the context of the relevant larger scale. As well as combining scales of analysis, combining different approaches may also help answer specific questions, for example use of field or mapping techniques alongside modelling, or direct comparison of palaeo and contemporary ice streams.

8. Conclusions

This thesis has provided a unique insight into the basal characteristics and processes of seven palaeo-ice streams. Use of multiple scales of analysis has allowed two of these ice streams to be characterised to a level of detail that has rarely been achieved before. The resultant outcomes can be summarised as follows.

- Subglacial lineation elongation ratio depicts spatial heterogeneity at the macroscale across palaeo-ice stream beds. The three characteristics observed in all of the ice streams examined were: decreases in maximum elongation ratio towards the ice stream lateral margins; clustering of subglacial lineations according to elongation ratio; and low elongation ratios distributed throughout the ice stream bed. The drop in elongation ratios at the lateral margins results from expected velocity changes here, which is seen in contemporary ice streams. The other observed variabilities may relate to ice velocity, degree of coupling of the ice to its bed, or substrate strain rate. Topography was identified as a factor that can affect elongation ratio, as well as subglacial lineation abundance, allowing topographic sticky spots to be identified on several of the ice streams examined. The observed variations in elongation ratios may provide a useful guide to test future models of ice streams and subglacial lineations. At meso and micro scales, variability is apparent in terms of sediment properties and pore water pressure and supports the idea that heterogeneity in hydrology and flow mechanisms are commonplace in subglacial environments (e.g. Piotroswki and Kraus, 1997; van der Meer *et al*., 2003; Evans *et al*., 2006a).

- Examination of bed variables indicated that the most common characteristics of the ice stream beds were: widespread till, fine grained sedimentary bedrock with a moderate permeability, low relief and a flat topographic curvature. Whilst these characteristics were variable across the ice stream beds examined, these features were also the most common for areas of high bedform clustering. Therefore, this combination of characteristics is favourable for subglacial lineation formation.

- A range of subglacial processes were identified from the examined palaeo-ice streams and of these, deformation and high pore water pressures were particularly significant. Deformation was observed at all scales and ductile and brittle deformation structures were common but not ubiquitous. Multiple lines of evidence indicate that pore water pressures were high and that they fluctuated. This finding is consistent with studies of contemporary ice streams and the fact that high pore water pressures is synonymous with ice stream flow, suggests that it may provide an additional criterion for the identification of palaeo-ice streams (Stokes and Clark, 1999). Schematic models for the Tweed and Central Alberta ice streams are given and these may provide a guide for future studies and an indication of the characteristics that may be associated with subglacial deformation and subglacial sliding.

- Fast flow mechanisms were identified in both the Tweed and Central Alberta ice streams. Subglacial deformation was considered to have been a key flow mechanism in the Tweed Ice Stream based on the evidence for till deformation and homogenisation especially in the upper layers of sediment, as well as macroscale evidence for extensive subglacial lineations. Some limited areas with no surficial sediments and elongated bedforms indicate that subglacial sliding was also operating in the ice stream. In the Central Alberta Ice Stream subglacial lineations were few and instead much of the bed was characterised by a very low amplitude, streamlined relief. Its sediments displayed some evidence for deformation, but the preservation of structures and intraclasts indicated that strain was low. This suggests that decoupling and subglacial sliding operated at these sites and may have also been dominant across much of the ice stream, which could explain the lack of subglacial lineations.

- Analysis of three scales of analysis provided an effective means to fully characterise the Tweed and Central Alberta ice streams. Many processes were corroborated between the different scales and this provided a significantly greater level of detail, compared to use of only one scale. A multiscale approach reduces the possibility of misleading results, which may occur through use of only one scale. A summary of the findings and interpretations that are possible from each of the spatial scales is presented, which provides a useful guide for future studies.

References

Abdalati, W. and Krabill, W. 1999. Calculation of ice velocities in the Jakobshavn Isbrae area using airborne laser altimetry. *Remote Sensing of Environment* 67, 194-204.

Aber, J. S. 1988: Ice-shoved hills of Saskatchewan compared with Mississippi Delta mudlumps: implications for glaciotectonic models. In Croot, D. G., editor, *Glaciotectonic Forms and Processes*, Rotterdam: Balkema, 1-9.

Aber, J. S. and Ber, A. 2007: *Glaciotectonism*. Oxford: Elsevier.

Alberta Geological Survey. 2009. Compilation of Alberta Research Council's Hydrogeology Maps [shapefile geospatial data] From: http://www.ags.gov.ab.ca/publications/DIG/ZIP/DIG_2009_0003.zip

Alley, R. B. 1989. Water-Pressure Coupling of Sliding and Bed Deformation: I. Water System *Journal of Glaciology* 119, 108-118.

Alley, R. B. 1991. Deforming-bed origin for southern Laurentide till sheets? *Journal of Glaciology* 37, 125.

Alley, R. B. 1993. In search of ice-stream sticky spots. *Journal of Glaciology* 39, 447-454.

Alley, R. B., Anandakrishnan, S., Dupont, T. K. and Parizek, B. R. 2004. Ice streams--fast, and faster? *Comptes Rendus Physique* 5, 723-734.

Alley, R. B., Blankenship, D. D., Bentley, C. R. and Rooney, S. T. 1986. Deformation of till beneath ice stream B, West Antarctica. *Nature* 322, 57-59.

Alley, R. B., Blankenship, D. D., Rooney, S. T. and Bently, C. R. 1987. Till beneath ice stream B 4. a coupled ice-till flow model. *Journal of Geophysical Research* 92, 8931-8940.

Alley, R. B., Clark, P. U., Huybrechts, P. and Joughin, I. 2005. Ice-Sheet and Sea-Level Changes. *Science* 310, 456-460.

Alley, R. B. and Whillans, I. M. 1991. Changes in the West Antarctic Ice Sheet. *Science* 254, 959-963.

Anandakrishnan, S. 2003. Dilatant till layer near the onset of streaming flow of Ice Stream C, West Antarctica, determined by AVO (amplitude vs offset) analysis. *Annals of Glaciology* 36, 283-286.

Anandakrishnan, S. and Alley, R. B. 1997. Stagnation of ice stream C, West Antarctica by water piracy. *Geophysical Research Letters* 24, 265-268.

Anandakrishnan, S., Blankenship, D. D., Alley, R. B. and Stoffa, P. L. 1998. Influence of subglacial geology on the position of a West Antarctic ice stream from seismic observations. *Nature* 394, 62-65.

Anderson, R. S. and Anderson, S. P. 2010: *Geomorphology: The mechanics and chemistry of landscapes*. Cambridge Cambridge University Press.

Anderson, J. B. and Fretwell, L. O. 2008. Geomorphology of the onset area of a paleo-ice stream, Marguerite Bay, Antarctic Peninsula. *Earth Surface Processes and Landforms* 33, 503-512.

Andreassen, K., Laberg, J. S. and Vorren, T. O. 2008. Seafloor geomorphology of the SW Barents Sea and its glaci-dynamic implications. *Geomorphology* 97, 157-177.

Andrews, J. T. and King, C. A. M. 1968. Comparative till fabrics and till fabric variability in a till sheet and a drumlin: a small-scale study. *Proceedings of the Yorkshire Geological and Polytechnic Society* 36, 435-461.

Andrews, J. T. and MacLean, B. 2003. Hudson Strait ice streams: a review of stratigraphy, chronology and links with North Atlantic Heinrich events. *Boreas* 32, 4-17.

Arch, J., Maltman, A. J. and Knipe, R. J. 1988. Shear-zone geometries in experimentally deformed clays: the influence of water content, strain rate and primary fabric. *Journal of Structural Geology* 10, 91-99.

Atre, S. R. and Bentley, C. R. 1993. Laterally varying basal conditions beneath Ice Streams B and C, West Antarctica. *Journal of Glaciology* 39, 507-514.

Ballantyne, C. K. and Benn, D. I. 1994. Paraglacial slope adjustment and resedimentation following recent glacier retreat, Fåbergstølsdalen, Norway. *Arctic and Alpine Research*, 255-269.

Ballantyne, C. K. and Harris, C. 1994: *The Periglaciation of Great Britain*. Cambridge: Cambridge University Press.

Bamber, J. L., Alley, R. B. and Joughin, I. 2007. Rapid response of modern day ice sheets to external forcing. *Earth and Planetary Science Letters* 257, 1-13.

Bamber, J. L., Vaughan, D. G. and Joughin, I. 2000. Widespread Complex Flow in the Interior of the Antarctic Ice Sheet. *Science* 287, 1248-1250.

Barker, A. J. 1998: *Introduction to Metamorphic Textures and Microstructures*. Cheltenham: Stanley Thornes.

Baroni, C. and Fasano, F. 2006. Micromorphological evidence of warm-based glacier deposition from the Ricker Hills Tillite (Victoria Land, Antarctica). *Quaternary Science Reviews* 25, 976-992.

Beaney, C. L. and Shaw, J. 2000. The subglacial geomorphology of southeast Alberta: evidence for subglacial meltwater erosion. *Canadian Journal of Earth Sciences* 37, 51-61.

Beem, L. H. J., Ken C.; Van Der Veen, C.J. 2010. Basal melt rates beneath Whillans Ice Stream, West Antarctica. *Journal of Glaciology* 56, 647-654.
Bell, R. E., Blankenship, D. D., Finn, C. A., Morse, D. L., Scambos, T. A., Brozena, J. M. and Hodge, S. M. 1998. Influence of subglacial geology on the onset of a West Antarctic ice stream from aerogeophysical observations. *Nature* 394, 58-62.
Bell, R. E., Studinger, M., Shuman, C. A., Fahnestock, M. A. and Joughin, I. 2007. Large subglacial lakes in East Antarctica at the onset of fast-flowing ice streams. *Nature* 445, 904-907.
Benedict, J. B. 1976. Frost creep and gelifluction features: A review. *Quaternary Research* 6, 55-76.
Benn, D. I. 1994. Fluted moraine formation and till genesis below a temperate valley glacier: Slettmarkbreen, Jotunheimen, southern Norway. *Sedimentology* 41, 279-292.
Benn, D. I. 1995. Fabric signature of subglacial till deformation, Breidamerkurjokull, Iceland. *Sedimentology* 42, 735-747.
Benn, D. I. 2004a: Clast morphology. In Evans, D. J. A. and Benn, D. I., editors, A p*ractical guide to the Study of Glacial Sediments*, London: Arnold, 78-92.
Benn, D. I. 2004b: Macrofabric. In Evans, D. J. A. and Benn, D. I., editors, *A practical guide to the study of glacial sediments*, London: Arnold, 93-144.
Benn, D. I., Ballantyne, C. K., 1993. The description and representation of particle shape. *Earth Surface Processes and Landforms* 18, 665-672.
Benn, D. I. and Evans, D. J. A. 1996. The interpretation and classification of subglacially-deformed materials. *Quaternary Science Reviews* 15, 23-52.
Benn, D. I. and Evans, D. J. A. 1998: *Glaciers & glaciation*. Arnold.
Benn, D. I. and Evans, D. J. A. 2006. Subglacial Megafloods: Outrageous Hypothesis or Just Outrageous? In Knight, P. G. editor, *Glacier Science And Environmental Change*, 42-50.
Benn, D. I. and Evans, D. J. A. 2010: *Glaciers and glaciation*. Arnold.
Bennett, M. R. 2003. Ice streams as the arteries of an ice sheet: their mechanics, stability and significance. *Earth-Science Reviews* 61, 309-339.
Bennett, M. R. and Glasser, N. F. 1996: *Glacial Geology: Ice Sheets and Landforms*. London: Wiley.
Bentley, C. R. 1987. Antarctic ice streams-A review. *Journal of Geophysical Research* 92, 8843-8858.
Bentley, C. R., Lord, N. and Liu, C. 1998. Radar reflections reveal a wet bed beneath stagnant Ice Stream C and a frozen bed beneath ridge BC, West Antarctica. *Journal of Glaciology* 44, 149-156.
Bertran, P. 1993. Deformation-induced microstructures in soils affected by mass movements. *Earth Surface Processes and Landforms* 18, 645-660.
Bertran, P. and Texier, J. P. 1999. Facies and microfacies of slope deposits. *Catena* 35, 99-121.
Bindschadler, R., Vornberger, P., Blankenship, D., Scambos, T. and Jacobel, R. 1996. Surface velocity and mass balance of Ice Streams D and E, West Antarctica. *Journal of Glaciology* 42, 461-475.
Bindschadler, R. A. and Scambos, T. A. 1991. Satellite-image-derived velocity field of an Antarctic Ice Stream. *Science* 252, 242-246.
Bingham, R. G. and Siegert, M. J. 2007. Radar-derived bed roughness characterization of Institute and Moller ice streams, West Antarctica, and comparison with Siple Coast ice streams. *Geophysical Research Letters* 34, L21504.
Blank, R. R. and Fosberg, M. A. 1990: Micromorphology and classification of secondary calcuim carbonate accumulations that surround or occur on the undersides of coarse fragments in Idaho (U.S.A). In Douglas, L. A. editor, *Soil micromorphology: a basic and applied science*: Elsevier, 341-346.
Blankenship, D. D., Bentley, C. R., Rooney, S. T. and Alley, R. B. 1986. Seismic measurements reveal a saturated porous layer beneath an active Antarctic ice stream. *Nature* 322, 54-57.
Blankenship, D. D., Bentley, C. R., Rooney, S. T. and Alley, R. B. 1987. Till beneath ice stream B. I-Properties derived from seismic travel times. II-Structure and continuity. III-Till deformation-Evidence and implications. IV-A coupled ice-till flow model. *Journal of Geophysical Research* 92, 8903-8940.
Blott, S. J. and Pye, K. 2001. GRADISTAT: a grain size distribution and statistics package for the analysis of unconsolidated sediments. *Earth Surface Processes and Landforms* 26, 1237-1248.
Bougamont, M., Tulaczyk, S. and Joughin, I. 2003. Numerical investigations of the slow-down of Whillans Ice Stream, West Antarctica: is it shutting down like Ice Stream C? *Annals of Glaciology* 37, 239-246.
Boulton, G. S. and Hagdorn, M. 2006. Glaciology of the British Isles Ice Sheet during the last glacial cycle: form, flow, streams and lobes. *Quaternary Science Reviews* 25, 3359-3390.
Boulton, G. S. 1978. Boulder shapes and grain-size distributions of debris as indicators of transport paths through a glacier and till genesis. *Sedimentology* 25, 773-799.
Boulton, G. S. 1979. Processes of glacier erosion on different substrata. *Journal of Glaciology* 23, 15-38.
Boulton, G. S. 1986. Geophysics: A paradigm shift in glaciology? *Nature* 322, 18-18.
Boulton, G. S. 1987: A theory of drumlin formation by subglacial sediment deformation. In Menzies, J. and Rose, J., editors, *Drumlin symposium* Rotterdam: Balkema, 25-80.

Boulton, G. S. 1996a. The origin of till sequences by subglacial sediment deformation beneath mid-latitude ice sheets. *Annals of Glaciology* 22, 75-84.
Boulton, G. S. 1996b. Theory of glacial erosion, transport and deposition as a consequence of subglacial sediment deformation. *Journal of Glaciology* 42, 43-62.
Boulton, G. S. and Clark, C. D. 1990. A highly mobile Laurentide ice sheet revealed by satellite images of glacial lineations. *Nature* 346, 813-817.
Boulton, G. S., Dobbie, K. E. and Zatsepin, S. 2001. Sediment deformation beneath glaciers and its coupling to the subglacial hydraulic system. *Quaternary International* 86, 3-28.
Boulton, G. S. and Hindmarsh, R. C. A. 1987. Sediment deformation beneath glaciers: rheology and geological consequeces. *Journal of Geophysical Research* 92, 9059-9082.
Boulton, G. S. and Jones, A. S. 1979. Stability of temperate ice caps and ice sheets resting on beds of deformable sediment. *Journal of Glaciology* 24.
Bradwell, T. 2005. Bedrock megagrooves in Assynt, NW Scotland. *Geomorphology* 65, 195-204.
Bradwell, T., Stoker, M. and Larter, R. 2007. Geomorphological signature and flow dynamics of The Minch palaeo-ice stream, northwest Scotland. *Journal of Quaternary Science* 22, 609-617.
Brewer, R. 1976. Fabric and mineral analysis of soils. New York, RE Krieger, 482p.
Briner, J. 2007. Supporting evidence from the New York drumlin field that elongate subglacial bedforms indicate fast ice flow. *Boreas* 36, 2, 143-147.
British Geological Survey (1977), Quaternary Geology map of the UK, scale: 1:625000, [shapefile geospatial data], accessed using: Edina Geology Digimap Service, http://edina.ac.uk/digimap, downloaded: May 2008
British Geological Survey (2007), Bedrock Geology map of the UK, scale: 1:625000, [shapefile geospatial data], accessed using: Edina Geology Digimap Service, http://edina.ac.uk/digimap, downloaded: May 2008
Burke, M. J. 1969. The Forth Valley: an ice-moulded lowland. *Transactions of the Institute of British Geographers*, 51-59.
Canals, M., Urgeles, R. and Calafat, A. M. 2000. Deep sea-floor evidence of past ice streams off the Antarctic Peninsula. *Geology* 28, 31-34.
Carr, S. J. 1999. The micromorphology of Last Glacial Maximum sediments in the Southern North Sea. *Catena* 35, 123-145.
Carr, S. J. 2001. Micromorphological criteria for discriminating subglacial and glacimarine sediments: evidence from a contemporary tidewater glacier, Spitsbergen. *Quaternary International* 86, 71-79.
Carr, S. J. 2004. Micro-scale features and structures. In *Evans D. J. A, Benn D. I. editors. A Practical Guide to the Study of Glacial Sediments,. Arnold: London*, 115–144.
Carr, S. J. and Goddard, M. A. 2007. Role of particle size in till-fabric characteristics: systematic variation in till fabric from Vestari-Hagafellsjökull, Iceland. *Boreas* 36, 371-385.
Carr, S. J., Holmes, R., van der Meer, J. J. M. and Rose, J. 2006. The Last Glacial Maximum in the North Sea Basin: micromorphological evidence of extensive glaciation. *Journal of Quaternary Science* 21, 131-153.
Carr, S. J. and Lee, J. A. 1998. Thin-section production of diamicts; problems and solutions. *Journal of Sedimentary Research* 68, 217.
Carr, S. J. and Rose, J. 2003. Till fabric patterns and significance: particle response to subglacial stress. *Quaternary Science Reviews* 22, 1415-1426.
Carr, S. J., Haflidason. H. and Sejrup. H. P. 2000. Micromorphological evidence supporting Late Weichselian glaciation of the Northern North Sea. *Boreas* 29, 315-328.
Chaolu, Y. and Zhijiu, C. 2001. Subglacial deformation: evidence from microfabric studies of particles and voids in till from the upper Urumqi river valley, Tien Shan, China. *Journal of Glaciology* 47, 607-612.
Christoffersen, P. and Tulaczyk, S. 2003a. Signature of palaeo-ice-stream stagnation: till consolidation induced by basal freeze-on. *Boreas* 32, 114-129.
Christoffersen, P. and Tulaczyk, S. 2003b. Response of subglacial sediments to basal freezeon: 1. Theory and comparison to observations from beneath the West Antarctic Ice Sheet. *Journal of Geophysical Research* 108, 2222.
Clapperton, C. M. 1968. Channels Formed by the Superimposition of Glacial Meltwater Streams, with Special Reference to the East Cheviot Hills, North-East England. *Geografiska Annaler. Series A, Physical Geography* 50, 207-220.
Clapperton, C. M. 1970a. The Evidence for a Cheviot Ice Cap. *Transactions of the Institute of British Geographers*, 115-127.
Clapperton, C. M. 1970b. Channels Formed by the Superimposition of Meltwater Streams. A Reply to Comments by Thorsten Stenborg, 1969: Channel Formation and Glacier Drainage. *Geografiska Annaler. Series A, Physical Geography* 52, 94-95.

Clark, C. D. 1999. Glaciodynamic context of subglacial bedform generation and preservation. *Annals of Glaciology* 28, 23-32.
Clark, C., Evans, D., Khatwa, A., Bradwell, T., Jordan, C., Marsh, S., Mitchell, W. and Bateman, M. 2004. Map and GIS database of glacial landforms and features related to the last British Ice Sheet. *Boreas* 33, 359-375.
Clark, C. D. 1993. Mega-scale glacial lineations and cross-cutting ice-flow landforms. *Earth Surface Processes and Landforms* 18, 1–29.
Clark, C. D., Hughes, A. L. C., Greenwood, S. L., Spagnolo, M. and Ng, F. S. L. 2009. Size and shape characteristics of drumlins, derived from a large sample, and associated scaling laws. *Quaternary Science Reviews* 28, 677-692.
Clark, C. D., Knight, J. K. and Gray, J. T. 2000. Geomorphological reconstruction of the Labrador Sector of the Laurentide Ice Sheet. *Quaternary Science Reviews* 19, 1343-1366.
Clark, C. D. and Stokes, C. R. 2001. Extent and basal characteristics of the M'Clintock Channel Ice Stream. *Quaternary International* 86, 81-101.
Clark, C. D. and Stokes, C. R. 2003: Palaeo-ice stream landsystem. In Evans, D. J. A., editor, *Glacial Landsystems*, London: Arnold, 204-227.
Clark, C. D., Tulaczyk, S. M., Stokes, C. R. and Canals, M. 2003. A groove-ploughing theory for the production of mega-scale glacial lineations, and implications for ice-stream mechanics. *Journal of Glaciology* 49, 240-256.
Clark, P. U. and Walder, J. S. 1994. Subglacial drainage, eskers, and deforming beds beneath the Laurentide and Eurasian ice sheets. *Bulletin of the Geological Society of America* 106, 304-314.
Clarke, G. K. C. 1987. Fast glacier flow: Ice streams, surging, and tidewater glaciers. *Journal of Geophysical Research* 92, 8835-8842.
Clarke, G. K. C. 2005. Subglacial Processes. *Annual Review of Earth and Planetary Sciences* 33, 247-276.
Clarke, G. K. C., Leverington, D. W., Teller, J. T., Dyke, A. S. and Marshall, S. J. 2005. Fresh arguments against the Shaw megaflood hypothesis. A reply to comments by David Sharpe on 'Paleohydraulics of the last outburst flood from glacial Lake Agassiz and the 8200 BP cold event'. *Quaternary Science Reviews* 24, 1533-1541.
Clarke, T. S. and Echelmeyer, K. 1996. Seismic-reflection evidence for a deep subglacial trough beneath Jakobshavns Isbræ, West Greenland. *Journal of Glaciology* 42, 219-232.
Clayton, C. R. I., Abbireddy, C. O. R. and Schiebel, R. 2009. A method of estimating the form of coarse particulates. *Géotechnique*, 1-9.
Common, R. 1954. The geomorphology of the east Cheviot area. *Scottish Geographical Journal* 70, 124-138.
Courty, M. A., Goldberg, P., McPhail, R.,. 1989: *Soils and micromorphology in archaeology*. Cambrigde, UK: Cambridge University Press.
Croot, D. G. and Sims, P. C. 1996. Early stages of till genesis: an example from Fanore, County Clare, Ireland. *Boreas* 25, 37-46.
Dalrymple, J. B. and Jim, C. Y. 1984. Experimental study of soil microfabrics induced by isotropic stresses of wetting and drying. *Geoderma* 34, 43-68.
Davis, G. H., Bump, A. P., García, P. E. and Ahlgren, S. G. 2000. Conjugate Riedel deformation band shear zones. *Journal of Structural Geology* 22, 169-190.
De Angelis, H. 2007. Glacial geomorphology of the east-central Canadian Arctic. *Journal of Maps* v2007, 323-341.
De Angelis, H. and Kleman, J. 2005. Palaeo-ice streams in the northern Keewatin sector of the Laurentide ice sheet. *Annals of Glaciology* 42, 135-144.
De Angelis, H. and Kleman, J. 2007. Palaeo-ice streams in the Foxe/Baffin sector of the Laurentide Ice Sheet. *Quaternary Science Reviews* 26, 1313-1331.
De Angelis, H. D. and Kleman, J. 2008. Palaeo-ice-stream onsets: examples from the north-eastern Laurentide Ice Sheet. *Earth Surface Processes and Landforms* 33, 560-572.
de Smith, M. J., Goodchild, M. F. and Longley, P. A. 2012: Geospatial analysis: a comprehensive guide to principles, techniques and software tools. (http://www.spatialanalysisonline.com/)
Derbyshire, E. 1961. Subglacial Col Gullies and the Deglaciation of the North-East Cheviots. *Transactions and Papers (Institute of British Geographers)*, 31-46.
Dockal, J. A. (2003). Grain Morphology Roundness, Surface Features, and Sphericity of Grains. Retrieved March 2010, from http://people.uncw.edu/dockal/gly312/grains/grains.htm.
Domack, E., Amblàs, D., Gilbert, R., Brachfeld, S., Camerlenghi, A., Rebesco, M., Canals, M. and Urgeles, R. 2006. Subglacial morphology and glacial evolution of the Palmer deep outlet system, Antarctic Peninsula. *Geomorphology* 75, 125-142.
Dowdeswell, J. A., Cofaigh, C. O. and Pudsey, C. J. 2004. Thickness and extent of the subglacial till layer beneath an Antarctic paleo-ice stream. *Geology* 32, 13-16.

Dowdeswell, J. A. and Sharp, M. J. 1986. Characterization of pebble fabrics in modern terrestrial glacigenic sediments. *Sedimentology* 33, 699-710.
Dunlop, P. and Clark, C. D. 2006. The morphological characteristics of ribbed moraine. *Quaternary Science Reviews* 25, 1668-1691.
Dyke, A. S., Moore, A. and Robertson, K. 2003: Deglaciation of North America. Geological Survey of Canada Open File 1574.
Dyke, A. S. and Morris, T. F. 1988. Drumlin fields, dispersal trains, and ice streams in Arctic Canada. *Canadian Geographer* 32, 86–90.
Dyke, A. S., Morris, T. F., Green, D. E. C. and England, J. H. 1992. Quaternary geology of Prince of Wales Island, central Canadian Arctic. *Geological Survey of Canada, Memoir* 433.
Echelmeyer, K. A. and Harrison, W. D. 1999. Ongoing margin migration of Ice Stream B, Antarctica. *Journal of Glaciology* 45, 361-369.
Echelmeyer, K. A., Harrison, W. D., Larsen, C. and Mitchell, J. E. 1994. The role of the margins in the dynamics of an active ice stream. *Journal of Glaciology* 40, 527-538.
Engelhardt, H., Humphrey, N., Kamb, B. and Fahnestock, M. 1990. Physical Conditions at the Base of a Fast Moving Antarctic Ice Stream. *Science* 248, 57-59.
Engelhardt, H. and Kamb, B. 1997. Basal hydraulic system of a West Antarctic ice stream: constraints from borehole observations. *Journal of Glaciology* 43, 207-230.
Engelhardt, H. and Kamb, B. 1998. Basal sliding of Ice Stream B, West Antarctica. *Journal of Glaciology* 44, 223-230.
Environment Agency. 2012. Aquifer map of England, Accessed 6th September 2012. From: http://maps.environment-agency.gov.uk/wiyby/wiybyController?x=357683.0&y=355134.0&scale=1&layerGroups=default&ep=map&textonly=off&lang=_e&topic=groundwater
Evans, A. J. 1998: The causes and implications of microstructures in glacial sediments. Thesis (PhD). The University of Leeds.
Evans, D. J. A. 1991. A gravel/diamicton lag on the south Albertan prairies, Canada: Evidence of bed armoring in early deglacial sheet-flood/spillway courses. *Geological Society of America Bulletin* 103, 975-982.
Evans, D. J. A. 1994: The stratigraphy and sedimentary structures associated with complex subglacial thermal regimes at the south-west margin of the Laurentide ice sheet, southern Alberta, Canada. In Warren, W. P. and Croot, D. G., editors, *Formation and deformation of glacial deposits*, Rotterdam: Balkema, 203-220.
Evans, D. J. A. 1996. A possible origin for a mega-fluting complex on the southern Alberta prairies, Canada. *Zeitschrift für Geomorphologie, Supplement* 106, 125–148.
Evans, D. J. A. 2003: *Glacial Landsystems*. Arnold.
Evans, D. J. A. and Benn, D. I. 2004. Facies description and the logging of sedimentary exposures. In Evans, D. J. A. and Benn, D. I. editors, *A Practical Guide to the Study of Glacial Sediments. Arnold*, 11–50.
Evans, D. J. A. and Campbell, I. A. 1992. Glacial and postglacial stratigraphy of Dinosaur Provincial Park and surrounding plains, southern Alberta, Canada. *Quaternary Science Reviews* 11, 535-555.
Evans, D. J. A. and Campbell, I. A. 1995. Quaternary stratigraphy of the buried valleys of the lower Red Deer River, Alberta, Canada. *Journal of Quaternary Science* 10, 123-148.
Evans, D. J. A., Clark, C. D. and Mitchell, W. A. 2005. The last British Ice Sheet: A review of the evidence utilised in the compilation of the Glacial Map of Britain. *Earth-Science Reviews* 70, 253-312.
Evans, D. J. A., Clark, C. D. and Rea, B. R. 2008. Landform and sediment imprints of fast glacier flow in the southwest Laurentide Ice Sheet. *Journal of Quaternary Science* 23, 249-272.
Evans, D. J. A. and Cofaigh, C. 2003. Depositional evidence for marginal oscillations of the Irish Sea ice stream in southeast Ireland during the last glaciation. *Boreas* 32, 76-101.
Evans, D. J. A., Phillips, E. R., Hiemstra, J. F. and Auton, C. A. 2006a. Subglacial till: Formation, sedimentary characteristics and classification. *Earth-Science Reviews* 78, 115-176.
Evans, D. J. A., Rea, B. R. and Benn, D. I. 1998. Subglacial deformation and bedrock plucking in areas of hard bedrock. *Glacial Geology and Geomorphology* 4, 1-22.
Evans, D. J. A., Rea, B. R., Hiemstra, J. F. and O´ Cofaigh, C. 2006b. A critical assessment of subglacial mega-floods: a case study of glacial sediments and landforms in south-central Alberta, Canada. *Quaternary Science Reviews* 25, 1638-1667.
Evans, D. J. A., Rea, B. R., and Lemmen, D. S. 1999. Glacial landsystems of the southwest Laurentide Ice Sheet: modern Icelandic analogues. *Journal of Quaternary Science* 14, 673-691.
Evans, D. J. A. and Twigg, D. R. 2002. The active temperate glacial landsystem: a model based on Breiðamerkurjökull and Fjallsjökull, Iceland. *Quaternary Science Reviews* 21, 2143-2177.
Evenson, E. B. 1971: Macro-and Microfabric of Till and the Genesis of Glacial Landforms in Jefferson County, Wisconsin. Ohio State University Press, 345.

Everest, J., Bradwell, T. and Golledge, N. 2005. Subglacial landforms of the Tweed Palaeo-Ice Stream. *Scottish Geographical Journal* 121, 163-173.
Eyles, C. H. 1988. A model for striated boulder pavement formation on glaciated, shallow-marine shelves; an example from the Yakataga Formation, Alaska. *Journal of Sedimentary Research* 58, 62-71.
Eyles, N., Boyce, J. I. and Barendregt, R. W. 1999. Hummocky moraine: sedimentary record of stagnant Laurentide Ice Sheet lobes resting on soft beds. *Sedimentary Geology* 123, 163-174.
Eyles, N., Eyles, C. H. and Miall, A. D. 1983. Lithofacies types and vertical profile models; an alternative approach to the description and environmental interpretation of glacial diamict and diamictite sequences. *Sedimentology* 30, 393-410.
Eyles, N. and Lazorek, M. 2007: Glacial Landforms, Sediments | Glacigenic Lithofacies. In Scott, A. E., editor, *Encyclopedia of Quaternary Science*, Oxford: Elsevier, 920-932.
Eyles, N., McCabe, A. M. and Bowen, D. Q. 1994. The stratigraphic and sedimentological significance of Late Devensian Ice Sheet surging in Holderness, Yorkshire, U.K. *Quaternary Science Reviews* 13, 727-759.
Finlayson, A., Merritt, J., Browne, M., Merritt, J., McMillan, A. and Whitbread, K. 2010. Ice sheet advance, dynamics, and decay configurations: evidence from west central Scotland. *Quaternary Science Reviews* 29, 969-988.
Fischer, U. H. and Clarke, G. K. C. 2001. Review of subglacial hydro-mechanical coupling: Trapridge Glacier, Yukon Territory, Canada. *Quaternary International* 86, 29-43.
Fisher, T. G. and Shaw, J. 1992. A depositional model for Rogen moraine, with examples from the Avalon Peninsula, Newfoundland. *Canadian Journal of Earth Sciences* 29, 669-686.
Fowler, A. C. 2000. An instability mechanism for drumlin formation. *Geological Society London Special Publications* 176, 307.
Fowler, A. C. 2003. On the rheology of till. *Annals of Glaciology* 37, 55-59.
French, H. 2007: *The Periglacial Environment*. Chichester: Wiley.
Fricker, H. A., Scambos, T., Bindschadler, R. and Padman, L. 2007. An active subglacial water system in West Antarctica mapped from space. *Science* 315, 1544.
Fullerton, D. S., Colton, R. B. and Bush, A. 2004: Limits of mountain and continental glaciations east of the Continental Divide in northern Montana and north-western North Dakota, U.S.A. In Jürgen Ehlers and Gibbard, P. L., editors, *Quaternary glaciations: extent and chronology, Part 2*
Gades, A. M., Raymond, C. F., Conway, H. and Jacobel, R. W. 2000. Bed properties of Siple Dome and adjacent ice streams, West Antarctica, inferred from radio-echo sounding measurements. *Journal of Glaciology* 46, 88-94.
Gale, S. J. and Hoare, P. G. 1991: *Quaternary sediments*. Belhaven Press New York.
Gazetteer for Scotland http://www.scottish-places.info/ Visited between June 2008 and September 2011
Geikie, A. 1865: The Scenery and Geology of Scotland. London, Macmillan & Co.
Gordon, S. J. and Dorn, R. I. 2004: Rind, Weathering. In Goudie, A., editor, *Encyclopedia of geomorphology, Volume 2*, London: Routledge, 853 - 855.
Graham, A. G. C., Larter, R. D., Gohl, K., Hillenbrand, C. D., Smith, J. A. and Kuhn, G. 2009. Bedform signature of a West Antarctic palaeo-ice stream reveals a multi-temporal record of flow and substrate control. *Quaternary Science Reviews* 28, 2774-2793.
Graham, A. G. C., Lonergan, L. and Stoker, M. S. 2007. Evidence for Late Pleistocene ice stream activity in the Witch Ground Basin, central North Sea, from 3D seismic reflection data. *Quaternary Science Reviews* 26, 627-643.
Graham, D. J. and Midgley, N. G. 2000. Graphical representation of particle shape using triangular diagrams: an Excel spreadsheet method. *Earth Surface Processes and Landforms* 25, 1473-1477.
Gray, L., Joughin, I., Tulaczyk, S., Spikes, V. B., Bindschadler, R. and Jezek, K. 2005. Evidence for subglacial water transport in the West Antarctic Ice Sheet through three-dimensional satellite radar interferometry. *Geophysical Research Letters* 32. L03501
Greenwood, S. L. Clark, C. D. and Hughes, A. L. C. 2007. Formalising an inversion methodology for reconstructing ice-sheet retreat patterns from meltwater channels: application to the British Ice Sheet. *Journal of Quaternary Science* 22, 637-645.
Gregory, J. W. 1915. The tweed valley and its relations to the Clyde and Solway. *Scottish Geographical Journal* 31, 478-486.
Greve, R. 2000. On the Response of the Greenland Ice Sheet to Greenhouse Climate Change. *Climatic Change* 46, 289-303.
Gudmundsson, G. and Jenkins, A. 2009. Ice-flow velocities on Rutford Ice Stream, West Antarctica, are stable over decadal timescales. *Journal of Glaciology* 55, 339-344.
Gudmundsson, G. H., Raymond, C. F. and Bindschadler, R. 1998. The origin and longevity of flow-stripes on Antarctic ice streams. *Annals of Glaciology* 27, 145-152.
Gunn, W., Clough, C. T. and Watts, W. W. 1895: *The Geology of Part of Northumberland, Including the Country Between Wooler and Coldstream*. For Her Majesty's Stationery Office.

Haldorsen, S. 1981. Grain-size distribution of subglacial till and its realtion to glacial crushing and abrasion. *Boreas* 10, 91-105.
Ham, N. R. and Mickelson, D. M. 1994. Basal till fabric and deposition at Burroughs Glacier, Glacier Bay, Alaska. *Bulletin of the Geological Society of America* 106, 1552-1559.
Hamilton, W. N., Price, M. C. and Langenberg, C. W. 1999: Geological Map of Alberta *Alberta Geological Survey, Alberta Energy and Utilities Board, Map No. 236*.
Harris, C. 1990: Micromorphology and microfabrics of sorted circles, Front Range, Colorado, U.S.A. In Burgess, M. M., Harry, D. G. and Sego, D. C., editors, *Proceedings of the 5th Canadian Permafrost Conference*, Ottawa: National Research Council of Canada, 89-94.
Harris, C. 1998. The micromorphology of paraglacial and periglacial slope deposits: a case study from Morfa Bychan, West Wales, UK. *Journal of Quaternary Science* 13, 73-84.
Harris, C. 2007: Periglacial Landforms: Slope Deposits and Forms. In Elias, S., A. , editor, *Encyclopedia of Quaternary Science*, Oxford: Elsevier, 2207-2217.
Harris, C., Smith, J. S., Davies, M. C. R. and Rea, B. 2008. An investigation of periglacial slope stability in relation to soil properties based on physical modelling in the geotechnical centrifuge. *Geomorphology* 93, 437-459.
Harrison, J. C. St-Onge, M. R. Petrov, O. Strelnikov, S. Lopatin, B. Wilson, F. Tella, S. Paul, D. Lynds, T. Shokalsky, S. Hults, C. Bergman, S. Jepsen, H F. Solli, A. 2008. Geological map of the Arctic. Geological Survey of Canada, Open File, 5816
Hart, J., K. . 1994. Till fabric associated with deformable beds. *Earth Surface Processes and Landforms* 19, 15-32.
Hart, J. K. 1995. Subglacial erosion, deposition and deformation associated with deformable beds. *Progress in Physical Geography* 19, 173-191.
Hart, J. K. 1997. The relationship between drumlins and other forms of subglacial glaciotectonic deformation. *Quaternary Science Reviews* 16, 93-107.
Hart, J. K. 1999. Identifying fast ice flow from landform assemblages in the geological record: a discussion. *Annals of Glaciology* 28, 59-66.
Hart, J. K. 2007. An investigation of subglacial shear zone processes from Weybourne, Norfolk, UK. *Quaternary Science Reviews* 26, 2354-2374.
Hart, J. K., Khatwa, A. and Sammonds, P. 2004. The effect of grain texture on the occurrence of microstructural properties in subglacial till. *Quaternary Science Reviews* 23, 2501-2512.
Hättestrand, C. 1997. Ribbed moraines in Sweden - distribution pattern and palaeoglaciological implications. *Sedimentary Geology* 111, 41-56.
Hättestrand, C. and Kleman, J. 1999. Ribbed moraine formation. *Quaternary Science Reviews* 18, 43-61.
Hess, D., P,. and Briner, J., P,. . 2009. Geospatial analysis of controls on subglacial bedform morphometry in the New York Drumlin Field - implications for Laurentide Ice Sheet dynamics. *Earth Surface Processes and Landforms* 34, 1126–1135.
Hicock, S. R. 1991. On subglacial stone pavements in till. *The Journal of Geology*, 607-619.
Hicock, S. R. 1992. Lobal interactions and rheologic superposition in subglacial till near Bradtville, Ontario, Canada. *Boreas* 21, 73-88.
Hicock, S. R. and Dreimanis, A. 1992. Deformation till in the Great Lakes region: implications for rapid flow along the south-central margin of the Laurentide Ice Sheet. *Canadian Journal of Earth Sciences* 29, 1565-1579.
Hicock, S. R. and Fuller, E. A. 1995. Lobal interactions, rheologic superposition, and implications for a Pleistocene ice stream on the continental shelf of British Columbia. *Geomorphology* 14, 167-184.
Hicock, S. R., Goff, J. R., Lian, O. B. and Little, E. C. 1996. On the interpretation of subglacial till fabric. *Journal of Sedimentary Research* 66, 928-934.
Hiemstra, J. F., Evans, D. J. A. and Ó Cofaigh, C. 2007. The role of glacitectonic rafting and comminution in the production of subglacial tills: examples from southwest Ireland and Antarctica. *Boreas* 36, 386-399.
Hiemstra, J. F., Evans, D. J. A., Scourse, J. D., McCarroll, D., Furze, M. F. A. and Rhodes, E. 2006. New evidence for a grounded Irish Sea glaciation of the Isles of Scilly, UK. *Quaternary Science Reviews* 25, 299-309.
Hiemstra, J. F. and Rijsdijk, K. F. 2003. Observing artificially induced strain: implications for subglacial deformation. *Journal of Quaternary Science* 18, 373-383.
Hiemstra, J. F., Rijsdijk, K. F., Evans, D. J. A. and van der Meer, J. J. M. 2005. Integrated micro and macro scale analyses of Last Glacial Maximum Irish Sea Diamicts from Abermawr and Traeth y Mwnt, Wales, UK. *Boreas* 34, 61-74.
Hindmarsh, R. C. 1997. Deforming beds: Viscous and plastic scales of deformation. *Quaternary Science Reviews* 16, 1039-1056.
Hindmarsh, R. C. 1998a. Drumlinization and drumlin-forming instabilities: viscous till mechanisms. *Journal of Glaciology* 44, 293-314.

Hindmarsh, R. C. A. 1998b. Ice-stream surface texture, sticky spots, waves and breathers: the coupled flow of ice, till and water. *Journal of Glaciology* 44, 589-614.
Hindmarsh, R. C. and Stokes, C. R. 2008. Formation mechanisms for ice-stream lateral shear margin moraines. *Earth Surface Processes and Landforms* 33, 610.
Hodgson, D. A. 1994. Episodic ice streams and ice shelves during retreat of the northwesternmost sector of the Late Wisconsinan Laurentide Ice Sheet over the central Canadian Arctic archipelago. *Boreas* 23, 14–28.
Hoey, T. 2004: The size of sedimentary particles. In Evans, D. J. A. and Benn, D. I., editors, *A Practical Guide to the Study of Glacial Sediments*, London: Arnold, 51-76.
Holland, D. M., Thomas, R. H., De Young, B., Ribergaard, M. H. and Lyberth, B. 2008. Acceleration of Jakobshavn Isbrae triggered by warm subsurface ocean waters. *Nature Geoscience* 1, 659-664.
Hollingworth, S. E. 1931. The glaciation of western Edenside and adjoining areas and the drumlins of Edenside and the Solway basin. *Quarterly Journal of the Geological Society* 87, 281.
Hooke, R., Hanson, B., Iverson, N. R., Jansson, P. and Fischer, U. H. 1997. Rheology of till beneath Storglaciären, Sweden. *Journal of Glaciology* 43, 172-179.
Hooke, R. L. and Iverson, N. R. 1995. Grain-size distribution in deforming subglacial tills; role of grain fracture. *Geology* 23, 57-60.
How Spatial Autocorrelation (Global Moran's I) works. (2011) Accessed 5th December 2011. From http://help.arcgis.com/en/arcgisdesktop/10.0/help/index.html#/How_Spatial_Autocorrelation_Global_Moran_s_I_works/005p0000000t000000/
Hooyer, T. S. and Iverson, N. R. 2000. Clast-fabric development in a shearing granular material: Implications for subglacial till and fault gouge. *Geological Society of America Bulletin* 112, 683-692.
Hooyer, T. S., Iverson, N. R., Lagroix, F. and Thomason, J. F. 2008. Magnetic fabric of sheared till: A strain indicator for evaluating the bed deformation model of glacier flow. *Journal of Geophysical Research* 113, F02002.
Hubbard, A., Bradwell, T., Golledge, N., Hall, A., Patton, H., Sugden, D., Cooper, R. and Stoker, M. 2009. Dynamic cycles, ice streams and their impact on the extent, chronology and deglaciation of the British-Irish ice sheet. *Quaternary Science Reviews* 28, 758-776.
Intermap Technologies. NEXTMap Britain: Digital terrain mapping of the UK, [Internet]. NERC Earth Observation Data Centre, 2007, Available from http://badc.nerc.ac.uk/view/neodc.nerc.ac.uk__ATOM__dataent_11658383444211836
Iverson, N. R., Hooyer, T. S., Fischer, U. H., Cohen, D., Moore, P. L., Jackson, M., Lappegard, G. and Kohler, J. 2007. Soft-bed experiments beneath Engabreen, Norway: regelation infiltration, basal slip and bed deformation. *Journal of Glaciology* 53, 323.
Iverson, N. R., Hooyer, T. S., Thomason, J. F., Graesch, M, and Shumway, J. R.. 2008. The experimental basis for interpreting particle and magnetic fabrics of sheared till. *Earth Surface Processes and Landforms* 33, 627-645.
Iverson, R. M., Logan, M., LaHusen, R. G. and Berti, M. 2010. The perfect debris flow? Aggregated results from 28 large-scale experiments. *Journal of Geophysical Research.* 115, F03005.
Jackson , L. E., Phillips, F. M., Shimamura, K. and Little, E. C. 1997. Cosmogenic 36Cl dating of the Foothills erratics train, Alberta, Canada. *Geology* 25, 195-198.
Jacobson, H. P. and Raymond, C. F. 1998. Thermal effects on the location of ice stream margins. *Journal of Geophysical Research-Solid Earth* 103, 12111-12122.
Jansson, K. N., Stroeven, A. P. and Kleman, J. 2003. Configuration and timing of Ungava Bay ice streams, Labrador-Ungava, Canada. *Boreas* 32, 256-262.
Jeffery, G. B. 1922. The Motion of Ellipsoidal Particles Immersed in a Viscous Fluid. *Proceedings of the Royal Society of London. Series A, Containing Papers of a Mathematical and Physical Character (1905-1934)* 102, 161-179.
Jenness, J. 2007. Longest Straight Lines Across Interior of Polygons. ESRI Downloads.
Jenness, J. 2012. DEM Surface Tools. Jenness Enterprises. Accessed 24th July 2012. From: http://www.jennessent.com/arcgis/surface_area.htm
Jennings, C. E. 2006. Terrestrial ice streams--a view from the lobe. *Geomorphology* 75, 100-124.
Jørgensen, F. and Piotrowski, J. A. 2003. Signature of the Baltic Ice Stream on Funen Island, Denmark during the Weichselian glaciation. *Boreas* 32, 242-255.
Joughin, I., Abdalati, W. and Fahnestock, M. 2004a. Large fluctuations in speed on Greenland's Jakobshavn Isbrae glacier. *Nature* 432, 608-610.
Joughin, I., Bamber, J. L., Scambos, T., Tulaczyk, S., Fahnestock, M. and MacAyeal, D. R. 2006. Integrating satellite observations with modelling: basal shear stress of the Filcher-Ronne ice streams, Antarctica. *Philosophical Transactions of the Royal Society A: Mathematical, Physical and Engineering Sciences* 364, 1795-1814.

Joughin, I., Fahnestock, M., MacAyeal, D., Bamber, J. and Goginenei, P. 2001. Observation and analysis of ice flow in the largest Greenland ice stream. *Journal of Geophysical Research. D. Atmospheres* 106, 34.
Joughin, I., Gray, L., Bindschadler, R., Price, S., Morse, D., Hulbe, C., Mattar, K. and Werner, C. 1999. Tributaries of West Antarctic Ice Streams Revealed by RADARSAT Interferometry. *Science* 286, 283-286.
Joughin, I., MacAyeal, D. R. and Tulaczyk, S. 2004b. Basal shear stress of the Ross ice streams from control method inversions. *J. Geophys. Res* 109.
Joughin, I. and Tulaczyk, S. 2002. Positive Mass Balance of the Ross Ice Streams, West Antarctica. *Science* 295, 476-480.
Joughin, I., Tulaczyk, S., Bindschadler, R. and Price, S. F. 2002. Changes in West Antarctic ice stream velocities: Observation and analysis. *Journal of Geophysical Research* 107, 2289.
Kalvans, A. and Saks, T. 2008. Two-dimensional apparent microfabric of the basal Late Weichselian till and associated shear zone: case study from western Latvia. *Estonian Journal of Earth Sciences* 57, 241-255.
Kamb, B. 1991. Rheological nonlinearity and flow instability in the deforming bed mechanism of ice stream motion. *Journal of Geophysical Research* 96, 16585-16595.
Kamb, B. 2001. Basal zone of the West Antarctic ice streams and its role in lubrication of their rapid motion. *The West Antarctic Ice Sheet: Behavior and Environment* 77, 157–199.
Kavanaugh, J. L. and Clarke, G. K. C. 2006. Discrimination of the flow law for subglacial sediment using in situ measurements and an interpretation model. *J. Geophys. Res.* 111, F01002.
Kemp, R. A. 2007: Palaeosols and wind-blown sediments. Soil Micromorphology. In Elias, S. A., editor, *Encyclopedia of Quaternary Science*, Oxford: Elsevier, 2103-2114.
Kendall, P. F. and Muff, H. B. 1901. VIII. Evidences of Ancient Glacier-dammed Lakes in the Cheviots. *Geological Magazine (Decade IV)* 8, 513-515.
Kerr, R. J. 1978. The nature and derivation of glacial till in part of the Tweed basin. Thesis (PhD). University of Edinburgh
Khatwa, A. and Tulaczyk, S. 2001. Microstructural interpretations of modern and Pleistocene subglacially deformed sediments: the relative role of parent material and subglacial processes. *Journal of Quaternary Science* 16, 507-517.
Kilfeather, A., Ó Cofaigh, C., Dowdeswell, J., van der Meer, J. and Evans, D. 2010. Micromorphological characteristics of glacimarine sediments: implications for distinguishing genetic processes of massive diamicts. *Geo-Marine Letters* 30, 77-97.
Kilfeather, A. A. 2004. Glaciation, deformation and till porosity: County Laois, Ireland. Thesis (PhD). Queen Mary, University of London.
Kilfeather, A. A. and van der Meer, J. J. M. 2008. Pore size, shape and connectivity in tills and their relationship to deformation processes. *Quaternary Science Reviews* 27, 250-266.
King, E. C., Hindmarsh, R. C. A. and Stokes, C. R. 2009. Formation of mega-scale glacial lineations observed beneath a West Antarctic ice stream. *Nature Geoscience* 2, 585-588.
King, E. C., Woodward, J. and Smith, A. M. 2007. Seismic and radar observations of subglacial bed forms beneath the onset zone of Rutford Ice Stream, Antarctica. *Journal of Glaciology* 53, 665-672.
Kjær, K. H., Houmark-Nielsen, M. and Richardt, N. 2003. Ice-flow patterns and dispersal of erratics at the southwestern margin of the last Scandinavian Ice Sheet: signature of palaeo-ice streams. *Boreas* 32, 130-148.
Kjær, K. H., Larsen, E., van der Meer, J., Ingolfsson, O., Kruger, J., Orn Benediktsson, I., Knudsen, C. G. and Schomacker, A. 2006. Subglacial decoupling at the sediment/bedrock interface: a new mechanism for rapid flowing ice. *Quaternary Science Reviews* 25, 2704-2712.
Kleman, J. and Borgström, I. 1994. Glacial land forms indicative of a partly frozen bed. *Journal of Glaciology* 40, 255-264.
Kohler, J. 2007. Glaciology: Lubricating lakes. *Nature* 445, 830-831.
Krinsley, D. and Takahashi, T. 1962. Surface Textures of Sand Grains - an Application of Electron Microscopy: Glaciation. *Science* 138, 1262-1264.
Krüger, J. and Thomsen, H. H. 1984. Morphology, stratigraphy, and genesis of small drumlins in front of the glacier Myrdalsjökull, south Iceland. *Journal of Glaciology* 30, 94-105.
Lachniet, M., S,. Larson, G. J,. Lawson, D. E,. Evenson, E. B,. Alley, R. B. 2001. Microstructures of sediment flow deposits and subglacial sediments: a comparison. *Boreas* 30, 254-264.
Lachniet, M. S., Larson, G. J., Strasser, J. C., Lawson, D. E., Evenson, E. B. and Alley, R. B. 1999. Microstructures of glacigenic sediment-flow deposits, Matanuska Glacier, Alaska. *Geological Society of America Special Papers* 337, 45-57.
Larsen, N. K. and Piotrowski, J. A. 2003: Fabric Pattern in a Basal Till Succession and Its Significance for Reconstructing Subglacial Processes. Journal of Sedimentary Research, 725-734.

Larsen, N. K., Piotrowski, J. A. and Christiansen, F. 2006b. Microstructures and microshears as proxy for strain in subglacial diamicts: Implications for basal till formation. *Geology* 34, 889-892.
Larsen, N. K., Piotrowski, J. A., Christoffersen, P. and Menzies, J. 2006a. Formation and deformation of basal till during a glacier surge; Elisebreen, Svalbard. *Geomorphology* 81, 217-234.
Larsen, N. K., Piotrowski, J. A., Menzies, J.,. 2007. Microstructural evidence of low-strain, time-transgressive subglacial deformation. *Journal of Quaternary Science* 22, 593-608.
Larsen, N. K., Piotrowski, J. A. and Kronborg, C. 2004. A multiproxy study of a basal till: a time-transgressive accretion and deformation hypothesis. *Journal of Quaternary Science* 19, 9-21.
Lawson, D. E. 1979. Semdimentological analysis of the western terminus region of the Matanuska Glacier, Alaska. *CRREL Report*, 79-79.
Lee, J. R. and Phillips, E. R. 2008. Progressive soft sediment deformation within a subglacial shear zone--a hybrid mosaic-pervasive deformation model for Middle Pleistocene glaciotectonised sediments from eastern England. *Quaternary Science Reviews* 27, 1350-1362.
Lian, O. B. and Hicock, S. R. 2000. Thermal conditions beneath parts of the last Cordilleran Ice Sheet near its centre as inferred from subglacial till, associated sediments, and bedrock. *Quaternary International* 68-71, 147-162.
Lian, O. B., Hicock, S. R. and Dreimanis, A. 2003. Laurentide and Cordilleran fast ice flow: some sedimentological evidence from Wisconsinan subglacial till and its substrate. *Boreas* 32, 102-113.
Linch, L. D. 2010. The micromorphology of iceberg scour. Thesis (PhD) Queen Mary, University of London.
Lindén, M., Möller, P. E. R. and Adrielsson, L. 2008. Ribbed moraine formed by subglacial folding, thrust stacking and lee-side cavity infill. *Boreas* 37, 102-131.
Liverman, D. G. E., Catto, N. R. and Rutter, N. W. 1989. Laurentide glaciation in west-central Alberta: a single (Late Wisconsinan) event. *Canadian Journal of Earth Sciences* 26, 266-274.
Livingstone, S. J., Cofaigh, C. O. and Evans, D. J. A. 2008. Glacial geomorphology of the central sector of the last British-Irish Ice Sheet. *Journal of Maps* 358-377.
Lowe, A. L. and Anderson, J. B. 2002. Reconstruction of the West Antarctic ice sheet in Pine Island Bay during the Last Glacial Maximum and its subsequent retreat history. *Quaternary Science Reviews* 21, 1879-1897.
Lowe, A. L. and Anderson, J. B. 2003. Evidence for abundant subglacial meltwater beneath the paleo-ice sheet in Pine Island Bay, Antarctica. *Journal of Glaciology* 49, 125-138.
MacAyeal, D. R. 1989. Large-scale ice flow over a viscous basal sediment-Theory and application to ice stream B, Antarctica. *Journal of Geophysical Research* 94, 4071-4087.
MacAyeal, D. R. 1993. Binge/purge oscillations of the Laurentide ice sheet as a cause of the North Atlantic's Heinrich events. *Paleoceanography* 8, 775-784.
MacAyeal, D. R., Bindschadler, R. A. and Scambos, T. A. 1995. Basal friction of ice stream E, west Antarctica. *Journal of Glaciology* 41, 247-262.
MacDonald, A. M., Ball, D.F., Dochartaigh, D.E.O. 2004. A GIS of aquifer productivity in Scotland: explanatory notes. *British Geological Survey Comissioned Report* CR/04/047N, 21pp.
MacKenzie, W. S. and Adams, A. E. 1994: *A color atlas of rocks and minerals in thin section*. Wiley.
Mahaney, W. C. and Kalm, V. 2000. Comparative scanning electron microscopy study of oriented till blocks, glacial grains and Devonian sands in Estonia and Latvia. *Boreas* 29, 35-51.
Maizels, J. 1993. Lithofacies variations within sandur deposits: the role of runoff regime, flow dynamics and sediment supply characteristics. *Sedimentary Geology* 85, 299-325.
March, A. 1932. Mathematische Theorie der Regelung nach der Korngestalt bei affiner Deformation. *Z. Kristallogr* 81, 285-297.
Mark, D. M. 1973. Analysis of Axial Orientation Data, Including Till Fabrics. *Geological Society of America Bulletin* 84, 1369-1374.
McCarroll, D. and Rijsdijk, K.F. 2003. Deformation styles as a key for interpreting glacial depositional environments. *Journal of Quaternary Science* 18, 473-489.
Menzies, J. 1979. A review of the literature on the formation and location of drumlins. *Earth Science Reviews* 14, 315–359.
Menzies, J. 1989. Subglacial hydraulic conditions and their possible impact upon subglacial bed formation. *Sedimentary Geology* 62, 125-150.
Menzies, J. 1990. Sand intraclasts within a diamicton mélange, southern Niagara Peninsula, Ontario, Canada. *Journal of Quaternary Science* 5, 189-206.
Menzies, J. 1996. Glasgow's drumlins. *Scottish Geographical Journal* 112, 188-193.
Menzies, J. 2000. Micromorphological analyses of microfabrics and microstructures indicative of deformation processes in glacial sediments. *Geological Society, London, Special Publications* 176, 245-257.

Menzies, J., Meer, J. J. M., Domack, E. and Wellner, J. S. 2010. Micromorphology: as a tool in the detection, analyses and interpretation of (glacial) sediments and man-made materials. *Proceedings of the Geologists' Association* 121, 281-292.
Menzies, J. and Taylor, J. 2003. Seismically induced soft-sediment microstructures (seismites) from Meikleour, western Strathmore, Scotland. *Boreas* 32, 314-327.
Menzies, J., van der Meer, J. J. M. and Rose, J. 2006. Till--as a glacial "tectomict", its internal architecture, and the development of a "typing" method for till differentiation. *Geomorphology* 75, 172-200.
Menzies, J. and Zaniewski, K. 2003. Microstructures within a modern debris flow deposit derived from Quaternary glacial diamicton--a comparative micromorphological study. *Sedimentary Geology* 157, 31-48.
Menzies, J., Zaniewski, K. and Dreger, D. 1997. Evidence, from microstructures, of deformable bed conditions within drumlins, Chimney Bluffs, New York State. *Sedimentary Geology* 111, 161-175.
Miall, A. D. 1978. Lithofacies types and vertical profile models in braided river deposits: a summary. *Fluvial sedimentology* 597, 604.
Migon, P. and Lidmar-Bergström, K. 2001. Weathering mantles and their significance for geomorphological evolution of central and northern Europe since the Mesozoic. *Earth-Science Reviews* 56, 285-324.
Millar, S. W. S. and Nelson, F. E. 2001. Clast Fabric in Relict Periglacial Colluvium, Salamanca Re-Entrant, Southwestern New York, USA. *Geografiska Annaler. Series A, Physical Geography* 83, 145-156.
Millar, S. W. S. and Nelson, F. E. 2003. Influence of clast axial ratio on macrofabric strength in periglacial colluvium. *Journal of Sedimentary Research* 73, 720.
Möller, P. 2006. Rogen moraine: an example of glacial reshaping of pre-existing landforms. *Quaternary Science Reviews* 25, 362-389.
Motyka, R. J., Truffer, M., Fahnestock, M., Mortensen, J., Rysgaard, S. and Howat, I. 2011. Submarine melting of the 1985 Jakobshavn Isbræ floating tongue and the triggering of the current retreat. *Journal of Geophysical Research (Earth Surface)* 116, 01007.
Muller, B. U. and Schluchter, C. 2000. Influence of the glacier bed lithology on the formation of a subglacial till sequence -- ring-shear experiments as a tool for the classification of subglacial tills. *Quaternary Science Reviews* 20, 1113-1125.
Munro-Stasiuk, M. J. 2000. Rhythmic Till Sedimentation: Evidence for Repeated Hydraulic Lifting of a Stagnant Ice Mass. *Journal of Sedimentary Research* 70, 94-106.
Munro-Stasiuk, M. J. 2003. Subglacial Lake McGregor, south-central Alberta, Canada. *Sedimentary Geology* 160, 325-350.
Munro-Stasiuk, M. J. and Shaw, J. 2002. The Blackspring Ridge Flute Field, south-central Alberta, Canada: : evidence for subglacial sheetflow erosion. *Quaternary International* 90, 75-86.
Munro, M. and Shaw, J. 1997. Erosional origin of hummocky terrain in south-central Alberta, Canada. *Geology* 25, 1027-1030.
Murray, T. 1997. Assessing the paradigm shift: Deformable glacier beds. *Quaternary Science Reviews* 16, 995-1016.
Murray, T., Corr, H., Forieri, A. and Smith, A. M. 2008. Contrasts in hydrology between regions of basal deformation and sliding beneath Rutford Ice Stream, West Antarctica, mapped using radar and seismic data. *Geophysical Research Letters* 35, L12504.
Murray, T. and Dowdeswell, J. A. 1992. Water Throughflow and the Physical Effects of Deformation on Sedimentary Glacier Beds. *Journal of Geophysical Research(B)* 97, 8993-9002.
National Topographic Data Base, [shapefile geospatial data]. Natural Resources Canada. Downloaded from Geogratis. http://geogratis.cgdi.gc.ca/geogratis/en/collection/F3D83500-2564-D61E-4F37-FEF860E6DDC0.html;jsessionid=D9A7C1DE618B70633AEBC32CC994866D
Downloaded: May 2011
Ng, F. 2000. Canals under sediment-based ice sheets. *Annals of Glaciology* 30, 146-152.
Nye, J. F. 1957. The Distribution of Stress and Velocity in Glaciers and Ice-Sheets. *Proceedings of the Royal Society of London. Series A. Mathematical and Physical Sciences* 239, 113-133.
Ó Cofaigh, C., Jeffrey, E., Dowdeswell, J. A. and Larter, R. D. 2007. Till characteristics, genesis and transport beneath Antarctic paleo-ice streams. *Journal of Geophysical Research* 112.
Ó Cofaigh, C., Dowdeswell, J. A., Allen, C. S., Hiemstra, J. F., Pudsey, C. J., Evans, J. and Evans, D. J. A. 2005. Flow dynamics and till genesis associated with a marine-based Antarctic palaeo-ice stream. *Quaternary Science Reviews* 24, 709-740.
Ó Cofaigh, C. and Evans, D. J. A. 2001. Sedimentary evidence for deforming bed conditions associated with a grounded Irish Sea glacier, southern Ireland. *Journal of Quaternary Science* 16, 435-454.
Ó Cofaigh, C., Pudsey, C. J. and Dowdeswell, J. 2002. Evolution of subglacial bedforms along a paleo-ice stream, Antarctic Peninsula continental shelf. *Geophysical Research Letters* 29, 41-41.

Ó Cofaigh, C., Taylor, J., Dowdeswell, J. A. and Pudsey, C. J. 2003. Palaeo-ice streams, trough mouth fans and high-latitude continental slope sedimentation. *Boreas* 32, 37-55.
Ordnance Survey data shapefiles, accessed using: Edina Geology Digimap Service, http://edina.ac.uk/digimap, downloaded: May 2008
Ostry, R. C. and Deane, R. E. 1963. Microfabric Analyses of Till. *Geological Society of America Bulletin* 74, 165-168.
Ottesen, D., Dowdeswell, J. A. and Rise, L. 2005a. Submarine landforms and the reconstruction of fast-flowing ice streams within a large Quaternary ice sheet: The 2500-km-long Norwegian-Svalbard margin (57°-80°N). *Geological Society of America Bulletin* 117, 1033-1050.
Ottesen, D., Rise, L., Knies, J., Olsen, L. and Henriksen, S. 2005b. The Vestfjorden-Traenadjupet palaeo-ice stream drainage system, mid-Norwegian continental shelf. *Marine Geology* 218, 175-189.
Ottesen, D., Stokes, C. R., Rise, L. and Olsen, L. 2008. Ice-sheet dynamics and ice streaming along the coastal parts of northern Norway. *Quaternary Science Reviews* 27, 922-940.
Overpeck, J. T., Otto-Bliesner, B. L., Miller, G. H., Muhs, D. R., Alley, R. B. and Kiehl, J. T. 2006. Paleoclimatic Evidence for Future Ice-Sheet Instability and Rapid Sea-Level Rise. *Science* 311, 1747-1750.
Owen, G. 1996. Experimental soft-sediment deformation: structures formed by the liquefaction of unconsolidated sands and some ancient examples. *Sedimentology* 43, 279-293.
Owen, G. 2003. Load structures: gravity-driven sediment mobilization in the shallow subsurface. *Geological Society, London, Special Publications* 216, 21.
Passchier, S., Laban, C., Mesdag, C. S. and Rijsdijk, K. F. 2010. Subglacial bed conditions during Late Pleistocene glaciations and their impact on ice dynamics in the southern North Sea. *Boreas* 39, 633-647.
Paterson, W. S. B. 1994: *The Physics of Glaciers*. Oxford: Butterworth-Heinemann.
Patterson, C. J. 1998. Laurentide glacial landscapes; the role of ice streams. *Geology* 26, 643-646.
Patterson, D. 2008: Bounding Containers ArcScript. ESRI Downloads.
Payne, A. J. 1999. A thermomechanical model of ice flow in West Antarctica. *Climate Dynamics* 15, 115-125.
Peters, L. E., Anandakrishnan, S., Alley, R. B. and Smith, A. M. 2007. Extensive storage of basal meltwater in the onset region of a major West Antarctic ice stream. *Geology* 35, 251.
Phillips, E. 2006. Micromorphology of a debris flow deposit: evidence of basal shearing, hydrofracturing, liquefaction and rotational deformation during emplacement. *Quaternary Science Reviews* 25, 720-738.
Phillips, E., Everest, J. and Diaz-Doce, D. 2010. Bedrock controls on subglacial landform distribution and geomorphological processes: Evidence from the Late Devensian Irish Sea Ice Stream. *Sedimentary Geology* 232, 98-118.
Phillips, E., Merritt, J., Auton, C. and Golledge, N. 2007. Microstructures in subglacial and proglacial sediments: understanding faults, folds and fabrics, and the influence of water on the style of deformation. *Quaternary Science Reviews* 26, 1499-1528.
Phillips, E., van der Meer, J. J. M. and Ferguson, A. 2011. A new microstructural mapping methodology for the identification, analysis and interpretation of polyphase deformation within subglacial sediments. *Quaternary Science Reviews* 30, 2570-2596.
Piotrowski, J. A., Kraus, A.M.,. 1997. Response of sediment to ice sheet loading in northwestern Germany: effective stresses and glacierbed stability. *Journal of Glaciology* 43, 495–502.
Piotrowski, J. A., Larsen, N. K. and Junge, F. W. 2004. Reflections on soft subglacial beds as a mosaic of deforming and stable spots. *Quaternary Science Reviews* 23, 993-1000.
Piotrowski, J. A., Larsen, N. K., Menzies, J. and Wysota, W. 2006. Formation of subglacial till under transient bed conditions: deposition, deformation, and basal decoupling under a Weichselian ice sheet lobe, central Poland. *Sedimentology* 53, 83-106.
Piotrowski, J. A., Mickelson, D. M., Tulaczyk, S., Krzyszkowski, D. and Junge, F. W. 2001. Were deforming subglacial beds beneath past ice sheets really widespread? *Quaternary International* 86, 139-150.
Piotrowski, J. A. and Tulaczyk, S. 1999. Subglacial conditions under the last ice sheet in northwest Germany: ice-bed separation and enhanced basal sliding? *Quaternary Science Reviews* 18, 737-751.
Porta, J. and Herrero, J. 1990: Micromorphology of soils enriched with gypsum. In Douglas, L. A. editor, *Soil micromorphology: a basic and applied science*: Elsevier, 321-339.
Powers, M. C. 1953. A new roundness scale for sedimentary particles. *Journal of Sedimentary Research* 23, 117.
Prest, V. K., Grant, D. R. and Rampton, V. N. 1968: Glacial map of Canada. Map 1253A (1:5000000). Ottawa: Geological Survey of Canada.
Price, R. J. 1960. Glacial Meltwater Channels in the Upper Tweed Drainage Basin. *The Geographical Journal* 126, 483-489.
Price, S. F., Bindschadler, R. A., Hulbe, C. L. and Blankenship, D. D. 2002. Force balance along an inland tributary and onset to Ice Stream D, West Antarctica. *Journal of Glaciology* 48, 20-30.

Ragg, J. 1960: *The Soils of the Country Round Kelso and Lauder: Sheets 25 and 26*. Edinburgh: Her Majesty's Stationery Office.
Rains, B., Shaw, J., Skoye, R., Sjogren, D. and Kvill, D. 1993. Late Wisconsin subglacial megaflood paths in Alberta. *Geology* 21, 323-326.
Rathert, D. 2003: Linear Properties ArcScript. ESRI Downloads.
Rattas, M. and Piotrowski, J. A. 2003. Influence of bedrock permeability and till grain size on the formation of the Saadjärve drumlin field, Estonia, under an east-Baltic Weichselian ice stream. *Boreas* 32, 167-177.
Raymond, C., Echelmeyer, K., Whillans, I., Doake, C. 2001. Ice stream shear margins. In R.B. Alley, and Bindschadler, R. A., editors, The West Antarctic ice sheet: behavior and environment. Washington DC: American Geophysical Union, 137-155.
Reinardy, B. T. I., Hiemstra, J. F., Murray, T., Hillenbrand, C.-D. and Larter, R. D. 2011. Till genesis at the bed of an Antarctic Peninsula palaeo-ice stream as indicated by micromorphological analysis. *Boreas* 40, 498-517.
Retzlaff, R. and Bentley, C. R. 1993. Timing of stagnation of Ice Stream C, West Antarctica, from short-pulse radar studies of buried surface crevasses. *Journal of Glaciology* 39, 553-561.
Retzlaff, R., Lord, N. and Bentley, C. R. 1993. Airborne-radar studies: Ice Streams A, B and C, West Antarctica. *Journal of Glaciology* 39, 495-506.
Rijsdijk, K. F. 2001. Density-driven deformation structures in glacigenic consolidated diamicts: examples from Traeth y Mwnt, Cardiganshire, Wales, UK. *Journal of Sedimentary Research* 71, 122.
Rippin, D. M., Bamber, J. L., Siegert, M. J., Vaughan, D. G. and Corr, H. F. J. 2006. Basal conditions beneath enhanced-flow tributaries of Slessor Glacier, East Antarctica. *Journal of Glaciology* 52, 481-490.
Roberts, D. and Long, A. 2005. Streamlined bedrock terrain and fast ice flow, Jakobshavns Isbrae, West Greenland: implications for ice stream and ice sheet dynamics. *Boreas* 34, 25-42.
Roberts, D. H. 2007. Palaeo-ice streaming in the central sector of the British–Irish Ice Sheet during the Last Glacial Maximum: evidence from the northern Irish Sea Basin. *Boreas* 36, 115-129.
Rooney, S. T., Blankenship, D. D., Alley, R. B. and Bently, C. R. 1987. Till beneath ice stream B 2. structure and continuity. *Journal of Geophysical Research* 92, 8913-8920.
Rose, J. 1987: Drumlins as part of glacier bedform continuum. In Menzies, J. and Rose, J., editors, *Drumlin Symposium*, Rotterdam: Balkema, 103-116.
Rose, J. and Smith, M. J. 2008. Glacial geomorphological maps of the Glasgow region, western central Scotland. *Journal of Maps* 399, 416.
Ross, M., Campbell, J. E., Parent, M. and Adams, R. S. 2009. Palaeo-ice streams and the subglacial landscape mosaic of the North American mid-continental prairies. *Boreas* 38, 421-439.
Schoof, C. 2002. Mathematical Models of Glacier Sliding and Drumlin Formation. *PhD thesis*.
Schoof, C. 2004. On the mechanics of ice-stream shear margins. *Journal of Glaciology* 50, 208-218.
Sejrup, H. P., Eiliv, L., Haflidi, H., Ida, M. B., Berit, O. H., Hafdis, E. J., Edward, L. K., Jon, L., Oddvar, L., Atle, N., Aring, rd, Ottesen, D. A. G., St, le, R., Leif, R. and Knut, S. 2003. Configuration, history and impact of the Norwegian Channel Ice Stream. *Boreas* 32, 18-36.
Sergienko, O. V. and Hulbe, C. L. 2011. 'Sticky spots' and subglacial lakes under ice streams of the Siple Coast, Antarctica. *Annals of Glaciology* 52, 18.
Sergienko, O. V., MacAyeal, D. R. and Bindschadler, R. A. 2009. Stickslip behavior of ice streams: modeling investigations. *Annals of Glaciology* 50, 87-94.
Shaw, J. 2002. The meltwater hypothesis for subglacial bedforms. *Quaternary International* 90, 5-22.
Shaw, J. 2009. In defence of the meltwater (megaflood) hypothesis for the formation of subglacial bedform fields. *Journal of Quaternary Science* 25, 3, 249-260.
Shaw, J. and Freschauf, R. C. 1973. A kinematic discussion of the formation of glacial flutings. *The Canadian Geographer* 17, 19-35.
Shaw, J., Kvill, D. and Rains, B. 1989. Drumlins and catastrophic subglacial floods. *Sedimentary Geology* 62, 177-202.
Shetsen, I. 1987: Quaternary geology, southern Alberta. Edmonton, Canada: Alberta Research Council.
Shetsen, I. 1990: Quaternary Geology, central Alberta. Edmonton, Canada: Alberta Research Council.
Shetsen, I. 2002: Quaternary Geology of Southern Alberta - Deposits (GIS data, polygon features). *Digital Data*, Edmonton, Alberta, Canada: Alberta Geological Survey.
Shipp, S. and Anderson, J. B. 1997. Paleo ice-streams and icestreams boundaries, Ross Sea, Antarctica. *Glaciated Continental Margins: An Atlas of Acoustic Images. London, Chapman and Hall*, 106-109.
Siegert, M. J. and Bamber, J. L. 2000. Subglacial water at the heads of Antarctic ice-stream tributaries. *Journal of Glaciology* 46, 702-703.
Siegert, M. J., Taylor, J., Payne, A. J. and Hubbard, B. 2004. Macro-scale bed roughness of the siple coast ice streams in West Antarctica. *Earth Surface Processes and Landforms* 29, 1591-1596.
Sissons, J. B. 1960. Some aspects of glacial drainage channels in Britain: Part I. *Scottish Geographical Journal* 76, 131-146.

Sissons, J. B. 1961. Some aspects of glacial drainage channels in Britain. Part II. *Scottish Geographical Journal* 77, 15-36.
Smith, A. M. 1997. Basal conditions on Rutford Ice Stream, West Antarctica, from seismic observations. *Journal of Geophysical Research* 102, 543-552.
Smith, A. M., Murray, T., Nicholls, K. W., Makinson, K., Aðalgeirsdóttir, G., Behar, A. E. and Vaughan, D. G. 2007. Rapid erosion, drumlin formation, and changing hydrology beneath an Antarctic ice stream. *Geology* 35, 127-130.
Smith, J. A., Hillenbrand, C.D., Larter, R. D., Graham, A. G. C. and Kuhn, G. 2009. The sediment infill of subglacial meltwater channels on the West Antarctic continental shelf. *Quaternary Research* 71, 190-200.
Smith, M., J., Clark, Chris, D. 2005. Methods for the visualization of digital elevation models for landform mapping. *Earth Surface Processes and Landforms* 30, 885-900.
Sneed, E. D. and Folk, R. L. 1958. Pebbles in the lower Colorado River, Texas a study in particle morphogenesis. *The Journal of Geology* 66, 114-150.
Soils of Canada. 2012. Orders: Cryosolic. Accessed 13th December 2012. From: http://www.soilsofcanada.ca/orders/cryosolic/index.php
Stalker, A. 1956. The Erratics Train, Foothills of Alberta. *Geological Survey of Canada Bulletin* 37, 32.
Stalker, A. 1960. Ice-pressed drift forms and associated deposits in Alberta. *Geological Survey of Canada Bulletin* 57, Department of Mines and Technical Surveys
Stalker, A. M. 1983: Quaternary stratigraphy in southern Alberta report III: the Cameron Ranch Section. *Geological Survey of Canada Paper*
Stalker, A. M. S. 1977. The probable extent of classical Wisconsin ice in southern and central Alberta. *Canadian Journal of Earth Sciences* 14, 2614-2619.
Stalsberg, K., Larsen, E., Ottesen, D. and Sejrup, H. P. 2003. Middle to Late Weichselian Norwegian Channel Ice Stream deposits and morphology on Jæren, southwestern Norway and the eastern North Sea area. *Boreas* 32, 149-166.
Stanford, S. D. and Mickelson, D. M. 1985. Till fabric and deformational structures in drumlins near Waukesha, Wisconsin, USA. *Journal of Glaciology* 31, 220-228.
Stokes, C. R. 2006. Geomorphological Map of Ribbed Moraines on the Dubawnt Lake Palaeo-Ice Stream Bed: A Signature of Ice Stream Shut-down? *Journal of Maps*, 1-9.
Stokes, C. R. and Clark, C. D. 1999. Geomorphological criteria for identifying Pleistocene ice streams. *Annals of Glaciology* 28, 67-74.
Stokes, C. R. and Clark, C. D. 2001. Palaeo-ice streams. *Quaternary Science Reviews* 20, 1437-1457.
Stokes, C. R. and Clark, C. D. 2002a. Are long subglacial bedforms indicative of fast ice flow? *Boreas* 31, 239-249.
Stokes, C. R. and Clark, C. D. 2002b. Ice stream shear margin moraines. *Earth Surface Processes and Landforms* 27, 547-558.
Stokes, C. R. and Clark, C. D. 2003a. The Dubawnt Lake palaeo-ice stream: evidence for dynamic ice sheet behaviour on the Canadian Shield and insights regarding the controls on ice-stream location and vigour. *Boreas* 32, 263-279.
Stokes, C. R. and Clark, C. D. 2003b. Laurentide ice streaming on the Canadian Shield: A conflict with the soft-bedded ice stream paradigm? *Geology* 31, 347-350.
Stokes, C. R., Clark, C. D., Darby, D. A. and Hodgson, D. A. 2005. Late Pleistocene ice export events into the Arctic Ocean from the M'Clure Strait Ice Stream, Canadian Arctic Archipelago. *Global and Planetary Change* 49, 139-162.
Stokes, C. R., Clark, C. D., Lian, O. B. and Tulaczyk, S. 2007. Ice stream sticky spots: A review of their identification and influence beneath contemporary and palaeo-ice streams. *Earth-Science Reviews* 81, 217-249.
Stokes, C. R., Clark, C. D. and Winsborrow, M. C. M. 2006. Subglacial bedform evidence for a major palaeo-ice stream and its retreat phases in Amundsen Gulf, Canadian Arctic Archipelago. *Journal of Quaternary Science* 21, 399-412.
Stokes, C. R., Lian, O. B. Tulaczyk, S. Clark, C. D. 2008. Superimposition of ribbed moraines on a palaeo-ice-stream bed: implications for ice stream dynamics and shutdown. *Earth Surface Processes and Landforms* 33, 593-609.
Stokes, C. R., Spagnolo, M. and Clark, C. D. 2011. The composition and internal structure of drumlins: Complexity, commonality, and implications for a unifying theory of their formation. *Earth-Science Reviews* 107, 398-422.
Storrar, R., and Stokes, C. R. 2007. A Glacial Geomorphological Map of Victoria Island, Canadian Arctic. *Journal of Maps*, 191-210.
Sugden, D. E., Denton, G. H. and Marchant, D. R. 1991. Subglacial meltwater channel systems and ice sheet overriding, Asgard Range, Antarctica. *Geografiska Annaler. Series A, Physical Geography* 73, 109-121.

Swithinbank, C. W. M. 1954. Ice streams. *Polar Record 7 (48)*, 185–186.
Tarnocai, C. and Smith, C. A. S. 1989. Micromorphology and development of some central Yukon paleosols, Canada. *Geoderma* 45, 145-162.
Tarplee, M. F. V., van der Meer, J. J. M. and Davis, G. R. 2011. The 3D microscopic 'signature'of strain within glacial sediments revealed using X-ray computed microtomography. *Quaternary Science Reviews* 30, 3501-3532.
Taylor, G. I. 1923. The Motion of Ellipsoidal Particles in a Viscous Fluid. *Proceedings of the Royal Society of London. Series A* 103, 58-61.
Thomas, R. H., Stephenson, S. N., Bindschadler, R. A., Shabtaie, S. and Bentley, C. R. 1988. Thinning and grounding-line retreat on Ross Ice Shelf, Antarctica. *Annals of Glaciology* 11, 165-172.
Thomason, J. F. and Iverson, N. R. 2006. Microfabric and microshear evolution in deformed till. *Quaternary Science Reviews* 25, 1027-1038.
Trotter, F. M. 1929. The Glaciation of Eastern Edenside, the Alston Block, and the Carlisle Plain. *Quarterly Journal of the Geological Society* 85, 549.
Truffer, M. and Echelmeyer, K. A. 2003. Of isbrae and ice streams. *Annals of Glaciology* 36, 66-72.
Tulaczyk, S. 1999. Basal mechanics and geological record of ice streaming, West Antarctica. *Thesis* (PhD). California Institute of Technology
Tulaczyk, S. 2006a. Fast glacier flow and ice streaming. *In P. G. Knight, editor, Glacier Science And Environmental Change*, 353-359.
Tulaczyk, S. 2006b. Scale independence of till rheology. *Journal of Glaciology* 52, 377-380.
Tulaczyk, S., Kamb, B. and Engelhardt, H. F. 2001. Estimates of effective stress beneath a modern West Antarctic ice stream from till preconsolidation and void ratio. *Boreas* 30, 101-114.
Tulaczyk, S., Kamb, B., Scherer, R. P. and Engelhardt, H. F. 1998. Sedimentary processes at the base of a West Antarctic ice stream; constraints from textural and compositional properties of subglacial debris. *Journal of Sedimentary Research* 68, 487-496.
Tulaczyk, S., Kamb, W. B. and Engelhardt, H. F. 2000a. Basal mechanics of Ice Stream B, West Antarctica 1. Till mechanics. *Journal of Geophysical Research* 105, 463-482.
Tulaczyk, S., Kamb, W. B. and Engelhardt, H. F. 2000b. Basal mechanics of Ice Stream B, West Antarctica 2. Undrained plastic bed model. *Journal of Geophysical Research* 105, 483-494.
van der Meer, J. J. M. 1993. Microscopic evidence of subglacial deformation. *Quaternary Science Reviews* 12, 553-587.
van der Meer, J. J. M. and Hiemstra, J. F. 1998. Micromorphology of Miocene diamicts, indications of grounded ice. *Terra Antartica, 5 (3), 363-366.*
van der Meer, J. J. M. 1987. Micromorphology of glacial sediments as a tool in distinguishing genetic varieties of till. *Geological Survey of Finland Special Paper* 3, 77–89.
van der Meer, J. J. M. 1996. Micromorphology. *Past Glacial Environments–Sediments, Forms and Techniques* 2, 335–356.
van der Meer, J. J. M., Carr, S. J., Kjær, K. H., Anders Schomacker, J. K. and Kurt, H. K. 2010: 10 Mýrdalsjökull's Forefields Under the Microscope. The Micromorphology of Meltout and Subglacial Tills. *Developments in Quaternary Science*: Elsevier, 159-180.
van der Meer, J. J. M., Menzies, J. and Rose, J. 2003. Subglacial till: the deforming glacier bed. *Quaternary Science Reviews* 22, 1659-1685.
van der Veen, C. J. 1999: *Fundamentals of glacier dynamics*. Balkema.
van Vliet-Lanoë, B. 1998. Frost and soils: implications for paleosols, paleoclimates and stratigraphy. *Catena* 34, 157-183.
Vandenberghe, J. 2007: Periglacial Landforms: Cryoturbation Structures. In Elias, S. A., editor, *Encyclopedia of Quaternary Science*, Oxford: Elsevier, 2147-2153.
Vaughan, D. 2008. West Antarctic Ice Sheet collapse – the fall and rise of a paradigm. *Climatic Change* 91, 65-79.
Vaughan, D. G., Smith, A. M., Nath, P. C. and Le Meur, E. 2003. Acoustic impedance and basal shear stress beneath four Antarctic ice streams. *Annals of Glaciology* 36, 225-232.
Vogel, S. W., Tulaczyk, S. and Joughin, I. R. 2003. Distribution of basal melting and freezing beneath tributaries of Ice Stream C: implication for the Holocene decay of the West Antarctic ice sheet. *Annals of Glaciology* 36, 273-282.
Walder, J. S. and Fowler, A. 1994. Channelized subglacial drainage over a deformable bed. *Journal of Glaciology* 40, 3-15.
Waller, R., Murton, J. and Whiteman, C. 2009. Geological evidence for subglacial deformation of Pleistocene permafrost. *Proceedings of the Geologists' Association* 120, 155-162.
Waller, R., Phillips, E., Murton, J., Lee, J. and Whiteman, C. 2011. Sand intraclasts as evidence of subglacial deformation of Middle Pleistocene permafrost, North Norfolk, UK. *Quaternary Science Reviews* 30, 3481-3500

Warren, W. P. and Ashley, G. M. 1994. Origins of the ice-contact stratified ridges (eskers) of Ireland. *Journal of Sedimentary Research Section A: Sedimentary Petrology and Processes*, 433-449.
Washburn, A. L. 1980: *Geocryology*. New York: Wiley.
Weertman, J. 1968. Diffusion law for the dispersion of hard particles in an ice matrix that undergoes simple shear deformation. *Journal of Glaciology* 7, 161-165.
Weertman, J. 1974. Stability of the junction of an ice sheet and an ice shelf. *Journal of Glaciology* 13, 3-11.
Wellner, J. S., Heroy, D. C. and Anderson, J. B. 2006. The death mask of the antarctic ice sheet: Comparison of glacial geomorphic features across the continental shelf. *Geomorphology* 75, 157-171.
Wellner, J. S., Lowe, A. L., Shipp, S. S. and Anderson, J. B. 2001. Distribution of glacial geomorphic features on the Antarctic continental shelf and correlation with substrate: implications for ice behavior. *Journal of Glaciology* 47, 397-411.
Wentworth, C. K. 1922. A scale of grade and class terms for clastic sediments. *The Journal of Geology* 30, 377-392.
West, R. G. and Donner, J. J. 1956. The glaciations of East Anglia and the East Midlands: a differentiation based on stone-orientation measurements of the tills. *Quarterly Journal of the Geological Society* 112, 69.
Wheeler, J. O. Hoffman, P. F., Card, K. D., Davidson, A., Sanford, B. V., Okulitch, A. V. and Roest, W. R. 1996: Geological Map of Canada. *Series Map 1860A*: Geological Survey of Canada.
Whillans, I. M., Bolzan, J. and Shabtaie, S. 1987. Velocity of ice streams B and C, Antarctica. *Journal of Geophysical Research* 92, 8895-8902.
Whillans, I. M. and Van Der Veen, C. J. 1997. The role of lateral drag in the dynamics of Ice Stream B, Antarctica. *Journal of Glaciology* 43, 231-237.
White, S. H., Burrows, S. E., Carreras, J., Shaw, N. D. and Humphreys, F. J. 1980. On mylonites in ductile shear zones. *Journal of Structural Geology* 2, 175-187.
Winberry, J. P., Anandakrishnan, S. and Smith, A. M. 2007. Changes in speed near the onset of Bindschadler Ice Stream, West Antarctica. *Annals of Glaciology* 46, 83-86.
Wingham, D. J., Siegert, M. J., Shepherd, A. and Muir, A. S. 2006. Rapid discharge connects Antarctic subglacial lakes. *Nature* 440, 1033-1036.
Winsborrow, M. C. M., Clark, C. D. and Stokes, C. R. 2010. What controls the location of ice streams? *Earth-Science Reviews* 103, 45-59.
Winsborrow, M. C. M., Clark, C.D., Stokes, C.R. 2004. Ice Streams of the Laurentide Ice Sheet. *Géographie physique et Quaternaire* 58, 269-280.
Young, R. R., Burns, J. A., Smith, D. G., Arnold, L. D. and Rains, R. B. 1994. A single, late Wisconsin, Laurentide glaciation, Edmonton area and southwestern Alberta. *Geology* 22, 683.

Appendix A – Spatial autocorrelation

Table A.1 - Results of spatial autocorrelation conducted for subglacial lineation elongation ratio. The positive Morans I index value demonstrates that elongation ratio is clustered for all of the ice streams studied. Z scores are above the critical values for a 99 % significance level, which indicates that there is a less than 1 % likelihood that the clustered pattern is a result of random chance.

Ice Stream	Moran's I index	Z score (standard deviations)	P value (significance level) (critical value is given in brackets)	Result
Solway (n = 683)	0.18	13.28	0.01 (2.58)	Clustered
Forth (n = 2445)	0.24	28.8	0.01 (2.58)	Clustered
Crooked Lake (n = 1565)	0.24	16.72	0.01 (2.58)	Clustered
Transition Bay (n = 999)	0.16	11.76	0.01 (2.58)	Clustered
Haldane (n = 1458)	0.1	9.58	0.01 (2.58)	Clustered
Tweed (n = 1575)	0.15	19.04	0.01 (2.58)	Clustered
Central Alberta Ice Stream (n = 302)	0.1	10.02	0.01 (2.58)	Clustered

Appendix B – Particle Size Distribution

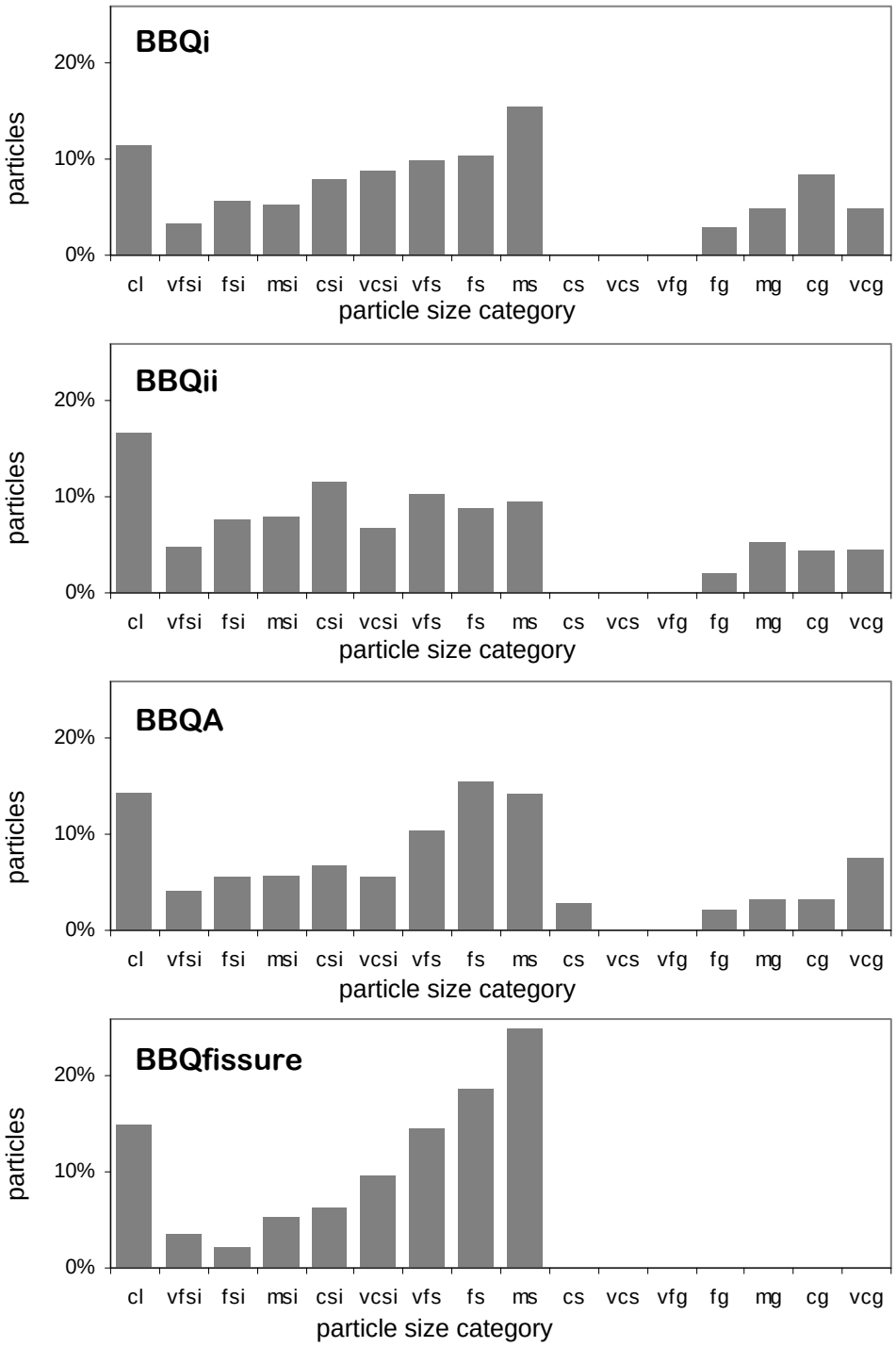

Figure B.1 – Blinkbonny Quarry particle size distribution histograms. Particle sizes are categorised according to the Wentworth size categories. Particle size abbreviations are as follows: cl = clay; vfsi = very fine silt; fsi = fine silt; msi = medium silt; csi = coarse silt; vcsi = very coarse silt; vfs = very fine sand; fs = fine sand; ms = medium sand; cs = coarse sand; vcs = very coarse sand; vfg = very fine gravel; fg = fine gravel; mg = medium gravel; cg = coarse gravel; vcg = very coarse gravel.

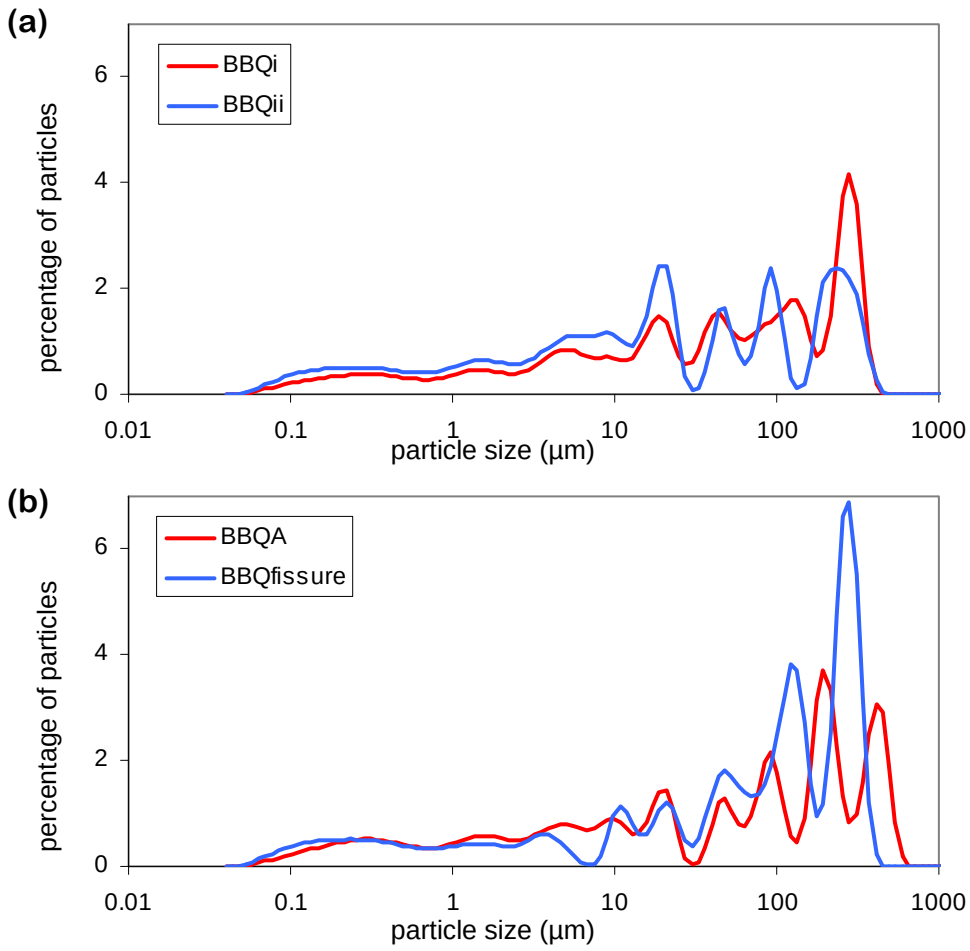

Figure B.2 – Blinkbonny Quarry particle size distribution line graphs for the fine sediment fraction (0.01 to 1000 µm, which includes clay to coarse sand sized particles) (note the logarithmic scales on the x axes). (a) Samples BBQi and BBQii; (b) Samples BBQA and BBQfissure (sampled from the diamict with a fissure in LF1).

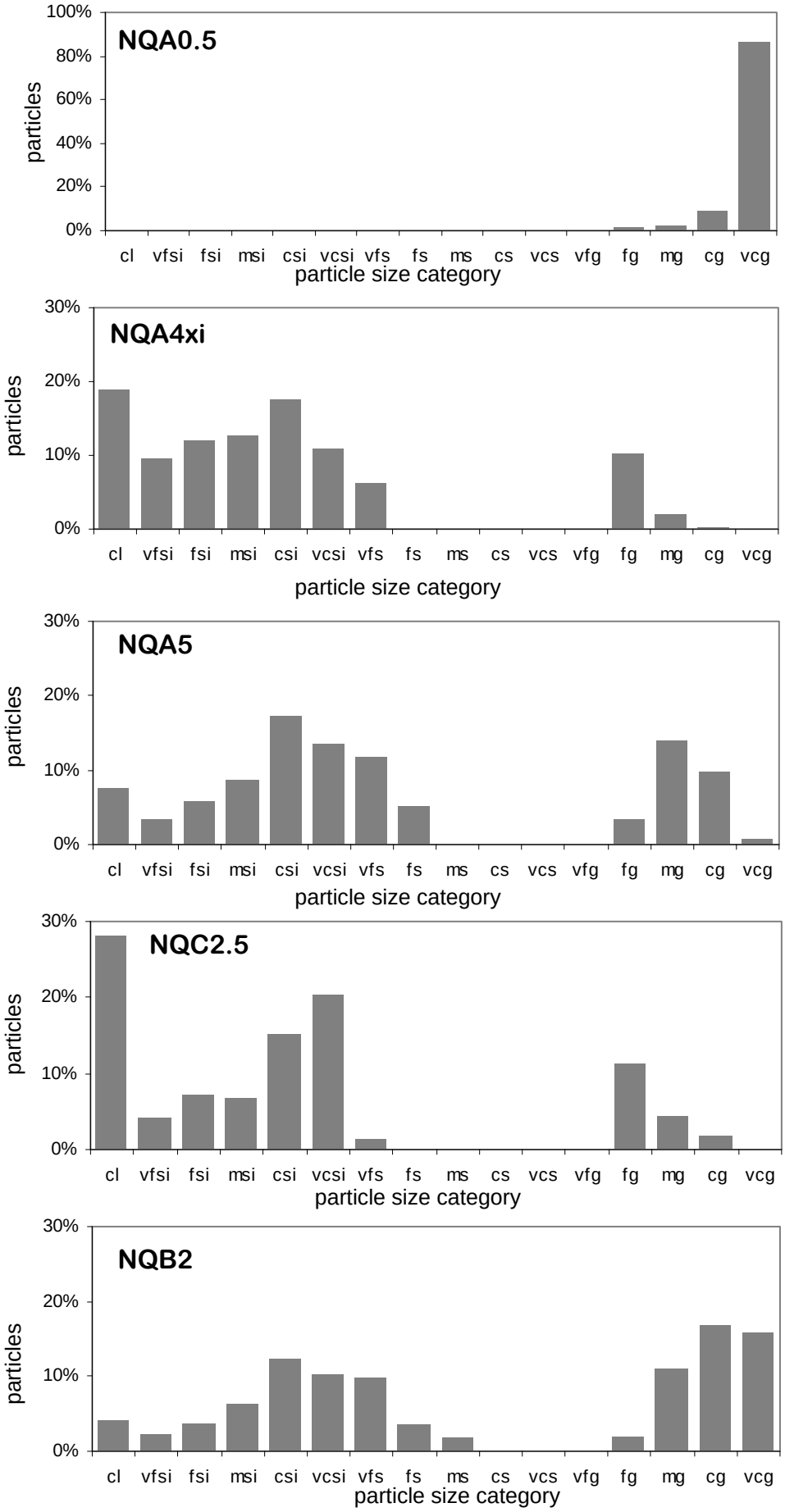

Figure B.3 – continued over the page

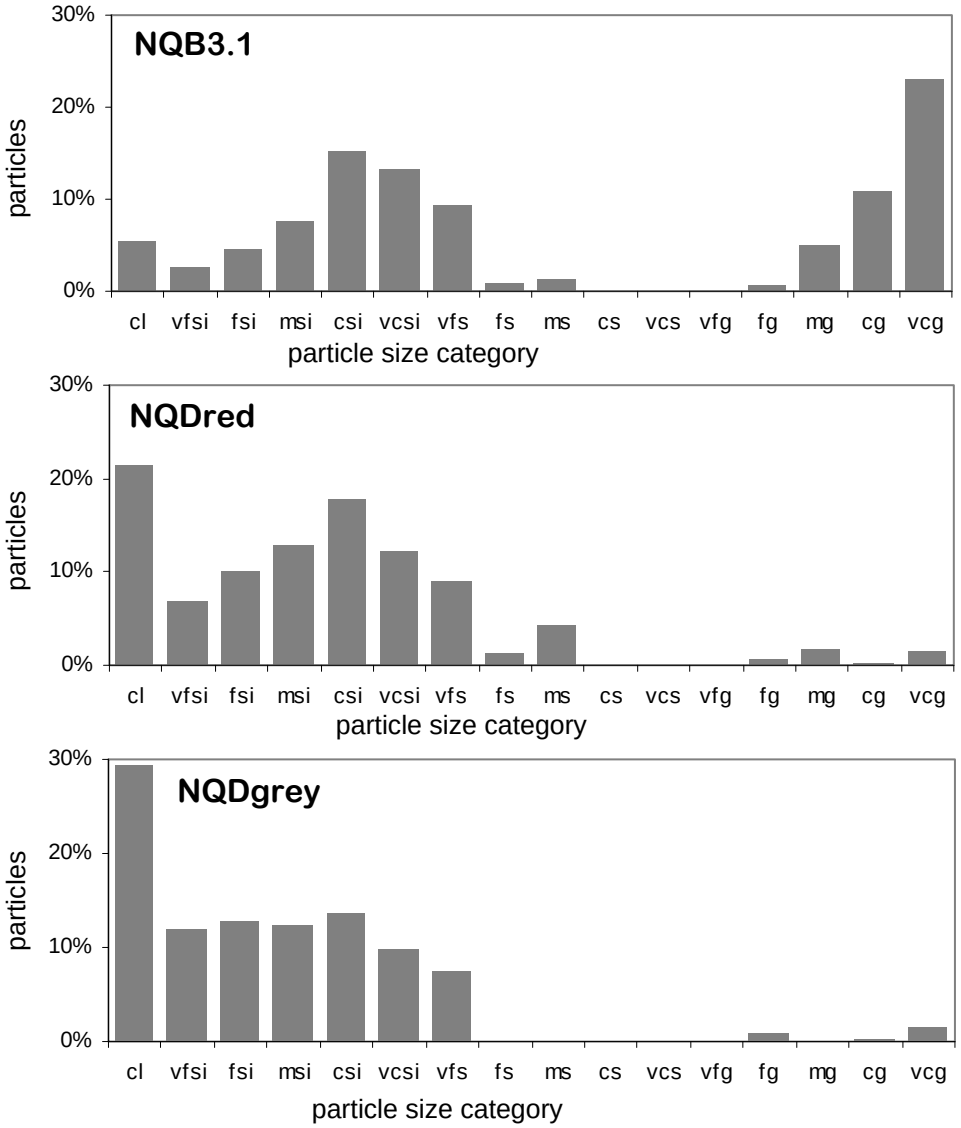

Figure B.3 – Newton Quarry particle size distribution histograms. Particle sizes are categorised according to the Wentworth size categories. Particle size abbreviations are as follows: cl = clay; vfsi = very fine silt; fsi = fine silt; msi = medium silt; csi = coarse silt; vcsi = very coarse silt; vfs = very fine sand; fs = fine sand; ms = medium sand; cs = coarse sand; vcs = very coarse sand; vfg = very fine gravel; fg = fine gravel; mg = medium gravel; cg = coarse gravel; vcg = very coarse gravel.

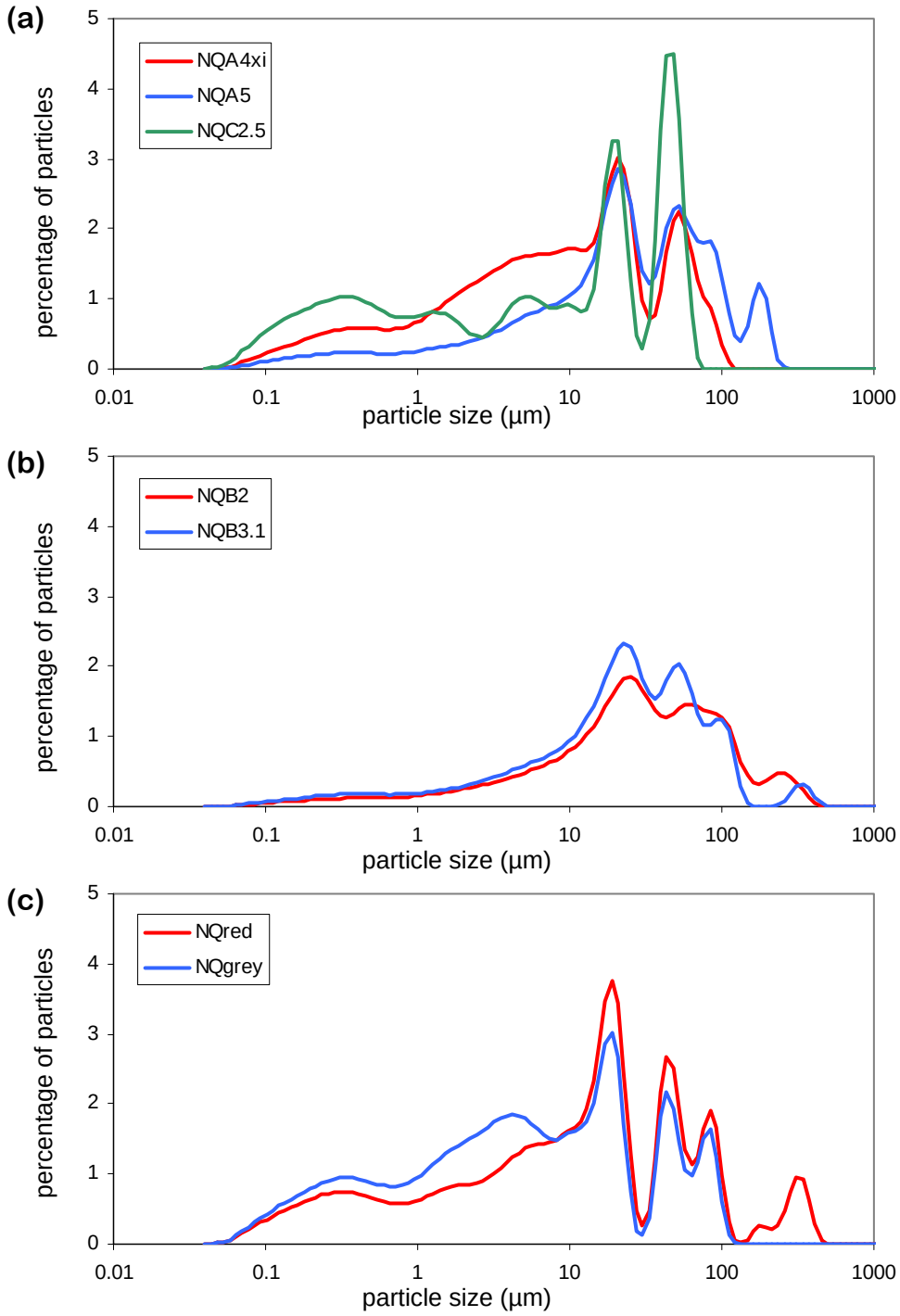

Figure B.4 – Newton Quarry particle size distribution line graphs for the fine sediment fraction (0.01 to 1000 µm, which includes clay to coarse sand sized particles) (note the logarithmic scales on the x axes). (a) Samples NQA4, NQA5, NQC2.5 (Lithofacies 2); (b) Samples NQB2 and NQB3.1 (Lithofacies 3); and (c) samples NQred and NQgrey (Lithofacies 4).

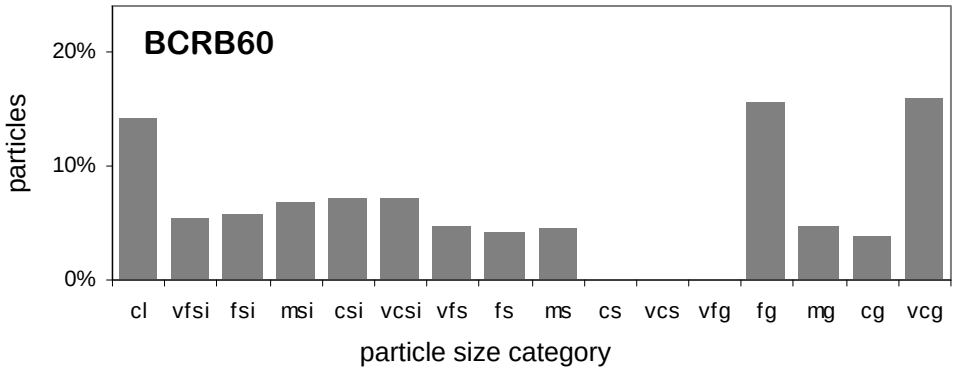

Figure B.5 – Berry Creek Reservoir particle size distribution histogram for LF4. Particle sizes are categorised according to the Wentworth size categories. Particle size abbreviations are as follows: cl = clay; vfsi = very fine silt; fsi = fine silt; msi = medium silt; csi = coarse silt; vcsi = very coarse silt; vfs = very fine sand; fs = fine sand; ms = medium sand; cs = coarse sand; vcs = very coarse sand; vfg = very fine gravel; fg = fine gravel; mg = medium gravel; cg = coarse gravel; vcg = very coarse gravel.

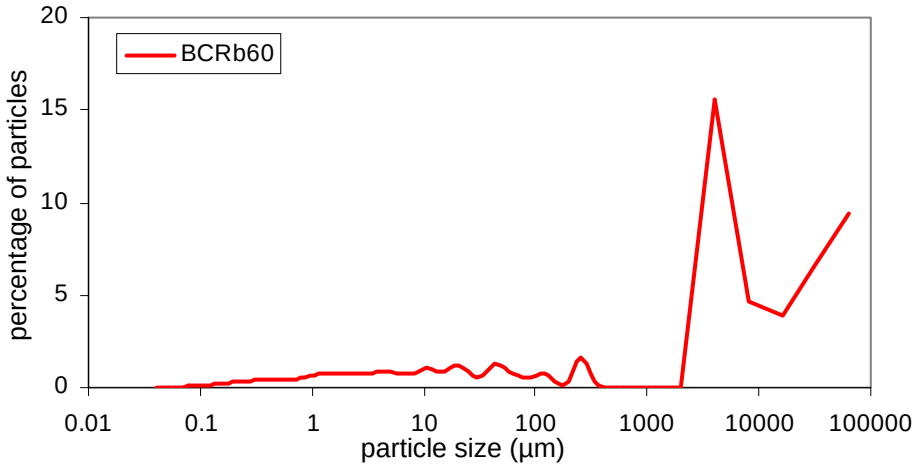

Figure B.6 – Berry Creek Reservoir particle size distribution line graph for the fine sediment fraction (0.01 to 1000 µm, which includes clay to coarse sand sized particles) of LF4 (note the logarithmic scales on the x axis).

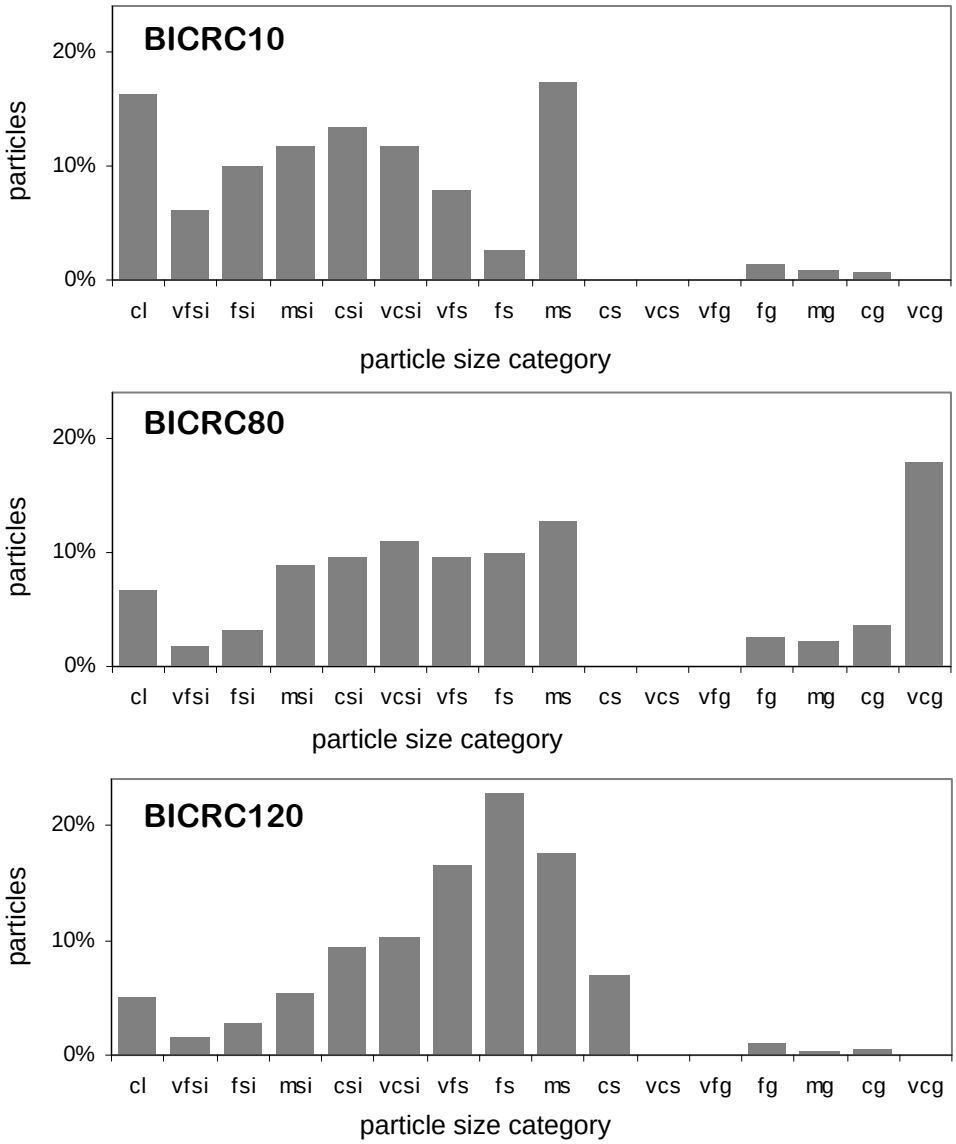

Figure B.7 – Blood Indian Creek Reservoir particle size distribution histograms, for LF1 (BICRc10) and LF3 (BICRc80and BICRC120). Particle sizes are categorised according to the Wentworth size categories. Particle size abbreviations are as follows: cl = clay; vfsi = very fine silt; fsi = fine silt; msi = medium silt; csi = coarse silt; vcsi = very coarse silt; vfs = very fine sand; fs = fine sand; ms = medium sand; cs = coarse sand; vcs = very coarse sand; vfg = very fine gravel; fg = fine gravel; mg = medium gravel; cg = coarse gravel; vcg = very coarse gravel.

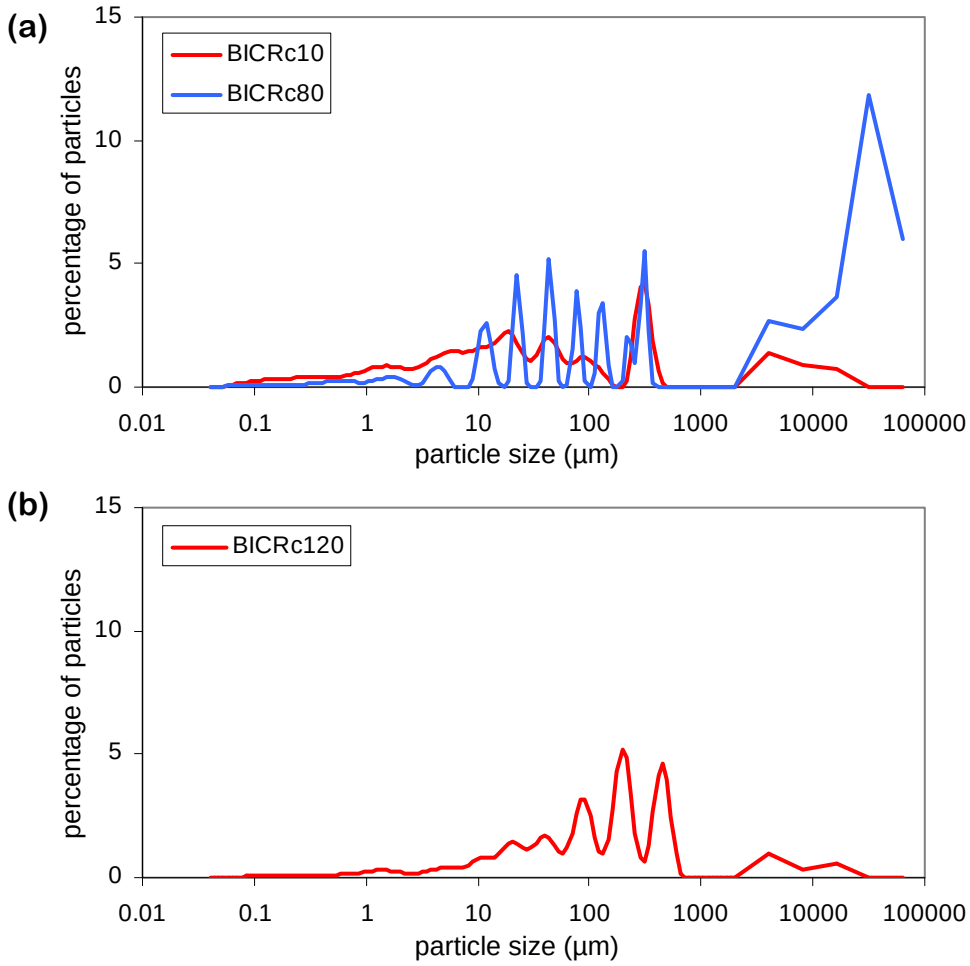

Figure B.8 – Blood Indian Creek Reservoir particle size distribution line graphs for the fine sediment fraction (0.01 to 1000 µm, which includes clay to coarse sand sized particles) (note the logarithmic scales on the x axes). (a) Samples BICRC10 (LF1) and BICRC80 (LF3); (b) Samples BICRC120 (LF3).

Appendix C – Micromorphology

C.1 Micromorphological descriptions

Table C.1 – Characteristics of sample BBQi, (regular size, a and b thin sections) Blinkbonny Quarry. Numbers in brackets indicate the relative abundance of each feature (1 = one or two present; 2 = medium abundance; 3 = high abundance).

Voids
Vughs (3) *Many vughs contain cutans.*
Fissures (2)
Structures/Features
Circular/arcuate grain alignments (3)
Iron staining (3) *There is strong, spatially variable, iron staining throughout the sample. Staining is not present in the grey domains or grey cutans.*
Grain lineations (3)
Cutans (3) *Small cutans (c. 0.8 mm diameter) are present throughout the sample, in association with voids.*
Clast weathering rinds (2)
Turbates (2)
Multiple domains (1) *Two types of matrix material are present in the sample. (1) An orangey brown matrix containing abundant quartz grains and larger clasts, which is heavily iron stained is dominant throughout the sample. (2) A grey matrix material comprised of silts and clays, with a grainy yellow birefringence is present in some localised areas. The grey domains have a similar appearance to the grey cutans observed.*
Intraclasts (1) *Intraclasts are mainly pebble type 3.*
Papules (1)
Plasmic fabric
Skelsepic (3) *Skelsepic fabric is present throughout the orange brown matrix.*
Masepic (2) *Grey domains and grey cutans have a strong yellow grainy masepic plasmic fabric.*
Unistrial (1)

Table C.2 – Characteristics of sample BBQii, (regular size, a and b thin sections) Blinkbonny Quarry. Numbers in brackets indicate the relative abundance of each feature (1 = one or two present; 2 = medium abundance; 3 = high abundance).

Voids
Fissures (2) *Fissures are usually concentrated in areas of fine-grained matrix.*
Vughs (2)
Structures/Features
Clast weathering rinds (3)
Grain lineations (3)
Spalling grains (3)
Turbates (3)
Cutans (3) *Orange and grey cutans are present at the edges of voids and clasts.*
Grain concentrations (2) *There are some grain rich areas in the sample which contain little or no matrix.*
Iron staining (2) *This sample has less iron staining than BBQi. It is fairly localised and is only present in the orange matrix material and is concentrated at the edges of large clasts.*
Multiple domains (2) *Orange and grey domains are present, similar to BBQi. Orange and grey domains cover approximately equal areas of the slide, with diffuse boundaries between the two.*
Intraclasts (1) *Intraclasts are mainly pebble type 3.*
Papules (1)
Plasmic fabric
Skelsepic (3)
Masepic (3) *Localised masepic fabric is present throughout this sample.*
Unistrial (1)

Table C.3 – Characteristics of sample BBQA, (regular size, a and b thin sections) Blinkbonny Quarry. Numbers in brackets indicate the relative abundance of each feature (1 = one or two present; 2 = medium abundance; 3 = high abundance).

Voids
Vughs (3)
Fissures (3)
Structures/Features
Cutans (3) *Cutans are pale orange to mid orange in colour, with a bright orange birefringence. The lighter orange cutans are usually situated inside of the darker orange cutans. Very few grey cutans are present which are inside of the orange cutans and this boundary is diffuse. A large area of cutans (c. 6 mm wide) is present in a circular area in BBQAa (profile view) this is surrounded by an area of concentrated quartz grains.*
Turbates (3)
Grain lineations (3)
Grain concentrations (2)
Spalling grains (2)
Iron staining (2)
Papules (2)
Clast weathering rinds (1)
Multiple Domains (1) *The sample predominantly consists of orange-brown matrix, with very few small localised areas of grey matrix.*
Intraclasts (1) *Intraclasts are mainly pebble type 3.*
Plasmic fabric
Skelsepic (3)
Masepic (2) *Strong masepic fabric is present in the cutans.*
Unistrial (2)

Table C.4 – Characteristics of sample BBQJ, (regular size, a and b thin sections) Blinkbonny Quarry. Numbers in brackets indicate the relative abundance of each feature (1 = one or two present; 2 = medium abundance; 3 = high abundance).

Voids
Fissures (3)
Vughs (3) *Small (<0.5 mm), smooth walled vughs are common. They are often associated with cutans.*
Structures/Features
Cutans (3) *Cutans are pervasive in this sample. They are present in discrete areas where they have horizontal laminations and they are present in between quartz grains.*
Iron staining (3)
Grain lineations (3)
Spalling grains and fragments (2) *Cutans may be present in the area where grains or fragments have spalled off clasts.*
Turbates (2)
Clast weathering rinds (1)
Multiple domains (1) *Most of the sample is dominated by fine texture, orange matrix, and there are some small areas of medium texture, grey matrix.*
Plasmic fabric
Skelsepic (3) *Strong, bright orange skelsepic plasmic fabric is pervasive in the orange matrix. Where it appears very similar to cutans. Weaker, yellow skelsepic plasmic fabric is present in the grey matrix domains.*
Masepic (3) *Strong masepic fabric is present in the cutans.*

Table C.5 – Characteristics of sample NQB, (regular size, a and b thin sections) Newton Quarry. Numbers in brackets indicate the relative abundance of each feature (1 = one or two present; 2 = medium abundance; 3 = high abundance).

Voids
Vughs (3)
Fissures (3)
Vesicles (1)
Structures/Features
Turbates (3)
Clast edge grading into matrix (3)
Multiple domains (2)
Intraclasts (2) *Pebble type 2 and 3 are present throughout the sample.*
Grain concentrations (2)
Spalling grains (2)
Grain lineations (2) *Common along the edges of clasts.*
Cutans (2) *The majority of cutans are orange and associated with voids. A small number of narrow grey cutans are present along the edges of rounded voids.*
Plasmic fabric
Masepic (3)
Skelsepic (2) *Skelsepic plasmic fabric is present around some quartz grains, often only along one or two edges of the grain.*
Unistrial (1)

Table C.6 – Characteristics of sample NQA, (regular size, a and b thin sections) Newton Quarry. Numbers in brackets indicate the relative abundance of each feature (1 = one or two present; 2 = medium abundance; 3 = high abundance).

Voids
Fissures (3)
Vughs (2) *Vughs are mostly circular or oval in shape. These are often found around clasts, where they may form a line. Commonly found in the fine-grained areas of the sample.*
Vesicles (2)
Structures/Features
Grain concentrations (3)
Multiple domains (3) *Multiple domains with poorly defined boundaries are present. Domains of fine grained material (similar in appearance to the local fine grained clasts) and domains of highly concentrated quartz grains are present.*
Grain lineations (3)
Clast edge grading into matrix (3)
Turbates (3)
Cutans (3) *Small areas of bright orange cutans and larger areas of pale orange cutans are present in this sample.*
Spalling grains (2)
Intraclasts (2)
Plasmic fabric
Masepic (3) *Masepic plasmic fabric is present within the cutans and in some areas within the matrix.*
Skelsepic (3)
Unistrial (1)

Table C.7 – Characteristics of sample NQAxi, (regular size, a and b thin sections) Newton Quarry. Numbers in brackets indicate the relative abundance of each feature (1 = one or two present; 2 = medium abundance; 3 = high abundance).

Voids
Vughs (3) *Vughs are smooth walled and usually circular or oval in shape. They range in size from 0.2 to 2 mm.*
Fissures (3) *Most fissures are relatively narrow (c. 0.4 mm thick), have coarse walls and form a well connected network across the fine grained areas of the sample. No fissures are present within the areas of grain concentrations.*
Vesicles (2)
Structures/Features
Grain concentrations (3) *Concentrations of quartz within the fine grained matrix and layers of quartz which form wavy structures.*
Cutans (3) *Cutans are pale to dark orange in colour.*
Multiple domains (2) *Different textural domains are present.*
Clast edge grading into matrix (2)
Clast weathering rinds (1)
Spalling grains (1)
Turbates (1)
Faulting (1)
Iron staining (1)
Grain lineations (1)
Plasmic fabric
Masepic (2)

Table C.8 – Characteristics of sample NQC, (regular size, a and b thin sections) Newton Quarry. Numbers in brackets indicate the relative abundance of each feature (1 = one or two present; 2 = medium abundance; 3 = high abundance).

Voids
Vughs (3) *Circular, ovate and elongate smooth walled vughs are abundant. Elongate shaped vughs are common in NQCb. Most vughs are not associated with cutans.*
Fissures (2) *A network of well connected, coarse walled fissures is present.*
Vesicles (2)
Structures/Features
Cutans (3) *Cutans are mid to pale orange in colour.*
Grain concentrations (2) *A large area of concentrated grains is present near the top of NQCa and in the centre of NQCb.*
Multiple domains (2) *Domains of grain concentrations, brecciated mudstones within a fine grained matrix and fine matrix are present.*
Clast edge grading into matrix (2)
Faulting (2)
Iron Staining (2)
Grain lineations (2)
Turbates (1)
Plasmic fabric
Masepic (3)
Skelsepic (2) *Skelsepic plasmic fabric is present around some quartz grains and mudstone clasts.*

Table C.9 – Characteristics of sample BCRa95, (mammoth size; two overlapping vertical (a) thin sections) Berry Creek Reservoir. Numbers in brackets indicate the relative abundance of each feature (1 = one or two present; 2 = medium abundance; 3 = high abundance).

Voids
Packing voids (3) *Pervasive within the sand domain.*
Fissures (2) *Common in the fine grained (diamict) domain.*
Vughs (2) *Present in sand lithofacies (sampling artefact).*
Structures/Features
Multiple domains (3) *Associated with the different lithofacies, including large sand intraclasts and diamict. Some mixing between the two is evident. A sharp, undulating boundary is evident between these domains, some encroachment of the diamict matrix into the sand domain can be seen.*
Turbates (1) *In the diamict domain.*
Grain lineations (2) *In the diamict domain.*
Clast brecciation (1) *In the diamict domain.*
Plasmic fabric
Skelsepic (3) *Pervasive in the diamict domain and present within a very thin layer of matrix in the sand domain.*
Masepic (2) *Present in the diamict domain.*
Other
Sample taken from melange and encompasses sand intraclasts and diamict. These domains have very different characteristics.

Table C.10 – Characteristics of sample BCRa145, (mammoth size; two overlapping vertical (a) thin sections) Berry Creek Reservoir. Numbers in brackets indicate the relative abundance of each feature (1 = one or two present; 2 = medium abundance; 3 = high abundance).

Voids
Fissures (3) *Range of orientations but the majority are consistent with the orientation of the stratification. Dendritic. From 0.05 – 1 mm wide.*
Vughs (2)
Structures/Features
Multiple domains /Stratification (3) *Clear stratification throughout the sample; deformed, irregular layers. Gradual contacts between the layers.*
Grain concentrations (3) *Sand rich layers within the stratification.*
Grain lineations (3) *Typically long and with the same orientation as the stratification.*
Turbates (3) *Typically with corestones.*
Intraclasts (2) *Sand intraclasts, with lenticular shapes (associated with the stratification).*
Gypsum (1) *Cluster near top of sample.*
Iron Staining (1)
Plasmic fabric
Skelsepic (3) *Well developed and abundant.*
Masepic (3)

Table C.11 – Characteristics of sample BCRa180, (regular size; a and b thin sections) Berry Creek Reservoir. Numbers in brackets indicate the relative abundance of each feature (1 = one or two present; 2 = medium abundance; 3 = high abundance).

Voids
Fissures (3) *Abundant short, poorly-connected fissures in slide a (< 0.5 mm wide). Large fissures trending widthways across slide b (likely sampling artefacts).*
Vughs (2)
Packing voids (2) *In localised areas of the slide.*
Structures/Features
Carbonate deposits (3) *Localised areas of carbonate, not associated with large clasts.*
Grain concentrations (2)
Grain lineations (2) *Alignments of grains.*
Gypsum (2) *Concentrations of gypsum present in slide b. Crystals are typically irregular and amorphous shapes.*
Turbates (1) *Observed in slide a.*
Iron Staining (1) *Minor iron staining, often associated with fissures*.
Organic matter (1)
Plasmic fabric
Skelsepic (3) *Pervasive and strong throughout a and b slides.*
Masepic (3) *Pervasive, Associated with skelsepic plasmic fabric and stronger in the finer grained areas.*
Other
Skeleton grains range from 0.2 – 10.6 mm. Grains >0.3 mm are typically rounded and well-rounded; grains <0.3 mm are typically sub-angular and sub-rounded.
Some stratification across slide a, evident as variations in skeleton grain density.

Table C.12 – Characteristics of sample BCRb10, (regular size, only vertical (a) thin section) Berry Creek Reservoir. Numbers in brackets indicate the relative abundance of each feature (1 = one or two present; 2 = medium abundance; 3 = high abundance).

Voids
Packing voids (3) *The sample is very matrix poor so packing voids are abundant throughout the sample.*
Fissures (2) *Well-connected fissures within the fine grained clasts.*
Structures/Features
Carbonate deposits (2) *Present in a layer underneath some of the hard granite clasts. None on the fine grained clasts.*
Clast edge grading into matrix (2)
Brecciation (2) *Larger mudstone clasts are brecciated in situ, they are broken into several smaller angular clasts.*
Plasmic fabric
Masepic (2) *Present in the majority of mudstone clasts*.
Skelsepic (2) *Present in the innermost layer of the thin layer of matrix around some of the grains.*
Unistrial (1) *Present within some of the mudstone clasts.*
Other
Very coarse texture, dominated by grains and clasts, with very little matrix.

Table C.13 – Characteristics of sample BCRb40, (regular size, a and b thin sections) Berry Creek Reservoir. Numbers in brackets indicate the relative abundance of each feature (1 = one or two present; 2 = medium abundance; 3 = high abundance).

Voids
Packing voids (3) *Packing voids are present consistently across the sample*.
Fissures (2) *Abundant in the mudstone clasts, where they typically match the clast fabric and may form a polygonal pattern.*
Structures/Features
Carbonate deposits (3) *Present in a and b slides, only on the hard lithologies and not the mudstone clasts. Found on certain sides of the clasts, and at the base of the clasts.*
Spalling grains (2) *Occur on the mudstone and quartzite clasts.*
Clast brecciation (2) *Brecciation of the mudstone clasts.*
Weathering rinds (1)
Clast edge grading into matrix (1) *Of the mudstone clasts.*
Plasmic fabric
Masepic (3) *Present to varying degrees in the mudstone clasts.*
Skelsepic (2)
Other
Coarse sediment, dominated by skeleton grains with very little matrix.

Table C.14 – Characteristics of sample BCRb80, (regular size, a and b thin sections) Berry Creek Reservoir. Numbers in brackets indicate the relative abundance of each feature (1 = one or two present; 2 = medium abundance; 3 = high abundance).

Voids
Packing voids (3) *Present across entire sample, but some heterogeneities in terms of how tightly packed the grains and sediment is.*
Fissures (3) *Present within the mudstone clasts, particularly the larger ones. Typically well-connected, polygonal and parallel to the clast fabric.*
Vughs (2) *Typically present in the areas where the sediment is loosest.*
Structures/Features
Carbonate deposits (3) *Found at the base and east side of the resistant clast lithologies.*
Spalling grains (3) *Most common on mudstone clasts, but also observed on the more resistant lithologies.*
Clast brecciation (3) *Mudstone clasts are brecciated to varying degrees.*
Clast edge grading into matrix (2) *Of the mudstone clasts.*
Intraclasts (2)
Plasmic fabric
Masepic (3) *Present in the mudstone clasts and the intraclasts.*
Skelsepic (3) *Present around some of the medium sized grains and within the intraclasts.*

Table C.15 – Characteristics of sample BICRa, (regular size, a and b thin sections) Blood Indian Creek Reservoir. Numbers in brackets indicate the relative abundance of each feature (1 = one or two present; 2 = medium abundance; 3 = high abundance).

Voids
Fissures (3) *Network of connected orthogonal fissures. Prominent across lower domain and b slide.*
Vughs (2) *Present in all domains.*
Structures/Features
Multiple domains (3) *Three domains each with different textures, in the upper, mid and lower parts of the a slide.*
Intraclasts (3) *Typically rounded/well-rounded and 0.4 - 2 mm in diameter.*
Gypsum (3) *Concentrated in discrete areas (4 – 13 mm wide). No matrix is present in-between the gypsum crystals. Lenticular, rounded and amorphous shaped crystals.*
Grain concentrations (2) *Different grain densities in different domains.*
Plasmic fabric
Masepic (2) *Common in the intraclasts.*
Skelsepic (2) *Especially present on the mid and larger sized grains. More developed in the lower domain than the upper domain (including the b slide).*

Table C.16 – Characteristics of sample BICRb, Blood Indian Creek Reservoir. Numbers in brackets indicate the relative abundance of each feature (1 = one or two present; 2 = medium abundance; 3 = high abundance).

Voids
Fissures (3) *Typically large and well connected in the upper domain and small and poorly connected in the lower domain.*
Vughs (3)
Vesicles (3) *Present throughout all three domains, some with organic matter in.*
Channels and chambers (3) *Elongate smooth walled voids of varying size and length. Some have bits of sediment or organic matter in them. Most common in the fine grained areas.*
Structures/Features
Multiple domains (3) *Three domains present, which correspond to the lithofacies sampled from. The lower domain is quite fine grained and matrix rich. The middle domain is fine grained with some textural variability, including laminations towards the top of the domain. Upper domain is grain rich with some matrix and heterogeneous.*
Carbonate deposits (3) *Present in all domains, with some variations in concentration between domains.*
Burrows/Bioturbation (3) *Present in all domains, especially abundant at the contacts between the domains.*
Organic matter (2)
Turbates (2) *Most turbates in lower domain.*
Laminations (2) *At top of middle domain. Sub-horizontal laminae of varying texture and colour. Discontinuous and some apparent postdepositional disturbance.*
Haloes (2) *Some haloes present near base of upper domain. Fine-grained sediment around medium sized grains.*
Grain lineations (1)
Intraclasts (1)
Crushed quartz (1)
Plasmic fabric
Skelsepic (3) *Abundant in lower domain; very slight in middle domain and present but weak in upper domain.*
Masepic (2) *Common in lower domain.*
Unistrial (1) *Present in lower domain.*

Table C.17 – Characteristics of sample BICRc10, (regular size, a and b thin sections) Berry Creek Reservoir. Numbers in brackets indicate the relative abundance of each feature (1 = one or two present; 2 = medium abundance; 3 = high abundance).

Voids
Fissures (3)
Vughs (2)
Structures/Features
Intraclasts (3) *Range from 0.4 – 4 mm diameter. Many pebble type 2 (strong masepic plasmic fabric within them).*
Grain lineations (3)
Turbates (3) *Typically arcuate alignments of grains trailing off a clast.*
Carbonate deposits (2)
Grain concentrations (1)
Iron Staining (1)
Plasmic fabric
Skelsepic (3) *Well developed in a and b slide. Present on grains 0.02 – 1.2 mm in size.*
Masepic (3)

Table C.18 – Characteristics of sample BICRc30, (regular size, vertical (a) thin section) Berry Creek Reservoir. Numbers in brackets indicate the relative abundance of each feature (1 = one or two present; 2 = medium abundance; 3 = high abundance).

Voids
Fissures (2) *Common in the lower domain and at the boundary between the two domains. Typically orientated parallel to the boundary between the lithofacies. Some of the smaller fissures have carbonate deposits in them.*
Vughs (2) *Common in the lower domain.*
Packing voids (2) *Common in the upper domain.*
Structures/Features
Multiple domains (3) *Sampled from the boundary between LF1 and LF3, so slide a is characterised by two domains. The lower domain (LF1) is fine grained and matrix rich, whilst the upper domain (LF3) has a much coarser texture and little matrix. Sharp, slightly undulating boundary between the two domains.*
Intraclasts (3) *Common in lower domain, few in upper domain. Typically rounded and well rounded, 0.2 – 3 mm in diameter.*
Carbonate deposits (3) *Found throughout sample, especially at contact between domains. Present in discrete areas, often forming concentric rings.*
Grain concentrations (2)
Turbates (1)
Grain lineations (1)
Organic matter (1)
Plasmic fabric
Skelsepic (3)
Masepic (2)

Table C.19 – Characteristics of sample BICRc50, (regular size, vertical (a) thin section) Blood Indian Creek Reservoir. Numbers in brackets indicate the relative abundance of each feature (1 = one or two present; 2 = medium abundance; 3 = high abundance).

Voids
Packing voids (3) *Small voids in-between the skeleton grains throughout the sample. Sediment is matrix poor.*
Vughs (2)
Fissures (1)
Structures/Features
Clast brecciation (2) *Of the fine-grained sedimentary clasts.*
Plasmic fabric
Skelsepic (2) *Apparent in the tiny amounts of matrix adhering to the grains.*
Other
Skeleton grains dominate the sample and matrix is minimal and spatially variable. Matrix is present in small clumps and on the tops of grains. Skeleton grains are typically rounded and well-rounded.

Table C.20 – Characteristics of sample BICRc80, (regular size, a and b thin sections) Blood Indian Creek Reservoir. Numbers in brackets indicate the relative abundance of each feature (1 = one or two present; 2 = medium abundance; 3 = high abundance).

Voids
Packing voids (3)
Fissures (2)
Vughs (2)
Vesicles (1) *Typically small (< 0.1 mm), present in fine grained areas.*
Structures/Features
Spalling grains (2) *Fragments observed that have spalled off large quartzite grains.*
Carbonate deposits (2) *Extensive around the edge and base of a large quartzite grain.*
Multiple domains (1)
Intraclasts (1)
Plasmic fabric
Skelsepic (2) *Typically on grains 0.2 – 3.3 mm diameter.*
Other
Discontinuous meandering layer within slide a, consisting of small grains and some matrix. Some textural banding is apparent within the layer.
Overall fining upwards trend to the sample.

Table C.21 – Characteristics of sample BICRc120, (regular size, a and b thin sections) Blood Indian Creek Reservoir. Numbers in brackets indicate the relative abundance of each feature (1 = one or two present; 2 = medium abundance; 3 = high abundance).

Voids
Vughs (3) *Relatively small (0.1 – 2 mm diameter) and typically have smooth walls and irregular shapes.*
Fissures (2) *Poorly connected, of varying size and thickness.*
Packing voids (2)
Vesicles (2)
Structures/Features
Grain lineations (3)
Multiple domains (2) *Areas of different matrix structure, typically with indistinct boundaries.*
Turbates (2) *Typically with core stones.*
Gypsum (2) *Small clusters in discrete areas*
Carbonate deposits (2) *At the base of some of the largest grains.*
Organic matter (1) *Some root fragments present.*
Burrows/bioturbation (1)
Plasmic fabric
Skelsepic (2) *More common in slide b than slide a.*

Table C.22 – Characteristics of sample BICRd, Blood Indian Creek Reservoir. Numbers in brackets indicate the relative abundance of each feature (1 = one or two present; 2 = medium abundance; 3 = high abundance).

Voids
Vughs (3)
Fissures (2) *Typically disconnected and some are filled with gypsum*.
Packing voids (2)
Structures/Features
Multiple domains (3) *Two large domains are present, which correspond to the two lithofacies that the sample crosses. The upper domain is grain rich with little matrix. The lower domain is more matrix rich, and has a heterogeneous structure and texture. The boundary between the domains is indistinct.*
Intraclasts (3) *Large intraclasts (up to 4 mm diameter) are present in the upper domain (typically pebble type 3). Intraclasts in the upper domain are the same material as the lower domain. Few intraclasts are present in the lower domain.*
Gypsum (3) *Abundant clusters in the lower domain, but rare in the upper domain. Crystal shapes are typically lenticular, with the larger crystals more prismatic and blocky. Crystals of similar size and shape are typically clustered together.*
Turbates (2) *Abundant in the lower domain. Typically have corestones.*
Grain lineations (1)
Plasmic fabric
Skelsepic (3) *Extensive and well developed around the majority of grains and clasts.*
Masepic (2)
Unistrial (2) *Common short shears depicted by unistrial plasmic fabric in the lower domain.*

C.2 Grain lineation mapping

(a) BBQAa

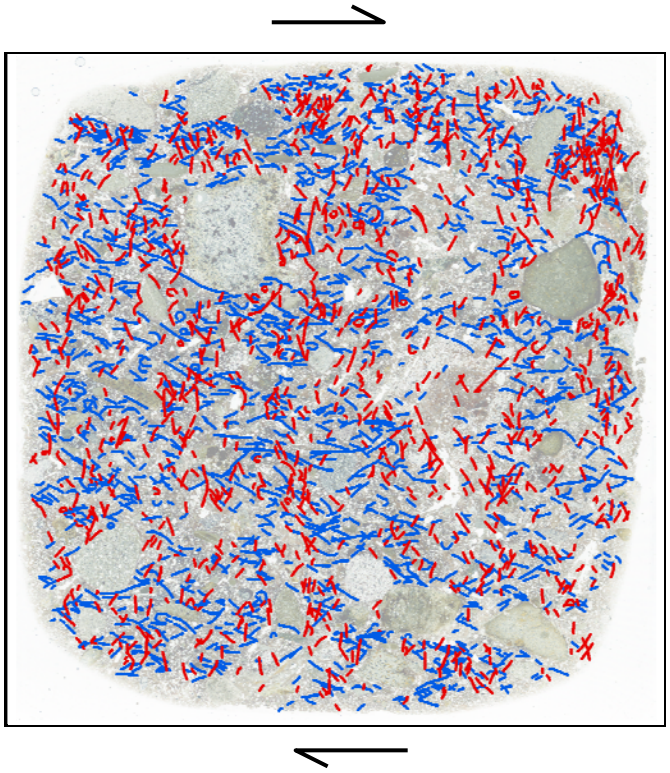

(b) BBQiia

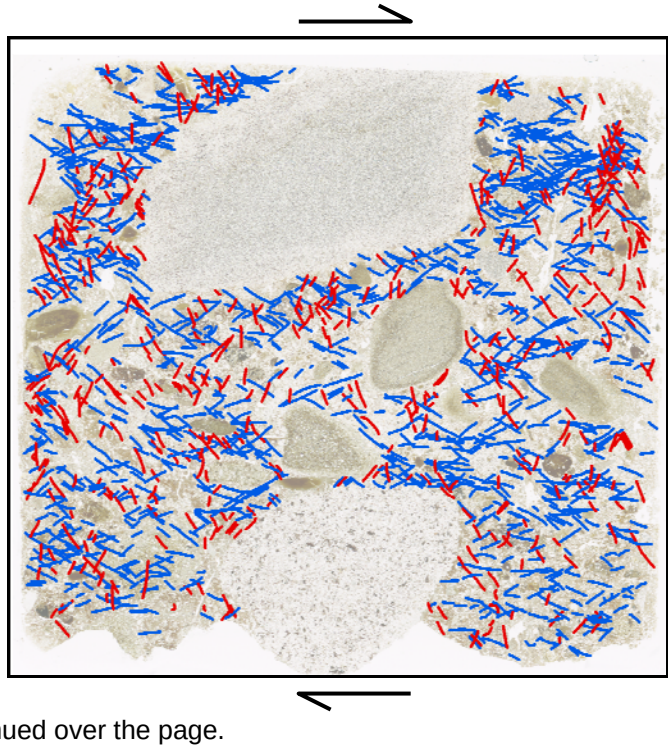

Figure C.1 – Continued over the page.

(c) BBQia

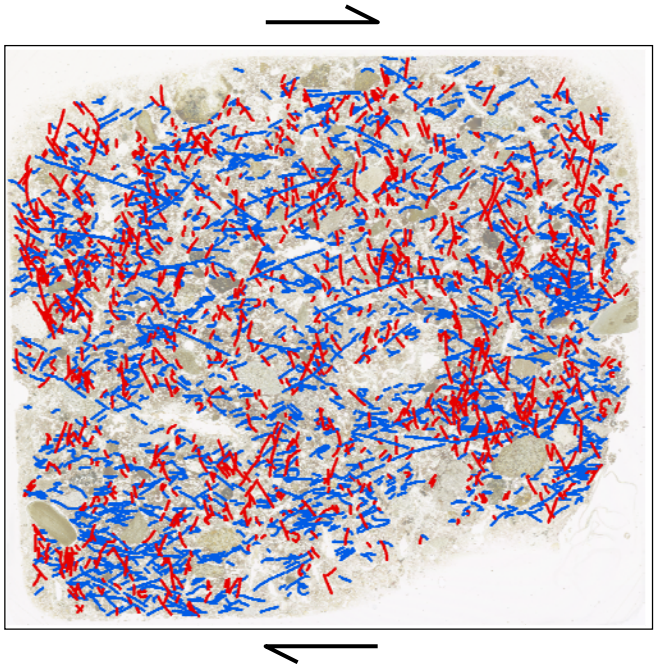

(d) BBQJa

Perpendicular to ice flow direction

Figure C.1 – Continued over the page.

(e) NQAc

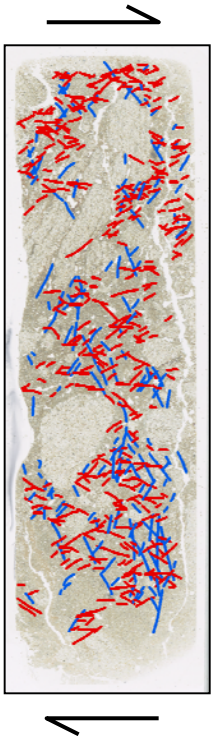

(f) NQAa

Perpendicular to ice flow direction

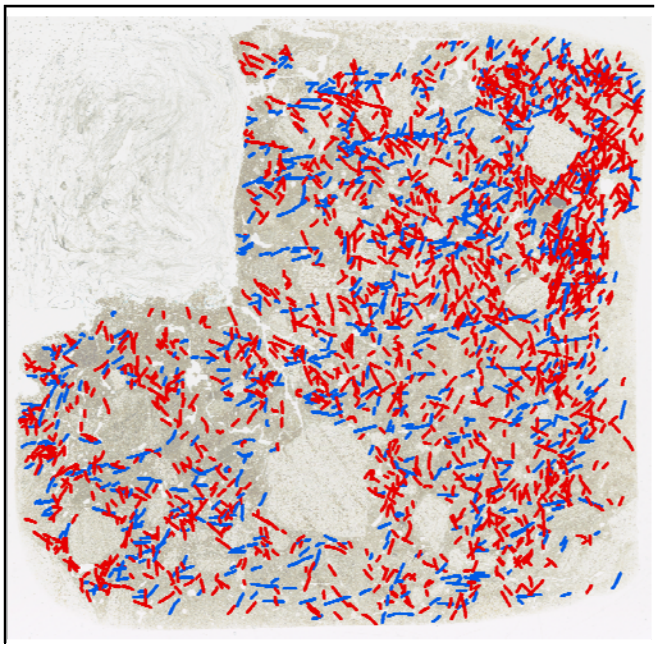

Figure C.1 – Grain lineation mapping for vertical thin sections. (a) BBQAa; (b) BBQiia; (c) BBQia; (d) BBQJa; (e) NQAc; (f) NQAa. Grain alignments with high angle dips (greater than 45º) are red and those with low angle dips (less than 45º) are blue. Relative sense of shear is indicated with arrows.

C.3 Microfabric statistics

Table C.9 – Vector mean and confidence interval (95 %) (i.e. 95 % of values fall within this range) for the azimuth microfabrics.

Sample	**Vector mean**	**Confidence interval (95 %)**
BBQi	56.1°	6.9°
BBQii	153.7°	26.6°
BBQJ	66.7°	7.4°
NQA	57.7°	1.6°
NQB	164°	7.9°
NQC	168.5°	7.7°
BCRa180	126.9°	3.2°
BCRb40	64.9°	24.8°
BICRa	77°	35.4°
BICRc10	28.6°	2.9°
BICRc80	18°	9.6°
BICRc120	26.9°	2.4°